Magnesium Ring-Opening Polymerisation Catalysts

Xinning Yin BSc (Hons) AMRSC



Thesis submitted to the University of Oxford for the degree of

Doctor of Philosophy, June 2016

The work described in this Thesis was carried out in the Chemistry Research Laboratory, University of Oxford from October 2012 to June 2016 under the supervision of Professor Philip Mountford. All work is my own unless stated to the contrary, and has not previously been submitted for any degree at this or any other university.

Xinning Yin

June 2016

Abstract

Xinning Yin June 2016
St Hilda's College D. Phil Thesis

This Thesis describes the synthesis and characterisation of new magnesium borohydride, alkoxide and amide complexes, and their uses as catalysts for the ring-opening polymerisation (ROP) of *rac*-, *L*-, *D*-, *meso*-lactide and ε-caprolactone.

Chapter One introduces cyclic esters and possible mechanistic pathways leading to polyesters by ROP. Common techniques for polymer characterisation are described and an overview of ROP from an industrial perspective is also given.

Chapter Two describes the synthesis and characterisation of a series of magnesium alkyl, halide, borohydride and alkoxide complexes supported by the 3-*tert*-butyl, 5-methyl tris(pyrazolyl)methane ligand. Computational analysis will be discussed to gain further understanding from the viewpoint of bonding and structures.

Chapter Three describes the activities of magnesium borohydride and benzyloxide catalysts in the ROP of cyclic esters. Detailed mechanistic studies for the ROP of LA using a magnesium borohydride catalyst are discussed.

Chapter Four describes the use of borate ester species as chain transfer agents in the immortal ROP of *rac*-LA and ε-CL. The effect of non-activated catalysts and borate ester species on the occurrence of transesterification side reactions is also discussed.

Chapter Five describes the synthesis and characterisation of a series of magnesium amide, borohydride and halide complexes supported by the chiral bis(oxazolinylphenyl)amine ligand. The catalytic activities of the magnesium borohydride complex in the living and immortal ROP of LA are also discussed.

Chapter Six contains experimental details and characterising data for the new complexes reported in this Thesis.

CD Appendix contains .CIF files for all the new crystallographically-characterised complexes and .xyz files containing the coordinates of the geometrically optimised structures.

Contents

	Declaration	i
	Abstract	ii
	Contents	iii
	Acknowledgements	vii
	Abbreviations	viii
	Notes	xi
Chapter One – Introduction		1
1.1	Overview	2
1.2	General introduction	2
1.2.1	Introduction to PCL	2
1.2.2	Introduction to PLA	3
1.3	Thermodynamic aspects of ROP	4
1.4	ROP mechanisms	5
1.4.1	Anionic ROP	5
1.4.2	Cationic ROP	7
1.4.3	Organocatalysis	8
1.4.4	Metal-mediated ROP	10
1.4.4.1	Coordination insertion mechanism	10
1.4.4.2	Activated monomer mechanism	12
1.4.5	Living and immortal ROP	14
1.5	Stereocontrol and tacticity of PLA	17
1.5.1	Characterisation of PLA stereosequences using NMR spectroscopy	19
1.6	Polymer characterisation	22
1.6.1	NMR spectroscopy	22
1.6.2	MALDI-ToF Mass Spectrometry	22
1.6.3	Definitions of polymer molecular weight	23
1.6.4	Gel Permeation Chromatography	24
1.7	Industrial ROP catalysts	25
1.8	Aims and outlook	27
1.9	References for Chapter One	27

Chapter Two – Synthesis, characterisation and DFT studies of tris(pyrazolyl)methanide magnesium complexes 40

2.1 Overview 41
2.2 Introduction 41
2.3 Synthesis and characterisation of Tpm*^{d} magnesium complexes 45
2.3.1 Synthesis and characterisation of (Tpm*^{d})Li(THF) (**1**), (Tpm*^{d})Mg(BH_4) (**2**) and (Tpm*^{d})MgMe (**3**) 46
2.3.2 Synthesis and characterisation of (Tpm*^{d})Mg(Bu) (**4**), (Tpm*^{d})Mg(OBn) (**5**) and (Tpm*^{d})Mg(BD_4) (**2-*d*$_4$**) 54
2.3.3 Synthesis and characterisation of (Tpm*^{d})Mg(Cl) (**6**), (Tpm*^{d})Mg(Br) (**7**) and [(Tpm*)Mg(Me)]Br (**8**) 57
2.4 Computational analysis of $Tp^{Me,Me}$ and Tpm^{d} ligand-supported magnesium alkoxide species 59
2.5 Summary and conclusions 64
2.6 References for Chapter Two 64

Chapter Three – Tris(pyrazolyl)methanide magnesium complexes for the ROP of *rac*-, *L*-, *meso*-LA and ε-CL and their mechanistic studies 68

3.1 Overview 69
3.2 Introduction 69
3.2.1 Alkaline earth complexes as ROP catalysts 69
3.2.2 Borohydride initiators for the ROP of cyclic esters 73
3.2.2.1 Lanthanide borohydride initiators for the ROP of cyclic esters 73
3.2.2.2 Alkaline earth borohydride initiators for the ROP of cyclic esters 76
3.2.3 Literature reported and newly revised borohydride initiating mechanisms 79
3.2.4 Borate ester species as chain transfer agents 84
3.3 ROP of ε-CL using (Tpm*^{d})Mg(OBn) (**5**) as a catalyst 85
3.4 ROP of LA using (Tpm*^{d})Mg(OBn) (**5**) as a catalyst 88
3.4.1 Catalytic activity of (Tpm*^{d})Mg(OBn) (**5**) in the ROP of LA 88
3.4.2 Mechanistic considerations of (Tpm*^{d})Mg(OBn) (**5**) in the ROP of LA 93
3.5 ROP of ε-CL using (Tpm*^{d})Mg(BH_4) (**2**) as a catalyst 94

3.5.1	Catalytic activity of (Tpm*^{d})Mg(BH_4) (**2**) for the ROP of ε-CL	94
3.5.2	Mechanistic considerations of (Tpm*^{d})Mg(BH_4) (**2**) for the ROP of ε-CL	96
3.6	ROP of *rac*-LA using (Tpm*^{d})Mg(BH_4) (**2**) as a catalyst	98
3.6.1	Catalytic activity of (Tpm*^{d})Mg(BH_4) (**2**) for the ROP of *rac*-LA	98
3.6.2	Mechanistic considerations of (Tpm*^{d})Mg(BH_4) (**2**) for the ROP of *rac*-LA	100
3.6.2.1	Identification of the first hydride transfer product	101
3.6.2.2	Polymer end group analysis	118
3.6.2.3	Chain transfer ability of "B(LA-H)$_3$"	123
3.6.3	Rate differences in the ROP of *rac*-LA using (Tpm*^{d})Mg(BH_4) (**2**) and (Tpm*^{d})Mg(OBn) (**5**)	126
3.7	Summary and conclusions	127
3.8	References for Chapter Three	130
Chapter Four – Borate ester species as chain transfer agents for the ROP of *rac*-LA and ε-CL		136
4.1	Overview	137
4.2	A novel approach to generate B(OBn)$_3$ *in-situ*	137
4.3	ROP of *rac*-LA using *in-situ* generated and externally added B(OBn)$_3$	139
4.4	ROP of ε-CL using *in-situ* generated and externally added B(OBn)$_3$	151
4.5	Chain transfer ability of bulky borate ester species in the ROP of ε-CL	156
4.6	The effect of non-activated catalysts on the occurrence of transesterification side reactions	159
4.7	Exchange processes between a borate ester and a metal alkoxide or metal polymeryl species	164
4.8	Summary and conclusions	168
4.9	References for Chapter Four	170

Chapter Five – Chiral bis(oxazolinylphenyl)amine ligand-supported magnesium catalysts for the ROP of *rac*-, *L*-, *D*- and *meso*-LA 172

5.1 Overview 173
5.2 Introduction 173
5.2.1 Achiral initiators for the isoselective ROP of LA 173
5.2.2 Chiral initiators for the isoselective ROP of LA 181
5.2.3 Oxazoline ligand-supported initiators for the ROP of LA 190
5.3 Synthesis and characterisation of BOPA ligand-supported magnesium complexes 193
5.3.1 Synthesis and characterisation of BOPA^{iPr}-supported magnesium complexes 194
5.3.2 Synthesis and characterisation of BOPA^{Ph}-supported magnesium complexes 200
5.4 ROP of *rac*-, *L*-, *D*- and *meso*-LA using magnesium catalysts 210
5.4.1 ROP of *rac*-LA using magnesium amide catalysts 210
5.4.2 ROP of *rac*-, *L*-, *D*- and *meso*-LA using magnesium borohydride catalysts 212
5.5 Summary and conclusions 231
5.6 References for Chapter Five 233

Chapter Six – Experimental details and characterising data 240

6.1 General methods and instrumentation 241
6.2 Literature preparations and reagent purification 242
6.3 X-ray data collection and processing parameters 243
6.4 Computational details 243
6.5 Experimental details and characterising data for Chapter Two 244
6.6 Experimental details and characterising data for Chapter Three 248
6.7 Experimental details and characterising data for Chapter Four 251
6.8 Experimental details and characterising data for Chapter Five 253
6.9 Polymerisation procedures 261
6.10 References for Chapter Six 264

Appendix xii

Acknowledgements

First and foremost, I would like to thank my supervisor, Prof. Philip Mountford, for his support and guidance throughout my DPhil studies. I have learnt a great deal from him and my studies and these experiences will undoubtedly be very beneficial for my later career and life. I am particularly grateful to Philip for allowing me to undertake an industrial placement during my studies, which I enjoyed and benefited from greatly.

I would like to express my sincere thanks to Dr Insun Yu for being a great mentor and friend, who provided valuable help and advice both chemistry-wise and life-wise. I am grateful for all the effort she has put into the ROP projects and the encouragement she has given me in the last two years. I must also thank Dr Matt Blake for the DFT calculations and for being a close friend who offered moral support, especially when chemistry was not going so well and during the stressful job hunting process. My ROP ancestor, Dr Junjuda Unruangsri, deserves my special mention for being my big sister in the lab. I think she will be very happy to know that I have inherited her "teasing" skills, which have been passed down to the later generations of the group. I truly appreciate Dr Andrey Protchenko, Dr Bryony Core, Dr Laura Stevenson, Drs (to be) Richard Collins and Phonpimon Wongmahasirikun, Ross Green, Adán Reyes, Ben Clough, Simona Mellino, Karen Gamero, Bowen Xie, Nichabhat Diteepeng, Theresa Scharbert, Martin Slusarczyk and Natália Vieira for making this group an enjoyable place to work in. I cannot finish without acknowledging Matt and Insun again for proofreading this Thesis.

Additionally, I must express my gratitude to Dr Amber Thompson, Collin Sparrow for their help with X-ray crystallography and mass spectrometry, Dr Nick Rees for NMR spectroscopy and his collection of J-pop music which made the basement NMR room more lively. I would also like to thank Dr Ben Ward of the University of Cardiff with whom I collaborated on the BOPA work.

Lastly, I reserve the deepest thanks for my parents and grandmother who have raised me well and always been there for me. I would not be who or where I am today without their unconditional love and support. I am grateful to all my other friends, especially those in chemistry for all the advice and understanding. I would also like to thank myself for being strong and surviving those seemingly hard moments, which become an integral part of my "painfully" happy time in Oxford when I look back.

Abbreviations

General

Å	Ångstrom
av.	average
ca.	*circa*, about
calcd	calculated
cal	calories
CTA	chain-transfer agent(s)
cf.	*confer*, compare
d	day(s)
°	degrees
℃	degrees Celsius
DFT	Density Functional Theory
equiv(s).	equivalent(s)
g	gram(s)
GPC	gel permeation chromatography
h	hour(s)
*i*ROP	immortal ring-opening polymerisation
η	intrinsic viscosity
J	Joule(s)
k	kilo
K	Kelvin
k_{obs}	observed rate constant
k_i	rate constant of initiation
k_p	rate constant of propagation
k_{tr}	rate constant of chain-transfer reaction
L	litre(s)
mg	milligram(s)
min	minute(s)
mL	millilitre(s)
μL	microliter(s)
ROP	ring-opening polymerisation
RT	room temperature
s	second(s)

SEC	Size Exclusion Chromatography
T	temperature
T_g	glass transition temperature
T_m	melting temperature

Chemical

Ar	aryl group
Bn	benzyl
BnOH	benzyl alcohol
BOPA	bis(oxazolinylphenyl)amine
Cp	C_5H_5
Cp*	C_5Me_5
$CzOx^{Me_2}$	2,2'-(3,6-di-*tert*-butyl-9λ^2-carbazole-1,8-diyl)bis(4,4-dimethyl-4,5-dihydrooxazole)
$CzOx^{iPr}$	2,2'-(3,6-di-*tert*-butyl-9λ^2-carbazole-1,8-diyl)bis(4-isopropyl-4,5-dihydrooxazole)
Cyh	cyclohexyl
D-lactide	(*R*,*R*)-cis-3,6-dimethyl-1,4-dioxane-2,5-dione
DMAP	4-dimethylaminopyridine
^{n}Bu	*n*-butyl
^{t}Bu	*tert*-butyl
^{i}Pr	*iso*-propyl
^{i}PrOH	isopropyl alcohol
L	a supporting ligand (set)
LA	lactide
L-lactide	(*S*,*S*)-cis-3,6-dimethyl-1,4-dioxane-2,5-dione
Me	methyl
meso-lactide	(*R*,*S*)-cis-3,6-dimethyl-1,4-dioxane-2,5-dione
M_n	number average molecular weight
M_p	peak molecular weight
M-OR	metal alkoxide
M_w	weight average molecular weight
PDI	poly dispersity index
Ph	phenyl
PhCHO	benzaldehyde
P_m	probability of *meso*- linkages

PLA	poly(lactic acid)
P_r	probability of racemic linkages
py	pyridine
pz	pyrazole
R	generic aryl or alkyl
rac-lactide	a racemic mixture of *D*- and *L*-lactide
$Sn(Oct)_2$	tin octanoate
THF	tetrahydrofuran
Tpm	tris(pyrazolyl)methane
Tpm^d	tris(pyrazolyl)methanide
Tpm*	3-*tert*-butyl, 5-methyl tris(pyrazolyl)methane
Tpm^{*d}	3-*tert*-butyl, 5-methyl tris(pyrazolyl)methanide

Mass Spectrometry

EI	electron impact
FI	field ionisation
m/z	mass to charge ratio
MS	mass spectrometry
MALDI-ToF MS	matrix-assisted laser desorption/ionization - time of flight mass spectrometry

Nuclear Magnetic Resonance Spectroscopy

$^{11}B\{^1H\}$	proton-decoupled ^{11}B
$^{13}C\{^1H\}$	proton-decoupled ^{13}C
app.	apparent
br	broad
COSY	correlation spectroscopy
d	doublet
dq	doublet of quartets
HETCOR	heteronuclear correlation
HMBC	heteronuclear multiple bond correlation
HMQC	heteronuclear single quantum correlation
i	*ipso*
J	coupling constant
m	*meta*

m	multiplet
NMR	nuclear magnetic resonance
nOe	nuclear Overhauser effect
NOESY	nuclear Overhauser effect spectroscopy
o	*ortho*
p	*para*
ppm	parts per million
q	quartet
ROESY	rotating-frame nuclear Overhauser Effect spectroscopy
s	singlet
sept	septet
t	triplet
VT	variable temperature
δ	chemical shift in ppm

Infrared Spectroscopy

br	broad
FT-IR	fourier transform infrared red
IR	infrared red
m	medium
s	strong
w	weak
ν	frequency

Note about numbering of compounds described in this Thesis

Literature compounds described in this Thesis are numbered **1.x**, **2.x**, **3.x**, **4.x**, according to the Chapter in which they first occur. The new compounds described in this Thesis are numbered **1 - 28**. MALDI-ToF mass spectroscopy was performed by Colin Sparrow, and elemental analysis were performed by Stephen Boyer at London Metropolitan University.

Chapter One

Introduction

1.1 Overview

This Chapter will provide a general introduction to the ring-opening polymerisation (ROP) of cyclic esters. The various initiating mechanisms for metal-mediated ROP will be discussed, with the emphasis on the concept of living and immortal polymerisation. A brief introduction on polymer microstructure will be discussed, as well as the analytical tools used for characterisation of polymers.

1.2 General Introduction

The last six decades have witnessed a continuous usage of polymeric materials derived from petrochemical feedstocks. Since the discovery of Ziegler Natta catalysts in the 1950s, there has been a surge in the commercial manufacture of various polyolefins. For example, poly(ethylene), which has found numerous applications in areas such as packaging, is being produced at an annual scale of 80 million tonnes globally.[1] However, it is predicted that petrochemical resources will arguably be depleted in the near future. It is therefore of significant interest to develop new polymeric materials derived from renewable resources.[2]

Despite the forthcoming shortage of petrochemical feedstocks, the search for alternative materials to polyolefins is also driven by the environmental impact that the production of polyolefins has brought upon; these polymers are not readily biodegradable and are usually disposed of in landfill sites where degradation takes a very long time.[3] In an effort to solve the aforementioned problems, significant attention has been paid to the development of biodegradable polymers. Of the variety of such polymers known, poly(ε-caprolactone) (PCL) and polylactide (PLA),[4-12] being linear aliphatic polyesters, have attracted particular interest due to their unique properties, allowing them to find applications in a number of areas such as packaging[13, 14] and biomedical materials.[15-19]

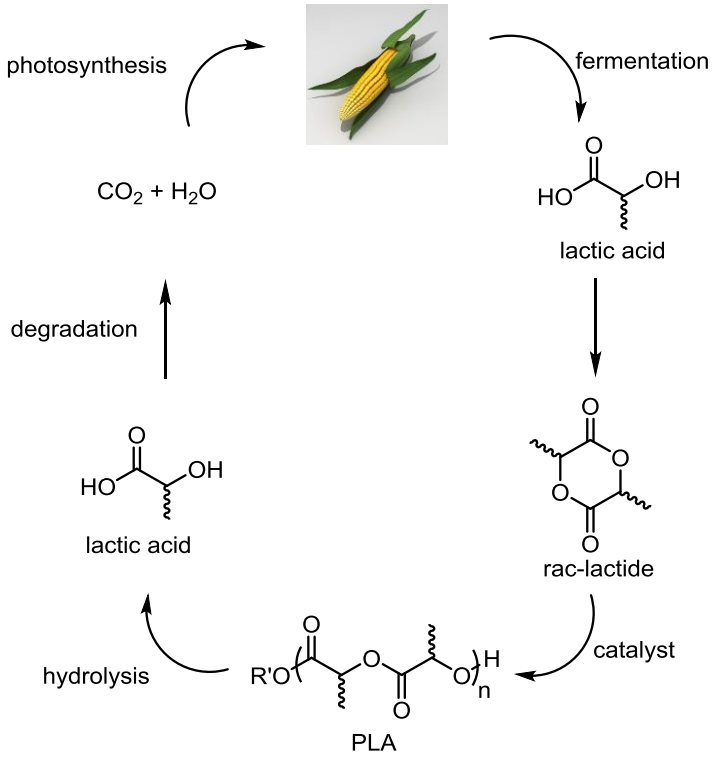
1.2.1 Introduction to PCL

PCL is a thermoplastic polymer derived from ε-caprolactone (ε-CL) monomers which are synthesised industrially through the Bayer Villiger oxidation of cyclohexanone with peracids or hydrogen peroxide.[20] PCL is semi-crystalline and possesses a low glass transition temperature (T_g) of -60 °C, a low melting point (T_m) of 60 °C and a high decomposition temperature of 350 °C, facilitating thermoplastic processing and

extrusion at a wide range of temperatures.[21] The most common use of PCL lies in the manufacture of polyurethanes,[22-24] although more recently, PCL has also been employed as a feedstock for 3D printing.[25-27] Furthermore, extensive *in vitro* and *in vivo* biocompatibility studies have led to the FDA approval of PCL to be used in a number of medical devices, such as drug delivery systems and sutures.[11]

1.2.2 Introduction to PLA

PLA is an aliphatic polyester which is derived from lactide (LA) monomers. In contrast to ε-CL which requires synthesis from non-renewable starting materials, LA can be readily derived from renewable resources. The fermentation of corn starch or sugar cane generates optically pure *L*-lactic acid which can undergo direct condensation to produce low molecular weight PLA oligomers (*vide infra*).[28] The cyclic dimer (LA) can then be obtained *via* the depolymerisation of these oligomers with loss of optical purity.[29, 30] This is followed by the ROP of LA to produce PLA. Once synthesised, PLA is easily hydrolysed to form lactic acid which can be metabolised both *in vivo* and in the environment to yield carbon dioxide and water, as depicted in Scheme 1.1.[9, 16, 31]



Scheme 1.1 Lifecycle of PLA.

As mentioned previously, PLA can also be synthesised from the direct condensation of lactic acid. However, this synthetic route is less desirable due to the formation of low molecular weight oligomers with a wide molecular weight distribution.[31] In addition, such processes typically involve the use of non-ambient conditions to remove water in order to achieve a high yield. One successful synthesis involves heating the lactic acid under reduced pressure with the addition of a catalyst while water is being continuously removed by Soxhlet extraction.[32] Given the above-mentioned limitations, the method used industrially is ROP which can be initiated by metal complexes, enzymes or organic compounds.[5, 7, 12, 33-35] This alternative route provides a much more controlled process, yielding high molecular weight polymers with narrow dispersities and desirable microstructures (*vide infra*).

The history of PLA production can be dated back to the 1930s. First reported by Carothers, PLA was synthesised *via* a condensation approach at elevated temperatures.[36] Following this breakthrough, Dupont advanced the technology in 1954, allowing high molecular weight PLA to be accessed.[37] However, it was not until 1972 that the first commercial application was brought about by Ethicon Inc., which developed a multifilament suture made of poly(lactide-co-glycolide).[38] There has been a surge in the demand of PLA in recent years. The leading producer in the market, NatureWorks LLC, reported an annual production capacity of 140,000 tonnes in 2008. Due to its biodegradability and biocompatibility, PLA has found a broad spectrum of applications in fields ranging from packaging to biomedical materials.[13-17, 19]

1.3 Thermodynamic aspects of ROP

The thermodynamic driving force for the ROP of cyclic esters is the alleviation of ring strain, which arises due to deviation from non-distorted bond angles, eclipsed hydrogen atoms and non-bonding interactions between substituents.[39] In some cases, the negligible interaction between monomer, polymer and solvent allows the enthalpy of polymerisation to be dependent solely on the ring strain. Most polymerisations of cyclic esters are disfavoured entropically, as a consequence of loss of translational degrees of freedom as the monomers polymerise. There are a few exceptions, an example being the ROP of tridecanolide (14-membered ring). This polymerisation was driven entropically due to the formation of highly flexible long polymer chains

from the less strained macrocyclic monomers. Generally speaking, the enthalphy contribution to ΔG must prevail in order for the polymerisation to be allowed thermodynamically (ΔG < 0).

The majority of six-membered ring monomers cannot be polymerised due to a low ring strain. For example, the theoretical polymerisation parameters for cyclohexane was determined as ΔH = 2.9 kJ mol^{-1} and ΔS = -10.5 J mol^{-1} K^{-1} whereas ΔH = -22.9 kJ mol^{-1} and ΔS = -41.1 J mol^{-1} K^{-1} were calculated for *L*-LA ROP catalysed by $Sn(Oct)_2$ in 1,4-dioxane.[40-42] In contrast to cyclohexane which adopts a chair conformation, the presence of ester functionalities in *L*-LA forces the molecule to adopt a less stable skewed boat conformation with a planar ester group in the solid state and a boat conformation in solution, leading to an increase in ring strain.[43] Despite the fact that these thermodynamic parameters are valid for *L*-, *D*- and *rac*-LA, *meso*-LA has to be considered separately. In contrast to enantiopure LA featuring two methyl groups *cis* to each other, *meso*-LA has two stereocentres with opposite configuration, leading to a *trans* conformation between the two methyl groups. Solid state structure of *meso*-LA shows that the molecule adopts a structure which is between a twist boat and a planar conformation.[44] Consistent valence force field calculations demonstrate that *meso*-LA is 0.4 kcal mol^{-1} less stable than *rac*-LA in the ground state.

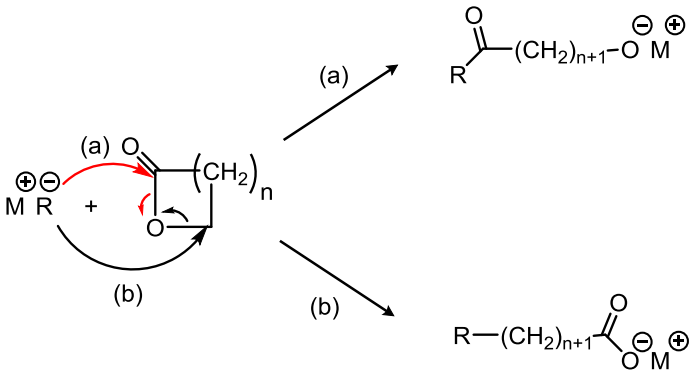
1.4 ROP mechanisms

Several mechanisms through which ROP of cyclic esters can occur have been reported in the literature, including anionic, cationic and organocatalytic, the details of which will be covered in this section. For a review of enzyme initiated ROP, the reader is referred to several articles in this area.[45-49] Metal-mediated ROP is the focus of this Thesis and typically proceeds through either coordination insertion or activated monomer pathways.

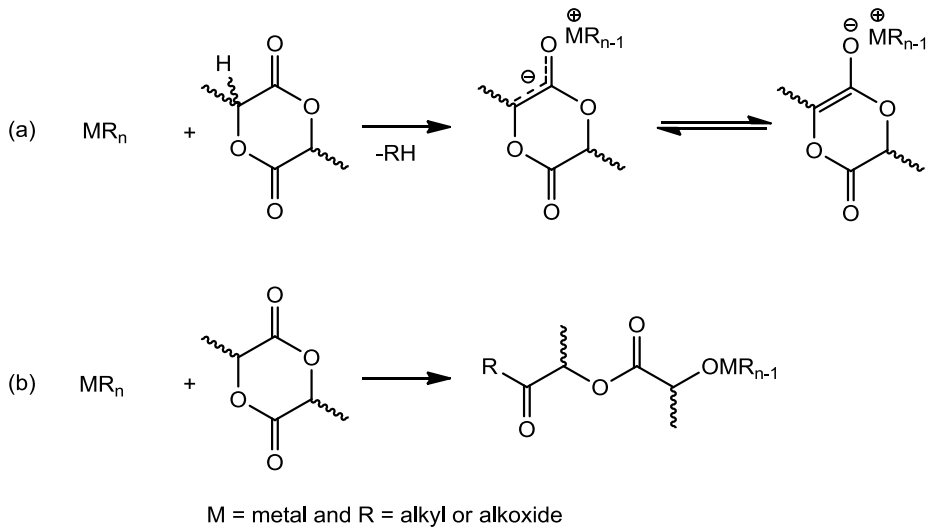
1.4.1 Anionic ROP

Anionic ROP is defined as the ROP process involving the use of a nucleophilic initiator, which can exist in a number of different forms, such as alkyllithiums, Grignard reagents, metal alkyls and alkoxides.[39, 50] These anionic initiators are highly active but lead to poorly-controlled polymerisations due to the strong

nucleophilic/basic nature of the initiators, inducing undesirable transesterification side reactions (*vide infra*). For smaller ring lactones such as β-lactones, the nucleophilic attack could occur at either the alkyl oxygen bond (alkyl oxygen bond cleavage) or the carbonyl carbon (acyl oxygen bond cleavage), resulting in the formation of polymers with carboxylate or alkoxide groups at the propagating chain end, respectively (Scheme 1.2).[51-54] For larger ring lactones such as LA, anionic ROP predominantly proceeds through an acyl oxygen bond cleavage, with the initiation step involving either deprotonation of the monomer or direct nucleophilic attack at the carbonyl carbon, as demonstrated in Scheme 1.3.[55] For example, Jhurry and co-workers have reported the ROP of LA using $LiN^{i}Pr_2$-THF which initiates LA *via* deprotonation reactions to give an enolate, which subsequently attacks another LA molecule followed by acyl oxygen bond cleavage to give the active species: an alkoxide anion. Walach and Kelen also independently reported LA ROP proceeding through the direct nucleophilic attack pathway using KOMe and $KO^{t}Bu$, respectively.[56, 57] These two routes could be distinguished *via* end group analysis; polymers derived from direct nucleophilic attack typically feature ester chain ends whereas such termini are not observed in polymers produced *via* a deprotonation pathway.



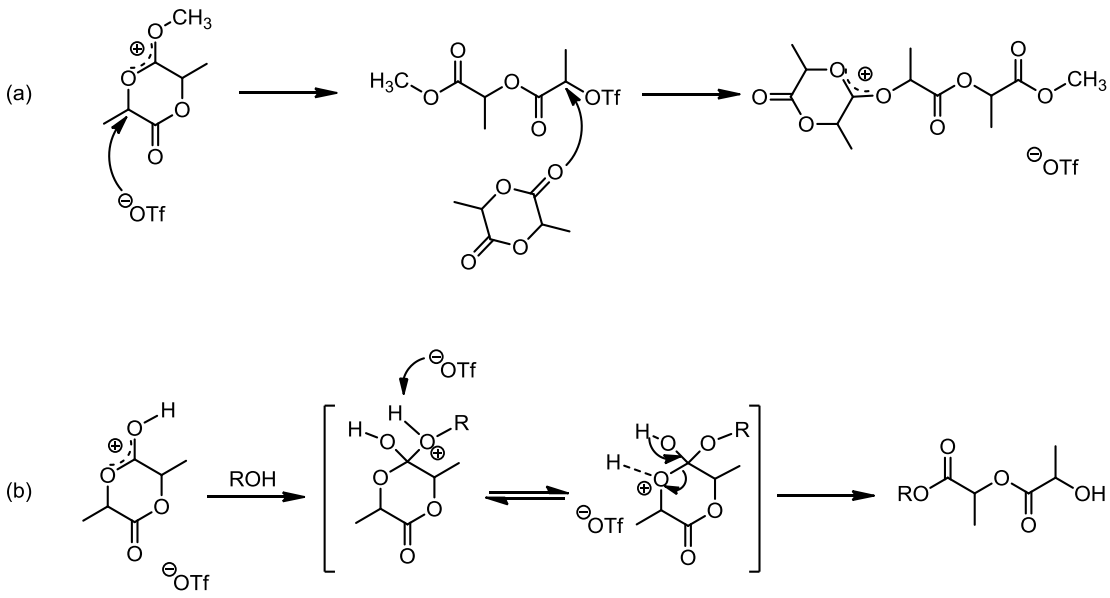
Scheme 1.2 Initiation of anionic ROP of β-lactone through (a) acyl oxygen bond cleavage or (b) alkyl oxygen bond cleavage.[51-54]



Scheme 1.3 Initiation of anionic ROP of LA through (a) deprotonation or (b) nucleophilic attack followed by ring-opening.[55-57]

1.4.2 Cationic ROP

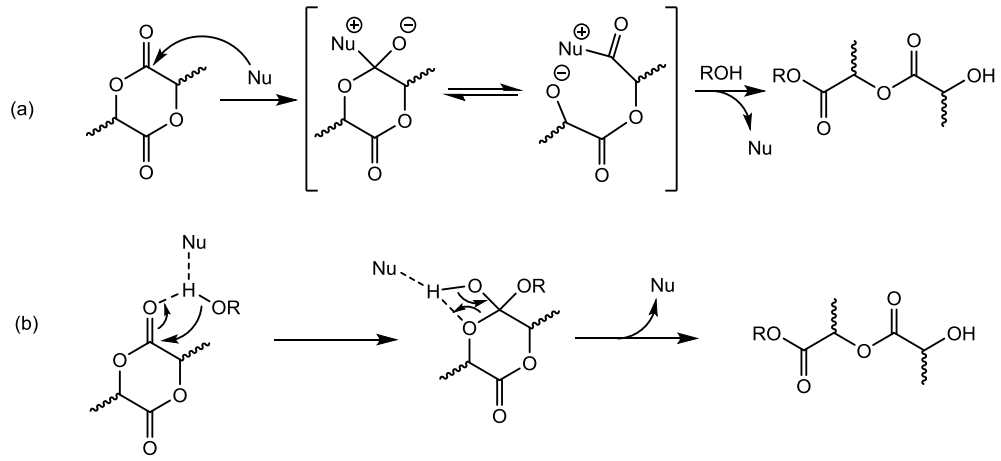
Cationic ROP involves the use of electrophilic initiators including Brønsted and Lewis acids to ring-open cyclic esters. Reported by Kircheldorf and co-workers in 1986, ROP of *L*-LA was successfully performed using triflic acid and methyl triflate as cationic initiators.[58, 59] The resulting polymer initiated by the latter was found to be terminated with a methyl ester end group, indicating that the initiation proceeded through an alkyl oxygen bond cleavage (Route a, Scheme 1.4), as opposed to an acyl oxygen bond cleavage. Bourissou *et al.* later reported a modified cationic ROP system, in which an exogenous alcohol, such as isopropanol was added, in conjunction with triflic acid.[60] The polymerisation was found to proceed through an activated monomer mechanism (*vide infra*), whereby the acid activates the LA monomer prior to attack by the alcohol. End group analysis of the resulting polymer revealed an isopropyl ester terminus, indicating that the polymerisation occurs *via* an acyl oxygen bond cleavage (Route b, Scheme 1.4), as opposed to an alkyl oxygen bond cleavage, which would result in the formation of an isopropyl ether chain end. This catalytic system initiated cationic polymerisation in a well-controlled manner with no occurrence of transesterification side reactions, forming PLA with narrow molecular weight distributions. The living nature (*vide infra*) of this catalytic system was supported by a second experiment in which further equivalents of LA monomers were added to the polymeryl chain to resume the polymerisation.



Scheme 1.4 Cationic ROP mechanisms using (a) methyl triflate (b) triflic acid and an exogenous alcohol.[58-60]

1.4.3 Organocatalysis

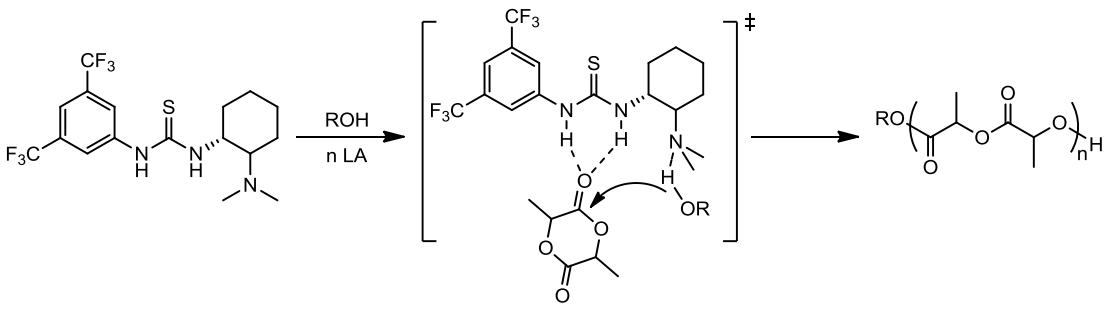
Organocatalysts have gained increasing popularity in recent years due to their promising potential as alternatives to metal-based initiators which have found limited applications in biomedical areas due to toxicity issues. In addition, organocatalysts can be readily available organic molecules which are easy to synthesise and are tolerant of air and moisture. The most common classes of organic molecules which were found to be active in the ROP of cyclic esters in the presence of an alcohol include N-heterocyclic carbenes, amines, phosphazenes and thioureaamines.[31, 61, 62] Polymerisations most likely proceed through either a nucleophilic monomer activation mechanism (Route a, Scheme 1.5) or a base-catalysed process (Route b, Scheme 1.5).



Scheme 1.5 Organocatalytic ROP proceeding through (a) nucleophilic monomer activation or (b) basic pathways, where Nu = amine, NHC, phosphazene or thioureaamines; ROH = initiating protic agent or growing polymer chain.[39]

The first example was reported by Hedrick *et al*. in 2001 employing 4-dimethylaminopyridine (DMAP) and 4-pyrrolidinopyridine (PPY) as organocatalysts for the ROP of LA.[63] Both were active in solution and in the melt with the addition of ethanol, producing PLA with narrow dispersities. The same group later introduced the use of guanidine and amidine species which were highly active and initiated ROP of LA in a controlled manner.[64, 65]

Hedrick also reported the initiating ability of an N-heterocyclic carbene 1,3-bis-(2,4,6-trimethylphenyl)imidazol-2-ylidene in the presence of benzyl alcohol for the ROP of *L*-LA, leading to the formation of polymers with well-controlled molecular weights.[66] Following this pioneering work, other NHCs with different steric and electronic properties, including imidazolium, imidazolinium, thiazolium and triazolium have shown to be highly active in the ROP of cyclic esters.[67-70] Introduced by the same group, thioureaamine species, in the presence of pyrenebutanol, also demonstrated moderate activity in the ROP of *rac*-LA, producing polymers whose experimental M_n agreed very well with the expected values.[71] This system was living, as evidenced by a second experiment, in which further LA monomers were added to extend the polymeryl chain. A bifunctional activated monomer mechanism was proposed, whereby the carbonyl oxygen of LA was activated through hydrogen bonding to the thiourea functionality whereas the alcohol was activated *via* hydrogen bonding to the amine group (Scheme 1.6).



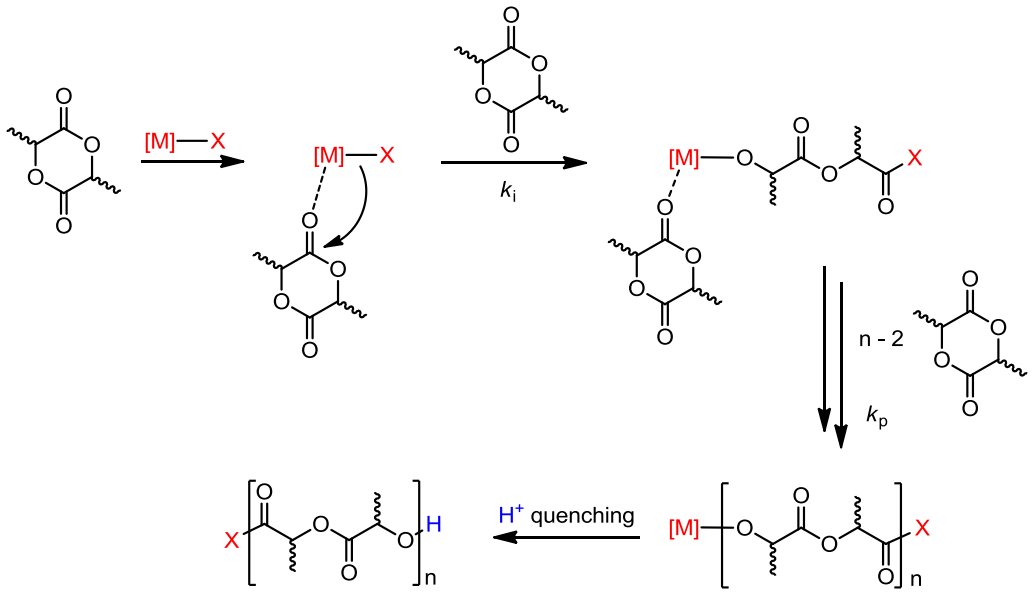
Scheme 1.6 Activated monomer mechanism through hydrogen bonding.[71]

1.4.4 Metal-mediated ROP

Typically, metal-mediated ROP of LA involves the use of a Lewis acidic metal supported by an ancillary ligand and a nucleophilic initiator. The appropriate combination of the three would initiate polymerisations in a well-controlled manner, producing polymers with good molecular weight and stereocontrol. The nucleophilic initiators are commonly limited to alkoxide, amide and borohydride species[31, 33] whereas the choice of metals is much more diverse, including alkali metals,[72-78] alkaline earth,[79-85] Group 3 metals,[86-90] lanthanides,[91-94] Group 4 metals,[95-102] iron,[103, 104] zinc,[105-107] tin[108-113] and Group 13 metals.[114-126] The two most common mechanisms for metal-mediated ROP of cyclic esters are the activated monomer mechanism and the most widely known coordination insertion mechanism.

1.4.4.1 Coordination insertion mechanism

First introduced in 1971 by Dittrich and Schulz, the coordination insertion mechanism is now the most widely accepted pathway for metal-mediated ROP and is supported experimentally and theoretically.[127-132] The first step involves the coordination of a monomer through the carbonyl oxygen to the Lewis acidic metal centre, activating the monomer towards a nucleophilic attack by the initiator.[16, 31, 39, 128, 133] The acyl oxygen bond is subsequently cleaved to form a metal alkoxide species prior to the coordination of a second monomer. The propagation process is continued to produce a polymer chain terminated with the corresponding initiator before the metal-oxygen bond is cleaved by quenching with a protic source.[31, 39, 134] A detailed coordination insertion pathway involving ROP of LA is depicted in Scheme 1.7.



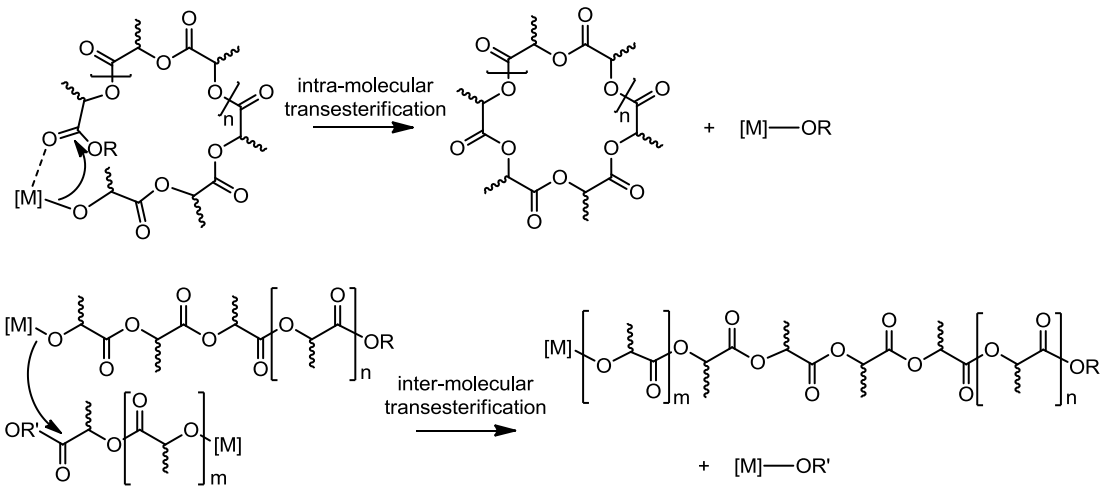
Scheme 1.7 Coordination insertion mechanism for the ROP of LA. [M] = metal and X = initiator, k_i and k_p are the rate constants of initiation and propagation, respectively.[31, 39]

In the coordination insertion mechanism, propagation is limited by both $[monomer]_0$ and $[catalyst]_0$. In order to obtain polymers with narrow molecular weight distribution and a good agreement between the experimental and theoretical molecular weights, a faster rate of initiation than that of propagation must be fulfilled. In other words, all initiators have to be consumed in the ring-opening event before bulk propagation occurs. If propagation and initiation rates are comparable, insertion of monomers into the growing polymeryl chain may be more favourable in comparison to insertion into the metal initiator bond, leading to partial catalyst activation and hence the formation of polymers with a broad molecular weight dispersity. This phenomenon is commonly observed in polymerisations induced by an inefficient initiator, such as metal amide or alkyl.[135-139]

Another criterion to achieve well-controlled polymerisations is the absence of irreversible chain transfer or termination events. However, polyesters produced from ROP are often subject to deleterious transesterification side reactions which may compete with monomer insertion, leading to the alteration of polymer structures. Transesterification can occur both intra- and intermolecularly.[31, 140, 141] The former involves the nucleophilic attack of the metal alkoxide bond on the internal ester group on the same growing polymeryl chain, generating a macrocyclic ester, in conjunction

with a new growing polymeryl chain. A similar nucleophilic attack can also occur between two distinct growing chains and is referred to as intermolecular transesterification.

Both transesterification side reactions in the ROP of LA can be detected *via* various techniques. For example, cyclic polymers are easily distinguished by the lack of end groups in the MALDI-ToF mass spectrum whereas the presence of peak envelopes with $\Delta m/z$ = 72 g mol^{-1} (half a LA unit) is indicative of intermolecular transesterification.[133] Despite MALDI-ToF MS being the most conclusive tool, transesterification in *rac*-LA ROP can also be identified by an increase in the *mrm* and the appearance of *mrr*/*rrm* tetrad resonances in the ^{1}H and ^{13}C{^{1}H} NMR spectra (*vide infra*).[140, 142, 143] Moreover, an increase in PDI and a decrease in M_n as polymerisations progress are also characteristic of such processes.[140]

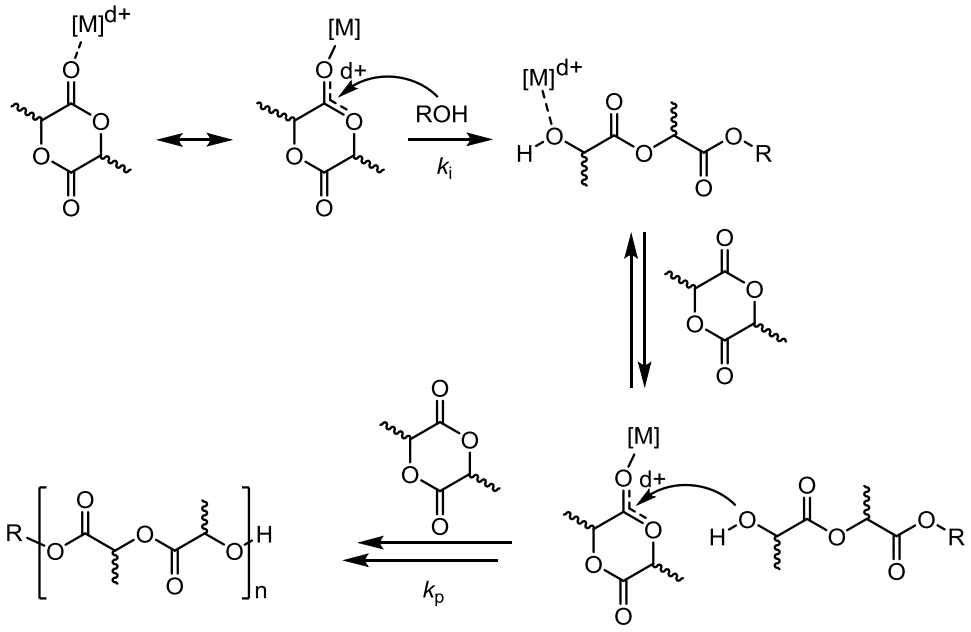


Scheme 1.8 Intramolecular and intermolecular transesterification side reactions. [M] = metal initiator. R and R' = alkyl group on the PLA chain.[31]

1.4.4.2 Activated monomer mechanism

The activated monomer mechanism is commonly observed in organocatalytic or cationic initiating systems involving simple Lewis acidic metal salts, such as metal triflates in the presence of an exogenous alcohol as the nucleophilic initiator.[10, 144-147] The mechanism involves the coordination of a monomer to the Lewis acidic metal centre through the carbonyl oxygen followed by a nucleophilic attack by an exogenous alcohol to ring-open the monomer. The resulting hydroxy terminated ring-opened monomer subsequently acts as a nucleophile, attacking further activated

monomers to continue the propagation cycle. An efficient initiation process enables the complete consumption of alcohol at the initiation stage, resulting in multiple chains being produced per metal centre (one chain per alcohol). Therefore, the molecular weight of the polymer is dependent on the initial ratio of $[monomer]_0$:$[alcohol]_0$, as opposed to $[monomer]_0$:$[metal]_0$ ratio for the coordination insertion mechanism.[148, 149] This concept is referred to as immortal polymerisation and will be introduced in Section 1.4.5.



Scheme 1.9 Activated monomer mechanism for the ROP of LA. [M] = metal initiator and ROH = exogenous alcohol. k_i and k_p are the rate constants of initiation and propagation, respectively.[144-147]

Nomura and Hedrick have independently reported the use of $Sc(OTf)_3$ in the ROP of ε-CL and δ-valerolactone in the presence of an alcohol.[144, 146] Nomura demonstrated that ε-CL ROP using $Sc(OTf)_3$ and benzyl alcohol produced PCL with a narrow molecular weight distribution and the molecular weight of the resulting polymer was inversely proportional to the amount of benzyl alcohol used. This polymerisation was proposed to proceed through the aforementioned activated monomer mechanism. In contrast, $Sn(OTf)_2$ and ethanol, reported by Hedrick *et al*., was postulated to induce the ROP of ε-CL *via* a coordination insertion pathway. Prior to propagation, an exchange process occurs between $Sn(OTf)_2$ and ethanol, generating the active alkoxide species.

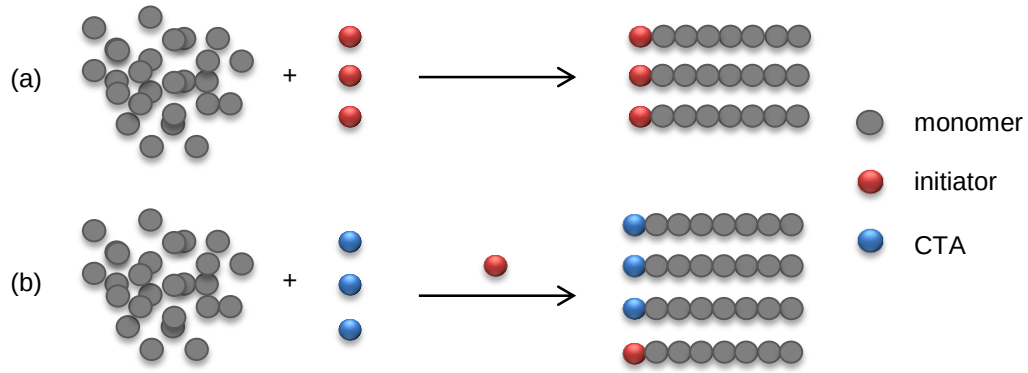
1.4.5 Living and immortal ROP

Living polymerisation is defined as the reaction which proceeds in the absence of chain transfer or chain termination events, featuring a sufficiently rapid initiation process so that the rate of initiation (k_i) is much faster than that of propagation (k_p).[150, 151] Characteristic features for living polymerisations include a linear growth of molecular weight as a function of % conversion, affording polymers with a good agreement between the experimental and calculated molecular weight based on one chain per initiator and a narrow molecular weight distribution. Moreover, living polymerisation is also capable of resuming the polymerisation upon sequential addition of monomers.[80, 152, 153] Such controlled processes allow the physical properties of the resulting polymer to be tuned by varying the quantity and the nature of the initiator. Living polymerisation is commonly observed in metal-mediated ROP.[5, 16, 29, 154]

The general rate law for a living ROP can be expressed as $-d[M]/dt = k_p[I][M]$, whereby [I] is the initiator concentration, [M] is the monomer concentration and k_p is the propagation rate constant.[31] Generally speaking, a living polymerisation demonstrates overall second order (first order with respect to both [I] and [M]) and the rate law can be expressed in terms of k_p since chain termination and transfer events are negligible.[155] It is important to note that k_p is independent of [I]. In order to evaluate k_p, it is common to carry out *pseudo* first order experiments at various [I] to determine k_{obs} (sometimes referred to as k_{app}) at a particular initiator concentration. The rate law can then be written as $-d[M]/dt = k_{obs}[M]$.[31] Whilst living polymerisation often shows first order dependence on monomer concentration, there is literature precedence for second or non-integer order dependence on monomer concentration.[80, 128, 156-162] In certain polymerisations, a latency period prior to a linear dependency (induction period) has been observed, which may be a consequence of initiator or polymer chain aggregates or ligand rearrangements.[163, 164]

Despite affording polymers in a well-controlled manner, conventional living polymerisation suffers from low efficiency and productivity since catalysts are known to convert a small amount of monomer and each metal centre can only produce one polymer chain.[165] This initiating mode has impeded the use of catalysts in industry since it is desirable that the catalytic system can generate as many chains as possible

with different functionalities. This is circumvented by "immortal" ROP whereby a chain transfer agent (CTA), commonly an alcohol or an amine, undergoes rapid exchange with the growing polymeryl chain, resulting in well-controlled polymerisations with the number of polymer chains generated exceeding the number of initiators used.[166, 167] The number of polymer chains generated in immortal ROP is determined by the $[M]_0$:$[CTA]_0$ ratio, as opposed to $[M]_0$:$[I]_0$ ratio, depicted in Scheme 1.10.

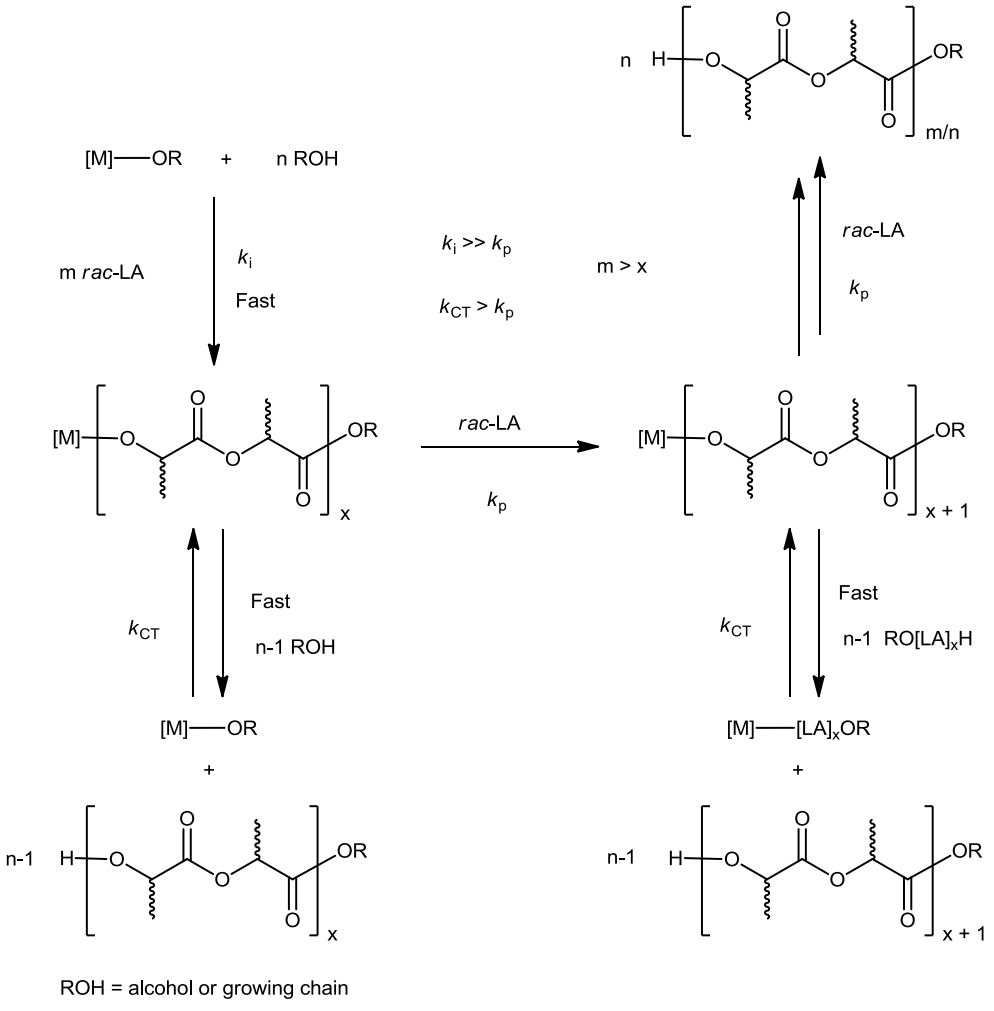


Scheme 1.10 Comparisons between living and immortal polymerisation.[144, 165]

The area of immortal ROP was pioneered by Inoue *et al*. in the 1980s, whereby epoxides were ring-opened in an immortal manner using porphyrin supported aluminium alkoxides with the aid of protic agents.[168-170] Following this breakthrough, immortal ROP has been performed on other systems involving various metals, such as Mg,[149, 171, 172] Ca,[149, 163, 173] Zn,[76, 149, 173] Al,[167, 174-176] Sn[177] and Y.[148, 178, 179]

Metal-mediated immortal ROP can proceed *via* either the coordination insertion or activated monomer mechanism.[165] Scheme 1.11 depicts a detailed coordination insertion mechanism for the ROP of LA. The pathway typically begins with the protonolysis reaction between a non-alkoxide species (L)[M](X) (L = ligand, [M] = metal, X = initiator) and the protic chain transfer agent ROH to produce (L)[M](OR) (OR = alkoxide) *in-situ*. This is followed by the insertion of lactide monomers into the [M]-OR bond, leading to the formation of a propagating species (L)[M]-pol-OR, which further undergoes exchange reactions with the protic chain transfer agent ROH to give a new initiator (L)[M](OR) and a dormant H-pol-OR chain. The propagation is continued employing the newly generated (L)[M](OR) as the initiator and H-pol-OR as a chain transfer agent. This process is maintained throughout the course of the polymerisation, affording multiple polymer chains per metal centre. Crucially, the

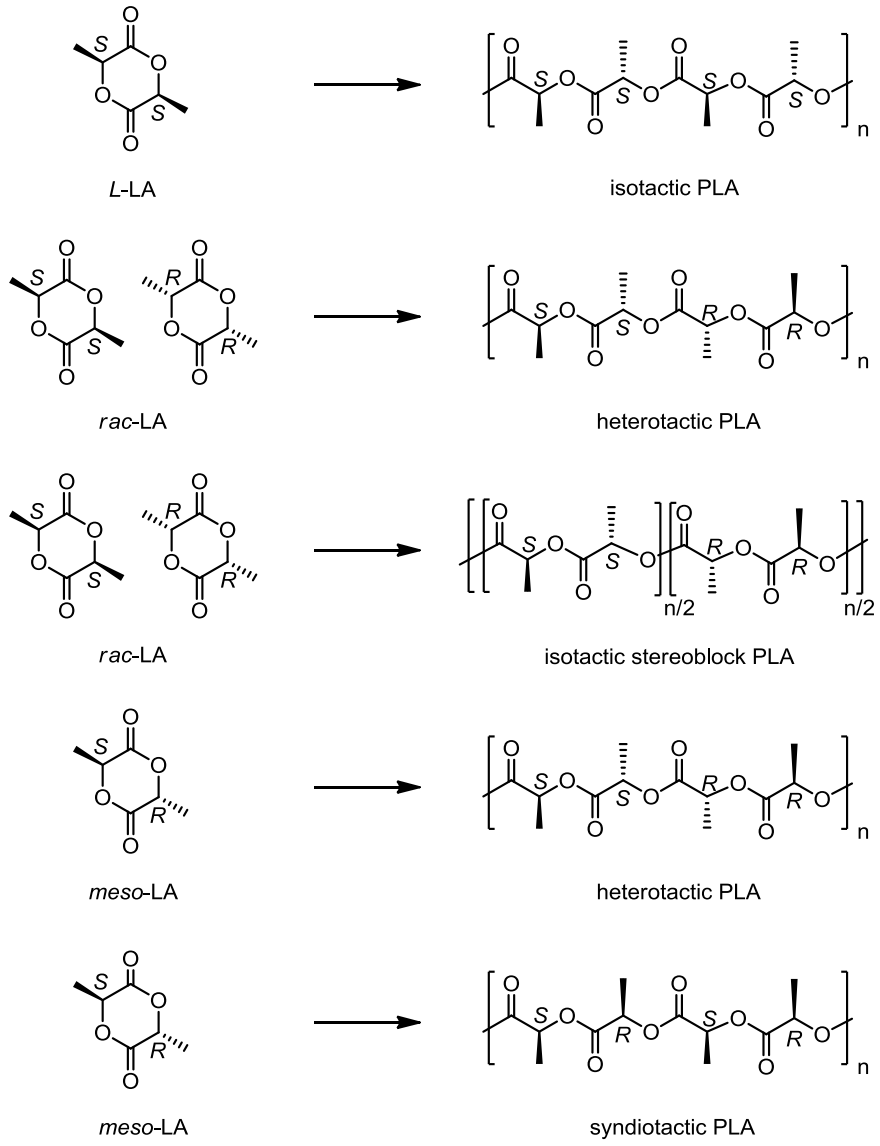
prerequisite to achieve efficient immortal ROP is the much faster rate of chain transfer than that of propagation ($k_{tr} > k_p$). If this is not fulfilled, inefficient chain transfer can lead to the formation of polymers with higher than expected molecular weight since the polymer chain remains bound to the metal centre for a longer time. In comparison to the classical living polymerisation, immortal ROP demonstrates several advantages; in addition to an improvement in productivity, polymers produced *via* this approach generally demonstrate narrower molecular weight distribution since the occurrence of transesterification side reactions is diminished (polymers predominantly exist as dormant chains).[180] In addition, end group functionalisation can be readily achieved by employing different chain transfer agents.



Scheme 1.11 Immortal ROP of LA in the presence of a chain transfer agent (ROH).[165, 179, 181]

1.5 Stereocontrol and tacticity of PLA

Since there are two stereogenic centres per LA molecule, three diastereotopic forms are present, namely *L*- and *D*-LA featuring two *S* and *R* stereocentres, respectively and *meso*-LA containing one *S* and one *R* stereocentre. A racemic mixture of *L*- and *D*-LA is referred to as *rac*-LA. Depending on the stereochemistry of the monomer and the catalyst used, four common PLA microstructures can be observed, namely isotactic, syndiotactic, heterotactic and atactic, shown in Scheme 1.12.[31]



Scheme 1.12 Lactide monomers and PLA microstructures.[31]

The microstructure of PLA imposes a significant effect on both the physical and mechanical properties of the polymer and as such it is often a primary objective to develop appropriate catalysts to produce highly stereo-regular polymers in order to

optimise these macromolecular properties.[14, 114] For *rac*-LA, random enchainment of *L*- and *D*-LA monomers results in the formation of atactic PLA which is amorphous and possesses a T_g of approximately 60 °C.[18, 182] In contrast, PLA formed from a single enantiomer in the absence of epimerisation is isotactic, featuring a T_m of around 180 °C and high tensile strength and slow degradation.[182-184] Isotactic PLA can also be derived from *rac*-LA with the use of an appropriate catalyst, forming stereoblock or stereocomplex PLA. The latter is produced *via* post-polymerisation blending of homochiral polymers PDLA and PLLA. Both stereoblock and stereocomplex PLA feature higher T_m than homochiral polymers alone.[185, 186] For example, Spassky *et al*. reported the preparation of a stereoblock PLA with a T_m of 187 °C[187] whilst an even higher T_m of 210 °C was observed for a stereoblock PLA synthesised by Nomura and co-workers.[125]

Heterotactic PLA is produced either from *rac*-LA by the alternative insertion of *D*-LA followed by *L*-LA[44, 80, 86-88, 135, 178, 181, 188-200] or from *meso*-LA if the system alternates between which stereocentre is ring-opened.[201-204] T_m measurement for heterotactic PLA is difficult since it is amorphous; however, $T_m \approx 130$ °C and $T_g > 45$ °C have been reported.[166, 205, 206] It is also possible to obtain syndiotactic PLA from *meso*-LA provided the catalyst shows a preference for either *R* or *S* stereocentres.[207]

Stereocontrol in ROP of *rac*-LA is achieved through two mechanisms, namely chain end and enantiomorphic site control.[208] In the former case, the stereochemistry of the last repeating LA unit determines the chirality of the monomer to be inserted. Achiral catalysts that induce stereoselective ROP typically operate under this mechanism and both isotatic and heterotactic PLA have been produced. Enantiomorphic site control, on the other hand, involves the selection of monomers according to the chirality of the ligand, and hence is commonly observed in ROP initiated by chiral catalysts. However, it is usually a combination of both chain end and enantiomorphic site control mechanisms that dictate the chirality of the incoming monomer in *rac*-LA ROP catalysed by chiral initiators. Under enantiomorphic site control, it is possible to synthesise stereoblock or stereocomplex PLA from *rac*-LA and an enantiopure[115, 187, 209] or a racemic catalyst,[114, 115, 209, 210] as well as syndiotactic PLA from *meso*-LA.[114, 211]

1.5.1 Characterisation of PLA stereosequences using NMR spectroscopy

According to Bernoullian statistics, there are five tetrad sequences (four sterocentres involving two LA monomer units) related to PLA derived from both *rac*- and *meso*-LA.[212] The relative ratios of these tetrad sequences are determined by the ability of the catalyst to enchain monomers in either a *racemic* or *meso* dyad (two stereocentres involving one LA molecule). The common notions used to describe dyad enchainment are *r* and *m*, where the former denotes a *racemic* dyad (-*SR*- or -*RS*-) and the latter refers to a *meso* dyad (-*SS*- or -*RR*-). Sometimes, it is also common to use the notion *s* and *i*, whereby *s* denotes syndiotactic dyad and *i* refers to isotatic dyad. The tacticity of PLA can be evaluated by analysis using either ^{1}H or ^{13}C NMR spectroscopy. This can be achieved by assessing the NMR resonances, at the tetrad level, corresponding to the methine region in the ^{1}H{^{1}H} NMR spectrum and the methine and carbonyl regions in the ^{13}C{^{1}H} NMR spectrum.[143, 213-218] These assignments were based on the work first introduced by Lillie *et al.*[219] in 1975 and then Schindler *et al.*[220] in the following year. Further studies were performed using two-dimensional NMR spectroscopy, such as HMQC and HMBC, confirming these initial assignments.[142, 213, 214, 216, 221-224] Figure 1.1 depicts the NMR assignments for PLA synthesised from *rac*- and *meso*-LA.[224] The probability of occurrence of a particular dyad can be calculated using Bernoullian statistics and equations related to each tetrad are shown in Table 1.1.[80]

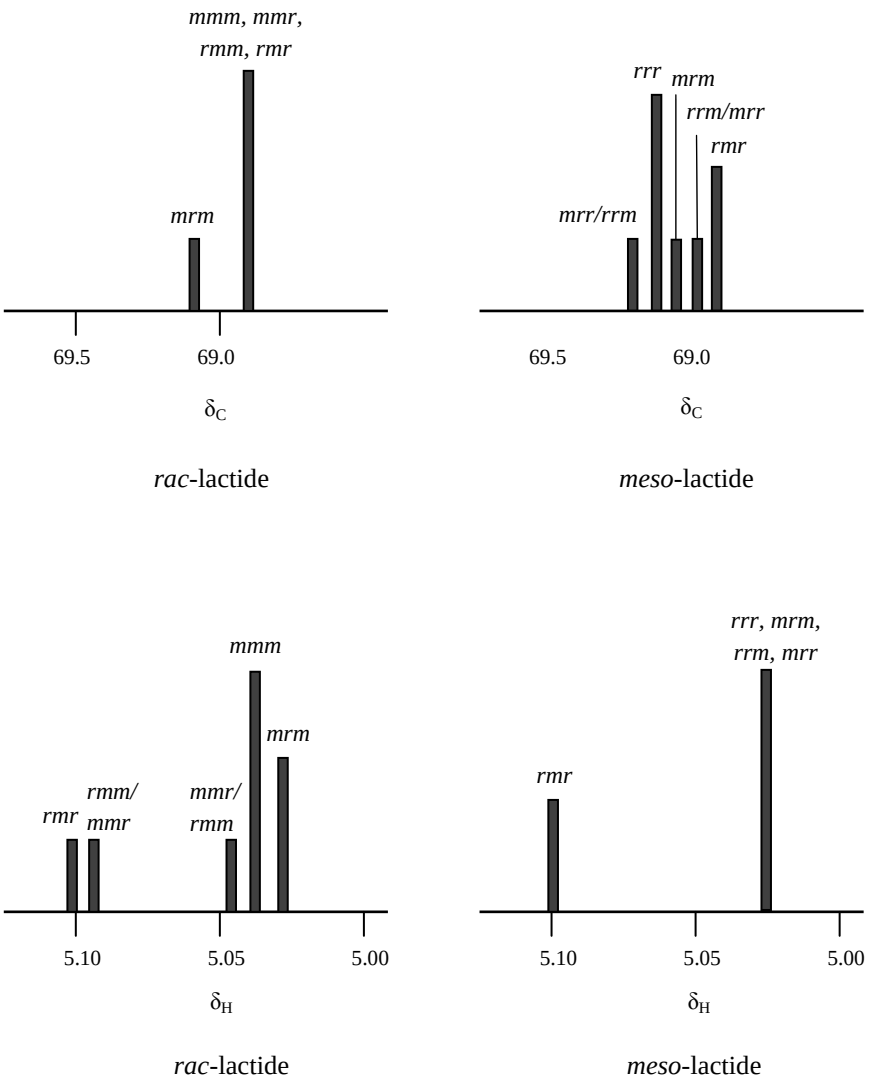


Figure 1.1 Schematic representation of the assignment of PLA tetrads in $^{13}C\{^{1}H\}$ and $^{1}H\{^{1}H\}$ NMR spectra.[224]

Table 1.1. Tetrad probabilities based on Bernoullian statistics.[80]

Tetrad	Probability	
	***rac*-LA**	***meso-LA***
[*mmm*]	$P_m^2 + \frac{P_r P_m}{2}$	0
[*mmr*]	$\frac{P_r P_m}{2}$	0
[*rmm*]	$\frac{P_r P_m}{2}$	0
[*rmr*]	$\frac{P_r^2}{2}$	$\frac{P_m^2 + P_r P_m}{2}$
[*rrr*]	0	$P_r^2 + \frac{P_r P_m}{2}$
[*rrm*]	0	$\frac{P_r P_m}{2}$
[*mrr*]	0	$\frac{P_r P_m}{2}$
[*mrm*]	$\frac{P_r^2 + P_r P_m}{2}$	$\frac{P_m^2}{2}$

As mentioned previously, it is possible to synthesise both heterotactic and isotactic PLA starting from *rac*-LA. The degree of heterotactic enrichment can be expressed as a probability, P_r, which is defined as the probability to form a *racemic* linkage whereas the corresponding degree of isotatic enrichment can be evaluated using P_m, namely the probability to form a *meso* dyad.[31] In addition, P_r can be expressed in terms of rate constants of enchainment; $P_r = k_{R/SS}/(k_{R/SS} + k_{R/RR}) = k_{S/RR}/(k_{S/RR} + k_{S/SS})$. Heterotactic enrichment occurs when the rate of enchainment *via* a *racemic* linkage is higher than that *via* a *meso* linkage. For a value of $0 < P_r < 0.5$, the polymerisation demonstrates an isotatic bias whereas a value of $0.5 < P_r < 1$ indicates heterotactic enrichment. A bias towards heterotactic enrichment is manifested by the dominant *rmr* and *mrm* tetrad signals corresponding to *RSSR* and *SSRR* sequences, respectively in the $^1H\{^1H\}$ NMR spectrum. In the case of *meso*-LA, both heterotactic and syndiotactic PLA can be produced depending on the preference to enchain LA *via* either a *racemic* linkage or a *meso* dyad. When enchainment *via racemic* linkage is in favour, syndiotactic PLA forms and $0.5 < P_r < 1$ whereas heterotactic PLA results when *meso* enchainment is preferred ($0 < P_r < 0.5$).

The dominant resonance for isotactic PLA is the *mmm* tetrad and the degree of isotatic enrichment is expressed as P_m, where P_m denotes the probability of forming a *meso* linkage. A value of $0.5 < P_m < 1$ corresponds to an isotatic bias whereas a value of $0 < P_m < 0.5$ indicates heterotactic enrichment.

1.6 Polymer characterisation

Various analytical techniques have been used to characterise polymers. These include ^{1}H, ^{1}H{^{1}H}, ^{13}C{^{1}H} NMR spectroscopy, Gel Permeation Chromatography (GPC) and Matrix Assisted Laser Desorption Ionisation - Time of Flight Mass Spectroscopy (MALDI-ToF MS).

1.6.1 NMR spectroscopy

^{1}H NMR spectroscopy allows the structural information of PLA to be obtained. For polymers with a sufficiently low molecular weight, it is possible to resolve end groups using this technique. Integration of the signal corresponding to polymer methine protons against that of the end group can lead to elucidation of M_n by NMR and is often used to support the M_n obtained from GPC measurements. However, this approach may be unreliable for high molecular weight polymers due to the very intense ^{1}H resonances corresponding to the backbone in comparison to those of end groups.[163] Another use of NMR spectroscopy in ROP studies is in kinetic analysis, whereby the % monomer conversion at a particular time during the course of the polymerisation can be determined by integrating the backbone signals of the polymer against those of the unreacted monomer. This facilitates the construction of a kinetic profile which can be very informative regarding the polymerisation mechanism. In addition, examining the plot of M_n *vs*. % conversion is a simple approach to determine if M_n grows in a linear fashion, an important characteristic of living polymerisation. Last but not least, ^{1}H{^{1}H} NMR spectroscopy is commonly used to study the microstructure of PLA, as introduced in Section 1.5.1.[144, 214-219]

1.6.2 MALDI-ToF Mass Spectrometry

MALDI-ToF MS is a soft ionisation technique commonly used in the analysis of biomolecules and synthetic polymers which tend to be fragile and would be fragmented when exposed to other conventional ionisation methods. The polymer sample is mixed with and embedded in a suitable matrix material containing organic

molecules with a strong optical absorption in the UV range, such as *trans*-2-[3-(4-*tert*-butylphenyl)-2-methyl-2-propenylidene]malononitrile or 4-hydroxy-3-methoxy-cinnamic acid.[225] The second step involves irradiation with a UV laser beam, causing the matrix to absorb the radiation energy and subsequently transferring it to the polymer molecules which are then desorbed into a stream comprising neutral and ionised matrix molecules. For relatively polar molecules, a cationic dopant such as sodium or potassium ions is incorporated with the polymer molecules which are accelerated and passed through a time-of-flight mass spectrometer, and resolved according to their mass-to-charge (m/z) ratio.

MALDI-ToF MS is a vital tool to accurately detect the end groups of a polymer. In addition, inter- and intramolecular transesterification side reactions can be discerned by the presence of peak envelopes with $\Delta\ m/z$ = 72 g mol^{-1} and the absence of end groups, respectively.[133] The MALDI-ToF mass spectrometer and techniques employed in this Thesis are described in detail in Chapter Six.

1.6.3 Definitions of polymer molecular weight

Synthetic polymers are typically non-uniform in length and exist as chains with a range of molecular weights, following a Gaussian distribution around an average value. The most common parameters used to describe molecular weight are number average molecular weight (M_n), weight average molecular weight (M_w) and polydispersity index (PDI).[226]

M_n can be calculated using Equation 1.1, in which N_i is the number of molecules having a molecular mass of M_i.

$$M_n = \frac{\sum M_i N_i}{\sum N_i}$$

Equation 1.1

M_w can be calculated using Equation 1.2, in which W_i is the total mass of molecules having a molecular mass of M_i.

$$M_w = \frac{\sum W_i M_i}{\sum W_i}$$

Equation 1.2

PDI measures the molecular weight distribution of polymer chains in a sample and is defined as the following shown in Equation 1.3.

$$PDI = \frac{M_w}{M_n}$$

Equation 1.3

In classical living polymerisations where only initiation and propagation occur (free of chain termination and transfer), polymer chains are expected to grow uniformly to give identical chain length and as such a PDI of unity. However, this is not observed in reality; M_w is biased towards polymers with high molecular weight and is therefore greater than M_n, resulting in PDI being greater than one even in extremely well-controlled polymerisations which may be described as living. Common causes which lead to deviation from non-uniform PDI include transesterification side reactions, irreversible chain transfer and termination events. A slow initiation compared to propagation can also contribute to polymers with a wide dispersity of molecular weights being produced. For ROP of cyclic esters, a PDI below 1.2 is classified as narrow molecular weight distribution whereas a value in the range of 1.2-1.8 and above 1.8 is considered as moderate and broad, respectively.

1.6.4 Gel Permeation Chromatography

Gel Permeation Chromatography (GPC), a type of size exclusion chromatography (SEC), is a useful tool to determine the molecular weight and polydispersity index of a polymer sample on the basis of their hydrodynamic volume.[227] In this technique, polymer samples are dissolved in an organic solvent (mobile phase), for example THF, and eluted through a chromatographic column (stationary phase), which is packed with porous beads of styrene divinyl benzene copolymer. Separation of polymer molecules is dependent on their size in solution relative to the pore; smaller molecules permeate through the pores with a longer retention time compared to larger molecules and as such are eluted at a later stage.[228] Detection of polymers can be achieved by using either concentration sensitive (eg. UV, refractive index (RI)) or molecular weight sensitive detectors (eg. Multi-angle light scattering), or both for the accurate molecular weight determination of copolymers.[229] Typically, a differential refractometer with refractive index method is used for linear polyesters. Polymer

molecular weights (M_w, M_n) and PDI are calculated using external standards such as polystyrene with known M_w, M_n and M_p (distribution maximum point) values.

Since polystyrene and polyesters with the same molecular weight have different hydrodynamic volumes at a particular concentration and condition, it is necessary to carry out corrections to relate the observed molecular weights to the absolute values. Mark-Houwink corrections are used, in which the hydrodynamic volume of a polymer is proportional to the product [η]M, where [η] is the intrinsic viscosity and M is the molecular weight.[226, 227, 230] The Mark-Houwink relationship relates [η] and M according to Equation 1.4.

$$[\eta] = KM^{\alpha}$$

Equation 1.4

The values for K and α can be determined from a linear plot of log[η] *vs*. logM, in which logK is the intercept at the log[η] axis and α is the gradient of the plot. α values usually range from 0 to 2, with 0 corresponding to a hard sphere, 1 helical structures or coils and 2 a rigid rod. Both K and α values are unique to individual polymer type and are solvent and temperature dependent. It is important to note that M_n and PDI for PCL and PLA reported in this Thesis are obtained in THF at 30 °C, with the application of Mark-Houwink corrections following calibrations with the appropriate polystyrene standards.[231] RI methods are only applicable to linear polyesters, and as such cyclic polyesters formed from transesterification side reactions are taken into account by approximation. For absolute molecular weight measurement, more advanced GPC instruments incorporating three detection methods are used, namely RI, viscometry and multi-angle light scattering.

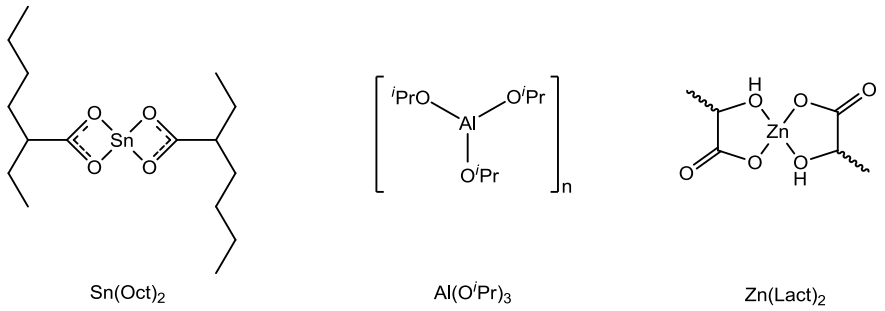
1.7 Industrial ROP catalysts

Tin octanoate ($Sn(Oct)_2$) is the most widely used ROP catalyst for the industrial production of PLA and related copolymers.[14, 16, 18, 39, 232] In conjunction with its ease of handling and good solubility in common organic solvents and bulk monomer in the melt, $Sn(Oct)_2$ demonstrates high catalytic activity, polymerising large quantities of lactide monomers in the melt ranging from minutes to hours in the presence of an alcohol as a co-initiator. High molecular weight PLA with M_n up to 10^6 Da can be produced.[14, 129] However, ROP catalysed with $Sn(Oct)_2$ is not without its drawbacks;

intra- and intermolecular transesterification side reactions are commonly observed in both solution state polymerisations and in the melt.[233] An activated monomer mechanism was proposed for $Sn(Oct)_2$ initiated LA ROP, whereby the exogenous alcohol nucleophilically attacks the activated LA molecule coordinated to the Sn metal centre.[16] Later work by Penczek *et al*. proposed an alternative coordination insertion mechanism involving the *in-situ* generation of an alkoxide initiator from $Sn(Oct)_2$ and alcohol prior to polymerisation.[234] This revised mechanism was supported by various investigations, including intermediate and kinetic studies, as well as end group analysis.[232, 235, 236] Despite the fact that $Sn(Oct)_2$ is FDA approved for its use as a food additive, limited biomedical applications have been found for PLA synthesised using $Sn(Oct)_2$ as a catalyst due to its potential toxicity.[237]

$Al(O^iPr)_3$, being less toxic than $Sn(Oct)_2$, has also been shown to be active in the ROP of LA.[142, 238, 239] A coordination insertion mechanism was proposed, producing PLA with molecular weight below 10^5 g mol^{-1} after several days under melt conditions, much less active than $Sn(Oct)_2$.[129] Moreover, an induction period is systematically observed, attributable to aggregation phenomenon.[240] It is notable that Al ions are bio-incompatible and suspected of causing Alzheimer's disease.

Due to the bio-incompatibility of Sn and Al rendering limited applications in biomedical areas, much attention has been devoted to the development of alternative initiators, an example being Zn alkoxide species.[237, 240-242] Typically, a reaction time of several days under melt conditions is required, similar to $Al(O^iPr)_3$. Among all zinc based catalysts, Zn lactate polymerises LA with a better degree of molecular weight control.



$Sn(Oct)_2$ $Al(O^iPr)_3$ $Zn(Lact)_2$

Figure 1.2 Industrially employed ROP catalysts.[16, 39]

1.8 Aims and outlook

Recent years have witnessed a considerable increase in the industrial production of PLA. The wide spectrum of applications associated with this material has led to an increasing interest in developing ROP catalysts with enhanced activity and stereoselectivity. Conventional industrial catalysts are mostly homoleptic species and suffer from poor control and low activity even under forcing conditions. In an effort to overcome these problems, numerous studies involving the development of catalysts have been reported, aimed at producing PLA with higher activity and improved molecular weight and stereocontrol. The work described in this Thesis is based on two catalytic systems supported by different ligands. Chapter Two and Three describe the synthesis and the catalytic activities of magnesium catalysts supported by a scorpionate ligand, with the emphasis on mechanistic studies regarding a magnesium borohydride initiator. This is followed by the use of borate ester species as chain transfer agents in immortal ROP, discussed in Chapter Four. The catalytic activities, as well as the stereoselectivities of a chiral magnesium catalyst will be described in Chapter Five.

1.9 References for Chapter One

1. A. L. Baner and O. G. Piringer, *Plastic Packaging: Interactions with Food and Pharmaceuticals*, Wiley, 2nd edn., 2008.
2. A. J. Ragauskas, C. K. Williams, B. H. Davison, G. Britovsek, J. Cairney, C. A. Eckert, W. J. Frederick, J. P. Hallett, D. J. Leak, C. L. Liotta, J. R. Mielenz, R. Murphy, R. Templer and T. Tschaplinski, *Science*, 2006, **311**, 484.
3. R. Mülhaupt, *Macromol. Chem. Phys.*, 2013, **214**, 159.
4. A. P. Gupta and V. Kumar, *Eur. Polym. J.*, 2007, **43**, 4053.
5. B. J. O'Keefe, M. A. Hillmyer and W. B. Tolman, *Dalton Trans.*, 2001, 2215.
6. C. K. Williams and M. A. Hillmyer, *Polym. Rev.*, 2008, **48**, 1.
7. C. A. Wheaton, P. G. Hayes and B. J. Ireland, *Dalton Trans.*, 2009, 4832.
8. E. Chiellini and R. Solaro, *Adv. Mater.*, 1996, **8**, 305.
9. S. Mecking, *Angew. Chem. Int. Ed.*, 2004, **43**, 1078.
10. M. Labet and W. Thielemans, *Chem. Soc. Rev.*, 2009, **38**, 3484.
11. M. A. Woodruff and D. W. Hutmacher, *Prog. Polym. Sci.*, 2010, **35**, 1217.
12. M. J. Stanford and A. P. Dove, *Chem. Soc. Rev.*, 2010, **39**, 486.

13. R. Auras, B. Harte and S. Selke, *Macromol. Biosci.*, 2004, **4**, 835.
14. R. E. Drumright, P. R. Gruber and D. E. Henton, *Adv. Mater.*, 2000, **12**, 1841.
15. Y. Ikada and H. Tsuji, *Macromol. Rapid Commun.*, 2000, **21**, 117.
16. O. Dechy-Cabaret, B. Martin-Vaca and D. Bourissou, *Chem. Rev.*, 2004, **104**, 6147.
17. H. Tamber, P. Johansen, H. P. Merkle and B. Gander, *Adv. Drug Deliv. Rev.*, 2005, **57**, 357.
18. A.-C. Albertsson and I. K. Varma, *Biomacromolecules*, 2003, **4**, 1466.
19. H. R. Kricheldorf, *Chemosphere*, 2001, **43**, 49.
20. R. Raja and J. Meurig Thomas, *Z. Anorg. Allg. Chem.*, 2005, **631**, 2942.
21. D. W. Hutmacher, T. Schantz, I. Zein, K. W. Ng, S. H. Teoh and K. C. Tan, *J. Biomed. Mater. Res*, 2001, **55**, 203.
22. D. Sarkar, J.-C. Yang, A. S. Gupta and S. T. Lopina, *J. Biomed. Mater. Res. Part A*, 2009, **90A**, 263.
23. P. Ping, W. Wang, X. Chen and X. Jing, *J. Polym. Sci. B: Polym. Phys.*, 2007, **45**, 557.
24. J. D. Fromstein and K. A. Woodhouse, *J. Biomed. Mater. Sci. Polym. Ed.*, 2002, **13**, 391.
25. S. A. Park, S. H. Lee and W. D. Kim, *Bioprocess Biosyst. Eng.*, 2010, **34**, 505.
26. C. X. F. Lam, X. M. Mo, S. H. Teoh and D. W. Hutmacher, *Mater. Sci. Eng.: C*, 2002, **20**, 49.
27. J. P. Temple, D. L. Hutton, B. P. Hung, P. Y. Huri, C. A. Cook, R. Kondragunta, X. Jia and W. L. Grayson, *J. Biomed. Mater. Res. Part A*, 2014, **102**, 4317.
28. A. N. Vaidya, R. A. Pandey, S. Mudliar, M. S. Kumar, T. Chakrabarti and S. Devotta, *Crit. Rev. Environ. Sci. Technol.*, 2005, **35**, 429.
29. M. Okada, *Prog. Polym. Sci.*, 2002, **27**, 87.
30. E. T. H. Vink, K. R. Rábago, D. A. Glassner and P. R. Gruber, *Polym. Deg. Stab.*, 2003, **80**, 403.
31. R. H. Platel, L. M. Hodgson and C. K. Williams, *Polym. Rev.*, 2008, **48**, 11.
32. M. H. Hartmann, *Biopolymers from Renewable Resources*, Springer-Verlag, 1998.
33. C. M. Thomas, *Chem. Soc. Rev.*, 2010, **39**, 165.

34. N. E. Kamber, W. Jeong, R. M. Waymouth, R. C. Pratt, B. G. G. Lohmeijer and J. L. Hedrick, *Chem. Rev.*, 2007, **107**, 5813.
35. A.-C. Albertsson and R. K. Srivastava, *Adv. Drug Deliv. Rev.*, 2008, **60**, 1077.
36. W. H. Carothers, G. L. Dorough and F. J. van Natta, *J. Am. Chem. Soc.*, 1932, **54**, 761.
37. C. E. Lowe, *Google Patents*, 1954.
38. B. Azimi, P. Nourpanah, M. Rabiee and S. Arbab, *J. Eng. Fiber Fabr.*, 2014, **9**, 47.
39. P. Dubois, O. Coulembier and J.-M. Raquez, *Handbook of Ring-Opening Polymerization*, Wiley-VCH, 2009.
40. F. S. Dainton and K. J. Ivin, *Q. Rev. Chem. Soc.*, 1958, **12**, 61.
41. A. A. Evstropov, B. V. Lebedev, T. G. Kulagina and N. K. Lebedev, *Vysokomol. Soedin. Ser. A*, 1982, **24**, 568.
42. A. Duda and S. Penczek, *Macromolecules*, 1990, **23**, 1636.
43. G. J. van Hummel, S. Harkema, F. E. Kohn and J. Feijen, *Acta Crystallogr. B*, 1982, **38**, 1679.
44. M. H. Chisholm, N. W. Eilerts, J. C. Huffman, S. S. Iyer, M. Pacold and K. Phomphrai, *J. Am. Chem. Soc.*, 2000, **122**, 11845.
45. D. Knani, A. L. Gutman and D. H. Kohn, *J. Polym. Sci. A: Polym. Chem.*, 1993, **31**, 1221.
46. A. Idris and A. Bukhari, *Biotechnol. Adv.*, 2012, **30**, 550.
47. J. Zhang, H. Shi, D. Wu, Z. Xing, A. Zhang, Y. Yang and Q. Li, *Process Biochem.*, 2014, **49**, 797.
48. E. Stavila, G. O. R. Alberda van Ekenstein, A. J. J. Woortman and K. Loos, *Biomacromolecules*, 2014, **15**, 234.
49. M. Sobczak, *J. Appl. Polym. Sci.*, 2012, **125**, 3602.
50. S. Penczek, M. Cypryk, A. Duda, P. Kubisa and S. Slomkowski, *Prog. Polym. Sci.*, 2007, **32**, 247.
51. Z. Jedlinski, P. Kurcok and M. Kowalczuk, *Macromolecules*, 1985, **18**, 2679.
52. Z. Jedlinski, M. Kowalczuk and P. Kurcok, *Macromolecules*, 1991, **24**, 1218.
53. Z. Jedliński, P. Kurcok, W. Walach, H. Janeczek and I. Radecka, *Die Makromolekulare Chemie*, 1993, **194**, 1681.
54. P. Kurcok, J. Penczek, J. Franek and Z. Jedlinski, *Macromolecules*, 1992, **25**, 2285.

55. A. Bhaw-Luximon, D. Jhurry, N. Spassky, S. Pensec and J. Belleney, *Polymer*, 2001, **42**, 9651.
56. Z. Jedliński, W. Wałach, P. Kurcok and G. y. Adamus, *Die Makromolekulare Chemie*, 1991, **192**, 2051.
57. L. Sipos, M. Zsuga and T. Kelen, *Polym. Bull.*, **27**, 495.
58. H. R. Kricheldorf and R. Dunsing, *Die Makromolekulare Chemie*, 1986, **187**, 1611.
59. H. R. Kricheldorf and I. Kreiser, *Die Makromolekulare Chemie*, 1987, **188**, 1861.
60. D. Bourissou, B. Martin-Vaca, A. Dumitrescu, M. Graullier and F. Lacombe, *Macromolecules*, 2005, **38**, 9993.
61. A. P. Dove, *Macro Lett.*, 2012, **1**, 1409.
62. H. A. Brown and R. M. Waymouth, *Acc. Chem. Res.*, 2013, **46**, 2585.
63. F. Nederberg, E. F. Connor, M. Möller, T. Glauser and J. L. Hedrick, *Angew. Chem. Int. Ed.*, 2001, **40**, 2712.
64. B. G. G. Lohmeijer, R. C. Pratt, F. Leibfarth, J. W. Logan, D. A. Long, A. P. Dove, F. Nederberg, J. Choi, C. Wade, R. M. Waymouth and J. L. Hedrick, *Macromolecules*, 2006, **39**, 8574.
65. R. C. Pratt, B. G. G. Lohmeijer, D. A. Long, R. M. Waymouth and J. L. Hedrick, *J. Am. Chem. Soc.*, 2006, **128**, 4556.
66. E. F. Connor, G. W. Nyce, M. Myers, A. Möck and J. L. Hedrick, *J. Am. Chem. Soc.*, 2002, **124**, 914.
67. G. W. Nyce, T. Glauser, E. F. Connor, A. Möck, R. M. Waymouth and J. L. Hedrick, *J. Am. Chem. Soc.*, 2003, **125**, 3046.
68. G. W. Nyce, S. Csihony, R. M. Waymouth and J. L. Hedrick, *Chem. Eur. J.*, 2004, **10**, 4073.
69. S. Csihony, D. A. Culkin, A. C. Sentman, A. P. Dove, R. M. Waymouth and J. L. Hedrick, *J. Am. Chem. Soc.*, 2005, **127**, 9079.
70. R. C. Pratt, B. G. G. Lohmeijer, D. A. Long, P. N. P. Lundberg, A. P. Dove, H. Li, C. G. Wade, R. M. Waymouth and J. L. Hedrick, *Macromolecules*, 2006, **39**, 7863.
71. A. P. Dove, R. C. Pratt, B. G. G. Lohmeijer, R. M. Waymouth and J. L. Hedrick, *J. Am. Chem. Soc.*, 2005, **127**, 13798.

72. M. H. Chisholm, C.-C. Lin, J. C. Gallucci and B.-T. Ko, *Dalton Trans.*, 2003, 406.
73. B.-T. Ko and C.-C. Lin, *J. Am. Chem. Soc.*, 2001, **123**, 7973.
74. A. K. Sutar, T. Maharana, S. Dutta, C.-T. Chen and C.-C. Lin, *Chem. Soc. Rev.*, 2010, **39**, 1724.
75. W.-Y. Lu, M.-W. Hsiao, S. C. N. Hsu, W.-T. Peng, Y.-J. Chang, Y.-C. Tsou, T.-Y. Wu, Y.-C. Lai, Y. Chen and H.-Y. Chen, *Dalton Trans.*, 2012, **41**, 3659.
76. Y. Huang, W. Wang, C.-C. Lin, M. P. Blake, L. Clark, A. D. Schwarz and P. Mountford, *Dalton Trans.*, 2013, **42**, 9313.
77. S.-C. Rosca, D.-A. Rosca, V. Dorcet, C. M. Kozak, F. M. Kerton, J.-F. Carpentier and Y. Sarazin, *Dalton Trans.*, 2013, **42**, 9361.
78. J. Zhang, C. Jian, Y. Gao, L. Wang, N. Tang and J. Wu, *Inorg. Chem.*, 2012, **51**, 13380.
79. M. G. Cushion and P. Mountford, *Chem. Commun.*, 2011, **47**, 2276.
80. B. M. Chamberlain, M. Cheng, D. R. Moore, T. M. Ovitt, E. Lobkovsky and G. W. Coates, *J. Am. Chem. Soc.*, 2001, **123**, 3229.
81. M. H. Chisholm and N. W. Eilerts, *Chem. Commun.*, 1996, 853.
82. V. Poirier, T. Roisnel, J.-F. Carpentier and Y. Sarazin, *Dalton Trans.*, 2009, 9820.
83. B. J. Ireland, C. A. Wheaton and P. G. Hayes, *Organometallics*, 2010, **29**, 1079.
84. R. A. Collins, J. Unruangsri and P. Mountford, *Dalton Trans.*, 2013, **42**, 759.
85. T. J. J. Whitehorne, B. Vabre and F. Schaper, *Dalton Trans.*, 2014, **43**, 6339.
86. C.-X. Cai, A. Amgoune, C. W. Lehmann and J.-F. Carpentier, *Chem. Commun.*, 2004, 330.
87. J. S. Klitzke, T. Roisnel, E. Kirillov, O. de Lázerro Casagrande and J.-F. Carpentier, *Organometallics*, 2014, **33**, 309.
88. C. Bakewell, T.-P.-A. Cao, X. F. Le Goff, N. J. Long, A. Auffrant and C. K. Williams, *Organometallics*, 2013, **32**, 1475.
89. C. Bakewell, T. P. A. Cao, N. Long, X. F. Le Goff, A. Auffrant and C. K. Williams, *J. Am. Chem. Soc.*, 2012, **134**, 20577.
90. B. M. Chamberlain, Y. Sun, J. R. Hagadorn, E. W. Hemmesch, V. G. Young, M. Pink, M. A. Hillmyer and W. B. Tolman, *Macromolecules*, 1999, **32**, 2400.
91. M. Visseaux and F. Bonnet, *Coord. Chem. Rev.*, 2011, **255**, 374.

92. A. Otero, J. Fernández-Baeza, A. Lara-Sánchez, C. Alonso-Moreno, I. Márquez-Segovia, L. F. Sánchez-Barba and A. M. Rodríguez, *Angew. Chem. Int. Ed.*, 2009, **48**, 2176.
93. A. Buchard, R. H. Platel, A. Auffrant, X. F. Le Goff, P. Le Floch and C. K. Williams, *Organometallics*, 2010, **29**, 2892.
94. J. Kratsch, M. Kuzdrowska, M. Schmid, N. Kazeminejad, C. Kaub, P. Oña-Burgos, S. M. Guillaume and P. W. Roesky, *Organometallics*, 2013, **32**, 1230.
95. M. D. Jones, S. L. Hancock, P. McKeown, P. M. Schafer, A. Buchard, L. H. Thomas, M. F. Mahon and J. P. Lowe, *Chem. Commun.*, 2014, **50**, 15967.
96. T. R. Forder, M. F. Mahon, M. G. Davidson, T. Woodman and M. D. Jones, *Dalton Trans.*, 2014, **43**, 12095.
97. S. L. Hancock, M. F. Mahon and M. D. Jones, *New J. Chem.*, 2013, **37**, 1996.
98. Z. R. Turner, J.-C. Buffet and D. O'Hare, *Organometallics*, 2014, **33**, 3891.
99. A. D. Schwarz, A. L. Thompson and P. Mountford, *Inorg. Chem.*, 2009, **48**, 10442.
100. R. L. Webster, N. Noroozi, S. G. Hatzikiriakos, J. A. Thomson and L. L. Schafer, *Chem. Commun.*, 2013, **49**, 57.
101. A. Sauer, A. Kapelski, C. Fliedel, S. Dagorne, M. Kol and J. Okuda, *Dalton Trans.*, 2013, **42**, 9007.
102. M. Jeong Go, J. Min Lee, K. Mun Lee, C. Hwa Oh, K. H. Park, S. H. Kim, M. Kim, H.-R. Park, M. H. Park, Y. Kim and J. Lee, *Polyhedron*, 2014, **67**, 286.
103. Y. Y. Kang, H.-R. Park, M. H. Lee, J. An, Y. Kim and J. Lee, *Polyhedron*, 2015, **95**, 24.
104. A. B. Biernesser, B. Li and J. A. Byers, *J. Am. Chem. Soc.*, 2013, **135**, 16553.
105. C. A. Wheaton, B. J. Ireland and P. G. Hayes, *Organometallics*, 2009, **28**, 1282.
106. H. Sun, J. S. Ritch and P. G. Hayes, *Inorg. Chem.*, 2011, **50**, 8063.
107. Z. Liu, W. Gao, J. Zhang, D. Cui, Q. Wu and Y. Mu, *Organometallics*, 2010, **29**, 5783.
108. H. R. Kricheldorf, K. Bornhorst and H. Hachmann-Thiessen, *Macromolecules*, 2005, **38**, 5017.
109. N. Nimitsiriwat, V. C. Gibson, E. L. Marshall and M. R. J. Elsegood, *Dalton Trans.*, 2009, 3710.

110. A. P. Dove, V. C. Gibson, E. L. Marshall, H. S. Rzepa, A. J. P. White and D. J. Williams, *J. Am. Chem. Soc.*, 2006, **128**, 9834.
111. A. Kowalski, J. Libiszowski, T. Biela, M. Cypryk, A. Duda and S. Penczek, *Macromolecules*, 2005, **38**, 8170.
112. N. Nimitsiriwat, E. L. Marshall, V. C. Gibson, M. R. J. Elsegood and S. H. Dale, *J. Am. Chem. Soc.*, 2004, **126**, 13598.
113. M. Lahcini, P. M. Castro, M. Kalmi, M. Leskelä and T. Repo, *Organometallics*, 2004, **23**, 4547.
114. T. M. Ovitt and G. W. Coates, *J. Am. Chem. Soc.*, 2002, **124**, 1316.
115. Z. Zhong, P. J. Dijkstra and J. Feijen, *Angew. Chem. Int. Ed.*, 2002, **41**, 4510.
116. S. L. Hancock, M. F. Mahon and M. D. Jones, *Dalton Trans.*, 2013, **42**, 9279.
117. I. Yu, A. Acosta-Ramírez and P. Mehrkhodavandi, *J. Am. Chem. Soc.*, 2012, **134**, 12758.
118. D. C. Aluthge, B. O. Patrick and P. Mehrkhodavandi, *Chem. Commun.*, 2013, **49**, 4295.
119. C. Bakewell, R. H. Platel, S. K. Cary, S. M. Hubbard, J. M. Roaf, A. C. Levine, A. J. P. White, N. J. Long, M. Haaf and C. K. Williams, *Organometallics*, 2012, **31**, 4729.
120. C. Bakewell, A. J. P. White, N. J. Long and C. K. Williams, *Inorg. Chem.*, 2013, **52**, 12561.
121. T. R. Forder and M. D. Jones, *New J. Chem.*, 2015, **39**, 1974.
122. I. dos Santos Vieira, E. L. Whitelaw, M. D. Jones and S. Herres-Pawlis, *Chem. Eur. J.*, 2013, **19**, 4712.
123. W. Zhang, Y. Wang, L. Wang, C. Redshaw and W.-H. Sun, *J. Organomet. Chem.*, 2014, **750**, 65.
124. Z. Tang and V. C. Gibson, *Eur. Polym. J.*, 2007, **43**, 150.
125. N. Nomura, R. Ishii, Y. Yamamoto and T. Kondo, *Chem. Eur. J.*, 2007, **13**, 4433.
126. M. P. Blake, A. D. Schwarz and P. Mountford, *Organometallics*, 2011, **30**, 1202.
127. V. W. Dittrich and R. C. Schulz, *Die Angewandte Makromolekulare Chemie*, 1971, **15**, 109.
128. P. Dubois, C. Jacobs, R. Jerome and P. Teyssie, *Macromolecules*, 1991, **24**, 2266.

129. P. Degée, P. Dubois, R. Jérŏme, S. Jacobsen and H.-G. Fritz, *Macromol. Symp.*, 1999, **144**, 289.
130. P. Degée, P. Dubois and R. Jérôme, *Macromol. Chem. Phys.*, 1997, **198**, 1973.
131. H. D. Dyer, S. Huijser, N. Susperregui, F. Bonnet, A. D. Schwarz, R. Duchateau, L. Maron and P. Mountford, *Organometallics*, 2010, **29**, 3602.
132. H. von Schenck, M. Ryner, A.-C. Albertsson and M. Svensson, *Macromolecules*, 2002, **35**, 1556.
133. H. R. Kricheldorf, M. Berl and N. Scharnagl, *Macromolecules*, 1988, **21**, 286.
134. P. J. Dijkstra, H. Du and J. Feijen, *Polym. Chem.*, 2011, **2**, 520.
135. M. H. Chisholm, J. Gallucci and K. Phomphrai, *Inorg. Chem.*, 2002, **41**, 2785.
136. M. H. Chisholm, J. C. Gallucci and K. Phomphrai, *Inorg. Chem.*, 2005, **44**, 8004.
137. H. Ma and J. Okuda, *Macromolecules*, 2005, **38**, 2665.
138. A. P. Dove, V. C. Gibson, E. L. Marshall, A. J. P. White and D. J. Williams, *Dalton Trans.*, 2004, 570.
139. M. S. Hill and P. B. Hitchcock, *Dalton Trans.*, 2002, 4694.
140. N. Spassky, V. Simic, M. S. Montaudo and L. G. Hubert-Pfalzgraf, *Macromol. Chem. Phys.*, 2000, **201**, 2432.
141. J. Baran, A. Duda, A. Kowalski, R. Szymanski and S. Penczek, *Macromol. Rapid Commun.*, 1997, **18**, 325.
142. M. Bero, J. Kasperczyk and Z. J. Jedlinski, *Die Makromolekulare Chemie*, 1990, **191**, 2287.
143. J. Coudane, C. Ustariz-Peyret, G. Schwach and M. Vert, *J. Polym. Sci. A: Polym. Chem.*, 1997, **35**, 1651.
144. N. Nomura, A. Taira, T. Tomioka and M. Okada, *Macromolecules*, 2000, **33**, 1497.
145. N. Nomura, A. Taira, A. Nakase, T. Tomioka and M. Okada, *Tetrahedron*, 2007, **63**, 8478.
146. M. Möller, R. Kånge and J. L. Hedrick, *J. Polym. Sci. A: Polym. Chem.*, 2000, **38**, 2067.
147. S. M. Weidner, F. Scheliga and H. R. Kricheldorf, *Macromol. Chem. Phys.*, 2013, **214**, 2043.
148. W. Zhao, D. Cui, X. Liu and X. Chen, *Macromolecules*, 2010, **43**, 6678.

149. Y. Sarazin, B. Liu, T. Roisnel, L. Maron and J.-F. Carpentier, *J. Am. Chem. Soc.*, 2011, **133**, 9069.
150. M. Szwarc, *Nature*, 1956, **178**, 1168.
151. M. Szwarc, *J. Polym. Sci. A: Polym. Chem.*, 1998, **36**, IX-XV.
152. T. Aida, *Prog. Polym. Sci.*, 1994, **19**, 469.
153. R. P. Quirk and B. Lee, *Polym. Int.*, 1992, **27**, 359.
154. C. K. Williams, *Chem. Soc. Rev.*, 2007, **36**, 1573.
155. L. Wang, M. Bochmann, R. D. Cannon, J.-F. Carpentier, T. Roisnel and Y. Sarazin, *Eur. J. Inorg. Chem.*, 2013, **2013**, 5896.
156. F. Bonnet, A. R. Cowley and P. Mountford, *Inorg. Chem.*, 2005, **44**, 9046.
157. H.-Y. Chen, B.-H. Huang and C.-C. Lin, *Macromolecules*, 2005, **38**, 5400.
158. B. J. O'Keefe, L. E. Breyfogle, M. A. Hillmyer and W. B. Tolman, *J. Am. Chem. Soc.*, 2002, **124**, 4384.
159. H.-Y. Chen, J. Zhang, C.-C. Lin, J. H. Reibenspies and S. A. Miller, *Green Chem.*, 2007, **9**, 1038.
160. A. Duda and S. Penczek, *Macromol. Rapid Commun.*, 1994, **15**, 559.
161. A. Duda and S. Penczek, *Polym. Prepr. (Am. Chem. Soc., Div. Polym. Chem.)*, 1990, **31**, 12.
162. T. Ouhadi, A. Hamitou, R. Jerome and P. Teyssie, *Macromolecules*, 1976, **9**, 927.
163. Z. Zhong, P. J. Dijkastra, C. Birg, M. Westerhausen and J. Feijen, *Macromolecules*, 2001, **34**, 3863.
164. Z. Zhong, S. Schneiderbauer, P. J. Dijkstra, M. Westerhausen and J. Feijen, *J. Polym. Environ.*, 2002, **9**, 31.
165. N. Ajellal, J.-F. Carpentier, C. Guillaume, S. M. Guillaume, M. Helou, V. Poirier, Y. Sarazin and A. A. Trifonov, *Dalton Trans.*, 2010, **39**, 8363.
166. A. P. Dove, *Chem. Commun.*, 2008, 6446.
167. Y.-C. Liu, B.-T. Ko and C.-C. Lin, *Macromolecules*, 2001, **34**, 6196.
168. S. Asano, T. Aida and S. Inoue, *J. Chem. Soc., Chem. Commun.*, 1985, 1148.
169. S. Inoue, *Makromol. Chem. M. Symp.*, 1986, **3**, 295.
170. S. Inoue and T. Aida, *Makromol. Chem. M. Symp.*, 1986, **6**, 217.
171. M. J. Walton, S. J. Lancaster and C. Redshaw, *ChemCatChem*, 2014, **6**, 1892.
172. Y. Wang, W. Zhao, X. Liu, D. Cui and E. Y. X. Chen, *Macromolecules*, 2012, **45**, 6957.

173. Y. Sarazin, V. Poirier, T. Roisnel and J.-F. Carpentier, *Eur. J. Inorg. Chem.*, 2010, 3423.
174. T. Aida, Y. Maekawa, S. Asano and S. Inoue, *Macromolecules*, 1988, **21**, 1195.
175. M. Lamberti, I. D'Auria, M. Mazzeo, S. Milione, V. Bertolasi and D. Pappalardo, *Organometallics*, 2012, **31**, 5551.
176. M.-L. Hsueh, B.-H. Huang and C.-C. Lin, *Macromolecules*, 2002, **35**, 5763.
177. L. Wang, V. Poirier, F. Ghiotto, M. Bochmann, R. D. Cannon, J.-F. Carpentier and Y. Sarazin, *Macromolecules*, 2014, **47**, 2574.
178. L. Clark, M. G. Cushion, H. D. Dyer, A. D. Schwarz, R. Duchateau and P. Mountford, *Chem. Commun.*, 2010, **46**, 273.
179. A. Amgoune, C. M. Thomas and J.-F. Carpentier, *Pure Appl. Chem.*, 2007, **79**, 2013.
180. I. Barakat, P. Dubois, R. Jérôme and P. Teyssié, *J. Polym. Sci. A: Polym. Chem.*, 1993, **31**, 505.
181. A. Amgoune, C. M. Thomas and J.-F. Carpentier, *Macromol. Rapid Commun.*, 2007, **28**, 693.
182. A. Södergård and M. Stolt, *Prog. Polym. Sci.*, 2002, **27**, 1123.
183. W. Amass, A. Amass and B. Tighe, *Polym. Int.*, 1998, **47**, 89.
184. N. Nomura, J. Hasegawa and R. Ishii, *Macromolecules*, 2009, **42**, 4907.
185. Y. Ikada, K. Jamshidi, H. Tsuji and S. H. Hyon, *Macromolecules*, 1987, **20**, 904.
186. N. Yui, P. J. Dijkstra and J. Feijen, *Die Makromolekulare Chemie*, 1990, **191**, 481.
187. N. Spassky, M. Wisniewski, C. Pluta and A. Le Borgne, *Macromol. Chem. Phys.*, 1996, **197**, 2627.
188. E. Grunova, E. Kirillov, T. Roisnel and J.-F. Carpentier, *Dalton Trans.*, 2010, **39**, 6739.
189. X. Liu, X. Shang, T. Tang, N. Hu, F. Pei, D. Cui, X. Chen and X. Jing, *Organometallics*, 2007, **26**, 2747.
190. M. Bouyahyi, N. Ajellal, E. Kirillov, C. M. Thomas and J.-F. Carpentier, *Chem. Eur. J.*, 2011, **17**, 1872.
191. H. Xie, Z. Mou, B. Liu, P. Li, W. Rong, S. Li and D. Cui, *Organometallics*, 2014, **33**, 722.

192. Z. Mou, B. Liu, X. Liu, H. Xie, W. Rong, L. Li, S. Li and D. Cui, *Macromolecules*, 2014, **47**, 2233.
193. A. Amgoune, C. M. Thomas, T. Roisnel and J.-F. Carpentier, *Chem. Eur. J.*, 2006, **12**, 169.
194. M. H. Chisholm, J. C. Gallucci and K. Phomphrai, *Inorg. Chem.*, 2004, **43**, 6717.
195. A. Stopper, K. Press, J. Okuda, I. Goldberg and M. Kol, *Inorg. Chem.*, 2014, **53**, 9140.
196. V. Balasanthiran, M. H. Chisholm, C. B. Durr and J. C. Gallucci, *Dalton Trans.*, 2013, **42**, 11234.
197. M. Cheng, A. B. Attygalle, E. Lobkovsky and G. W. Coates, *J. Am. Chem. Soc.*, 1999, **121**, 11583.
198. T. P. A. Cao, A. Buchard, X. F. Le Goff, A. Auffrant and C. K. Williams, *Inorg. Chem.*, 2012, **51**, 2157.
199. H. Ma, T. P. Spaniol and J. Okuda, *Inorg. Chem.*, 2008, **47**, 3328.
200. M. H. Chisholm, J. Gallucci and K. Phomphrai, *Chem. Commun.*, 2003, 48.
201. A. Sauer, J.-C. Buffet, T. P. Spaniol, H. Nagae, K. Mashima and J. Okuda, *Inorg. Chem.*, 2012, **51**, 5764.
202. J.-C. Buffet, A. N. Martin, M. Kol and J. Okuda, *Polym. Chem.*, 2011, **2**, 2378.
203. A. Pietrangelo, M. A. Hillmyer and W. B. Tolman, *Chem. Commun.*, 2009, 2736.
204. A. Pietrangelo, S. C. Knight, A. K. Gupta, L. J. Yao, M. A. Hillmyer and W. B. Tolman, *J. Am. Chem. Soc.*, 2010, **132**, 11649.
205. C. Romain, B. Heinrich, S. B. Laponnaz and S. Dagorne, *Chem. Commun.*, 2012, **48**, 2213.
206. J. M. Becker, R. J. Pounder and A. P. Dove, *Macromol. Rapid Commun.*, 2010, **31**, 1923.
207. J.-C. Buffet and J. Okuda, *Polym. Chem.*, 2011, **2**, 2758.
208. M. H. Chisholm, N. J. Patmore and Z. Zhou, *Chem. Commun.*, 2005, 127.
209. Z. Zhong, P. J. Dijkstra and J. Feijen, *J. Am. Chem. Soc.*, 2003, **125**, 11291.
210. T. M. Ovitt and G. W. Coates, *J. Polym. Sci. A: Polym. Chem.*, 2000, **38**, 4686.
211. T. M. Ovitt and G. W. Coates, *J. Am. Chem. Soc.*, 1999, **121**, 4072.

212. F. A. Bovey and P. A. Mirau, *NMR of Polymers*, Academic Press, San Diego, 1996.
213. J. E. Kasperczyk, *Macromolecules*, 1995, **28**, 3937.
214. M. H. Chisholm, S. S. Iyer, M. E. Matison, D. G. McCollum and M. Pagel, *Chem. Commun.*, 1997, 1999.
215. M. H. Chisholm, S. S. Iyer, D. G. McCollum, M. Pagel and U. Werner-Zwanziger, *Macromolecules*, 1999, **32**, 963.
216. K. A. M. Thakur, R. T. Kean, K. A. M. Thakur, M. T. Zell, B. E. Padden and E. J. Munson, *Chem. Commun.*, 1998, 1913.
217. M. Wei, D. T. Ivey and A. E. Tonelli, *Macromolecules*, 2002, **35**, 1976.
218. H. R. Kricheldorf, C. Boettcher and K.-U. Tönnes, *Polymer*, 1992, **33**, 2817.
219. E. Lillie and R. C. Schulz, *Makromol. Chem.*, 1975, **176**, 1901.
220. A. Schindler and D. Harper, *J. Polym. Sci. C: Polym. Lett.*, 1976, **14**, 729.
221. K. A. M. Thakur, R. T. Kean, E. S. Hall, J. J. Kolstad, T. A. Lindgren, M. A. Doscotch, J. I. Siepmann and E. J. Munson, *Macromolecules*, 1997, **30**, 2422.
222. J. E. Kasperczyk, *Polymer*, 1999, **40**, 5455.
223. I. Rashkov, J. L. Espartero, N. Manolova and M. Vert, *Macromolecules*, 1996, **29**, 57.
224. M. T. Zell, B. E. Padden, A. J. Paterick, K. A. M. Thakur, R. T. Kean, M. A. Hillmyer and E. J. Munson, *Macromolecules*, 2002, **35**, 7700.
225. T. Kinumi, T. Saisu, M. Takayama and H. Niwa, *J. Mass Spectrom.*, 2000, **35**, 417.
226. D. Walton and P. Lorimer, *Polymers, Oxford Chemistry Primers*, Oxford University Press, 2000.
227. A. Rudin and H. L. W. Hoegy, *J. Polym. Sci. A: Polym. Chem.*, 1972, **10**, 217.
228. D. A. Skoog, *Principle of Instrumental Analysis*, Thompson Brooks/Cole: Belmont, California, 6th edn., 2006.
229. B. Trathnigg, *Prog. Polym. Sci.*, 1995, **20**, 615.
230. P. C. Hiemenz and T. P. Lodge, *Polymer Chemistry*, CRC Press, New York, USA, 2nd edn., 2007.
231. J. R. Dorgan, J. Janzen, D. M. Knauss, S. B. Hait, B. R. Limoges and M. H. Hutchinson, *J. Polym. Sci. B: Polym. Phys.*, 2005, **43**, 3100.
232. H. R. Kricheldorf, I. Kreiser-Saunders and A. Stricker, *Macromolecules*, 2000, **33**, 702.

233. S. Gogolewski, M. Jovanovic, S. M. Perren, J. G. Dillon and M. K. Hughes, *Polym. Degrad. Stab.*, 1993, **40**, 313.

234. A. Kowalski, A. Duda and S. Penczek, *Macromolecules*, 2000, **33**, 7359.

235. A. Duda, S. Penczek, A. Kowalski and J. Libiszowski, *Macromol. Symp.*, 2000, **153**, 41.

236. J. Libiszowski, A. Kowalski, A. Duda and S. Penczek, *Macromol. Chem. Phys.*, 2002, **203**, 1694.

237. G. Schwach, J. Coudane, R. Engel and M. Vert, *Polym. Bull.*, 1996, **37**, 771.

238. C. Miola-Delaite, T. Hamaide and R. Spitz, *Macromol. Chem. Phys.*, 1999, **200**, 1771.

239. A. Kowalski, A. Duda and S. Penczek, *Macromolecules*, 1998, **31**, 2114.

240. G. Schwach, J. Coudane, R. Engel and M. Vert, *Polym. Int.*, 1998, **46**, 177.

241. G. Schwach, J. Coudane, R. Engel and M. Vert, *Polym. Bull.*, 1994, **32**, 617.

242. G. Schwach and M. Vert, *Int. J. Biol. Macromol.*, 1999, **25**, 283.

Chapter Two

Synthesis, characterisation and DFT studies of tris(pyrazolyl)methanide magnesium complexes

2.1 Overview

This Chapter will describe the detailed synthesis and characterisation of a series of magnesium complexes supported by the 3-*tert*-butyl, 5-methyl-tris(pyrazolyl)methane ligand (Tpm*). The solid state structures of the complexes have been elucidated by X-ray crystallography and compared with those of analogous compounds previously prepared in the Mountford group. DFT calculations will also be discussed to gain further understanding of the bonding and structures of these complexes. In this Chapter, nine new complexes will be presented, in conjunction with five solid state structures.

2.2 Introduction

The chemistry of tris(pyrazolyl)hydroborate (Tp) and tris(pyrazolyl)methane (Tpm) ligands has been extensively studied in the last few decades. First introduced by Trofimenko in 1967,[1] the former has become one of the most widely used classes of ligand in coordination chemistry.[2] For further information regarding the synthesis and reactivity of Tp and other scorpionate-type ligands, the reader is referred to several comprehensive reviews on the subject.[3-10] The latter Tpm ligand is the neutral analogue of Tp and is formally derived by replacing the anionic $\{BH\}^-$ moiety in the apical position with an isoelectronic CH group.[11] Despite its first introduction in 1937,[12] there has been much less attention regarding the development of Tpm-supported complexes[6] possibly due to the initial difficulties associated with the synthesis of the protio-ligand on a multi-gram scale, which have now been overcome.[13] Removal of the apical proton results in the formation of the anionic tris(pyrazolyl)methanide (Tpm^d), the ambidentate characteristics of which facilitates binding *via* two possible coordination sites, namely through the apical carbon or the pyrazolyl ring nitrogens.[14]

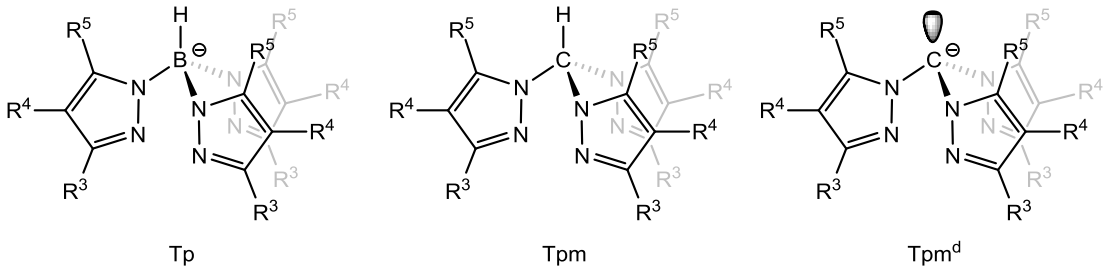


Figure 2.1 Tp, Tpm and Tpm^d ligands.

The first structurally authenticated Tpm^{d} derivative was reported by Stone *et al.* in 1990.[15, 16] Compound **2.1** (Figure 2.2) was formed as a side product in the synthesis of $WPt(\mu\text{-}CMe)(CO)_2(PMe_2Ph)_2\{(C_6F_5)AuC(pz)_3\}$ by reacting $Pt(norbonene)(PMe_2Ph)_2$ with *in-situ* generated $W(CMe)(CO)_2\{(C_6F_5)AuC(pz)_3\}$. The ambidentate nature of this complex through both the apical carbon and the 2-position nitrogens on the pyrazolyl ring was clearly established by X-ray crystallography.

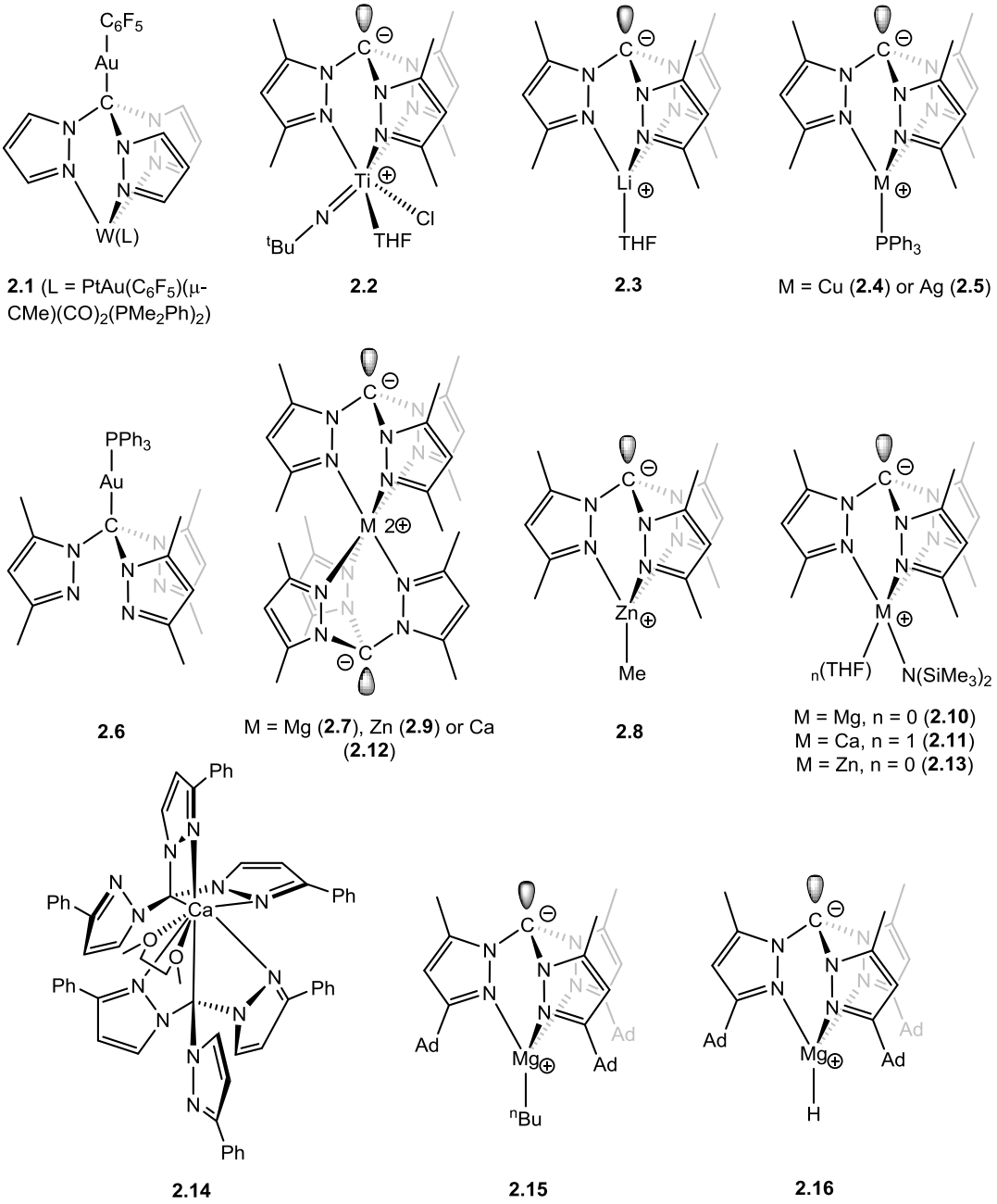


Figure 2.2 Examples of main group and transition metal Tpm^{d} complexes. [15-23]

Later in 2001, Mountford and co-workers pioneered the first example of a naked, sp^3 hybridised carbanion.[17] Complex **2.2** was synthesised *via* the reaction between $Ti(N^tBu)\{HC(Me_2pz)_3\}Cl_2$ and MeLi or LiN^iPr_2 in THF. NMR spectroscopy, X-ray crystallography and DFT calculations supported the zwitterionic nature of **2.2**. A similar compound (**2.3**) featuring a spatially separated carbanion and a lithium cation was prepared by deprotonating $HC(3,5\text{-}Me_2pz)_3$ with MeLi in THF. [17, 18, 24]

Breher *et al.* later reported a series of Tpm^d-supported metal complexes with different coordination modes.[19] Compounds **2.4** and **2.5** were obtained by reacting **2.3** with $[Ph_3PCuCl]_4$ and $[Ph_3PAg][NO_3]$, respectively. Both complexes possessed zwitterionic structures comprising the anionic Tpm^d as the κ^3-coordinated N_3-ligand. In contrast, the reaction between **2.3** and Ph_3PAuCl led to the formation of **2.6**, which featured a two-coordinate Au centre with a direct Au-C covalent bond. The difference in the coordination behaviour of Au compared to others was attributed to the fact that small, non-polarisable metals preferred to bind to the "hard" pyrazolyl nitrogens whereas softer metals, such as Au, would coordinate to the carbanion.

The choice of metals in Tpm^d ligand-supported complexes has also been extended to magnesium and zinc. Reported by Mountford *et al.*, compound **2.7** was synthesised by reacting 2 equiv. of $HC(3,5\text{-}Me_2pz)_3$ with 1 equiv. of $MgPh_2$ in Et_2O.[20] X-ray crystallography confirmed the formation of the homoleptic species in which the magnesium centre was sandwiched between the two ligands and coordinated to six pyrazolyl nitrogens. The synthesis of the heteroleptic compound $(Tpm^{(Me,Me)d})Mg(Ph)$ was attempted by using an excess of $MgPh_2$. However, the desired product was isolated in low yields due to the difficulties in the removal of the excess $MgPh_2$, required to suppress the formation of **2.7**. A similar reaction was performed between $HC(3,5\text{-}Me_2pz)_3$ and a small excess of $ZnMe_2$ in toluene under extended heating conditions, leading to the formation of complex **2.8**. No homoleptic species (**2.9**) was formed, in contrast to the zwitterionic magnesium analogue **2.7**. Complex **2.9** was later synthesised by reacting **2.3** with $ZnCl_2$ in a 2:1 stoichiometry in THF under extended heating conditions.[21]

Following the successful synthesis of the aforementioned compounds, complexes **2.10** and **2.11** were prepared *via* the protonolysis reaction between $HC(3,5\text{-}Me_2pz)_3$ and $M\{N(SiMe_3)_2\}_2(THF)_x$ (M = Mg, x = 0 for **2.10** and M = Ca, x = 2 for **2.11**) in a 1:1

stoichiometry.[21] Both complexes were zwitterionic in nature and possessed a cationic $\{M\text{-}N(SiMe_3)_2\}^+$ moiety. As expected, the homoleptic calcium species (**2.12**) could be obtained by using 2 equiv. of $HC(3,5\text{-}Me_2pz)_3$. The structure of **2.12** was analogous to that of the previously reported **2.7**. The synthesis of a heteroleptic Zn compound (**2.13**) *via* the protonolysis pathway between the protio-ligand and $Zn\{N(SiMe_3)_2\}_2$ was unsuccessful. Nevertheless, complex **2.13** was isolated in quantitative yields by reacting $(Tpm^{(Me,Me)d})Zn(Cl)$ with $NaN(SiMe_3)_2$. Complexes **2.10** and **2.11** were highly active in the ROP of *rac*-LA in both THF and toluene, polymerising 100 equiv. of *rac*-LA within 1 min at room temperature. A lower activity was observed for **2.13** under identical polymerisation conditions. In all polymerisations using **2.10**, **2.11** and **2.13**, a poor agreement between the experimental and theoretical M_n was observed, in conjunction with broad PDIs.

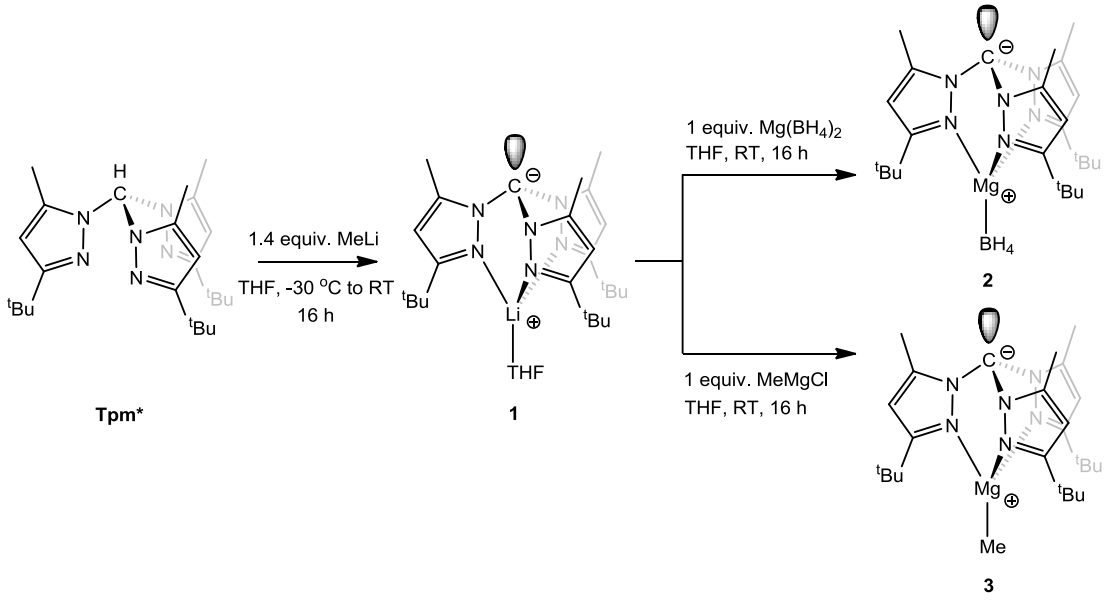
Westerhausen and co-workers later reported the synthesis of a calcium complex supported by a bulkier Tpm^d ligand.[22] Compound **2.14** was isolated in quantitative yields by reacting 2 equiv. of $HC(3\text{-}Phpz)_3$ with 1 equiv. of $Ca\{N(SiMe_3)_2\}_2(THF)_2$ in dimethoxyethane. Surprisingly, the calcium centre was bound to the Tpm^d ligand through a κ^2-N, κ^1-C coordination mode. This is the first example of such coordination mode being observed in Tpm^d alkaline earth complexes. The unexpected formation of the Ca-C bonds was facilitated by the elongation of the $Ca\text{-}N_{pz}$ bonds and the Ca-C distances were within the expected range for a dialkylcalcium complex.[25, 26]

While the work in this Thesis was in progress, Jones *et al.* reported a series of magnesium complexes supported by a Tpm^d ligand with a bulky adamantyl group at the 3-position of the pyrazolyl ring.[23] Compound **2.15** was obtained *via* the reaction between $HC(3\text{-}Ad,\ 5\text{-}Mepz)_3$ and $MgBu_2$ in toluene. No homoleptic species was generated, in contrast to the formation of **2.7** involving a less bulky ligand. Complex **2.15** served as an excellent precursor for the preparation of **2.16** by reacting with $LiAlH_4$. X-ray crystallography confirmed the monomeric nature of **2.16** with a terminal Mg-H bond.

2.3 Synthesis and characterisation of Tpm*^{d} magnesium complexes

Tpm*^{d}-supported magnesium complexes (Tpm*^{d} = C(3-^{t}Bu, 5-Mepz)$_3$) were synthesised and utilised as ROP catalysts for a number of reasons. The choice of magnesium as the metal centre will be justified in Chapter Three. One of the problems associated with alkaline earth metal complexes is their propensity to redistribute to form homoleptic species,[27] the formation of which can be circumvented by the use of a bulky supporting ligand.[28] As discussed in Section 2.2, complexes featuring a sterically congested Tpm^{d} ligand, such as compounds **2.15** and **2.16,** have shown to be highly stable towards redistribution to form homoleptic species. In addition, the sterically encumbered coordination sphere created by using a bulky ligand could potentially improve the stereoselectivity of the resulting catalysts. It is notable that previous work in the Mountford group has introduced a number of Tp ligand-supported alkaline earth catalysts which were shown to be active and stereoselective in the ROP of cyclic esters.[29, 30] It is a combination of the aforementioned reasons that drove the development of Tpm*^{d} magnesium complexes as ROP catalysts. Tpm* was synthesised according to the literature procedures by Reger *et al.* in 41% isolated yield.[13] The sterically demanding nature of the ligand provides a well-defined coordination environment that allows the formation of a range of deprotonated magnesium complexes.

2.3.1 Synthesis and characterisation of (Tpm*^{d})Li(THF) (1), (Tpm*^{d})Mg(BH$_4$) (2) and (Tpm*^{d})Mg(Me) (3)



Scheme 2.1 Synthesis of (Tpm*^{d})Li(THF) (**1**), (Tpm*^{d})Mg(BH$_4$) (**2**) and (Tpm*^{d})Mg(Me) (**3**).

The lithium salt (Tpm*^{d})Li(THF) (**1**) was synthesised as a precursor to access (Tpm*^{d})Mg(BH$_4$) (**2**) and (Tpm*^{d})Mg(Me) (**3**) *via* salt elimination pathways. The protio-ligand was deprotonated with MeLi in THF, affording **1** as a pink solid in 45% isolated yield. The H$_{pz}$, methyl and ^{t}Bu substituents on the pyrazolyl ring could be observed as singlets at 5.66, 2.58 and 1.26 ppm, respectively, in the ^{1}H NMR spectrum (C$_6$D$_6$) (Figure 2.3). Integration of the THF signals relative to the ligand backbone revealed the coordination of one THF.

Diffraction-quality crystals were grown from a mixture of THF and hexane at -30 °C. The structure identifies the monomeric nature of the complex, with the Li centre coordinated to the three pyrazolyl N donors and the O donor of THF (Figure 2.4 and Table 2.1), analogous to the literature reported (Tpm$^{(Me,Me)d}$)Li(THF) (**2.3**).[18] The geometry at the Li centre is best described as distorted tetrahedral, with N(1)-Li(1)-O(1) and N(1)-Li(1)-N(5) bond angles of 135.5(2) and 90.36(18)°, respectively, deviating significantly from the ideal tetrahedral structure. The N-C(25)-N angles of 108.73(18)-112.22(19)° are in good agreement with the *pseudo*-tetrahedral geometry at the carbanionic centre, comparable with those found in **2.3** (109.2(1)-109.7(1)°).

The bond distances and inner ring angles within the pyrazolyl ring, in conjunction with the average C(25)-N distance of 1.444(2) Å, show that no charge delocalisation into the pyrazolyl ring occurs. The Li(1)···C(25) distance was found to be 2.885(5) Å, which is 0.7 Å longer than a direct Li-C bond commonly observed in lithium organyl compounds.[31-34] This indicates that there is no covalent interaction between the carbanion and the Li cation. The Li-O bond distance of **1** (2.015(5) Å) is significantly longer than that of **2.3** (1.908(3) Å), presumably due to the bulkier ^{t}Bu substituents at the 3-position of the pyrazolyl ring in **1**.[18]

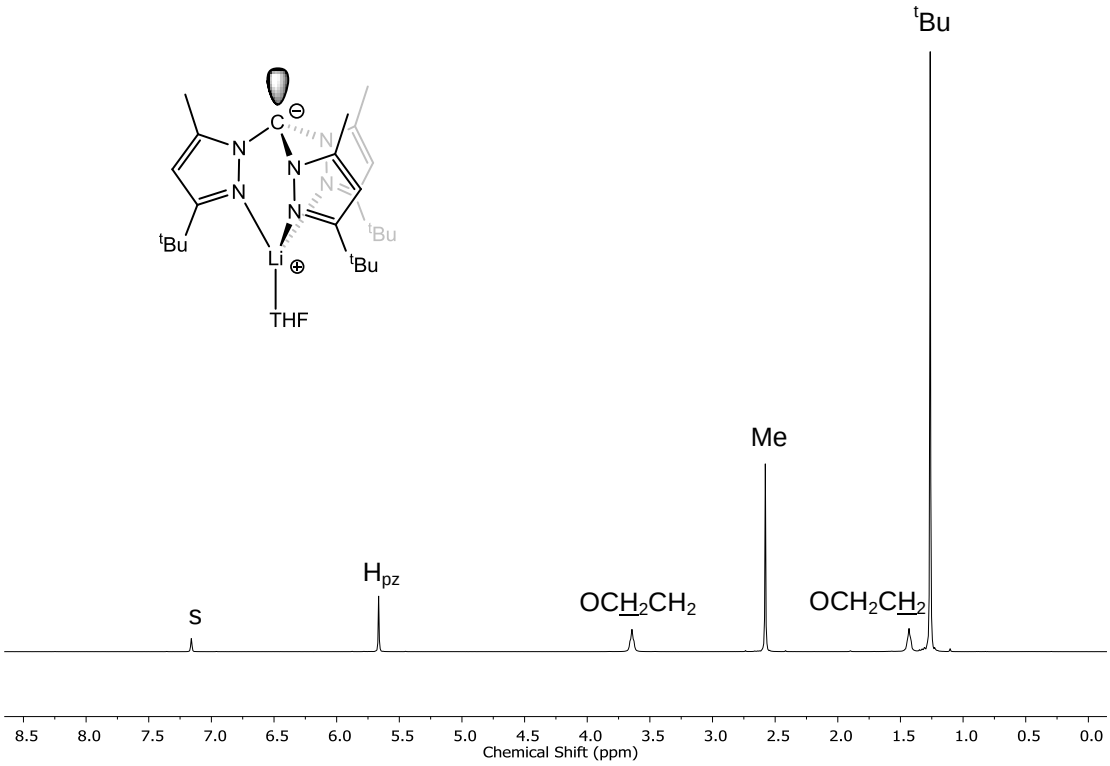


Figure 2.3 ^{1}H NMR spectrum (C_6D_6, 400.2 MHz, 298 K) of (Tpm*^{d})Li(THF) (**1**). "s" denotes protio-solvent.

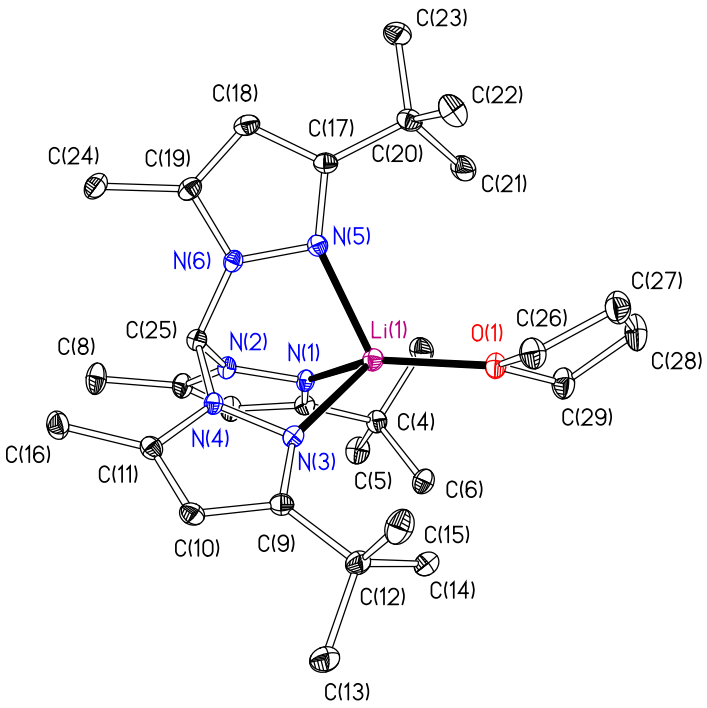


Figure 2.4 Displacement ellipsoid plot of (Tpm*^{d})Li(THF) (**1**). H atoms omitted for clarity. Ellipsoids are drawn at the 20% probability level.

Table 2.1 Selected bond lengths (Å) and angles (°) for (Tpm*^{d})Li(THF) (**1**).

Li(1)-N(1)	2.053(5)	Li(1)-N(3)	2.100(5)
Li(1)-N(5)	2.067(4)	Li(1)-O(1)	2.015(5)
Li(1)···C(25)	2.885(5)	C(25)-N(2)	1.449(3)
C(25)-N(4)	1.449(3)	C(25)-N(6)	1.434(3)
N(3)-N(4)	1.377(3)	N(3)-C(9)	1.342(3)
C(9)-C(10)	1.404(4)	C(10)-C(11)	1.373(4)
C(11)-N(4)	1.356(3)		
N(1)-Li(1)-N(3)	91.00(18)	N(1)-Li(1)-N(5)	90.36(18)
N(3)-Li(1)-N(5)	100.62(18)	N(1)-Li(1)-O(1)	135.5(2)
N(2)-C(25)-N(4)	108.73(18)	N(4)-C(25)-N(6)	112.22(19)
N(2)-C(25)-N(6)	110.81(19)	N(4)-N(3)-C(9)	105.33(19)
N(3)-C(9)-C(10)	110.3(2)	C(9)-C(10)-C(11)	106.2(2)
C(10)-C(11)-N(4)	107.1(2)	C(11)-N(4)-N(3)	111.06(19)

(Tpm*^{d})Mg(BH_4) (**2**) was obtained as a THF-free white solid in 76% isolated yield *via* the salt elimination reaction between **1** and Mg(BH_4)$_2$ in THF. The characteristic

signals corresponding to B$\underline{H}_4$ could be observed as a broad quartet in the region of 1.16-1.79 ppm in the ^{1}H NMR spectrum (C_6D_6). This is the result of the rapid exchange between the terminal B-H_t and bridging B-H_b on the NMR timescale. The $^1J_{B\text{-}H}$ coupling constant of 83 Hz is therefore an average value for both B-H_t and B-H_b. The ^{11}B NMR spectrum (C_6D_6) showed a quintet at -38.7 ppm, in good agreement with a typical borohydride signal.[29, 30, 35-38]

Complex **2** was also characterised by X-ray crystallography using diffraction-quality crystals grown from a toluene/hexane mixture at -30 °C. Complex **2** possesses *pseudo*-tetrahedral geometry with the Mg centre coordinated to the three pyrazolyl N donors and the κ^3-BH_4 moiety (Figure 2.5 and Table 2.2). The Mg(1)···C(25) distance was found to be 2.948(2) Å, much longer than that of a typical Mg-C bond in a magnesium alkyl complex,[39] indicating the absence of covalent interaction between the carbanion and the Mg cation. The BH_4 moiety coordinates to the magnesium centre *via* a κ^3-coordination mode in the solid state, similar to an analogous compound ($Tp^{tBu,Me}$)Mg(BH_4) (**2.17**) prepared previously in the Mountford group.[30] The Mg(1)···B(1) distance of 2.278(3) Å is consistent with the value expected for a κ^3-bound BH_4 (2.22-2.34 Å).[40] The hydrogen atoms in the BH_4 moiety were located in a Fourier difference map and positionally and isotropically refined, giving the Mg···H distances in the usual range of 1.90-2.32 Å.[40] The average Mg-N_{pz} bond length of 2.1042(10) Å is very similar to that found in **2.17** (2.1121(9) Å).[30]

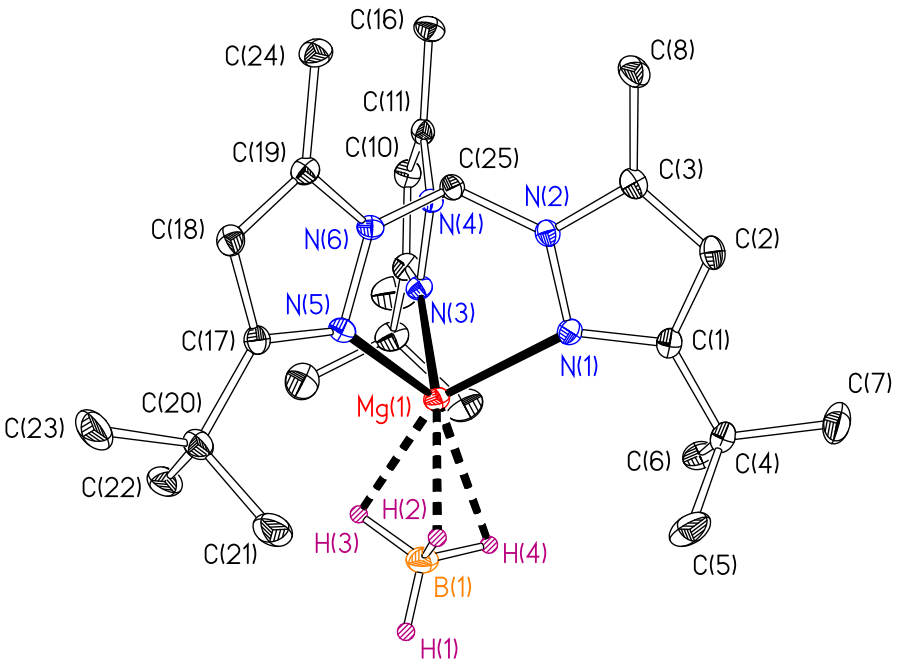


Figure 2.5 Displacement ellipsoid plot of (Tpm*^{d})Mg(BH$_4$) (**2**). Ellipsoids are drawn at the 20% probability level.

Table 2.2 Selected bond lengths (Å) and angles (°) for (Tpm*^{d})Mg(BH$_4$) (**2**).

Mg(1)-N(1)	2.1102(17)	Mg(1)-N(3)	2.0924(18)
Mg(1)-N(5)	2.1100(17)	Mg(1)-H(2)	1.97(2)
Mg(1)-H(3)	2.15(2)	Mg(1)-H(4)	2.43(2)
Mg(1)···C(25)	2.948(2)	Mg(1)···B(1)	2.278(3)
B(1)-H(1)	1.01(3)	B(1)-H(2)	1.174(17)
B(1)-H(3)	1.177(17)	B(1)-H(4)	1.145(17)
N(1)-Mg(1)-N(3)	89.03(6)	N(1)-Mg(1)-H(3)	152.2(5)
N(1)-Mg(1)-H(4)	104.2(5)	H(3)-B(1)-H(4)	108.8(8)
H(1)-B(1)-H(4)	109.4(9)		

Apart from X-ray diffraction, various other techniques can be used to structurally characterise the coordination modes of borohydrides, such as neutron diffraction, NMR and IR spectroscopy. Diffraction with any kind of radiation has its limitations in providing useful structural information in the solution state. NMR spectroscopy, on the other hand, has too slow a timescale to gain understanding of the coordination modes of borohydrides. The superior technique is IR spectroscopy, allowing useful information on the M-BH$_4$ coordination environment to be obtained. It has the

advantage of distinguishing the four coordination modes drawn in Figure 2.6 in both the solid and solution state.[41] The structurally diagnostic bands are in the range of 1000-2600 cm^{-1} and assigning these B-H stretching bands according to their frequencies and shapes enables the differentiation of the various coordination modes. Table 2.3 lists the criteria for structural assignments.

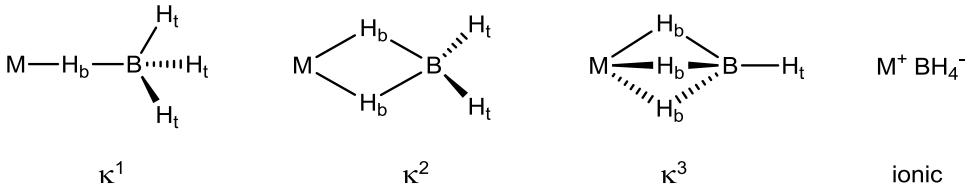


Figure 2.6 Different coordination modes of borohydrides.

Table 2.3 IR active fundamental vibrational transitions commonly observed for mononuclear M-BH_4 configurations.[41]

Structure	Freq. (cm^{-1})	Normal mode	Symmetry	Comments
Monodentate	2450-2300	B–H_t	A_1, E	Strong doublet
	~2000	B–H_b stretching	A_1	Strong
	~2000-1700	M–H_b stretching	A_1	Often broad
	1150-1000	BH_3 deformation	A_1, E	Strong band
Bidentate	2600-2400	B–H_t stretching	A_1, B_1	Strong doublet (50-80 cm^{-1})
	2150-1650	B–H_b stretching	A_1, B_2	Strong band, possible shoulder
	1500-1300	M–H_b stretching	A_1	Strong band
	1200-1100	BH_2 deformation	B_2	Strong
Tridentate	2600-2450	B–H_t stretching	A_1	Strong singlet
	2200-2100	B–H_b stretching	A_1, E	Doublet (50-80 cm^{-1})
	1250-1150	Bridge deformation	E	Strong
Ionic	2300-2200	B–H_t stretching	T_2	Strong broad
	1100-1050	BH_2 deformation	T_2	Strong broad

The solid state IR spectrum of **2** supported the findings based on crystallographic data, further confirming the κ^3-coordination mode of the BH_4 moiety. The absorption at 2359 cm^{-1} (singlet) was assigned to the terminal ν(B-H_t) stretching mode whilst the

bridging ν(B-H_b) stretching mode was observed as a doublet at 2225 and 2176 cm^{-1} (49 cm^{-1} splitting). The κ^3-coordination mode remained unchanged in the solution state (THF). The strong singlet at 2386 cm^{-1} and the doublet at 2232 and 2175 cm^{-1} (57 cm^{-1} splitting) are characteristic of the terminal and bridging ν(B-H) stretching modes, respectively.

κ^3-coordination modes have been observed in other systems containing a magnesium borohydride moiety, including (^{t}BuO)Mg(BH_4)(OEt_2),[42] (^{Dipp}NacNac)Mg(BH_4)(THF),[36] (^{Dipp}NacNac)Mg(BH_4)(Et_2O),[43] Mg(BH_4)$_2$($Me_2NC_2H_4NMe_2$),[42] and (CzOx^{iPr})Mg(BH_4)(THF).[35] This coordination mode is far more common in lanthanide borohydride complexes.[38, 44-50] There is also literature precedence for borohydrides adopting a κ^2-coordination mode, examples being Mg(BH_4)$_2$(py)$_4$,[51] (PhO)Mg(BH_4)(THF)$_2$,[42] (2,6-OC_6H_3 ^{t}Bu$_2$)Mg(BH_4)(THF)(DME) [42] and {(Me_3TACD)Al(^{i}Bu)$_3$}Mg(BH_4).[52] Interestingly, (^{Dipp}NacNac)Mg(BH_4)(THF) undergoes a significant change from κ^3- to κ^2-coordination upon dissolving in THF as a consequence of an additional THF ligand in the coordination sphere.[36]

The salt elimination reaction between **1** and MeMgCl in THF led to the formation of (Tpm*^{d})Mg(Me) (**3**), which was obtained as a cream powder in 87% isolated yield. The Mg-<u>Me</u> protons were clearly observed as a sharp singlet at -0.11 ppm in the ^{1}H NMR spectrum (C_6D_6). No coordinated THF signal was present. Crystals suitable for X-ray diffraction were grown from a mixture of THF and hexane at -30 °C. Complex **3** has crystallographically imposed C_3 symmetry, crystallising in the cubic space group $I\bar{4}3d$. Complex **3** is four-coordinate with the Mg coordinated to the three pyrazolyl N donors and the C atom of the Me moiety (Figure 2.7 and Table 2.4). The coordination geometry at the Mg centre is best described as distorted tetrahedral with the average C-Mg-N and N-Mg-N angles of 124.57(2)° and 90.98(2)°, respectively. The Mg(1)-C(10) bond distance of 2.1371(19) Å is comparable to those found in other known compounds containing a Mg-Me moiety in the literature.[53-57]

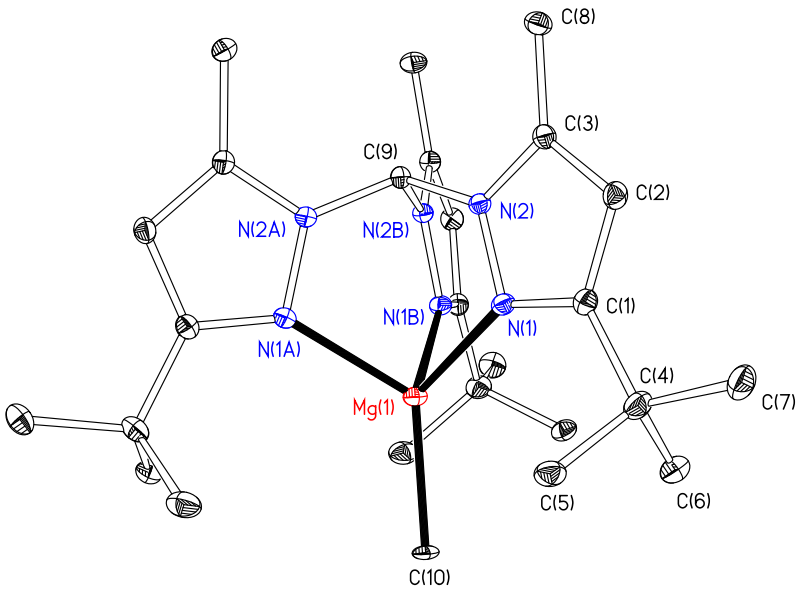
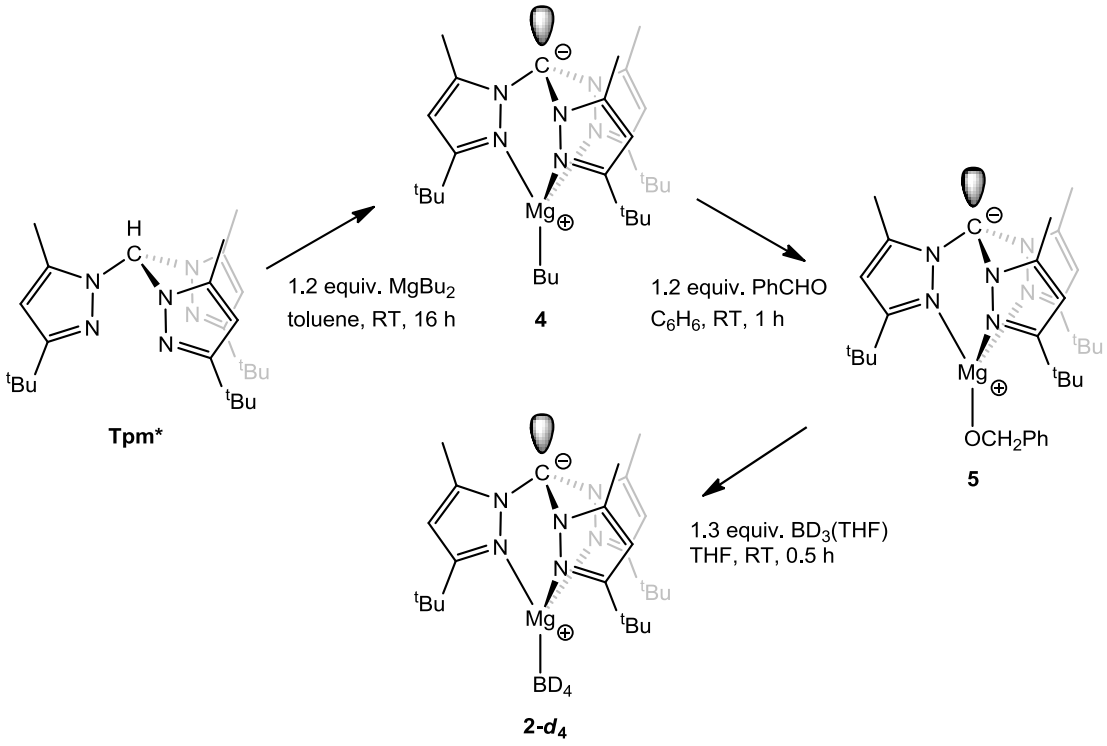


Figure 2.7 Displacement ellipsoid plot of (Tpm*^{d})Mg(Me) (**3**). H atoms omitted for clarity. Ellipsoids are drawn at the 20% probability level.

Table 2.4 Selected bond lengths (Å) and angles (°) for (Tpm*^{d})Mg(Me) (**3**).

Mg(1)-N(1)	2.1083(11)	Mg(1)-C(10)	2.1371(19)
Mg(1)···C(9)	2.997(2)		
N(1)-Mg(1)-N(1A)	90.98(4)	N(1)-Mg(1)-C(10)	124.57(3)

2.3.2 Synthesis and characterisation of (Tpm*^{d})Mg(Bu) (4), (Tpm*^{d})Mg(OBn) (5) and (Tpm*^{d})Mg(BD$_4$) (2-*d*$_4$)



Scheme 2.2 Synthesis of (Tpm*^{d})Mg(Bu) (**4**), (Tpm*^{d})Mg(OBn) (**5**) and (Tpm*^{d})Mg(BD$_4$) (**2-*d*$_4$**).

(Tpm*^{d})Mg(Bu) (**4**) was synthesised as a precursor to access (Tpm*^{d})Mg(OBn) (**5**) and subsequently (Tpm*^{d})Mg(BD$_4$) (**2-*d*$_4$**). Complex **4** was obtained as a cream solid in 56% isolated yield *via* the reaction between Tpm* and MgBu$_2$ in toluene at room temperature. Diffraction-quality crystals were grown from a saturated hexane solution at -30 °C. Compound **4** is four-coordinate with the Mg coordinated to three pyrazolyl N donors and the carbon from the Bu moiety (Figure 2.8 and Table 2.5). The coordination environment at the Mg centre is best described as distorted tetrahedral with N-Mg-N and N-Mg-C angles of 88.55(13)-91.77(13)º and 121.8(2)-130.00(19)º, respectively, in close agreement with those found in (Tp^{tBu,Me})Mg(Bu) (**2.18**) prepared previously in the Mountford group.[30] The Mg(1)-C(26) bond distance in **4** is longer than that observed in **2.18** (2.121(5) Å for **4** *cf.* 2.070(4) Å for **2.18**) whereas the average Mg-N$_{pz}$ distances are identical within error (2.123(2) Å for **4** *cf.* 2.1311(9) Å for **2.18**). The average Mg(1)-N$_{pz}$ bond distance of 2.123(2) Å in **4** is longer than that

in **3** (2.1083(11) Å), presumably due to the smaller size of the Me group in comparison to that of the ^{n}Bu group.

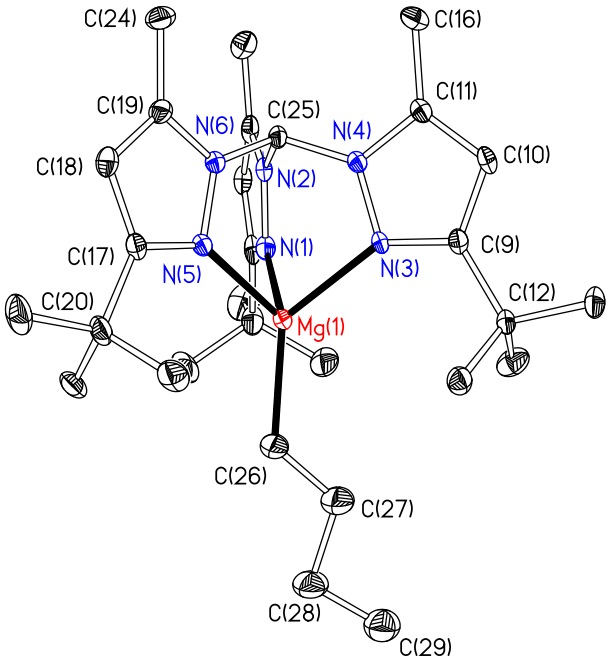


Figure 2.8 Displacement ellipsoid plot of (Tpm*^{d})Mg(Bu) (**4**). H atoms omitted for clarity. Ellipsoids are drawn at the 20% probability level.

Table 2.5 Selected bond lengths (Å) and angles (°) for (Tpm*^{d})Mg(Bu) (**4**).

Mg(1)-N(1)	2.136(4)	Mg(1)-N(3)	2.116(3)
Mg(1)-N(5)	2.116(3)	Mg(1)-C(26)	2.121(5)
C(26)-C(27)	1.492(7)	Mg(1)···C(25)	3.033(4)
N(1)-Mg(1)-N(3)	88.65(14)	N(1)-Mg(1)-N(5)	91.77(13)
N(3)-Mg(1)-N(5)	88.55(13)	N(1)-Mg(1)-C(26)	124.7(2)
N(3)-Mg(1)-C(26)	130.00(19)	N(5)-Mg(1)-C(26)	121.8(2)
Mg(1)-C(26)-C(27)	126.1(4)		

Following the successful synthesis of two magnesium alkyl species, attention was focused on the development of alkoxide complexes, which according to the literature, have demonstrated superiority compared to other initiators for the ROP of cyclic esters.[58-60] The most common synthetic pathway to access a metal alkoxide species is *via* the protonolysis reaction between a metal alkyl complex and an alcohol. However, the addition of benzyl alcohol to **4** led to decomposition due to the sensitivity of the

carbanion, forming the Tpm* protio-ligand. An alternative approach was therefore carried out by reacting **4** with benzaldehyde through a β-H transfer mechanism, producing (Tpm*^{d})Mg(OBn) (**5**) as a light yellow solid in 65% isolated yield. The formation of a six-membered ring transition state in a chair conformation (Figure 2.9) is expected during the course of the reaction, whereby a β-H is transferred from the Bu moiety to the carbonyl carbon of benzaldehyde. Chisholm *et al.* recently reported the NMR tube scale synthesis of (^{Dipp}NacNac)Mg(OBn) using this approach.[61] Six-membered ring transition states are also found in other reactions, an example being Meerwein-Ponndorf-Verley reduction, during which a hydride is transferred from a sacrificial alcohol to an aldehyde to generate a new alcohol with the aid of an aluminium alkoxide catalyst.[62]

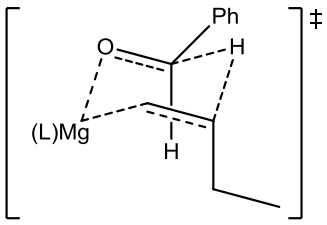
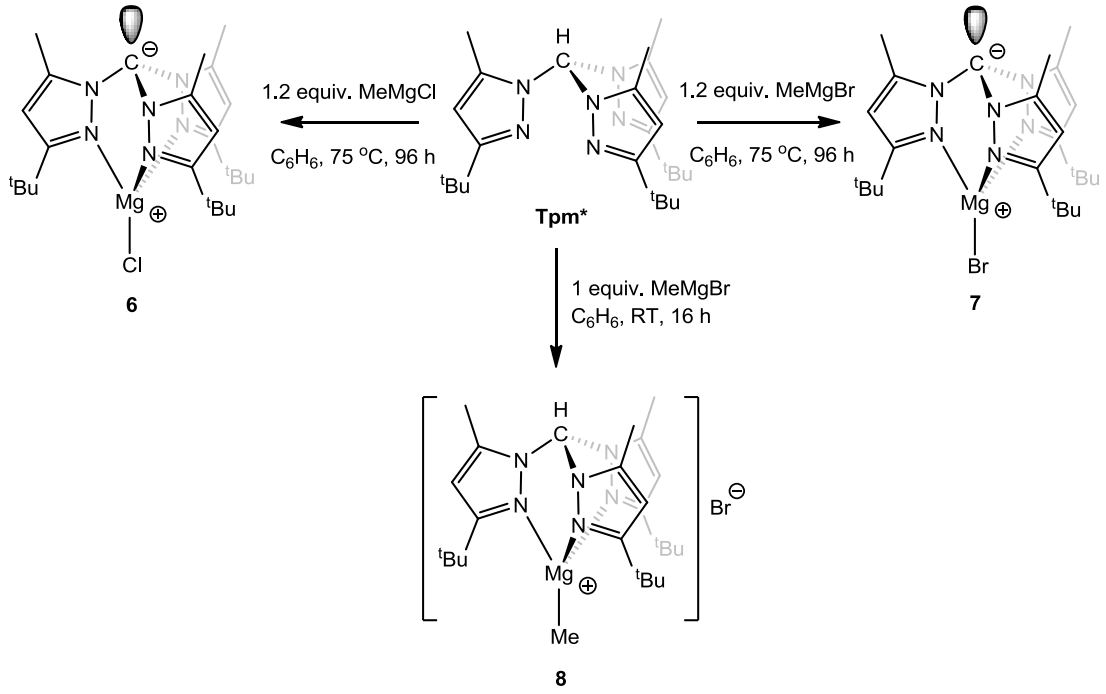


Figure 2.9 β-H transfer from the methylene group of the butyl moiety.

The successful synthesis of **5** facilitated the formation of (Tpm*^{d})Mg(BD_4) (**2-*d*$_4$**) *via* an exchange reaction between **5** and BD_3(THF). The reason for the interest in **2-*d*$_4$** will be justified in Chapter Three. Complex **2-*d*$_4$** was obtained as a white solid in 74% isolated yield. The ^{1}H NMR spectrum (C_6D_6) was reminiscent of that for **2**, with the absence of the quartet signal corresponding to $B\underline{H}_4$ whilst the ^{2}H NMR spectrum (C_6H_6) showed a quartet in the region of 1.23-1.72 ppm. The observed $^{1}J_{B\text{-}D}$ coupling constant of 13 Hz is in good agreement with the calculated value of 12.7 Hz ($^{1}J_{B\text{-}H}$ = 83 Hz for **2**, γ_D/γ_H = 0.154). Additionally, the ^{11}B NMR spectrum clearly revealed a multiplet at -39.3 ppm, characteristic of $\underline{B}D_4$. The BD_4 ligand of **2-*d*$_4$** possesses a κ^3-coordination mode in both the solid and solution state, confirmed by IR spectroscopic analysis. In comparison to **2**, B-D stretching frequencies are shifted to lower wavenumbers due to an increased reduced mass. In a nujol mull, the singlet at 1834 cm^{-1} and the doublet at 1771 and 1733 cm^{-1} (38 cm^{-1} splitting) were assigned to the terminal and bridging ν(B-D) stretching modes, respectively. The THF solution state IR spectrum revealed a singlet at 1970 cm^{-1} (ν(B-H$_t$)) and a doublet at 1793 and 1735 cm^{-1} (ν(B-H$_b$)) with 58 cm^{-1} splitting, characteristic of a κ^3-coordination mode.

2.3.3 Synthesis and characterisation of (Tpm*^{d})Mg(Cl) (6), (Tpm*^{d})Mg(Br) (7) and [(Tpm*)Mg(Me)]Br (8)

Scheme 2.3 depicts the synthesis of (Tpm*^{d})Mg(Cl) (**6**) and (Tpm*^{d})Mg(Br) (**7**) *via* the protonolysis reactions of Tpm* with the corresponding methyl Grignard reagents under heating conditions. A cationic species, [(Tpm*)Mg(Me)]Br (**8**), was also prepared by reacting the protio-ligand with MeMgBr at room temperature.



Scheme 2.3 Synthesis of (Tpm*^{d})Mg(Cl) (**6**), (Tpm*^{d})Mg(Br) (**7**) and [(Tpm*)Mg(Me)]Br (**8**).

Complex **6** was synthesised *via* the reaction between the protio-ligand and 1.2 equiv. of MeMgCl at 75 °C for 96 h, affording **6** as a light yellow solid in 26% isolated yield. The low yield was attributed to the repeated recrystallisation required to remove the remaining Tpm* protio-ligand. Using a larger excess of MeMgCl resulted in the formation of (Tpm*^{d})Mg(Me) (**3**) which was difficult to remove. Crystals of **6** suitable for X-ray crystallography were grown from a saturated benzene solution at room temperature. Compound **6** is four-coordinate with the Mg coordinated to the three pyrazolyl N donors and the Cl moiety (Figure 2.10 and Table 2.6). The coordination geometry at the Mg centre is best described as distorted tetrahedral, with N-Mg-N and N-Mg-Cl angles of 92.26(5)-93.36(7)^{o} and 123.30(4)-123.55(6)^{o}, respectively. The Mg(1)-Cl(1) and the average Mg(1)-N_{pz} bond lengths were found to

be 2.2634(8) and 2.0830(9) Å, in close agreement with those found in ($Tp^{tBu,Me}$)Mg(Cl) (**2.19**) (2.2587(9) and 2.0992(6) Å, respectively).[30] As expected, the average Mg(1)-N_{pz} bond length of 2.0830(9) Å in **6** is shorter than those in **3** (2.1083(6) Å) and **4** (2.123(2) Å) due to the more electronegative nature of Cl than C, resulting in a stronger interaction between the electropositive Mg and the pyrazolyl nitrogens.

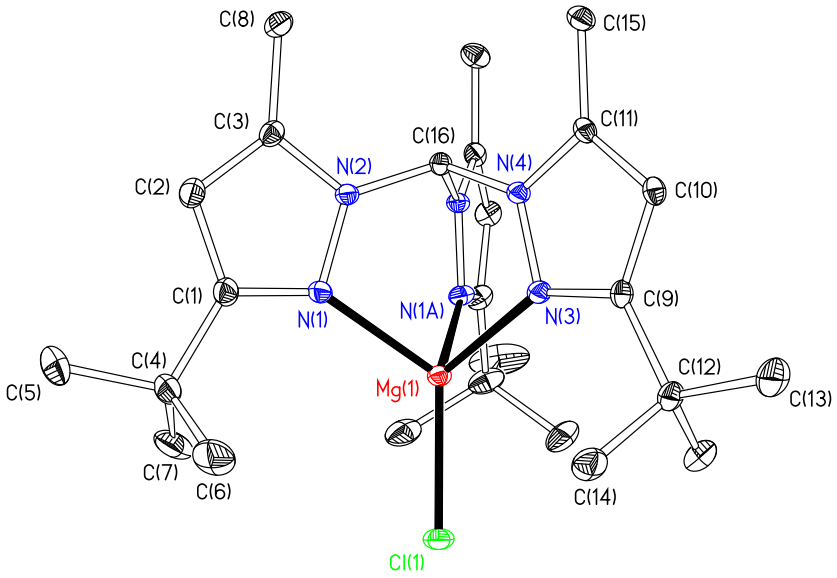


Figure 2.10 Displacement ellipsoid plot of (Tpm*^{d})Mg(Cl) (**6**). H atoms omitted for clarity. Ellipsoids are drawn at the 20% probability level.

Table 2.6 Selected bond lengths (Å) and angles (°) for (Tpm*^{d})Mg(Cl) (**6**).

Mg(1)-N(1)	2.0842(13)	Mg(1)-N(3)	2.0806(18)
Mg(1)-N(1A)	2.0842(13)	Mg(1)-Cl(1)	2.2634(8)
Mg(1)···C(16)	2.945(2)		
N(1)-Mg(1)-N(3)	92.26(5)	N(1)-Mg(1)-N(1A)	93.36(7)
N(3)-Mg(1)-N(1A)	92.26(5)	N(1)-Mg(1)-Cl(1)	123.30(4)
N(3)-Mg(1)-Cl(1)	123.55(6)	N(1A)-Mg(1)-Cl(1)	123.30(4)

An analogous reaction between the protio-ligand and 1.2 equiv. of MeMgBr was also carried out, in an attempt to access (Tpm*^{d})Mg(Br) (**7**). The same problem encountered in the synthesis of **6** persisted (protio-ligand was present). Unfortunately, multiple purification attempts *via* repeated recrystallisation were unsuccessful in this case. Using a larger excess of MgMgBr resulted in the formation of an unknown side

product which was difficult to remove. Pure complex **7** was therefore not isolated and NMR characterisation was carried out in the presence of the protio-ligand. In contrast, the equimolar reaction between Tpm* and MeMgBr at room temperature resulted in the formation of [(Tpm*)Mg(Me)]Br (**8**) as a white solid. Due to the poor solubility of **8** in non-polar solvents, NMR characterisation was performed in CD_2Cl_2. The apical proton could be observed as a singlet at 8.19 ppm in the ^{1}H NMR spectrum whereas the Mg-Me protons were significantly shielded (-0.77 ppm), similar to those observed in **3**. The presence of $[(Tpm^*)Mg(Me)]^+$ was further confirmed by electrospray mass spectrometry. The spectrum revealed a peak centred at 463 *m/z* with the correct isotope distribution, indicative of the cation. Jones *et al.* recently reported an analogous compound $[(Tpm^{Ad})Mg(Me)]I$ through the reaction between HC(3-Ad, 5-Mepz)$_3$ and MeMgI at room temperature.[23]

2.4 Computational analysis of $Tp^{Me,Me}$ and Tpm^{d} ligand-supported magnesium alkoxide species

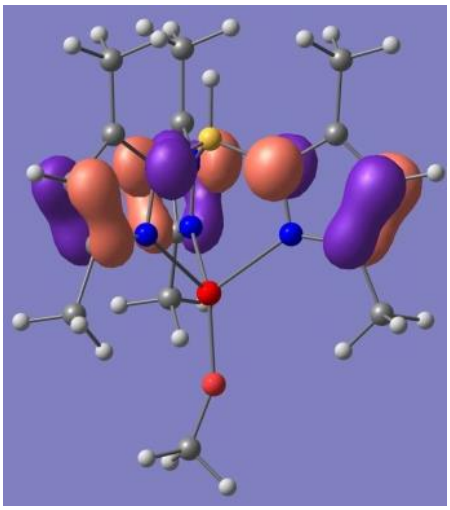
As will be discussed in Chapter Three, $(Tp^{tBu,Me})Mg(OBn)$ (**2.20**) and $(Tpm^{*d})Mg(OBn)$ (**5**) demonstrate significantly different activities in the ROP of *rac*-LA.[30] The latter polymerises *rac*-LA at a rate which is 1550 times higher than the former under identical conditions. In order to gain a more comprehensive understanding of the structures and bonding of both $Tp^{tBu,Me}$ and Tpm^{*d} ligand-supported magnesium alkoxide species, Density Functional Theory (DFT) as well as Quantum Theory of Atoms in Molecules (QTAIM) calculations were carried out by Dr Matthew Blake of the University of Oxford. Geometry optimisations were first performed on a model compound $(Tp^{Me,Me})Mg(OMe)$ (**Q2.21**), starting from geometries based on the X-ray crystal structure of $(Tp^{tBu,Me})Mg(OMe)$ (**2.22**) synthesised previously by Dr J. Unruangsri.[30] The *tert*-butyl substituents at the 3-position of the pyrazolyl ring were replaced with the less computationally demanding methyl groups. The computed geometry for **Q2.21** is in good agreement with that determined experimentally for **2.22**. The Mg-O distance of 1.834 Å is only 0.033 Å longer than that found in the X-ray crystal structure of **2.22** (1.801(2) Å). In addition, the average N-Mg-O angle of 125.5° is also comparable to that found in **2.22** (124.01(7)°). $(Tpm^{(Me,Me)d})Mg(OMe)$ (**Q2.23**), a model compound for **5**, was geometrically optimised starting from the same X-ray structure by further replacing the B-H fragment with a carbon atom, giving a calculated structure whose geometry at

the magnesium centre is in close agreement with that determined experimentally for **2.22**.

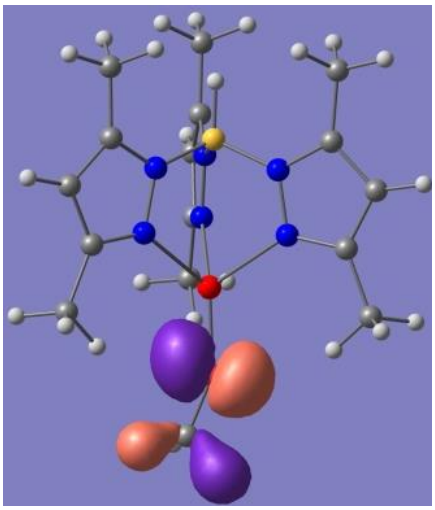
Bond dissociation enthalpies (BDE) were computed since the insertion of LA molecules in the polymerisation involves breaking the Mg-O bond (either Mg-alkoxide or Mg-polymeryl). The BDEs for **Q2.21** and **Q2.23** ((L)Mg(OMe) → (L)Mg + OMe in their relaxed geometries) were calculated to be very similar (412.4 kJ mol^{-1} for **Q2.21** and 408.8 kJ mol^{-1} for **Q2.23**), shown in Table 2.7.

Figures 2.11 and 2.12 illustrate the isosurfaces for the selected molecular orbitals (MOs) for both **Q2.21** and **Q2.23**, as well as their associated energies. Whilst the HOMO-2 (ligand π, -5.45 eV) and LUMO (ligand π*, -0.87 eV) for **Q2.21** are primarily pyrazolyl ring-based, the HOMO (-4.33 eV) and HOMO-1 (-4.40 eV) have 72% and 70% oxygen 2p character, respectively. These two occupied MOs find their counterparts as HOMO-1 (-4.32 eV, 71% O 2p) and HOMO-2 (-4.40 eV, 71% O 2p) in **Q2.23**. As expected, the HOMO in **Q2.23** is localised on the apical carbon, with 77% C 2s and 2p character (-4.23 eV). Bonding parameters and atomic charges were calculated using QTAIM calculations and the selected data are shown in Table 2.8. Very similar Mg-O bond critical point parameters and charges (excluding apical C and BH moieties) were obtained in **Q2.21** and **Q2.23**, suggesting very similar bonding situations.

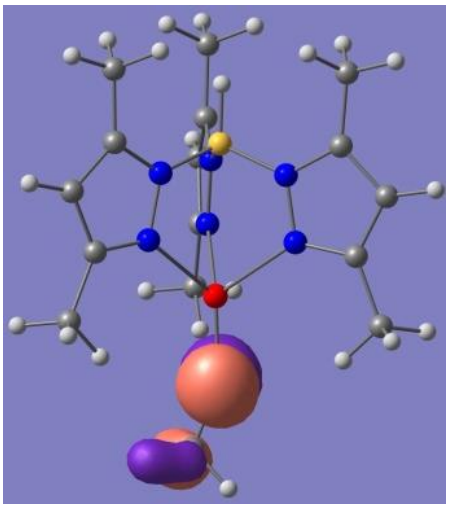
Despite the fact that DFT and QTAIM computational analysis suggested near-identical electronic structures of **Q2.21** and **Q2.23**, ground state geometries were analysed in order to investigate whether steric factors played an important role in the *rac*-LA ROP activities of **2.20** and **5**. The Mg-O and Mg···B/C distances of 1.834 Å and 3.097 Å in **Q2.21** were comparable to those found in **Q2.23** (1.830 Å and 3.063 Å, respectively). Furthermore, the distances between Mg and the plane formed by the three coordinating N atoms at the 2-position of the pyrazolyl ring for **Q2.21** and **Q2.23** were calculated to be 1.231 and 1.256 Å, respectively, suggesting negligible steric differences. It was thus concluded based on the aforementioned computational studies that very minor electronic and steric differences existed between **Q2.21** and **Q2.23** in their ground state structures. The significant differences in *rac*-LA ROP activities between **5** and **2.20** will be further discussed in Chapter Three.



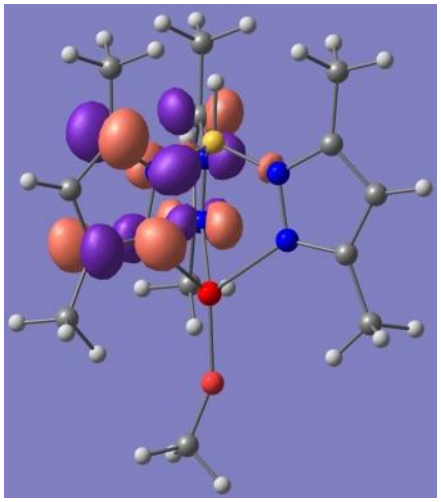
HOMO-2: -5.45 eV



HOMO-1: -4.40 eV

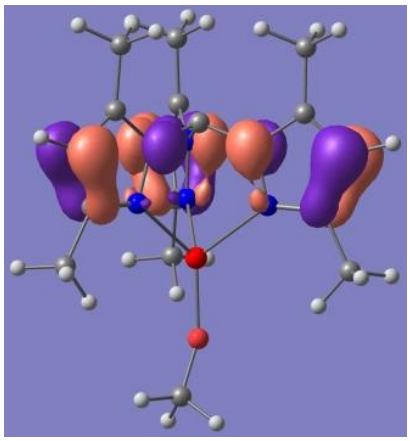


HOMO: -4.33 eV

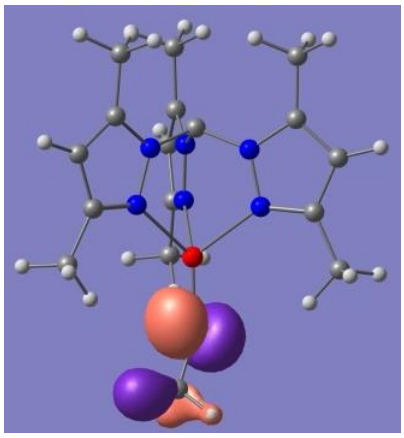


LUMO: -0.87 eV

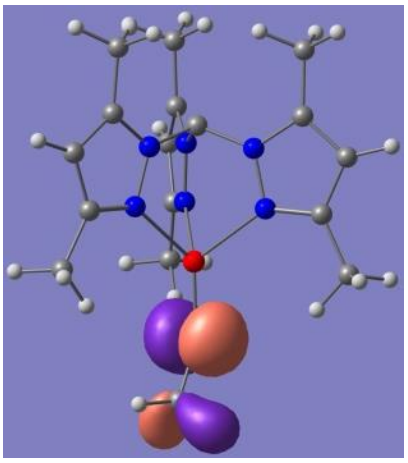
Figure 2.11 Isosurfaces and associated energies of selected molecular orbitals of ($Tp^{Me,Me}$)Mg(OMe) (**Q2.21**).



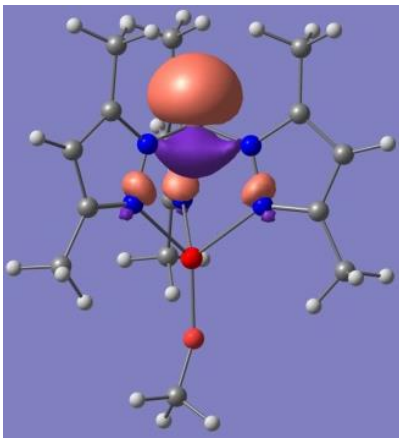
HOMO-3: -5.49 eV



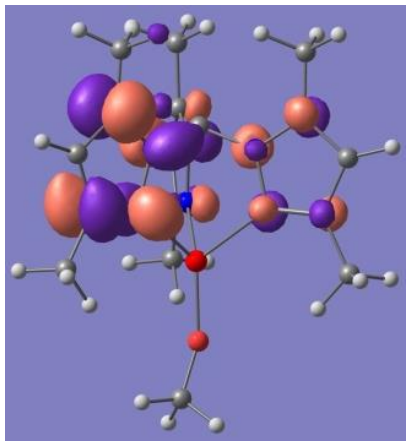
HOMO-2: -4.40 eV



HOMO-1: -4.32 eV



HOMO: -4.23 eV



LUMO: -0.97 eV

Figure 2.12 Isosurfaces and associated energies of selected molecular orbitals of ($Tpm^{(Me,Me)d}$)Mg(OMe) (**Q2.23**).

Table 2.7 Bond dissociation enthalpies for ($Tp^{Me,Me}$)Mg(OMe) (**Q2.21**) and ($Tpm^{(Me,Me)d}$)Mg(OMe) (**Q2.23**).

Complex	Fragments	BDE to non-relaxed fragments / kJ mol^{-1}	BDE to relaxed fragments / kJ mol^{-1}
Q2.21	($Tp^{Me,Me}$)Mg + OMe	417.3	412.4
Q2.23	(Tpm^{d})Mg + OMe	413.7	408.8

Table 2.8 Selected QTAIM data (atomic units) for ($Tp^{Me,Me}$)Mg(OMe) (**Q2.21**) and ($Tpm^{(Me,Me)d}$)Mg(OMe) (**Q2.23**).

Complex	Mg charges	OMe charges	Sum of $Tp^{tBu,Me}$ or Tpm^{d} charges	Sum of apical BH or C charges	ρ [a]	$\nabla^2\rho$ [a]	H [a]	δ (Mg-O) [a]
Q2.21	1.729	-0.873	-0.858	1.437	0.060	0.594	0.022	0.230
Q2.23	1.731	-0.873	-0.859	0.796	0.061	0.603	0.023	0.233

[a] Values for ρ (electron density), $\nabla^2\rho$ (electron density Laplacian), H (energy density) and δ (delocalisation index) were obtained at the Mg-O bond critical points.

2.5 Summary and conclusions

This Chapter described the synthesis and characterisation of a series of Tpm*^{d} ligand-supported magnesium complexes. Deprotonating the protio-ligand with MeLi afforded (Tpm*^{d})Li(THF) (**1**). (Tpm*^{d})Mg(BH_4) (**2**) and (Tpm*^{d})Mg(Me) (**3**) were prepared *via* salt elimination pathways by reacting **1** with $Mg(BH_4)_2$ and MeMgCl, respectively. The protonolysis reaction between the protio-ligand and $MgBu_2$ resulted in the formation of (Tpm*^{d})Mg(Bu) (**4**), which served as a precursor for the synthesis of (Tpm*^{d})Mg(OBn) (**5**). (Tpm*^{d})Mg(BD_4) (**2-*d*$_4$**) was accessed by reacting **5** with an excess amount of BD_3(THF). (Tpm*^{d})Mg(Cl) (**6**) and (Tpm*^{d})Mg(Br) (**7**) were prepared from the protonolysis reaction between the protio-ligand and the corresponding methyl Grignard reagents under heating conditions although **6** was obtained in low yields and **7** could not be isolated. Performing the reaction between the protio-ligand and MeMgBr at room temperature afforded [(Tpm*)Mg(Me)]Br (**8**). The X-ray crystal structures of **1**, **2**, **3**, **4** and **6** were obtained and discussed. DFT and QTAIM calculations were performed, suggesting very similar geometries and bonding situations between the two model compounds (Tp^{Me,Me})Mg(OMe) (**Q2.21**) and (Tpm$^{(Me,Me)d}$)Mg(OMe) (**Q2.23**). These two calculated structures show negligible electronic and steric differences in their ground state forms.

2.6 References for Chapter Two

1. S. Trofimenko, *J. Am. Chem. Soc.*, 1967, **89**, 3170.
2. S. Trofimenko, *Scorpoinates: the Coordination Chemistry of Polypyrazolylborate Ligands*, Imperial College Press, London, 1998.
3. S. Trofimenko, *Chem. Rev.*, 1993, **93**, 943.
4. S. Trofimenko, *Chem. Rev.*, 1972, **72**, 497.
5. N. Marques, A. Sella and J. Takats, *Chem. Rev.*, 2002, **102**, 2137.
6. H. R. Bigmore, S. C. Lawrence, P. Mountford and C. S. Tredget, *Dalton Trans.*, 2005, 635.
7. C. Pettinari and R. Pettinari, *Coord. Chem. Rev.*, 2005, **249**, 525.
8. C. Pettinari and R. Pettinari, *Coord. Chem. Rev.*, 2005, **249**, 663.
9. S. Trofimenko, *Polyhedron*, 2004, **23**, 197.
10. A. Otero, J. Fernandez-Baeza, A. Antinolo, J. Tejeda and A. Lara-Sanchez, *Dalton Trans.*, 2004, 1499.

11. D. L. Reger, *Comm. Inorg. Chem.*, 1999, **21**, 1.
12. W. HücKel and H. B. Chneider, *Chem. Ber.*, 1937, **70**, 2024.
13. D. L. Reger, T. C. Grattan, K. J. Brown, C. A. Little, J. J. S. Lamba, A. L. Rheingold and R. D. Sommer, *J. Organomet. Chem.*, 2000, **607**, 120.
14. I. Kuzu, I. Krummenacher, J. Meyer, F. Armbruster and F. Breher, *Dalton Trans.*, 2008, 5836.
15. P. K. Byers, N. Carr and F. G. A. Stone, *J. Chem. Soc., Dalton Trans.*, 1990, 3701.
16. P. K. Byers and F. G. A. Stone, *J. Chem. Soc., Dalton Trans.*, 1991, 93.
17. S. C. Lawrence, M. E. G. Skinner, J. C. Green and P. Mountford, *Chem. Commun.*, 2001, 705.
18. F. Breher, J. Grunenberg, S. C. Lawrence, P. Mountford and H. Rüegger, *Angew. Chem. Int. Ed.*, 2004, **43**, 2521.
19. I. Krummenacher, H. Ruegger and F. Breher, *Dalton Trans.*, 2006, 1073.
20. H. R. Bigmore, J. Meyer, I. Krummenacher, H. Rüegger, E. Clot, P. Mountford and F. Breher, *Chem. Eur. J.*, 2008, **14**, 5918.
21. M. G. Cushion, J. Meyer, A. Heath, A. D. Schwarz, I. Fernández, F. Breher and P. Mountford, *Organometallics*, 2010, **29**, 1174.
22. C. Müller, H. Görls, S. Krieck and M. Westerhausen, *Eur. J. Inorg. Chem.*, 2013, **2013**, 5679.
23. R. Lalrempuia, A. Stasch and C. Jones, *Chem. Asian J.*, 2015, **10**, 447.
24. I. Fernandez, P. Ona-Burgos, F. Armbruster, I. Krummenacher and F. Breher, *Chem. Commun.*, 2009, 2586.
25. M. P. Coles, S. E. Sözerli, J. D. Smith, P. B. Hitchcock and I. J. Day, *Organometallics*, 2009, **28**, 1579.
26. F. G. N. Cloke, P. B. Hitchcock, M. F. Lappert, G. A. Lawless and B. Royo, *J. Chem. Soc., Chem. Commun.*, 1991, 724.
27. W. Schlenk and W. Schlenk Jr, *Ber. Dtsch. Chem. Ges.*, 1929, **62**, 920.
28. S. Harder, *Chem. Rev.*, 2010, **110**, 3852.
29. M. G. Cushion and P. Mountford, *Chem. Commun.*, 2011, **47**, 2276.
30. J. Unruangsri, *D.Phil Thesis, University of Oxford*, 2014.
31. M. A. Nichols and P. G. Williard, *J. Am. Chem. Soc.*, 1993, **115**, 1568.
32. T. Kottke and D. Stalke, *Angew. Chem.*, 1993, **105**, 619.
33. T. Kottke and D. Stalke, *Angew. Chem. Int. Ed. Engl.*, 1993, **32**, 580.

34. S. S. Al-Juaid, C. Eaborn, P. B. Hitchcock, M. S. Hill and J. D. Smith, *Organometallics*, 2000, **19**, 3224.
35. B. A. Core, *DPhil Thesis, University of Oxford*, 2015.
36. R. A. Collins, J. Unruangsri and P. Mountford, *Dalton Trans.*, 2013, **42**, 759.
37. M. Schmid, S. M. Guillaume and P. W. Roesky, *Organometallics*, 2014, **33**, 5392.
38. M. Kuzdrowska, L. Annunziata, S. Marks, M. Schmid, C. G. Jaffredo, P. W. Roesky, S. M. Guillaume and L. Maron, *Dalton Trans.*, 2013, **42**, 9352.
39. X. Xu, Y. Chen, G. Zou, Z. Ma and G. Li, *J. Organomet. Chem.*, 2010, **695**, 1155.
40. D. A. Fletcher, R. F. McMeeking and D. Parkin, *J. Chem. Inf. Comput. Sci.*, 1996, **36**, 746.
41. T. J. Marks and J. R. Kolb, *Chem. Rev.*, 1977, **77**, 263.
42. M. Bremer, G. Linti, H. Nöth, M. Thomann-Albach and G. E. W. J. Wagner, *Z. Anorg. Allg. Chem.*, 2005, **631**, 683.
43. J. Prust, K. Most, I. Müller, E. Alexopoulos, A. Stasch, I. Usón and H. W. Roesky, *Z. Anorg. Allg. Chem.*, 2001, **627**, 2032.
44. J. Jenter, P. W. Roesky, N. Ajellal, S. M. Guillaume, N. Susperregui and L. Maron, *Chem. Eur. J.*, 2010, **16**, 4629.
45. J. Kratsch, M. Kuzdrowska, M. Schmid, N. Kazeminejad, C. Kaub, P. Oña-Burgos, S. M. Guillaume and P. W. Roesky, *Organometallics*, 2013, **32**, 1230.
46. H. D. Dyer, S. Huijser, N. Susperregui, F. Bonnet, A. D. Schwarz, R. Duchateau, L. Maron and P. Mountford, *Organometallics*, 2010, **29**, 3602.
47. W. Li, M. Xue, J. Tu, Y. Zhang and Q. Shen, *Dalton Trans.*, 2012, **41**, 7258.
48. N. Meyer, J. Jenter, P. W. Roesky, G. Eickerling and W. Scherer, *Chem. Commun.*, 2009, 4693.
49. M. A. Sinenkov, G. K. Fukin, A. V. Cherkasov, N. Ajellal, T. Roisnel, F. M. Kerton, J.-F. Carpentier and A. A. Trifonov, *New J. Chem.*, 2011, **35**, 204.
50. M. Visseaux and F. Bonnet, *Coord. Chem. Rev.*, 2011, **255**, 374.
51. M. Bremer, H. Nöth and M. Warchhold, *Eur. J. Inorg. Chem.*, 2003, **2003**, 111.
52. S. Schnitzler, T. P. Spaniol, L. Maron and J. Okuda, *Chem. Eur. J.*, 2015, **21**, 11330.

53. O. Michel, K. Yamamoto, H. Tsurugi, C. Maichle-Mössmer, K. W. Törnroos, K. Mashima and R. Anwander, *Organometallics*, 2011, **30**, 3818.
54. S. R. Neal, A. Ellern and A. D. Sadow, *J. Organomet. Chem.*, 2011, **696**, 228.
55. M. Westerhausen, T. Bollwein, N. Makropoulos, S. Schneiderbauer, M. Suter, H. Nöth, P. Mayer, H. Piotrowski, K. Polborn and A. Pfitzner, *Eur. J. Inorg. Chem.*, 2002, **2002**, 389.
56. I. J. Blackmore, V. C. Gibson, P. B. Hitchcock, C. W. Rees, D. J. Williams and A. J. P. White, *J. Am. Chem. Soc.*, 2005, **127**, 6012.
57. J. F. Dunne, D. B. Fulton, A. Ellern and A. D. Sadow, *J. Am. Chem. Soc.*, 2010, **132**, 17680.
58. R. H. Platel, L. M. Hodgson and C. K. Williams, *Polym. Rev.*, 2008, **48**, 11.
59. C. M. Thomas, *Chem. Soc. Rev.*, 2010, **39**, 165.
60. M. J. Stanford and A. P. Dove, *Chem. Soc. Rev.*, 2010, **39**, 486.
61. M. H. Chisholm, K. Choojun, J. C. Gallucci and P. M. Wambua, *Chem. Sci.*, 2012, **3**, 3445.
62. J. J. Li, *Name Reactions*, Springer, 4th edition edn., 2009.

Chapter Three

Tris(pyrazolyl)methanide magnesium complexes for the ROP of *rac*-, *L*-, *meso*-LA and ε-CL and their mechanistic studies

3.1 Overview

This Chapter will describe the in-depth study of the ROP of cyclic esters using (Tpm*^{d})Mg(OBn) (**5**) and (Tpm*^{d})Mg(BH_4) (**2**) introduced in Chapter Two. An introduction to alkaline earth ROP catalysts and the previously reported mechanism for ROP initiated by borohydride complexes will precede the presentation of results. Detailed investigations into the ROP of *rac*-, *L*-, *meso*-LA and ε-CL using **5** will be discussed. Furthermore, the *rac*-LA ROP activity of **2** will be presented, followed by a revised mechanistic study using various NMR spectroscopic techniques.

3.2 Introduction

3.2.1 Alkaline earth complexes as ROP catalysts

The field of homogeneous catalysis has been dominated by transition metal based catalysts over the last few decades, promoting many chemical transformations.[1-12] However, not only are some transition metal catalysts expensive, but also their toxicity is less desirable from the viewpoint of safety and sustainable green chemistry. Therefore, the replacement of toxic catalysts with less harmful materials has been of great interest in the chemical society. Moreover, the use of abundant metals instead of rare ones has also been promoted in recent years, driving cost reduction in chemical processes. Alkaline earth metals are considered to fulfil the above-mentioned criteria. They are among the most abundant elements in nature, being found both in the earth crust and in the sea.[13] Magnesium and calcium, in particular, demonstrate low toxicity and biocompatibility, making them ideal for catalyst development from a ROP point of view. In addition, alkaline earth metals, located between Group 1 and Group 3, demonstrate nucleophilicity and Lewis acidity, both of which are necessary for monomer binding and activation.[14, 15] Nevertheless, the chemistry of alkaline earth complexes was relatively underdeveloped and it was not until the last decade that there had been a significant surge in the interest of these complexes in areas such as organic transformations[16-20] and polymerisations.[21-25]

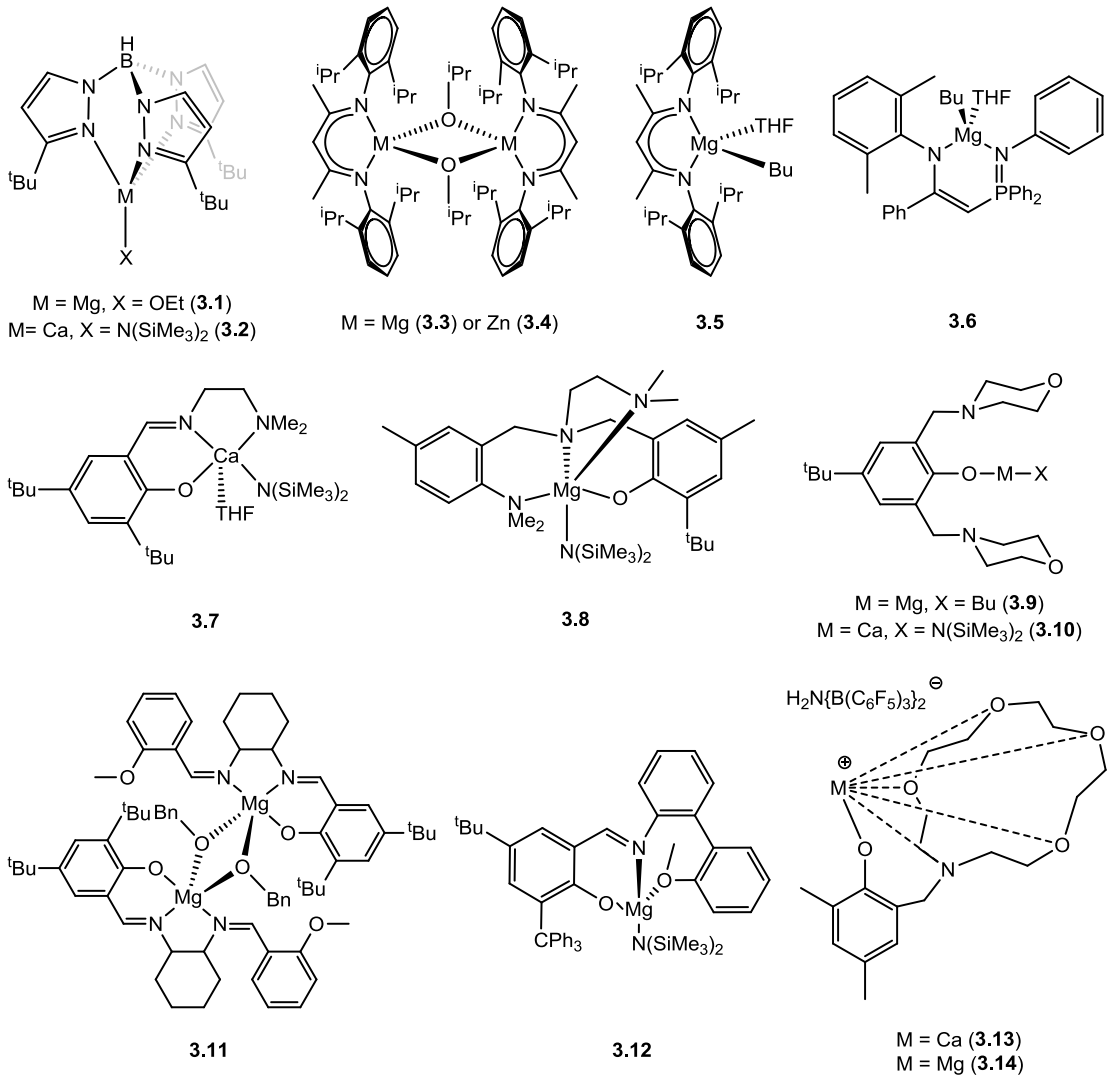


Figure 3.1 Literature examples of alkaline earth initiators for LA ROP. [26-37]

The development of ROP catalysts using alkaline earth metal complexes was pioneered by Chisholm *et al.*[26, 27] and Coates *et al.*[28], who independently synthesised a series of Mg and Ca amide and alkoxide complexes supported by tris(pyrazolyl)borate (Tp) and β-diketiminate (NacNac) ligands (Figure 3.1). (Tp^{tBu})Mg(OEt) (**3.1**), prepared by the protonolysis reaction between (Tp^{tBu})Mg(Me) and EtOH, was able to polymerise up to 1000 equiv. of *L*-LA (CH_2Cl_2, room temperature) while maintaining a narrow PDI of 1.2.[26] A linear relationship between the experimental M_n and % conversion was observed, together with a good agreement between the experimental and theoretical M_n, indicating the well-controlled nature of the ROP using **3.1**. Later on, a series of (Tp^{tBu})CaX complexes, where X = amide and aryloxide, were shown to be highly active towards *rac*-LA ROP.[27] For example, (Tp^{tBu})CaN($SiMe_3$)$_2$ (**3.2**) was able to polymerise 200 equiv. of *rac*-LA within 1 min (THF, room temperature) and

showed a high level of stereoselectivity, resulting in the formation of highly heterotactic PLA (P_r = 0.90).

In 2001, Coates *et al.* reported a series of Mg and Zn amide and alkoxide complexes supported by NacNac ligands, among which [(^{Dipp}NacNac)Mg(μ-O^{i}Pr)]$_2$ (**3.3**) was highly active, polymerising 200 equiv. of *rac*-LA within 2 min in CH_2Cl_2 to yield atactic PLA.[28] Nonetheless, a moderate PDI of 1.59 was observed, subsequently improved by the addition of ^{i}PrOH (PDI = 1.29). A superior agreement between the experimental and calculated M_n was also observed upon addition of ^{i}PrOH whereas no apparent change in polymerisation rates and polymer tacticity was found. In contrast, the Zn analogue (**3.4**) was less active, reaching 95% conversion within 20 min under identical polymerisation conditions. However, the polymerisation using **3.4** was much better controlled (PDI = 1.10) and the resulting PLA was highly heterotactically enriched (P_r = 0.90), as a result of a chain end control mechanism. Chisholm and co-workers later reported a monomeric species (^{Dipp}NacNac)Mg(Bu)(THF) (**3.5**), which was capable of reaching 92% conversion (100 equiv. of *rac*-LA) within 1.5 min in CH_2Cl_2 at room temperature.[29] A solvent effect was found when the polymerisation was performed in THF, in which case a lower polymerisation rate was observed (60% conversion in 1.5 min). Concomitantly, a dramatic improvement in heterotacticity was achieved (P_r = 0.96 in THF *cf.* 0.56 in CH_2Cl_2). The influence of THF has been observed in many other instances due to its coordinating nature, competing with monomer coordination and thus, resulting in a reduced rate and improved stereoselectivity.[38-40]

Recently, phosphinimino-amine ligands have been developed by modifying the NacNac framework by replacing the carbon at the 1-position with a phosphorus atom. Cui *et al.* subsequently synthesised a series of magnesium complexes and examined the ligand effects on the ROP of *rac*-LA.[30] The steric hindrance of the substituents was shown to have negligible impact on the catalytic activity but affected stereoselectivity considerably. Complex **3.6**, supported by the least sterically bulky ligand among the series, led to the formation of PLA with the highest heterotacticity (P_r = 0.92). Crystallographic investigations were subsequently undertaken to obtain further insight into this observation. It was concluded that the repulsions between large substituents created more space around the metal centre, allowing monomers to coordinate more freely and hence resulting in poorer stereoselectivity. The P_r of the

resulting polymer obtained using **3.6** was further improved to 0.98 when the polymerisation was performed at 0 °C, the highest value documented to date for a magnesium based catalyst.

Half-salen calcium complexes reported by Darensbourg and co-workers demonstrated excellent activities in producing high molecular weight polymers with narrow PDIs (1.02-1.05).[31] Complex **3.7**, synthesised by the one-pot reaction of the protio-ligand with $NaN(SiMe_3)_2$ and CaI_2, was able to polymerise up to 700 equiv. of *L*-LA within 30 min while maintaining a PDI of 1.04 in the melt. PLA produced from *rac*-LA ROP performed in THF was atactic with the exception when the polymerisation was conducted at -33 °C (P_r = 0.73). Unexpectedly, the rate of polymerisation was much higher in THF than in $CHCl_3$ as a consequence of increased nucleophilicity of the initiator due to the coordination of THF. The slower rate associated with the ROP performed in $CHCl_3$ also led to heterotactic PLA being produced (P_r = 0.66 in $CHCl_3$ *cf.* 0.52 in THF at room temperature). Ma *et al.* later reported a series of magnesium complexes supported by aminophenolate ligands.[32] For example, complex **3.8** was able to polymerise up to 10,000 equiv. of *rac*-LA in 15 min (toluene, room temperature) to afford slightly isotactic PLA (P_m = 0.58) with a moderate PDI of 1.28. The ROP activity was further improved upon addition of 1 equiv. of ^{i}PrOH, polymerising 10,000 equiv. of *rac*-LA in 5 min. However, a negligible impact on polymer tacticity (P_m = 0.57) and PDI (1.23) was observed.

In 2009, Carpentier and Sarazin synthesised a magnesium n-butyl complex (**3.9**) supported by 4-*tert*-butyl-2,6-bis(morpholinomethyl)phenoxy ligand.[33] Complex **3.9** was shown to be highly active, polymerising 200 equiv. of *L*-LA in 10 min (toluene, 60 °C). Moderate molecular weight distribution (PDI = 1.63) was observed, subsequently improved by the addition of ^{i}PrOH. Complex **3.9** was able to polymerise up to 5000 equiv. of *L*-LA in the presence of up to 100 equiv. of ^{i}PrOH, giving polymers with excellent agreement between the calculated and experimental M_n and narrow PDIs (1.1-1.2). This indicated that the immortal polymerisation proceeded in a well-controlled manner, with the rate of chain transfer being much faster than that of propagation. A calcium complex (**3.10**) supported by the same ligand was also shown to be very active despite producing polymers with less well-controlled molecular weight distribution (PDI = 1.2-1.4).

The first magnesium iminophenolate complex [(SalenOMe)Mg(μ-OBn)]$_2$ (**3.11**) used for *rac*-LA ROP was introduced by Lin *et al.*[34] Compound **3.11** showed moderate activity, producing PLA with well-controlled M_n and narrow PDIs. However, only slightly heterotactic PLA (P_r = 0.57) was produced even when the polymerisation was conducted in THF. Ma *et al.* recently reported a series of magnesium amide complexes supported by modified iminophenolate ligands.[35] In particular, complex **3.12** exhibited high activity, polymerising 200 equiv. of *rac*-LA within 1.5 min in THF. Gratifyingly, the resulting polymer showed a moderate degree of heterotacticity (P_r = 0.72), which was further improved by carrying out the polymerisation at -38 °C (P_r = 0.81). Generally, the difficulties associated with the use of amide initiators are well-known; low initiation efficiency resulting in the formation of polymers with higher than expected M_n was found in a number of systems.[41-43] This was also observed in this case where **3.12** was used alone as the initiator. Upon addition of 1 equiv. of ^{i}PrOH to form an alkoxide species *in-situ*, a much better agreement between the theoretical and experimental M_n values was observed, in conjunction with a narrower PDI.

Sarazin and Carpentier later reported the synthesis of a series of alkaline earth metal cationic species $[(L)M]^{+}[H_2N\{B(C_6F_5)_3\}_2]^{-}$, among which the calcium complex **3.13**, in the presence of benzyl alcohol, demonstrated good activity and molecular weight control in the ROP of *L*-LA.[36, 37] Up to 3000 equiv. of *L*-LA could be polymerised within 24 h (toluene, 60 °C), producing P*L*LA with a good agreement between the experimental and calculated M_n and narrow PDIs (1.06-1.12). It is notable that **3.13** polymerised *rac*-LA *via* an activated monomer mechanism. In contrast to the good activity of **3.13**, the magnesium analogue **3.14** only produced traces of polymer after heating the reaction mixture at 100 °C for 3 h, the origin of which was not discussed in the publication.

3.2.2 Borohydride initiators for the ROP of cyclic esters

3.2.2.1 Lanthanide borohydride initiators for the ROP of cyclic esters

Compared to metal alkoxides and amides which are by far the most widely used initiators for the ROP of cyclic esters, catalysts bearing a borohydride moiety are relatively scarce. In the last decade, lanthanide borohydrides have caught much research interest and have shown to be superior to their amide counterparts and

comparable to alkoxides in terms of initiating efficiency and molecular weight control.[40, 44-49]

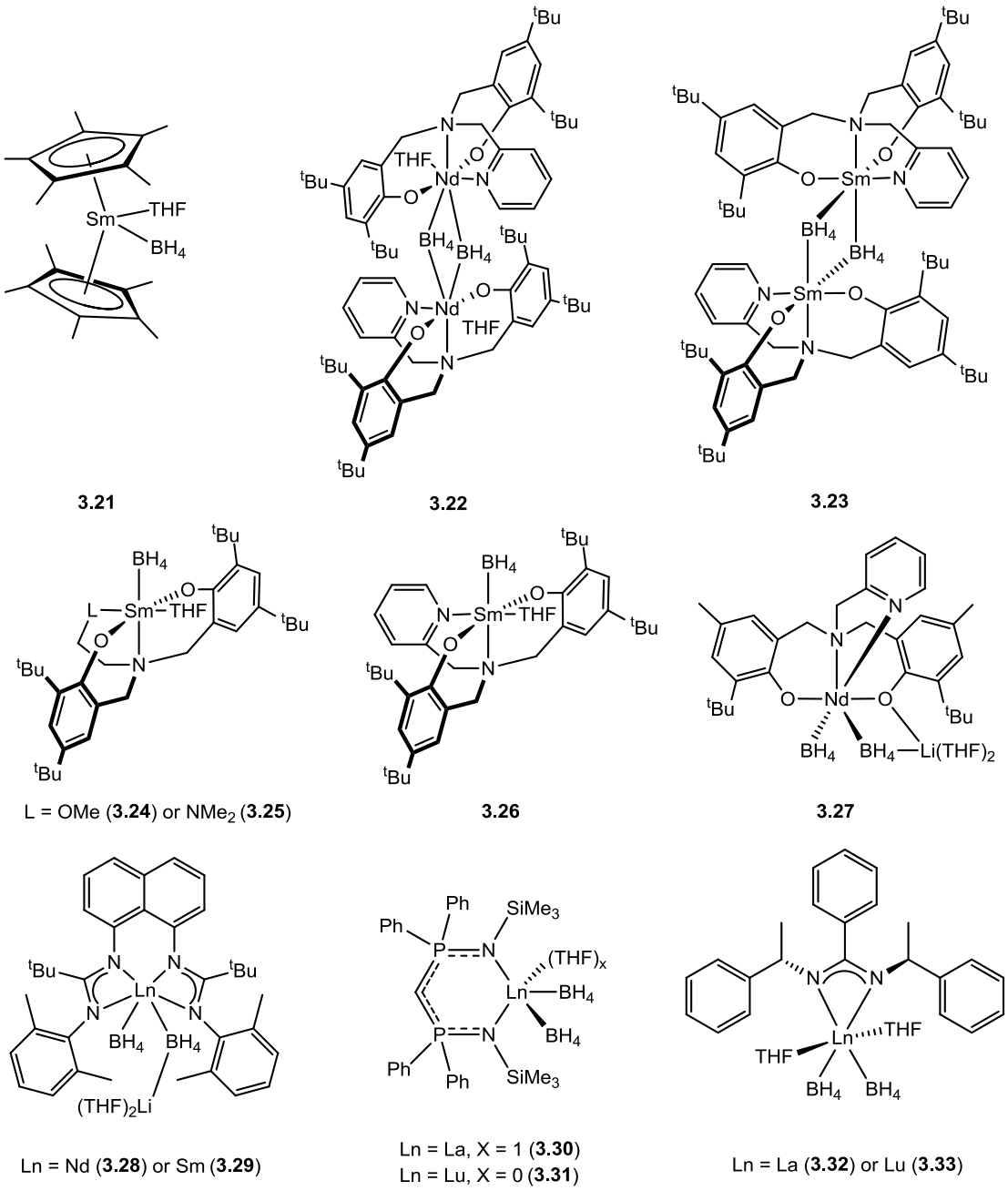


Figure 3.2 Literature examples of lanthanide borohydride initiators for the ROP of cyclic esters.[40, 44-49]

Initially pioneered by Guillaume *et al.* in 2003, $Ln(BH_4)_3(THF)_3$ complexes (Ln = La (**3.15**), Nd (**3.16**) and Sm(**3.17**)) were shown to be highly active for the ROP of ε-CL, resulting in the formation of α,ω-dihydroxytelechelic PCL (THF, room temperature).[50] In all cases, a good agreement between the calculated and

experimental M_n was observed at the beginning of the polymerisation followed by a slight deviation towards the end. This was accompanied by a narrow molecular weight distribution (PDI = 1.1-1.3) throughout the course of the polymerisation. The corresponding cationic species $[Ln(BH_4)_2(THF)_5][BPh_4]$ (Ln = La (**3.18**), Nd (**3.19**) or Sm (**3.20**)), developed by Okuda *et al.*, showed higher activity than their neutral parent compounds but similar molecular weight control (PDI = 1.2-1.4).[51] Interestingly, the ROP of ε-CL initiated by $Cp^*_2Sm(BH_4)(THF)$ (**3.21**) (Figure 3.2) produced PCL with lower than expected M_n values, the origin of which was inconclusive at the time of publication.[40] More importantly, preliminary studies regarding borohydride initiating mechanisms were carried out based on NMR spectroscopic observations using **3.21** (Section 3.2.3).[52]

Mountford and co-workers subsequently reported a series of complexes supported by a diaminobis(phenoxide) ligand, examples being $[(O_2NN')M(\mu\text{-}BH_4)(THF)_x]_2$ (M = Nd, x = 1 (**3.22**) or M = Sm, x = 0 (**3.23**)).[44] Both complexes were prepared *via* the salt elimination reactions between Na_2O_2NN' and the corresponding $Ln(BH_4)_3(THF)_3$ in THF. Both complexes were highly active towards the ROP of ε-CL in toluene, giving PCL with well-controlled M_n and moderate PDIs (1.6-1.8). In terms of *rac*-LA ROP, **3.23** was found to be more active than **3.22** in THF, producing heterotactically enriched PLA (P_r = 0.72). However, the observed M_n values were much lower than those expected for both catalysts, attributed to the presence of chain transfer events. Later in 2010, a detailed study on Sm borohydride compounds $(O_2N^L)Sm(BH_4)(THF)$ (L = OMe (**3.24**), NMe_2 (**3.25**) or py (**3.26**)) supported by a range of bis(phenolate)amine ligands with different pendant arms was reported.[45] It was found that the pendant arm had an effect on both the *rac*-LA ROP activity and the molecular weight control. Complex **3.25** demonstrated the highest activity while maintaining the best agreement between the calculated and experimental M_n and giving the narrowest PDI (1.41). Highly heterotactic PLA was produced using **3.24**-**3.26** (P_r = 0.78-0.84).

Later in 2011, a heterobimetallic Nd complex $[OONN]Nd(BH_4)(\mu\text{-}BH_4)Li(THF)_2$ (**3.27**) bearing borohydride initiators was reported by Trifonov *et al.*[46] Complex **3.27** was active in the ROP of both *rac*-BBL and *rac*-LA. The former resulted in the formation of polymers whose experimental M_n was in close agreement with the calculated value based on one chain per metal centre, suggesting the single-site character of **3.27** in *rac*-BBL ROP. However, a much lower than expected M_n was

observed in *rac*-LA ROP, indicating that both borohydride moieties might play a role in the initiation stage. This behaviour was also observed in catalytic systems employing analogous Nd (**3.28**) and Sm (**3.29**) compounds bearing an ansa-bis(amidinate) ligand.[47] The M_n of PLA obtained matched well with the calculated value based on two chains per metal centre at the early stage of the polymerisation. No significant stereocontrol was observed, as indicated by the formation of atactic polymers, in contrast to the previously introduced compounds **3.24**-**3.26** by Mountford *et al.*[45]

Reported by Roesky *et al.* in 2010, bis(phosphinimino)methanide-supported Ln borohydride complexes $\{CH(PPh_2NSiMe_3)_2\}Ln(BH_4)_2(THF)_x$ (Ln = La, x = 1 (**3.30**) or Ln = Lu, x = 0 (**3.31**)) were synthesised *via* the salt elimination reactions between $K\{CH(PPh_2NSiMe_3)_2\}$ and the corresponding $Ln(BH_4)_3(THF)_3$ in THF.[48] Complexes **3.30** and **3.31** were highly active for the ROP of ε-CL, affording α,ω-dihydroxytelechelic PCL with well-controlled M_n and narrow PDIs (1.1-1.3). The same group later reported lanthanide borohydride complexes {(S)-PEBA}$Ln(BH_4)_2(THF)_2$ (Ln = La (**3.32**) or Lu(**3.33**)) supported by the chiral N,N'-bis((S)-1-phenylethyl)benzamidine ligand.[49] Both complexes showed good activities in the ROP of *rac*-LA (THF, 60 ºC), producing PLA with moderate PDIs (1.1-1.3). The experimental M_n values were in close agreement with the calculated ones based on two chains per metal centre, indicating that both borohydride groups were active in the initiation process. It is worth noting that the chiral ligand hardly imposed any stereocontrol, producing atactic PLA with P_r = 0.5-0.6.

3.2.2.2 Alkaline earth borohydride initiators for the ROP of cyclic esters

The efficient and well-controlled nature of lanthanide borohydride complexes in the ROP of cyclic esters has resulted in an expansion of the borohydride catalysts library. Given the low toxicity and high abundance of Group 2 metals, recent years have witnessed an increase in the interest of employing alkaline earth borohydride complexes as catalysts for the ROP of cyclic esters.[53-56] Some of the examples are shown in Figure 3.3.

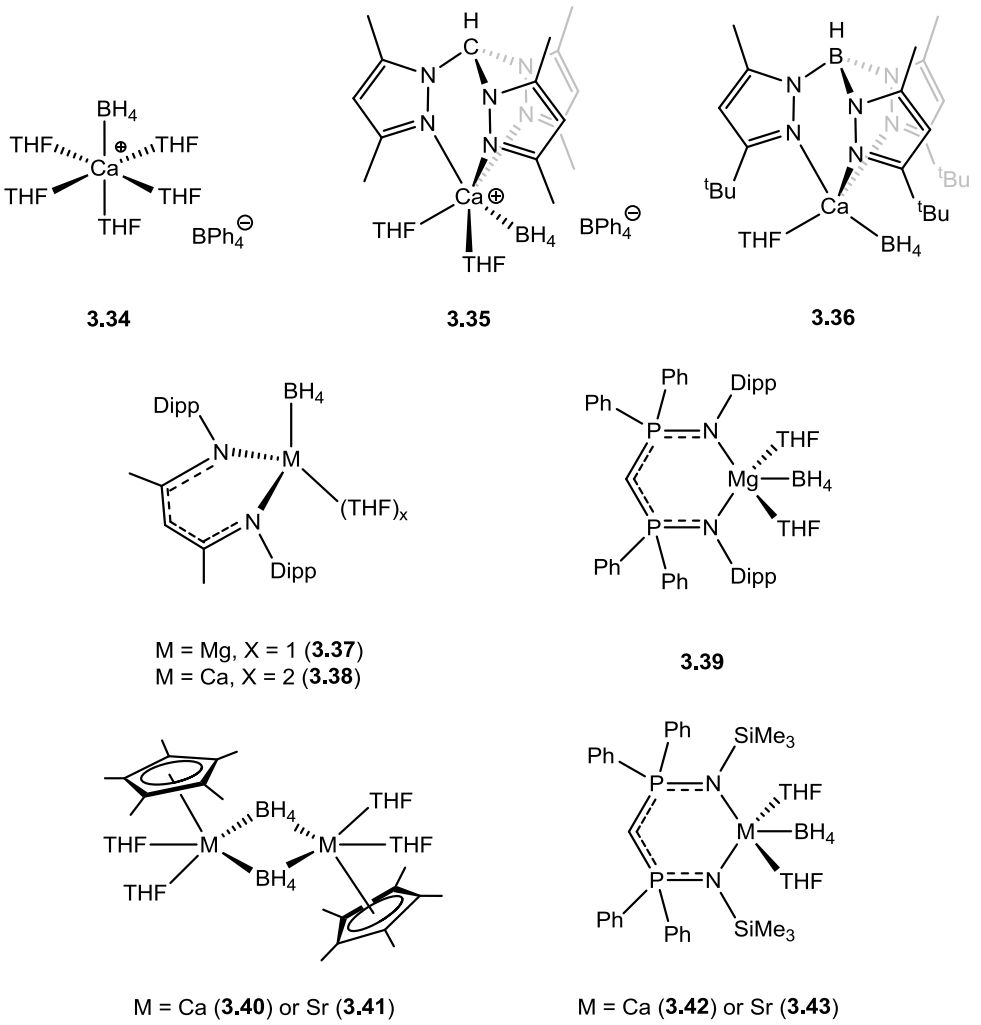


Figure 3.3 Examples of alkaline earth borohydride initiators for the ROP of cyclic esters.[53-56]

In 2011, Mountford *et al.* reported the first examples of cationic main group borohydride complexes and investigated their activities in the ROP of both ε-CL and *rac*-LA.[53] $[Ca(BH_4)(THF)_5]$**[**BPh_4] (**3.34**) (Figure 3.3) was synthesised *via* the reaction between $Ca(BH_4)_2(THF)_2$ and $[Et_3NH][BPh_4]$ in THF at -78 °C. Regarding the ROP of ε-CL using **3.34**, complete conversion was reached within 2 min (200 equiv. of ε-CL, THF, room temperature) whereas a longer polymerisation time (3 h) and heating at 70 °C was required for the ROP of *rac*-LA. This was improved by using $[(Tpm^{Me,Me})Ca(BH_4)(THF)_2][BPh_4]$ (**3.35**), obtained by reacting **3.34** with $Tpm^{Me,Me}$ protio-ligand. Complex **3.35** was able to polymerise up to 250 equiv. of *rac*-LA within 2 h (THF, room temperature), producing PLA with moderate PDIs (1.2-1.4). It was concluded that the $Tpm^{Me,Me}$ ligand provided a better-defined coordination environment, preventing the formation of dinuclear species or polymeryl

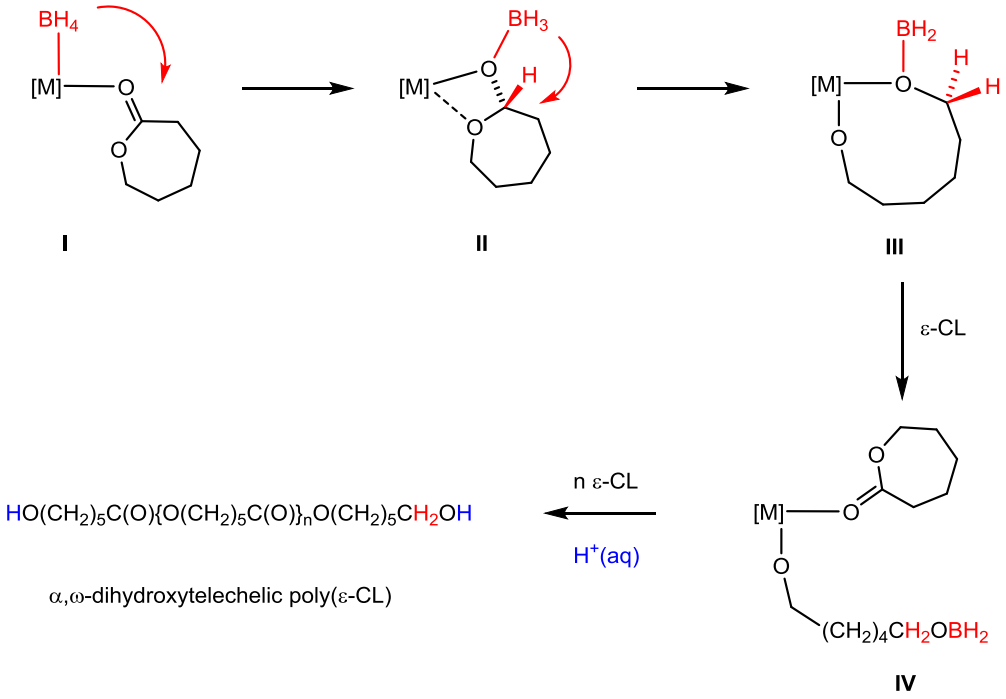
chain chelating resting state and as such led to a faster polymerisation. In addition, a linear relationship between the experimental M_n and % conversion was observed, with the gradient of the best fit line in excellent agreement with that calculated based on one chain per metal centre, clearly indicating the well-controlled nature of the ROP using **3.35**. Neither of the above-mentioned catalysts were found to induce hetereotactic enrichment of the resulting PLA. In contrast to this, ($Tp^{tBu,Me}$)Ca(BH_4)(THF) (**3.36**), synthesised by reacting K[$Tp^{tBu,Me}$] with $Ca(BH_4)_2(THF)_2$, exhibited high heteroselectivity (P_r = 0.88-0.90) due to the sterically more demanding nature of $Tp^{tBu,Me}$ in comparison to $Tpm^{Me,Me}$ ligand, consequently inducing stereoselectivity through a chain end control mechanism. Moreover, complex **3.36** initiated fast polymerisation (over 90% conversion achieved within 5 min), affording PLA with close to expected M_n and moderate PDIs (1.6-1.7).

Mountford *et al.* later reported the synthesis of NacNac ligand-supported borohydride complexes (^{Dipp}NacNac)M(BH_4)$(THF)_x$ (M = Mg, x = 1 (**3.37**) or M = Ca, x = 2 (**3.38**)) by reacting the corresponding metal bis(borohydride) with the potassiated ligand.[54] Complexes **3.37** and **3.38** exhibited good activities in the ROP of ε-CL, giving α,ω-dihydroxytelechelic PCL. In terms of *rac*-LA ROP, complex **3.37** displayed excellent activity, reaching 88% conversion (100 equiv. of *rac*-LA) within 5 min. Heterotactic PLA with a good agreement between the calculated and the observed M_n was produced, indicative of the well-controlled nature of the polymerisation. Nevertheless, transesterification side reactions were apparently present, as evidenced by the moderate PDIs in the range of 1.4-1.8 and the presence of repeating units of $\Delta m/z$ = 72 g mol^{-1} in the MALDI-ToF mass spectrum of the resulting polymer. PLA formed from the ROP using **3.38** showed lower heterotacticity and broader molecular weight distribution. For comparison purposes, {$CH(PPh_2NDipp)_2$}Mg(BH_4)$(THF)_2$ (**3.39**) supported by a bis(phosphinimino)methanide ligand was synthesised. Complex **3.39** was similar to **3.37** in terms of activity in ε-CL ROP but led to PCL with a poorer agreement between the calculated and observed M_n due to a mismatch between the rates of initiation and propagation. Complex **3.39** induced much slower *rac*-LA ROP in comparison to **3.37**, reaching 90% conversion in 7 h. Disappointingly, PLA produced was atactic and displayed a much lower than expected M_n, suggesting the presence of chain transfer events.

In the same year, Roesky, Guillaume and Maron reported the synthesis of $[Cp^*M(BH_4)(THF)_n]_2$ (M = Ca (**3.40**), Sr (**3.41**)) and $\{CH(PPh_2NSiMe_3)_2\}M(BH_4)(THF)_2$ (M = Ca (**3.42**), Sr (**3.43**)), all of which showed good molecular weight control in ε-CL ROP, producing PCL with a good agreement between the calculated and observed M_n and moderate PDIs (1.3-1.8).[55, 56] Complex **3.40** was able to polymerise 500 equiv. of ε-CL to complete conversion within 20 min (THF, room temperature) whereas under analogous conditions, only 75% conversion was reached after 180 min using **3.41**. In contrast, the strontium analogue **3.43** was found to be more active than **3.42**, polymerising ε-CL in a shorter time and giving PCL with narrower PDIs. The same trends were also observed in *rac*-LA ROP. In general, these complexes exhibited significantly lower activity and degree of control compared to their lanthanide counterparts **3.30** and **3.31**.[48]

3.2.3 Literature reported and newly revised borohydride initiating mechanisms

Mechanistic studies of borohydride initiators were pioneered by Guillaume, Maron, Roesky and Mountford following the successful employment of lanthanide borohydrides as catalysts for the ROP of cyclic esters.[50, 52, 57] Detailed experimental studies and DFT calculations led to the establishment of a proposed mechanism, shown in Scheme 3.1.



Scheme 3.1 Literature reported borohydride initiating mechanism for ε-CL.[50, 52, 57]

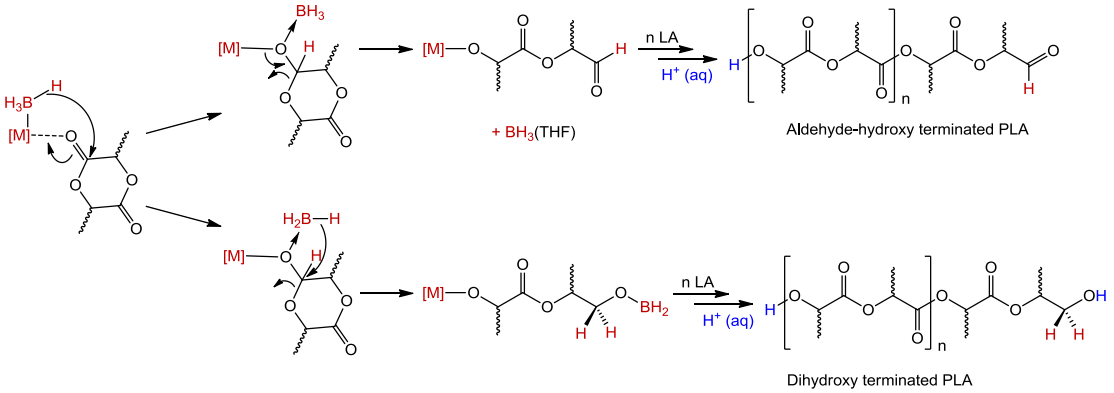
The proposed mechanism begins with the coordination of a ε-CL monomer to the Lewis acidic metal centre, activating the monomer towards a nucleophilic attack by the BH_4 initiator, forming Adduct **I**. A hydride is subsequently transferred from the BH_4 moiety to the carbonyl carbon of ε-CL, followed by the migration of BH_3 to the formally anionic oxygen, generating **II**. A second hydride transfer takes place, resulting in the formation of **III**, which features a fully reduced alkoxide chain end. Subsequent ring opening occurs and propagation is continued by the successive coordination of the monomer (**IV**). Hydrolysis of the [M]-O bond at one chain end and the $-OBH_2$ group at the other using a protic agent generates a α,ω-dihydroxytelechelic polymer.

Early mechanistic studies carried out by Guillaume *et al.* using 1 equiv. of $Nd(BH_4)_3(THF)_3$ (**3.16**) and 3 equiv. of ε-CL afforded a white solid which was identified as $Nd\{O(CH_2)_5CH_2OBH_2\}_3$ (reminiscent of **IV**) by elemental analysis.[50] Subsequent hydrolysis resulted in the formation of 1,6-hexanediol, which was confirmed by ^1H, $^{13}C\{^1H\}$ NMR spectroscopy, gas chromatography and mass spectrometry. Furthermore, polymer characterisation using NMR spectroscopic techniques was carried out after quenching a growing chain with benzyl alcohol. Only the hydroxy end group was observed, suggesting the dihydroxytelechelic nature of the isolated polymer. These experimental results provided clear evidence that $Nd\{O(CH_2)_5CH_2OBH_2\}_3$, produced *via* double hydride transfer, could act as the active initiator for ε-CL ROP. A similar study performed by using an equimolar amount of $Cp^*_2Sm(BH_4)(THF)$ (**3.21**) and ε-CL also supported the above proposed mechanism.[52] The initial formation of the intermediate $Cp^*_2Sm(BH_4)$(ε-CL) rapidly evolved towards $Cp^*_2Sm[O(CH_2)_6OBH_2]$ *via* double hydride transfer. Hydrolysis led to a mixture of ε-CL (from the coordinated ε-CL on $Cp^*_2Sm(BH_4)$(ε-CL)) and 1,6-hexanediol, confirming the identity of both the intermediate and $Cp^*_2Sm\{O(CH_2)_6OBH_2\}$. In addition, characterisation of the isolated polymer synthesised from the reaction between $Cp^*_2Sm\{O(CH_2)_6OBH_2\}$ and further ε-CL monomers suggested that both chain ends were terminated with hydroxy groups, providing strong evidence for the active initiation ability of $Cp^*_2Sm\{O(CH_2)_6OBH_2\}$.

The above-discussed initiating mechanism was first supported by DFT calculations carried out by Maron, Guillaume and Mountford using $Cp_2Eu(H)$, $Cp_2Eu(BH_4)$ and $(N_2NN')Eu(BH_4)$ (N_2NN'=(2-C_5H_4N)$CH_2(CH_2CH_2NMe)_2$) as model compounds.[58]

For all systems, the mechanistic pathways were calculated to be thermodynamically and kinetically favourable with respect to the separate initiator and ε-CL. DFT investigations were fully consistent with the two-step process, namely hydride transfer followed by ring opening, leading to $Cp_2Eu\{O(CH_2)_5C(O)H\}$ for $Cp_2Eu(H)$ and $(L)Eu\{O(CH_2)_6OBH_2\}$ for $Cp_2Eu(BH_4)$ and $(N_2NN')Eu(BH_4)$. Theoretical studies on other systems, such as **3.40** and **3.42** were also present in the literature.[56]

Despite the fact that both experimental work and DFT calculations have provided strong evidence for the formation of α,ω-dihydroxytelechelic PCL, chain ends for other polymers formed *via* ROP processes are not restricted to hydroxy groups only. The synthesis of a α-hydroxy,ω-formatetelechelic PTMC by employing $Sm(BH_4)_3(THF)_3$ (**3.17**) as the catalyst was documented by Guillaume *et al.* whereas Carpentier and Trifonov have reported the preparation of a PLA chain which was terminated with a hydroxy group at one end and an ambiguous group at the other.[59, 60] Mountford *et al.* have also found the presence of two types of end groups in one PLA polymer chain, namely alcohol and apparently aldehyde, in conjunction with the dominant α,ω-dihydroxytelechelic PLA.[45] The formation of the unexpected aldehyde end group was subsequently investigated by DFT calculations using $(O_2'N^{NMe2})Eu(BH_4)$ as the model compound. It was confirmed that the reaction pathway leading to $-CH(Me)CH_2OBH_2$ growing chain end was indeed kinetically accessible and thermodynamically favourable. The first step involving a hydride transfer to the carbonyl carbon of the LA monomer is of close resemblance to that found in the calculations for ε-CL ROP. The difference lies in the next step; whilst a concerted second hydride transfer followed by ring opening is possible (postulated in ε-CL ROP), it is kinetically more favourable to form a ring-opened species ($[M]OCH(Me)C(O)OCH(Me)CHO\cdot BH_3$) with an aldehyde end group initially, before the chelating BH_3 further undergoes hydride transfer to reduce the aldehyde. This revised LA ROP mechanism was consistent with the experimental work which confirmed the formation of both α,ω-dihydroxytelechelic and aldehyde-hydroxy terminated PLA through MALDI-ToF mass spectrometry. Scheme 3.2 depicts the different pathways leading to the formation of different polymer end groups.

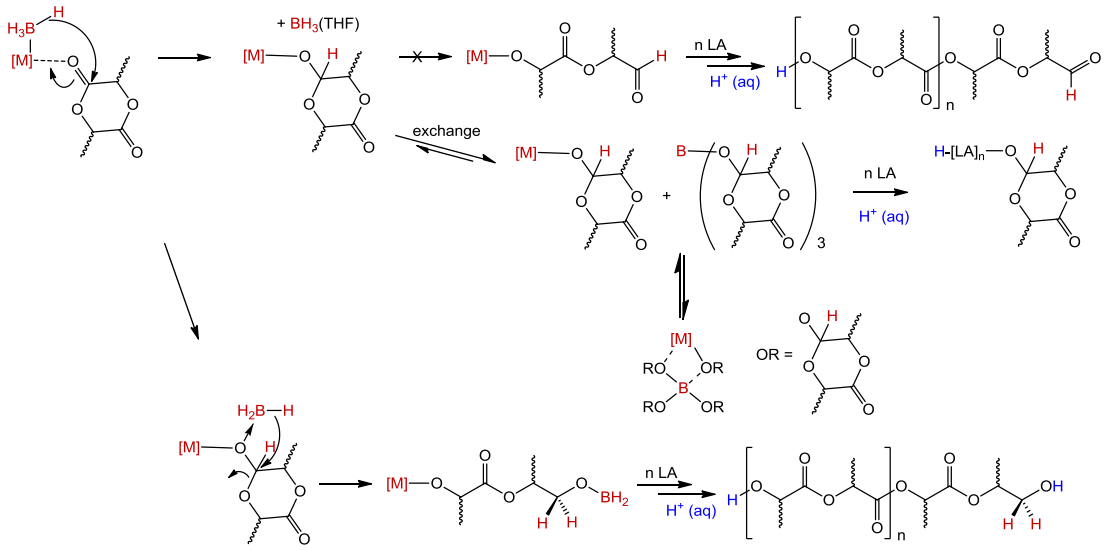


Scheme 3.2 Literature reported borohydride initiating mechanism for the ROP of LA.[45]

Over the following years, the Mountford group has pursued a continuous interest in borohydride initiated LA ROP and synthesised a considerable number of PLA samples using a range of borohydride initiators supported by different ligands. Whilst the presence of an aldehyde end group was consistent with the MALDI-ToF mass spectrometric data, the aldehyde proton and carbon signals were never observed in the respective ^{1}H and ^{13}C{^{1}H} NMR spectra. Additionally, a significant amount of literature has suggested that borane species is capable of reducing carbonyl groups. For example, Pelter and Levitt reported the reduction of 2 equiv. of acetone by 1 equiv. of BH_3(THF) to give diisopropoxyborane.[61] Moreover, the reduction of a range of aliphatic and aromatic ketones by BH_3(THF) was documented by Brown *et al.*[62] Weiss and co-workers also reported the reductive nature of diborane in aldehyde-containing compounds.[63] Asymmetric reduction of ketones with excellent enantioselectivity has also been studied extensively using borane species, typically BH_3(THF) or $BH_3(Me_2S)$, in the presence of a ligand.[64-69] The literature information mentioned above, in conjunction with the experimental data obtained in the Mountford group, has led to doubts regarding the initial assignments for an aldehyde end group of the resulting PLA. Further investigations regarding the mechanism for the ROP of LA employing borohydride initiators were subsequently conducted.

Initial studies were performed by Dr J. Unruangsri using ($Tp^{tBu,Me}$)Mg(BH_4) (**2.17**) as the initiator.[70] Unexpectedly, complex **2.17** was inactive towards the ROP of *rac*-LA at room temperature in THF. Heating at 70 °C was required for the polymerisation to proceed (induction period of 2 h, 86% conversion in 4.5 h). Peculiarly, the experimental M_n was approximately half of the calculated value for one chain being produced per metal centre. MALDI-ToF analysis of the polymer produced showed a

mixture of dihydroxy and apparently hydroxy-aldehyde end groups, the latter was eventually disproved based on various NMR spectroscopic studies. Instead, it was established that the resulting PLA was terminated with a non-opened LA ring (LA-H) chain end, giving identical isotopic distribution pattern as an aldehyde end group. Hence, these two termini could not be distinguished unambiguously using MALDI-ToF mass spectrometry. A revised mechanism was proposed, illustrated in Scheme 3.3.



Scheme 3.3 Revised mechanism for LA ROP using ($Tp^{tBu,Me}$)Mg(BH_4) (**2.17**) in THF.[70]

Identical to the previously reported mechanism, the first hydride transfer from the BH_4 moiety to the carbonyl carbon of LA leads to the formation of a sterically bulky alkoxide species ($Tp^{tBu,Me}$)Mg(LA-H) (**3.44**) featuring a non-opened LA ring, in conjunction with BH_3(THF).[70] As mentioned previously, subsequent ring-opening to form an aldehyde species is not very likely given the reductive nature of BH_3(THF) widely documented in the literature. Instead, **3.44** and BH_3(THF) undergo exchange reactions to form a borate ester, "B(LA-H)$_3$", which could be used as a potential chain transfer agent. The identity of "B(LA-H)$_3$" will be discussed later. Compound **3.44** could act as an initiator under heating conditions, resulting in the formation of a non-opened LA ring-terminated polymer. The other reaction pathway, proceeding through [M]OCH(Me)C(O)OCH(Me)CH_2OBH_2, was only supported by the formation of dihydroxy-terminated polymers as determined by MALDI-ToF mass spectrometry. Unfortunately, no previous NMR spectroscopic evidence was obtained.

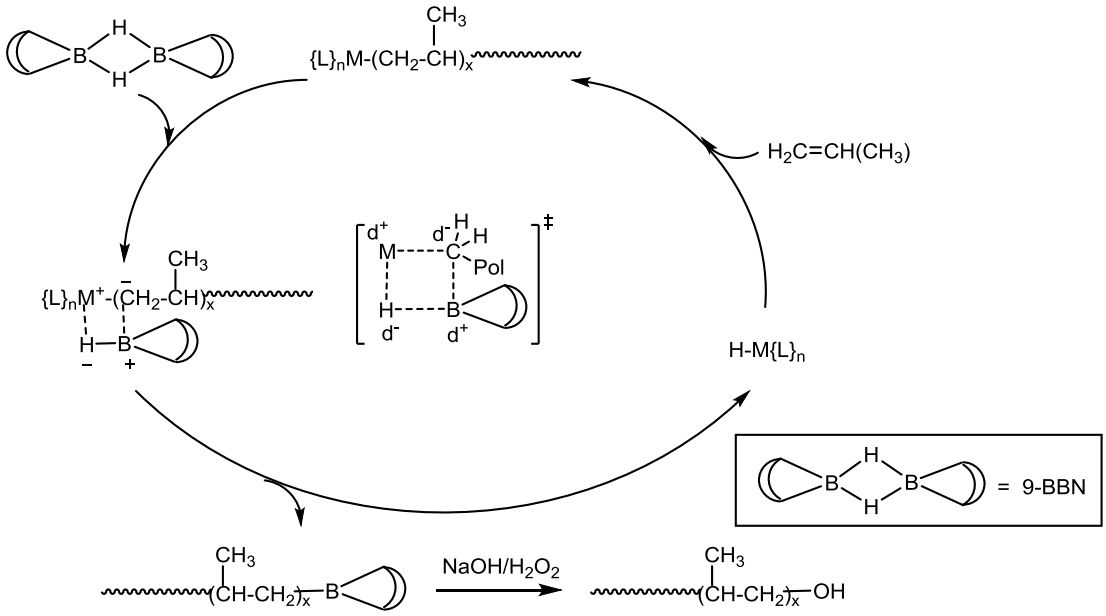
3.2.4 Borate esters species as chain transfer agents

Boron-containing compounds have been widely utilised in numerous areas in organic synthesis,[71-75] such as cross-coupling reactions,[76-78] hydroboration[79] and Diels-Alder reactions.[75, 80] For further information, the reader is directed to several recent review articles in the literature.[81-87] The use of boron-containing species in polymerisations was pioneered by Ewen and Marks *et al.*, who independently reported the use of $B(C_6F_5)_3$ containing metal compounds as catalysts for olefin polymerisation. The alkyl abstraction reactions between the Lewis acidic $B(C_6F_5)_3$ and zirconocene dimethyl precursors afforded a variety of cationic zirconocene monomethyl compounds which demonstrated high activity in ethylene polymerisation.[88]

Recent discoveries by Chung *et al.* suggested the use of organoboranes containing H-B or Me-B moieties as chain transfer agents in metallocene-mediated olefin polymerisation (Scheme 3.4).[89] Rapid ligand exchange between R-M (M = transition metal, R = polymeryl chain) and H-B or Me-B facilitated by favourable acid-base interaction resulted in the formation of a borane-terminated polymer and regeneration of a vacant active site. The appropriate combination of the organoborane and the metallocene catalytic system under optimised polymerisation conditions could lead to the expansion of this method to a wide range of olefin homo- and co-polymerisations, producing polyethylene, polypropylene, syndiotactic polystyrene, poly(ethylene-co-styrene), poly(ethylene-co-1-octene) and poly(ethylene-co-propylene). The molecular weight of the resulting polyolefin was directly proportional to the molar ratio of [olefin]/[borane]. Moreover, functionalisation of the polymer chain end could be achieved due to the reactive nature of the borane end group. For example, a hydroxy-terminated polyolefin was obtained by quenching with $NaOH/H_2O_2$.

It was not until recently that boron-containing species have been used as chain transfer agents in the ROP of cyclic esters. Sun *et al.* introduced the one-pot approach in which lanthanide borohydrides were treated with a range of carbonyl compounds followed by feeding of ε-CL to produce polymers with various chain ends.[90] Initial mechanistic studies have suggested the formation of $Ln(OR)_3$ and $B(OR)_3$ (OR = corresponding alkoxide). The former was unambiguously identified as the real active species whereas the role of the latter as chain transfer agents was not recognised at the time of publication. In light of this approach, Dr J. Unruangsri developed a new

method whereby the addition of benzaldehyde to a metal borohydride species led to the *in-situ* formation of a metal alkoxide and $B(OBn)_3$, which could be employed as an initiator and a chain transfer agent, respectively (Chapter Four).[70]



Scheme 3.4 Synthesis of a chain functionalised polyolefin using a borane derivative (9-BBN) chain transfer agent.[89]

3.3 ROP of ε-CL using (Tpm*^{d})Mg(OBn) (5) as a catalyst

Research has shown that metal alkoxide species have demonstrated superiority compared to other initiators in terms of exerting better polymerisation control.[91-93] A primary objective of this work is to evaluate the ROP activities of (Tpm*^{d})Mg(OBn) (**5**) and to study the properties of the resulting polymer. The ROP of ε-CL was performed in THF at room temperature. Aliquots were taken at regular intervals and quenched with wet THF to monitor the % conversion of the monomer. Polymer samples were subsequently analysised by NMR spectroscopy, MALDI-ToF mass spectrometry and GPC techniques.

Compound **5** was highly active, polymerising 200 equiv. of ε-CL in 2 min (Table 3.1, Entry 1). Surprisingly, the polymerisation was found to exhibit a zeroth order dependence on ε-CL concentration, as evidenced by the linear growth (R^2 = 0.997) of conversion (%) *vs.* time (Figure 3.4). Zeroth order dependence on monomer concentration is rare but not unprecedented in the literature; a similar observation was reported in the ROP of *rac*-LA in toluene using an yttrium alkoxide initiator,

subsequently rationalised by the non-involvement of the monomer in the rate-determining step.[94] It is postulated that this is also the case in the ε-CL ROP using **5**. A linear relationship between the % conversion and the experimental M_n was observed, in conjunction with narrow PDIs (1.12-1.19). In addition, the experimental M_n was close to the calculated value based on one chain being produced per metal centre, indicating the well-controlled nature of the polymerisation using **5** (Figure 3.5). Polymer end group analysis was carried out using MALDI-ToF mass spectrometry which revealed the presence of OBn end groups (Figure 3.6). Consistently, the ^{1}H NMR spectrum ($CDCl_3$, 298 K) of the isolated polymer showed a singlet at 5.11 ppm and a multiplet at 3.65 ppm, corresponding to the methylene protons at the OBn and the hydroxy chain ends, respectively. These assignments are in good agreement with those reported in the literature.[95, 96] Following the successful use of **5** with 200:1 [ε-CL]:[**5**], monomer loadings were subsequently increased to 500 and 1000:1 (Table 3.1, Entries 2, 3 and 4), under which conditions PCL was produced within 4 min and 10 min, respectively, while maintaining narrow PDIs (1.13-1.25). A very good agreement between the calculated and experimental M_n was observed in the former case whereas transesterification side reactions were present at high % conversions in the latter, leading to tailing-off in M_n. Zeroth order dependence on ε-CL concentration was also observed in both cases. The results of ε-CL ROP with different monomer loadings were summarised in Table 3.1.

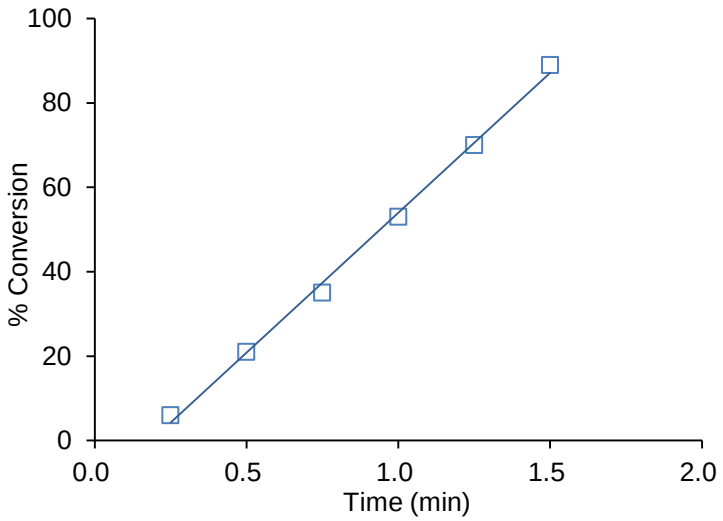


Figure 3.4 Data for the ROP of ε-CL using (Tpm*^{d})Mg(OBn) (**5**). % Conversion *vs.* time plot. Conditions: $[\varepsilon\text{-CL}]_0$:$[\mathbf{5}]_0$ = 200:1, $[\varepsilon\text{-CL}]_0$ = 1.0 M, $[\mathbf{5}]_0$ = 0.005 M, 3.4 mL THF at room temperature. R^2 = 0.997.

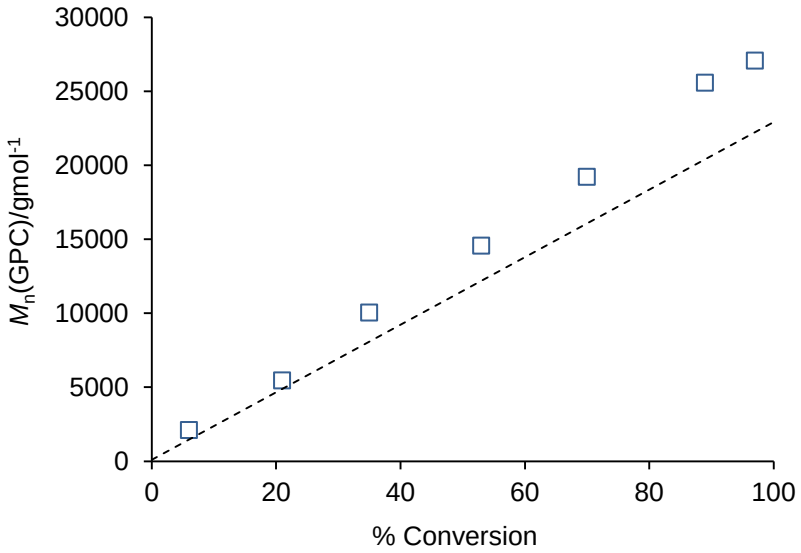


Figure 3.5 Data for the ROP of ε-CL using (Tpm*^{d})Mg(OBn) (**5**). M_n (GPC) *vs.* % conversion plot. The dashed line represents the M_n expected for one chain per metal centre. Conditions: $[\varepsilon\text{-CL}]_0$:$[\mathbf{5}]_0$ = 200:1, $[\varepsilon\text{-CL}]_0$ = 1.0 M, $[\mathbf{5}]_0$ = 0.005 M, 3.4 mL THF at room temperature.

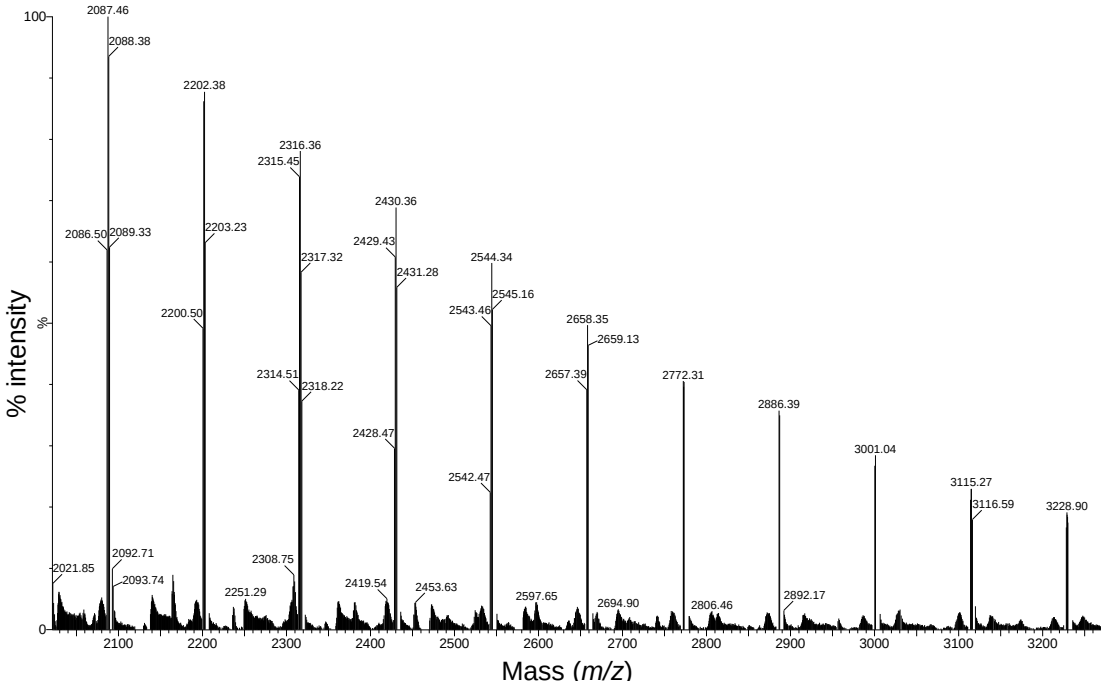


Figure 3.6 MALDI-ToF MS of PCL synthesised using (Tpm*^{d})Mg(OBn) (**5**). M_n by GPC = 2100 g mol^{-1}. Conditions: $[\varepsilon\text{-CL}]_0$:$[\mathbf{5}]_0$ = 200:1, $[\varepsilon\text{-CL}]_0$ = 1.0 M, $[\mathbf{5}]_0$ = 0.005 M, 3.4 mL THF at room temperature. K^+ dopant, Δ(*m/z*) = 114 g mol^{-1}.

Table 3.1 Selected data for the ROP of ε-CL using (Tpm*^{d})Mg(OBn) (**5**) in THF.

Entry	$[\varepsilon\text{-CL}]_0$:$[\mathbf{5}]_0$[a]	Conv.[b] (%)	Time (min)	M_n obs[c] (g mol^{-1})	M_n calc[d] (g mol^{-1})	PDI[e]	Yield (%)[f]
1	200:1	97	2	27,070	22,251	1.15	86
2	500:1	94	4	55,320	53,754	1.20	90
3	1000:1	58	6	68,230	66,309	1.13	/
4	1000:1	90	11	86,670	102,834	1.25	75

[a] Conditions: $[\varepsilon\text{-CL}]_0$ = 1.0 M, 3.4 mL THF at room temperature. [b] Measured by ^{1}H NMR ($CDCl_3$) analyses. [c] Molecular weights (g mol^{-1}) determined from GPC using Mark-Houwink corrections. [d] Expected M_n (g mol^{-1}) for one chain per metal centre; M_n (calc for Entry 1) = conversion (%) × 200 × 114.1 + 108.1; M_n (calc for Entry 2) = conversion (%) × 500 × 114.1 + 108.1; M_n (calc for Entries 3 & 4) = conversion (%) × 1000 × 114.1 + 108.1. [e] PDI = M_w/M_n. [f] Isolated yield.

3.4 ROP of LA using (Tpm*^{d})Mg(OBn) (5) as a catalyst

3.4.1 Catalytic activity of (Tpm*^{d})Mg(OBn) (5) in the ROP of LA

Following the successful use of **5** as the initiator for the ROP of ε-CL, its catalytic activities were subsequently probed in the ROP of *rac*-, *L*- and *meso*-LA. All polymerisations were performed in THF at room temperature with a $[LA]_0$:$[\mathbf{5}]_0$ ratio of 100:1 ($[LA]_0$ = 0.5 M).

The high activity of **5** was also manifested in the ROP of *rac*-LA, reaching 94% conversion within 1 min. The polymerisation was found to be first order with respect to *rac*-LA concentration, with an observed rate constant (k_{obs}) of 0.0536(27) s^{-1} (R^2 = 0.990), shown in Figure 3.7. This was in contrast to the ROP results obtained using (Tp^{tBu,Me})Mg(OBn) (**2.20**), where k_{obs} = 0.124(3) h^{-1}.[70] As discussed in Section 2.4, there are no significant electronic and steric differences in the ground state structures of Tpm$^{(Me,Me)d}$ and Tp^{Me,Me} ligand-supported alkoxide species according to DFT calculations. A subsequent control experiment was carried out in order to evaluate the ability of the apical carbanion to initiate ROP. (Tpm*^{d})Mg(Cl) (**6**) was found to be inactive in the ROP of *rac*-LA under identical polymerisation conditions. This is consistent with the previous work reported by Dr M. Cushion in the Mountford group,[97] whereby the zwitterionic sandwich compounds Mg{C(Me$_2$pz)$_3$}$_2$ (**2.7**), Ca{C(Me$_2$pz)$_3$}$_2$ (**2.12**) and Zn{C(Me$_2$pz)$_3$}$_2$ (**2.9**) featuring two methyl groups at

both the 3- and 5-positions of the pyrazolyl ring were shown to be inactive towards the ROP of *rac*-LA. In contrast, Mg{C(Me_2pz)$_3$}{C(pz)$_3$} (**3.45**), Ca{C(Me_2pz)$_3$}{C(pz)$_3$} (**3.46**), Mg{C(Me_2pz)$_3$}{C(4-Etpz)$_3$} (**3.47**) and Ca{C(Me_2pz)$_3$}{C(4-Etpz)$_3$} (**3.48**) demonstrated moderate activities under identical polymerisation conditions, due to the fact that C(pz)$_3$ (no substituents on the pyrazolyl ring) and C(4-Etpz)$_3$ (ethyl group at the 4-position) offered less steric protection to the carbanion compared to C(Me_2pz)$_3$, allowing the ROP of *rac*-LA to proceed *via* an anionic pathway. Breher *et al*. also reported the reactivity of the carbanion of the sandwich compounds with $AlEt_3$.[98] For example, the reaction between **3.45** and $AlEt_3$ resulted in the formation of a bond between the carbanionic carbon of C(pz)$_3$ and $AlEt_3$ whilst the other carbanion on {C(Me_2pz)$_3$} remained unreacted. Additionally, no reaction was observed between **2.7** and $AlEt_3$. Based on these results, it was postulated that the significant difference in the observed rate constants of **5** and **2.20** might be due to the difference in the size or flexibility of the coordination sphere during the polymerisation process (larger and more flexible coordination sphere for **5**).

Broad PDIs in the range of 1.76-2.63 were observed for the *rac*-LA ROP initiated by **5**, indicating the formation of PLA chains with a wide M_n dispersity. One would expect that this is a result of transesterification side reactions. However, close examination of the MALDI-ToF mass spectrum (Figure 3.8) of the resulting polymer revealed the presence of OBn end groups only. Neither cyclic PLA nor repeating units with $\Delta m/z$ = 72 g mol^{-1} were observed, indicating the absence of intra- or intermolecular transesterification. Instead, the broad PDI was attributed to a much faster rate of propagation than that of initiation, leading to the formation of polymers of various chain lengths. This was consistent with the M_n data obtained (Figure 3.9); even though a linear relationship between % conversion and M_n was observed with a gradient of 157(9) g mol^{-1} (% conversion)$^{-1}$, the experimental M_n was slightly higher than the expected value based on one polymer chain being produced per metal centre.

The ^{1}H NMR spectrum ($CDCl_3$, 298 K) of the isolated polymer revealed a broad signal at 2.71 ppm and a quartet at 4.35 ppm, corresponding to the hydroxy and BnO[LA]$_n$C(O)CH(Me)OC(O)C<u>H</u>(Me)OH protons, respectively. Unfortunately, the methylene protons at the OBn end group could not be clearly distinguished due to overlapping signals with the methine protons of PLA. The above-mentioned ^{1}H NMR data are fully consistent with those reported in the literature.[96, 99] The microstructure

of the polymer was analysed by $\{^1H\}^1H$ NMR spectroscopy in $CDCl_3$, revealing a moderate degree of heterotacticity (P_r = 0.69-0.75). This indicated the preference of the catalyst to insert *via* a *racemic* dyad as a result of a chain end control mechanism.

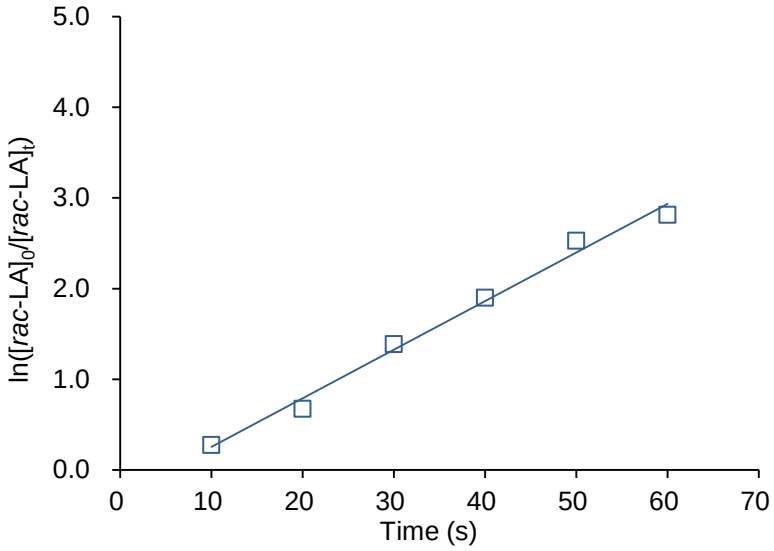


Figure 3.7 Data for the ROP of *rac*-LA using (Tpm*^{d})Mg(OBn) (**5**). Semilogarithmic first-order plot of ln([*rac*-LA]$_0$/[*rac*-LA]$_t$) *vs*. time (k_{obs} = 0.0536(27) s^{-1}, R^2 = 0.990). Conditions: [*rac*-LA]$_0$:[**5**]$_0$ = 100:1, [*rac*-LA]$_0$ = 0.5 M, [**5**]$_0$ = 0.005 M, 6 mL THF at room temperature.

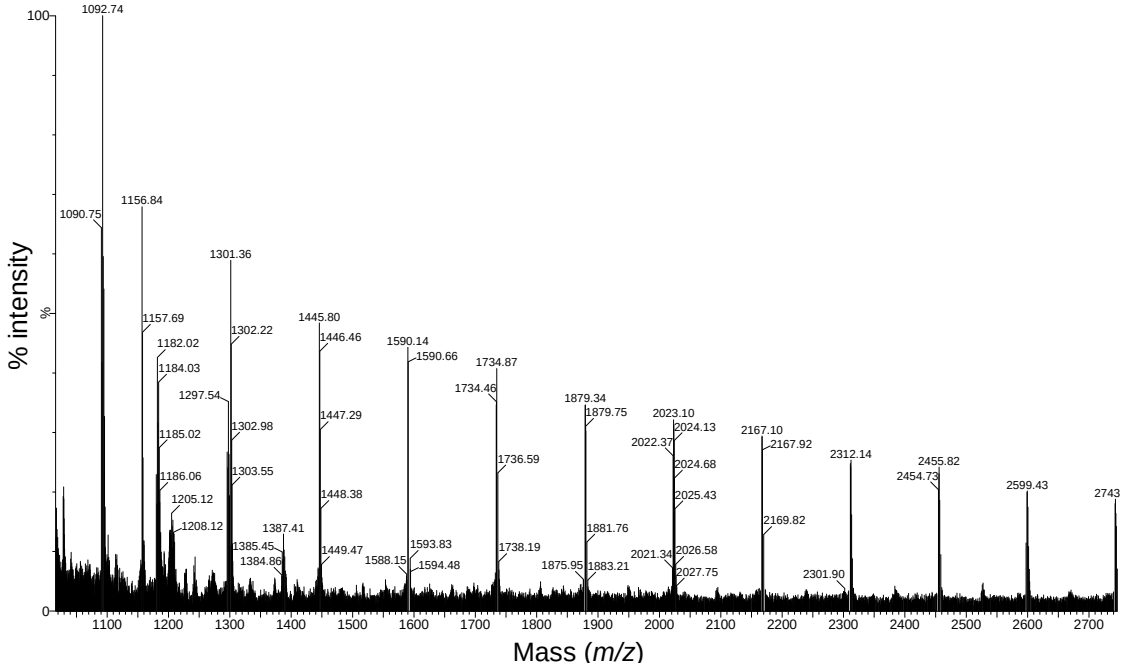


Figure 3.8 MALDI-ToF MS of PLA synthesised using (Tpm*^{d})Mg(OBn) (**5**). Conditions: [*rac*-LA]$_0$:[**5**]$_0$ = 100:1, [*rac*-LA]$_0$ = 0.5 M, [**5**]$_0$ = 0.005 M, 6 mL THF at room temperature. K^+ dopant, $\Delta(m/z)$ = 144 g mol^{-1}.

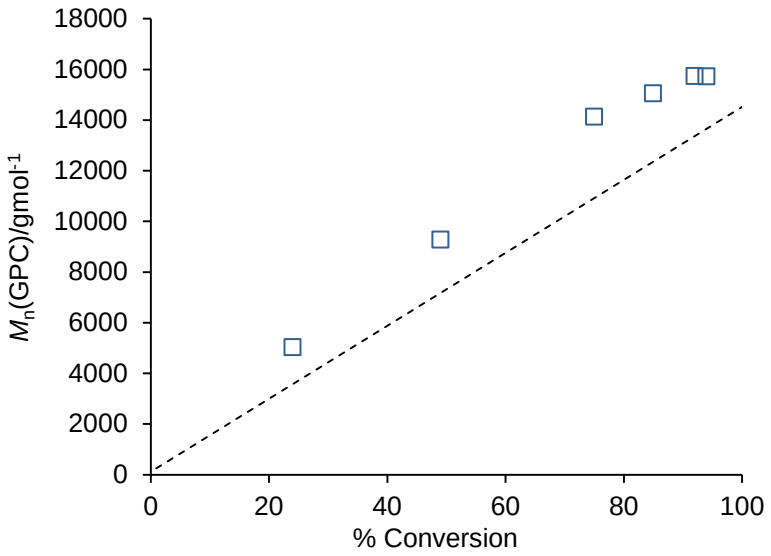


Figure 3.9 Data for the ROP of *rac*-LA using (Tpm*^{d})Mg(OBn) (**5**). M_n (GPC) *vs.* % conversion plot. The dashed line represents the M_n expected for one chain per metal centre. Conditions: [*rac*-LA]$_0$:[**5**]$_0$ = 100:1, [*rac*-LA]$_0$ = 0.5 M, [**5**]$_0$ = 0.005 M, 6 mL THF at room temperature.

Following the preliminary study of **5** in the ROP of *rac*-LA, investigations into its activities with *L*- and *meso*-LA were subsequently carried out. A summary of results is shown in Table 3.2. The ROP of *L*-LA proceeded slower than that of *rac*-LA, reaching 88% conversion within 5 min. This was expected since **5** preferred the enchainment of monomers *via* a *racemic* dyad (*RS* or *SR*) as opposed to a *meso* dyad (*SS* or *RR*), as evidenced by the formation of heterotactically enriched PLA produced from the ROP of *rac*-LA. Employing an enantiomerically pure monomer in this case only allowed the insertion *via* the less favourable *meso* linkage, therefore slowing the rate of the polymerisation. A first order dependence on *L*-LA concentration was found, with an observed rate constant (k_{obs}) of 0.00794(50) s^{-1} (R^2 = 0.988) (*cf.* 0.0536(27) s^{-1}, R^2 = 0.990 for *rac*-LA ROP). In good agreement with this was a narrower PDI being produced, due to the smaller mismatch between the rates of propagation and initiation. Similarly, the experimental M_n was higher than the expected value based on one chain being produced per metal centre.

Table 3.2 Selected data for the ROP of *rac*-, *L*- and *meso*-LA using (Tpm*[d])Mg(OBn) (**5**) in THF.

Monomer [a]	Conv.[b] (%)	Time (s)	M_n obs[c] (g mol^{-1})	M_n calc[d] (g mol^{-1})	PDI[e]	P_r [b]
rac-LA	94	60	15,720	13,656	2.55	0.69
L-LA	88	300	19,100	12,790	1.83	/
meso-LA	92	90	19,590	13,368	2.49	0.66

[a] Conditions: $[LA]_0$:$[\mathbf{5}]_0$ = 100:1, $[LA]_0$ = 0.5 M, $[\mathbf{5}]_0$ = 0.005 M, 6 mL THF at room temperature. [b] Measured by ^{1}H NMR ($CDCl_3$) analyses. [c] Molecular weights (g mol^{-1}) determined from GPC using the appropriate Mark-Houwink corrections. [d] Expected M_n (g mol^{-1}) for one polymer chain growing per metal centre, M_n = conversion (%) × 100 × 144.1 + 108.1. [e] PDI = M_w/M_n.

Complex **5** was shown to be highly active in the ROP of *meso*-LA, reaching 92% conversion within 1.5 min. Unexpectedly, the polymerisation (first order rate constant k_{obs} = 0.0338(21) s^{-1}, R^2 = 0.985) was slightly slower than that of *rac*-LA, as opposed to several other systems reported in the literature, which found otherwise.[100-105] In the literature, the faster rate of polymerisation associated with *meso*-LA was rationalised by its greater ring strain and this was supported by PC MODEL and constant valence force field calculations carried out by Chisholm *et al.*, indicating that *meso*-LA was less stable in its ground state compared to *L*- and *D*-LA.[106] However, Feijen *et al.* reported a series of Schiff based ligand-supported aluminium catalysts which polymerised *rac*-LA ROP faster than *meso*-LA.[107] This was accounted for by the chain end selection effect caused by the presence of both *R*- and *S*- stereocentres in the last repeating unit on the propagating chain. Similar observations were reported in other catalytic systems present in the literature.[28, 108, 109] The origin for the faster rate of *rac*-LA ROP in comparison to that of *meso*-LA polymerisation using **5** remains unclear to date. Given the fact that heterotactic PLA was produced from the ROP of *rac*-LA using **5**, it is therefore not surprising that *meso*-LA ROP afforded syndiotactic PLA due to the preferred enchainment *via* a *racemic* dyad over a *meso* dyad.

3.4.2 Mechanistic considerations of (Tpm*^{d})Mg(OBn) (5) in the ROP of LA

In order to gain further insight into the behaviour of **5** in the ROP of LA, an NMR tube scale reaction between **5** and 5 equiv. of *L*-LA was undertaken in C_6D_6. *L*-LA was used due to its superior solubility over *rac*-LA in C_6D_6. The reaction was complete within 5 min, affording a short polymeryl chain (Tpm*^{d})Mg[LA]$_5$OBn (**9**). Diagnostic regions in the ^{1}H NMR spectrum were identified, illustrated in Figure 3.10.

The two methine protons (H_a and H_b) on the last inserted LA unit were observed at 5.19 and 5.45 ppm as multiplets, as opposed to well-defined quartets due to the formation of polymers of various chain lengths. In contrast, the methine protons on the reminder of the polymeryl chain were observed as a multiplet at 5.04 ppm, with an integration of 8 relative to H_a and H_b. In addition, the diastereotopic methylene protons on the OBn moiety became chemically inequivalent upon *L*-LA insertion and therefore appeared as two mutually coupled doublets at 4.81 and 4.91 ppm, with $^2J_{H\text{-}H}$ coupling constants of 9.6 and 10.0 Hz, respectively. It is notable that the signals corresponding to **5** were still present in the ^{1}H NMR spectrum recorded 5 min after the reaction, indicative of partial catalyst activation (66% of **5** activated). Slight catalyst decomposition (9%) was observed, which could also account for the higher than expected M_n obtained in the corresponding large scale polymerisation, as discussed previously in Section 3.4.1.

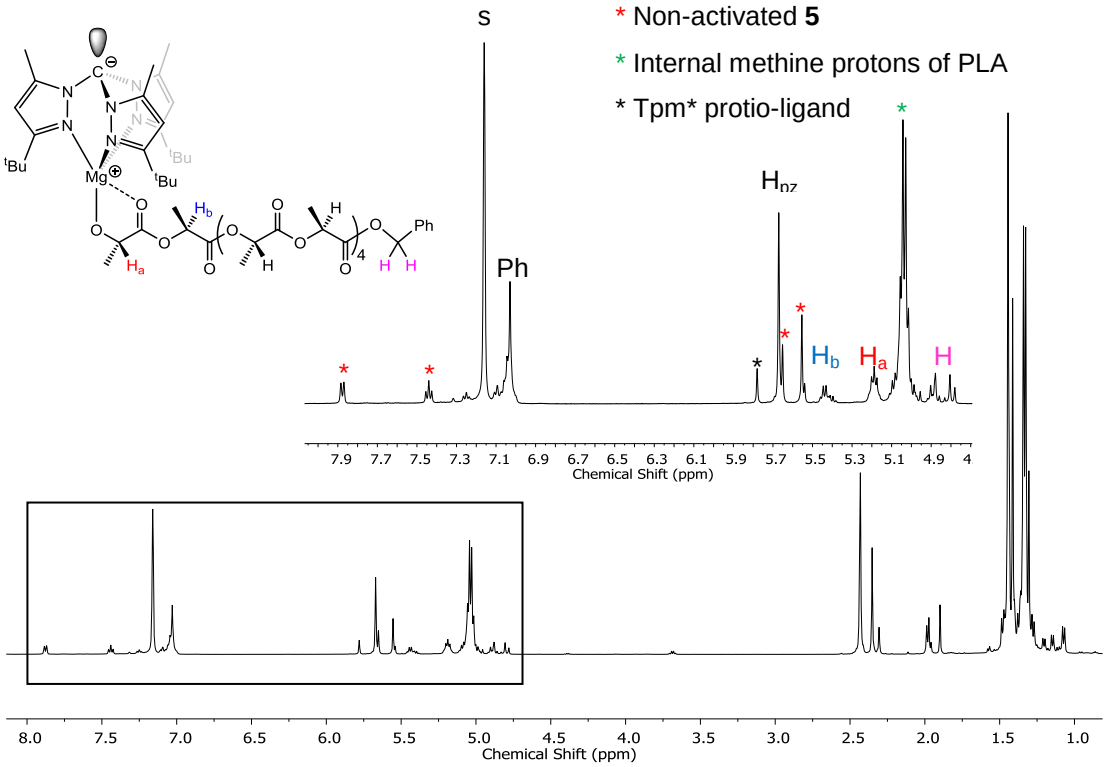


Figure 3.10 ^{1}H NMR spectrum (C_6D_6, 400.2 MHz, 298 K) of (Tpm*^{d})Mg[LA]$_5$OBn (**9**) generated by reacting (Tpm*^{d})Mg(OBn) (**5**) with 5 equiv. of *L*-LA. "*" denotes non-activated **5**. "*" denotes protio-ligand. "*" denotes methine protons of PLA. "s" denotes residual protio-solvent.

3.5 ROP of ε-CL using (Tpm*^{d})Mg(BH$_4$) (2) as a catalyst

3.5.1 Catalytic activity of (Tpm*^{d})Mg(BH$_4$) (2) for the ROP of ε-CL

Following the pioneering work by Mountford *et al.* using alkaline earth metal borohydride complexes in the ROP of cyclic esters, the catalytic activity of (Tpm*^{d})Mg(BH$_4$) (**2**) was probed in the ROP of ε-CL. Complex **2** was shown to be highly active, reaching 90% conversion (200 equiv. of ε-CL) within 10 min in THF at room temperature. Kinetic analysis demonstrated a dependence on ε-CL concentration that was neither first nor second order. Regrettably, the experimental M_n was poorly controlled, as evidenced by the broad PDIs (1.82-2.55) and the non-linear growth of M_n *vs.* % conversion (Figure 3.11). In order to gain an understanding of the nature of polymer end groups, another polymerisation with [ε-CL]$_0$:[**2**]$_0$ = 50:1 was performed, producing PCL with low M_n suitable for MALDI-ToF MS analysis. The resulting polymer was shown to be α,ω-dihydroxytelechelic (Figure 3.12). The ^{1}H NMR

spectrum ($CDCl_3$, 298 K) of the isolated polymer revealed a multiplet at 3.65 ppm, corresponding to the methylene protons at the hydroxy chain ends, consistent with the literature reported results using a lanthanide borohydride catalyst (**3.21**).[52]

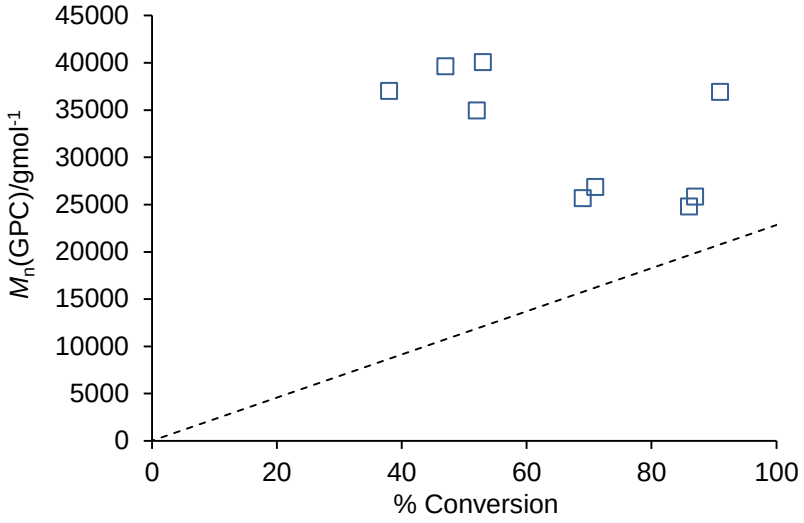


Figure 3.11 Data for the ROP of ε-CL using (Tpm*^{d})Mg(BH_4) (**2**). M_n (GPC) *vs.* % conversion plot. The dashed line represents the M_n expected for one chain per metal centre. Conditions: $[\varepsilon\text{-CL}]_0$:$[\mathbf{2}]_0$ = 200:1, $[\varepsilon\text{-CL}]_0$ = 1.0 M, $[\mathbf{2}]_0$ = 0.005 M, 3.4 mL THF at room temperature.

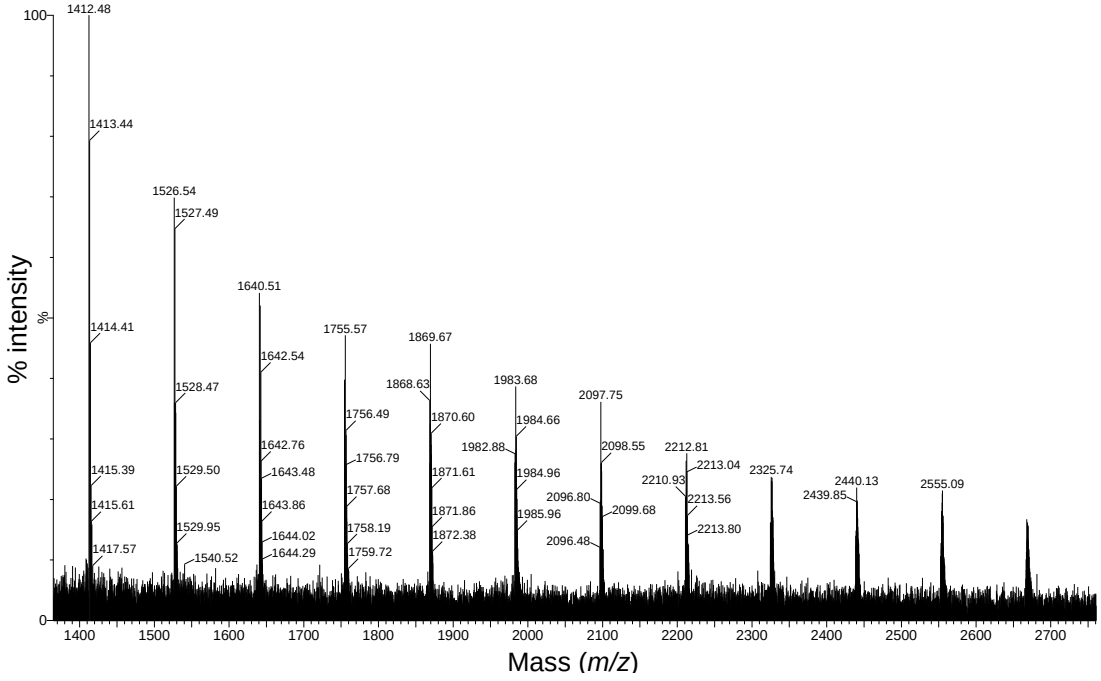


Figure 3.12 MALDI-ToF MS of PCL synthesised using (Tpm*^{d})Mg(BH_4) (**2**). M_n by GPC = 1392 g mol^{-1}. Conditions: $[\varepsilon\text{-CL}]_0$:$[\mathbf{2}]_0$ = 50:1, $[\varepsilon\text{-CL}]_0$ = 1.0 M, $[\mathbf{2}]_0$ = 0.02 M, 3.4 mL THF at room temperature. K^+ dopant, Δ(*m/z*) = 114 g mol^{-1}.

In contrast to the poor molecular weight control imposed by **2**, the analogous ($Tp^{tBu,Me}$)Mg(BH_4) (**2.17**) produced PCL whose experimental M_n was in good agreement with the calculated value for one chain being produced per metal centre.[70] In addition, a linear relationship between M_n *vs*. % conversion was observed, in conjunction with narrow PDIs (1.1-1.3), indicating the well-controlled behaviour of the catalyst. However, the polymerisation employing **2.17** proceeded more slowly, reaching 82% conversion in 2 h. First order dependence on ε-CL concentration was found, with an observed rate constant (k_{obs}) of 0.0170(6) min^{-1} (R^2 = 0.991).

3.5.2 Mechanistic considerations of (Tpm*^{d})Mg(BH_4) (2) for the ROP of ε-CL

Mechanistic studies using NMR spectroscopic techniques were carried out, in an attempt to account for the non-ideal behaviour of **2** in ε-CL ROP. An NMR tube scale reaction between **2** and 15 equiv. of ε-CL was performed in C_6D_6 and monitored by ^1H and ^{11}B NMR spectroscopy. The methylene protons closest to the metal centre of the polymeryl chain could be clearly observed as a triplet at 4.50 ppm in the ^1H NMR spectrum recorded 5 min after the reaction (Figure 3.13, a). Close examination of the ^{11}B NMR spectrum revealed the disappearance of the $\underline{B}H_4$ signal at -38.7 ppm, in conjunction with the emergence of two new peaks at 18.3 and 3.0 ppm, of which the former was assigned to $B(OR)_3$ where -OR most likely corresponded to ring opened ε-CL units. This was confirmed by the reaction between 1 equiv. of BH_3(THF) and 3 equiv. of ε-CL in C_6D_6, the ^{11}B NMR spectrum of which after 7 h clearly showed a peak at 18.2 ppm ($BH(OR)_2$ signal at 27.6 ppm diminishing over time). The presence of borate ester compounds in the literature also supported this assignment.[110] However, the exact identity of $B(OR)_3$ remains elusive to date. According to the literature and the previous work carried out in the Mountford group, the peak at 3.0 ppm was postulated to correspond to a tetra-coordinated species (Tpm*^{d})Mg{$B(OR)_4$}, formed *via* the reversible association of $B(OR)_3$ to (Tpm*^{d})Mg(OR).[70] This was supported by the literature evidence reported by Williamson *et al.*, who confirmed the precedence of $\{B(OMe)_4\}^-$ species in solution, giving rise to a signal at 5.1 ppm in the ^{11}B NMR spectrum.[111]

In order to gain further mechanistic insight, deuterium labelling experiments using (Tpm*^{d})Mg(BD_4) (**2-*d*$_4$**) were performed, in an attempt to pinpoint the positions of the deuterium atoms on the polymeryl chain. This was achieved by the addition of 15

equiv. of ε-CL to a solution of **2-*d*$_4$** in C_6D_6, the ^{1}H NMR spectrum (Figure 3.13, b) of which after 5 min showed resemblance to that obtained previously using **2**. Additionally, the ^{2}H NMR spectrum (C_6H_6) (Figure 3.13, c) revealed a broad peak at 3.95 ppm, indicating that the deuteride was transferred to the methylene group adjacent to the ether oxygen ($OCD_2(CH_2)_4C(O)$). Unfortunately, the corresponding proton (from BH_4 of **2**) in the ^{1}H NMR spectrum of the reaction between **2** and 15 equiv. of ε-CL was obscured by the $\{OC\underline{H}_2(CH_2)_4C(O)\}_n$ signal of the PCL chain, hampering complete signal assignments. The exact mechanism for the ROP of ε-CL using **2** remains unclear to date.

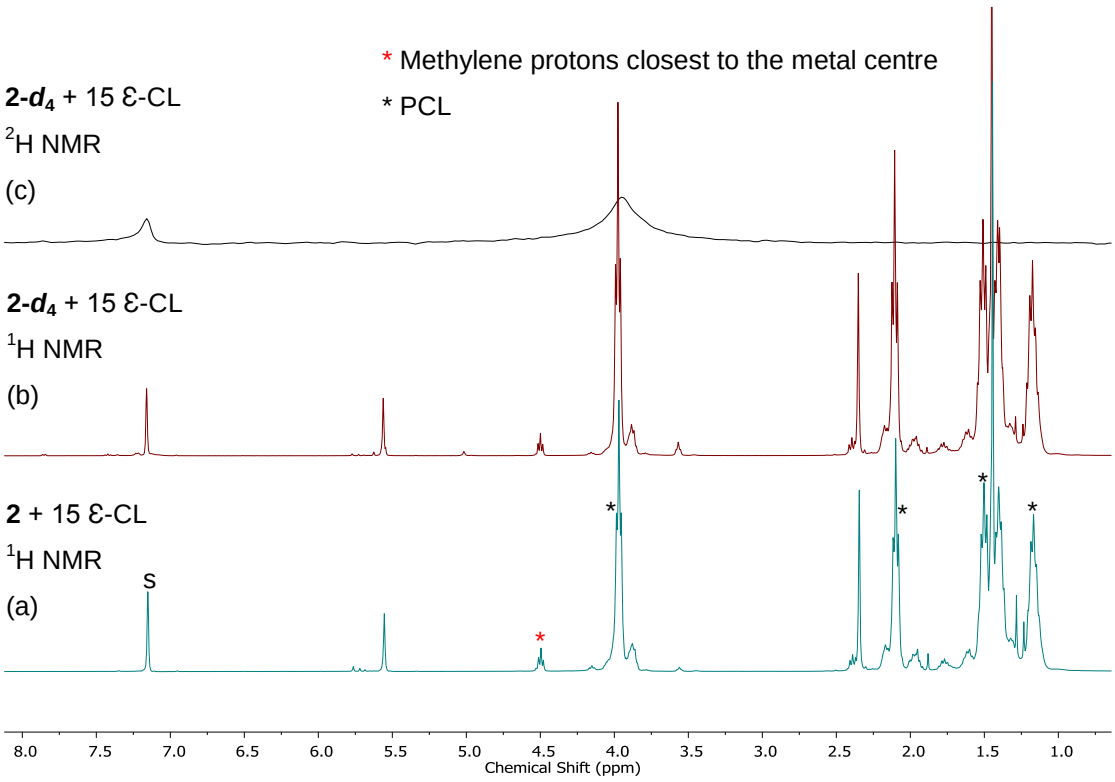


Figure 3.13 ^{1}H NMR spectra (C_6D_6, 400.2 MHz, 298 K) of the reactions between (a) (Tpm*^{d})Mg(BH_4) (**2**) or (b) (Tpm*^{d})Mg(BD_4) (**2-*d*$_4$**) and 15 equiv. of ε-CL. ^{2}H NMR spectrum (C_6H_6, 76.7 MHz, 298 K) (c) of the reaction between (Tpm*^{d})Mg(BD_4) (**2-*d*$_4$**) and 15 equiv. of ε-CL. "*" denotes the methylene protons closest to the metal centre. "*" denotes PCL. "s" denotes residual protio-solvent.

3.6 ROP of *rac*-LA using (Tpm*^{d})Mg(BH$_4$) (2) as a catalyst

3.6.1 Catalytic activity of (Tpm*^{d})Mg(BH$_4$) (2) for the ROP of *rac*-LA

The catalytic activity of **2** was also probed in the ROP of *rac*-LA. Complex **2** was moderately active, reaching 90% conversion (100 equiv. of *rac*-LA) within 6 h in THF at room temperature. A significant induction period of approximately 2 h was observed, after which time the polymerisation demonstrated first order dependence on *rac*-LA concentration (k_{obs} = 0.624(26) h^{-1}, R^2 = 0.993), shown in Figure 3.14. As mentioned previously, the analogous (Tp^{tBu,Me})Mg(BH$_4$) (**2.17**) was inactive towards the ROP of *rac*-LA at room temperature; heating at 70 °C was required for the polymerisation to proceed (THF, 86% conversion in 4.5 h).[70] These results indicated the presence of a possible energy barrier before the propagation step.

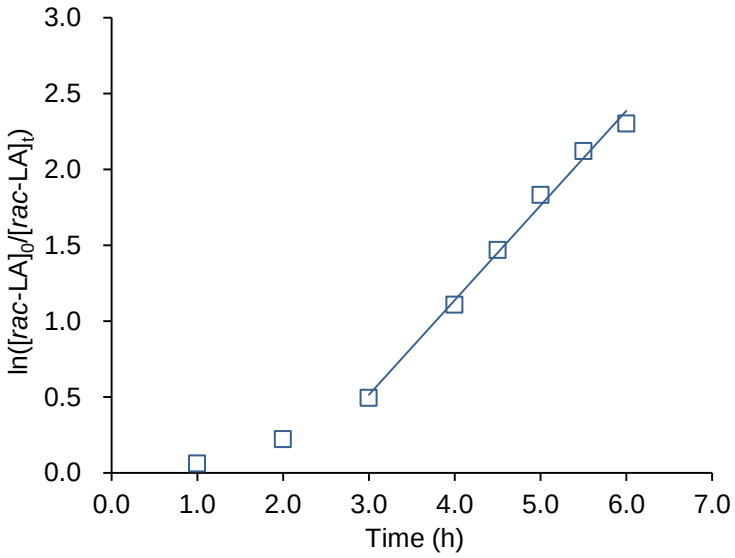


Figure 3.14 Data for the ROP of *rac*-LA using (Tpm*^{d})Mg(BH$_4$) (**2**). Semilogarithmic first-order plot of ln([*rac*-LA]$_0$/[*rac*-LA]$_t$) *vs*. time (k_{obs} = 0.624(26) h^{-1}, R^2 = 0.993). Conditions: [*rac*-LA]$_0$:[**2**]$_0$ = 100:1, [*rac*-LA]$_0$ = 0.5 M, [**2**]$_0$ = 0.005 M, 6 mL THF at room temperature.

Analysis of the resulting polymer using ^{1}H{^{1}H} NMR spectroscopy demonstrated the preference of the catalyst to insert LA *via* a *racemic* linkage, giving a P_r of 0.62. In addition, the MALDI-ToF mass spectrum (Figure 3.15) revealed the presence of two types of end groups, namely hydroxy and non-opened LA ring, consistent with the previously reported results using (Tp^{tBu,Me})Mg(BH$_4$) (**2.17**) and the revised

mechanism. For example, the peak envelope centered at 2922 g mol^{-1} could be assigned to a polymer chain containing 19 LA repeating units with a hydroxy group at one end and a non-opened LA ring at the other whereas the corresponding α,ω-dihydroxytelechelic PLA could be observed at 2924 g mol^{-1}. In addition, the predominant peak distribution with repeating units of $\Delta m/z$ = 72 g mol^{-1} suggested the presence of intermolecular transesterification. No cyclic PLA was observed.

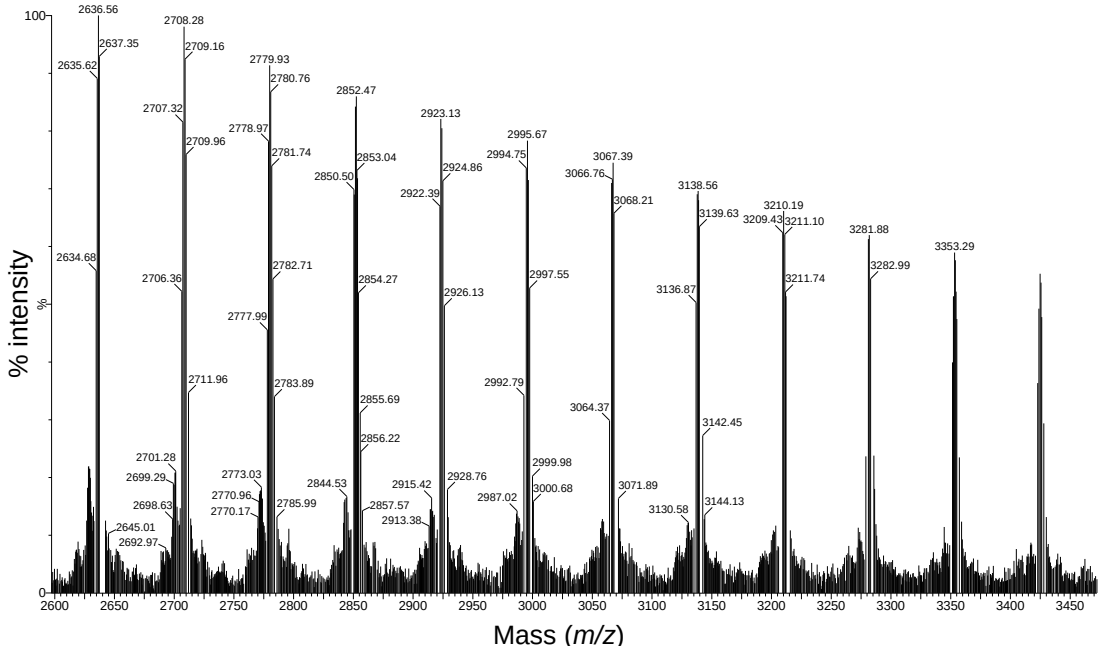


Figure 3.15 MALDI-ToF MS of PLA synthesised using (Tpm*^{d})Mg(BH$_4$) (**2**). M_n by GPC = 2290 g mol^{-1}. Conditions: [*rac*-LA]$_0$:[**2**]$_0$ = 100:1, [*rac*-LA]$_0$ = 0.5 M, [**2**]$_0$ = 0.005 M, 6 mL THF at room temperature. K^+ dopant.

The growth of M_n *vs.* % conversion (Figure 3.16) was found to be linear in the ROP of *rac*-LA initiated by **2**, with a gradient of 67(1) g mol^{-1} (% conversion)$^{-1}$, almost half of the value expected (144 g mol^{-1} (% conversion)$^{-1}$) for one chain being produced per metal centre. This could be attributed to two possible reasons, namely transesterification side reactions or chain transfer events. Although intermolecular transesterification was evident from the MALDI-ToF mass spectrum, its presence does not justify the lower than expected experimental M_n values. These results were thus reflective of possible chain transfer events, leading to multiple polymer chains being produced per metal centre. As discussed in Section 3.2.3, such observations have been reported previously in the Mountford group and initial mechanistic studies have provided evidence for the occurrence of chain transfer events in alkaline earth metal borohydride initiated *rac*-LA ROP.[70]

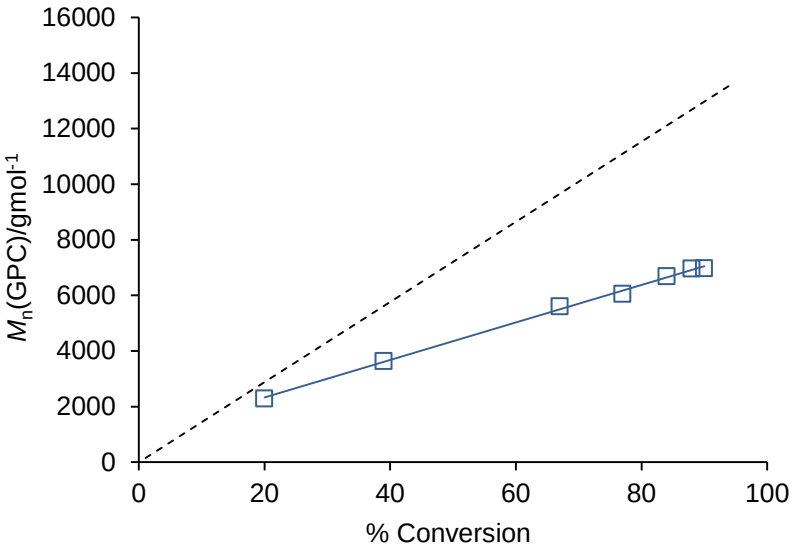


Figure 3.16 Data for the ROP of *rac*-LA using (Tpm*^{d})Mg(BH$_4$) (**2**). M_n (GPC) *vs.* % conversion plot. The dashed line represents the M_n expected for one chain per metal centre. Conditions: [*rac*-LA]$_0$:[**2**]$_0$ = 100:1, [*rac*-LA]$_0$ = 0.5 M, [**2**]$_0$ = 0.005 M, 6 mL THF at room temperature.

3.6.2 Mechanistic considerations of (Tpm*^{d})Mg(BH$_4$) (2) for the ROP of *rac*-LA

Following the *rac*-LA ROP studies using **2** which revealed the unexpected behaviour of the catalyst in terms of giving lower than expected M_n and possessing a long induction period, further mechanistic investigations were subsequently undertaken using various NMR spectroscopic techniques. A good starting point was to build on the initial pioneering work carried out by Dr J. Unruangsri on the mechanisms for the ROP of LA initiated by (Tp^{tBu,Me})Mg(BH$_4$) (**2.17**) (Section 3.2.3).[70] In order to determine whether this proposed mechanism is valid for **2**, there are three main questions that need to be addressed. Firstly, the first step, according to the proposed mechanism, involves the transfer of one hydride to form a non-opened LA alkoxide species. It is therefore crucial to verify the generation of this first hydride transfer product. Secondly, given the fact that such species can act as an initiator, it is necessary to investigate whether the non-opened LA ring can be observed on the polymer chain end. Thirdly, the chain transfer ability of "B(LA-H)$_3$" in the ROP of LA requires investigation.

3.6.2.1 Identification of the first hydride transfer product

NMR tube scale reactions between **2** and 5 equiv. of *L*-LA were performed in both THF-d_8 and C_6D_6 at room temperature, giving similar results. For the purpose of NMR structural assignments, the latter was employed as the preferred NMR solvent to give superior signal separation. *L*-LA, as opposed to *rac*-LA, was used because of its higher solubility in C_6D_6.

The addition of 5 equiv. of *L*-LA to **2** in C_6D_6 led to the instantaneous formation of the first hydride transfer product (Tpm*^{d})Mg(*L*-LA-H) (**10**), in conjunction with a mixture of species denoted as "B(LA-H)$_3$" and other unidentifiable products. Figure 3.17 illustrates the ^{1}H NMR spectrum recorded 5 min after the reaction. Signals corresponding to the pyrazolyl, methyl and *tert*-butyl protons on the Tpm*^{d} ligand could be clearly observed at 5.54, 2.31 and 1.32 ppm, respectively. Close examination of the region between 4.00 and 6.00 ppm revealed the presence of three characteristic signals corresponding to the non-opened LA alkoxide unit. The MgOC<u>H</u> proton, H_a, could be observed at 5.80 ppm as a doublet ($^3J_{H\text{-}H}$ = 2.0 Hz) due to coupling with the adjacent methine proton H_b, which appeared as a doublet of quartets at 4.59 ppm. H_b was coupled to both H_a and the Me protons with $^3J_{H\text{-}H}$ coupling constants of 2.0 and 6.5 ppm, respectively. The other methine proton, H_c, possessed a chemical shift of 4.45 ppm and appeared as a quartet ($^3J_{H\text{-}H}$ = 6.5 Hz) due to coupling with the adjacent Me protons. A relative integration of 1:1:1 (H_a:H_b:H_c) provided further evidence for the assignments of these three protons on the non-opened LA unit. Additionally, the methyl protons were visible as two doublets at 1.69 and 1.63 ppm. It is worth noting that no PLA was formed in this reaction.

Through comparing the ^{1}H NMR spectrum of the *in-situ* generated **10** to that of **9**, it is apparent that the two species displayed very different resonances and patterns, providing further structural authentication that the first hydride transfer product (**10**) did not feature ring-opened LA units. The reaction between **2** and 5 equiv. of *L*-LA was monitored by ^{1}H and ^{11}B NMR spectroscopy over the course of 3 h, the details of which will be discussed later. Unfortunately, the large scale synthesis and isolation of **10** were unsuccessful due to the difficulties associated with the removal of unknown side products.

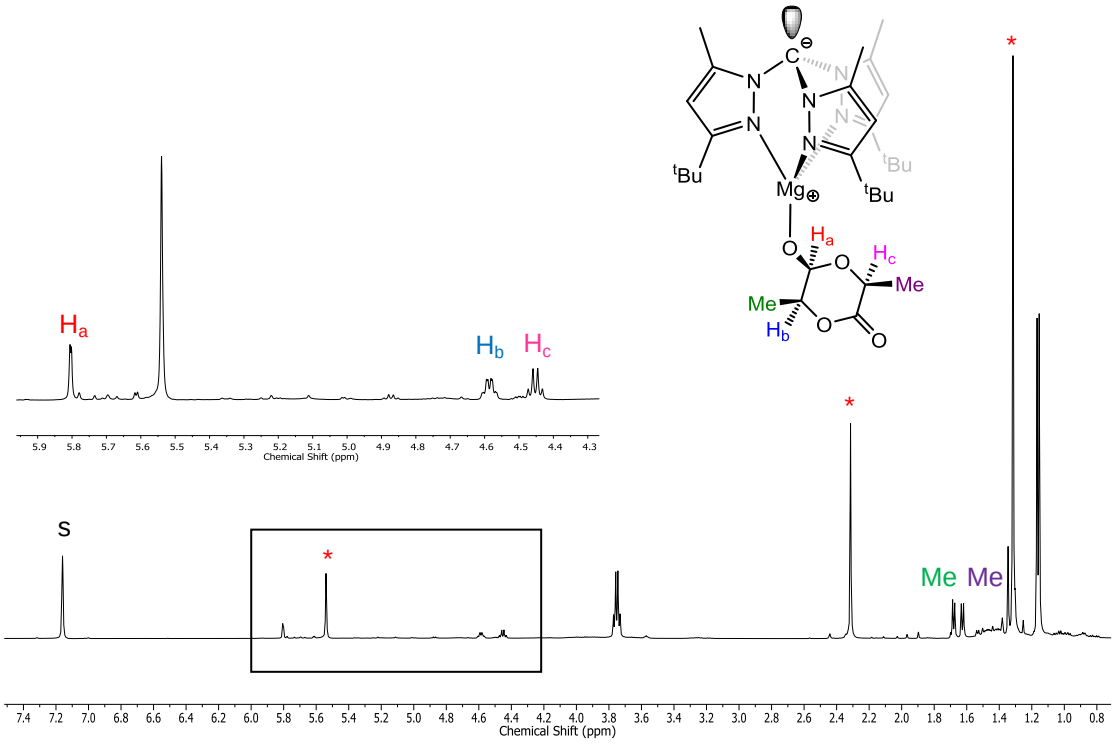


Figure 3.17 ^{1}H NMR spectrum (C_6D_6, 500.0 MHz, 298 K) of (Tpm*^{d})Mg(*L*-LA-H) (**10**) generated *in-situ* by reacting (Tpm*^{d})Mg(BH_4) (**2**) with 5 equiv. of *L*-LA. "*" denotes Tpm*^{d} ligand signals. "s" denotes residual protio-solvent.

A complementary deuterium labelling experiment (Figure 3.18) between **2-*d*$_4$** and 5 equiv. of *L*-LA was subsequently performed in C_6D_6 so as to further confirm the formation of the first hydride transfer product. As expected, the transfer of a deuteride from the BD_4 moiety to the carbonyl group was very rapid, generating the deuterium analogue (Tpm*^{d})Mg(*L*-LA-D) (**10-*d*$_1$**) within 5 min. The ^{1}H NMR spectrum showed close resemblance to that obtained from **2** and 5 equiv. of *L*-LA, with the exception that the doublet signal at 5.80 ppm was significantly diminished, clearly indicating the replacement of H_a with a deuterium atom. In addition, the coupling pattern for H_b was simplified to a quartet (*cf.* doublet of quartets for **10**) due to unobserved $^{3}J_{H\text{-}D}$ coupling.

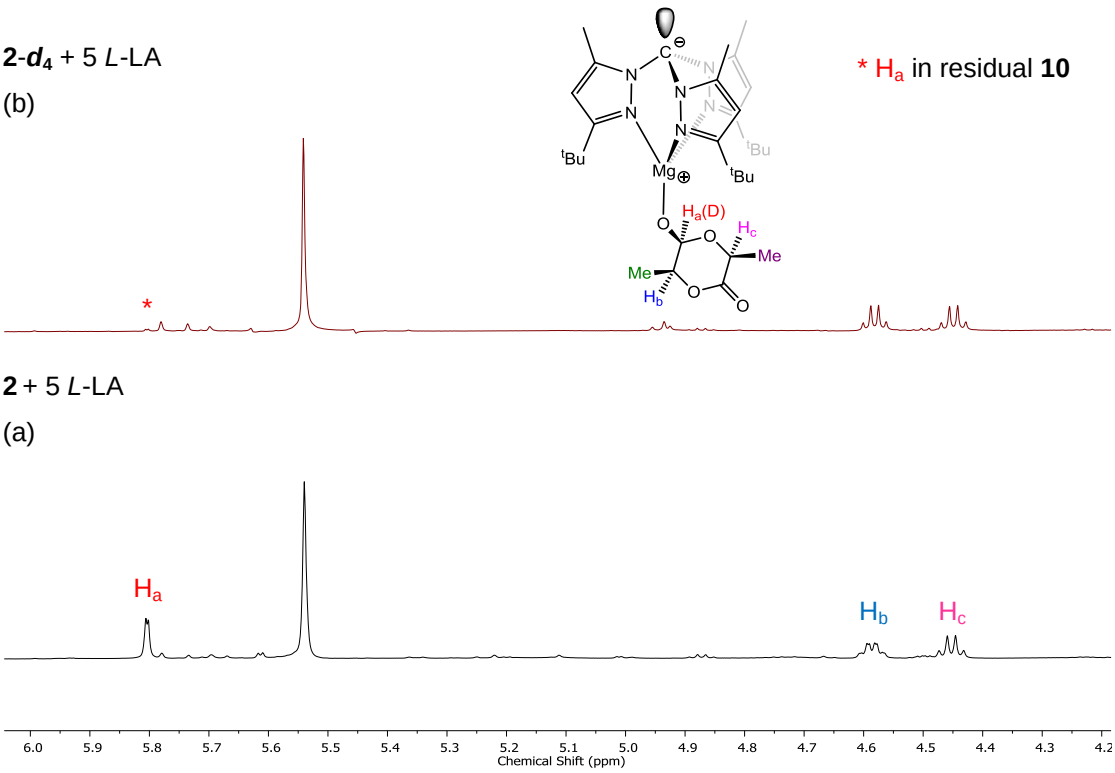


Figure 3.18 ^{1}H NMR spectra (C_6D_6, 500.0 MHz, 298 K) of (a) (Tpm*^{d})Mg(*L*-LA-H) (**10**) and (b) (Tpm*^{d})Mg(*L*-LA-D) (**10-*d*$_1$**) generated *in-situ* by reacting (Tpm*^{d})Mg(BH_4) (**2**) and (Tpm*^{d})Mg(BD_4) (**2-*d*$_4$**) with 5 equiv. of *L*-LA, respectively. "*" denotes H_a in residual **10**.

1D nOe NMR spectroscopy was also employed in order to gain further insight into the structure of **10** (Figure 3.20). A nOe was observed to both H_b and H_c when H_a was irradiated. This is in good agreement with the DFT calculations performed in collaboration with Prof. Laurent Maron on the structurally and electronically similar (Tp^{tBu,Me})Mg(LA-H) (**3.44**), the geometrically optimised structure of which is depicted in Figure 3.19. It is apparent that the MgOC<u>H</u> and two methine protons on the non-opened LA ring are all aligned towards the same direction (*cis*) and their calculated through-space distances are within the nOe range (H_a-H_c = 2.36 Å and H_a-H_b = 2.44 Å). Based on the DFT calculations and the experimental nOe results, the stereochemistry of the chiral centres on the non-opened LA unit for **10** could be elucidated. The MgO<u>C</u>H carbon possesses an *R* conformation, opposite to those at the two methine carbons (*S*). The *cis* orientation of H_a and H_b was also consistent with the vicinal coupling constant of 2.0 Hz observed in the ^{1}H NMR spectrum, suggesting a dihedral angle of 60-90° according to the Karplus equation.[112-114] In addition to the

nOe observed within the non-opened LA ring, a through-space correlation was also present between H_a and the *tert*-butyl groups on the ligand, consistent with the DFT calculations which revealed the shortest H_a-^{t}Bu through-space distance of 2.29 Å.

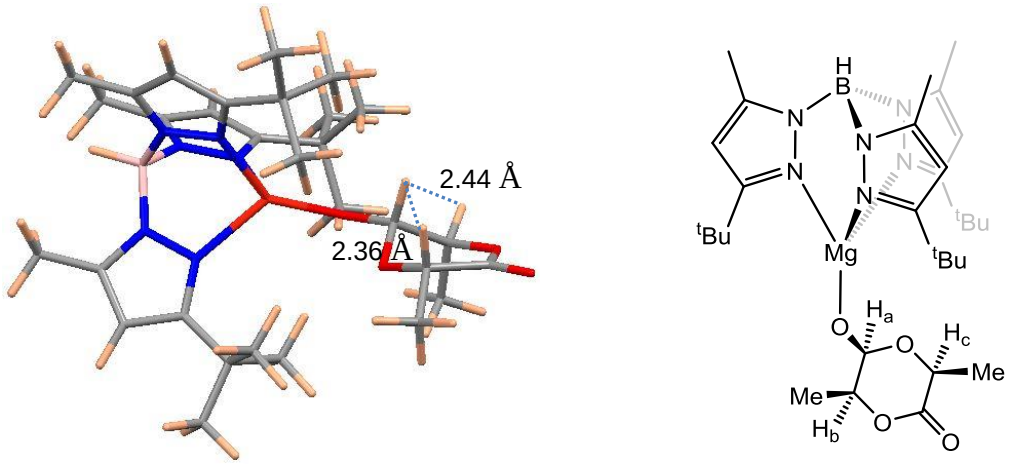


Figure 3.19 Geometrically optimised structure of (Tp^{tBu,Me})Mg(LA-H) (**3.44**).

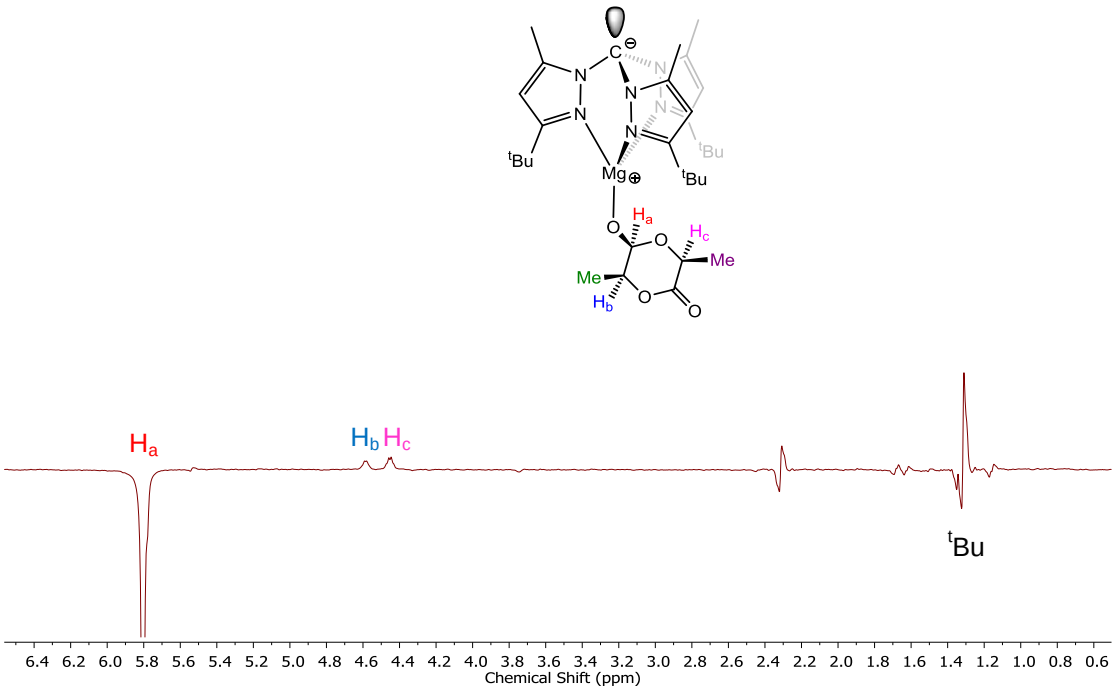


Figure 3.20 1D nOe NMR spectrum (C_6D_6, 500.0 MHz, 298 K) of the *in-situ* generated (Tpm*^{d})Mg(*L*-LA-H) (**10**). See Figure 3.17 for the reference ^{1}H NMR spectrum of **10**.

Quantitative distance determination was subsequently performed based on the nOe data. Through-space distances were calculated using the equation $r_{ij} = r_{ref}\,(a_{ref}/a_{ij})^{1/6}$,

where r_{ij} is the through-space distance of the two protons i and j, a_{ij} is the nOe cross-peak volume, r_{ref} is a known distance between two protons and a_{ref} is a known nOe volume.[115] Table 3.3 displays the detailed results obtained from the nOe data of **10**. The calculated distances are in close agreement with those obtained from the DFT calculations of **3.44**.

Table 3.3 Selective qualitative H-H distance calculated by 1D NOESY spectroscopy of **10**.

	r_{ref} (Å)		r_{ij} (Å)	
	$r_{Hb\text{-}Me}$	$r_{Hc\text{-}Me}$	$r_{Ha\text{-}Hb}$	$r_{Ha\text{-}Hc}$
DFT calculations of **3.44**	2.49 (r_{ref})	2.47 (r_{ref})	2.44	2.36
nOe calculations	/	/	2.52	2.39

The first hydride transfer product obtained from the reaction between **2** and 5 equiv. of *D*-LA in C_6D_6 gave very similar nOe results, suggesting an *S* conformation at the MgOCH carbon (*cf. R* for two methine groups). Following these initial studies, an NMR tube scale reaction between **2** and 5 equiv. of *meso*-LA in C_6D_6 was also performed in order to gain further structural understanding of the first hydride transfer product (Tpm*^{d})Mg(*meso*-LA-H) (**10'**). The ^{1}H NMR spectrum (Figure 3.21) recorded 5 min after the reaction revealed the presence of H_b and H_c, appearing as an apparent quintet and a quartet at 4.53 and 4.39 ppm, respectively. Interestingly, a significant upfield shift was observed for H_a, which was visible as a doublet with $^{3}J_{H\text{-}H}$ = 7.0 Hz. This was perhaps reflective of a change in the orientation of H_a relative to H_b and H_c, giving rise to a considerably lower chemical shift at 5.22 ppm (*cf.* 5.80 ppm for **10**). Moreover, the $^{3}J_{H\text{-}H}$ vicinal coupling constant of 7.0 Hz was much larger than that observed in **10** (2.0 Hz), suggesting a dihedral angle of either 120-150° or 0-30° between H_a and H_b according to the Karplus equation.[112-114] Since the relative spatial arrangement between H_a and H_b in **10'** could not be unambiguously determined, thorough-space studies using 1D nOe NMR spectroscopy were also carried out (Figure 3.22). A nOe between H_a and H_c was observed, indicative of their *cis* orientation. In other words, the stereochemistry at their attached carbons was opposite. In contrast, H_a and H_b were *trans* to each other (same stereochemistry at the attached carbons), resulting in the absence of any correlation between the two protons.

As observed with **10**, a nOe was also present between H_a and the *tert*-butyl protons on the Tpm*^{d} ligand.

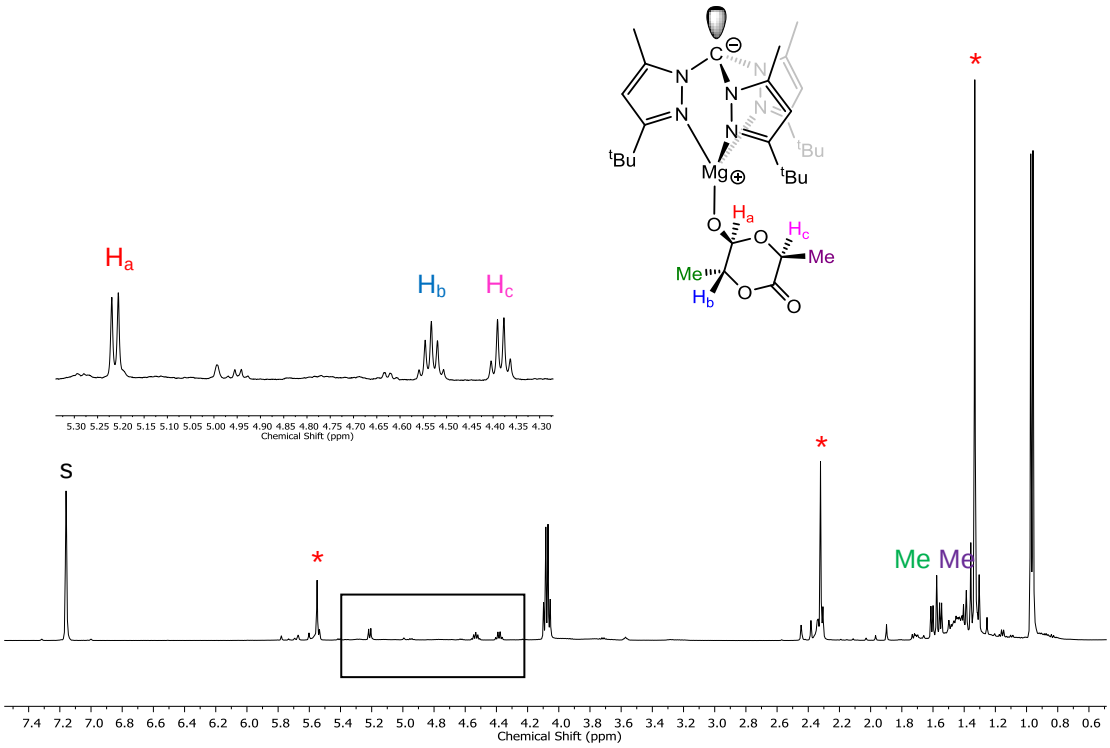


Figure 3.21 ^{1}H NMR spectrum (C_6D_6, 500.0 MHz, 298 K) of (Tpm*^{d})Mg(*meso*-LA-H) (**10'**) generated by reacting (Tpm*^{d})Mg(BH_4) (**2**) with 5 equiv. of *meso*-LA. "*" denotes Tpm*^{d} ligand. "s" denotes residual protio-solvent.

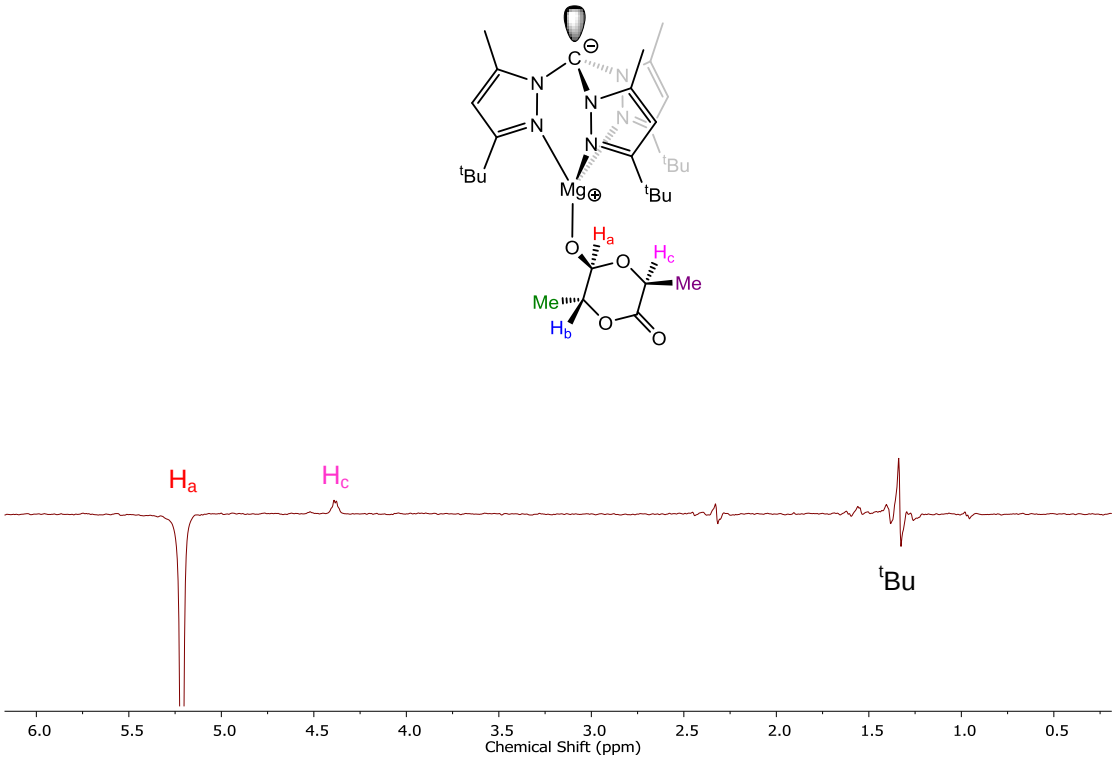


Figure 3.22 1D nOe NMR spectrum (C_6D_6, 500.0 MHz, 298 K) of the *in-situ* generated (Tpm*^{d})Mg(*meso*-LA-H) (**10'**). See Figure 3.21 for the reference ^{1}H NMR spectrum of **10'**.

According to the proposed mechanism for the ROP of LA, one should expect to observe NMR spectroscopic evidence for the generation of "B(LA-H)$_3$", in conjunction with (Tpm*^{d})Mg(*L*-LA-H) (**10**). "B(LA-H)$_3$" can be formed either by the exchange reaction between **10** and BH_3(THF) or *via* the direct reduction of LA by BH_3(THF). The former was reminiscent of the synthetic route employed for the preparation of (Tpm*^{d})Mg(BD_4) (**2-*d*$_4$**) discussed previously in Chapter Two. (Tpm*^{d})Mg(OBn) (**5**) was reacted with BH_3(THF), generating **2-*d*$_4$** and B(OBn)$_3$ as a by-product. The feasibility of this synthetic route provided evidence for the *in-situ* formation of "B(LA-H)$_3$" *via* the exchange reaction between **10** and BH_3(THF). However, reacting **2** with 5 equiv. of *L*-LA did not yield clearly identifiable signals corresponding to "B(LA-H)$_3$" in the ^{1}H NMR spectrum (Figure 3.23, a).

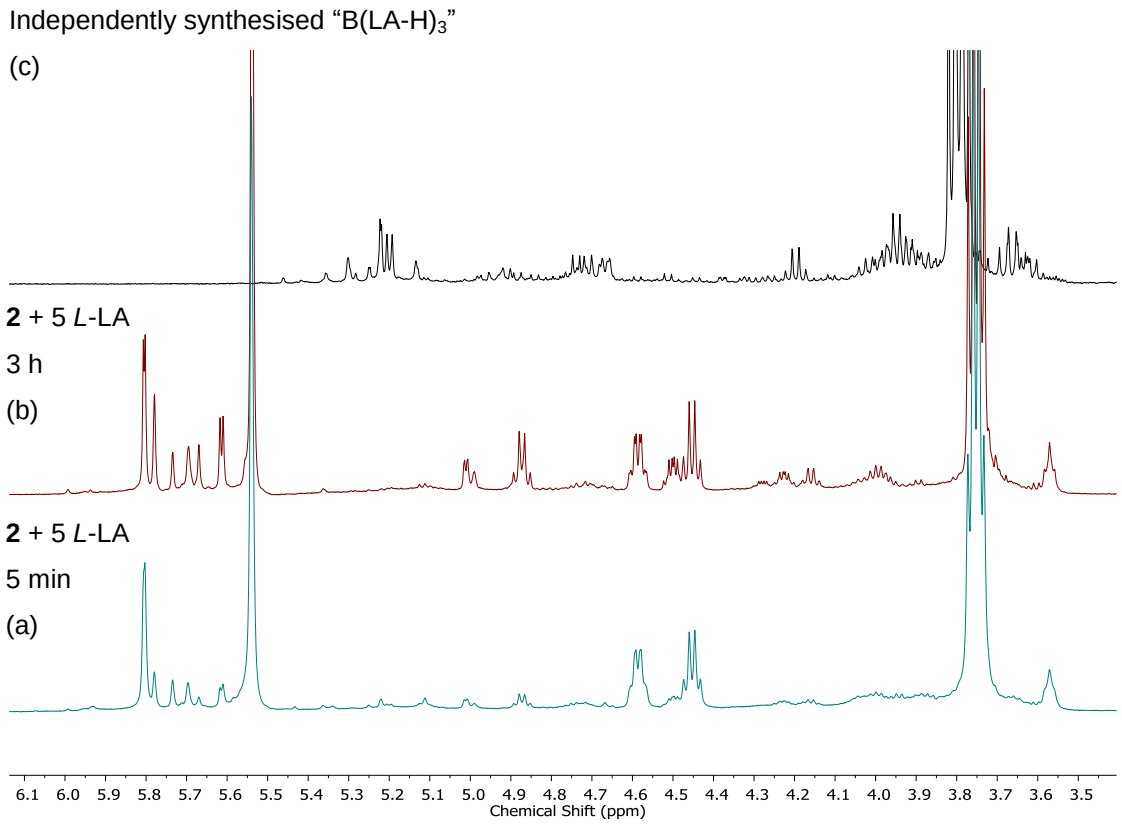


Figure 3.23 ^{1}H NMR spectra (C_6D_6, 500.0 MHz, 298 K) of the reaction between (Tpm*^{d})Mg(BH_4) (**2**) and 5 equiv. of *L*-LA after (a) 5 min and (b) 3 h. ^{1}H NMR spectrum (C_6D_6, 500.0 MHz, 298 K) (c) of the *in-situ* generated "B(LA-H)$_3$" by heating BH_3(THF) with 5 equiv. of *L*-LA at 60 °C for 3 h.

A control experiment between 1 equiv. of BH_3(THF) and 5 equiv. of *L*-LA in C_6D_6 was subsequently attempted in order to independently synthesise "B(LA-H)$_3$". The ^{11}B{^{1}H} NMR spectrum recorded 5 min after the reaction revealed the presence of the remaining BH_3(THF) and the formation of a minor peak at 23.1 ppm and two major peaks in the region of 27-29 ppm, corresponding to "B(LA-H)$_3$" and "BH(LA-H)$_2$" type species, respectively. This suggested that the reduction of the first and second LA was facile whereas that of the third appeared to be rate-determining. In addition, a broad signal was also observed at 18.6 ppm, tentatively attributed to "BH_2(LA-H)". Literature precedence of $BH(OR)_2$ species (OR = alkoxide) was documented by Nöth and Wrackmeyer *et al.*[110] whereas the only compound of BH_2(OR) type reported was BH_2OMe, identified by microwave spectroscopy.[116] A high level of conversion to "B(LA-H)$_3$" was achieved by heating the reaction at 60 °C for 3 h, after which time the ^{11}B{^{1}H} NMR spectrum showed the presence of a major peak at 23.1 ppm

("B(LA-H)$_3$"), in conjunction with signals corresponding to "BH(LA-H)$_2$" and "BH$_2$(LA-H)" type species. The corresponding ^{1}H NMR spectrum (Figure 3.23, c) revealed several sets of signals, suggesting the formation of multiple reduction products. A large amount of unreacted LA was also observed. It is important to note that the exact identity of "B(LA-H)$_3$" remains unclear and is not restricted to the borate ester containing three non-opened LA alkoxides. It was postulated that borate ester species with ring-opened LA units were also present.

The reaction between **2** and 5 equiv. of *L*-LA (C_6D_6) was monitored by ^{1}H NMR spectroscopy over the course of 3 h. It was found that some of the signals initially hidden underneath the baseline were gradually intensified (Figure 3.23, b). For example, an increase in the integration of the doublet at 5.62 ppm, the quartet at 4.88 ppm and the multiplet at 4.50 ppm was indicative of the formation of a new species featuring a non-opened LA ring.

The reaction between **2** and 5 equiv. of *L*-LA (C_6D_6) was also monitored by ^{11}B NMR spectroscopy over the course of 3 h. The absence of the signal at -38.7 ppm after 5 min indicated the complete consumption of **2**, confirming that the first hydride transfer process was rapid. Five signals were observed, of which the major singlet at 23.1 ppm was assigned to "B(LA-H)$_3$", consistent with the chemical shift observed from the control experiment between BH$_3$(THF) and 5 equiv. of *L*-LA. The rapid appearance of this peak at room temperature (*cf.* heating required in the independent synthesis) clearly indicated the direct involvement of the metal centre in the *in-situ* generation of "B(LA-H)$_3$". The peak at 7.5 ppm was initially postulated to correspond to a tetra-coordinated species (Tpm*^{d})Mg(*L*-LA-H){"B(LA-H)$_3$"} (**11**), generated by the reversible association of "B(LA-H)$_3$" to **10** (Figure 3.24). However, later results have provided contradictory evidence, leading to doubts regarding the possibility for the formation of **11** (*vide infra*). The identities of the other three peaks at 18.4, 2.5 and -18.9 ppm remain unclear. No apparent change in the ^{11}B NMR spectrum was observed over the course of 3 h.

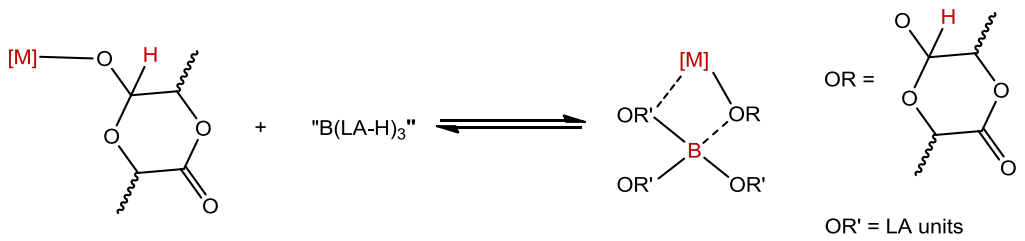


Figure 3.24 Reversible adduct formation of (Tpm*[d])Mg(LA-H){"B(LA-H)$_3$"} (**11**).

In order to gain a better understanding of the formation of multiple products in the NMR tube scale reaction between 1 equiv. of BH_3(THF) and 5 equiv. of *L*-LA and to further investigate the precise role of the former, a series of control experiments aimed at evaluating the reduction ability of BH_3(THF) with various carbonyl groups were performed. These experiments were carried out by Dr Insun Yu from the Mountford group. The reaction between 1 equiv. of BH_3(THF) and 3 equiv. of 2-methylcyclohexanone in THF-d_8 revealed the formation of BH(Cy-H)$_2$ and B(Cy-H)$_3$ (26.8 ppm and 17.8 ppm in $^{11}B\{^1H\}$ NMR spectrum, respectively) after 16 h. In addition, the -OC<u>H</u> protons were clearly observed as multiplets at 4.21 ppm in the ^{1}H NMR spectrum (Figure 3.25, a). BH_3(THF) was also capable of reducing *p*-tolualdehyde in THF-d_8, giving rise to a peak at 18.9 ppm corresponding to <u>B</u>(OCH$_2$Ph(Me))$_3$ in the $^{11}B\{^1H\}$ NMR spectrum after 16 h. Moreover, the methylene protons were visible at 4.96 ppm whereas the phenyl protons appeared as two doublets at 7.02 and 7.25 ppm, respectively, in the ^{1}H NMR spectrum (Figure 3.25, b). These results clearly demonstrated the reductive nature of BH_3(THF) towards aldehydes and ketones.

Furthermore, the reduction of *rac*-LA by BH_3(THF) in a 3:1 stoichiometry was re-evaluated in THF-d_8, forming multiple products. The $^{11}B\{^1H\}$ NMR spectrum recorded after 16 h revealed the presence of four peaks at 28.4, 22.9, 18.1 and -0.5 ppm, corresponding to "BH(LA-H)$_2$", "B(LA-H)$_3$", "BH$_2$(LA-H)" and BH_3(THF), respectively. The reaction was left at room temperature for another 32 h, after which time only "B(LA-H)$_3$" and "BH$_2$(LA-H)" were observed in the $^{11}B\{^1H\}$ NMR spectrum. One striking feature was the much higher than expected integration of *rac*-LA monomer signal in the ^{1}H NMR spectrum, suggesting the presence of a considerable amount of unreacted *rac*-LA. Based on these NMR spectroscopic observations, it was suspected that BH_3(THF) might be capable of reducing both

carbonyl groups of *rac*-LA. This hypothesis was tested by reacting 3 equiv. of terephthalaldehyde featuring two aldehyde groups with 1 equiv. of BH_3(THF) in THF-d_8. Two signals were observed at 29.9 and 20.4 ppm in the $^{11}B\{^1H\}$ NMR spectrum after 16 h, corresponding to $BH(OR)_2$ and $B(OR)_3$ species (OR = reduced alkoxide), respectively. A large excess of terephthalaldehyde remained unreacted after 16 h, providing evidence for the possible reduction at both aldehyde groups (Figure 3.25, c).

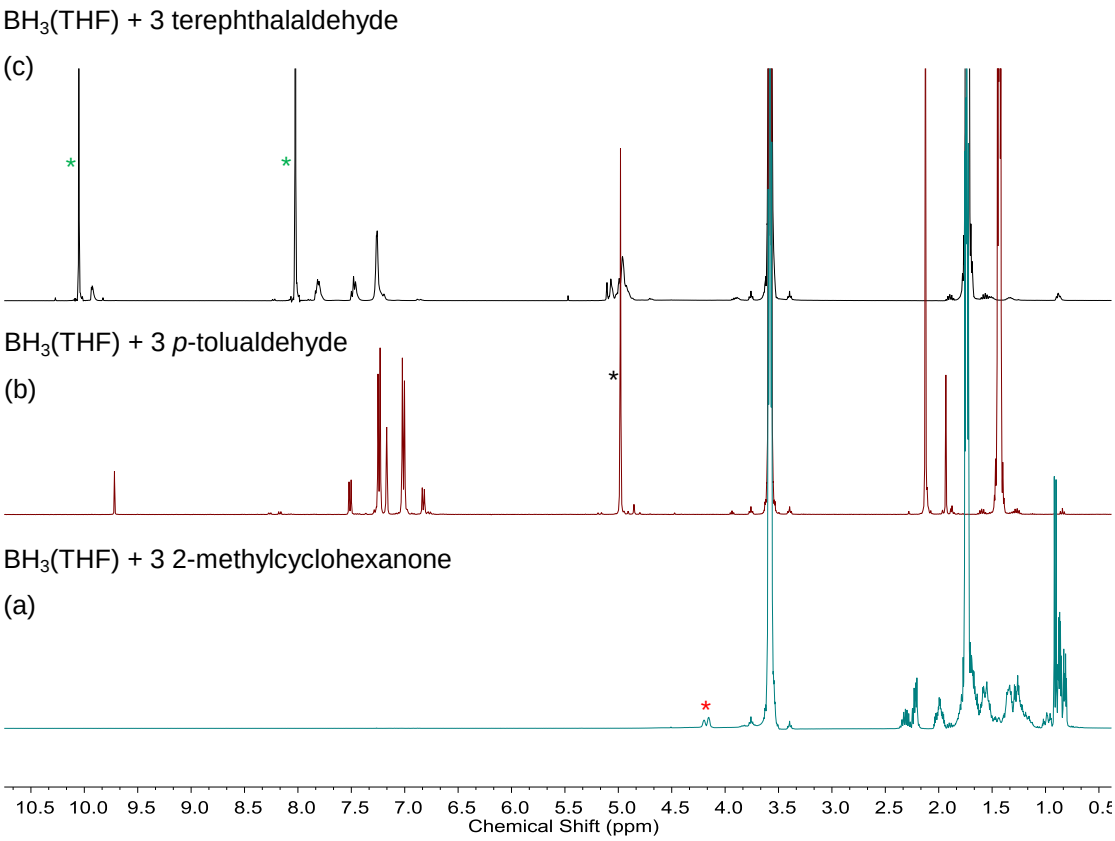
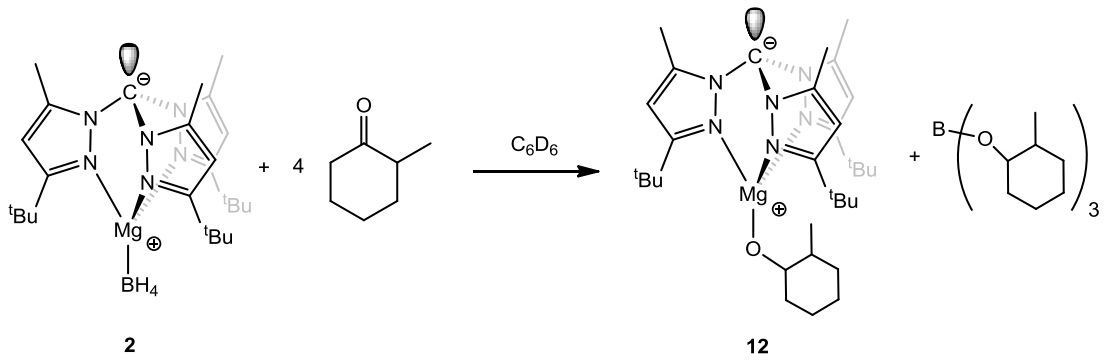


Figure 3.25 ^1H NMR spectra (THF-d_8, 400.2 MHz, 298 K) of the reactions between BH_3(THF) and 3 equiv. of (a) 2-methylcyclohexanone, (b) *p*-tolualdehyde and (c) terephthalaldehyde after 16 h. "*" denotes OC<u>H</u> protons for $BH(Cy\text{-}H)_2$ and $B(Cy\text{-}H)_3$. "*" denotes $B(OC\underline{H}_2Ph(Me))_3$. "*" denotes unreacted terephthalaldehyde.

In order to gain further insight into the reaction between **2** and LA and to avoid the formation of multiple products resulting in difficult NMR elucidation, a model study was performed by reacting 1 equiv. of **2** with 4 equiv. of 2-methylcyclohexanone. This particular ketone was used for three main reasons. Firstly, it is representative of a LA molecule given their similar size. Moreover, the possible reduction at both

carbonyl groups found in the reaction between BH_3(THF) and LA will not be encountered in this case since the molecule only possesses one carbonyl group. Lastly, the resulting alkoxide (Tpm*^{d})Mg(Cy-H) (**12**) could serve as a representative model for the propagating species in the ROP initiated by **2**.



Equation 3.1

The addition of 4 equiv. of 2-methylcyclohexanone to **2** in C_6D_6 resulted in the instantaneous formation of **12** and B(Cy-H)$_3$. Interestingly, the ^{1}H NMR spectrum revealed the presence of two sets of H_{pz} and *tert*-butyl proton resonance signals, suggesting the formation of diastereomers (Figure 3.26, a). This arose due to the fact the incoming hydride could attack from either the same or opposite side as the methine proton (C<u>H</u>Me), resulting in the formation of *cis* and *trans* isomers. It is worth noting that the two sets of signals did not integrate to 1:1, indicative of the preferable formation of one isomer over the other. This suggested that the trajectory of the incoming hydride was biased, favouring a specific spatial arrangement with the C<u>H</u>Me proton. This was in contrast to the extremely stereospecific reaction between **2** and 5 equiv. of *L*-LA discussed previously, whereby the hydride exclusively attacked from the same side as the C<u>H</u>Me proton to minimise steric repulsions with the two methyl groups, forming the *cis* isomer only. Unfortunately, assignments for the characteristic OC<u>H</u> protons for **12** were inconclusive due to the presence of overlapping signals corresponding to B(Cy-H)$_3$. Resonances for the protons on the backbone of the cyclohexanoxide ring were visible in the region of 0.9-2.5 ppm.

As observed for **12**, B(Cy-H)$_3$ was also formed as a mixture of diastereomers with the OC<u>H</u> protons appearing as multiplets at 4.46 and 3.91 ppm. These assignments were confirmed by the independent synthesis and isolation of B(Cy-H)$_3$ involving 1 equiv. of BH_3(THF) and 3.2 equiv. of 2-methylcyclohexanone, giving identical resonances

(Figure 3.26, c). Deuterium labelling experiments were also carried out by reacting 1 equiv. of **2-*d*$_4$** with 4 equiv. of 2-methylcyclohexanone in C_6D_6 (Figure 3.26, b). As expected, the OC<u>H</u> protons for both **12** and B(Cy-H)$_3$ were absent in the ^{1}H NMR spectrum, confirming the replacement of protons with deuterium nuclei.

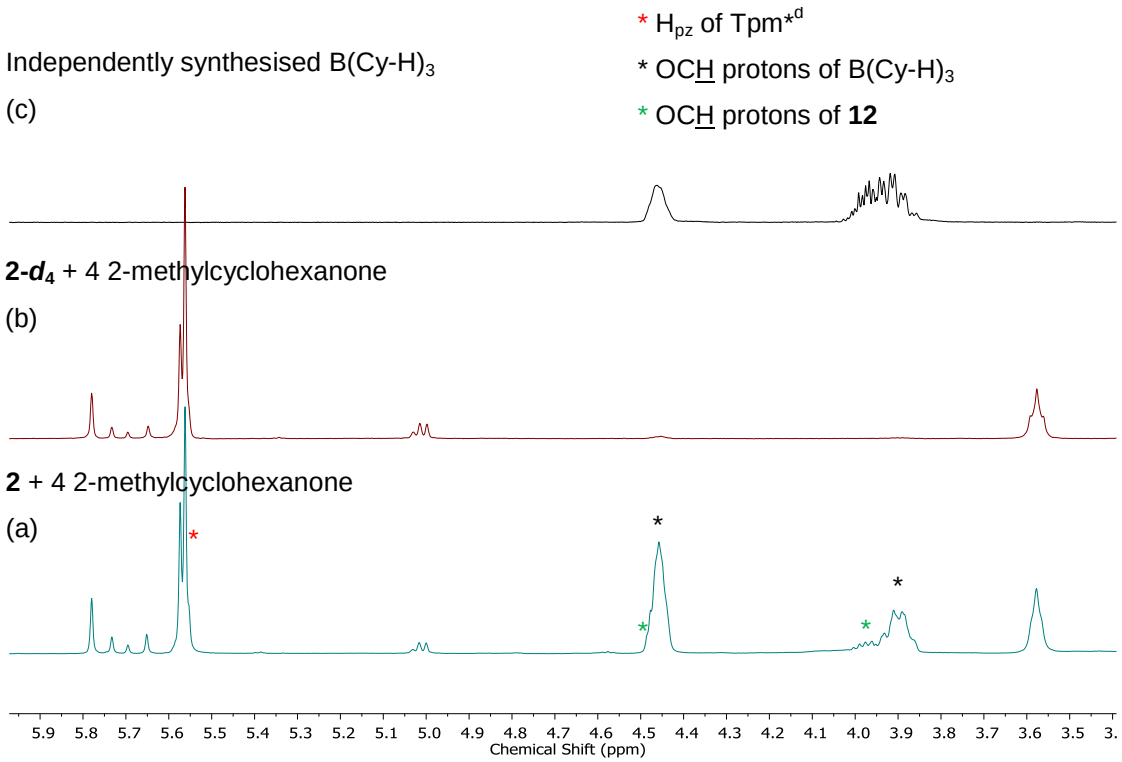


Figure 3.26 ^{1}H NMR spectra (C_6D_6, 400.2 MHz, 298 K) of the reactions between (a) (Tpm*^{d})Mg(BH$_4$) (**2**) or (b) (Tpm*^{d})Mg(BD$_4$) (**2-*d*$_4$**) and 4 equiv. of 2-methylcyclohexanone. ^{1}H NMR spectrum (C_6D_6, 400.2 MHz, 298 K) (c) of the independently synthesised and isolated B(Cy-H)$_3$. "*" denotes H$_{pz}$ protons of Tpm*^{d}. "*" denotes OC<u>H</u> protons for B(Cy-H)$_3$. "*" denotes OC<u>H</u> protons for **12**.

The ^{11}B NMR spectrum (C_6D_6) recorded after 5 min showed a distinct singlet at 18.1 ppm, corresponding to B(Cy-H)$_3$. The absence of any signals at approximately 7.5 ppm has led to doubts regarding the previous assignment for the tetra-coordinated species (Tpm*^{d})Mg(*L*-LA-H){"B(LA-H)$_3$"} (**11**) formed in the reaction between **2** and 5 equiv. of *L*-LA. Given the similar size of a non-opened LA ring alkoxide and a 2-methylcyclohexanoxide, it could be assumed based on the model study that the formation of such four-coordinate boron species was questionable due to the steric bulk imposed by the *tert*-butyl groups on the supporting Tpm*^{d} ligand. No change in the ^{11}B NMR spectrum was observed over the course of 3 h.

As mentioned previously, another reason for performing the model study was to employ **12** as a mimic for the propagating species in the ROP of LA initiated by **2**. However, the large scale synthesis and isolation of **12** by reacting **2** with 4 equiv. of 2-methylcyclohexanone was problematic. Multiple recrystallisation attempts failed due to the sensitive nature of the carbanion. In order to gain a deeper understanding of the propagating ability of **12**, 15 equiv. of *L*-LA was added to the *in-situ* generated **12** and $B(Cy\text{-}H)_3$ in C_6D_6, the ^1H NMR spectrum of which after 5 min is illustrated in Figure 3.27 (b). 98% conversion was reached within 5 min, as evidenced by the major quartet at 5.04 ppm, corresponding to the methine protons of PLA (*cf.* LA monomer signal at 3.72 ppm). As observed previously in the case of $(Tpm^{*d})Mg[LA]_5OBn$ (**9**), the two methine protons on the last inserted LA unit (H_a (5.18 ppm) and H_b (5.43 ppm)) could not be unambiguously distinguished as quartets due to overlapping signals with polymer chains of various chain lengths. Interestingly, only one set of signals for the Tpm^{*d} ligand was observed due to the fact that the relative spatial orientation of the -OC<u>H</u> and C<u>H</u>Me protons on the chain end made negligible difference to the chemical shifts of the resulting polymeryl chain. Clear identification of the -OC<u>H</u> and C<u>H</u>Me protons on the 2-methylcyclohexanoxide chain end was hampered by the presence of overlapping signals for $B(Cy\text{-}H)_3$. Quenching the reaction with HCl in Et_2O resulted in the generation of a polymer chain which was end-capped with a hydroxy group at one end and a 2-methylcyclohexanoxide terminus at the other. The hydroxy proton could be observed as a broad signal at 2.85 ppm whereas the OC<u>H</u> proton on the 2-methylcyclohexanoxide terminus was obscured by $B(Cy\text{-}H)_3$. As expected, the disappearance of the peaks at 5.43 and 5.18 ppm was consistent with the breakage of Mg-O bond, resulting in only one PLA methine signal in the ^1H NMR spectrum (Figure 3.27, c).

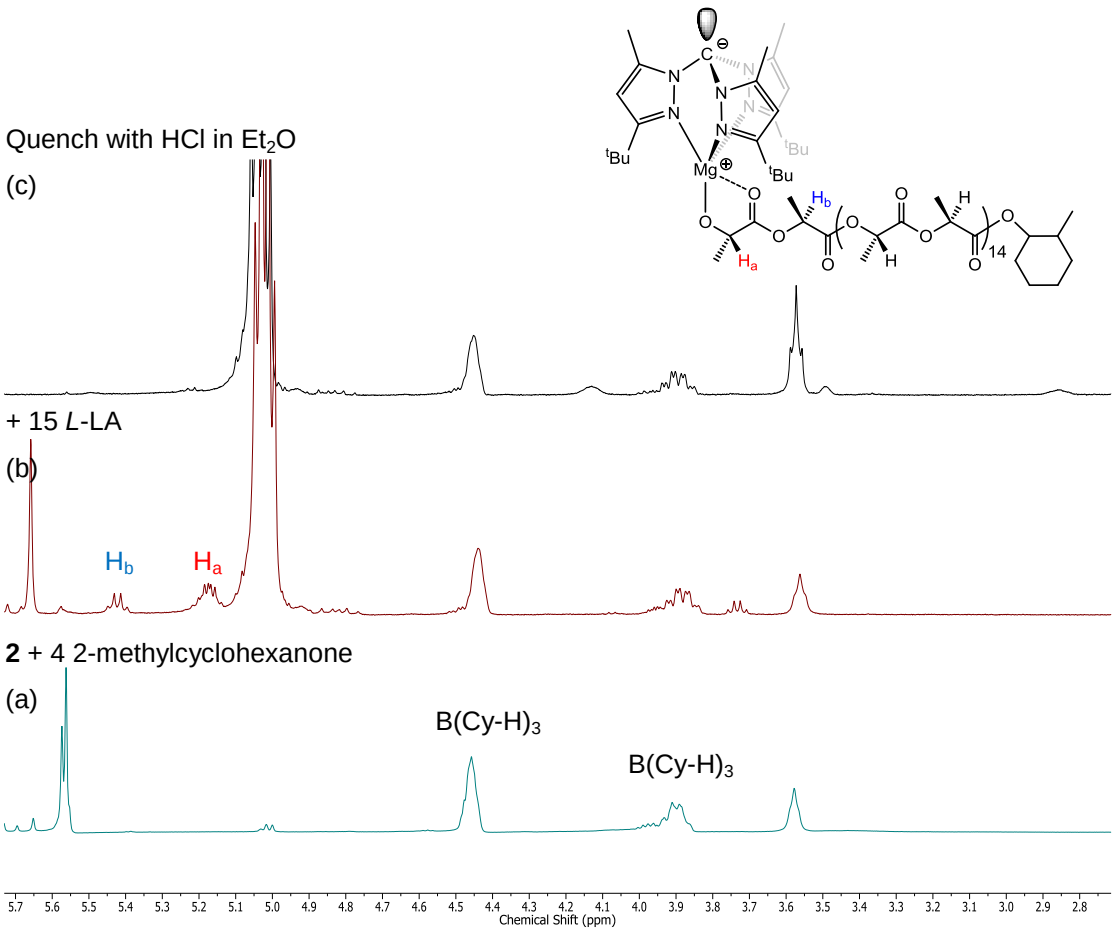


Figure 3.27 ^{1}H NMR spectrum (C_6D_6, 400.2 MHz, 298 K) (a) of the reaction between (Tpm*^{d})Mg(BH_4) (**2**) and 4 equiv. of 2-methylcyclohexanone. ^{1}H NMR spectrum (C_6D_6, 400.2 MHz, 298 K) (b) of (Tpm*^{d})Mg[LA]$_{15}$Cy-H formed after the addition of 15 equiv. of *L*-LA to the *in-situ* generated (Tpm*^{d})Mg(Cy-H) (**12**). ^{1}H NMR spectrum (C_6D_6, 400.2 MHz, 298 K) (c) of H[LA]$_{15}$Cy-H obtained after quenching (Tpm*^{d})Mg[LA]$_{15}$Cy-H with HCl in Et_2O.

MALDI-ToF mass spectrometry analysis of the quenched polymer subsequently confirmed the identity of the 2-methylcyclohexanoxide end group, in conjunction with the presence of intermolecular transesterification, as evidenced by repeating units with $\Delta(m/z)$ = 72 g mol^{-1}. The peak at 1451 g mol^{-1} was assigned to a polymer containing 9 LA repeating units with a 2-methylcyclohexanoxide terminus at one end and a hydroxy group at the other. These results, as well as the NMR spectroscopic observations, clearly confirmed the ability of the bulky 2-methylcyclohexanoxide to act as an initiator. The corresponding large scale polymerisation using the *in-situ* generated **12** and B(Cy-H)$_3$ will be discussed in Section 3.6.2.3.

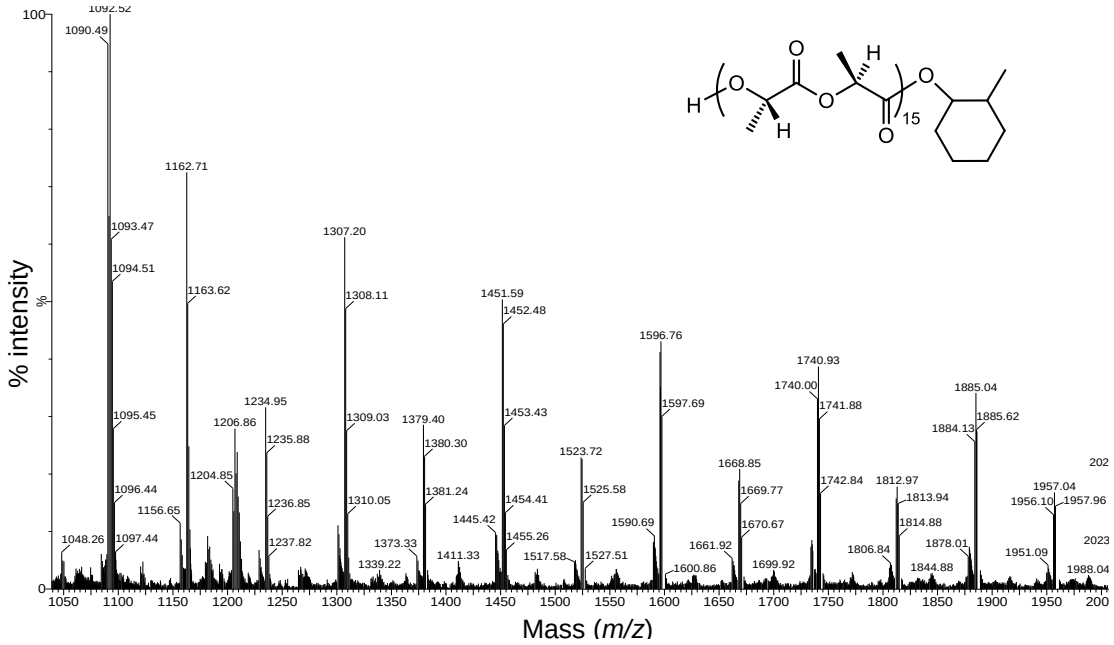
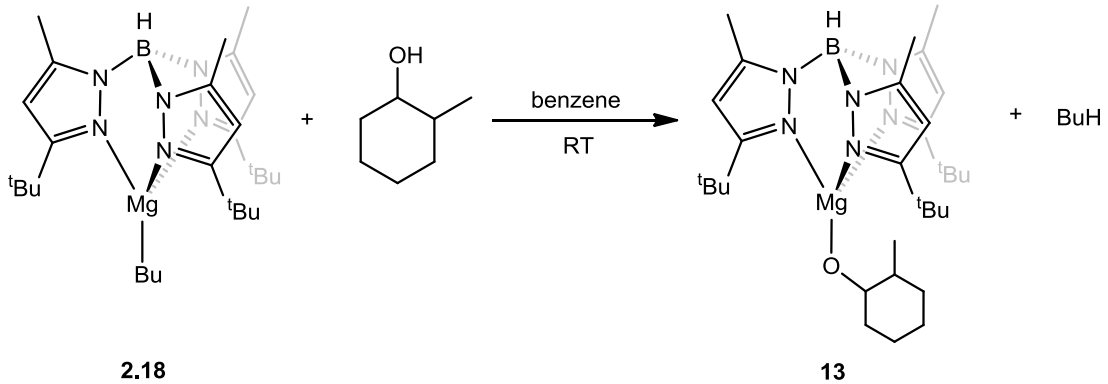


Figure 3.28 MALDI-ToF MS of the PLA synthesised by adding 15 equiv. of *L*-LA to the *in-situ* generated (Tpm*^{d})Mg(Cy-H) (**12**) and B(Cy-H)$_3$. K^+ dopant, Δ(*m/z*) = 72 g mol^{-1}.

Hampered by the difficulties encountered in the isolation of (Tpm*^{d})Mg(Cy-H) (**12**), synthesis of an analogous compound (Tp^{tBu,Me})Mg(Cy-H) (**13**) was attempted in order to gain further structural understanding of such alkoxide species. This was achieved *via* the protonolysis reaction between (Tp^{tBu,Me})Mg(Bu) (**2.18**) and a mixture of *cis* and *trans* 2-methylcyclohexanol in 1:1 stoichiometry in benzene. Compound **13** was obtained as a white solid in 75% isolated yield after washing with pentane.



Equation 3.2

The ^{11}B NMR spectrum (C_6D_6) of **13** revealed a single resonance (doublet) at -9.4 ppm, characteristic of the apical B-H. The presence of two chiral centres gave rise to four diastereomers (two sets of enantiomers), leading to the evolution of two distinct sets of signals (*cis* and *trans* isomers) in a 1:1 ratio in the ^{1}H NMR spectrum in C_6D_6 (Figure 3.29, c). The OCH proton of the *cis* isomer was observed as a doublet of triplets ($^3J_{H\text{-}H}$ = 10.4 Hz and 4.0 Hz) at 4.47 ppm, due to coupling with the neighbouring CHMe and OCHCH$_2$ protons. The CHMe proton for the *cis* isomer appeared as a multiplet with a chemical shift of 2.60 ppm whilst signals corresponding to the diastereotopic OCHCH$_2$ protons could be observed at 1.94 and 1.70 ppm. The distinct doublet at 1.43 ppm ($^3J_{H\text{-}H}$ = 7.0 Hz) could be attributed to the CHMe protons on the 2-methylcyclohexanoxide ring for the *cis* isomer.

In contrast, a triplet of doublets corresponding to the OCH proton for the *trans* isomer was visible at 3.93 ppm, with $^3J_{H\text{-}H}$ = 8.8 Hz and 4.0 Hz. The diastereotopic OCHCH$_2$ protons for the *trans* isomers were observed as multiplets at 2.52 and 1.75 ppm whereas the signal for the CHMe proton appeared as a multiplet at 1.86 ppm. The corresponding CHMe protons on the 2-methylcyclohexanoxide ring were clearly identified as a doublet ($^3J_{H\text{-}H}$ = 6.6 Hz) at 1.48 ppm.

1D nOe NMR spectroscopy (Figure 3.29, a and b) was subsequently performed to gain further understanding of the relative spatial arrangements of the protons on the 2-methylcyclohexnoxide unit. A nOe was observed between the OCH and CHMe protons for the *cis* isomer whereas no through-space correlation existed between these two protons for the *trans* isomer (red squares in Figure 3.29), providing strong evidence for the aforementioned assignments. A nOe was also observed between the OCH and the OCHCH$_2$ at 1.94 ppm for the *cis* isomer, as well as the OCH and the OCHCH$_2$ at 2.52 ppm for the *trans* isomer (blue squares).

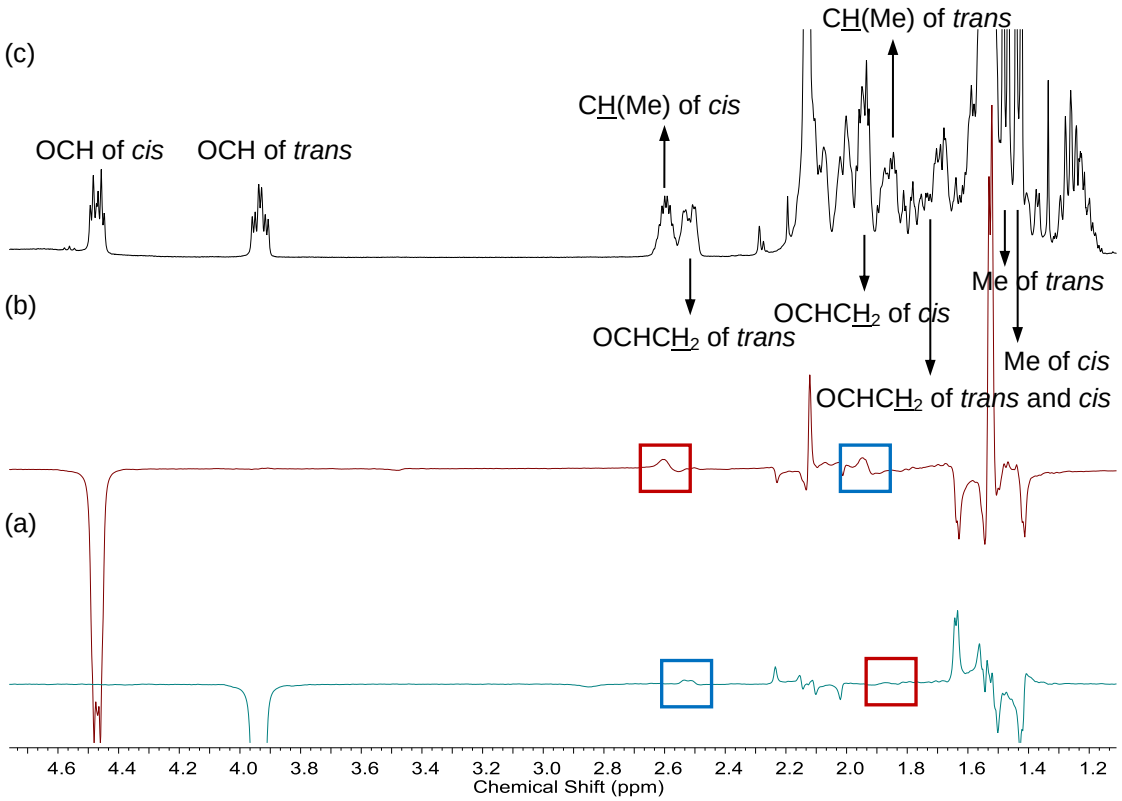


Figure 3.29 1D nOe NMR spectra (C_6D_6, 500.0 MHz, 298 K) (a) and (b) of ($Tp^{tBu,Me}$)Mg(Cy-H) (**13**). ^{1}H NMR spectrum (C_6D_6, 500.0 MHz, 298 K) (c) of **13**.

3.6.2.2 Polymer end group analysis

Following the successful identification of (Tpm*^{d})Mg(*L*-LA-H) (**10**) using various NMR spectroscopic techniques, investigations were carried out to evaluate its initiating ability in LA ROP. This was indirectly achieved *via* end group analysis of the resulting polymer obtained by adding 15 equiv. of *L*-LA to **2** in THF-d_8. The ^{1}H NMR spectrum (Figure 3.30, a) recorded after 16 h revealed the presence of two doublets at 5.62 and 5.52 ppm, corresponding to the OC<u>H</u> protons of the non-opened LA ring end group and "B(LA-H)$_3$", respectively. These assignments were confirmed by deuterium labelling experiments using **2-*d*$_4$** and 15 equiv. of *L*-LA, the ^{1}H NMR spectrum (Figure 3.30, b) of which after 16 h revealed the absence of such doublets at 5.62 and 5.52 ppm. The ^{2}H NMR spectrum (Figure 3.30, c) in protio-THF demonstrated the presence of several signals. As expected, the OC<u>D</u> deuterium nuclei were observed as two overlapping broad humps in the region of 5.50-5.70 ppm, in good agreement with the corresponding proton signals observed in the ^{1}H NMR spectrum of **2** and 15 equiv. of *L*-LA. In conjunction with this, a broad signal was present at 4.19 ppm, which was assigned to the methylene deuterium nuclei

M[LA]$_n$OCH(Me)C(O)OCH(Me)C<u>D</u>$_2$OH in α,ω-dihydroxytelechelic PLA. As mentioned previously in Section 3.2.3, an α,ω-dihydroxytelechelic PLA was formed *via* two successive hydride transfers followed by ring-opening of LA. The observed chemical shift at 4.19 ppm in this case was in good agreement with that (4.10 ppm) for the PLA obtained using an oxazoline ligand-supported magnesium borohydride catalyst previously reported in the group.[117] The signal at 3.62 ppm in the ^{2}H NMR spectrum was attributed to residual THF-d_8.

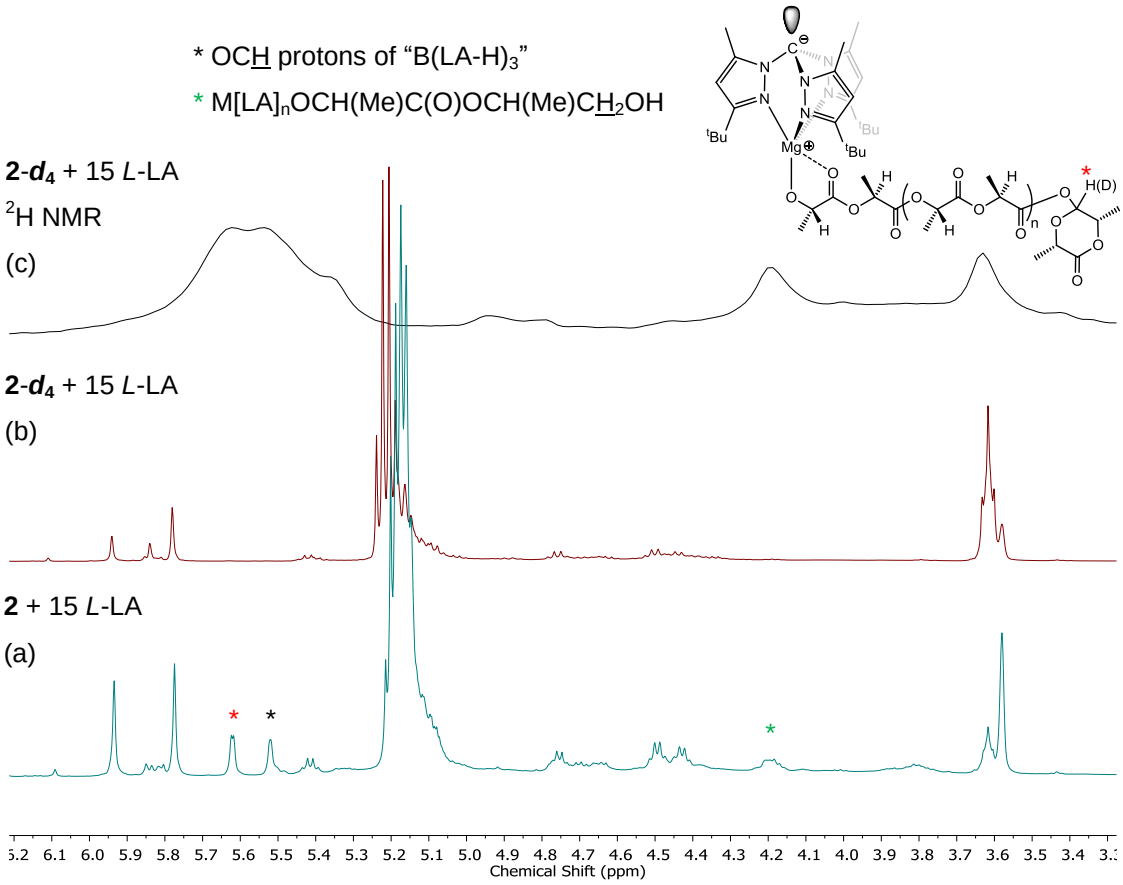


Figure 3.30 ^{1}H NMR spectrum (THF-d_8, 500.0 MHz, 298 K) of the reaction between (a) (Tpm*^{d})Mg(BH$_4$) (**2**) or (b) (Tpm*^{d})Mg(BD$_4$) (**2-*d*$_4$**) and 15 equiv. of *L*-LA. ^{2}H NMR spectrum (THF, 76.7 MHz, 298 K) (c) of the reaction between (Tpm*^{d})Mg(BD$_4$) (**2-*d*$_4$**) and 15 equiv. of *L*-LA. "*" denotes the OC<u>H</u> proton of the non-opened LA ring chain end. "*" denotes the OC<u>H</u> protons of "B(LA-H)$_3$". "*" denotes M[LA]$_n$OCH(Me)C(O)OCH(Me)C<u>H</u>$_2$OH.

Large scale polymerisations of *rac*-LA ([*rac*-LA]$_0$:[**2** or **2-*d*$_4$**]$_0$ = 100:1) initiated by **2-*d*$_4$** were subsequently performed and compared with the results obtained using **2**. Complex **2-*d*$_4$** was moderately active, reaching 88% conversion in 6 h (*cf.* 90%

conversion in 6 h for **2**). Close examination of the kinetic plots revealed the absence of any kinetic isotope effect. This provided further evidence that the first hydride transfer step was not rate-limiting. The polymerisation using **2-*d*$_4$** was found to demonstrate a first order dependence on *rac*-LA concentration after an initial induction period (k_{obs} = 0.598(13) h^{-1}, R^2 = 0.998 using **2-*d*$_4$** *cf.* k_{obs} = 0.624(26) h^{-1}, R^2 = 0.993 using **2**). A linear relationship between % conversion and M_n was observed, with a gradient of 70(2) g mol^{-1} (% conversion)$^{-1}$ (*cf.* 67(1) g mol^{-1} (% conversion)$^{-1}$ using **2**). However, the experimental M_n was lower than that expected based on one chain being produced per metal centre, suggesting possible chain transfer effects. Comparisons of both M_n and kinetic data using **2** and **2-*d*$_4$** are presented in Figures 3.31 and 3.32, respectively.

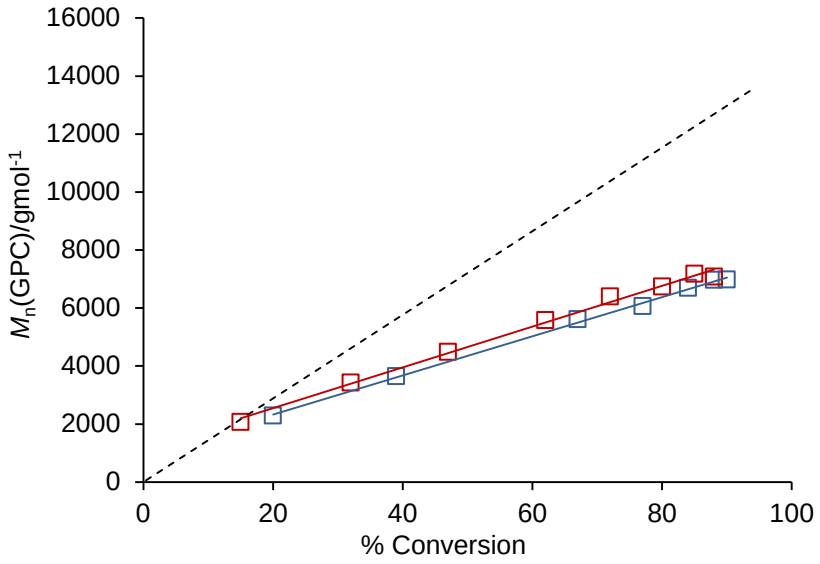


Figure 3.31 Data for the ROP of *rac*-LA using (Tpm*^{d})Mg(BH$_4$) (**2**) and (Tpm*^{d})Mg(BD$_4$) (**2-*d*$_4$**). M_n (GPC) *vs.* % conversion plot. The dashed line represents the M_n expected for one chain per metal centre. Blue squares represent data for **2**. Red squares represent data for **2-*d*$_4$**. Conditions: [*rac*-LA]$_0$:[**2** or **2-*d*$_4$**]$_0$ = 100:1, [*rac*-LA]$_0$ = 0.5 M, [**2** or **2-*d*$_4$**]$_0$ = 0.005 M, 6 mL THF at room temperature. Gradient = 67(1) g mol^{-1} (% conversion)$^{-1}$ for **2** and 70(2) g mol^{-1} (% conversion)$^{-1}$ for **2-*d*$_4$**.

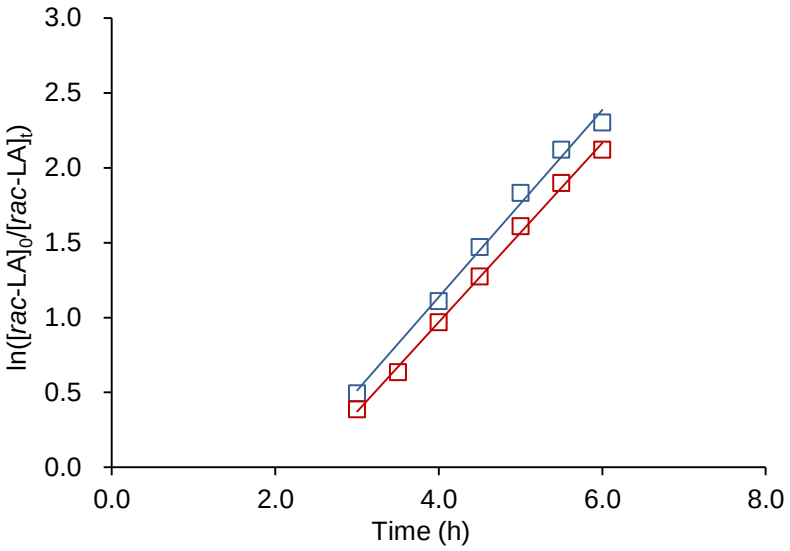


Figure 3.32 Data for the ROP of *rac*-LA using (Tpm*^{d})Mg(BH$_4$) (**2**) and (Tpm*^{d})Mg(BD$_4$) (**2-*d*$_4$**). Semilogarithmic first-order plot of ln([*rac*-LA]$_0$/[*rac*-LA]$_t$) *vs*. time (k_{obs} = 0.624(26) h^{-1}, R^2 = 0.993 using **2** *cf.* k_{obs} = 0.598(13) h^{-1}, R^2 = 0.998 using **2-*d*$_4$**). Blue squares represent data for **2**. Red squares represent data for **2-*d*$_4$**. Conditions: [*rac*-LA]$_0$:[**2** or **2-*d*$_4$**]$_0$ = 100:1, [*rac*-LA]$_0$ = 0.5 M, [**2** or **2-*d*$_4$**]$_0$ = 0.005 M, 6 mL THF at room temperature.

Further attempts to characterise polymer end groups were undertaken using NMR spectroscopy and MALDI-ToF mass spectrometry. Large scale polymerisations with [*rac*-LA]$_0$:[**2** or **2-*d*$_4$**]$_0$ = 15:1 were performed in THF followed by polymer isolation. For the polymerisation where **2** was used as the catalyst, multiple doublet signals corresponding to the OC<u>H</u> proton on the non-opened LA chain end were observed in the diagnostic region of 5.40-5.60 ppm in the ^{1}H NMR spectrum ($CDCl_3$, 298 K) (Figure 3.33, a), suggesting the formation of polymers with various chain lengths. The assignments for these protons were confirmed by deuterium labelling experiments using **2-*d*$_4$**, revealing the absence of such doublets in the ^{1}H NMR spectrum (Figure 3.33, b) and the presence of a broad signal in the ^{2}H NMR spectrum (Figure 3.33, c) of the isolated polymer. The two C<u>H</u>Me protons on the non-opened LA ring chain end of both H[LA]$_n$(LA-H) and H[LA]$_n$(LA-D) could be observed as overlapping multiplets at 4.34 ppm in the ^{1}H NMR spectrum. In addition, the peak at 4.17 ppm in the ^{1}H NMR spectrum of the isolated polymer obtained using **2** was postulated to correspond to the methylene protons H[LA]$_n$OCH(Me)C(O)OCH(Me)C<u>H$_2$</u>OH for the α,ω-dihydroxytelechelic PLA formed *via* two successive hydride transfer. In good

agreement with this was the presence of a broad signal with an identical chemical shift in the ^{2}H NMR spectrum (Figure 3.33, c) of the final polymer obtained using **2-*d*$_4$**. The hydroxy chain ends of the polymer could be observed in the region of 2.70-2.72 ppm as two overlapping broad signals in the ^{1}H NMR spectrum (Figure 3.33, a and b).

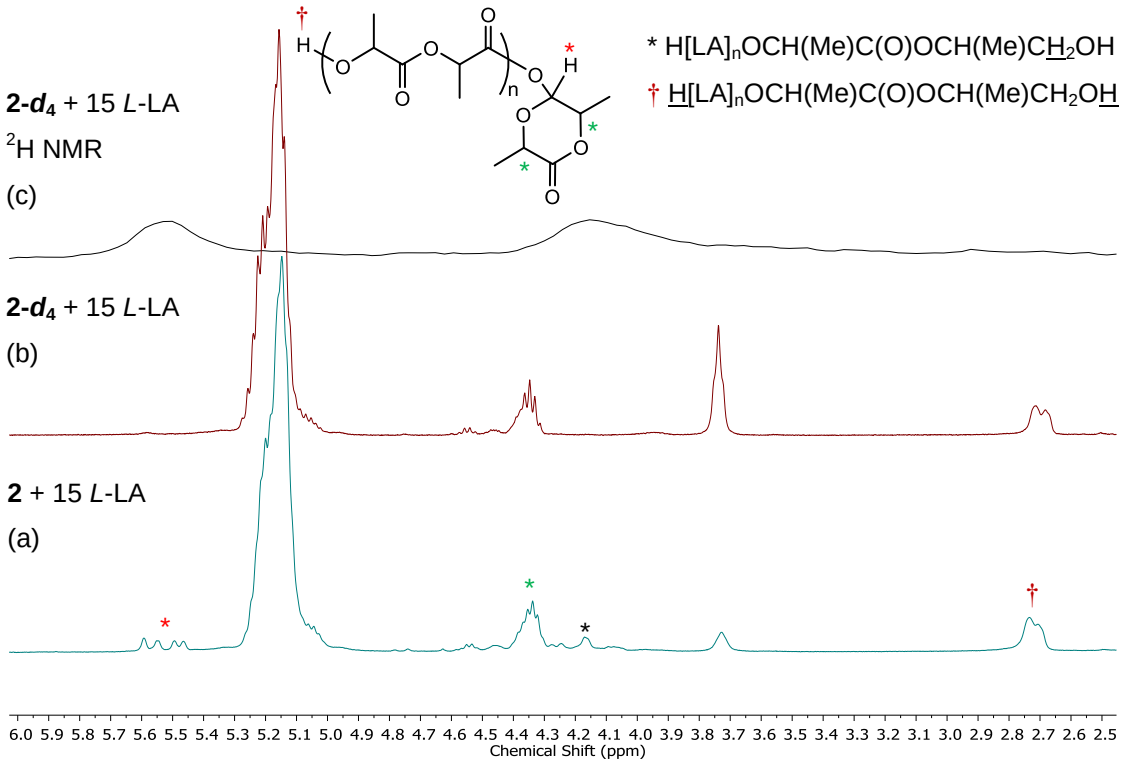


Figure 3.33 ^{1}H NMR spectra ($CDCl_3$, 500.0 MHz, 298 K) of the isolated (a) H[LA]$_n$(LA-H) and (b) H[LA]$_n$(LA-D) obtained *via* the large scale polymerisations of **2** or **2-*d*$_4$** with 15 equiv. of *rac*-LA. ^{2}H NMR spectrum ($CHCl_3$, 76.7 MHz, 298 K) (c) of the isolated H[LA]$_n$(LA-D). Conditions: [*rac*-LA]$_0$:[**2** or **2-*d*$_4$**]$_0$ = 15:1, [*rac*-LA]$_0$ = 0.5 M, [**2** or **2-*d*$_4$**]$_0$ = 0.033 M, 2.8 mL THF at room temperature. "*" and "*" denote OCH and CHMe protons of the non-opened LA ring chain end, respectively. "*" denotes H[LA]$_n$OCH(Me)C(O)OCH(Me)CH$_2$OH. "†" denotes hydroxy end groups.

MALDI-ToF MS analysis of the isolated polymer obtained using **2** or **2-*d*$_4$** and 15 equiv. of *rac*-LA showed peaks corresponding to both α,ω-dihydroxytelechelic PLA and H[LA]$_n$(LA-H/D). Figure 3.34 illustrates a MALDI-ToF mass spectrum of the polymer obtained using **2-*d*$_4$.** For example, the peak envelope centred at 907 g mol^{-1} could be assigned to a polymer chain containing 5 LA units with a hydroxy group terminated at one end and a LA-D unit at the other whereas the corresponding α,ω-

dihydroxytelechelic PLA was visible at around 909 g mol^{-1}. Intermolecular transesterification side reactions were also observed with peak envelopes of $\Delta(m/z)$ = 72 g mol^{-1}.

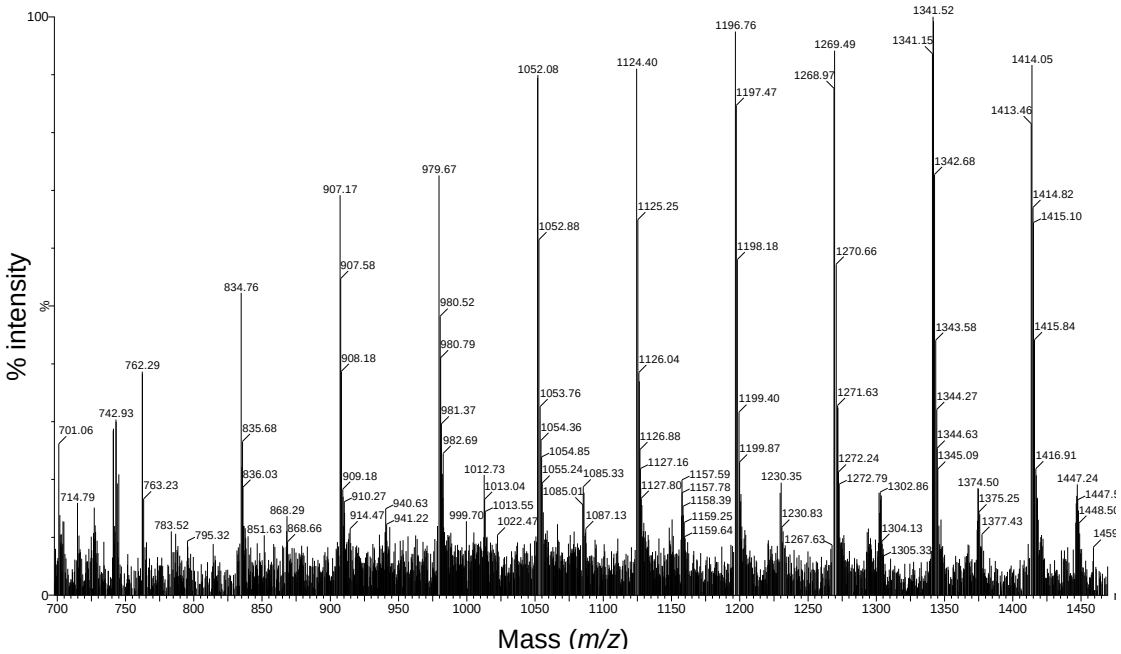


Figure 3.34 MALDI-ToF MS of the PLA obtained from the large scale polymerisation of (Tpm*^{d})Mg(BD$_4$) (**2-*d*$_4$**) with 15 equiv. of *rac*-LA. Conditions: [*rac*-LA]$_0$:[**2-*d*$_4$**]$_0$ = 15:1, [*rac*-LA]$_0$ = 0.5 M, [**2-*d*$_4$**]$_0$ = 0.033 M, 2.8 mL THF at room temperature. K^+ dopant.

3.6.2.3 Chain transfer ability of "B(LA-H)$_3$"

As mentioned previously, the large scale ROP results for *rac*-LA using both **2** and **2-*d*$_4$** as initiators suggested the occurrence of chain transfer events, as evidenced by the lower than expected M_n based on one chain being produced per metal centre. The role of "B(LA-H)$_3$" as a chain transfer agent was initially proposed by Dr J. Unruangsri based on detailed studies using a range of borate ester species and various Tp^{tBu,Me}-supported magnesium initiators.[70] However, the chain transfer ability of bulky borate ester species has never been thoroughly studied. Due to the difficulties encountered in the isolation of the borate ester featuring three non-opened LA units, an alternative approach was adopted by adding 15 equiv. of *L*-LA to the *in-situ* generated (Tpm*^{d})Mg(Cy-H) (**12**) and B(Cy-H)$_3$, obtained by reacting **2** with 4 equiv. of 2-methylcyclohexanone in C_6D_6. 1 equiv. of 1,4-dimethoxybenzene was also added to the reaction mixture as an internal standard to facilitate quantitative comparison.

Assuming observable chain transfer, it was expected that signals corresponding to $B(Cy\text{-}H)_n(Polym)_{3-n}$ would arise upon addition of 15 equiv. of *L*-LA as a result of the exchange between $B(Cy\text{-}H)_3$ and the growing polymeryl chain. However, no evidence for the formation of such species was obtained and very minor changes in the integration of $B(Cy\text{-}H)_3$ signals were observed before and after LA addition, indicating negligible chain transfer effect, shown in Figure 3.35.

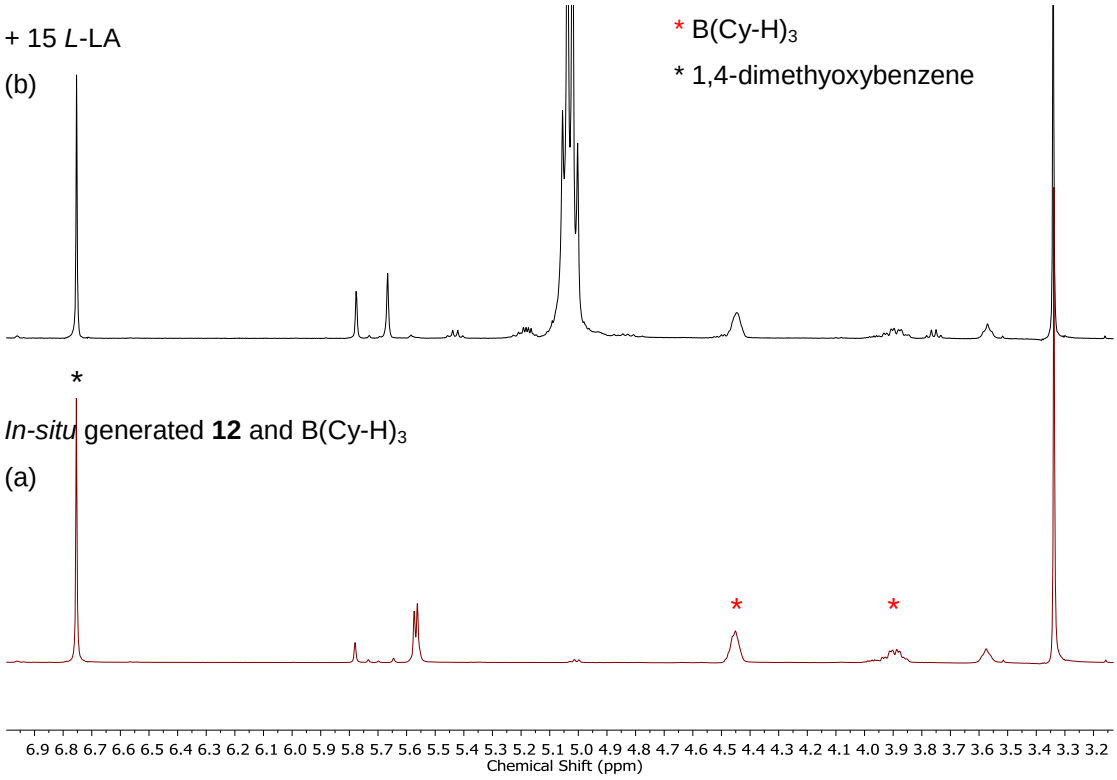


Figure 3.35 ^1H NMR spectrum (C_6D_6, 400.2 MHz, 298 K) (a) of the *in-situ* generated (Tpm*^{d})Mg(Cy-H) (**12**) and $B(Cy\text{-}H)_3$. ^1H NMR spectrum (C_6D_6, 400.2 MHz, 298 K) (b) of the resulting polymeryl chain after addition of 15 equiv. of *L*-LA. "*" denotes $B(Cy\text{-}H)_3$ generated *in-situ*. "*" denotes 1,4-dimethoxybenzene.

The corresponding large scale polymerisation was subsequently investigated ([*rac*-LA]$_0$:[**2**]$_0$:[2-methylcyclohexanone]$_0$ = 100:1:4). 92% of *rac*-LA (100 equiv.) was polymerised within 7 min, indicating the high activity of this *in-situ* generated catalytic system. The polymerisation was found to demonstrate a first order dependence on *rac*-LA concentration (k_{obs} = 0.0067(2) s^{-1}, R^2 = 0.994). A linear relationship (gradient = 96(2) g mol^{-1} (% conversion)$^{-1}$, R^2 = 0.997) between % conversion and M_n was observed up to 80% conversion, after which tailing-off occurred due to transesterification side reactions. The experimental M_n was much

higher than the expected value based on four chains being produced per metal centre. These large scale polymerisation results were consistent with the NMR studies discussed previously, confirming that bulky borate ester species, such as $B(Cy\text{-}H)_3$, demonstrated poor chain transfer ability for the ROP of LA using Tpm*^{d} systems.

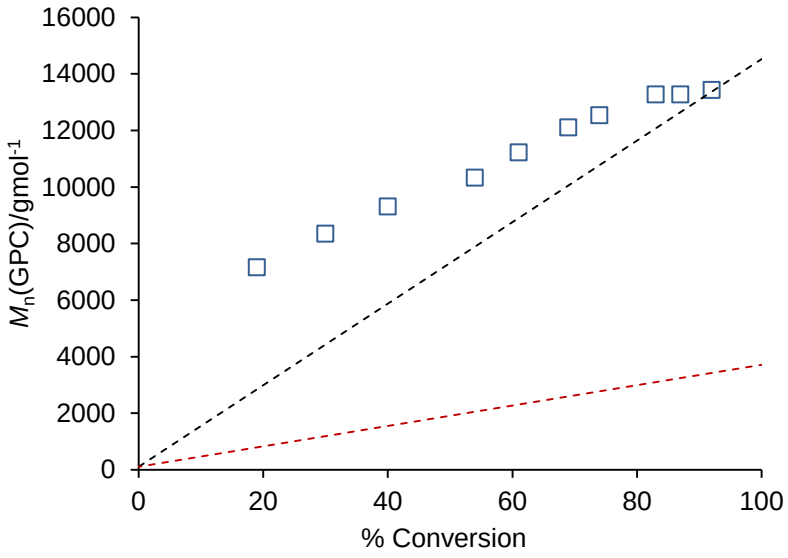


Figure 3.36 Data for the ROP of *rac*-LA using (Tpm*^{d})Mg(BH_4) (**2**) and 4 equiv. of 2-methylcyclohexanone. M_n (GPC) *vs.* % conversion plot. The dashed lines represent the M_n expected for one chain (black) or four chains (red) per metal centre. Conditions: [*rac*-LA]$_0$:[**2**]$_0$:[2-methylcyclohexanone]$_0$ = 100:1:4, [*rac*-LA]$_0$ = 0.5 M, [**2**]$_0$ = 0.005 M, 6 mL THF at room temperature.

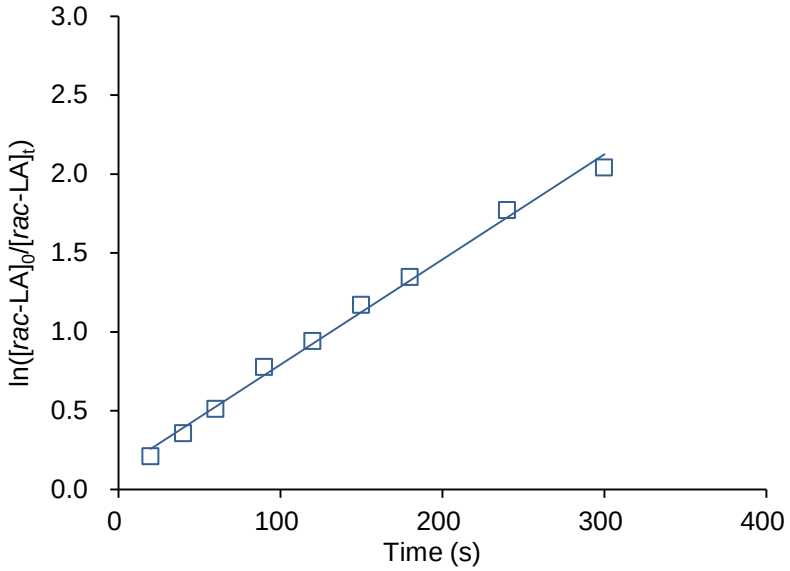


Figure 3.37 Data for the ROP of *rac*-LA using (Tpm*^{d})Mg(BH$_4$) (**2**) and 4 equiv. of 2-methylcyclohexanone. Semilogarithmic first-order plot of ln([*rac*-LA]$_0$/[*rac*-LA]$_t$) *vs*. time (k_{obs} = 0.0067(2) s^{-1}, R^2 = 0.994). Conditions: [*rac*-LA]$_0$:[**2**]$_0$:[2-methylcyclohexanone]$_0$ = 100:1:4, [*rac*-LA]$_0$ = 0.5 M, [**2**]$_0$ = 0.005 M, 6 mL THF at room temperature.

3.6.3 Rate differences in the ROP of *rac*-LA using (Tpm*^{d})Mg(BH$_4$) (2) and (Tpm*^{d})Mg(OBn) (5)

Detailed mechanistic studies discussed above have shown clear evidence that the active species for the ROP of *rac*-LA initiated by **2** is the alkoxide species (Tpm*^{d})Mg(LA-H). Therefore, it was expected that the rate of polymerisation for **2** should be comparable to that for **5** after the initial induction period. Nevertheless, the observed first order rate constant (k_{obs}) of the latter was found to be 300 times greater than that of the former. The origin of the significant difference was attributed to partial activation of **2**. As evidenced by the ^{1}H NMR spectrum between **2** and 5 equiv. of *L*-LA in C_6D_6, the spontaneous generation of **10** was accompanied by the occurrence of side reactions, liberating other unidentifiable species over the course of 3 h. Consistently, the ^{11}B NMR spectrum revealed the presence of several other signals apart from the major peak corresponding to "B(LA-H)$_3$". It was therefore postulated that not all of **2** was converted to the active catalyst **10**. The formation of other side products would result in a lower concentration of **10** and hence, a lower polymerisation rate. Typically, a decrease in the concentration of the active catalyst

would result in the formation of polymers with higher than expected M_n based on all complexes acting as active initiators. However, this was not observed; the experimental M_n was almost half of the calculated value based on one chain per metal centre, which was attributed to chain transfer effects induced by "B(LA-H)$_3$". NMR experiments and large scale polymerisations using the *in-situ* generated model system have demonstrated the inefficient chain transfer capacity of B(Cy-H)$_3$. However, it is important to note that the exact identity of "B(LA-H)$_3$" remains unclear. Even though the borate ester featuring three non-opened LA ring alkoxides possesses poor chain transfer ability, the same cannot be assumed for smaller species with ring-opened LA units. It is therefore proposed that these smaller borate ester species possess superior chain transfer ability, resulting in the formation of PLA with lower than expected M_n.

3.7 Summary and conclusions

This Chapter described the catalytic activities of both (Tpm*^{d})Mg(OBn) (**5**) and (Tpm*^{d})Mg(BH$_4$) (**2**) in the ROP of ε-CL and *rac*-LA. Compound **5** was highly active in the ROP of ε-CL and demonstrated well-controlled nature, as evidenced by the linear growth in % conversion *vs.* experimental M_n and narrow PDIs. Up to 1000 equiv. of ε-CL could be polymerised within minutes while maintaining good molecular weight control. The activity of **5** was also probed in the ROP of *rac*-, *L*- and *meso*-LA. Complex **5** was highly active in the ROP of *rac*-LA, in contrast to the electronically and structurally similar (Tp^{tBu,Me})Mg(OBn) (**2.20**). A three orders of magnitude difference in observed rate constants was found (k_{rel} = 1550) and this was attributed to the difference in the size or flexibility of the coordination sphere of the catalysts during the polymerisation. A higher than expected M_n was observed, in conjunction with a broad PDI. These results indicated that the rate of initiation was much slower than that of propagation, therefore resulting in the formation of polymers of various chain lengths. Analysis using MALDI-ToF mass spectrometry clearly revealed the presence of the anticipated -OBn end group. No transesterification was observed due to the mismatch between the rates of propagation and exchange. ^{1}H{^{1}H} NMR spectroscopy demonstrated the microstructure of the polymer to be heterotactic, indicating the presence of a chain end control mechanism. This is consistent with the fact that the ROP of *rac*-LA was faster than that of *L*-LA, suggesting the preference of the catalyst to enchain LA *via* a *racemic* as opposed to a *meso* linkage. The ROP of *meso*-LA was also performed, leading to the formation of syndiotactic PLA, as

expected. ^{1}H NMR studies were subsequently carried out to gain mechanistic insight into the ROP of LA using **5**. This was achieved by the addition of 5 equiv. of *L*-LA to **5** in C_6D_6 to generate a short polymeryl chain (Tpm*^{d})Mg[LA]$_5$OBn (**9**). Slight catalyst decomposition was found, which could also explain the higher than expected M_n observed in the large scale polymerisation.

The catalytic activity of (Tpm*^{d})Mg(BH_4) (**2**) was probed in the ROP of ε-CL. Complex **2** was found to be highly active despite demonstrating poor molecular weight control in terms of producing polymers with higher than expected M_n and broad PDIs. In addition, end group analysis through MALDI-ToF MS confirmed the resulting polymer to be α,ω-dihydroxytelechelic. Mechanistic studies were subsequently carried out by adding 15 equiv. of ε-CL to **2** in C_6D_6. The ^{11}B NMR spectrum revealed the presence of a "B(OR)$_3$" type species (OR = ring-opened ε-CL units) and (Tpm*^{d})Mg{B(OR)$_4$}. Deuterium labelling experiments employing **2-*d*$_4$** were subsequently attempted but provided little insight.

Compound **2** was moderately active in the ROP of *rac*-LA, yielding slightly heterotactic PLA. However, a long induction period was present and lower than expected M_n was observed throughout the course of the polymerisation. Mechanistic studies were therefore carried out to shed light on the unexpected behaviour of **2** in *rac*-LA ROP. The addition of 5 equiv. of *L*-LA to **2** in C_6D_6 resulted in the immediate formation of (Tpm*^{d})Mg(*L*-LA-H) (**10**) which was characterised by various NMR spectroscopic techniques. The diagnostic signals corresponding to the MgOC<u>H</u> and methine protons on the non-opened LA alkoxide were clearly identified in the ^{1}H NMR spectrum. Deuterium labelling experiments using **2-*d*$_4$** provided further evidence for the formation of the first hydride transfer product. Complexes **10** and (Tpm*^{d})Mg(*meso*-LA-H) (**10'**) were also investigated by 1D nOe NMR spectroscopy, giving expected correlation results. The reaction between **2** and 5 equiv. of *L*-LA was followed by ^{1}H and ^{11}B NMR spectroscopy over the course of 3 h, during which time side reactions occurred.

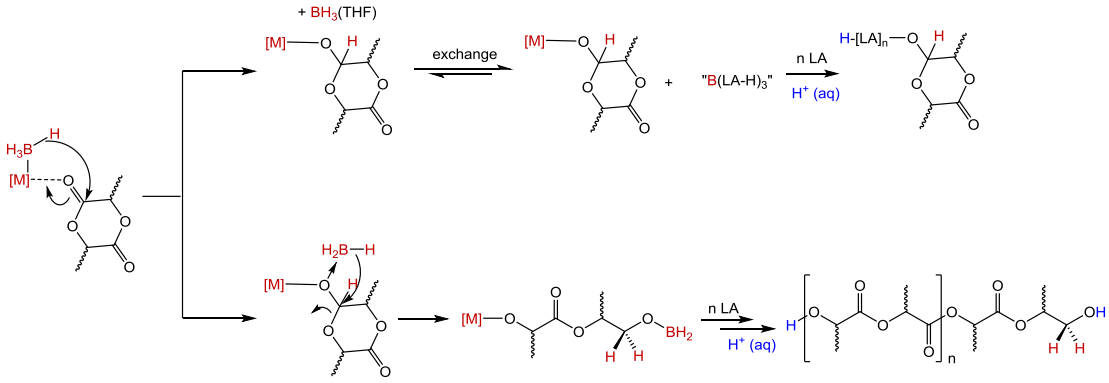
A model study was performed by reacting **2** with 4 equiv. of *L*-LA in C_6D_6 to generate (Tpm*^{d})Mg(Cy-H) (**12**) and B(Cy-H)$_3$ *in-situ*. The ^{1}H NMR spectrum clearly showed the presence of two sets of signals corresponding to **12**, the assignments of which were hampered by overlapping signals for B(Cy-H)$_3$. The

initiating ability of **12** was subsequently studied by adding 15 equiv. of *L*-LA to the *in-situ* generated catalytic system to generate a growing polymeryl chain, which was characterised by ^{1}H NMR spectroscopy. MALDI-ToF mass spectrometry analysis showed the presence of a 2-methylcyclohexanoxide end group. An analogous compound ($Tp^{tBu,Me}$)Mg(Cy-H) (**13**) was synthesised *via* a protonolysis pathway and fully characterised by NMR spectroscopic techniques.

The end groups of the resulting polymer obtained using **2** as the initiator were studied by adding 15 equiv. of *L*-LA to **2** in THF-d_8, giving rise to two characteristic doublets, corresponding to the OC<u>H</u> protons of the non-opened LA ring chain end of the polymeryl chain and "B(LA-H)$_3$". These assignments were confirmed by deuterium labelling experiments using **2-*d*$_4$**. A large scale polymerisation using **2-*d*$_4$** was carried out and compared with that using **2**. No kinetic isotope effect was observed, leading to the conclusion that the first hydride transfer step is not rate-limiting. NMR studies and MALDI-ToF MS analysis of the isolated PLA obtained using both **2** and **2-*d*$_4$** revealed the presence of a non-opened LA ring terminated polymer and α,ω-dihydroxytelechelic PLA.

The chain transfer ability of bulky borate ester species was evaluated by adding 15 equiv. of *L*-LA to the *in-situ* generated **12** and B(Cy-H)$_3$. Very minor changes in the integration of the latter were observed in the ^{1}H NMR spectrum upon addition of *L*-LA, indicating the inefficient nature of B(Cy-H)$_3$ as a chain transfer agent. This is consistent with the results obtained from the corresponding large scale polymerisation, resulting in the formation of PLA with much higher than expected M_n based on four chains being produced per metal centre.

In conclusion, the mechanism of *rac*-LA ROP initiated by **2** was thoroughly studied. The first hydride transfer step is facile, resulting in the *in-situ* generation of (Tpm*^{d})Mg(LA-H) and BH_3(THF). These two species undergo rapid exchange reactions to liberate "B(LA-H)$_3$". (Tpm*^{d})Mg(LA-H) can act as an initiator, leading to the formation of a final polymer which is terminated with a non-opened LA ring alkoxide at one end and a hydroxy group at the other. Two successive hydride transfers followed by ring-opening also occurs to generate α,ω-dihydroxytelechelic PLA.



Scheme 3.5 Mechanisms for the ROP of LA initiated by **2** in THF.

3.8 References for Chapter Three

1. P. Loxq, E. Manoury, R. Poli, E. Deydier and A. Labande, *Coord. Chem. Rev.*, 2016, **308**, 131.
2. S. Kaufhold, L. Petermann, R. Staehle and S. Rau, *Coord. Chem. Rev.*, 2015, **304–305**, 73.
3. M. S. Khan, A. Haque, M. K. Al-Suti and P. R. Raithby, *J. Organomet. Chem.*, 2015, **793**, 114.
4. Y.-Y. Li, S.-L. Yu, W.-Y. Shen and J.-X. Gao, *Acc. Chem. Res.*, 2015, **48**, 2587.
5. D. Zhang and Q. Wang, *Coord. Chem. Rev.*, 2015, **286**, 1
6. M. Amatore and C. Aubert, *Eur. J. Org. Chem.*, 2015, **2015**, 265.
7. Y.-M. He, Y. Feng and Q.-H. Fan, *Acc. Chem. Res.*, 2014, **47**, 2894.
8. Q.-H. Deng, R. L. Melen and L. H. Gade, *Acc. Chem. Res.*, 2014, **47**, 3162.
9. C.-X. Zhuo, C. Zheng and S.-L. You, *Acc. Chem. Res.*, 2014, **47**, 2558.
10. J. S. Arnold, Q. Zhang and H. M. Nguyen, *Eur. J. Org. Chem.*, 2014, **2014**, 4925.
11. A. Pradal, S. Gladiali, V. Michelet and P. Y. Toullec, *Chem. Eur. J.*, 2014, **20**, 7128.
12. Z.-J. Yao and G.-X. Jin, *Coord. Chem. Rev.*, 2013, **257**, 2522.
13. S. Harder, *Chem. Rev.*, 2010, **110**, 3852.
14. C. A. Wheaton, P. G. Hayes and B. J. Ireland, *Dalton Trans.*, 2009, 4832.
15. B. J. Ireland, C. A. Wheaton and P. G. Hayes, *Organometallics*, 2010, **29**, 1079.

16. A. Torvisco, A. Y. O'Brien and K. Ruhlandt-Senge, *Coord. Chem. Rev.*, 2011, **255**, 1268.
17. Y. Yamashita, T. Tsubogo and S. Kobayashi, *Chem. Sci.*, 2012, **3**, 967.
18. S. Kobayashi and Y. Yamashita, *Acc. Chem. Res.*, 2011, **44**, 58.
19. A. G. M. Barrett, M. R. Crimmin, M. S. Hill and P. A. Procopiou, *Proceedings of the Royal Society of London A: Mathematical, Physical and Engineering Sciences*, 2010, **466**, 927.
20. J. Penafiel, L. Maron and S. Harder, *Angew. Chem. Int. Ed.*, 2015, **54**, 201.
21. C. Gallegos, V. Tabernero, M. E. G. Mosquera, T. Cuenca and J. Cano, *Eur. J. Inorg. Chem.*, 2015, **2015**, 5124.
22. R. K. Kottalanka, A. Harinath and T. K. Panda, *RSC Adv.*, 2015, **5**, 37755.
23. M. Lamberti, A. Botta and M. Mazzeo, *Appl. Organomet. Chem.*, 2014, **28**, 140.
24. J. Wojtaszak, K. Mierzwicki, S. Szafert, N. Gulia and J. Ejfler, *Dalton Trans.*, 2014, **43**, 2424.
25. Y. Wang, B. Liu, X. Wang, W. Zhao, D. Liu, X. Liu and D. Cui, *Polym. Chem.*, 2014, **5**, 4580.
26. M. H. Chisholm and N. W. Eilerts, *Chem. Commun.*, 1996, 853.
27. M. H. Chisholm, J. Gallucci and K. Phomphrai, *Chem. Commun.*, 2003, 48.
28. B. M. Chamberlain, M. Cheng, D. R. Moore, T. M. Ovitt, E. Lobkovsky and G. W. Coates, *J. Am. Chem. Soc.*, 2001, **123**, 3229.
29. M. H. Chisholm, K. Choojun, J. C. Gallucci and P. M. Wambua, *Chem. Sci.*, 2012, **3**, 3445.
30. H. Xie, Z. Mou, B. Liu, P. Li, W. Rong, S. Li and D. Cui, *Organometallics*, 2014, **33**, 722.
31. D. J. Darensbourg, W. Choi, O. Karroonnirun and N. Bhuvanesh, *Macrmolecules*, 2008, **41**, 3493.
32. L. Wang and H. Ma, *Macromolecules*, 2010, **43**, 6535.
33. V. Poirier, T. Roisnel, J.-F. Carpentier and Y. Sarazin, *Dalton Trans.*, 2009, 9820.
34. J.-C. Wu, B.-H. Huang, M.-L. Hsueh, S.-L. Lai and C.-C. Lin, *Polymer*, 2005, **46**, 9784.
35. W. Yi and H. Ma, *Inorg. Chem.*, 2013, **52**, 11821.

36. Y. Sarazin, B. Liu, T. Roisnel, L. Maron and J.-F. Carpentier, *J. Am. Chem. Soc.*, 2011, **133**, 9069.
37. Y. Sarazin, V. Poirier, T. Roisnel and J.-F. Carpentier, *Eur. J. Inorg. Chem.*, 2010, 3423.
38. W. Yi and H. Ma, *Dalton Trans.*, 2014, **43**, 5200.
39. A. Amgoune, C. M. Thomas and J.-F. Carpentier, *Pure Appl. Chem.*, 2007, **79**, 2013.
40. I. Palard, A. Soum and S. M. Guillaume, *Macromolecules*, 2005, **38**, 6888.
41. S. D. Bennett, B. A. Core, M. P. Blake, S. J. A. Pope, P. Mountford and B. D. Ward, *Dalton Trans.*, 2014, **43**, 5871.
42. D. J. Darensbourg and O. Karroonnirun, *Inorg. Chem.*, 2010, **49**, 2360.
43. Y. Chapurina, J. Klitzke, O. d. L. Casagrande Jr, M. Awada, V. Dorcet, E. Kirillov and J.-F. Carpentier, *Dalton Trans.*, 2014, **43**, 14322.
44. F. Bonnet, A. R. Cowley and P. Mountford, *Inorg. Chem.*, 2005, **44**, 9046.
45. H. D. Dyer, S. Huijser, N. Susperregui, F. Bonnet, A. D. Schwarz, R. Duchateau, L. Maron and P. Mountford, *Organometallics*, 2010, **29**, 3602.
46. M. A. Sinenkov, G. K. Fukin, A. V. Cherkasov, N. Ajellal, T. Roisnel, F. M. Kerton, J.-F. Carpentier and A. A. Trifonov, *New J. Chem.*, 2011, **35**, 204.
47. M. V. Yakovenko, A. A. Trifonov, E. Kirillov, T. Roisnel and J.-F. Carpentier, *Inorg. Chim. Acta*, 2012, **383**, 137.
48. J. Jenter, P. W. Roesky, N. Ajellal, S. M. Guillaume, N. Susperregui and L. Maron, *Chem. Eur. J.*, 2010, **16**, 4629.
49. J. Kratsch, M. Kuzdrowska, M. Schmid, N. Kazeminejad, C. Kaub, P. Oña-Burgos, S. M. Guillaume and P. W. Roesky, *Organometallics*, 2013, **32**, 1230.
50. S. M. Guillaume, M. Schappacher and A. Soum, *Macromolecules*, 2003, **36**, 54.
51. D. Robert, M. Kondracka and J. Okuda, *Dalton Trans.*, 2008, 2667.
52. I. Palard, A. Soum and S. M. Guillaume, *Chem. Eur. J.*, 2004, **10**, 4054.
53. M. G. Cushion and P. Mountford, *Chem. Commun.*, 2011, **47**, 2276.
54. R. A. Collins, J. Unruangsri and P. Mountford, *Dalton Trans.*, 2013, **42**, 759.
55. S. Marks, M. Kuzdrowska, P. W. Roesky, L. Annunziata, S. M. Guillaume and L. Maron, *ChemPlusChem* 2012, **77**, 350.
56. M. Kuzdrowska, L. Annunziata, S. Marks, M. Schmid, C. G. Jaffredo, P. W. Roesky, S. M. Guillaume and L. Maron, *Dalton Trans.*, 2013, **42**, 9352.

57. I. Palard, M. Schappacher, A. Soum and S. M. Guillaume, *Polym. Int.*, 2006, **55**, 1132.
58. N. Barros, P. Mountford, S. M. Guillaume and L. Maron, *Chem. Eur. J.*, 2008, **14**, 5507.
59. I. Palard, M. Schappacher, B. Belloncle, A. Soum and S. M. Guillaume, *Chem. Eur. J.*, 2007, **13**, 1511.
60. G. G. Skvortsov, M. V. Yakovenko, P. M. Castro, G. K. Fukin, A. V. Cherkasov, J.-F. Carpentier and A. A. Trifonov, *Eur. J. Inorg. Chem.*, 2007, 3260.
61. A. Pelter and T. E. Levitt, *Tetrahedron*, 1970, **26**, 1545.
62. H. C. Brown, P. Heim and N. M. Yoon, *J. Am. Chem. Soc.*, 1970, **92**, 1637.
63. W. A. Remers, R. H. Roth and M. J. Weiss, *J. Am. Chem. Soc.*, 1964, **86**, 4612.
64. D.-M. Du, T. Fang, J. Xu and S.-W. Zhang, *Org. Lett.*, 2006, **8**, 1327.
65. J. Xu, T. Wei and Q. Zhang, *J. Org. Chem.*, 2003, **68**, 10146.
66. A.-L. Zhang, Z.-d. Yu, L.-W. Yang and N.-F. Yang, *Tetrahedron: Asymmetry*, 2015, **26**, 173.
67. G. Qin, Y. Chen, L. Yang, N. Yang and Z. Yang, *Chirality*, 2015, **27**, 422.
68. M. Azizoglu, A. Erdogan, N. Arslan and Y. Turgut, *Chirality*, 2014, **26**, 21.
69. A. Pinaka, D. Dimotikali, B. Chankvetadze, K. Papadopoulos and G. C. Vougioukalakis, *Synlett*, 2013, **24**, 2401.
70. J. Unruangsri, *D.Phil Thesis, University of Oxford*, 2014.
71. D. G. Hall, *Boronic acids: Preparation, Application in Organic Synthesis and Medicine*, Wiley, Weiheim, 2nd edn., 2011.
72. K. Ishihara and H. Yamamoto, *Eur. J. Org. Chem.*, 1999, **1999**, 527.
73. A. Pelter, K. Smith and H. C. Brown, *Borane Reagents*, Academic Press, 1988.
74. W. E. Piers, *Advances in Organometallic Chemistry*, Academic Press, 2004.
75. M. Yasuda, H. Nakajima, R. Takeda, S. Yoshioka, S. Yamasaki, K. Chiba and A. Baba, *Chem. Eur. J.*, 2011, **17**, 3856.
76. N. Miyaura and A. Suzuki, *Chem. Rev.*, 1995, **95**, 2457.
77. A. Suzuki, *Angew. Chem. Int. Ed.*, 2011, **50**, 6722.
78. B. W. Glasspoole and C. M. Crudden, *Nat. Chem.*, 2011, **3**, 912.
79. A. A. Oluyadi, S. Ma and C. N. Muhoro, *Organometallics*, 2013, **32**, 70.

80. M. C. Redondo, M. Veguillas, M. Ribagorda and M. C. Carreño, *Angew. Chem. Int. Ed.*, 2009, **48**, 370.
81. Y. H. Zhu and N. S. Hosmane, *Coord. Chem. Rev.*, 2015, **293**, 357.
82. C. Zhu and J. R. Falck, *Adv. Synth. Catal.*, 2014, **356**, 2395.
83. Z. H. Lu, Q. Yao, Z. J. Zhang, Y. W. Yang and X. S. Chen, *J. Nanomater.*, 2014, 11.
84. D. Olid, R. Nunez, C. Vinas and F. Teixidor, *Chem. Soc. Rev.*, 2013, **42**, 3318.
85. J. Jiao and Y. Nishihara, *J. Organomet. Chem.*, 2012, **721**, 3.
86. J. Cid, H. Gulyas, J. J. Carbo and E. Fernandez, *Chem. Soc. Rev.*, 2012, **41**, 3558.
87. W. E. Piers and T. Chivers, *Chem. Soc. Rev.*, 1997, **26**, 345.
88. X. Yang, C. L. Stern and T. J. Marks, *J. Am. Chem. Soc.*, 1991, **113**, 3623.
89. T. C. M. Chung, *Macromolecules*, 2013, **46**, 6671.
90. G. Wu, W. Sun and Z. Shen, *React. Func. Polym.*, 2008, **68**, 822.
91. R. H. Platel, L. M. Hodgson and C. K. Williams, *Polym. Rev.*, 2008, **48**, 11.
92. C. M. Thomas, *Chem. Soc. Rev.*, 2010, **39**, 165.
93. M. J. Stanford and A. P. Dove, *Chem. Soc. Rev.*, 2010, **39**, 486.
94. T. V. Mahrova, G. K. Fukin, A. V. Cherkasov, A. A. Trifonov, N. Ajellal and J.-F. Carpentier, *Inorg. Chem.*, 2009, **48**, 4258.
95. H.-L. Han, Y. Liu, J.-Y. Liu, K. Nomura and Y.-S. Li, *Dalton Trans.*, 2013, **42**, 12346.
96. Y. Wang, W. Zhao, D. Liu, S. Li, X. Liu, D. Cui and X. Chen, *Organometallics*, 2012, **31**, 4182.
97. M. G. Cushion, *D.Phil Thesis, University of Oxford*, 2011.
98. J. Meyer, I. Kuzu, S. González-Gallardo and F. Breher, *Z. Anorg. Allg. Chem.*, 2013, **639**, 301.
99. T. Athar and A. Hakeem, *Arabian J. Chem.*, 2014, **7**, 209.
100. A. Kapelski, J.-C. Buffet, T. P. Spaniol and J. Okuda, *Chem. Asian J.*, 2012, **7**, 1320.
101. J.-C. Buffet, J. P. Davin, T. P. Spaniol and J. Okuda, *New J. Chem.*, 2011, **35**, 2253.
102. A. Pilone, N. De Maio, K. Press, V. Venditto, D. Pappalardo, M. Mazzeo, C. Pellecchia, M. Kol and M. Lamberti, *Dalton Trans.*, 2015, **44**, 2157.

103. H. Du, A. H. Velders, P. J. Dijkstra, J. Sun, Z. Zhong, X. Chen and J. Feijen, *Chem. Eur. J.*, 2009, **15**, 9836.
104. A. Pietrangelo, S. C. Knight, A. K. Gupta, L. J. Yao, M. A. Hillmyer and W. B. Tolman, *J. Am. Chem. Soc.*, 2010, **132**, 11649.
105. J.-C. Buffet and J. Okuda, *Chem. Commun.*, 2011, **47**, 4796.
106. M. H. Chisholm, N. W. Eilerts, J. C. Huffman, S. S. Iyer, M. Pacold and K. Phomphrai, *J. Am. Chem. Soc.*, 2000, **122**, 11845.
107. H. Du, *PhD thesis, University of Twente*, 2009.
108. A. Amgoune, C. M. Thomas, T. Roisnel and J.-F. Carpentier, *Chem. Eur. J.*, 2006, **12**, 169.
109. H. Du, A. H. Velders, P. J. Dijkstra, Z. Zhong, X. Chen and J. Feijen, *Macromolecules*, 2009, **42**, 1058.
110. H. Nöth and B. Wrackmeyer, *Nuclear Magnetic Resonance Spectroscopy of Boron Compounds*, Springer-Verlag, Berlin, Heidelberg Germany, 1st edition edn., 1978.
111. J. H. Golden, C. Schreier, B. Singaram and S. M. Williamson, *Inorg. Chem.*, 1992, **31**, 1533.
112. M. Karplus, *J. Chem. Phys.*, 1959, **30**, 11.
113. M. Karplus, *J. Am. Chem. Soc.*, 1963, **85**, 2870.
114. M. J. Minch, *Concept. Magnetic. Res.*, 1994, **6**, 41.
115. B. A. Borgias, M. Gochin, D. J. Kerwood and T. L. James, *Prog. Nucl. Mag. Res. Sp.* , 1990, **22**, 83.
116. Y. Kawashima, H. Takeo and C. Matsumura, *J. Mol. Spectrosc.*, 1986, **116**, 23.
117. B. A. Core, *DPhil Thesis, University of Oxford*, 2015.

Chapter Four

Borate ester species as chain transfer agents for the ROP of *rac*-LA and ε-CL

4.1 Overview

This Chapter will describe the use of borate ester species as chain transfer agents in the ROP of cyclic esters. A recently developed approach was applied to generate $B(OBn)_3$ *in-situ*, which was utilised as a chain transfer agent in the ROP of *rac*-LA and ε-CL. The results were compared to those obtained using externally added $B(OBn)_3$. Chain transfer efficiency will also be investigated using NMR spectroscopic techniques. This will be followed by an evaluation of the effect of non-activated catalysts on inducing transesterification side reactions. In addition, the exchange reactions between a borate ester and a metal alkoxide or metal polymeryl species will also be discussed.

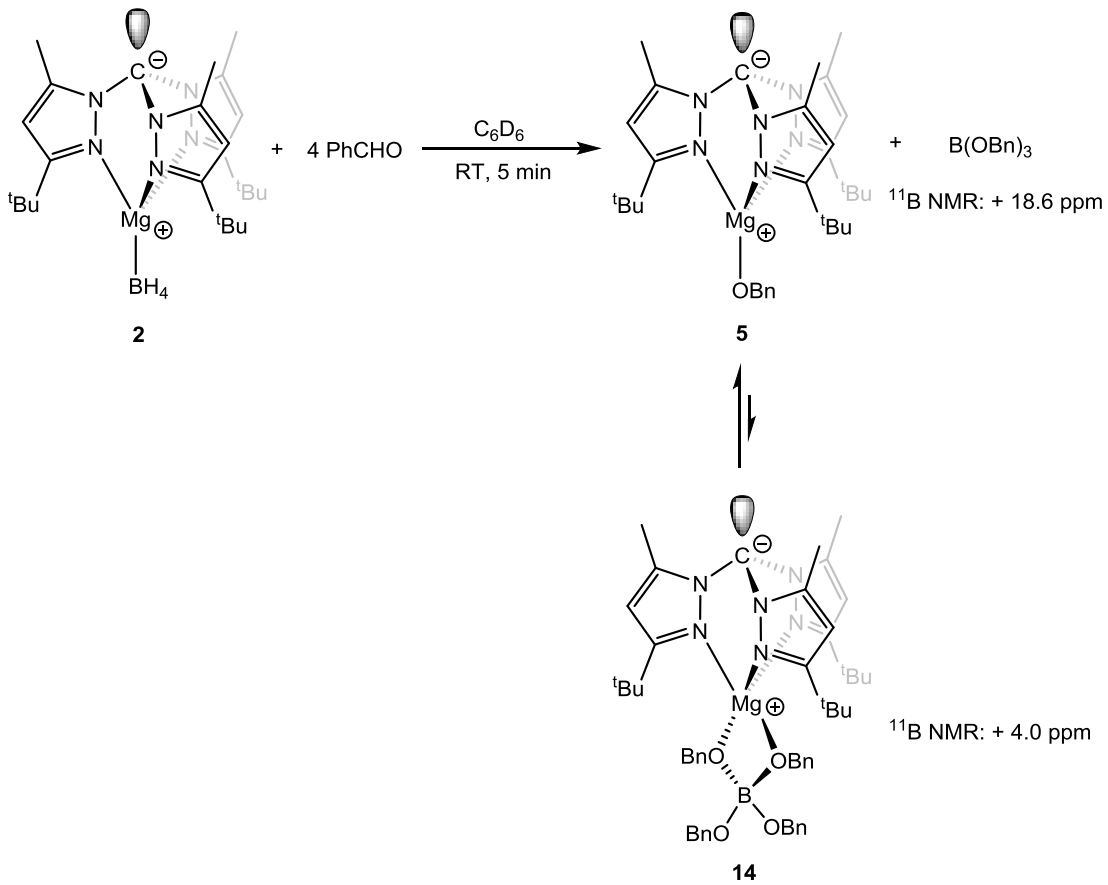
4.2 A novel approach to generate $B(OBn)_3$ *in-situ*

Following the mechanistic studies for the ROP of LA initiated by $(Tpm^{*d})Mg(BH_4)$ (**2**) described in Chapter Three, the inefficient initiating nature of borohydride species has stimulated the development of alternative approaches to circumvent such initiation process. Additionally, given the fact that bulky borate ester species, such as $B(Cy\text{-}H)_3$, have demonstrated poor chain transfer ability in the ROP of *rac*-LA, attention was subsequently focused on smaller borate ester analogues. Inspired by Sun *et al.* who reported the use of an *in-situ* generated lanthanide alkoxide species in the ROP of ε-CL, a similar approach was developed by Dr J. Unruangsri, involving the addition of an aldehyde to a borohydride species to generate an alkoxide and a borate ester *in-situ* (Scheme 4.1).[1, 2]

An NMR tube scale experiment was performed by adding 4 equiv. of benzaldehyde to a solution of **2** in C_6D_6, leading to the instantaneous formation of **5** and $B(OBn)_3$. The ^1H NMR spectrum (Figure 4.1, a) recorded after 5 min revealed the evolution of $B(OBn)_3$, as evidenced by the presence of signals at 4.94 ppm and in the region of 7.10-7.30 ppm, corresponding to the methylene and aromatic protons, respectively. In contrast to the *in-situ* generated $(Tpm^{*d})Mg(Cy\text{-}H)$ (**12**) and $B(Cy\text{-}H)_3$ which were found to remain as discrete species, **5** and $B(OBn)_3$ existed in equilibrium with $(Tpm^{*d})Mg(OBn)\{B(OBn)_3\}$ (**14**) due to the smaller size of the OBn substituents. These two different boron coordination environments could be unambiguously distinguished in the ^{11}B NMR spectrum, which revealed a major singlet at 18.6 ppm and a minor one at 4.0 ppm (ratio *ca.* 7:1 by integration) corresponding to $B(OBn)_3$

and **14**, respectively. In contrast to this was the analogous system ($Tp^{tBu,Me}$)Mg(OBn) (**2.20**) and $B(OBn)_3$ generated *in-situ*, which exclusively exist as separate species.[2] This may be reflective of the differences in the size or flexibility of the coordination sphere of $Tp^{tBu,Me}$ and Tpm^{*d} ligand-supported magnesium alkoxide species in the solution state.

It is worth emphasising that immortal ROP is particularly difficult to perform for alkaline earth systems due to the catalysts' sensitive nature. Conventional chain transfer agents such as alcohols and amines would normally lead to catalyst decomposition. However, the novel approach discussed above has allowed borate ester species to be used as a new type of aprotic chain transfer agent, the presence of which in several alkaline earth catalytic systems has shown no evidence of catalyst decomposition.[2, 3]



Scheme 4.1 *In-situ* generated (Tpm^{*d})Mg(OBn) (**5**) and $B(OBn)_3$.

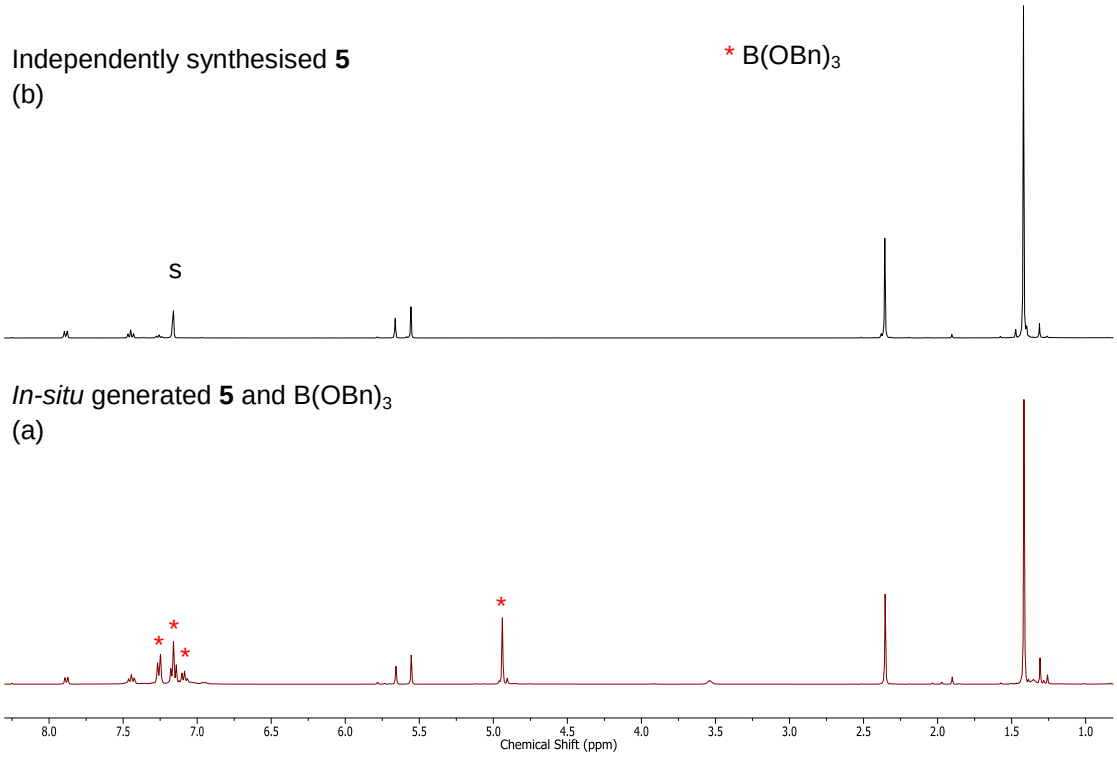


Figure 4.1 ^{1}H NMR spectra (C_6D_6, 400.2 MHz, 298 K) of (a) *in-situ* generated **5** and $B(OBn)_3$ and (b) independently synthesised (Tpm*^{d})Mg(OBn) (**5**). "*" denotes $B(OBn)_3$. "s" denotes residual protio-solvent.

4.3 ROP of *rac*-LA using *in-situ* generated and externally added $B(OBn)_3$

The *in-situ* generated **5** and $B(OBn)_3$, obtained by reacting **2** with 4 equiv. of benzaldehyde, were found to be highly active, reaching 88% conversion (100 equiv. of *rac*-LA) within 5 min in THF at room temperature (Table 4.1, Entry 3). The polymerisation was determined to be second order with respect to *rac*-LA concentration, with an observed rate constant (k_{obs}) of 0.0594(22) M^{-1} s^{-1} (R^2 = 0.992) (Figure 4.2). The rate acceleration observed in this case in comparison to the ROP initiated by **2** clearly indicated a more efficient initiation process induced by converting a borohydride to an alkoxide species. As discussed previously, the addition of benzaldehyde to **2** cleanly generated **5** and $B(OBn)_3$, the former could subsequently act as an initiator, following the coordination insertion mechanism to produce PLA. This is in contrast to the ROP of LA initiated by **2**, whereby multiple unidentifiable side products were generated, in conjunction with the active species (Tpm*^{d})Mg(LA-H). These unknown side products were postulated to be the inactive species, leading

to a decrease in the effective concentration of (Tpm*[d])Mg(LA-H) and therefore, reducing the rate of the polymerisation considerably. Unfortunately, negligible chain transfer effect was observed in the *rac*-LA ROP using *in-situ* generated **5** and $B(OBn)_3$, as evidenced by the close agreement between the experimental and calculated M_n based on one chain per metal at the beginning of the polymerisation (Figure 4.3). A tailing off effect in M_n was observed from 50% conversion onwards, due to the presence of transesterification side reactions. This is consistent with the results obtained from MALDI-ToF mass spectrometry, revealing the presence of repeating units with $\Delta(m/z)$ of 72 g mol^{-1} and cyclic PLA (Figure 4.4). The isolated polymer was determined to be heterotactically enriched (P_r = 0.65), presumably as a result of a chain end control mechanism.

Table 4.1 Selected data for the ROP of *rac*-LA using **2**, **5** and various additives in THF.

Entry	Catalyst[a]	Additive	Conv.[b] %	Time (s)	M_n obs[c] (g mol^{-1})	M_n calc[d] (g mol^{-1})	PDI[e]	P_r[b]
1	**5**	/	94	60	15,720	13,656	2.55	0.69
2	**5**	$B(OBn)_3$	88	300	9,740	3,279	1.58	0.66
3	**2**	4 PhCHO	89	300	6,960	3,315	1.65	0.65

[a] Conditions: $[rac\text{-LA}]_0$:$[initiator]_0$ = 100:1, $[rac\text{-LA}]_0$ = 0.5 M, $[initiator]_0$ = 0.005 M, 6 mL THF at room temperature. [b] Measured by ^{1}H NMR ($CDCl_3$) analyses. [c] Molecular weights (g mol^{-1}) determined from GPC using the appropriate Mark-Houwink corrections. [d] Expected M_n (g mol^{-1}) for one polymer chain growing per metal centre, M_n (calc for Entry 1) = conversion (%) × 100 × 144.1 + 108.1; Expected M_n (g mol^{-1}) for four polymer chains growing per metal centre, M_n (calc for Entries 2 and 3) = 1/4 (conversion (%) × 100 × 144.1) + 108.1. [e] PDI = M_w/M_n.

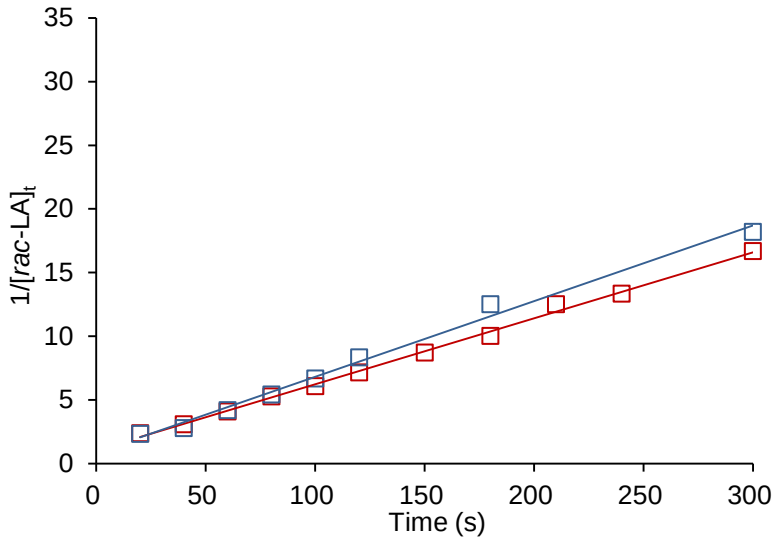


Figure 4.2 Data for the ROP of *rac*-LA in the presence of $B(OBn)_3$. Semilogarithmic second order plot of $1/[rac\text{-LA}]_t$ *vs*. time. Conditions: $[rac\text{-LA}]_0$ = 0.5 M, 6 mL THF at room temperature. $[rac\text{-LA}]_0$:[**2**]$_0$:$[PhCHO]_0$ = 100:1:4, k_{obs} = 0.0594(22) M^{-1} s^{-1} (R^2 = 0.992), blue squares; $[rac\text{-LA}]_0$:[**5**]$_0$:$[B(OBn)_3]_0$ = 100:1:1, k_{obs} = 0.0519(10) M^{-1} s^{-1} (R^2 = 0.997), red squares.

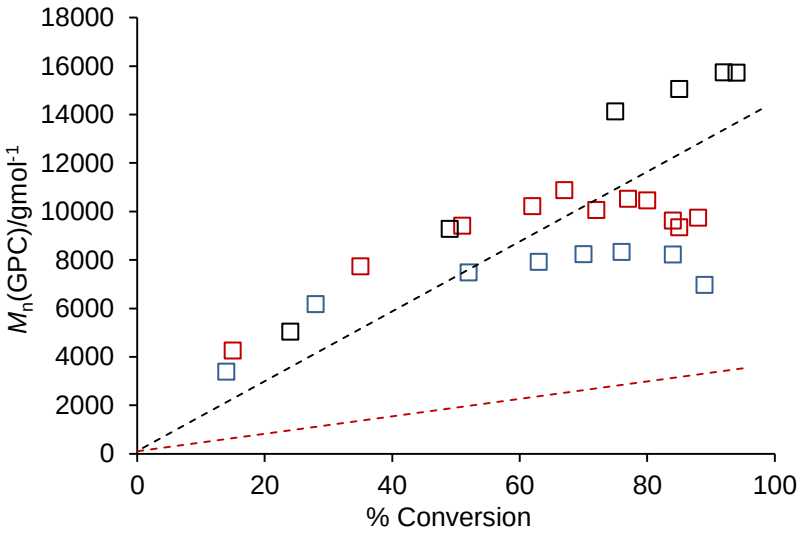


Figure 4.3 Data for the ROP of *rac*-LA with and without the addition of $B(OBn)_3$. M_n (GPC) *vs*. % conversion plot. The dashed lines represent M_n expected for one (black) and four (red) chains per metal centre, respectively. Conditions: $[rac\text{-LA}]_0$ = 0.5 M, 6 mL THF at room temperature. $[rac\text{-LA}]_0$:[**5**]$_0$ = 100:1, black squares; $[rac\text{-LA}]_0$:[**2**]$_0$:$[PhCHO]_0$ = 100:1:4, blue squares; $[rac\text{-LA}]_0$:[**5**]$_0$:$[B(OBn)_3]_0$ = 100:1:1, red squares.

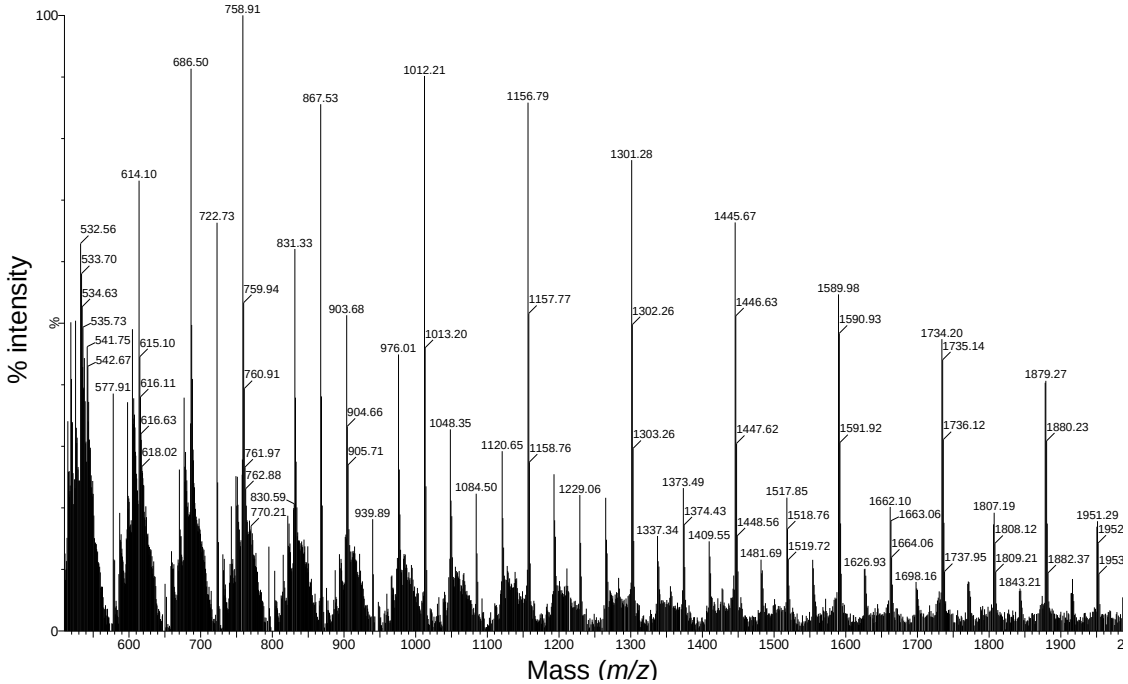


Figure 4.4 MALDI-ToF MS of PLA synthesised using *in-situ* generated **5** and $B(OBn)_3$. Conditions: $[rac\text{-LA}]_0:[\mathbf{2}]_0:[PhCHO]_0 = 100:1:4$, $[rac\text{-LA}]_0 = 0.5$ M, $[\mathbf{2}]_0 = 0.005$ M, 6 mL THF at room temperature. K^+ dopant.

The above polymerisation results using the *in-situ* generated catalytic system were compared to those obtained by using the independently synthesised **5** and externally added $B(OBn)_3$ (Table 4.1, Entry 2). As expected, a very similar second order rate constant was observed (k_{obs} = 0.0519(10) M^{-1} s^{-1}, R^2 = 0.997) (Figure 4.2). The experimental M_n was close to that expected based on one chain per metal centre at low % conversions followed by tailing-off effects towards the end of the polymerisation (Figure 4.3).

By comparing the ROP results which involved the use of $B(OBn)_3$ (both *in-situ* generated and externally added) to those which did not, it is apparent that the addition of $B(OBn)_3$ resulted in a decrease in the polymerisation rate and a shift of the reaction order (with respect to *rac*-LA concentration) from being first to second (Table 4.1, Entries 1-3). As discussed previously, **5** and $B(OBn)_3$ exist in equilibrium with a tetra-coordinated adduct **14**. It is postulated that **14** is the catalyst resting state and propagation could only occur upon dissociation into the discrete species **5** and $B(OBn)_3$. The presence of **14** as the resting state during the polymerisation would therefore result in a decrease in the concentration of the active catalyst, leading to a reduced polymerisation rate. Consistently, a narrower PDI was observed upon

incorporation of $B(OBn)_3$, presumably due to a decrease in the difference between the rates of propagation and initiation. Similar results have been observed in other catalytic systems reported in the Mountford group.[3]

Second order dependencies with respect to LA concentration are relatively rare but not unprecedented in the literature. For example, Wu *et al.* recently reported the ROP of *rac*-LA initiated by a tetra-nuclear Mg system.[4] The second order dependence in LA concentration was attributed to the simultaneous activation of two lactide molecules. Employing a more congested trinuclear magnesium catalyst only allowed activation of one lactide monomer at a time, therefore resulting in a shift in polymerisation order (with respect to LA concentration) to being first. Moreover, *rac*-LA ROP initiated by an indium lithium "ate" complex reported by Mountford and co-workers also demonstrated a second order rate dependence with respect to LA concentration. This was rationalised by the possible monomer activation at both the indium and lithium metal centres.[5] Other examples involving second order kinetics in LA concentration include a trinuclear zinc alkoxide catalyst and a lanthanide phenolate compound reported by Lin and Delbridge, respectively.[6, 7] Based on these previous studies, it is postulated that **14** might play a role in the coordination of LA molecules despite its inactive nature in initiating LA ROP. It is worth noting that the addition of $B(OBn)_3$ had a minor impact on the heterotacticity of the resulting polymer.

The close agreement between the experimental and calculated M_n (based on one chain per metal centre) observed in the large scale LA polymerisations using **5** and $B(OBn)_3$ could be attributed to two possible reasons. Studies in Chapter Three have demonstrated that borate ester species with bulky substituents, such as $B(Cy\text{-}H)_3$, possess poor chain transfer ability. It is therefore rational to hypothesise that $B(OBn)_3$ might still be too bulky to undergo rapid exchange with the growing polymeryl chain. Nevertheless, previous ROP studies using *in-situ* generated $(Tp^{tBu,Me})Mg(OBn)$ (**2.20**) and $B(OBn)_3$ have shown clear but contradictory results.[2] The experimental M_n was very close to the theoretical value based on four chains per metal centre, indicative of efficient chain transfer. This suggested that the lack of chain transfer in Tpm^{*d} catalytic systems was not related to the size of $B(OBn)_3$. Instead, given the significant difference in the observed rate constants (k_{obs}) between the two systems, it is

postulated that any potential chain transfer effect imposed by $B(OBn)_3$ might be suppressed by the fast rate of propagation associated with the Tpm*[d] systems.

Following the successful synthesis of ($Tp^{tBu,Me}$)Mg(Cy-H) (**13**) introduced in Chapter Three, a series of large scale polymerisations involving **13** and borate ester species were performed, shown in Table 4.2. Complex **13** exhibited moderate activity, reaching 93% monomer conversion after 47 h (100 equiv. of *rac*-LA, THF, room temperature; Table 4.2, Entry 1). Close examination of the kinetic plot (Figure 4.5) revealed the presence of a major induction period of approximately 16 h, after which time the polymerisation demonstrated a first order dependence on *rac*-LA concentration, with an apparent rate constant (k_{obs}) of 0.0882(81) h^{-1} (R^2 = 0.991). The rate-limiting step of the polymerisation was determined to be the first insertion of LA into the bulky alkoxide group, consistent with the presence of an induction period. In addition, a linear relationship between the experimental M_n and % conversion (Figure 4.6) was observed, with a gradient of 130(4) g mol^{-1} (% conversion)$^{-1}$ (R^2 = 0.997), corresponding to one chain being produced per metal centre. The resulting polymer was determined to be slightly heterotactically enriched (P_r = 0.64) according to $^1H\{^1H\}$ NMR spectroscopy. As expected, MALDI-ToF analysis clearly revealed the presence of a Cy-H chain end and intermolecular transesterification.

Table 4.2 Selected data for the ROP of *rac*-LA using **13** and various borate esters in THF.

Entry	Catalyst[a]	Additive	Conv.[b] %	Time (h)	M_n obs[c] (g mol^{-1})	M_n calc[d] (g mol^{-1})	PDI[e]	P_r[b]
1	**13**	/	93	47	12,360	13,518	1.22	0.64
2	**13**	$B(Cy\text{-}H)_3$	91	47	13,370	3,423	1.22	0.65
3	**13**	$B(OBn)_3$	95	39	6,790	3,531	1.22	0.64

[a] Conditions: $[rac\text{-LA}]_0:[\mathbf{13}]_0$ = 100:1, $[rac\text{-LA}]_0$ = 0.5 M, $[\mathbf{13}]_0$ = 0.005 M, 6 mL THF at room temperature. [b] Measured by ^1H NMR ($CDCl_3$) analyses. [c] Molecular weights (g mol^{-1}) determined from GPC using the appropriate Mark-Houwink corrections. [d] Expected M_n (g mol^{-1}) for one polymer chain growing per metal centre, M_n (calc for Entry 1) = conversion (%) × 100 × 144.1 + 114.2; Expected M_n (g mol^{-1}) for four polymer chains growing per metal centre, M_n (calc for Entry 2) = 1/4 (conversion (%) × 100 × 144.1) + 114.2, M_n (calc for Entry 3) = 1/4 (conversion (%) × 100 × 144.1) + 108.1. [e] PDI = M_w/M_n.

The addition of 1 equiv. of $B(Cy\text{-}H)_3$ had negligible impact on the rate of the polymerisation as 91% conversion was achieved after 47 h (Table 4.2, Entry 2). The polymerisation was found to be first order with respect to *rac*-LA concentration after a major induction period of 17 h (k_{obs} = 0.0766(78) h^{-1}, R^2 = 0.980) (Figure 4.5). Crucially, the experimental M_n was in very close agreement with the expected value based on one chain per metal centre, indicating the poor chain transfer ability of $B(Cy\text{-}H)_3$ (Figure 4.6). The gradient of the line of best fit was found to be 126(4) g mol^{-1} (% conversion)$^{-1}$ (R^2 = 0.996), very close to that obtained using **13** alone (130(4) g mol^{-1} (% conversion) $^{-1}$ (R^2 = 0.997)). No observable effect on heteroselectivity or molecular weight distribution was found upon addition of $B(Cy\text{-}H)_3$. An NMR tube scale reaction between **13** and $B(Cy\text{-}H)_3$ in a 1:1 ratio was conducted in C_6D_6, revealing two singlets at 18.1 and -9.3 ppm in the $\{^1H\}^{11}B$ NMR spectrum, corresponding to $\underline{B}(Cy\text{-}H)_3$ and the apical boron on the ligand, respectively. No tetra-coordinated adduct was formed and therefore, negligible rate reduction was observed upon addition of $B(Cy\text{-}H)_3$ in the large scale polymerisation. Moreover, no alteration in kinetics was found, in contrast to the previous case where $B(OBn)_3$ was added to **5**. These findings further serve to confirm the impact of tetra-coordinated species on LA coordination despite its inactive initiating nature.

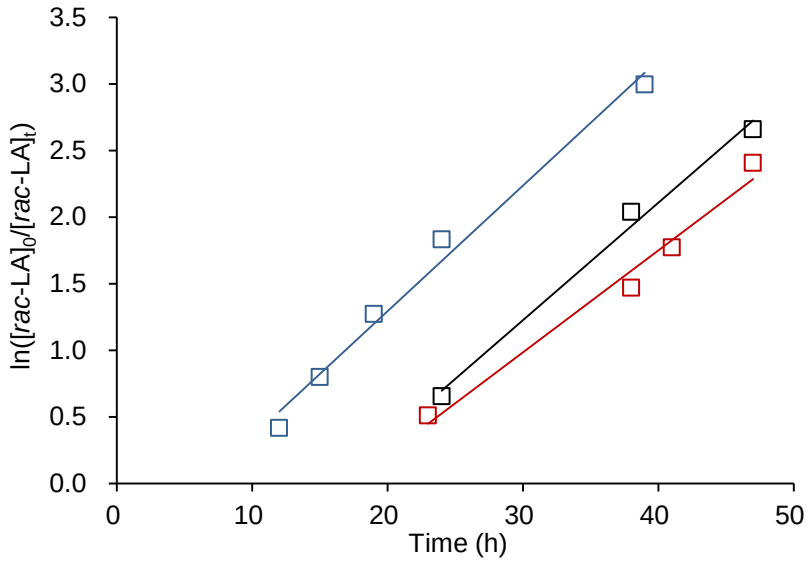


Figure 4.5 Data for the ROP of *rac*-LA using ($Tp^{tBu,Me}$)Mg(Cy-H) (**13**) and various borate ester species. Semilogarithmic first order plot of ln([*rac*-LA]$_0$/[*rac*-LA]$_t$) *vs.* time. Conditions: [*rac*-LA]$_0$ = 0.5 M, 6 mL THF at room temperature. [*rac*-LA]$_0$:[**13**]$_0$ = 100:1, k_{obs} = 0.0882(81) h^{-1} (R^2 = 0.991), black squares; [*rac*-LA]$_0$:[**13**]$_0$:[B(Cy-H)$_3$]$_0$ = 100:1:1, k_{obs} = 0.0766(78) h^{-1} (R^2 = 0.980), red squares; [*rac*-LA]$_0$:[**13**]$_0$:[B(OBn)$_3$]$_0$ = 100:1:1, k_{obs} = 0.0944(49) h^{-1} (R^2 = 0.989), blue squares.

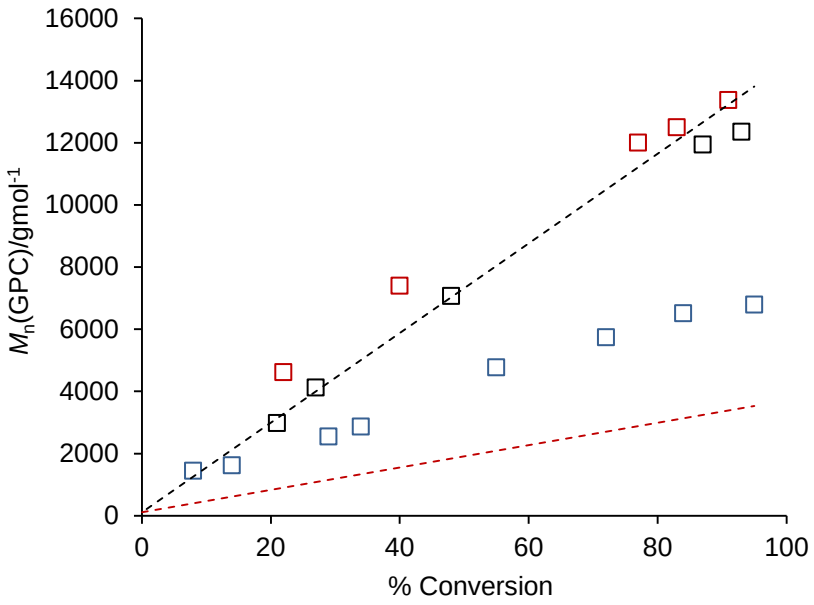


Figure 4.6 Data for the ROP of *rac*-LA using (Tp^{tBu,Me})Mg(Cy-H) (**13**) and various borate ester species. M_n (GPC) *vs*. % conversion plot. The dashed lines represent M_n expected for one (black) and four (red) chains per metal centre, respectively. Conditions: [*rac*-LA]$_0$ = 0.5 M, 6 mL THF at room temperature. [*rac*-LA]$_0$:[**13**]$_0$ = 100:1, black squares; [*rac*-LA]$_0$:[**13**]$_0$:[B(Cy-H)$_3$]$_0$ = 100:1:1, red squares; [*rac*-LA]$_0$:[**13**]$_0$:[B(OBn)$_3$]$_0$ = 100:1:1, blue squares.

A complementary NMR tube scale polymerisation (C_6D_6) was performed by adding 15 equiv. of *L*-LA to **13** and B(Cy-H)$_3$ in the presence of 1,4-dimethoxybenzene as an internal standard. Very minor changes in the integration of B(Cy-H)$_3$ were observed over the course of 16 h, suggesting negligible exchange between B(Cy-H)$_3$ and the polymeryl chain. This is fully consistent with the results obtained from the large scale polymerisation.

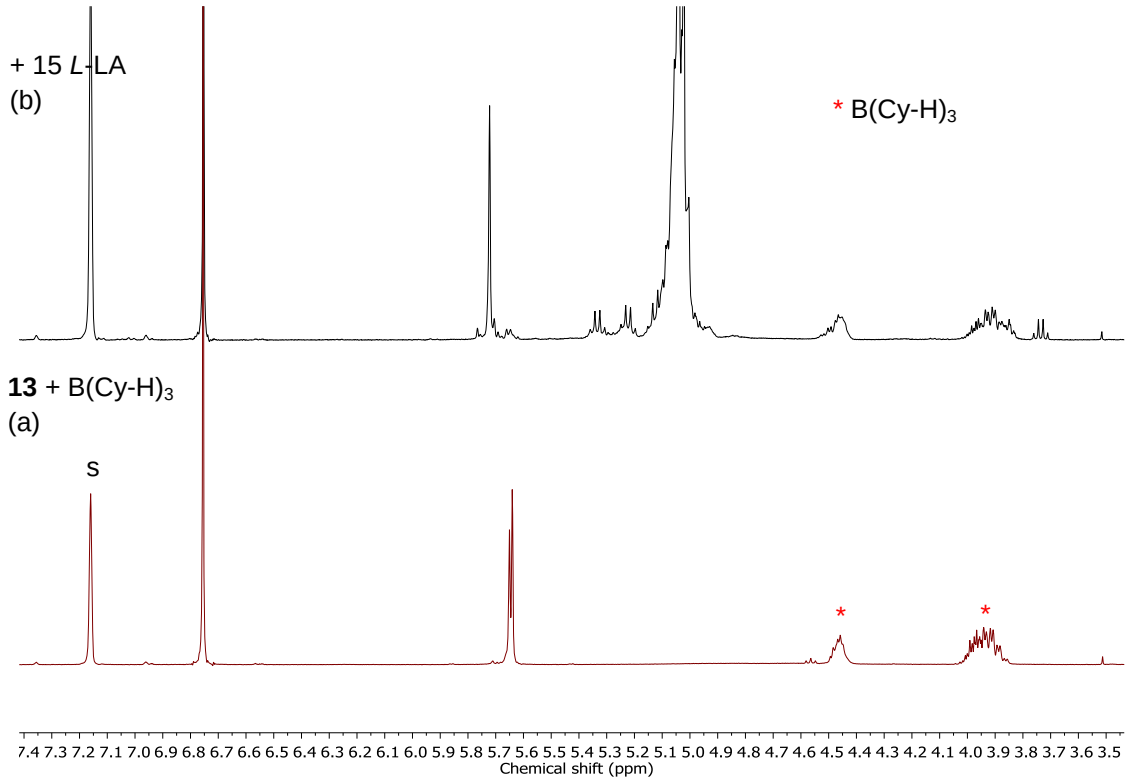


Figure 4.7 ^{1}H NMR spectrum (C_6D_6, 400.2 MHz, 298 K) (a) of the equimolar reaction between ($Tp^{tBu,Me}$)Mg(Cy-H) (**13**) and B(Cy-H)$_3$. ^{1}H NMR spectrum (C_6D_6, 400.2 MHz, 298 K) (b) of the resulting polymeryl chain obtained 16 h after addition of 15 equiv. of *L*-LA to **13** and B(Cy-H)$_3$. "*" denotes B(Cy-H)$_3$. "s" denotes residual protio-solvent.

In contrast to B(Cy-H)$_3$, the addition of a smaller borate ester analogue B(OBn)$_3$ led to a faster polymerisation; 95% conversion was reached after 39 h (Table 4.2, Entry 3). The induction period was reduced to 6 h, after which time the polymerisation demonstrated a first order dependence on *rac*-LA concentration (k_{obs} = 0.0944(49) h^{-1}, R^2 = 0.989). Interestingly, the experimental M_n values were in close agreement with the theoretical ones based on two chains per metal centre. In order to gain insight into the origin of the reduced M_n values, an NMR tube scale polymerisation was performed by adding 1 equiv. of B(OBn)$_3$ to **13** in C_6D_6 followed by 15 equiv. of *L*-LA. The reaction between **13** and B(OBn)$_3$ resulted in the instantaneous formation of ($Tp^{tBu,Me}$)Mg(OBn) (**2.20**), in conjuction with B(OBn)$_n$(Cy-H)$_{3-n}$. The ^{1}H NMR spectrum (Figure 4.8, a) recorded 5 min after the reaction revealed the presence of several methylene and phenyl proton environments in the region of 4.96-5.00 and 7.08-7.34 ppm, respectively, suggesting the formation of multiple B(OBn)$_n$(Cy-H)$_{3-n}$

species. It is apparent that **13** was completely converted to **2.20**, as evidenced by the disappearance of signals corresponding to the former. The ^{11}B NMR spectrum showed two singlets at 18.6 and -9.2 ppm, corresponding to $\underline{B}(OBn)_n(Cy\text{-}H)_{3-n}$ and the apical boron on the ligand, respectively. Subsequent addition of 15 equiv. of *L*-LA resulted in full conversion to PLA after 16 h. The ^{1}H NMR spectrum (Figure 4.8, b) revealed the presence of two quartets at 5.33 and 5.23 ppm, which were assigned to the two methine protons on the last inserted LA unit. In addition, the methylene protons on the OBn chain end could be clearly identified as two mutually coupled doublets with a roofing effect at 4.79 and 4.90 ppm. The above-discussed NMR data have identified **2.20** as the active species during the polymerisation, as opposed to **13**. This is consistent with the shorter induction period observed in the polymerisation using **13** and $B(OBn)_3$ (6 h) in comparison to that obtained employing **13** and $B(Cy\text{-}H)_3$ (17 h), presumably due to a reduction in sterics of the active alkoxide initiator. Unfortunately, little information regarding the chain transfer ability of $B(OBn)_n(Cy\text{-}H)_{3-n}$ could be obtained from the ^{1}H NMR spectrum. It is postulated that such borate ester species possesses limited chain transfer ability, resulting in two polymer chains being produced per metal centre. Consistently, the MALDI-ToF mass spectrum (Figure 4.9) of the resulting PLA obtained from the large scale polymerisation revealed the presence of two types of end groups. For example, the peak at 3604 g mol^{-1} could be attributed to an OBn terminated PLA (major) containing 24 LA units whereas the corresponding Cy-H terminated PLA (minor) was visible at 3610 g mol^{-1}.

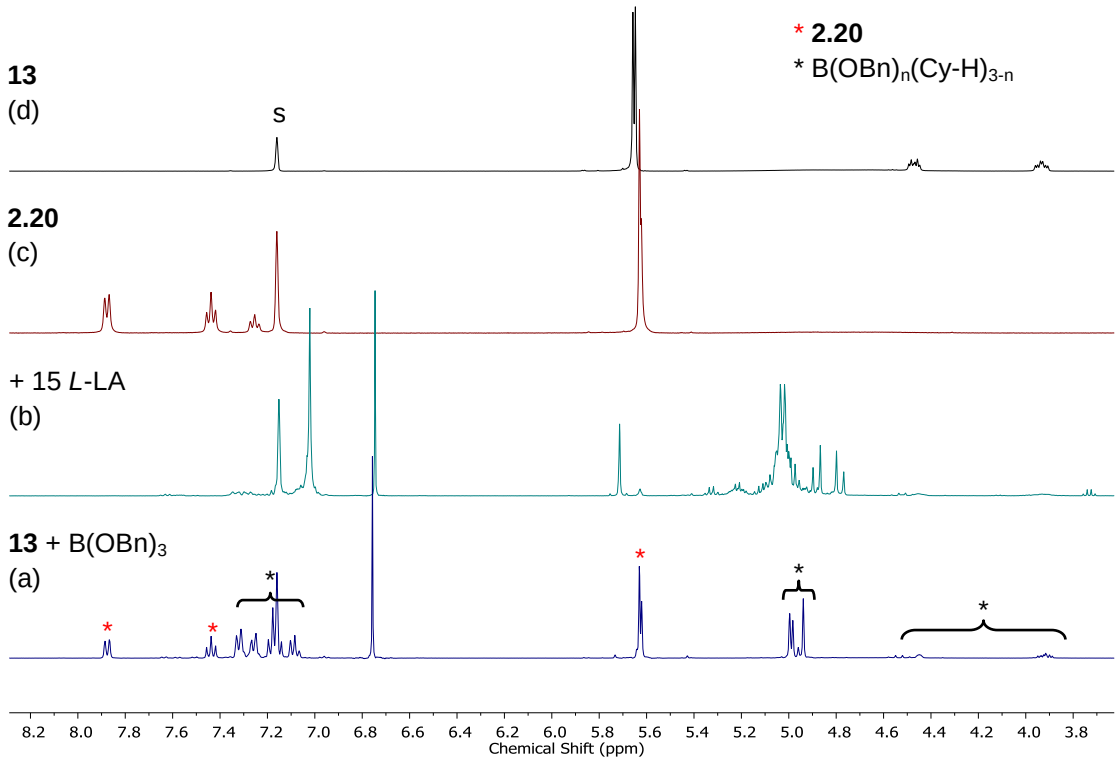


Figure 4.8 ^{1}H NMR spectrum (C_6D_6, 400.2 MHz, 298 K) (a) of the equimolar reaction between ($Tp^{tBu,Me}$)Mg(Cy-H) (**13**) and $B(OBn)_3$. ^{1}H NMR spectrum (C_6D_6, 400.2 MHz, 298 K) (b) of the resulting polymer obtained 16 h after the addition of 15 equiv. of *L*-LA. ^{1}H NMR spectra (C_6D_6, 400.2 MHz, 298 K) of (c) ($Tp^{tBu,Me}$)Mg(OBn) (**2.20**) and (d) **13**. "*" denotes **2.20**. "*" denotes $B(OBn)_n(Cy\text{-}H)_{3\text{-}n}$. "s" denotes residual protio-solvent.

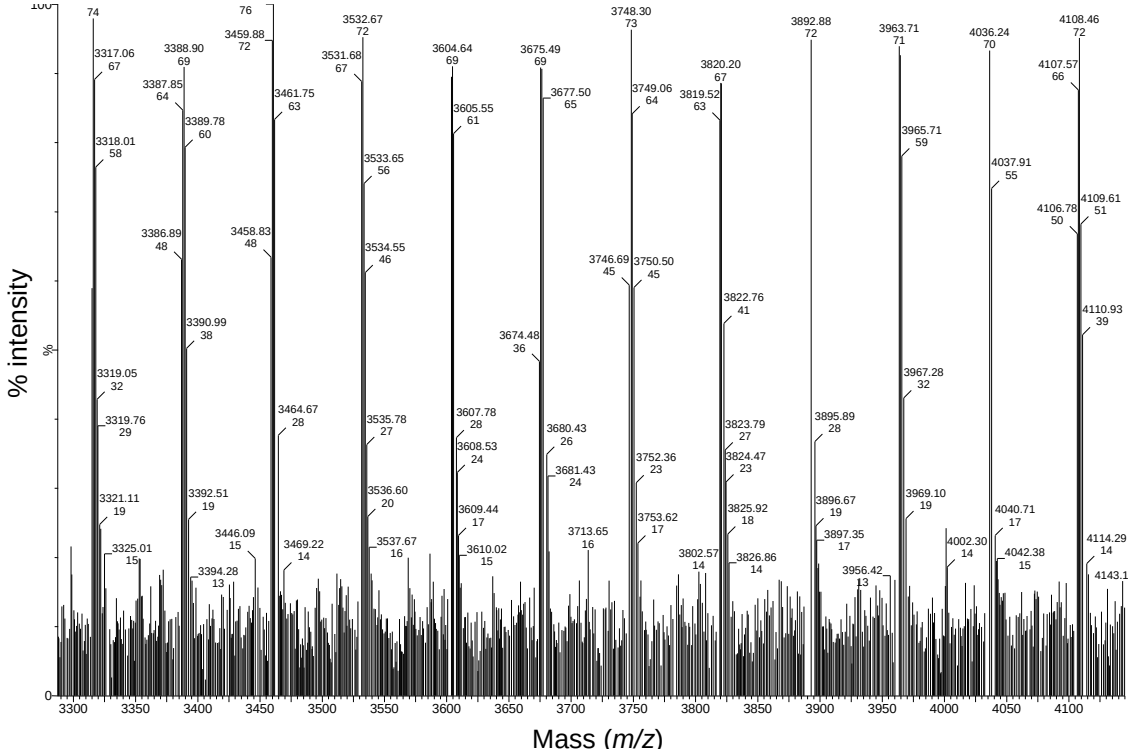


Figure 4.9 MALDI-ToF MS of PLA synthesised using *in-situ* generated **13** and $B(OBn)_3$. Conditions: $[rac\text{-LA}]_0$:$[\mathbf{13}]_0$:$[B(OBn)_3]_0$ = 100:1:1, $[rac\text{-LA}]_0$ = 0.5 M, $[\mathbf{13}]_0$ = 0.005 M, 6 mL THF at room temperature. K^+ dopant.

4.4 ROP of ε-CL using *in-situ* generated and externally added $B(OBn)_3$

Given the inefficient chain transfer ability of $B(OBn)_3$ in the ROP of *rac*-LA using **5**, further studies were also undertaken to investigate whether the use of $B(OBn)_3$ could lead to efficient immortal ε-CL ROP. Detailed kinetic and M_n analysis using catalytic systems containing both *in-situ* generated and externally added $B(OBn)_3$ were carried out and compared.

The ε-CL ROP activity of **5** was previously discussed in Chapter Three. Up to 1000 equiv. of ε-CL could be polymerised within 11 min, giving PCL with well-controlled M_n and low PDIs. The addition of external $B(OBn)_3$ (Table 4.3, Entry 2) had a minor effect on the rate of the polymerisation; 92% conversion was reached within 2 min, comparable to the polymerisation where no chain transfer agent was added (Table 4.3, Entry 1). Kinetic analysis showed the polymerisation to follow neither a first nor second order dependence on ε-CL concentration. Non-integer order is unusual but not unprecedented in the literature. For example, early work in the Mountford group has introduced (^{Dipp}NacNac)Mg(BH_4)(THF) (**3.37**) which demonstrated neither first nor

second order dependence on *rac*-LA concentration.[8] This was attributed to the presence of different types of species equilibrating over the course of the polymerisation. Later, non-integer order was also observed in the ROP of *rac*-LA using a carbazole ligand-supported magnesium benzyloxide catalyst and $B(OBn)_3$ previously reported in the Mountford group.[3] This was rationalised by the possible association and dissociation of $B(OR)_3$ (OR = OBn or polymeryl) to the metal centre, resulting in the formation of a complex pre-equilibrium prior to and following LA insertion. In light of these previous studies, it was postulated that such pre-equilibrium also existed in this particular catalytic system containing **5** and $B(OBn)_3$.

Table 4.3 Selected data for the ROP of ε-CL using **2**, **5** and various additives in THF.

Entry	Catalyst[a]	Additive	Conv.[b] %	Time (min)	M_n obs[c] (g mol^{-1})	M_n calc[d] (g mol^{-1})	PDI[e]
1	**5**	/	97	2	27,070	22,251	1.15
2	**5**	$B(OBn)_3$	92	2	8,780	5,359	1.69
3	**2**	4 PhCHO	99	2.5	7,950	5,758	1.67

[a] Conditions: $[\varepsilon\text{-CL}]_0$:$[\text{initiator}]_0$ = 200:1, $[\varepsilon\text{-CL}]_0$ = 1.0 M, $[\text{initiator}]_0$ = 0.005 M, 3.4 mL THF at room temperature. [b] Measured by ^{1}H NMR ($CDCl_3$) analyses. [c] Molecular weights (g mol^{-1}) determined from GPC using the appropriate Mark-Houwink corrections. [d] Expected M_n (g mol^{-1}) for one polymer chain growing per metal centre, M_n (calc for Entry 1) = conversion (%) × 200 × 114.1 + 108.1; Expected M_n (g mol^{-1}) for four polymer chains growing per metal centre, M_n (calc for Entries 2 and 3) = 1/4 (conversion (%) × 200 × 114.1) + 108.1. [e] PDI = M_w/M_n.

Close examination of the M_n data for the ROP using **5** and external $B(OBn)_3$ showed strong evidence for efficient chain transfer (Figure 4.10), as evidenced by the close agreement between the experimental and calculated M_n values (four chains per metal centre). This was reflective of the higher rate of chain transfer than that of propagation, in contrast to the ROP of *rac*-LA in the presence of $B(OBn)_3$ discussed previously. A moderate PDI was observed and MALDI-ToF MS results confirmed the formation of an OBn terminated PCL.

As expected, the ROP of ε-CL using *in-situ* generated **5** and $B(OBn)_3$ obtained by reacting **2** and 4 equiv. of benzaldehyde afforded very similar results. Full conversion was reached after 2.5 min, affording PCL with moderate PDIs (Table 4.3, Entry 3).

Again, a rate acceleration compared to the ROP initiated by **2** was observed, suggesting the more efficient initiation process by converting a borohydride to an alkoxide species upon addition of benzaldehyde. Neither first nor second-order dependence on ε-CL concentration was observed, due to the presence of a complex pre-equilibrium formed by the association and dissociation of the borate ester. The experimental M_n was consistent with the calculated value based on four chains per metal centre, indicating efficient chain transfer (Figure 4.10).

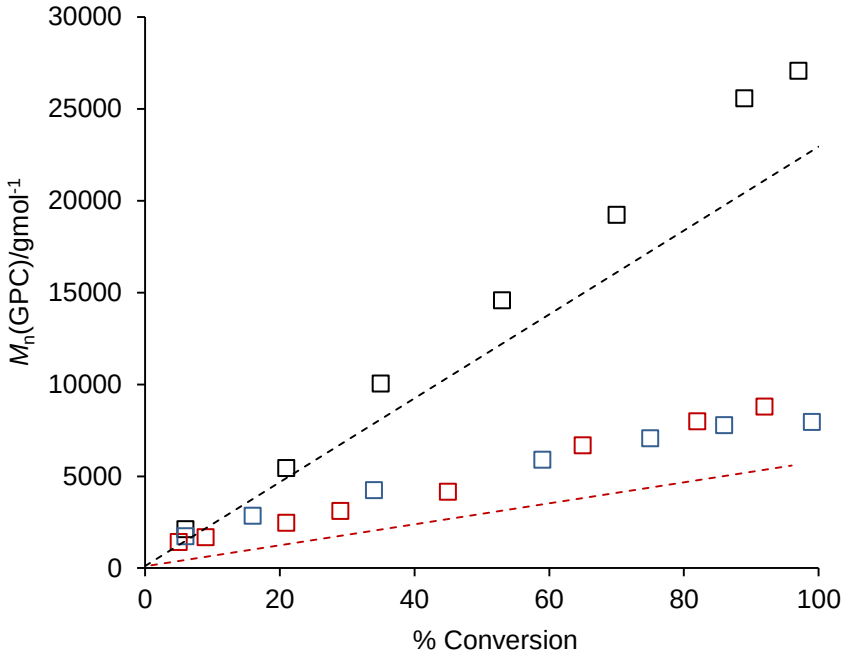


Figure 4.10 Data for the ROP of ε-CL with and without the addition of $B(OBn)_3$ in THF. M_n (GPC) *vs.* % conversion plot. The dashed lines represent M_n expected for one (black) and four (red) chains per metal centre, respectively. Conditions: $[\varepsilon\text{-CL}]_0$ = 1.0 M, 3.4 mL THF at room temperature. $[\varepsilon\text{-CL}]_0$:[**5**]$_0$ = 200:1, black squares; $[\varepsilon\text{-CL}]_0$:[**2**]$_0$:$[PhCHO]_0$ = 200:1:4, blue squares; $[\varepsilon\text{-CL}]_0$:[**5**]$_0$:$[B(OBn)_3]_0$ = 200:1:1, red squares.

In order to gain further evidence for the presence of chain transfer effects, an NMR tube scale polymerisation was carried out by adding 15 equiv. of ε-CL to a solution of *in-situ* generated **5** and $B(OBn)_3$ in C_6D_6. Prior to the addition of ε-CL, 1 equiv. of 1,4-dimethoxybenzene was also added to allow quantitative analysis. The ^{1}H NMR spectrum (C_6D_6) recorded after 5 min (Figure 4.11, b) suggested the complete conversion of the monomer to PCL. The methylene protons closest to the metal centre

appeared as a triplet ($^3J_{H\text{-}H}$ = 6.8 Hz) at 4.50 ppm. Crucially, the signal corresponding to $B(OBn)_3$ at 4.94 ppm was significantly diminished. In contrast, a broad peak at 5.03 ppm was observed, which was attributed to the methylene protons on the OBn fragment of $B(OBn)_n(polymeryl)_{3\text{-}n}$. This is indicative of the rapid exchange process between $B(OBn)_3$ and the growing polymeryl chain, consistent with the efficient chain transfer effect observed in the corresponding large scale polymerisation.

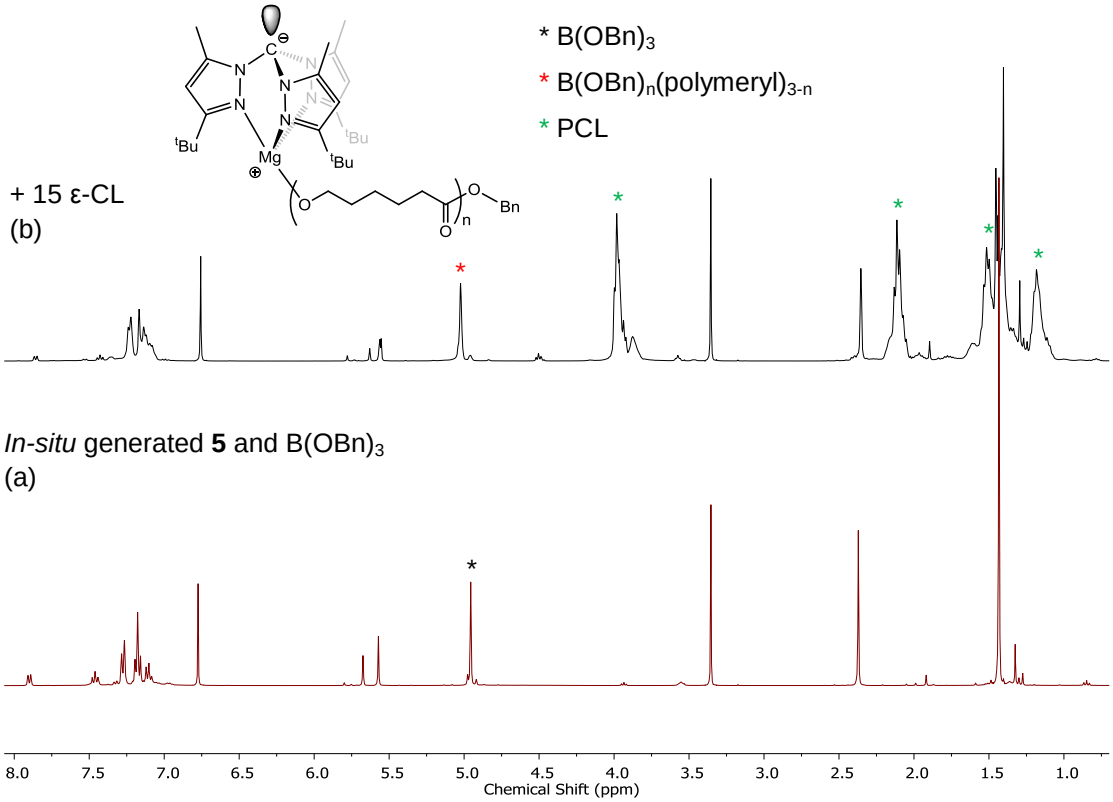


Figure 4.11 ^{1}H NMR spectrum (C_6D_6, 400.2 MHz, 298 K) (a) of the *in-situ* generated (Tpm*^{d})Mg(OBn) (**5**) and $B(OBn)_3$. ^{1}H NMR spectrum (C_6D_6, 400.2 MHz, 298 K) (b) of the resulting polymeryl chain obtained after addition of 15 equiv. of ε-CL to **5** and $B(OBn)_3$. "*" denotes $B(OBn)_n(polymeryl)_{3\text{-}n}$. "*" denotes $B(OBn)_3$. "*" denotes PCL.

Polymerisations were also carried out in toluene to probe for any solvent effects. All three polymerisations with and without the addition of $B(OBn)_3$ were slightly slower in toluene than in THF, shown in Table 4.4. The exact rate constants could not be obtained since neither first nor second order kinetics were observed. Literature has shown a number of examples where the use of donor solvents, such as THF, would lead to slower polymerisations compared to non-donor solvents due to their coordinating nature to the metal centre, therefore competing with monomer coordination.[9-16] However, there are only limited examples in the literature where the

reverse has been observed.[16, 17] For instance, Ma and Okuda have reported a series of yttrium and lutetium bis(phenolate) complexes for the ROP of *rac*-LA, which demonstrated strong solvent effects.[18] Polymerisations in THF were complete within several hours whereas those in toluene only afforded traces of polymers after several days. The exact origin for the rate difference was not discussed. Lamberti and co-workers also reported an *in-situ* generated dimeric magnesium alkoxide complex which showed higher ε-CL ROP activity in THF than in CH_2Cl_2.[19] This was rationalised by the formation of monomeric species, which was proposed to be more active than the dimer. Minor solvent effects were observed using **5** (both in the presence and absence of $B(OBn)_3$) and the origin for the slightly reduced rate in toluene remains unclear. A close agreement between the experimental and calculated M_n (Figure 4.12) was observed in all three polymerisations conducted in toluene, similar to those in THF. In addition, a decrease in PDI (1.7 in THF *cf.* 1.5 in toluene for polymerisations involving $B(OBn)_3$) was observed as a result of a lower propagation rate, indicating a more controlled polymerisation process.

Table 4.4 Selected data for the ROP of ε-CL using **2**, **5** and various additives in toluene.

Entry	Catalyst[a]	Additive	Conv.[b] %	Time (min)	M_n obs[c] (g mol^{-1})	M_n calc[d] (g mol^{-1})	PDI[e]
1	**5**	/	97	2.5	24,770	22,251	1.08
2	**5**	$B(OBn)_3$	89	3	6,900	5,187	1.52
3	**2**	4 PhCHO	89	3	6,090	5,187	1.51

[a] Conditions: $[\varepsilon\text{-CL}]_0$:$[\text{initiator}]_0$ = 200:1, $[\varepsilon\text{-CL}]_0$ = 1.0 M, $[\text{initiator}]_0$ = 0.005 M, 3.4 mL toluene at room temperature. [b] Measured by ^{1}H NMR ($CDCl_3$) analyses. [c] Molecular weights (g mol^{-1}) determined from GPC using the appropriate Mark-Houwink corrections. [d] Expected M_n (g mol^{-1}) for one polymer chain growing per metal centre, M_n (calc for Entry 1) = conversion (%) × 200 × 114.1 + 108.1; Expected M_n (g mol^{-1}) for four polymer chains growing per metal centre, M_n (calc for Entry 2 and 3) = 1/4 (conversion (%) × 200 × 114.1) + 108.1. [e] PDI = M_w/M_n.

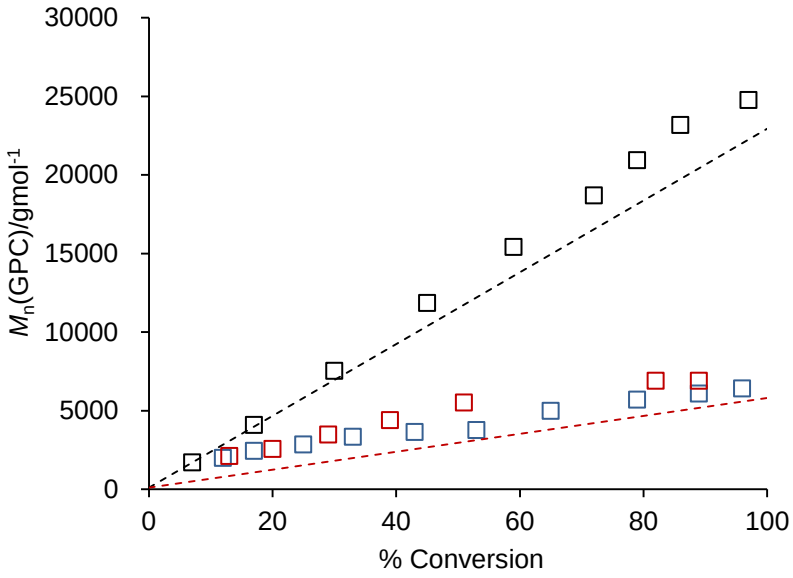


Figure 4.12 Data for the ROP of ε-CL with and without the addition of $B(OBn)_3$ in toluene. M_n (GPC) *vs*. % conversion plot. The dashed lines represent M_n expected for one (black) and four (red) chains per metal centre, respectively. Conditions: $[\varepsilon\text{-CL}]_0$ = 1.0 M, 3.4 mL toluene at room temperature. $[\varepsilon\text{-CL}]_0$:[**5**]$_0$ = 200:1, black squares; $[\varepsilon\text{-CL}]_0$:[**2**]$_0$:$[PhCHO]_0$ = 200:1:4, blue squares; $[\varepsilon\text{-CL}]_0$:[**5**]$_0$:$[B(OBn)_3]_0$ = 200:1:1, red squares.

4.5 Chain transfer ability of bulky borate ester species in the ROP of ε-CL

It is concluded from Chapter Three that the bulky $B(Cy\text{-}H)_3$ demonstrates poor chain transfer ability in the ROP of *rac*-LA. However, it remains unclear whether such bulky borate ester species could be efficiently used as a chain transfer agent in the ROP of ε-CL. Following the model studies described in Section 3.6.2.3, 4 equiv. of 2-methylcyclohexanone was added to **2** in order to generate (Tpm*^{d})Mg(Cy-H) (**12**) and $B(Cy\text{-}H)_3$ *in-situ*, which were subsequently applied as the catalytic system for the ROP of ε-CL. The polymerisation was rapid, reaching 94% conversion (200 equiv. of ε-CL) within 3 min. The reaction conformed to neither first nor second order with respect to ε-CL concentration, as previously observed in ε-CL ROP where $B(OBn)_3$ was used as the chain transfer agent. The experimental M_n values were in good agreement with the calculated ones based on one chain being produced per metal centre, indicating inefficient chain transfer (Figure 4.13). Analysis *via* MALDI-ToF MS revealed the presence of the anticipated Cy-H end group, shown in Figure 4.14.

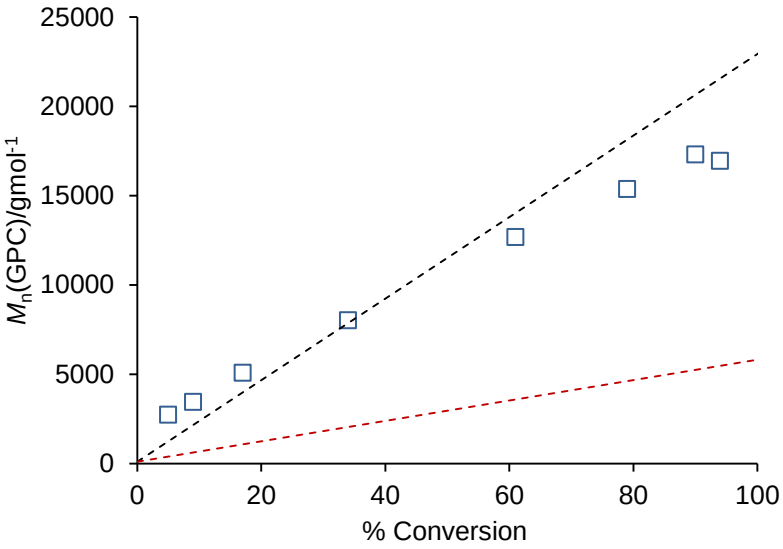


Figure 4.13 Data for the ROP of ε-CL using the *in-situ* generated (Tpm*^{d})Mg(Cy-H) (**12**) and B(Cy-H)$_3$. M_n (GPC) *vs.* % conversion plot. The dashed lines represent M_n expected for one (black) and four (red) chains per metal centre, respectively. Conditions: [ε-CL]$_0$:[**2**]$_0$:[2-methylcyclohexanone]$_0$ = 200:1:4, [ε-CL]$_0$ = 1.0 M, [**2**]$_0$ = 0.005 M, 3.4 mL THF at room temperature.

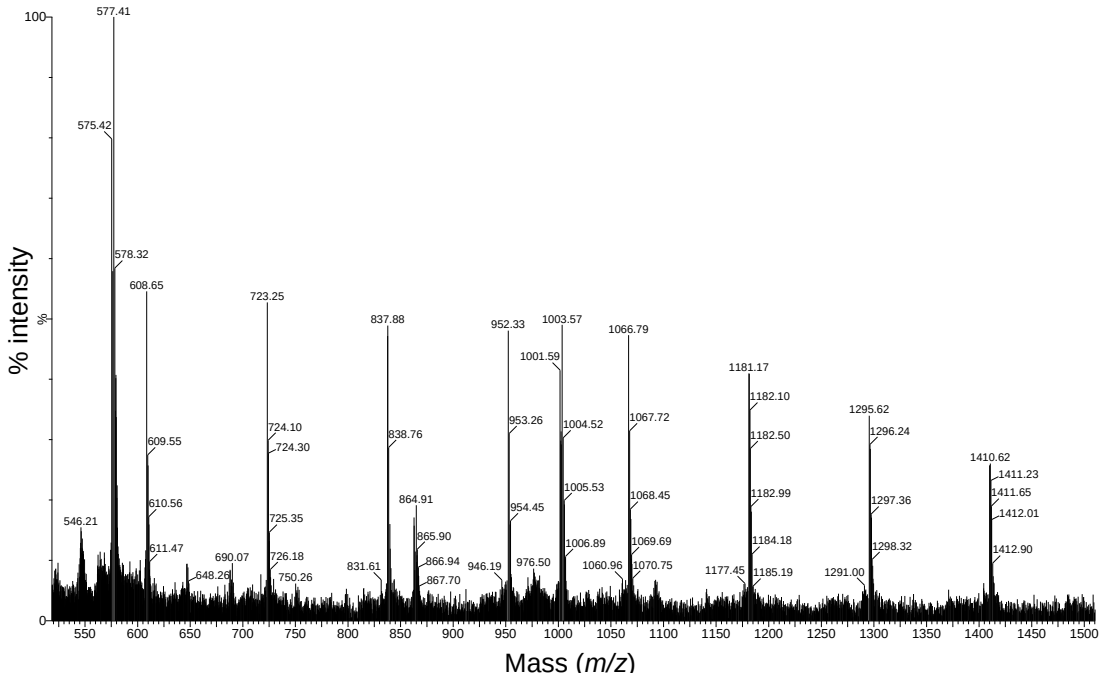


Figure 4.14 MALDI-ToF MS of PCL synthesised using the *in-situ* generated (Tpm*^{d})Mg(Cy-H) (**12**) and B(Cy-H)$_3$. Conditions: [ε-CL]$_0$:[**2**]$_0$:[2-methylcyclohexanone]$_0$ = 200:1:4, [ε-CL]$_0$ = 1.0 M, [**2**]$_0$ = 0.005 M, 3.4 mL THF at room temperature. K^+ dopant.

15 equiv. of ε-CL was added to the *in-situ* generated **12** and B(Cy-H)$_3$ on an NMR tube scale in C_6D_6 in order to gain spectroscopic evidence for the lack of chain transfer events observed in the corresponding large scale polymerisation. 1,4-dimethoxybenzene was used as an internal standard so as to obtain quantitative information. Upon addition of 15 equiv. of ε-CL, complete conversion was achieved within 10 min. The methylene protons closest to the metal centre could be observed as a triplet at 4.49 ppm with a $^3J_{H\text{-}H}$ coupling constant of 6.4 Hz in the ^{1}H NMR spectrum (C_6D_6) (Figure 4.15, b). In addition, signals corresponding to the OC<u>H</u> proton on the Cy-H chain end appeared as a characteristic triplet of doublets ($^3J_{H\text{-}H}$ = 10.0 and 4.0 Hz) at 4.59 ppm. A very minor change was observed in the integration of B(Cy-H)$_3$ before and after the addition of ε-CL, indicating negligible exchange between B(Cy-H)$_3$ and the polymeryl chain. This mirrored the absence of chain transfer effects observed in the corresponding large scale polymerisation.

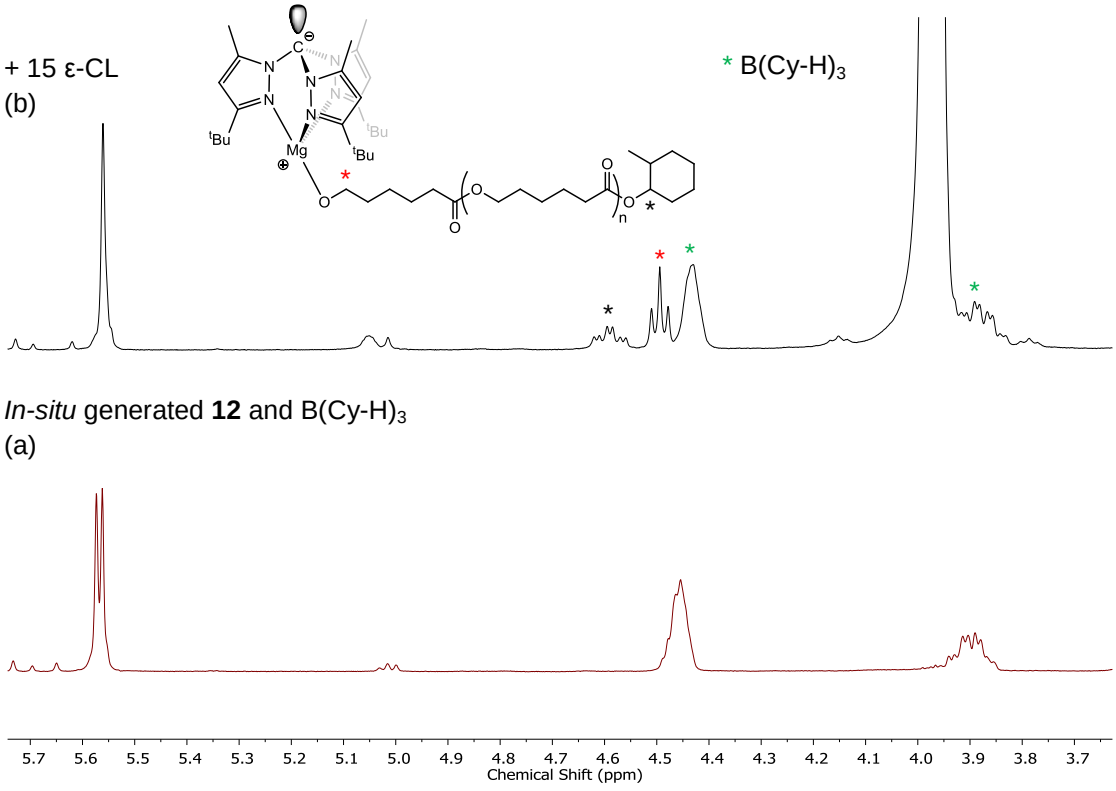


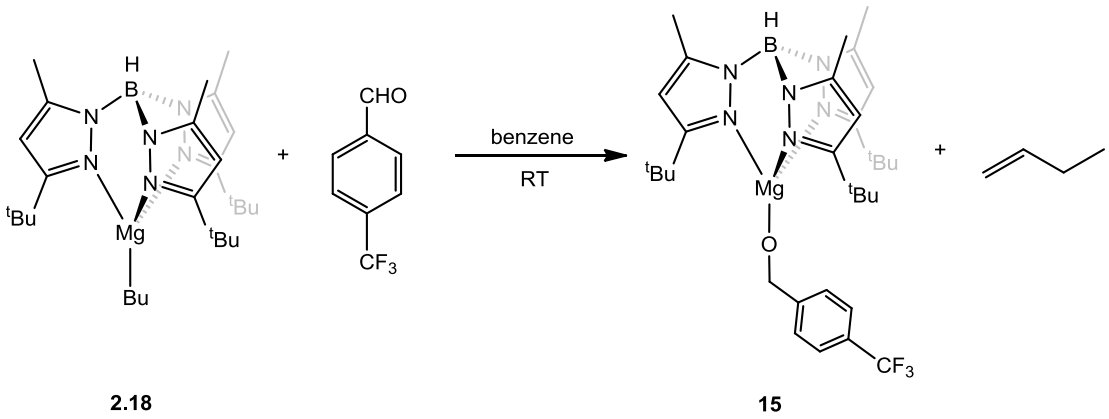
Figure 4.15 ^{1}H NMR spectrum (C_6D_6, 400.2 MHz, 298 K) (a) of the *in-situ* generated (Tpm*^{d})Mg(Cy-H) (**12**) and B(Cy-H)$_3$. ^{1}H NMR spectrum (C_6D_6, 400.2 MHz, 298 K) (b) of the resulting polymeryl chain obtained after the addition of 15 equiv. of ε-CL to **12** and B(Cy-H)$_3$. "*" denotes methylene protons closest to the metal centre. "*" denotes the OC<u>H</u> proton on the Cy-H chain end. "*" denotes B(Cy-H)$_3$.

4.6 The effect of non-activated catalysts on the occurrence of transesterification side reactions

As discussed previously in Chapter Three, the rates of the *rac*-LA ROP using (Tpm*^{d}) and (Tp^{tBu,Me}) ligand-supported alkoxides vary significantly. For example, **5** was able to polymerise 100 equiv. of *rac*-LA within 1 min (k_{obs} = 0.0536(27) s^{-1}) whereas the analogous compound (Tp^{tBu,Me})Mg(OBn) (**2.20**) required 18 h to reach a high level of conversion (k_{obs} = 0.124(3) h^{-1}). Interestingly, the polymerisation initiated by the former was found to be free of any transesterification side reactions as a result of the considerable mismatch between the rates of propagation and exchange. Moreover, the growing polymeryl chain was immediately quenched once a high level of conversion was reached in order to avoid any post-polymerisation intermolecular exchange or back-biting. In contrast, the much slower propagation rate associated with **2.20** facilitated the occurrence of exchange reactions during the ongoing polymerisation. An induction period of approximately 2 h was observed, during which time a high concentration of non-activated catalysts and a low concentration of growing polymeryl chains were simultaneously present in solution. This led to transesterification side reactions, as evidenced by the presence of peak envelopes with $\Delta(m/z)$ of 72 g mol^{-1} in the MALDI-ToF mass spectrum. In order to gain a deeper understanding of the effect of non-activated catalysts on the occurrence of transesterification side reactions, a series of NMR tube scale experiments were performed. The work in this section and Section 4.7 was carried out in collaboration with Dr Insun Yu.

50 equiv. of *L*-LA was added to a solution of (Tp^{tBu,Me})Mg(OMe) (**2.22**) in C_6D_6 to produce a growing polymeryl chain followed by the subsequent addition of 3 equiv. of (Tp^{tBu,Me})Mg($OCH_2C_6H_4CF_3$) (**15**). Complex **2.22** was first synthesised and fully characterised by Dr J. Unruangsri.[2] Complex **15** was selected as the model compound since the CF_3 group allowed monitoring of the exchange processes *via* ^{19}F NMR spectroscopy. Complex **15** was synthesised *via* the β-hydride transfer reaction between (Tp^{tBu,Me})Mg(Bu) (**2.18**) and 4-trifluoromethylbenzylaldehyde and obtained as a white solid in 71% isolated yield. The two phenyl proton environments could be observed as mutually coupled doublets at 7.78 and 7.65 ppm in the ^{1}H NMR spectrum (C_6D_6), with a $^{3}J_{H-H}$ coupling constant of 8.0 Hz. Furthermore, the characteristic

methylene protons on the OC<u>H</u>$_2$C$_6$H$_4$CF$_3$ moiety appeared as a distinct singlet at 5.54 ppm. The ^{19}F NMR spectrum revealed a sharp singlet at -61.42 ppm.



Equation 4.1

The addition of 50 equiv. of *L*-LA to **2.22** in C_6D_6 led to the formation of a growing polymeryl chain. The ^{1}H NMR spectrum recorded 16 h (Figure 4.16, a) after the reaction revealed the two methine protons on the last inserted LA unit as two quartets at 5.33 and 5.22 ppm due to coupling with the adjacent methyl protons. The methyl protons on the O<u>Me</u> chain end were visible as a singlet at 3.15 ppm. Upon addition of 3 equiv. of **15**, the reaction was monitored by ^{1}H NMR spectroscopy at regular intervals over the course of 12 h. The spectrum recorded after 30 min (Figure 4.16, b) revealed the evolution of several new species. Two major phenyl proton resonances were observed at 7.27 and 6.89 ppm, corresponding to ($Tp^{tBu,Me}$)Mg[LA]$_n$(OCH$_2$C$_6$<u>H</u>$_4$CF$_3$). The intensities of these two signals were gradually diminished over the course of 12 h, after which time multiple sets of signals were present in the region of 6.80-7.25 ppm, highlighting the formation of polymer chains of various chain lengths. In good agreement with this was the appearance of multiple signals in the region of 4.65-4.85 ppm, signifying the presence of multiple ($Tp^{tBu,Me}$)Mg[LA]$_n$(OC<u>H</u>$_2$C$_6$H$_4$CF$_3$) environments. Furthermore, the distinct quartets corresponding to the methine protons on the last inserted LA unit slowly merged with other signals, resulting in more complex patterns.

The reaction was also monitored by ^{19}F NMR spectroscopy, revealing the gradual disappearance of **15** over time (Figure 4.17). In contrast, three major resonances corresponding to ($Tp^{tBu,Me}$)Mg[LA]$_n$(OCH$_2$C$_6$H$_4$C<u>F</u>$_3$) of various chain lengths were

visible at -62.36, -62.41 and -62.42 ppm, with the latter two being observed as overlapping signals, which increased in intensity over time whereas the former was diminished in 12 h. These NMR spectroscopic observations clearly indicated the ongoing intermolecular exchange processes between a polymeryl chain and a metal alkoxide species, resulting in the generation of new polymeryl chains of various lengths.

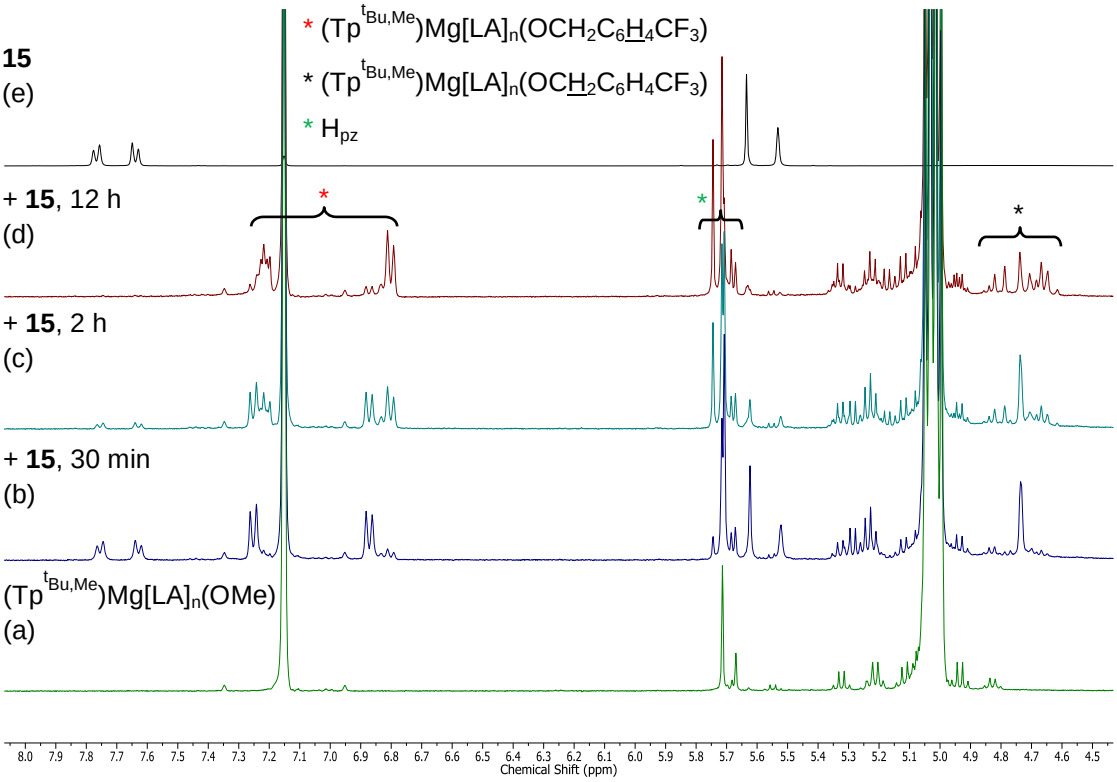


Figure 4.16 ^{1}H NMR spectrum (C_6D_6, 400.2 MHz, 298 K) (a) of ($Tp^{tBu,Me}$)Mg[LA]$_{50}$(OMe) obtained *via* reacting ($Tp^{tBu,Me}$)Mg(OMe) (**2.22**) with 50 equiv. of *L*-LA. ^{1}H NMR spectra (C_6D_6, 400.2 MHz, 298 K) of the resulting polymeryl chain obtained (b) 30 min, (c) 2 h and (d) 12 h after the addition of ($Tp^{tBu,Me}$)Mg($OCH_2C_6H_4CF_3$) (**15**). ^{1}H NMR spectrum (C_6D_6, 400.2 MHz, 298 K) (e) of **15**. "*" denotes ($Tp^{tBu,Me}$)Mg[LA]$_n$($OCH_2C_6\underline{H}_4CF_3$). "*" denotes ($Tp^{tBu,Me}$)Mg[LA]$_n$($OC\underline{H}_2C_6H_4CF_3$). "*" denotes H_{pz} signals.

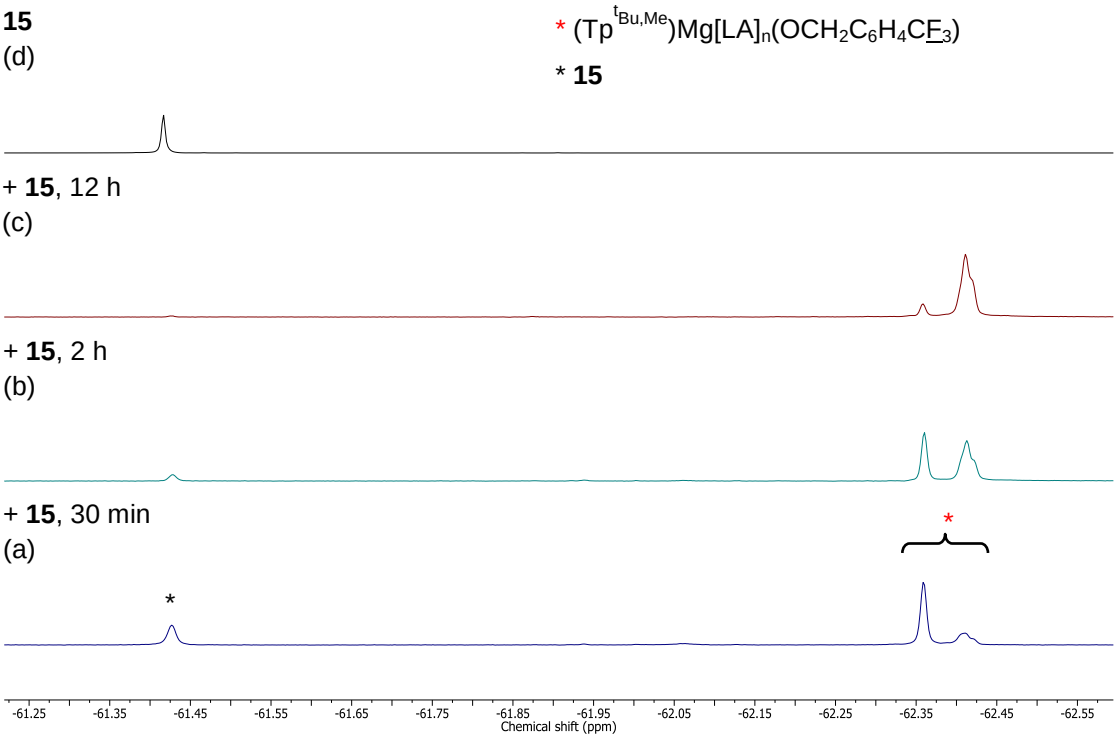


Figure 4.17 ^{19}F NMR spectra (C_6D_6, 176.5 MHz, 298 K) of (Tp^{tBu,Me})Mg[LA]$_n$(OCH$_2$C$_6$H$_4$CF$_3$) obtained (a) 30 min, (b) 2 h and (c) 12 h after the addition of (Tp^{tBu,Me})Mg(OCH$_2$C$_6$H$_4$CF$_3$) (**15**) to (Tp^{tBu,Me})Mg[LA]$_{50}$(OMe). ^{19}F NMR spectrum (C_6D_6, 176.5 MHz, 298 K) (d) of **15**. "*" denotes (Tp^{tBu,Me})Mg[LA]$_n$(OCH$_2$C$_6$H$_4$C<u>F</u>$_3$). "*" denotes (Tp^{tBu,Me})Mg(OCH$_2$C$_6$H$_4$C<u>F</u>$_3$).

Following this preliminary investigation, further studies were undertaken to evaluate whether the length of a growing polymeryl chain would have an impact on the rate of such exchange processes. (Tp^{tBu,Me})Mg[LA](OMe) containing one LA unit was therefore generated *via* the reaction between **2.22** and *L*-LA in a 1:1 stoichiometry and characterised by ^{1}H NMR spectroscopy (Figure 4.18, a). The two methine protons were visible as overlapping quartets in the region of 5.20-5.26 ppm whereas the methyl protons appeared as two doublets at 2.00 and 1.21 ppm ($^3J_{H\text{-}H}$ = 7.2 Hz). In addition, the OC<u>H</u>$_3$ protons could be clearly identified as a singlet at 3.22 ppm. Upon addition of 1 equiv. of **15**, the majority of **15** remained unreacted after 2 h but slowly underwent intermolecular exchange with the short polymeryl chain over the course of 20 h to produce (Tp^{tBu,Me})Mg[LA]$_n$(OCH$_2$C$_6$H$_4$CF$_3$) species, as evidenced by the evolution of two major sets of doublets in the aromatic region. Further evidence for the formation of polymeryl chains of various lengths was the presence of multiple sets

of H_{pz} and $(Tp^{tBu,Me})Mg[LA]_n(OC\underline{H}_2C_6H_4CF_3)$ signals in the region of 5.69-5.76 and 4.71-4.83 ppm, respectively. The aforementioned ^1H NMR spectroscopic observations mirrored those obtained from ^{19}F NMR studies, which revealed a gradual decrease in intensity of the peak at -61.42 ppm, corresponding to **15**. In contrast, gradually intensifying signals associated with $(Tp^{tBu,Me})Mg[LA]_n(OCH_2C_6H_4C\underline{F}_3)$ were visible at -62.36 and -62.41 ppm. These NMR data indicated the occurrence of intermolecular exchange between a short polymeryl chain and a metal alkoxide species. However, these exchange reactions occur at a much lower rate in comparison to those involving longer polymeryl chains, presumably due to the steric hindrance imposed by the bulky $Tp^{tBu,Me}$ ligand.

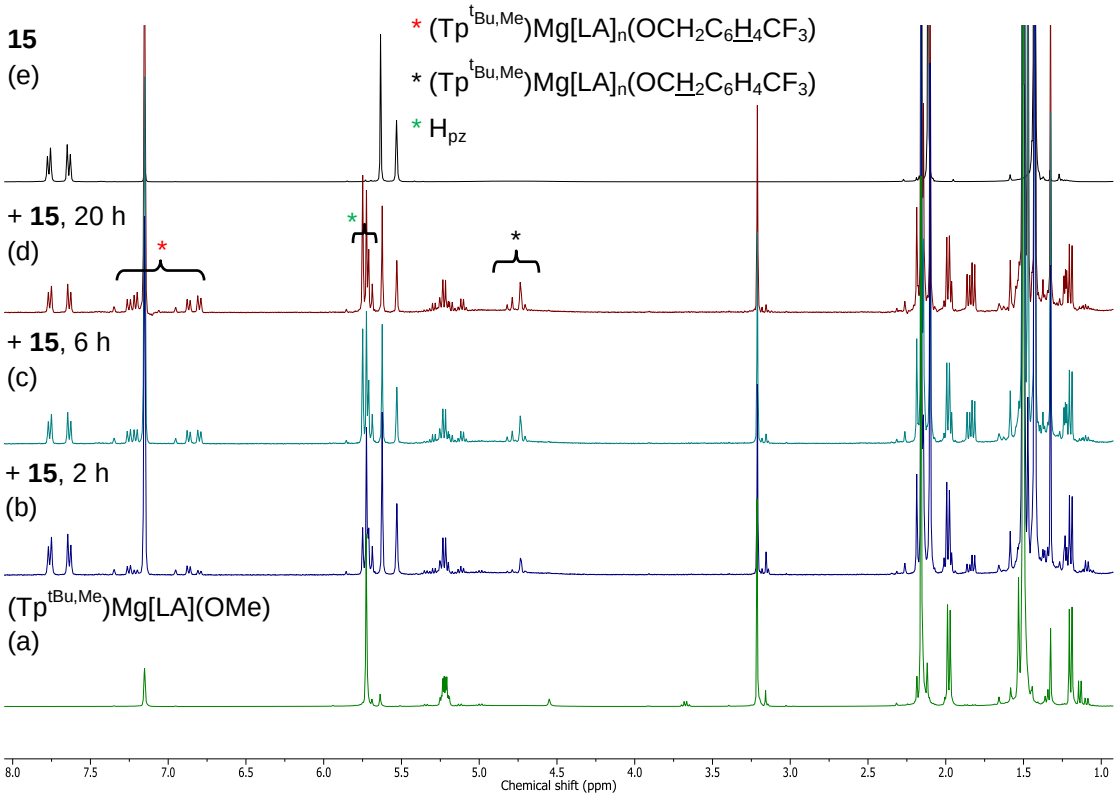


Figure 4.18 ^1H NMR spectrum (C_6D_6, 400.2 MHz, 298 K) (a) of $(Tp^{tBu,Me})Mg[LA](OMe)$ obtained *via* reacting $(Tp^{tBu,Me})Mg(OMe)$ (**2.22**) with 1 equiv. of *L*-LA. ^1H NMR spectra (C_6D_6, 400.2 MHz, 298 K) of $(Tp^{tBu,Me})Mg[LA]_n(OCH_2C_6H_4CF_3)$ obtained (b) 2 h, (c) 6 h and (d) 20 h after the addition of $(Tp^{tBu,Me})Mg(OCH_2C_6H_4CF_3)$ (**15**) to $(Tp^{tBu,Me})Mg[LA](OMe)$. ^1H NMR spectrum (C_6D_6, 400.2 MHz, 298 K) (e) of **15**. "*" denotes $(Tp^{tBu,Me})Mg[LA]_n(OCH_2C_6\underline{H}_4CF_3)$. "*" denotes $(Tp^{tBu,Me})Mg[LA]_n(OC\underline{H}_2C_6H_4CF_3)$. "*" denotes H_{pz} signals.

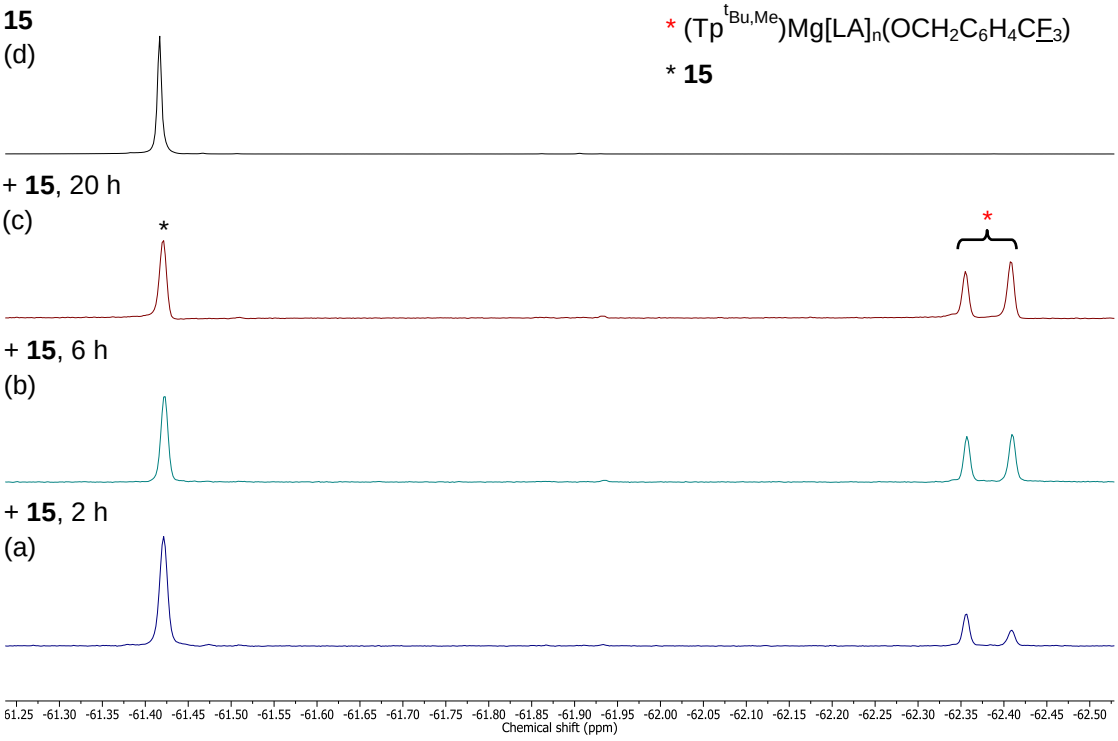


Figure 4.19 ^{19}F NMR spectra (C_6D_6, 176.5 MHz, 298 K) of ($Tp^{tBu,Me}$)Mg[LA]$_n$($OCH_2C_6H_4CF_3$) obtained (a) 2 h, (b) 6 h and (c) 20 h after the addition of ($Tp^{tBu,Me}$)Mg($OCH_2C_6H_4CF_3$) (**15**) to ($Tp^{tBu,Me}$)Mg[LA](OMe). ^{19}F NMR spectrum (C_6D_6, 176.5 MHz, 298 K) (d) of **15**. "*" denotes ($Tp^{tBu,Me}$)Mg[LA]$_n$($OCH_2C_6H_4C\underline{F}_3$). "*" denotes **15**.

4.7 Exchange processes between a borate ester and a metal alkoxide or metal polymeryl species

Whilst attempts to utilise borate ester species as efficient chain transfer agents failed in the Tpm*[d]-supported catalytic systems, previous work in the Mountford group has found two other systems where borate ester species were successfully used to induce immortal ROP. As mentioned previously, the polymerisation using *in-situ* generated ($Tp^{tBu,Me}$)Mg(OBn) (**2.20**) and $B(OBn)_3$ yielded PLA whose experimental M_n was very close to the theoretical value based on four chains per metal centre, indicative of efficient chain transfer.[2] Moreover, ($CzOx^{Me2}$)Mg(OBn) (**4.1**), in the presence of $B(OBn)_3$, induced immortal ROP in a well-controlled manner, affording heterotactic PLA with a good agreement between the experimental and calculated M_n.[3] These results have introduced borate ester species as a new type of aprotic chain transfer

agent, the promising potential of which could be extended to other catalytic systems, particularly those which demonstrated high sensitivity towards protic species.

In order to gain further insight into the occurrence of chain transfer events, an NMR tube scale reaction (C_6D_6) was performed by adding 1 equiv. of $B(OBn)_3$ to ($Tp^{tBu,Me}$)Mg[LA]$_5$(OMe), obtained by reacting **2.22** with 5 equiv. of *L*-LA. A minor amount of ($Tp^{tBu,Me}$)Mg(OBn) (**2.20**) was observed after 10 min, as evidenced by the two doublets at 7.87 and 7.43 ppm in the ^{1}H NMR spectrum (Figure 4.20, b), corresponding to the aromatic protons. The formation of **2.20** was postulated to proceed through a tetra-coordinated adduct species, shown in Scheme 4.2.

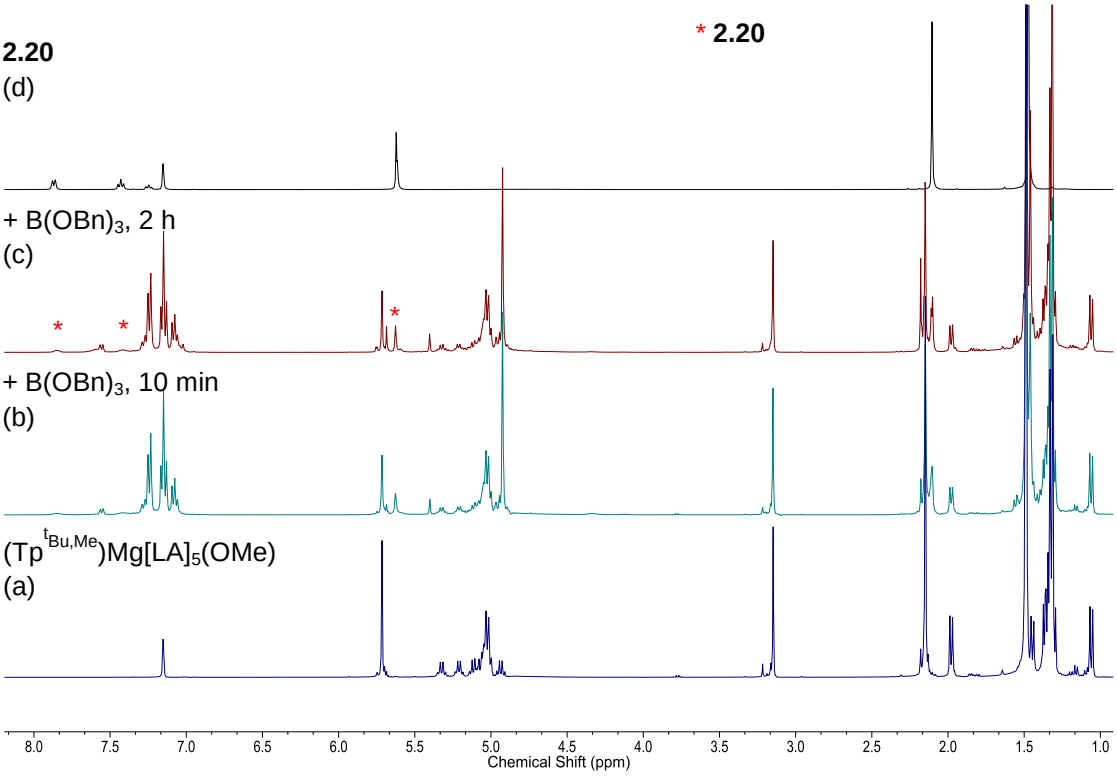
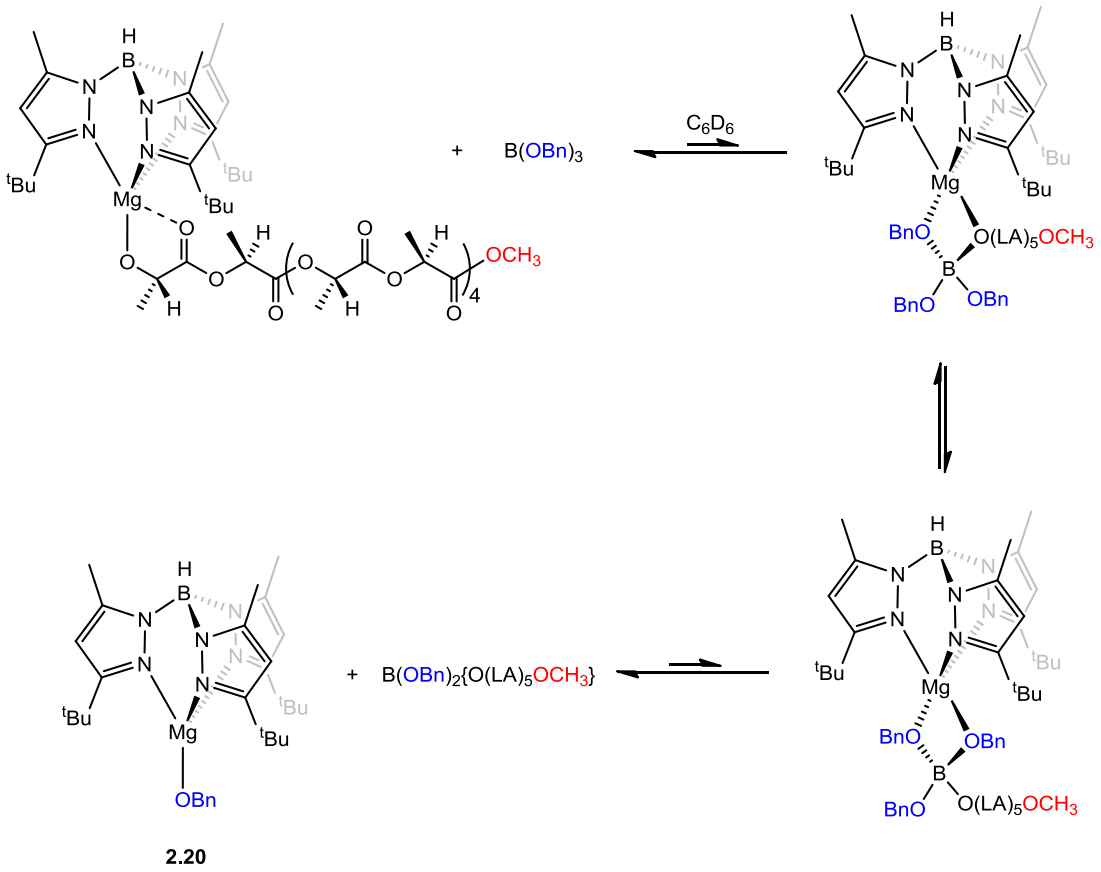


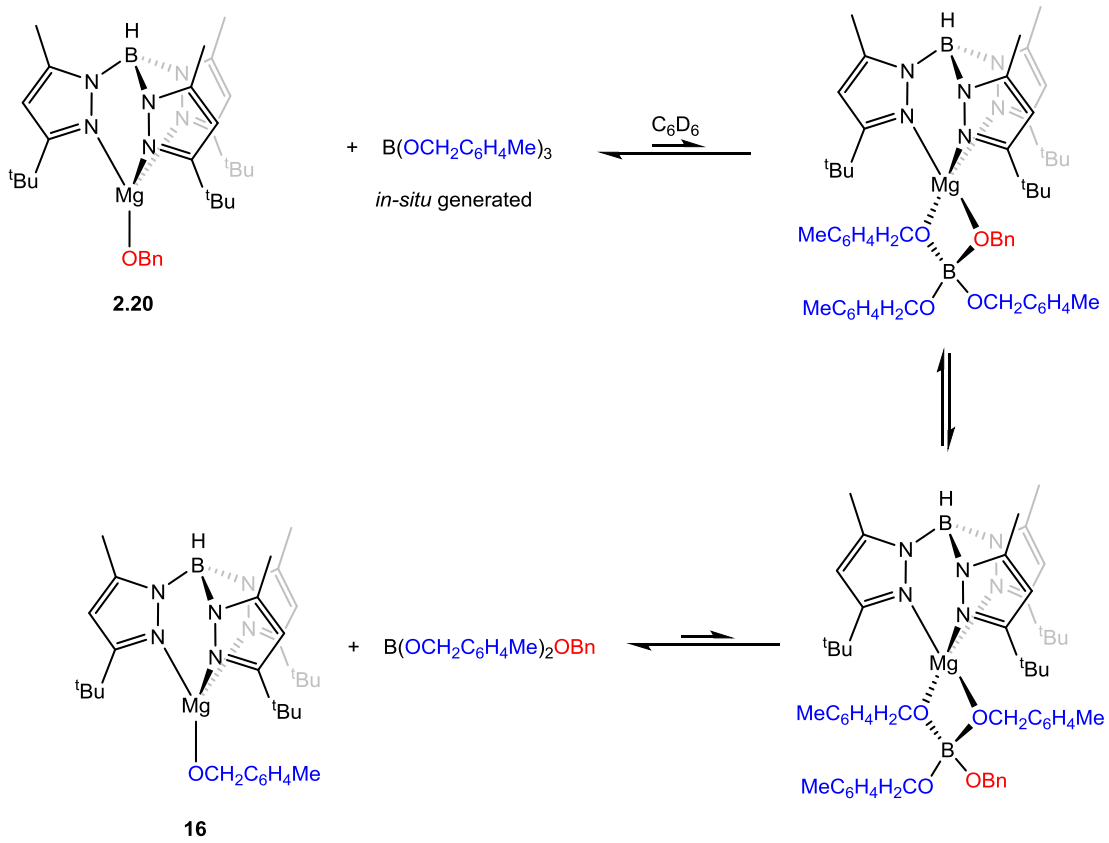
Figure 4.20 ^{1}H NMR spectrum (C_6D_6, 400.2 MHz, 298 K) (a) of ($Tp^{tBu,Me}$)Mg[LA]$_5$(OMe) obtained *via* reacting ($Tp^{tBu,Me}$)Mg(OMe) (**2.22**) with 5 equiv. of *L*-LA. ^{1}H NMR spectra (C_6D_6, 400.2 MHz, 298 K) of the polymeryl chain obtained (b) 10 min and (c) 2 h after the addition of $B(OBn)_3$ to ($Tp^{tBu,Me}$)Mg[LA]$_5$(OMe). ^{1}H NMR spectrum (C_6D_6, 400.2 MHz, 298 K) (d) of ($Tp^{tBu,Me}$)Mg(OBn) (**2.20**). "*" denotes **2.20**.



Scheme 4.2 Exchange between $B(OBn)_3$ and $(Tp^{tBu,Me})Mg[LA]_5(OMe)$.

Following this preliminary investigation, the exchange process between a borate ester and a metal alkoxide species was further studied by the equimolar reaction between $(Tp^{tBu,Me})Mg(OBn)$ (**2.20**) and $B(OCH_2C_6H_4Me)_3$. The latter was generated *in-situ* by reacting $BH_3(THF)$ with 3.2 equiv. of *p*-tolualdehyde in C_6D_6. After 16 h, full conversion to $B(OCH_2C_6H_4Me)_3$ was reached, with the two aromatic protons appearing as doublets at 7.01 and 7.24 ppm in the ^1H NMR spectrum (Figure 4.21, c). The *in-situ* generated $B(OCH_2C_6H_4Me)_3$, in the presence of unreacted *p*-tolualdehyde, was subsequently added to a C_6D_6 solution of **2.20** and the reaction was studied by ^1H NMR spectroscopy (Figure 4.21, a). Exchange occurred rapidly to generate $(Tp^{tBu,Me})Mg(OCH_2C_6H_4Me)$ (**16**) and $B(OBn)_n(OCH_2C_6H_4Me)_{3-n}$ within 10 min. One of the aromatic proton environments for **16** could be clearly identified as a doublet at 7.81 ppm whereas the other was obscured by overlapping signals assigned to borate ester species. The region of 4.93-4.98 ppm revealed the formation of several methylene proton environments, signifying the presence of multiple

$B(OBn)_n(OCH_2C_6H_4Me)_{3-n}$ species. It is notable that signals corresponding to **2.20** and $B(OCH_2C_6H_4Me)_3$ were also present in the ^1H NMR spectrum.



Scheme 4.3 Exchange between $B(OCH_2C_6H_4Me)_3$ and $(Tp^{tBu,Me})Mg(OBn)$ (**2.20**).

In order to confirm the formation of **16** during the above-discussed exchange process, an independent synthesis was carried out by reacting $(Tp^{tBu,Me})Mg(Bu)$ (**2.18**) with *p*-tolualdehyde in a 1:1 stoichiometry in benzene. Complex **16** was obtained as a white solid in 92% isolated yield. By comparing the ^1H NMR spectrum of the independently synthesised **16** (Figure 4.21, d) with that of the reaction between **2.20** and $B(OCH_2C_6H_4Me)_3$, it is evident that **16** was indeed formed as a product in the exchange process.

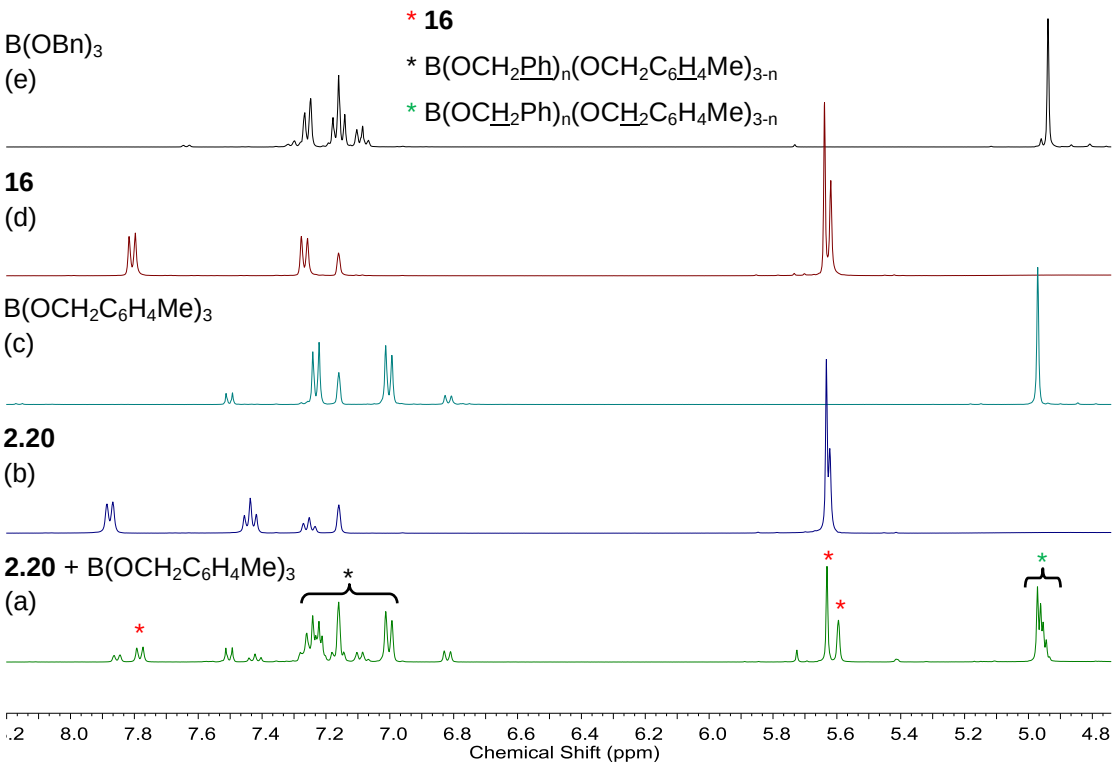


Figure 4.21 ^{1}H NMR spectrum (C_6D_6, 400.2 MHz, 298 K) (a) of the equimolar reaction between ($Tp^{tBu,Me}$)Mg(OBn) (**2.20**) and $B(OCH_2C_6H_4Me)_3$. ^{1}H NMR spectra (C_6D_6, 400.2 MHz, 298 K) of (b) **2.20**, (c) *in-situ* generated $B(OCH_2C_6H_4Me)_3$, (d) independently synthesised ($Tp^{tBu,Me}$)Mg($OCH_2C_6H_4Me$) (**16**) and (e) $B(OBn)_3$. "*" denotes **16**. "*" denotes $B(OCH_2\underline{Ph})_n(OCH_2C_6\underline{H}_4Me)_{3-n}$. "*" denotes $B(OC\underline{H}_2Ph)_n(OC\underline{H}_2C_6H_4Me)_{3-n}$.

4.8 Summary and conclusions

This Chapter evaluated the chain transfer ability of $B(OBn)_3$ in the ROP of *rac*-LA initiated by (Tpm^{*d})Mg(OBn) (**5**). $B(OBn)_3$ was found to be a poor chain transfer agent due to the significant mismatch between the rates of propagation and chain transfer, leading to the formation of polymers whose experimental M_n was close to the expected value based on one chain per metal centre. The incorporation of $B(OBn)_3$ also led to a decrease in polymerisation rate, due to the formation of a tetra-coordinated adduct which was postulated to be the catalyst resting state. This led to a decrease in the concentration of the active catalysts, therefore slowing the rate of the polymerisation. The addition of $B(OBn)_3$ also led to a shift of polymerisation kinetics from being first to second order with respect to *rac*-LA concentration, suggesting the non-innocent role of $B(OBn)_3$ in monomer coordination.

In contrast, $B(OBn)_3$ could be successfully used as a chain transfer agent in the ROP of ε-CL; the experimental M_n was in good agreement with the calculated value based on four chains per metal centre. An NMR tube scale polymerisation was also performed to confirm the efficient chain transfer ability of $B(OBn)_3$. Neither first nor second order kinetics were observed, presumably due to the presence of a complex pre-equilibrium upon association and dissociation of borate esters prior to and following LA insertion. Solvent effects were subsequently investigated by performing the polymerisations in toluene. Interestingly, the reaction proceeded slightly faster in THF than in toluene, the origin of which remains unclear.

The ROP of *rac*-LA using $(Tp^{tBu,Me})Mg(Cy\text{-}H)$ (**13**) was also studied. Complex **13** exhibited moderate activity, affording heterotactic PLA whose experimental M_n agreed well with the expected value based on one chain per metal centre. Upon addition of $B(Cy\text{-}H)_3$, no rate reduction was observed. This was attributed to the fact that $B(Cy\text{-}H)_3$ and **13** remained as separate species as opposed to a tetra-coordinated adduct. In addition, no chain transfer effect was observed, as evidenced by the close to expected M_n based on one chain per metal centre. This is in contrast to the polymerisation involving the use of **13** and $B(OBn)_3$. The active species was determined to be $(Tp^{tBu,Me})Mg(OBn)$ (**2.20**), formed by the exchange reaction between **13** and $B(OBn)_3$. $B(OBn)_n(Cy\text{-}H)_{3-n}$ was also generated, inducing chain transfer effects to produce PLA with an experimental M_n corresponding to two chains being produced per metal centre. Furthermore, $B(Cy\text{-}H)_3$ was found to be a poor chain transfer agent in the ROP of ε-CL, confirmed by both NMR studies and large scale polymerisations.

The effect of non-activated catalysts on the occurrence of transesterification side reactions was also investigated. $(Tp^{tBu,Me})Mg(OCH_2C_6H_4CF_3)$ (**15**) was added to a long polymeryl chain $(Tp^{tBu,Me})Mg[LA]_{50}(OMe)$, synthesised by the reaction between $(Tp^{tBu,Me})Mg(OMe)$ (**2.22**) and 50 equiv. of *L*-LA in C_6D_6. Intermolecular transesterification was observed within 30 min, as evidenced by the formation of multiple sets of signals corresponding to $(Tp^{tBu,Me})Mg[LA]_n(OCH_2C_6H_4CF_3)$ of various chain lengths in the ^1H NMR spectrum. This is in good agreement with the results obtained from ^{19}F NMR spectroscopy, revealing the presence of three major peaks corresponding to $(Tp^{tBu,Me})Mg[LA]_n(OCH_2C_6H_4C\underline{F}_3)$. Following this preliminary investigation, **15** was added to a short polymeryl chain

($Tp^{tBu,Me}$)Mg[LA](OMe) in order to evaluate the effect of polymer chain length on the degree of intermolecular exchange reactions. ($Tp^{tBu,Me}$)Mg[LA](OMe) was synthesised on the NMR tube scale by adding 1 equiv. of *L*-LA to **2.22** in C_6D_6. Intermolecular transesterification did occur albeit slowly upon addition of **15**. Both ^{1}H and ^{19}F NMR spectra revealed a significant quantity of unreacted **15** after 20 h.

The exchange process between a borate ester and a polymeryl species was also investigated. The ^{1}H NMR spectrum (C_6D_6) of the reaction between $B(OBn)_3$ and ($Tp^{tBu,Me}$)Mg[LA]$_5$(OMe) revealed the generation of ($Tp^{tBu,Me}$)Mg(OBn) (**2.20**), proceeding through a tetra-coordinated adduct.

The exchange process between a borate ester and a metal alkoxide species was also investigated by the NMR tube scale reaction (C_6D_6) between **2.20** and $B(OCH_2C_6H_4Me)_3$. The latter was synthesised *in-situ* by reacting BH_3(THF) with *p*-tolualdehyde. The exchange process occurred very rapidly following the addition of $B(OCH_2C_6H_4Me)_3$ to **2.20**, producing ($Tp^{tBu,Me}$)Mg($OCH_2C_6H_4Me$) (**16**) and $B(OBn)_n(OCH_2C_6H_4Me)_{3-n}$. An independent synthesis of **16** was subsequently carried out by reacting ($Tp^{tBu,Me}$)Mg(Bu) (**2.18**) with *p*-tolualdehyde to confirm its formation in the above-mentioned exchange process.

4.9 References for Chapter Four

1. G. Wu, W. Sun and Z. Shen, *React. Func. Polym.*, 2008, **68**, 822.
2. J. Unruangsri, *D.Phil Thesis, University of Oxford*, 2014.
3. B. A. Core, *DPhil Thesis, University of Oxford*, 2015.
4. Y. Gao, Z. Dai, J. Zhang, X. Ma, N. Tang and J. Wu, *Inorg. Chem.*, 2014, **53**, 716.
5. M. P. Blake, A. D. Schwarz and P. Mountford, *Organometallics*, 2011, **30**, 1202.
6. H.-Y. Chen, B.-H. Huang and C.-C. Lin, *Macromolecules*, 2005, **38**, 5400.
7. P. I. Binda and E. E. Delbridge, *Dalton Trans.*, 2007, 4685.
8. R. A. Collins, J. Unruangsri and P. Mountford, *Dalton Trans.*, 2013, **42**, 759.
9. M. H. Chisholm, J. Gallucci and K. Phomphrai, *Inorg. Chem.*, 2002, **41**, 2785.
10. M. H. Chisholm, J. C. Gallucci and K. Phomphrai, *Inorg. Chem.*, 2005, **44**, 8004.
11. I. Palard, A. Soum and S. M. Guillaume, *Macromolecules*, 2005, **38**, 6888.

12. P. Ravi, T. Gröb, K. Dehnicke and A. Greiner, *Macromolecules*, 2001, **34**, 8649.
13. S. Agarwal and M. Puchner, *Eur. Polym. J.*, 2002, **38**, 2365.
14. K. Nie, L. Fang, Y. Yao, Y. Zhang, Q. Shen and Y. Wang, *Inorg. Chem.*, 2012, **51**, 11133.
15. T. V. Mahrova, G. K. Fukin, A. V. Cherkasov, A. A. Trifonov, N. Ajellal and J.-F. Carpentier, *Inorg. Chem.*, 2009, **48**, 4258.
16. N. Ajellal, D. M. Lyubov, M. A. Sinenkov, G. K. Fukin, A. V. Cherkasov, C. M. Thomas, J.-F. Carpentier and A. A. Trifonov, *Chem. Eur. J.*, 2008, **14**, 5440.
17. H. Ma and J. Okuda, *Macromolecules*, 2005, **38**, 2665.
18. H. Ma, T. P. Spaniol and J. Okuda, *Inorg. Chem.*, 2008, **47**, 3328.
19. A. Pilone, M. Lamberti, M. Mazzeo, S. Milione and C. Pellecchia, *Dalton Trans.*, 2013, **42**, 13036.

Chapter Five

Chiral bis(oxazolinylphenyl)amine ligand-supported magnesium catalysts for the ROP of *rac*-, *L*-, *D*- and *meso*-LA

5.1 Overview

This Chapter will describe the synthesis and characterisation of a series of chiral bis(oxazolinylphenyl)amine (BOPA)-supported magnesium complexes. The catalytic activities of five of the compounds will be examined in the living or immortal ROP of *rac*-, *L*-, *D*- and *meso*-LA followed by an investigation of solvent effects. Thirteen new complexes will be presented in this Chapter, along with six solid state structures.

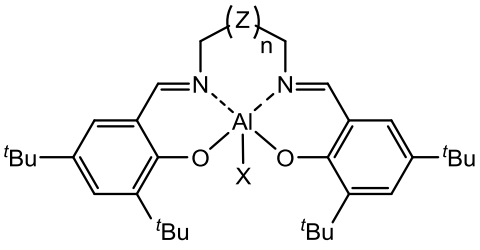
5.2 Introduction

The stereoselective ROP of *rac*-LA initiated by various catalytic systems has been of considerable interest in the last two decades due to the fact that polymer microstructure plays an important role in the physical and mechanical properties of the resulting PLA.[1-15] For example, atactic PLA is amorphous and possesses a glass transition temperature (T_g) of approximately 60 °C whereas the melting point (T_m) of isotatic PLA can be higher than 180 °C.[16-22] In theory, the production of isotactic PLA can be achieved by the ROP of enantiomerically pure LA in the absence of epimerisation. However, the use of *rac*-LA not only results in cost reduction but also opens up the possibility of producing stereoblock or stereocomplex PLA, which feature higher T_m than homochiral polymers alone.[21, 22] It is therefore not surprising that numerous efforts have been made to develop catalysts for the stereoselective ROP of LA, particularly those which can produce isotatic PLA from *rac*-LA.

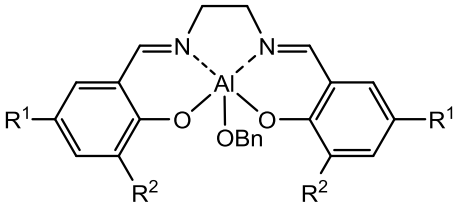
5.2.1 Achiral initiators for the isoselective ROP of LA

The area of stereoselective ROP of LA was pioneered by Spassky *et al.* who developed a chiral aluminium catalyst, the details of which will be discussed in Section 5.2.2.[23] Following this breakthrough, Nomura *et al.* prepared a series of aluminium benzyloxide complexes **5.1**-**5.4** (Figure 5.1) supported by salen ligands with different substituents on the backbone.[24] These catalysts were prepared *in-situ* by reacting the protio-ligands with 1 equiv. of triethylaluminium in toluene at 70 °C for 3 h followed by the addition of 1 equiv. of benzyl alcohol. The resulting catalyst solution was treated with 100 equiv. of *rac*-LA in toluene at 70 °C. It was found that incorporating two methyl groups on the backbone increased the catalytic activities while maintaining a high level of isoselectivity (94% conversion at 14 h for **5.1** *vs*. 90% conversion at 6 h for **5.2**, P_m = 0.80 for both). In contrast, the introduction of even

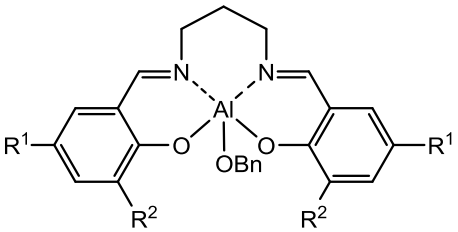
bulkier ligand backbones (**5.3** and **5.4**) resulted in a reduction in both activity and stereoselectivity. Compound **5.2** was subsequently examined in the ROP of *rac*-LA under melt conditions, yielding crystalline stereoblock PLA (P_m = 0.84) at an industrially favoured high temperature (180 °C) *via* a chain end control mechanism. In the same year, Chen and co-workers reported a similar aluminium alkyl complex **5.5**, which produced stereoblock PLA (P_m = 0.9) with a T_m as high as 201 °C in the presence of one equiv. of isopropanol in toluene at 70 °C, also as a result of a chain end control mechanism.[25] The polymerisation was found to exhibit moderate molecular weight control, with a linear growth of M_n *vs.* % conversion and narrow PDIs (1.05-1.21). The active isopropoxide species **5.6** was independently synthesised by heating the protio-ligand with $Al(O^iPr)_3$ in toluene and probed in the ROP of *rac*-LA, giving similar polymerisation results as expected.[26]



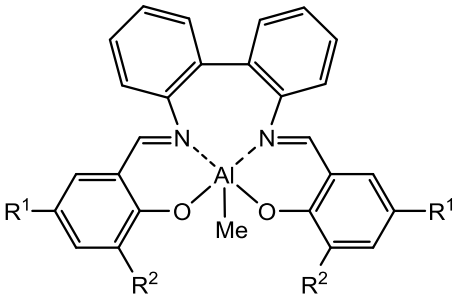
Z = CH_2, X = OBn (**5.1**)
Z = CMe_2, X = OBn (**5.2**)
Z = CEt_2, X = OBn (**5.3**)
Z = CBn_2, X = OBn (**5.4**)
Z = CMe_2, X = Et (**5.5**)
Z = CMe_2, X = O^iPr (**5.6**)



$R^1 = R^2$ = H (**5.7**)
$R^1 = R^2 = {}^tBu$ (**5.8**)
R^1 = Cl, R^2 = H (**5.9**)
$R^1 = R^2$ = Cl (**5.10**)



$R^1 = R^2$ = H (**5.11**)
$R^1 = R^2 = {}^tBu$ (**5.12**)
$R^1 = R^2$ = Cl (**5.13**)



$R^1 = R^2$ = H (**5.14**)
$R^1 = R^2 = {}^tBu$ (**5.15**)
$R^1 = R^2$ = Cl (**5.16**)

Figure 5.1 Literature examples of achiral initiators for the isoselective ROP of *rac*-LA.[24-27]

Reported by Gibson *et al*. in 2006, a series of *in-situ* generated aluminium complexes **5.7**-**5.16** supported by Schiff base ligands with various backbones and substituents on

the phenyl rings were examined as *rac*-LA ROP catalysts in toluene at 70 °C.[27] For initiators with a C_2 backbone, a significant steric effect upon incorporation of bulky substituents at the *ortho* position of the phenoxy group was observed. Comparisons of the kinetic data for polymerisations using **5.7** and **5.8** revealed a dramatic rate difference, with the former being sixty times faster than the latter. In addition, an electronic effect induced by the *para* chloro substituents in **5.9** was present, leading to a less pronounced but still noticeable rate enhancement; ROP employing **5.9** was twice as fast as that using **5.7**. Incorporation of an extra chloro substituent at the *ortho* position led to a further increase in the activity of the catalyst (**5.10**), presumably due to a combination of steric and electronic effects. All PLA produced using the aforementioned catalysts displayed a bias towards isotactic enrichment, with the highest P_m value (0.83) being observed for PLA obtained using the most sterically encumbered **5.8**. Interestingly, compound **5.9** afforded PLA with the lowest isotacticity despite the presence of bulky chloro substituents at the *ortho* position of the phenoxy ring. Lengthening the backbone to a C_3 linker resulted in a dramatic increase in the polymerisation rate. For example, comparisons between compounds **5.7** and **5.11** revealed an eleven-fold rate enhancement whilst an even more significant effect (k_{rel} = 130) was observed between di-*tert*-butyl substituted **5.8** and **5.12**. A concomitant increase in isoselectivity was also detected for compounds **5.11**-**5.13** upon lengthening the backbone. *Rac*-LA ROP activities of *in-situ* generated catalysts **5.14**-**5.16** featuring a diphenyl linker were also investigated in toluene at 70 °C. A considerable decrease in activity was observed, presumably due to reduced nucleophilicity of the metal centre as a result of delocalisation of the phenyl rings, therefore slowing down the LA insertion process. Unexpectedly, the dichloro-substituted complex **5.16** led to the formation of heterotactic PLA, the only example in this series of catalysts which demonstrated heteroselectivity.

Nomura *et al*. later carried out a similar structure-activity analysis regarding the effect of backbone and substituents on the polymerisation rates and degree of stereocontrol.[28] Among the series, *in-situ* generated **5.17** (Figure 5.2) with a sterically demanding $^tBuMe_2Si$ substituent at the *ortho* position of the phenoxy ring produced a stereoblock PLA with the highest P_m value reported to date using an achiral catalyst (P_m = 0.98, T_m = 210 °C).

In 2005, Chen and co-workers reported a series of aluminium complexes supported by Schiff base ligands derived from β-diketones.[29] For example, complexes **5.18** and **5.19** were generated *in-situ* by reacting the corresponding aluminium ethyl complexes with 1 equiv. of isopropanol in toluene. Their *rac*-LA ROP activities were subsequently investigated by treating the catalyst solution with 65 equiv. of *rac*-LA in toluene at 70 °C. As observed previously, the length of the backbone was found to have an influence on the catalytic activity, with **5.18** inducing polymerisation at a lower rate than **5.19** featuring a C_3 linker. This was rationalised by the less rigid nature of the backbone for the latter, resulting in more facile monomer coordination and subsequent insertion. Interestingly, incorporation of a longer linker also led to the formation of more isotactically enriched PLA (P_m = 0.76 using **5.19** *vs.* P_m = 0.70 using **5.18**). Complex **5.20**, synthesised by reacting the aluminium ethyl complex with 1 equiv. of isopropanol, demonstrated the highest activity and isoselectivity among the series, affording PLA with a narrow PDI and a P_m value of 0.78. For all polymerisations employing **5.18**-**5.20**, a linear growth of M_n *vs.* % conversion was observed, in conjunction with narrow PDIs (1.07-1.27).

Following these promising results, the same group extended the scope of study by investigating the effect of substituents at the enol position of the ligand.[29] It was found that the introduction of electron-withdrawing groups led to an increase in the activity of the catalysts. Compound **5.23**, generated *in-situ*, was found to induce faster polymerisation than its counterparts **5.21** and **5.22** bearing methyl and phenyl substituents, respectively, as a consequence of increased Lewis acidity at the metal centre, hence facilitating monomer coordination. The electron-withdrawing CF_3 group also led to the production of more isotactic PLA (P_m = 0.75 for **5.23** *vs*. 0.68 for **5.21** and 0.69 for **5.22**).

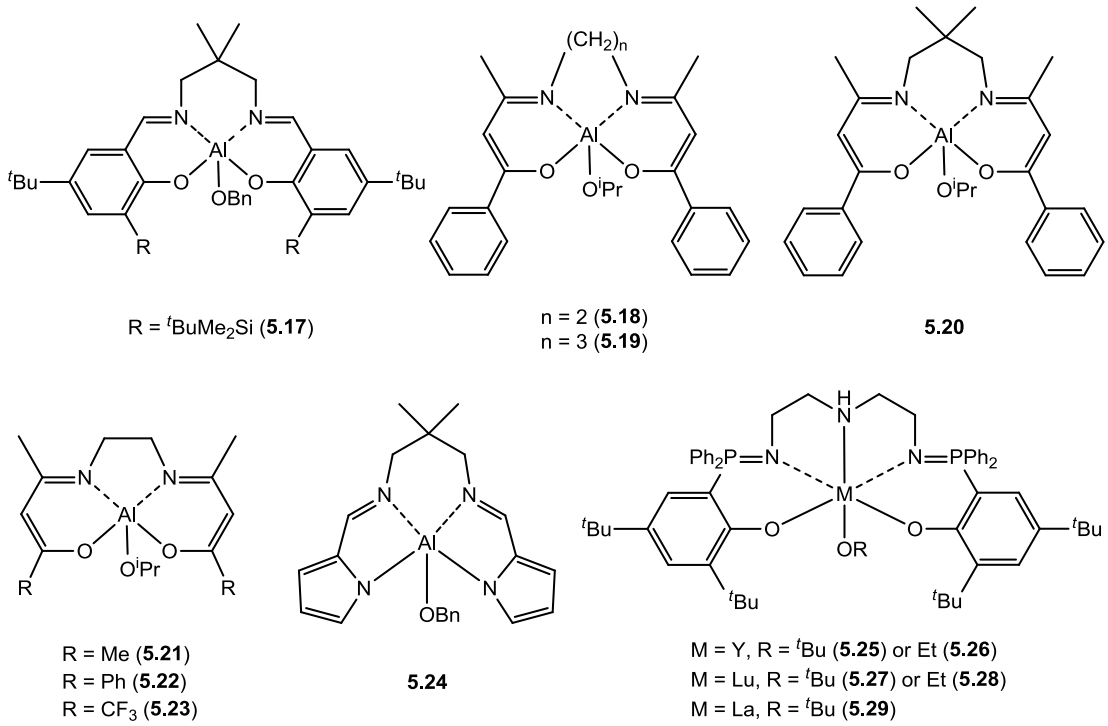


Figure 5.2 Further literature examples of achiral initiators for the isoselective ROP of *rac*-LA.[28-32]

Aluminium complexes featuring a bis(pyrrolidene) Schiff base ligand were also applied as catalysts for the ROP of *rac*-LA.[30] Complex **5.24**, generated *in-situ* by reacting the corresponding methyl complex with 1 equiv. of benzyl alcohol, was able to polymerise 100 equiv. of *rac*-LA within 1 h in toluene at 70 °C, producing PLA with the highest isotacticity (P_m = 0.80) among the series. In good agreement with this was the faster polymerisation rate for *L*-LA, indicating the catalyst's preference to enchain monomers *via* a *meso* linkage. Furthermore, an excellent agreement between the experimental and calculated M_n was observed for both *rac*- and *L*-LA ROP, in conjunction with narrow PDIs (1.03-1.06).

Following the promising potential of the aforementioned Schiff base ligand-supported catalysts, Williams *et al*. reported a series of phosphasalen ligand-supported yttrium complexes featuring ethoxide and *tert*-butoxide initiators.[31] The introduction of a diethylamine backbone resulted in the formation of hexa-coordinate complexes **5.25** and **5.26**, which exhibited high activity and isoselectivity. Analysis of the polymer microstructure revealed the generation of a stereoblock PLA with P_m values in the range of 0.74-0.84, as a result of a chain end control mechanism. In addition, both complexes gave excellent molecular weight control, producing PLA with narrow

PDIs and close agreement between the experimental and calculated M_n. The scope of study was also extended to other metals, such as lutetium and lanthanum.[32] The analogous compounds **5.27** and **5.28** were shown to be less active than their yttrium counterparts but induced higher level of isoselectivity (P_m = 0.80-0.89), leading to the conclusion that the size of the metal centre played an important role in polymerisation rates and isotacticity of the resulting polymer. Interestingly, PLA obtained using **5.29** was heterotactically enriched (P_r = 0.72).

In 2006, Gibson *et al.* reported a series of bis(phenolate) ligand-supported aluminium complexes **5.30**-**5.33** (Figure 5.3) with various substituents on the phenoxy rings.[33] These compounds, generated from the reaction between the corresponding aluminium methyl complexes and 1 equiv. of benzyl alcohol *in-situ*, were treated with 50 equiv. of *rac*-LA in toluene at 70 °C. Complex **5.30**, being the least sterically encumbered, was found to induce the fastest polymerisation while producing PLA with the highest isotacticity (P_m = 0.73). In contrast, the most sterically bulky complex **5.33** demonstrated slight heterotactic bias (P_r = 0.57) whereas the chloro-substituted **5.32** produced essentially atactic PLA.

Ma *et al*. reported a series of magnesium complexes **5.34**-**5.37** supported by an unsymmetrical aminophenolate ligand with different substituents and backbones.[34] The replacement of *tert*-butyl substituents with bulkier cumyl groups at both the *ortho* and *para* positions of the phenoxy ring had minor influence on the *rac*-LA ROP activities in both toluene and THF. For example, 84% conversion (200 equiv. of *rac*-LA) was achieved after 5 min using both **5.34** and **5.35** in THF at room temperature. However, the introduction of electron-withdrawing chloro substituents (**5.36**) resulted in a significant decrease in the polymerisation rate, in accordance with other catalytic systems reported in the literature.[35-38] Furthermore, adopting a longer backbone (**5.37**) also led to a considerable reduction in activity, particularly when the polymerisation was performed in toluene. The incorporation of different substituents and backbones was found to impart negligible influence on the stereoselectivity of the catalysts, yielding isotactic PLA with P_m values in the range of 0.61-0.68 in toluene and, surprisingly, heterotactic polymers in THF (P_r = 0.56-0.62). Disappointingly, polymerisations using **5.34**-**5.37** were found to display poor molecular weight control as a consequence of the sluggish initiating ability of amide initiators. This was subsequently improved by the addition of isopropanol, under which conditions

narrower PDIs were observed despite the negligible change in polymer microstructure, as expected.

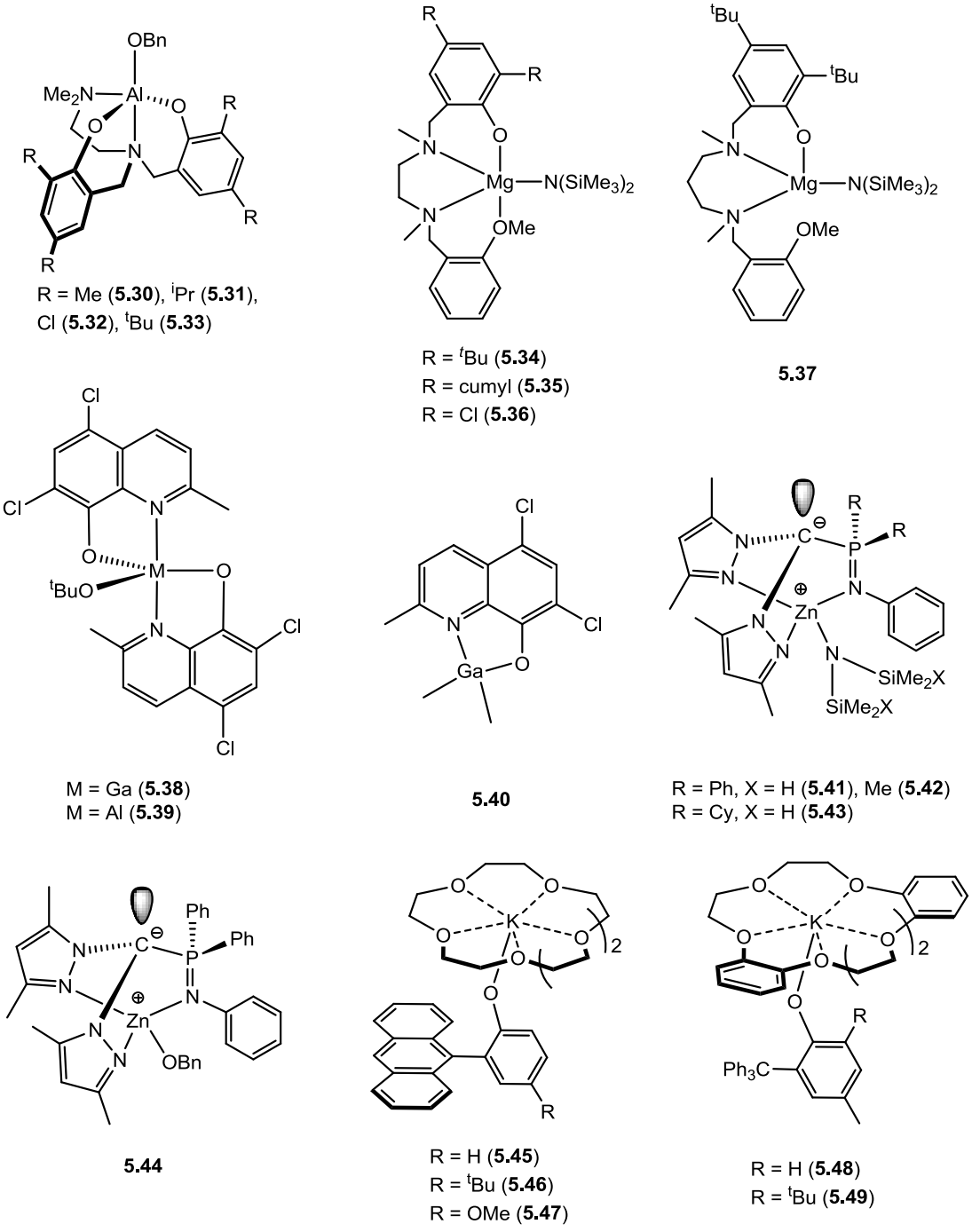


Figure 5.3 Further literature examples of achiral initiators for the isoselective ROP of *rac*-LA.[33, 34, 39-43]

Introduced by Williams and co-workers in 2013, complex **5.38** supported by an 8-quinoline ligand was capable of polymerising 100 equiv. of *rac*-LA in excess of 50 h in toluene at 75 °C.[39] Despite the seemingly sluggish activity, **5.38** induced

polymerisation at a much faster rate than its *in-situ* generated aluminium analogue **5.39** (91 % conversion at 137 h).[40] In addition to a beneficial rate enhancement, **5.38** also demonstrated good isoselectivity (P_m = 0.70) and excellent molecular weight control. It is worth mentioning that compound **5.38** was one of the few gallium complexes which demonstrated isoselectivity towards the ROP of *rac*-LA.[44, 45] The mono-ligated gallium complex **5.40** was also synthesised and probed in the ROP of *rac*-LA in the presence of 1 equiv. of isopropanol in toluene at 75 °C.[39] The polymerisation was marginally faster than that initiated by **5.38** at the expense of loss of stereoselectivity (P_m = 0.50), as a consequence of the reduced steric influence of the ligand in this mono-ligated catalytic system.

Cui *et al.* recently reported a number of heteroscorpionate ligand-supported zinc complexes **5.41**-**5.44**, which were subsequently treated with 200 equiv. of *rac*-LA in THF at room temperature.[41] Compound **5.41** was found to possess the highest activity and isoselectivity (P_m = 0.85) among the series, producing PLA with a good agreement between the calculated and experimental M_n. By comparing the polymerisation rates using **5.41** and **5.42**, it was concluded that the less bulky amide initiator resulted in a significant increase in the activity (91% conversion at 10 h for **5.41** *vs.* 73% conversion at 36 h for **5.42**). Varying the ligand backbone had a less pronounced effect on the activities of the catalyst, as evidenced by the negligible difference in the polymerisation rates between **5.41** and **5.43**. Interestingly, a solvent effect was observed; polymerisations performed in non-donor solvents such as toluene showed higher isoselectivity than those in THF, attributed to the reduced discrimination of the incoming monomer upon coordination of THF. In addition, the polymerisation control mechanism was studied using complex **5.44**. The observed rate constants for both *D*- and *L*-LA were very similar within error and P_m values remained in the range of 0.76-0.78 throughout the course of the polymerisation. These observations were indicative of the presence of a chain end control mechanism.

Wu and co-workers reported a series of potassium *o*-(9-anthryl)phenolate complexes **5.45**-**5.47** which induced *rac*-LA ROP *via* an activated monomer mechanism in the presence of benzyl alcohol.[42] Complex **5.45** was able to convert 93% of *rac*-LA (100 equiv.) within 2 min in the presence of 1 equiv. of benzyl alcohol (toluene, room temperature), affording isotactic PLA (P_m = 0.72). The isotacticity of the resulting polymer could be further improved by conducting the polymerisation at -70 ºC (P_m =

0.94). The incorporation of an electron-donating substituent at the *para* position of the phenoxy ring resulted in a minor increase in the polymerisation rate (99% at 2 min for **5.46** and 99% at 1.5 min for **5.47**) whilst no apparent change in the isotacticity of the polymer was observed. All three complexes induced *rac*-LA ROP in a well-controlled manner, producing PLA with an excellent agreement between the experimental and theoretical M_n and narrow PDIs (1.11-1.12). The same group later introduced complexes **5.48** and **5.49** featuring dibenzo 18-crown-6.[43] The latter bearing a bulky ^{t}Bu group at the *ortho* position of the phenoxy ring was found to be less stereoselective than the former (P_m = 0.77 for **5.48** *cf.* 0.60 for **5.49**). It was postulated that the "sandwich" structure constructed by the plane of the crown ether and the triphenyl methyl group played an important role in monomer coordination. The incorporation of a bulky ^{t}Bu substituent in **5.49** deformed this "sandwich" structure and as such resulted in a decrease in the isotacticity of the resulting polymer.

5.2.2 Chiral initiators for the isoselective ROP of LA

As mentioned previously (Section 5.2.1), the field of stereoselective ROP of LA was pioneered by Spassky and co-workers who developed a chiral Schiff base ligand-supported aluminium complex **(*R*)-5.50** (Figure 5.4), which was found to preferentially polymerise *D*-LA over *L*-LA with a relative rate ratio ($k_{rel} = k_{D\text{-LA}}/k_{L\text{-LA}}$) of 20:1 in toluene at 70 °C.[23] When treated with 75 equiv. of *rac*-LA, the polymer was found to contain mostly *D*-LA units at low % conversions whereas the less favourable insertion of *L*-LA occurred at a later stage of the polymerisation, eventually forming a stereoblock PLA which possessed a T_m of 187 °C, higher than that of homochiral polymers (180 °C). In addition to a high level of isoselectivity, **(*R*)-5.50** initiated *rac*-LA with good molecular weight control, with narrow PDIs and a close agreement between the calculated and experimental M_n, suggesting the catalyst's well-controlled nature. Following this breakthrough, Coates and Ovitt synthesised the racemic version of an analogous complex ***rac*-5.51**, which was postulated to lead to the formation of stereocomplex PLA when treated with *rac*-LA.[46] However, analysis of tetrads using ^{1}H{^{1}H} NMR spectroscopy revealed the polymer microstructure to be stereoblock as a result of polymer exchange processes. This was in contrast to the re-evaluation carried out by Baker *et al.* using the same catalyst under identical polymerisation conditions.[47] Powder X-ray diffraction of the resulting polymer clearly suggested the formation of a stereocomplex as opposed to stereoblock PLA.

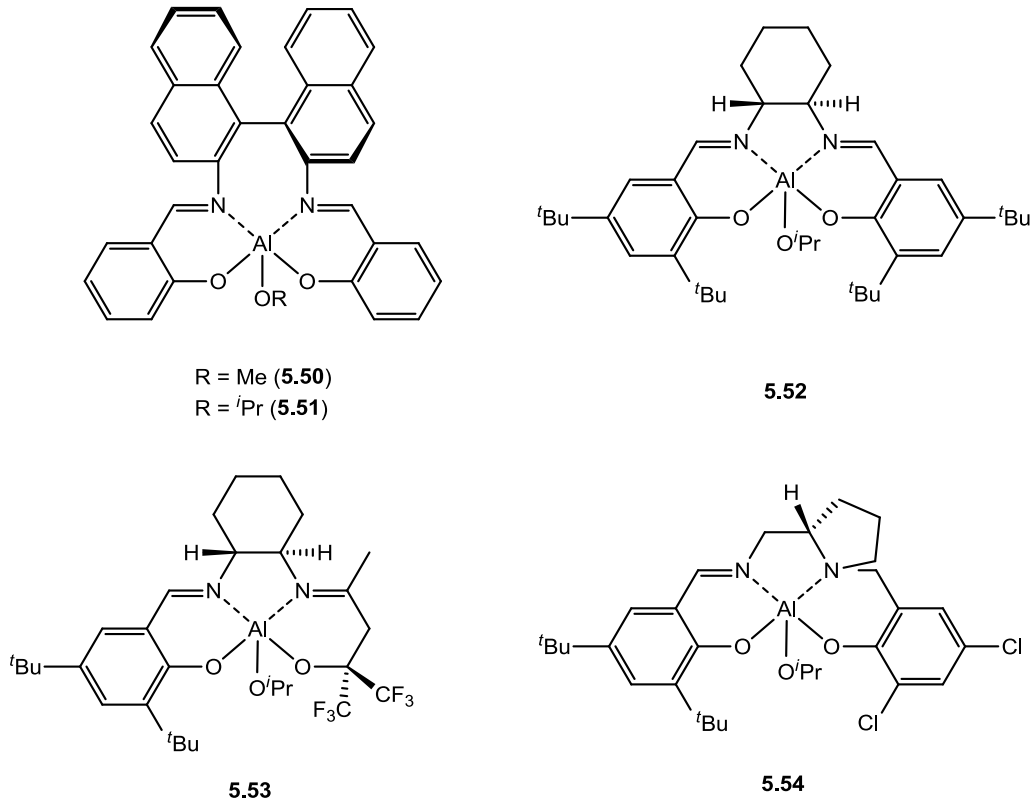
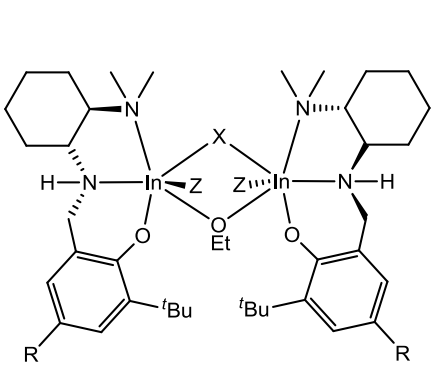


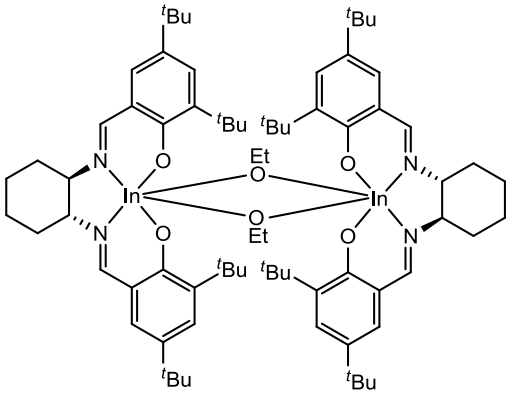
Figure 5.4 Literature examples of chiral initiators for the isoselective ROP of *rac*-LA.[23, 48-51]

In 2002, Feijen and co-workers synthesised an aluminium complex supported by a chiral Schiff base ligand both in an enantiomerically pure form and a racemic mixture.[48, 49] Complex **(*R*,*R*)-5.52** polymerised *L*-LA significantly faster than *D*-LA in toluene at 70 °C, with a relative propagation rate (k_{rel}) of approximately 14. This preference for the insertion of *L*-LA resulted in the formation of a stereoblock PLA when **(*R*,*R*)-5.52** was used to polymerise *rac*-LA; P_m values were found to be highest at low % conversions (P_m = 0.92 at 21% conversion) followed by a gradual decrease as the polymerisation proceeded. In contrast, ROP of *rac*-LA using ***rac*-5.52** yielded PLA whose microstructures were independent of % conversion, as evidenced by the very minor changes in the P_m values (0.92-0.93) observed throughout the course of the polymerisation. This was attributed to the parallel propagation of *L*-LA by **(*R*,*R*)-5.52** and *D*-LA by **(*S*,*S*)-5.52**, producing PLLA and PDLA sequences. The $^1H\{^1H\}$ NMR spectrum revealed the microstructure of the resulting polymer to be stereoblock, formed *via* a polymer exchange mechanism. High T_m was observed for PLA obtained using both **(*R*,*R*)-** (183 °C) and ***rac*-5.52** (185 °C).

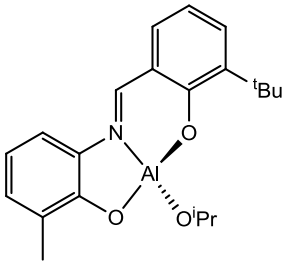
Five-coordinate aluminium complexes bearing non-symmetrical Schiff base ligands are also present in the literature.[50] Complex **(*R*,*R*)-5.53**, introduced by Carpentier and co-workers in 2009, was sluggish in activity, reaching 50% conversion (50 equiv. of *rac*-LA) in 7 days (toluene at 60 °C). However, **(*R*,*R*)-5.53** exhibited excellent molecular weight control, affording polymers with a good agreement between the calculated and experimental M_n, along with a narrow PDI of 1.04. Analysis with $^1H\{^1H\}$ NMR spectroscopy revealed the resulting PLA to be isotactically enriched, with a P_m value of 0.81. Following this work, Lamberti *et al.* synthesised compound **(*S*)-5.54**, which was able to polymerise 100 equiv. of *rac*-LA to a high level of conversion within 24 h at 80 °C in toluene, giving highly isotactic PLA (P_m = 0.81).[51] Consistently, kinetic studies with enantiomerically pure monomers revealed the preference of the catalyst to insert *L*-LA over *D*-LA, as evidenced by a substantial rate ratio (k_{rel}) of approximately 10. In addition, the minor difference in the polymerisation rates of *rac*- and *D*-LA was indicative of the insertion of *D*-LA being the rate-determining step. Moreover, first order kinetics persisted until 90% conversion for the ROP of *rac*-LA. Subsequent tetrad analysis of the polymer derived from *rac*-LA revealed the presence of *rmr* tetrads, indicating a single misinsertion leading to -*SSSSRRSSSS*- sequences. The intensity of *rmr* tetrads diminished towards the end of the polymerisation, indicating the formation of a polymer chain comprising longer blocks of PLLA with occasional misinsertions towards the isopropoxide terminus and longer blocks of PDLA free of misinsertions at the hydroxy chain end. These observations provided strong evidence for the operation of both enantiomorphic site and chain end control mechanisms, with the latter becoming increasingly dominant as the polymerisation proceeded. The same group recently reported an analogous compound with an achiral non-symmetrical ligand, demonstrating lower activity and isoselectivity.[52]



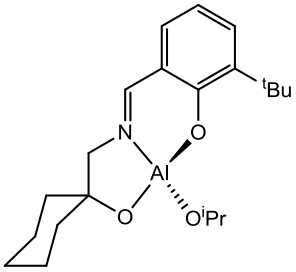
R = ^{t}Bu, X = Z = Cl (**5.55**)
R = Me, X = OEt, Z = I (**5.56**)



5.57



5.58



5.59

Figure 5.5 Further literature examples of chiral initiators for the isoselective ROP of *rac*-LA.[53-56]

Introduced by Mehrkhodavandi *et al*., the dinuclear indium complex ***rac*-5.55** (Figure 5.5) with an ethoxide bridge was synthesised by reacting 2 equiv. of the indium dichloride complex with 1 equiv. of sodium ethoxide in THF at room temperature.[53, 54, 57] Complex ***rac*-5.55** was determined to exist as a dimer in solution (CD_2Cl_2) by DOSY NMR spectroscopy and both (*S*,*S*)- and (*R*,*R*)- enantiomers were present. Complex ***rac*-5.55** was highly active, converting 200 equiv. of *rac*-LA within 30 min (CH_2Cl_2, room temperature) to produce slightly isotactic PLA (P_m = 0.53-0.62). Detailed kinetic analysis with enantiomerically pure monomers using **(*R*,*R*/*R*,*R*)-5.55** revealed a significant difference between the propagation rates of *L*- and *D*-LA (k_{rel} = 14). Complex **(*R*,*R*/*R*,*R*)-5.55** considerably favoured the insertion of *L*-LA over that of *D*-LA, whereas the opposite was observed when employing **(*S*,*S*/*S*,*S*)-5.55**. In good agreement with this was the presence of two kinetic regimes in the ROP of *rac*-LA initiated by **(*R*,*R*/*R*,*R*)-5.55**, indicating that the preferred monomer was polymerised first at a faster rate followed by insertion of the less favourable monomer. Peculiarly,

the resulting PLA obtained using enantiomerically pure catalysts was found to be atactic (P_m = 0.48). In contrast, the analogous dinuclear indium complex **(*R*,*R*/*R*,*R*)-5.56** featuring two bridging ethoxides polymerised *rac*-LA to produce PLA with moderate isotacticity (P_m = 0.65). As opposed to **(*R*,*R*/*R*,*R*)-5.55**, little monomer preference was found in the ROP of enantiomerically pure LA, with a k_{rel} of 2, indicating that the effect of enantiomorphic site control was much less pronounced compared to ROP using **(*R*,*R*/*R*,*R*)-5.55** and the isoselectivity demonstrated was mostly a result of a chain end control mechanism. The above-mentioned results were suggestive of the presence of different propagating species in the ROP initiated by **5.55** and **5.56**, subsequently confirmed by further NMR studies. It was concluded that both catalysts remained dinuclear during polymerisation, as opposed to mononuclear, which would essentially result in identical propagating species (identical selectivities).

Further studies by Mehrkhodavandi *et al*. introduced an analogous dinuclear indium complex (**5.57**) with two ethoxide bridges.[55] As observed with **5.55** and **5.56**, DOSY NMR spectroscopy analysis (CD_2Cl_2) of **5.57** confirmed the retention of a dinuclear structure in the solution state. **(*R*,*R*)-5.57** was able to polymerise 200 equiv. of *rac*-LA within 30 min in CH_2Cl_2 at room temperature, affording isotactic stereoblock PLA (P_m = 0.77) with excellent molecular weight control. **(*R*,*R*)-5.57** was also tolerant of high temperatures, inducing LA ROP in the melt at 130 °C under 10 min, much faster than analogous chiral aluminium catalyst systems.[12, 48] Detailed kinetic analysis with enantiomerically pure monomers revealed the catalyst's preference to insert *L*-LA over *D*-LA, as evidenced by the five-fold difference between the propagation rates. The rate-limiting step was determined to be the insertion of *D*-LA, since the propagation rate for *D*-LA was very close to that for *rac*-LA. Polymers at different % conversions were analysed by $^1H\{^1H\}$ NMR spectroscopy; P_m values reached maximum at lower than 20% or higher than 95% conversion whereas the lowest value was obtained at 50 % conversion, consistent with the formation of a stereoblock polymer. In contrast to **(*R*,*R*)-5.57**, complex ***rac*-5.57** polymerised *D*-, *L*- and *rac*-LA at very similar rates and minor changes in P_m values were observed throughout the course of the polymerisation. This was due to the presence of both enantiomers of **5.57**, leading to the consumption of *D*- and *L*-LA at the same rate. The aforementioned results were in close resemblance to those observed in polymerisations initiated by **5.52** reported by Feijen *et al*.[48, 49]

In 2011, Matsubara *et al*. reported a series of chiral aluminium isopropoxide complexes (chiral aluminium centre) supported by a Schiff base ligand.[56] Complex **5.58** was sluggish in activity when the polymerisation was performed in toluene at 70 °C, converting 100 equiv. of *rac*-LA after 96 h. This was subsequently improved by the use of pyridine as a solvent (96% conversion in 3 h), the origin of such rate enhancement remained controversial. However, the use of a donor solvent had negligible impact on the isotacticity of the resulting polymer (P_m = 0.80 in toluene *vs*. 0.79 in pyridine). A similar complex **5.59** was shown to possess the highest isoselectivity among the series (P_m = 0.92), while maintaining a moderate molecular weight control (PDI = 1.19).

Ma and co-workers later reported the synthesis of a series of chiral zinc and magnesium amide catalysts supported by an NNO-type aminophenolate ligand.[58] **(*S*$_C$*S*$_N$*R*$_N$*R*$_{Zn}$)-5.60** (Figure 5.6) was obtained by the protonolysis reaction between the enantiomerically pure (*S*)-protio-ligand and $Zn\{N(SiMe_3)_2\}_2$ in toluene. When treated with 200 equiv. of *rac*-LA in toluene at room temperature, the polymerisation reached a high level of conversion within 3 h, producing highly isotactic PLA (P_m = 0.80) with a good agreement between the calculated and experimental M_n. A moderate PDI of 1.66 was obtained, subsequently improved by the addition of 1 equiv. of isopropanol to convert **(*S*$_C$*S*$_N$*R*$_N$*R*$_{Zn}$)-5.60** to the corresponding isopropoxide. Polymerisations were also performed in THF under identical conditions, resulting in rate reduction yet superior molecular weight control. The addition of isopropanol and the use of different solvents were found to impose negligible impact on the microstructure of the resulting PLA. The origin for such high isoselectivity was subsequently investigated by kinetic analysis using *D*- and *L*-LA, revealing a four-fold difference which was characteristic of the operation of an enantiomorphic site control mechanism. In addition, analysis of the resulting polymer obtained from *rac*-LA at different % conversions suggested that the lowest P_m value was obtained at around 50% conversion, consistent with the formation of a stereoblock PLA. However, kinetic data were inconsistent with the operation of a pure enantiomorphic site control mechanism (rate decrease should be observed after the consumption of the favoured monomer); the presence of only one kinetic regime was observed throughout the course of the polymerisation, indicating that both enantiomorphic site and chain end control mechanisms were in operation. Interestingly, rather different

stereoselectivity was observed with the magnesium analogue **5.61**, which was obtained as a mixture of two diasteromers **($S_C S_N R_N R_{Mg}$)**- and **($S_C S_N S_N S_{Mg}$)-5.61** in a 7:1 ratio. Complex **5.61** was more active than its zinc counterpart in the ROP of *rac*-LA, producing highly heterotactic (P_r = 0.70-0.81) PLA with moderate molecular weight control. The degree of heterotacticity was determined to be solvent-dependent, with the higher P_r values being observed in toluene than in THF. Kinetic analysis with both *D*- and *L*-LA revealed hardly any preference (k_{rel} = 1.15), indicating a lack of enantiomorphic site control. As expected, the observed rate constant for *rac*-LA was more than twice as high as those for the enantiomerically pure monomers, consistent with the preference to insert LA alternatively (chain end control mechanism). The difference in stereoselectivity of **($S_C S_N R_N R_{Zn}$)-5.60** and **5.61** was rationalised by the larger atomic radius of magnesium in comparison to that of zinc, resulting in the coordination of monomers *via* two adjacent sites which preferred to choose LA monomers of opposite configurations.

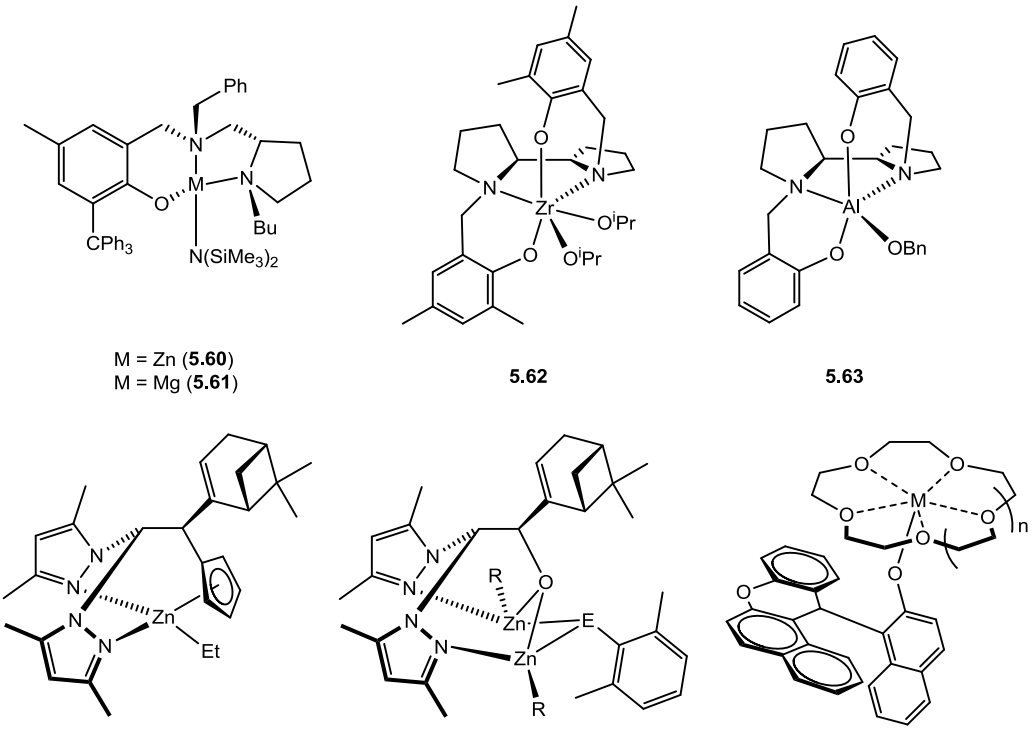


Figure 5.6 Literature examples of chiral initiators for the isoselective ROP of *rac*-LA.[58-63]

Jones *et al.* recently developed a series of bipyrolidine-salan derived zirconium complexes **(*R*,*R*)-**, **(*S*,*S*)-** and ***meso*-5.62**, synthesised by reacting the corresponding protio-ligand with $Zr(O^iPr)_4/^iPrOH$ in toluene.[59] All three catalysts exhibited moderate activities for the ROP of *rac*-LA, yielding isotactic PLA with P_m values in the range of 0.65-0.84. DSC analysis of the PLA obtained using ***meso*-5.62** showed an endothermic peak at 190 °C, indicative of the formation of a stereoblock polymer. This was consistent with the minor *rmr* tetrads in comparison to *rmm*, *mmr* and *mrm* tetrads in the $^1H\{^1H\}$ NMR spectrum. The origin for the high isoselectivity demonstrated by ***meso*-5.62** (P_m = 0.86) could be attributed to the catalyst's fluxional nature in solution, whereby an equilibrium existed between the (*R*,*S*) and (*S*,*R*) enantiomer. The operation of enantiomorphic site control discriminated selection of a preferred monomer to form a long block of PLLA or PDLA. However, the occasional misinsertions could trigger the complex to convert to its opposite configuration which went on to insert the other monomer, therefore enabling the formation of stereoblock PLA. The same group later reported the analogous hafnium and aluminium complexes, inducing isoselective and heteroselective polymerisations, respectively.[64] Kol and co-workers recently developed an analogous aluminium complex **5.63** which was generated *in-situ* and used as a catalyst for the ROP of *rac*-LA in toluene at 70 °C.[60] Complex **(*R*,*R*)-5.63** afforded isotactic PLA (P_m = 0.72) whereas ***rac*-5.63** led to a significant decrease in isotacticity (P_m = 0.56). This was attributed to the presence of polymeryl exchange processes, therefore compromising the effect of enantiomorphic site control.

The first example of a metal complex featuring an enantiomerically pure hybrid scorpionate/cyclopentadienyl ligand was introduced by Rodriguez *et al.*[61] Complex **5.64** was synthesised by deprotonating the cyclopentadienyl group of a 1:1 mixture of two protio-ligand regioisomers (both in (*R*,*R*) configuration) with diethylzinc. Complex **5.64** demonstrated moderate activity in *rac*-LA ROP in toluene, reaching 32% conversion in 15 h at room temperature. This could be improved by performing the polymerisation at 50 °C, converting 47% of the monomer within 4 h. In both cases, isotactic PLA (P_m = 0.73-0.77) with a good agreement between the calculated and experimental M_n was produced, in conjunction with narrow PDIs. Microstructural analysis of the PLA revealed the formation of a stereoblock polymer as a consequence of an enantiomorphic site control. Consistently, *L*-LA ROP using **5.64** proceeded at a

higher rate under identical polymerisation conditions, reaching 57% conversion in 12 h at room temperature.

Following this work, the same group later synthesised a series of dinuclear Zn complexes.[62] The reaction between the (*R*,*R*)-protio-ligand and 2 equiv. of $Zn(CH_2SiMe_3)_2$ followed by the addition of 1 equiv. of HO-2,6-$C_6H_3Me_2$ or HS-2,6-$C_6H_3Me_2$ afforded the enantiomerically pure **(*R*,*R*)-5.65** and **(*R*,*R*)-5.66**, respectively. Complex **(*R*,*R*)-5.65** demonstrated moderate activity for the ROP of *rac*-LA at 50 °C in THF, reaching 49% conversion in 4 h. Replacing the oxygen with a sulfur atom on the ligand (**(*R*,*R*)-5.66**) resulted in a decrease in the polymerisation rate, the origin of which was not specified. Both catalysts induced excellent molecular weight control and produced isotactic PLA (P_m = 0.71-0.74, T_m = 161-166 °C). Close examination of the tetrads in the $^1H\{^1H\}$ NMR spectrum revealed a ratio [*rmr*]:[*rmm*]:[*mmr*]:[*mrm*] of 1:1:1:2, indicating the operation of an enantiomorphic site control mechanism.

Wu and co-workers recently reported a crown ether complex of potassium naphthalenolates ***rac*-5.67**, which was shown to be highly active in the ROP of *rac*-LA in the presence of 1 equiv. of benzyl alcohol at room temperature.[63] 100 equiv. of *rac*-LA could be polymerised within 3 min in toluene, producing isotactic PLA (P_m = 0.71) with excellent molecular weight control. Further enhancement of isoselectivity was achieved by performing the polymerisation at 0 °C. Compared to other alkali metal catalysts present in the literature,[65-72] complex ***rac*-5.67** demonstrated higher isoselectivity, subsequently attributed to the presence of a "pocket", in which the K-O moiety was sandwiched between the crown ether and the planar benzoxanthenyl group. Tetrad analysis with $^1H\{^1H\}$ NMR spectroscopy suggested a combination of enantiomorphic site and chain end control, with the latter being the dominant mechanism. The analogous sodium complex ***rac*-5.68**, in the presence of 1 equiv. of benzyl alcohol, was less active under identical polymerisation conditions (100 equiv. of *rac*-LA, toluene, room temperature), reaching 57% conversion within 3 min. This was rationalised by the shorter Na-O bond, giving rise to a more sterically encumbered coordination sphere and therefore slowing down the monomer insertion process. A concomitant decrease in isotacticity was also observed (P_m = 0.65). It is notable that both complexes polymerised *rac*-LA *via* an activated monomer mechanism.

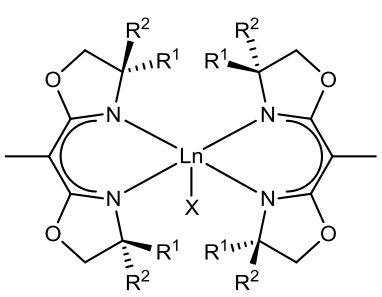
5.2.3 Oxazoline ligand-supported initiators for the ROP of LA

Among the number of ligand systems employed in molecular catalysis, the oxazoline ligands have attracted much research interest, especially in the area of asymmetric catalysis.[73-77] The success for the employment of such ligands could be attributed to several reasons. Firstly, oxazoline ligands are commonly derived from readily available α-amino acids, enabling facile synthesis from non-toxic and "green" starting materials. Secondly, their preparation is usually integrated with other molecular moieties, allowing a wide range of ligand environments to be accessed. In addition, the nitrogen donor atoms with moderate chemical "hardness" facilitate the coordination of various metals, extending the scope of study to a vast number of metal complexes. Last but not least, the introduction of chiral groups in proximity to the coordination nitrogen atom is an elegant method to transfer chiral information to the active site, thus providing a greater degree of stereocontrol during catalysis. Despite these advantages, the development of organometallic complexes based on oxazoline ligands and their applications in areas such as polymerisations and heterofunctionalisation are rather limited.[78-84] To be more specific, the utilisation of such ligands in the ROP of cyclic esters has been restricted to a handful of examples to date (Figures 5.7 and 5.8).

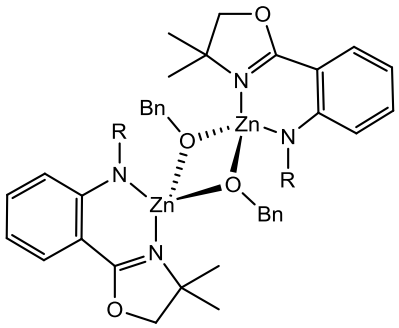
In 2006, Carpentier *et al*. reported a series of yttrium and lanthanum complexes (**5.69**-**5.71**) supported by chiral and achiral bis[bis(oxazolinato)] ligands.[85] Complex **5.69** polymerised 100 equiv. of *rac*-LA within 10 min in THF at room temperature, affording PLA with higher than expected M_n and moderate PDIs. The analogous lanthanum complex **5.70** demonstrated similar activity and molecular weight control, suggesting that the size of the metal had a minor effect on the polymerisation behaviour. Unfortunately, the incorporation of chiral groups (**5.71**) on the oxazoline moiety had no observable impact on the stereoselectivity of the catalysts; all catalysts resulted in the formation of atactic PLA.

Chen and co-workers later developed a number of monomeric or dimeric magnesium, zinc and aluminium complexes supported by oxazoline-containing ligands.[86-89] Complex **5.72** was moderately active in the ROP of *L*-LA, reaching 97% conversion (100 equiv. of *L*-LA, toluene, 50 °C) within 50 min while maintaining a narrow PDI of 1.07. However, higher than expected M_n was observed, presumably due to a faster

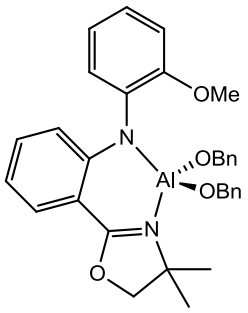
rate of propagation than that of initiation. The same group later reported the *L*-LA ROP results of an analogous complex **5.73** featuring a ^{n}Pr group on the amino moiety.[89] It was concluded that the incorporation of an aliphatic substituent resulted in an increase in activity under identical conditions (96% conversion at 25 min), presumably due to the less crowded coordination environment around the metal centre as a consequence of a decrease in ligand rigidity, therefore facilitating monomer coordination. Following this initial work, the catalytic activities of a series of monomeric aluminium complexes supported by similar ligands were investigated.[88] When treated with 100 equiv. of *L*-LA, *in-situ* generated **5.74** was much less active than its dimeric zinc analogue, reaching 29% conversion after 48 h in toluene at 50 °C.



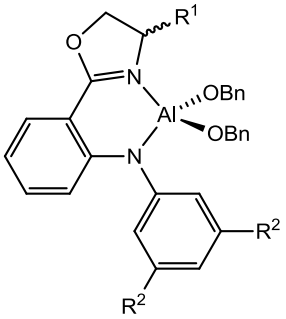
X = $N(SiMe_2H)_2$
Ln = Y, $R^1 = R^2$ = Me (**5.69**)
Ln = La, $R^1 = R^2$ = Me (**5.70**)
Ln = Y, $R^1 = {}^{i}$Pr, R^2 = H (**5.71**)



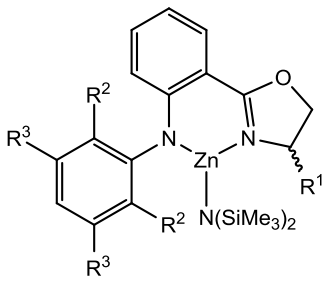
R = 2,4,6-mesityl (**5.72**)
R = ^{n}Pr (**5.73**)



5.74



R^1 = (*R*)-Ph, R^2 = H (**5.75**)
R^1 = (*S*)-^{i}Pr, R^2 = CF_3 (**5.76**)
R^1 = (*S*)-^{i}Pr, R^2 = H (**5.77**)
R^1 = (*R*)-^{t}Bu, R^2 = H (**5.78**)



R^1 = (*S*)-^{i}Pr, R^2 = Me, R^3 = H (**5.79**)
R^1 = (*R*)-Ph, R^2 = H, R^3 = CF_3 (**5.80**)

Figure 5.7 Oxazoline-containing catalysts for the ROP of LA.[85, 88-93]

While the work in this Thesis was in progress, Du *et al*. reported a range of *in-situ* generated aluminium benzyloxide complexes **5.75**-**5.78**, which were shown to be active in the stereoselective ROP of *rac*-LA.[90] For example, complex **5.75** induced

polymerisation of 50 equiv. of *rac*-LA after 24 h (toluene, 80 °C), producing slightly isotactic PLA (P_m = 0.60) with a good molecular weight control. The incorporation of an electron-withdrawing CF_3 group on the phenyl ring (**5.76**) had a minor impact on the polymerisation rate and isotacticity of the resulting polymer (P_m = 0.57). In contrast, complexes **5.77** and **5.78** exhibited heteroselectivity, affording PLA with P_r values of 0.69 and 0.74, respectively.

Later work by the same group introduced a series of analogous zinc amide complexes.[91] ROP of *rac*-LA using chiral **5.79** yielded highly isotactic PLA (P_m = 0.81, T_m = 189 °C) with higher than expected experimental M_n and a moderate PDI of 1.29. It is worth noting that the introduction of electron-withdrawing substituents on the phenyl ring (**5.80**) led to an increase in the isotacticity of the resulting PLA (P_m = 0.91, T_m = 212 °C).

The first example involving the use of chiral BOPA ligand-supported catalysts in the ROP of *rac*-LA was introduced by Ward and Mountford *et al*. (Figure 5.8).[92] A series of yttrium, samarium and lanthanum amide complexes were synthesised *via* the reaction between the protio-ligand and the corresponding metal tris(amide). Complexes **5.81**-**5.83** were moderately active in the ROP of *rac*-LA, producing PLA with higher than expected M_n. As anticipated, the use of more sterically demanding chiral groups on the oxazoline led to the formation of more heterotactic polymer (P_r = 0.70 for **5.81**, 0.71 for **5.82**, 0.80 for **5.83**). Such trends were also observed in samarium but not lanthanum complexes (minor difference in P_r).

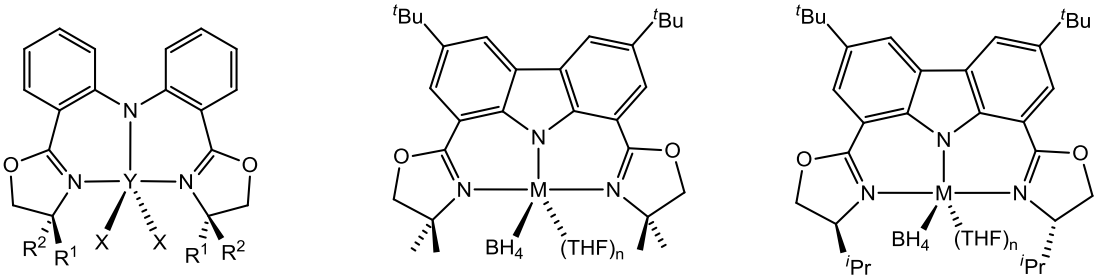


Figure 5.8 Further examples of oxazoline-containing catalysts for LA ROP.[85, 88-93]

Unpublished work in the Mountford group has introduced a series of magnesium and calcium complexes supported by chiral and achiral carbazole-bis(oxazoline) (CzOx) ligands.[93] Complex **5.84** was moderately active, converting 100 equiv. of *rac*-LA within 2 h (THF, room temperature) to afford heterotactic PLA with P_r values in the range of 0.82-0.84. In addition, an excellent agreement between the experimental and calculated M_n was observed, in conjunction with a narrow PDI of 1.14. The analogous calcium complex **5.85** was less active, producing PLA with less well-controlled molecular weight (PDI = 1.48) and reduced heterotacticity (P_r = 0.60-0.67). Interestingly, a significant decrease in polymerisation rate was observed upon incorporation of a chiral ligand. Complex **(*S*,*S*)-5.86** required 72 h to reach 92% conversion under identical polymerisation conditions, giving PLA featuring a lower than expected experimental M_n. The rate decrease was attributable to a stronger chelation of the monomer or growing polymeryl chain to the metal centre, as a result of reduced steric hindrance. Unfortunately, the rate reduction was not accompanied by an increase in heteroselectivity; the P_r values for the resulting PLA were in the range of 0.81-0.88. Kinetic analysis with *L*- and *D*-LA was also undertaken using **(*S*,*S*)-5.86**; 90% of *L*-LA was polymerised after 312 h whereas 89% conversion was reached after 384 h for *D*-LA ROP, indicating minor enantiomorphic site control. The slow polymerisation rates for the ROP of enantiomerically pure LA in comparison to that for *rac*-LA ROP was consistent with the heteroselectivity of **(*S*,*S*)-5.86**. Upon addition of 4.5 equiv. of benzaldehyde to convert **(*S*,*S*)-5.86** to the corresponding benzyloxide species and $B(OBn)_3$, a much more pronounced monomer enchainment preference was observed; 94% conversion was reached within 2 h for *D*-LA ROP whereas *L*-LA ROP required 120 h to reach 95% conversion, indicating strong enantiomorphic site control. The ROP of *rac*-LA proceeded faster (94% conversion in 0.75 h) than those of enantiomerically pure monomers and the resulting PLA was heterotactically enriched (P_r = 0.83-0.85). The chiral calcium complex **5.87** yielded slightly heterotactic PLA (P_r = 0.61) with poor molecular weight control (PDI = 1.91).

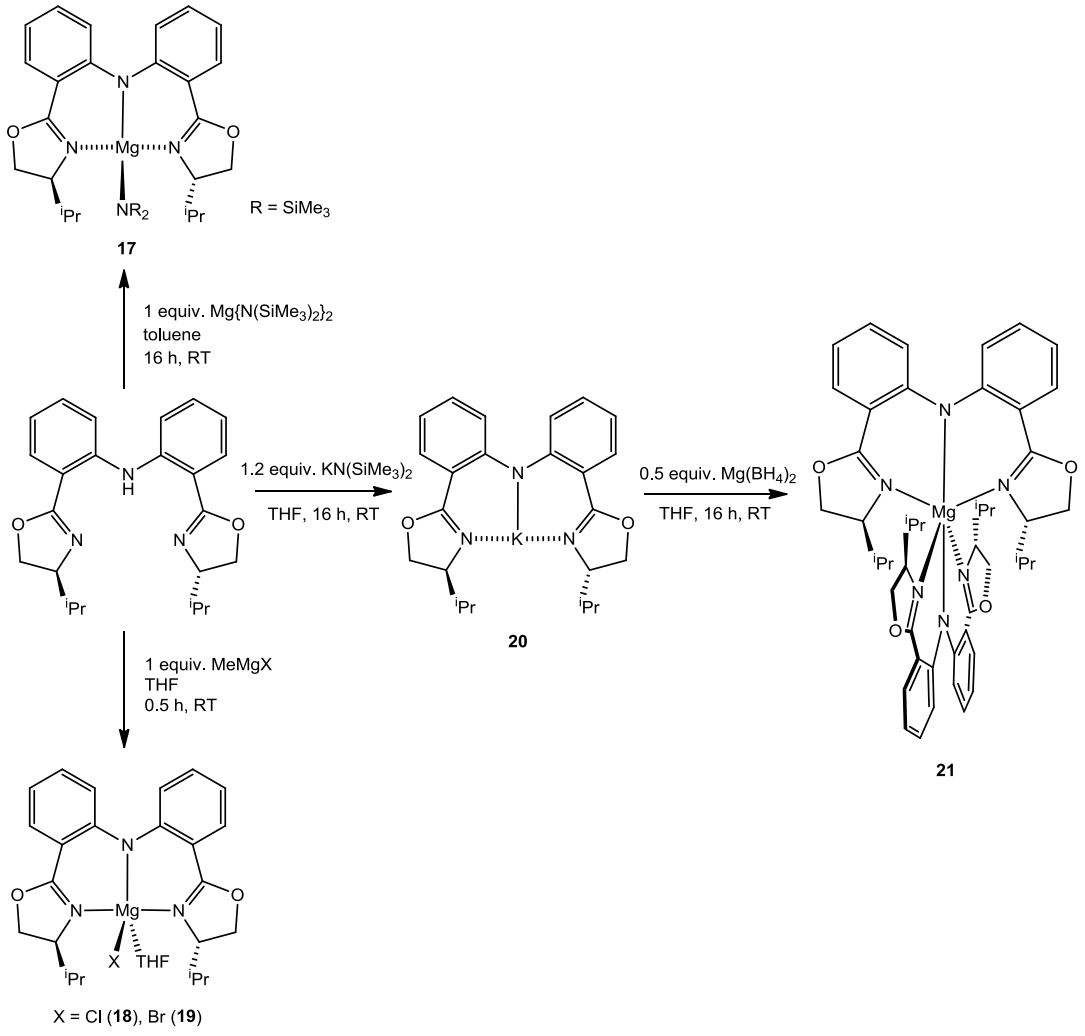
5.3 Synthesis and characterisation of BOPA-supported magnesium complexes

In comparison to the structurally similar carbazole-bis(oxazoline) (CzOx) ligand, it was anticipated that the incorporation of a BOPA ligand featuring a non-fused backbone in catalyst design would confer additional flexibility while retaining complex integrity, therefore leading to higher activity and improved stereoselectivity

of the resulting catalysts. The BOPA protio-ligand was synthesised in three steps according to literature procedures by Xu *et al*. and Gade *et al*. in 30% overall yield.[94, 95] Following the successful employment of BOPA-supported lanthanide complexes in the ROP of *rac*-LA by Ward and Mountford *et al*.,[92] the preparation of a range of magnesium complexes with different initiators was subsequently attempted *via* either protonolysis or salt elimination reactions starting from BOPA$^{i\text{Pr}}$-H or BOPA$^{\text{Ph}}$-H.

5.3.1 Synthesis and characterisation of BOPA$^{i\text{Pr}}$-supported magnesium complexes

Scheme 5.1 depicts the synthetic routes applied in order to generate a range of BOPA$^{i\text{Pr}}$-supported magnesium complexes. All compounds possess (*S*,*S*) configuration at the oxazoline moiety and the (*R*,*R*) enantiomers were not synthesised.



Scheme 5.1 Synthesis of magnesium complexes supported by the (*S*,*S*)-BOPA$^{i\text{Pr}}$ ligand.

Given the superior initiating efficiency of alkoxide species widely documented in the literature, the initial attempt was to employ (*S*,*S*)-(BOPA^{iPr})Mg{N(SiMe$_3$)$_2$} (**17**) as the starting material to access (*S*,*S*)-(BOPA^{iPr})Mg(OBn). Compound **17** was synthesised *via* the protonolysis reaction between an equimolar amount of (*S*,*S*)-BOPA^{iPr}-H and Mg{N(SiMe$_3$)$_2$}$_2$ in toluene at room temperature, affording a bright yellow powder in 63% isolated yield.

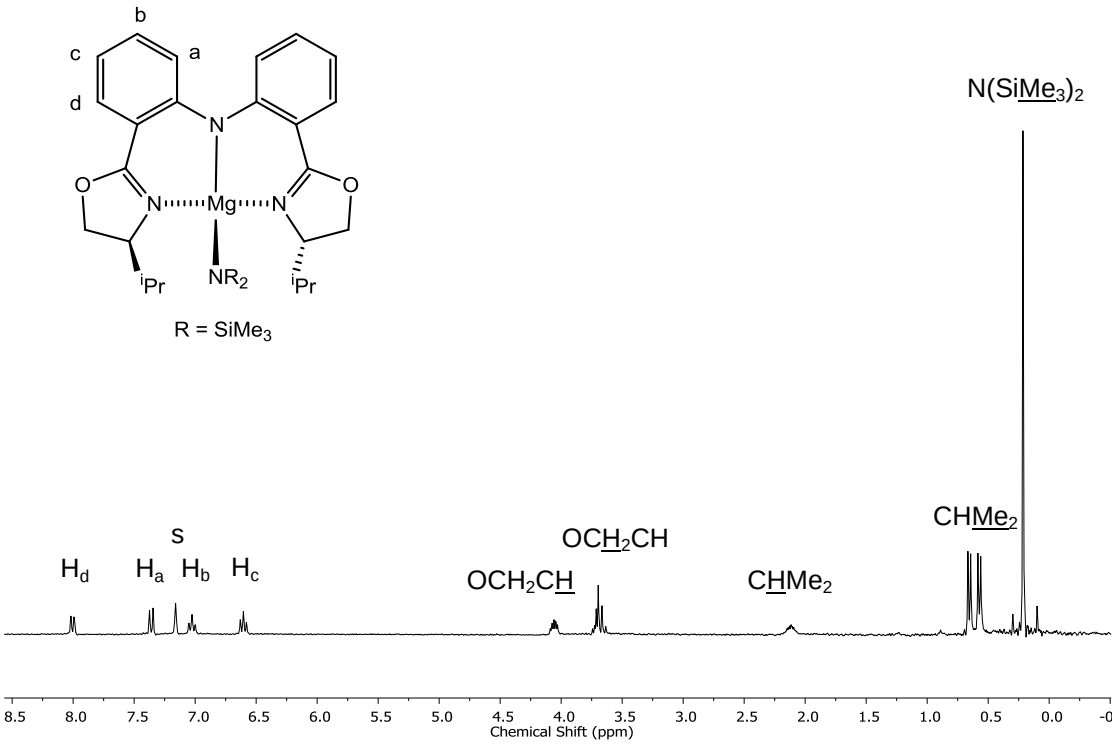


Figure 5.9 ^{1}H NMR spectrum (C_6D_6, 400.2 MHz, 298 K) of (*S*,*S*)-(BOPA^{iPr})Mg{N(SiMe$_3$)$_2$} (**17**). "s" denotes residual protio-solvent.

Close examination of the ^{1}H NMR spectrum (C_6D_6) of **17** (Figure 5.9) in comparison to that of (*S*,*S*)-BOPA^{iPr}-H revealed an upfield shift for the aromatic protons upon coordination to the metal centre. The methylene protons (OC$\underline{H}_2$CH) adjacent to the chiral centre on the oxazoline ring were diastereotopic, appearing as two overlapping multiplets in the region of 3.63-3.73 ppm. In addition, the OCH$_2$C$\underline{H}$ methine protons were visible as a multiplet at 4.06 ppm as a result of coupling to both the methine proton on the isopropyl group (C$\underline{H}$Me$_2$) and the two OC$\underline{H}_2$CH protons. The CH$\underline{Me}_2$ protons were also diastereotopic, giving rise to two doublets at 0.57 and 0.65 ppm, with a $^3J_{H\text{-}H}$ coupling constant of 6.6 Hz. It is worth noting that the analogous yttrium complex (*S*,*S*)-(BOPA^{iPr})Y{N(SiMe$_3$)$_2$}$_2$ synthesised *via* reacting the protio-ligand

with $Y\{N(SiMe_3)_2\}_3$ revealed two sets of signals in the ^{1}H NMR spectrum.[92] This was attributed to the presence of diastereomers arising from different senses of helical twist in the diphenylamine backbone, namely *exo* (^{i}Pr directed in mutually opposite directions) or *endo* (^{i}Pr close together in the same face of the coordination sphere). These two diastereomers possessed identical connectivity and were interconverting, confirmed by 2D correlation NMR spectroscopy and spin saturation transfer experiments, respectively. This phenomenon was not observed in **17**, presumably due to the smaller size of the metal (covalent radius = 1.41(7) Å for Mg *vs*. 1.90(7) Å for Y).[96]

Following the successful synthesis of **17**, the preparation for the corresponding alkoxide (*S*,*S*)-(BOPA^{iPr})Mg(OBn) was attempted by reacting **17** with 1 equiv. of benzyl alcohol in toluene at room temperature. Unfortunately, complex decomposition was observed, leading to the formation of (*S*,*S*)-BOPA^{iPr}-H, $Mg(OBn)_2$ and $HN(SiMe_3)_2$. The reaction was repeated under kinetic control by adding a dilute toluene solution of benzyl alcohol to a dilute toluene solution of **17** at -78 °C over the course of 3 h. Unfortunately, the same problem persisted.

An alternative approach to synthesise (*S*,*S*)-(BOPA^{iPr})Mg(OBn) involved the salt elimination reaction between a metal halide and KOBn. (*S*,*S*)-(BOPA^{iPr})Mg(Cl)(THF) (**18**) and (*S*,*S*)-(BOPA^{iPr})Mg(Br)(THF) (**19**) were subsequently synthesised by reacting the protio-ligand with the corresponding methyl Grignard reagents (THF, room temperature) and obtained as yellow solids with isolated yields of 82% and 83%, respectively. NMR characterisation of **18** was performed in THF-d_8 due to the compound's limited solubility in C_6D_6. The diastereotopic $OC\underline{H}_2CH$ protons were observed as a doublet of doublets ($^2J_{H\text{-}H}$ = 8.8 Hz, $^3J_{H\text{-}H}$ = 5.2 Hz) and an apparent triplet ($J_{H\text{-}H}$ = 9.6 Hz) at 4.35 and 4.21 ppm, respectively, in the ^{1}H NMR spectrum (THF-d_8). Compound **19**, on the contrary, was soluble in C_6D_6, allowing characterisation to be carried out in this solvent. As expected, the ^{1}H NMR spectrum of **19** (C_6D_6) showed the two diastereotopic methylene protons at 3.87 and 3.76 ppm, appearing as a doublet of doublets and an apparent triplet, respectively. The methylene protons adjacent to the oxygen on THF were also diastereotopic, appearing as two multiplets at 3.68 and 3.44 ppm (slow exchange on the NMR timescale). The effect of diastereotopicity for the other methylene protons on THF were less

pronounced, leading to a single multiplet at 1.01 ppm. Integration of THF signals relative to the ligand backbone revealed the coordination of only one THF.

Crystals of **19** suitable for X-ray diffraction were grown by Ward *et al*. The coordination of the bromide and THF moieties results in the removal of the two-fold symmetry associated with the (*S*,*S*)-BOPA^{iPr} ligand (Figure 5.10 and Table 5.1). Complex **19** possesses a five-coordinate geometry at the metal centre, with the Mg coordinating to the three N donors of the ligand, the Br and the O donor of THF. The geometry at the Mg centre could be described either as a square based pyramidal where the O donor occupies the axial position or as a distorted trigonal bipyramidal where the axial positions are occupied by N(2) and N(3). However, the N(2)-Mg(1)-N(3) and N(1)-Mg(1)-Br(1) bond angles of 159.14(7)° and 165.96(5)° deviate significantly from the ideal 180° and 120° for a trigonal bipyramidal geometry. Addison and co-workers have developed an approach to evaluate the degree of trigonality in a five-coordinate system using the equation $\tau = (\beta-\alpha)/60$, where β is the largest angle within the coordination sphere and α being the second largest.[97] In the case of square based pyramidal geometry, both α and β cannot involve inclusion of the apical donor, in this instance O(3). In an ideal square based pyramidal structure, $\alpha = \beta = 180°$, therefore $\tau = 0$ whereas $\tau = 1$ ($\alpha = 120°$ and $\beta = 180°$) in an ideal trigonal bipyramidal geometry. In the case of compound **19**, τ was calculated to be 0.1 ($\alpha = 159.14(7)°$ and $\beta = 165.96(5)°$), indicating the close to square based pyramidal structure of the complex. This is in good agreement with the bond angles of N(1)-Mg(1)-N(2), N(2)-Mg(1)-Br(1), Br(1)-Mg(1)-N(3) and N(3)-Mg(1)-N(1) being 85.96(6), 92.06(5), 92.21(5) and 84.97(6)°, respectively. In addition, the distance between Mg(1) and the plane formed by the four atoms on the base of the square based pyramid is 0.324 Å.

One of the most striking features in this structure is the non-coplanar conformation of the diphenylamine backbone. The two phenylene rings are twisted, giving rise to an angle of 59.4° between the planes formed by the two phenylene rings of the backbone. This is in contrast to a similar complex (CzOx^{Me2})Mg{N(SiMe$_3$)$_2$} reported previously in the Mountford group, revealing a co-planar backbone as a result of an extra bond between C(1) and C(13).[93] It is also notable that the phenylene and the oxazoline rings in **19** are co-planar, with inter-plane angles of 4.0° and 13.2°.

Interestingly, the bond distances of Mg(1)-N(1) and Mg(1)-N(2) are equivalent (2.1041(16) and 2.1104(17) Å, respectively), being slightly shorter than that for Mg(1)-N(3) (2.1535(17) Å). This was tentatively attributed to the steric hindrance imposed by THF and the bromide moiety, forcing the helical twist of the diphenylamine backbone. Mg(1)-O(3) and Mg(1)-Br(1) bond distances of 2.0572(15) and 2.5562(6) Å are comparable to those for analogous compounds reported in the literature.[98, 99]

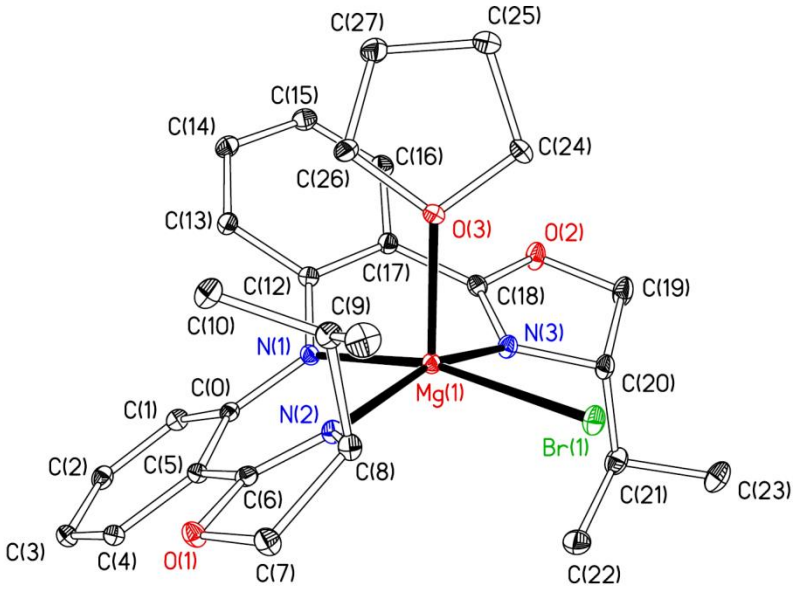


Figure 5.10 Displacement ellipsoid plot of (*S*,*S*)-(BOPA^{iPr})Mg(Br)(THF) (**19**). C-bound H atoms omitted for clarity. Ellipsoids are drawn at the 20% probability level.

Table 5.1 Selected bond lengths (Å) and angles (°) for (*S*,*S*)-(BOPA^{iPr})Mg(Br)(THF) (**19**).

Mg(1)-N(1)	2.1041(16)	Mg(1)-N(2)	2.1104(17)
Mg(1)-N(3)	2.1535(17)	Mg(1)-O(3)	2.0572(15)
Mg(1)-Br(1)	2.5562(6)	C(6)-N(2)	1.289(2)
O(1)-C(6)	1.363(2)	C(8)-N(2)	1.495(2)
N(1)-C(0)	1.384(2)	C(0)-C(1)	1.427(2)
O(3)-C(26)	1.457(2)		
N(1)-Mg(1)-O(3)	96.59(6)	O(3)-Mg(1)-Br(1)	97.39(4)
N(1)-Mg(1)-Br(1)	165.96(5)	N(2)-Mg(1)-N(3)	159.14(7)
N(1)-Mg(1)-N(2)	85.96(6)	N(2)-Mg(1)-Br(1)	92.06(5)
N(3)-Mg(1)-Br(1)	92.21(5)	N(1)-Mg(1)-N(3)	84.97(6)
O(1)-C(6)-N(2)	116.26(17)	O(1)-C(6)-C(5)	115.21(16)
C(6)-N(2)-C(8)	107.44(15)	N(2)-C(8)-C(9)	109.90(15)
C(6)-N(2)-Mg(1)	126.07(13)	Mg(1)-O(3)-C(24)	123.13(12)

Synthesis of (*S*,*S*)-(BOPA^{iPr})Mg(OBn) was not successful *via* the salt elimination route. No reaction was observed upon addition of 1 equiv. of KOBn to **18** or **19** at room temperature or 70 °C in THF.

As previously discussed, borohydride complexes have demonstrated superior polymerisation control compared to their amide and alkyl counterparts.[5, 6, 100-104] A two-step synthetic route was therefore attempted in order to synthesise (*S*,*S*)-(BOPA^{iPr})Mg(BH_4)(THF). Firstly, the potassium salt K(*S*,*S*)-(BOPA^{iPr}) (**20**) was obtained by reacting the protio-ligand with 1.2 equiv. of KN($SiMe_3$)$_2$ in THF. Compound **20** was isolated as a yellow powder in 68% yield. NMR spectroscopy analysis was carried out in THF-d_8 since the complex was only sparingly soluble in non-donor solvents.

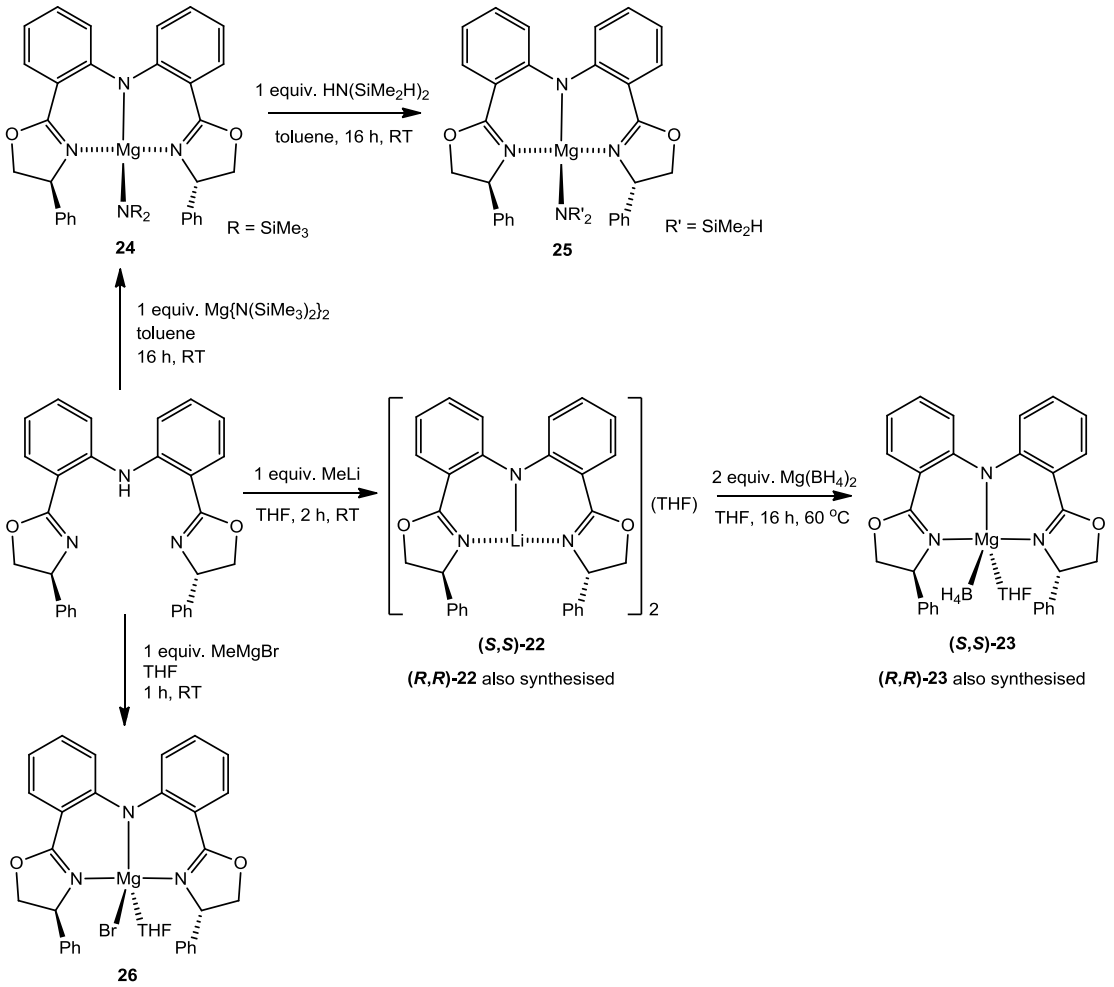
The synthesis of (*S*,*S*)-(BOPA^{iPr})Mg(BH_4) was attempted *via* the salt elimination reaction between an equimolar amount of **20** and Mg(BH_4)$_2$ in THF at room temperature, affording a yellow powder after toluene extraction and pentane wash. The ^{11}B NMR spectrum of the isolated compound showed no evidence for the presence of a borohydride moiety, leading to the postulation that the resulting complex was the homoleptic species {(*S*,*S*)-(BOPA^{iPr})}$_2$Mg (**21**). Alkaline earth

complexes are prone to redistribution according to Schlenk equilibria, facilitating ligand exchange in heteroleptic compounds to form homoleptic species.[105, 106] An independent synthesis was therefore carried out by reacting (*S*,*S*)-BOPA$^{i\text{Pr}}$-H with $Mg\{N(SiMe_3)_2\}_2$ in a 2:1 ratio at 70 °C for 48 h, affording a bright yellow solid which possessed identical NMR data as the compound obtained from the reaction between **20** and $Mg(BH_4)_2$. The formation of **21** was further confirmed by elemental analysis and the presence of a molecular ion peak at 805 *m/z* in the EI-MS spectrum. Although crystallographic data could not be obtained, it was postulated that the magnesium centre possesses an octahedral geometry and the two ligand moieties were orientated orthogonal to each other due to steric reasons. Ward *et al*. reported an analogous homoleptic compound $\{(S,S)\text{-}(BOPA^{Bn})\}_2Ca$, the X-ray crystal structure of which clearly revealed the orthogonal orientation of the two ligand moieties.[95] Each ligand occupies a plane passing through the metal centre (*mer*), with the amido nitrogens located *trans* to each other.

The stability of **21** in the presence of benzyl alcohol was probed in order to evaluate the possibility of performing ROP *via* an activated monomer mechanism. Unfortunately, the sensitivity of **21** led to complex decomposition upon addition of benzyl alcohol.

5.3.2 Synthesis and characterisation of BOPA^{Ph}-supported magnesium complexes

The unsuccessful attempt to synthesise (*S*,*S*)-(BOPA$^{i\text{Pr}}$)$Mg(BH_4)$ was attributed to the lack of steric hindrance imposed by the (*S*,*S*)-BOPA$^{i\text{Pr}}$ ligand, therefore facilitating redistribution to generate the homoleptic species **21**. This led to further investigation using the bulkier BOPA^{Ph} as the ligand framework so that such redistribution could be circumvented. A series of magnesium complexes was subsequently synthesised, as depicted in Scheme 5.2.



Scheme 5.2 Synthesis of magnesium complexes supported by the (*S*,*S*)-BOPA^{Ph} ligand.

Attempted synthesis of the potassium salt K(*S*,*S*)-(BOPA^{Ph}) *via* deprotonation of the protio-ligand with KN(SiMe$_3$)$_2$, KH or KBn yielded multiple products which were difficult to purify. Instead, the lithium salt [(*S*,*S*)-(BOPA^{Ph})Li]$_2$(THF) (**(*S*,*S*)-22**) was subsequently prepared by reacting the protio-ligand with methyl lithium in THF, affording a bright yellow powder in 78% isolated yield. The ^{1}H NMR spectrum in C_6D_6 revealed the presence of two sets of signals corresponding to the ligand backbone and one coordinated THF. Upon conducting the NMR characterisation in THF-d_8, complex **(*S*,*S*)-22** dissociates to a monomeric species (*S*,*S*)-(BOPA^{Ph})Li(THF) (**(*S*,*S*)-22′**), giving rise to one set of ligand signals in the ^{1}H NMR spectrum. This is consistent with the solid state structure grown from a mixture of THF and pentane at room temperature (*vide infra*). An analogous approach was used to prepare [(*R*,*R*)-(BOPA^{Ph})Li]$_2$(THF) (**(*R*,*R*)-22**) starting from (*R*,*R*)-BOPA^{Ph}-H.

Complex **(*S*,*S*)-22′** is four-coordinate in which the Li centre is coordinated to the three N donors of the $BOPA^{Ph}$ ligand and the O donor of THF (Figure 5.11 and Table 5.2). The geometry at the Li centre is best described as distorted tetrahedral, with N(2)-Li(1)-N(3) and N(2)-Li(1)-N(1) bond angles of 139.9(2) and 93.03(17)°, respectively, significantly deviating from an ideal tetrahedral geometry. All Li(1)-N bond distances fall within the expected range,[107] with Li(1)-N(1) (1.963(4) Å) and Li(1)-N(3) (1.974(4) Å) bond lengths being shorter than that of Li(1)-N(2) (2.016(4) Å). As observed previously, an angle of 56.0° was observed between the planes of the two phenylene rings on the backbone, in close agreement with the value obtained for **19**. Interestingly, the phenylene ring associated with C(21) is almost perpendicular to the phenyl ring associated with C(25), with an inter-plane angle of 86.8° whereas the corresponding value between the other phenylene and phenyl rings is 61.4°.

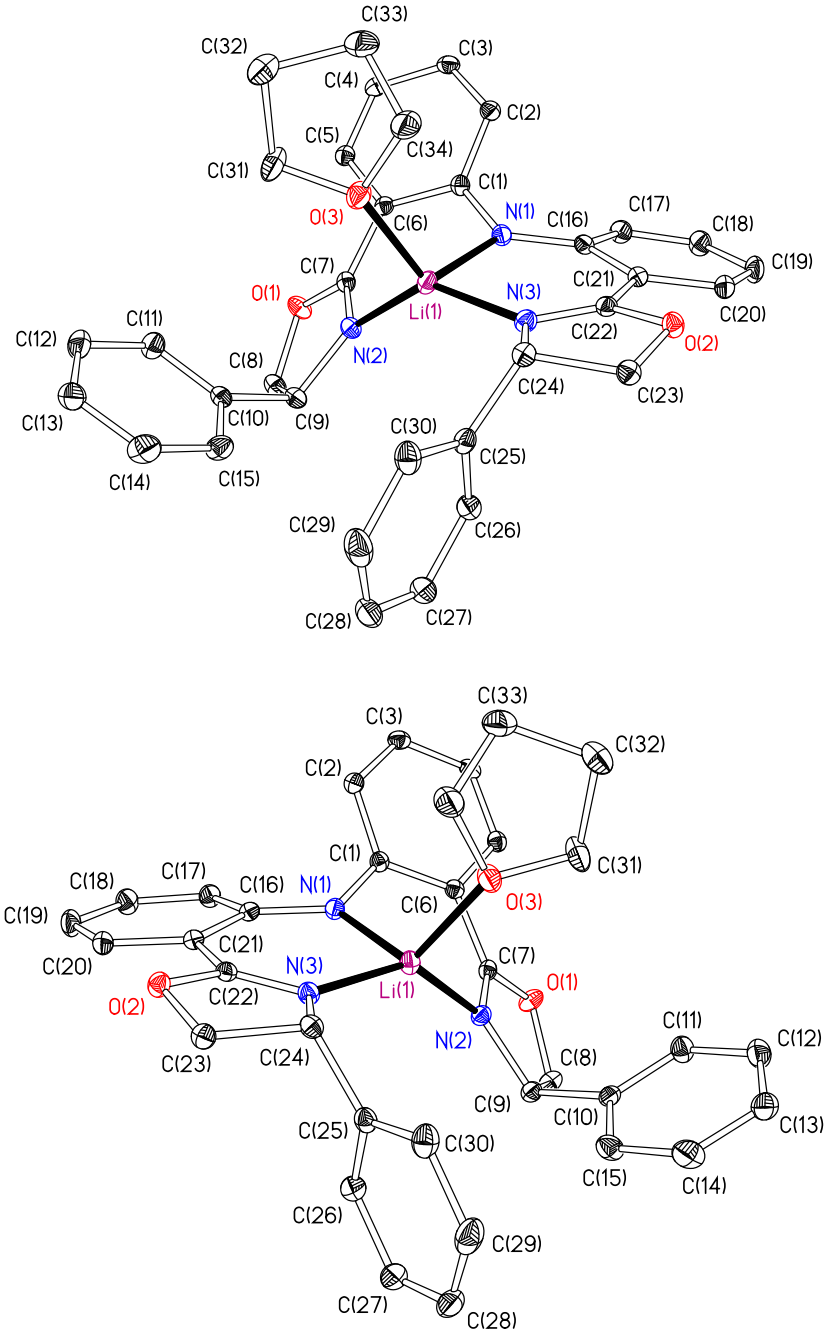


Figure 5.11 Displacement ellipsoid plots of (*S*,*S*)-(BOPA^{Ph})Li(THF) (**(*S*,*S*)-22′**) (top) and (*R*,*R*)-(BOPA^{Ph})Li(THF) (**(*R*,*R*)-22′**) (bottom). C-bound H atoms omitted for clarity. Ellipsoids are drawn at the 20% probability level.

Table 5.2 Selected bond lengths (Å) and angles (º) for (*S*,*S*)-(BOPA^{Ph})Li(THF) (**(*S*,*S*)-22′**).

Li(1)-N(1)	1.963(4)	Li(1)-N(2)	2.016(4)
Li(1)-N(3)	1.974(4)	Li(1)-O(3)	1.948(4)
C(7)-N(2)	1.282(3)	O(1)-C(7)	1.368(2)
C(1)-N(1)	1.382(3)	O(3)-C(31)	1.444(3)
N(1)-Li(1)-O(3)	114.0(2)	N(1)-Li(1)-N(3)	92.96(17)
N(2)-Li(1)-N(3)	139.9(2)	N(2)-Li(1)-O(3)	105.77(19)
N(1)-Li(1)-N(2)	93.03(17)	Li(1)-O(3)-C(31)	126.52(19)
N(2)-C(9)-C(10)	110.03(17)		

(*S*,*S*)-(BOPA^{Ph})Mg(BH_4)(THF) (**(*S*,*S*)-23**) was synthesised *via* a two-step process. The salt elimination reaction between [(*S*,*S*)-(BOPA^{Ph})Li]$_2$(THF) (**(*S*,*S*)-22**) and $Mg(BH_4)_2$ in THF at room temperature resulted in the formation of a lithium "ate" complex, which was extracted into toluene and heated at 60 ºC overnight. All volatile components were removed under reduced pressure and the resulting yellow solid was dried in *vacuo* for at least 2 h. Subsequent toluene extraction followed by washing with pentane afforded a yellow solid in 50% isolated yield. As observed previously, the diastereotopic protons on the oxazoline ring (OC$\underline{H}_2$CH) were visible as overlapping multiplets in the region of 3.83-3.92 ppm in the ^{1}H NMR spectrum (C_6D_6). Interestingly, the OCH$_2$C$\underline{H}$ proton was shifted downfield (5.87 ppm) whereas the opposite was observed for aromatic protons upon coordination to the metal centre. Furthermore, the diastereotopic protons adjacent to the oxygen on THF were observed as two multiplets at 2.97 and 3.29 ppm. The characteristic signals corresponding to B$\underline{H}_4$ were identified as a broad quartet with equal intensity ($^1J_{H\text{-}B}$ = 72 Hz) in the region of 0.30-1.07 ppm. This is the result of the rapid exchange between the terminal B-H$_t$ and bridging B-H$_b$ on the NMR timescale. Thus, the $^1J_{B\text{-}H}$ coupling constant of 72 Hz is an average value for both B-H$_t$ and B-H$_b$. The ^{11}B NMR (C_6D_6) spectrum showed a quintet at -37.9 ppm, in good agreement with a typical borohydride signal.[93, 100, 101, 108-110] (*R*,*R*)-(BOPA^{Ph})Mg(BH_4)(THF) (**(*R*,*R*)-23**) was also prepared *via* an analogous salt elimination synthetic route starting from **(*R*,*R*)-22**, giving an identical ^{1}H NMR spectrum.

Crystals of both **(*S*,*S*)-23** and **(*R*,*R*)-23** suitable for X-ray diffraction were grown from a mixture of THF and pentane at room temperature. Compound **(*S*,*S*)-23** is *pseudo*-five coordinate in which the Mg is coordinated to the three N donors of the ligand, the O donor of THF and a κ^2-BH_4 moiety (Figure 5.12 and Table 5.3). The geometry at the Mg centre is best described as *pseudo*-trigonal bipyramidal, with the oxazoline nitrogens occupying the axial positions. The bond angles of N(1)-Mg(1)-O(3), O(3)-Mg(1)···B(1) and B(1)···Mg(1)-N(1) are 105.78(5), 113.34(6) and 140.88(6)º, respectively, deviating from the ideal trigonal bipyramidal geometry. In addition, the N(2)-Mg(1)-N(3) bond angle of 166.31(6)º also shows a perturbation from linearity. As observed previously, a helical twist is present, giving rise to an inter-plane angle of 70.7° between the two phenylene rings on the backbone. This is significantly larger than that observed in **(*S*,*S*)-22′** (56.0°), presumably due to an increase in steric hindrance around the coordination sphere to accommodate the -BH_4 moiety. The bond length of Mg(1)-N(2) (2.1109(14) Å) is slightly shorter than that for Mg(1)-N(3) (2.1288(14) Å), but all fall within the normal range for Mg-N=C bonds of 1.99-2.27 Å.[107] The Mg(1)-N(1) bond distance was found to be 2.0648(13) Å, being shorter than those for Mg(1)-N(2) and Mg(1)-N(3). The Mg(1)-O(3) bond length of 2.0569(11) Å is in close agreement with that for an analogous compound ($CzOx^{Me2}$)Mg(BH_4)(THF) (**5.84**-**THF**) (2.083(2) Å) reported previously in the Mountford group.[93]

The borohydride moiety coordinates to the magnesium centre *via* a κ^2-coordination mode in the solid state. The hydrogen atoms were located in a Fourier difference map and positionally and isotropically refined, giving the Mg···H distances in the usual range.[107] The Mg(1)···B(1) length of 2.4678(19) Å is consistent with the value expected for a κ^2-bound borohydride (2.39-2.57 Å) and is significantly longer than the typical distance for a κ^3-bound -BH_4 (2.22-2.34 Å). For example, the crystal structure of **5.84**-**THF** revealed an κ^2-coordination mode of BH_4, possessing an Mg···B distance of 2.445(4) Å whereas (Tpm^{*d})Mg(BH_4) (**2**) discussed in Chapter Two had a κ^3-bound borohydride, giving rise to a Mg···B distance of 2.278(3) Å.[93]

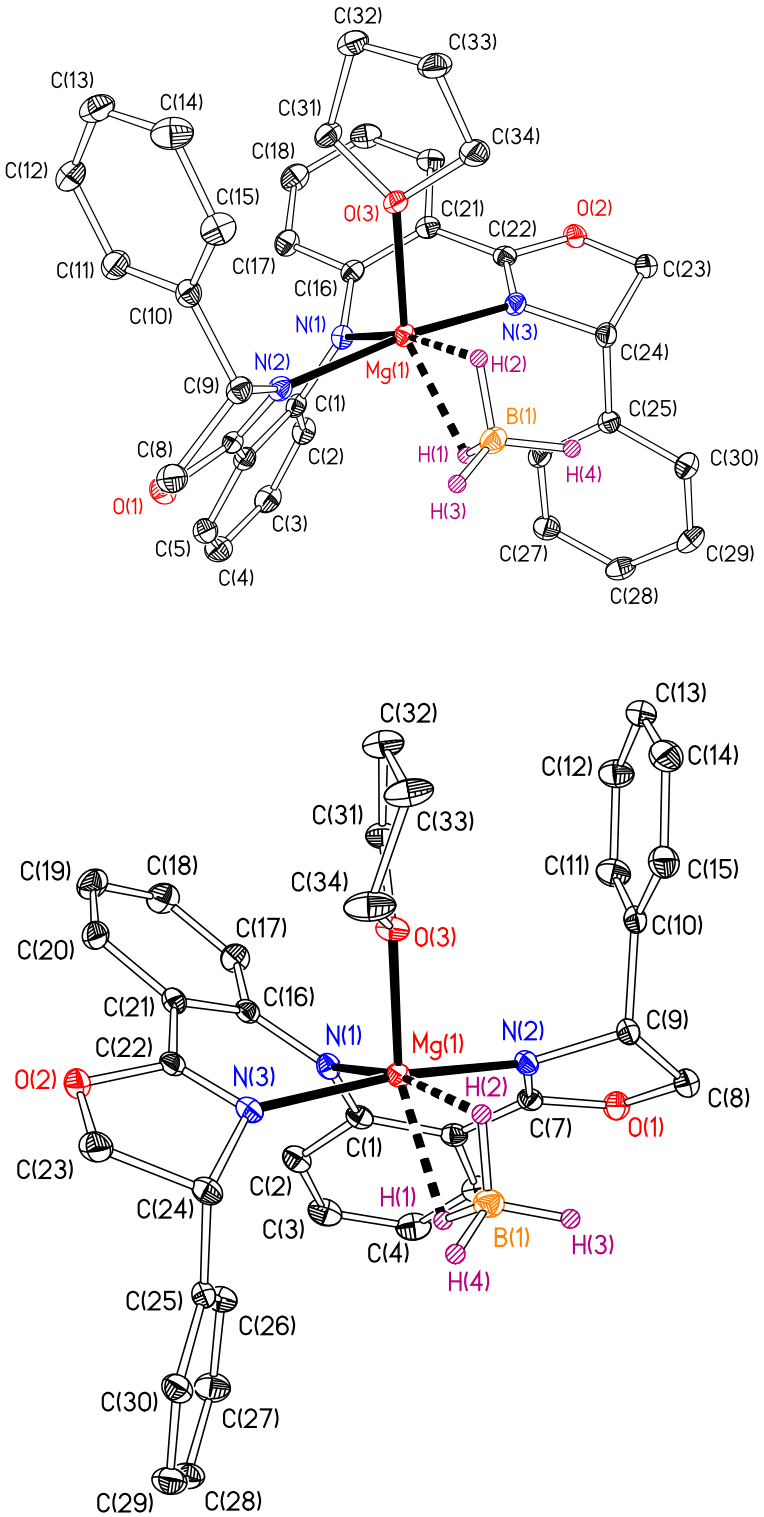


Figure 5.12 Displacement ellipsoid plots of (*S*,*S*)-(BOPA^{Ph})Mg(BH$_4$)(THF) (**(*S*,*S*)-23**) (top) and (*R*,*R*)-(BOPA^{Ph})Mg(BH$_4$)(THF) (**(*R*,*R*)-23**) (bottom). C-bound H atoms omitted for clarity. Ellipsoids are drawn at the 20% probability level.

Table 5.3 Selected bond lengths (Å) and angles (º) for (*S*,*S*)-(BOPA^{Ph})Mg(BH_4)(THF) (**(*S*,*S*)-23**).

Mg(1)-N(1)	2.0648(13)	Mg(1)-N(2)	2.1109(14)
Mg(1)-N(3)	2.1288(14)	Mg(1)-O(3)	2.0569(11)
Mg(1)···B(1)	2.4678(19)	Mg(1)···H(1)	2.029(18)
Mg(1)···H(2)	2.055(18)	B(1)-H(1)	1.121(19)
B(1)-H(2)	1.20(2)	B(1)-H(3)	1.07(2)
B(1)-H(4)	1.11(2)		
N(1)-Mg(1)-O(3)	105.78(5)	O(3)-Mg(1)···B(1)	113.34(6)
N(1)-Mg(1)···B(1)	140.88(6)	N(2)-Mg(1)-N(3)	166.31(6)
N(1)-Mg(1)-N(2)	84.88(5)	N(2)-Mg(1)···B(1)	89.13(6)
N(3)-Mg(1)···B(1)	94.12(6)	N(1)-Mg(1)-N(3)	84.22(5)
H(1)-B(1)-H(2)	110.0(13)	H(1)-B(1)-H(3)	111.0(15)
H(2)-B(1)-H(3)	106.8(14)	H(1)···Mg(1)···H(2)	55.5(7)

The solid state IR spectrum of **(*S*,*S*)-23** echoed the findings obtained from X-ray crystallographic data; strong absorptions corresponding to the terminal ν(B-H_t) stretching modes were observed at 2353 and 2305 cm^{-1} (48 cm^{-1} splitting), in conjunction with a strong band with a shoulder at 2194 cm^{-1} (bridging ν(B-H_b) stretching modes), further confirming the κ^2-coordination mode of the borohydride moiety.[111] The solid state coordination mode remained unchanged upon dissolving in THF, as evidenced by the strong absorptions at 2375 and 2324 cm^{-1} (51 cm^{-1} splitting) and the strong band at 2173 cm^{-1}, corresponding to the terminal and bridging ν(B-H) stretching modes, respectively.

(*S*,*S*)-(BOPA^{Ph})Mg{$N(SiMe_3)_2$} (**24**) was synthesised as a precursor to access the desired alkoxide complex. The protonolysis reaction between (*S*,*S*)-BOPA^{Ph}-H and Mg{$N(SiMe_3)_2$}$_2$ in toluene afforded **24** as a bright yellow powder in 54% isolated yield. Diffraction-quality crystals were grown from a mixture of THF and pentane at room temperature. Compound **24** is four-coordinate in which the Mg centre is coordinated to the N donors of the ligand and the -$N(SiMe_3)_2$ moiety (Figure 5.13 and Table 5.4). The geometry at the Mg centre is best described as distorted tetrahedral, with N(1)-Mg(1)-N(3) (89.83(5)º), N(1)-Mg(1)-N(2) (85.35(6)º), N(3)-Mg(1)-N(4) (124.24(6)º) and N(1)-Mg(1)-N(4) (123.92(6)º) deviating significantly from an ideal

tetrahedral geometry. The helical twist at the backbone is less pronounced than that in **(*S*,*S*)-23**, but is comparable to that found in **(*S*,*S*)-22′** (inter-plane angle of 61.9º for **24** *vs*. 70.7º for **(*S*,*S*)-23** and 56.0º for **(*S*,*S*)-22′**). The bond length of N(3)-Mg(1) (2.0669(13) Å) in **24** is significantly shorter than that for N(2)-Mg(1) (2.1322(15) Å), which is attributed to the steric repulsion between the oxazoline ring associated with N(2) and the -$N(SiMe_3)_2$ moiety. It is interesting to note that a hydrogen on C(32) is located in close proximity to the metal centre, with a Mg(1)···H distance of 2.89 Å. This is outside the sum of the van der Waals radii of 2.79 Å, therefore suggesting the absence of a γ-agostic interaction.[112, 113] The Mg(1)-N(4) bond length of 1.9912(13) Å is shorter than that for Mg(1)-N(1) (2.0415(14) Å) due to the less nucleophilic nature of N(1) as a result of charge delocalisation of the two phenylene rings. The Mg(1)-N(4) bond length of 1.9912(13) Å is slightly shorter than that found in ($CzOx^{Me2}$)Mg{$N(SiMe_3)_2$} (2.0261(17) Å), presumably due to the less sterically encumbered coordination environment as a consequence of less rigid ligand framework.[93]

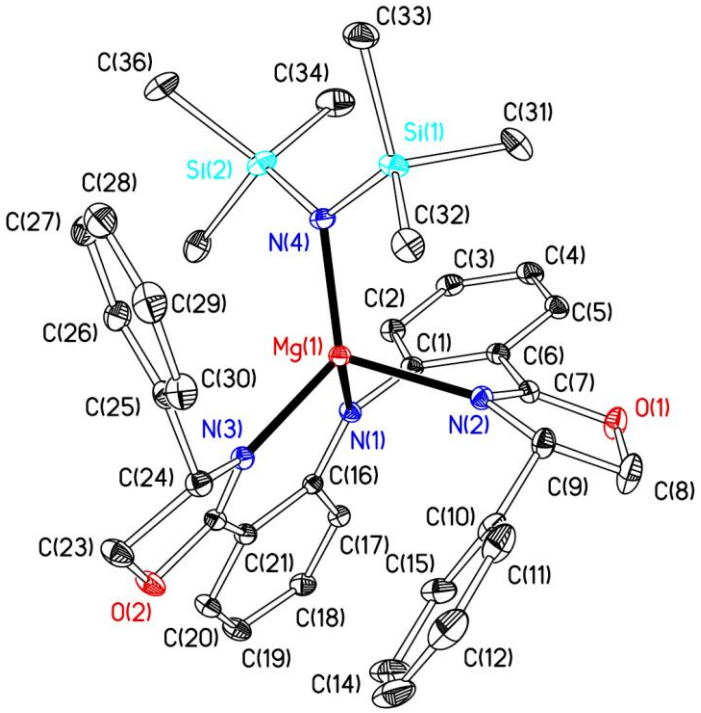


Figure 5.13 Displacement ellipsoid plot of (*S*,*S*)-($BOPA^{Ph}$)Mg{$N(SiMe_3)_2$} (**24**). C-bound H atoms omitted for clarity. Ellipsoids are drawn at the 20% probability level.

Table 5.4 Selected bond lengths (Å) and angles (°) for (*S*,*S*)-(BOPA^{Ph})Mg{N(SiMe$_3$)$_2$} (**24**)

Mg(1)-N(1)	2.0415(14)	Mg(1)-N(2)	2.1322(15)
Mg(1)-N(3)	2.0669(13)	Mg(1)-N(4)	1.9912(13)
N(4)-Si(1)	1.6971(15)	N(4)-Si(2)	1.6995(15)
N(1)-Mg(1)-N(2)	85.35(6)	N(1)-Mg(1)-N(3)	89.83(5)
N(2)-Mg(1)-N(3)	113.99(5)	N(2)-Mg(1)-N(4)	111.92(6)
N(3)-Mg(1)-N(4)	124.24(6)	N(1)-Mg(1)-N(4)	123.92(6)
Si(1)-N(4)-Mg(1)	115.05(7)	Si(2)-N(4)-Mg(1)	118.03(8)

The propensity to undergo redistribution to form homoleptic species was evaluated by reacting 2 equiv. of (*S*,*S*)-BOPA^{Ph}-H with 1 equiv. of Mg{N(SiMe$_3$)$_2$}$_2$ in toluene at 70 °C. A mixture of {(*S*,*S*)-(BOPA^{Ph})}$_2$Mg and **24** was observed in the ^{1}H NMR spectrum (C_6D_6) after heating for 16 h, in contrast to the previously discussed reaction between (*S*,*S*)-BOPA^{iPr}-H and Mg{N(SiMe$_3$)$_2$}$_2$, which only yielded the homoleptic species **21**. Extending the reaction time to 7 days did not result in the complete conversion to {(*S*,*S*)-(BOPA^{Ph})}$_2$Mg. Purification attempts such as repeated recrystallisation were unsuccessful.

Following the successful synthesis of **24**, a similar complex with a less bulky amide ligand (*S*,*S*)-(BOPA^{Ph})Mg{N(SiMe$_2$H)$_2$} (**25**) was prepared *via* the equimolar reaction between **24** and HN(SiMe$_2$H)$_2$ in toluene, affording a yellow solid in 78% isolated yield after washing with pentane to remove the HN(SiMe$_3$)$_2$ by-product. This synthetic pathway was reminiscent of the transamination reactions between Ca{N(SiMe$_3$)$_2$}$_2$ or M{N(SiMe$_3$)$_2$}$_3$ (M = Sc, Y, Sm, Nd and Lu) and HN(SiMe$_2$H)$_2$, reported by Carpentier[114] and Livinghouse[115], respectively. The formation of **25** was driven by the relief of steric hindrance around the magnesium centre. The ^{1}H NMR spectrum (C_6D_6) clearly revealed an apparent septet at 4.67 ppm ($^3J_{H\text{-}H}$ = 3.2 Hz) and two doublets at 0.05 and 0.12 ppm, corresponding to -N(SiMe$_2$<u>H</u>)$_2$ and the diastereotopic -N(Si<u>Me</u>$_2$H)$_2$ protons, respectively. In addition, the OCH$_2$C<u>H</u> proton could be observed as a doublet of doublets due to coupling with the neighbouring diastereotopic methylene protons (OC<u>H</u>$_2$CH), with $^3J_{H\text{-}H}$ coupling constants of 7.6 and 10.0 Hz. The OC<u>H</u>$_2$CH protons were visible as two doublets of doublets at 3.86 and 3.57 ppm.

The reaction between (*S*,*S*)-BOPA^{Ph}-H and MeMgBr in THF led to the formation of (*S*,*S*)-(BOPA^{Ph})Mg(Br)(THF) (**26**), which was isolated as a yellow powder in 75% yield after washing with pentane. As observed previously, the diastereotopic protons adjacent to the oxygen atom on THF were observed as two multiplets at 3.37 and 2.83 ppm in the ^{1}H NMR spectrum (C_6D_6). Integration of the THF signal relative to the ligand backbone was consistent with the coordination of one THF molecule.

Multiple attempts were made to synthesise the desired alkoxide complex (*S*,*S*)-(BOPA^{Ph})Mg(OBn) (**(*S*,*S*)-27**). The protonolysis reaction between **24** or **25** and benzyl alcohol in 1:1 stoichiometry led to catalyst decomposition even when the reaction was performed under kinetic control at -78 °C, generating the protio-ligand, $Mg(OBn)_2$ and the respective amine. No reaction was observed upon addition of KOBn to **26** in THF at 70 °C.

5.4 ROP of *rac*-, *L*-, *D*- and *meso*-LA using magnesium catalysts

5.4.1 ROP of *rac*-LA using magnesium amide catalysts

Following the successful synthesis of magnesium complexes bearing amide initiators, the catalytic activities of (*S*,*S*)-(BOPA^{iPr})Mg{N(SiMe$_3$)$_2$} (**17**), (*S*,*S*)-(BOPA^{Ph})Mg{N(SiMe$_3$)$_2$} (**24**) and (*S*,*S*)-(BOPA^{Ph})Mg{N(SiMe$_2$H)$_2$} (**25**) were subsequently probed for the ROP of *rac*-LA. All polymerisations were performed in THF at room temperature with a [*rac*-LA]$_0$:[catalyst]$_0$ ratio of 100:1 ([*rac*-LA]$_0$ = 1.0 M). The findings are summarised in Table 5.5.

Complex **17** was highly active, reaching 90% conversion within 1.5 min to produce slightly heterotactic PLA with a P_r value of 0.61. As mentioned previously, one of the problems commonly encountered for amide initiators is the much faster rate of propagation than that of initiation, leading to the formation of polymers with higher than expected M_n.[116-120] This was also observed in this case; the experimental M_n was almost 10 times that of the anticipated value. In addition, a non-linear growth of M_n *vs*. % conversion was observed, in conjunction with a moderate PDI (1.39), further indicating the catalyst's non-ideal behaviour in terms of molecular weight control. The reaction was found to conform to first order dependence on *rac*-LA concentration, with an observed rate constant (k_{obs}) of 0.0268(12) s^{-1} (R^2 = 0.990).

In comparison to **17**, the analogous complex **24** featuring bulkier phenyl substituents was slightly less active, reaching 92% conversion after 5 min. The polymerisation was also first order with respect to *rac*-LA concentration, with k_{obs} = 0.0088(2) s^{-1} (R^2 = 0.996). The decrease in activity of **24** compared to **17** could be attributed to the more congested coordination sphere arising from the incorporation of bulkier phenyl substituents, deterring the coordination and subsequent insertion of lactide monomers. The rate reduction was accompanied by a minor increase in the heterotacticity (P_r = 0.66) of the resulting polymer. Higher than expected experimental M_n values were observed throughout the course of the polymerisation, with tailing-off effects being present towards the end, presumably due to transesterification side reactions.

Complex **25**, featuring a less bulky amide initiator, was found to be slightly more active than **24** (90% conversion in 140 s), affording heterotactic PLA with a P_r value of 0.64. A first order rate dependence on *rac*-LA concentration was observed, with k_{obs} = 0.0177(6) s^{-1} (R^2 = 0.995) (*cf.* 0.0088(2) s^{-1} (R^2 = 0.996) for **24**). As observed with **17** and **24**, a higher than expected M_n was observed, in conjunction with a moderate PDI of 1.39. Unfortunately, end group investigations for the aforementioned polymerisations initiated by **17**, **24** and **25** were hampered by the high M_n values being out of the range for MALDI-ToF analysis. Further ROP studies by varying the $[monomer]_0$:$[initiator]_0$ ratio were not carried out.

Table 5.5 Selected data for the ROP of *rac*-LA using **17**, **24** and **25** in THF.

Entry	Catalyst [a]	Conv.[b] (%)	Time (s)	M_n obs[c] (g mol^{-1})	M_n calc[d] (g mol^{-1})	PDI[e]	P_r [b]
1	**17**	91	90	117,690	13,276	1.39	0.61
2	**24**	92	300	58,640	13,420	1.65	0.66
3	**25**	90	140	44,720	13,103	1.39	0.64

[a] Conditions: $[rac\text{-LA}]_0$:$[catalyst]_0$ = 100:1, $[LA]_0$ = 1.0 M, $[catalyst]_0$ = 0.01 M, 4 mL THF at room temperature. [b] Measured by ^1H NMR ($CDCl_3$) analyses. [c] Molecular weights (g mol^{-1}) determined from GPC using the appropriate Mark-Houwink corrections. [d] Expected M_n (g mol^{-1}) for one polymer chain growing per metal centre, M_n (calc for Entries 1 and 2) = conversion (%) × 100 × 144.1 + 160.4; M_n (calc for Entry 3) = conversion (%) × 100 × 144.1 + 132.3 . [e] PDI = M_w/M_n.

5.4.2 ROP of *rac*-, *L*-, *D*- and *meso*-LA using magnesium borohydride catalysts

A preliminary investigation into the ROP activity of (*S*,*S*)-(BOPA^{Ph})Mg(BH$_4$)(THF) (**(*S*,*S*)-23**) was performed by treating the catalyst with 100 equiv. of *rac*-LA in THF at room temperature. Complex **(*S*,*S*)-23** demonstrated moderate activity, reaching 92% conversion after 155 min (Table 5.6, Entry 1). This was in striking contrast to the analogous compound (*S*,*S*)-(CzOx^{iPr})Mg(BH$_4$)(THF) (**(*S*,*S*)-5.86**) supported by a carbazole-bis(oxazoline) ligand previously reported in the Mountford group, requiring 72 h to reach 92% conversion under identical polymerisation conditions.[93] Despite the fact that direct comparisons could not be made due to the difference in both the ligand backbone and the oxazoline substituents of **(*S*,*S*)-23** (Ph) and **(*S*,*S*)-5.86** (^{i}Pr), it was assumed based on studies conducted in Section 5.4.1 that catalysts bearing isopropyl groups at the chiral carbon would lead to faster polymerisations. The significant difference in rates observed for **(*S*,*S*)-23** and **(*S*,*S*)-5.86** could possibly be attributed to the difference in rigidity of the ligand backbone. Complex **(*S*,*S*)-23** featuring a non-fused diphenylamine linker could confer more flexibility due to the helical twist, creating more space around the coordination sphere. This was supported by the X-ray crystal structures shown earlier in this Chapter. In contrast, the co-planar backbone of **(*S*,*S*)-5.86** resulted in a sterically more encumbered environment around the magnesium centre, therefore hindering monomer coordination and insertion. Regrettably, the faster rate of propagation associated with **(*S*,*S*)-23** was accompanied by a significant decrease in heteroselectivity. The isolated PLA was only slightly heterotactically enriched (P_r = 0.60) in comparison to that obtained employing **(*S*,*S*)-5.86** (P_r = 0.81-0.88).

The ROP initiated by **(*S*,*S*)-23** demonstrated neither first nor second order dependence on *rac*-LA concentration. This was also observed in **(*S*,*S*)-5.86**, which was attributed to the presence of complex pre-equilibria arising from association and dissociation of "B(LA-H)$_3$" to the metal centre.[93] Complex **(*S*,*S*)-23** produced PLA with a close to expected (one chain per metal centre) M_n at low % conversions (Figure 5.14). Tailing-off effects were observed as the polymerisation proceeded, presumably due to transesterification side reactions. This was consistent with an increase in PDI from 1.21 at 10% conversion to 1.41 at 92% conversion.

Table 5.6 Selected data for the ROP of *rac*-, *L*-, *D*- and *meso*-LA using (*S*,*S*)-(BOPA^{Ph})Mg(BH$_4$)(THF) (**(*S*,*S*)-23**), (*R*,*R*)-(BOPA^{Ph})Mg(BH$_4$)(THF) (**(*R*,*R*)-23**) and *rac*-(BOPA^{Ph})Mg(BH$_4$)(THF) (***rac*-23**) in THF.

Entry	Catalyst [a]	Monomer (LA)	Conv.[b] (%)	Time (min)	M_n(obs)[c] (g mol^{-1})	M_n(calc)[d] (g mol^{-1})	PDI[e]	P_r[b]
1	**(*S*,*S*)-23**	*rac*	92	155	7,540	13,263	1.41	0.60
2	**(*S*,*S*)-23**	*L*	90	330	7,980	12,975	1.32	/
3	**(*S*,*S*)-23**	*D*	88	180	7,470	12,687	1.36	/
4	**(*R*,*R*)-23**	*rac*	91	155	7,340	13,119	1.44	0.63
5	**(*R*,*R*)-23**	*L*	88	180	7,960	12,687	1.37	/
6	**(*R*,*R*)-23**	*D*	93	330	8,200	13,408	1.38	/
7	***rac*-23**	*rac*	90	180	7,050	12,975	1.44	0.66
8	**(*S*,*S*)-23**	*meso*	89	5	10,490	12,831	1.47	0.68

[a] Conditions: $[LA]_0$:$[initiator]_0$ = 100:1, $[LA]_0$ = 1.0 M, $[initiator]_0$ = 0.01 M, 4 mL THF at room temperature. [b] Measured by ^{1}H NMR ($CDCl_3$) analyses. [c] Molecular weights (g mol^{-1}) determined from GPC using the appropriate Mark-Houwink corrections. [d] Expected M_n (g mol^{-1}) for one polymer chain growing per metal centre, M_n (calc for Entries 1-8) = conversion (%) × 100 × 144.1 + 4.0. [e] PDI = M_w/M_n

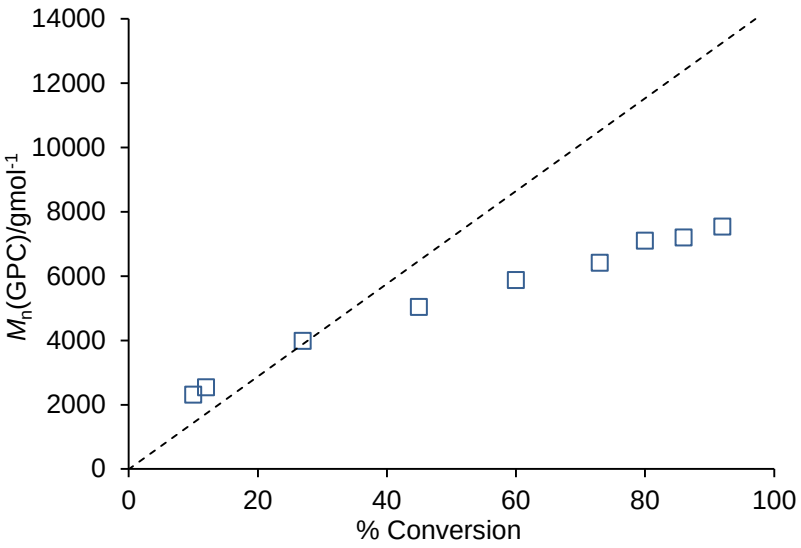
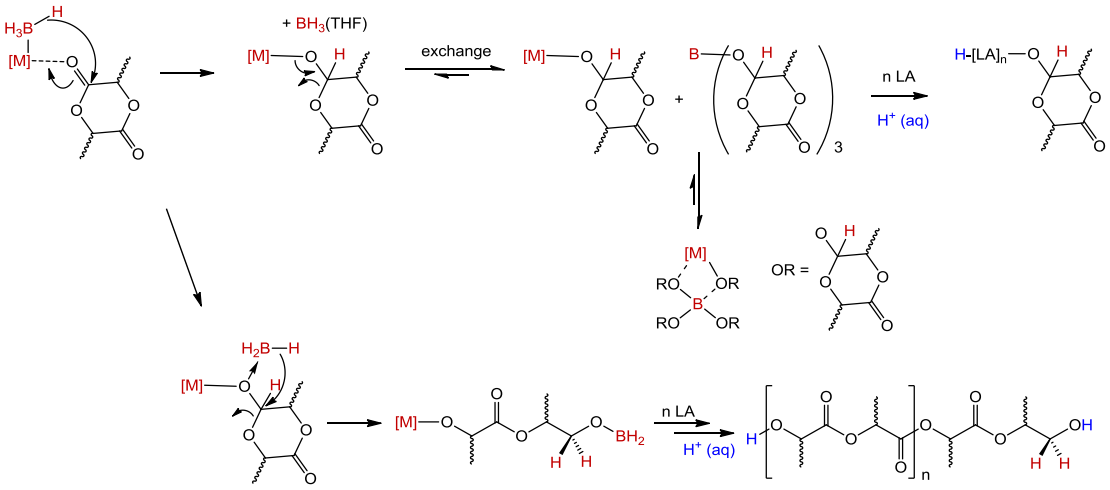


Figure 5.14 Data for the ROP of *rac*-LA using (*S*,*S*)-(BOPA^{Ph})Mg(BH$_4$)(THF) (**(*S*,*S*)-23**). M_n (GPC) *vs.* % conversion plot. The dashed line represents the M_n expected for one chain per metal centre. Conditions: [*rac*-LA]$_0$:[**(*S*,*S*)-23**]$_0$ = 100:1, [*rac*-LA]$_0$ = 1.0 M, [**(*S*,*S*)-23**]$_0$ = 0.01 M, 4 mL THF at room temperature.

In order to account for the unexpected polymerisation kinetics and to probe whether **(*S*,*S*)-23** initiated ROP *via* a similar mechanism as did (Tpm*^{d})Mg(BH$_4$) (**2**), an NMR tube-scale reaction between 1 equiv. of **(*S*,*S*)-23** and 10 equiv. of *rac*-LA was performed in THF-d_8. The ^{11}B NMR spectrum recorded 5 min after the reaction revealed the complete consumption of BH$_4$ and the presence of a major broad singlet at 7.2 ppm and another signal at 1.8 ppm, suggesting the formation of multiple tetra-coordinated adduct species. It is important to note that the peak at 22.7 ppm corresponding to the "free" "B(LA-H)$_3$" was very minor, indicating that the equilibrium favoured the side of the tetra-coordinated adduct. Analysis *via* ^{1}H NMR spectroscopy was hampered by broadening of the signals in the diagnostic region of 4.00-5.80 ppm. Although characteristic resonances corresponding to the non-opened LA ring alkoxide could not be unambiguously distinguished from the ^{1}H NMR spectrum, it was proposed based on ^{11}B NMR data that **(*S*,*S*)-23** followed a similar mechanism as **2**, shown in Scheme 5.3. That is, a single hydride transfer from the borohydride moiety to the carbonyl carbon of LA generated a non-opened LA ring alkoxide (*S*,*S*)-(BOPA^{Ph})Mg(LA-H) and BH$_3$(THF), which underwent exchange reactions to form "B(LA-H)$_3$". In contrast to (Tpm*^{d})Mg(LA-H) which featured a sterically bulky ligand framework, the flexible BOPA^{Ph} backbone gave rise to a less

congested coordination sphere, therefore enabling the coordination of "$B(LA\text{-}H)_3$" to (*S*,*S*)-BOPA^{Ph}Mg(LA-H). The resulting tetra-coordinated adduct was postulated to be the catalyst resting state and insertion of LA could only occur upon dissociation of "$B(LA\text{-}H)_3$". The neither first nor second order dependence on monomer concentration could be ascribed to the dissociation and association of "$B(LA\text{-}H)_3$" prior to and following LA insertion. Based on the results from Chapter Three which demonstrated the inefficient chain transfer capacity of bulky borate ester species, it was assumed that "$B(LA\text{-}H)_3$" also underwent negligible exchange with the growing polymeryl chain in the current catalytic system, leading to one chain being produced per metal centre. Unfortunately, there is no NMR spectroscopic evidence for the formation of α,ω-dihydroxytelechelic PLA proceeding through two successive hydride transfers.



Scheme 5.3 Proposed mechanisms for the ROP of LA initiated by **(*S*,*S*)-23**.

Polymer end group analysis was investigated by MALDI-ToF mass spectrometry which revealed two types of termini (Figure 5.15). For example, the peak envelope at 1194 g mol^{-1} could be assigned to PLA containing seven LA repeating units with a non-opened LA chain end whereas the corresponding α,ω-dihydroxytelechelic PLA could be observed at 1196 g mol^{-1}. In addition, intermolecular transesterification was also detected, as evidenced by the presence of peak envelopes of $\Delta m/z$ = 72 g mol^{-1}.

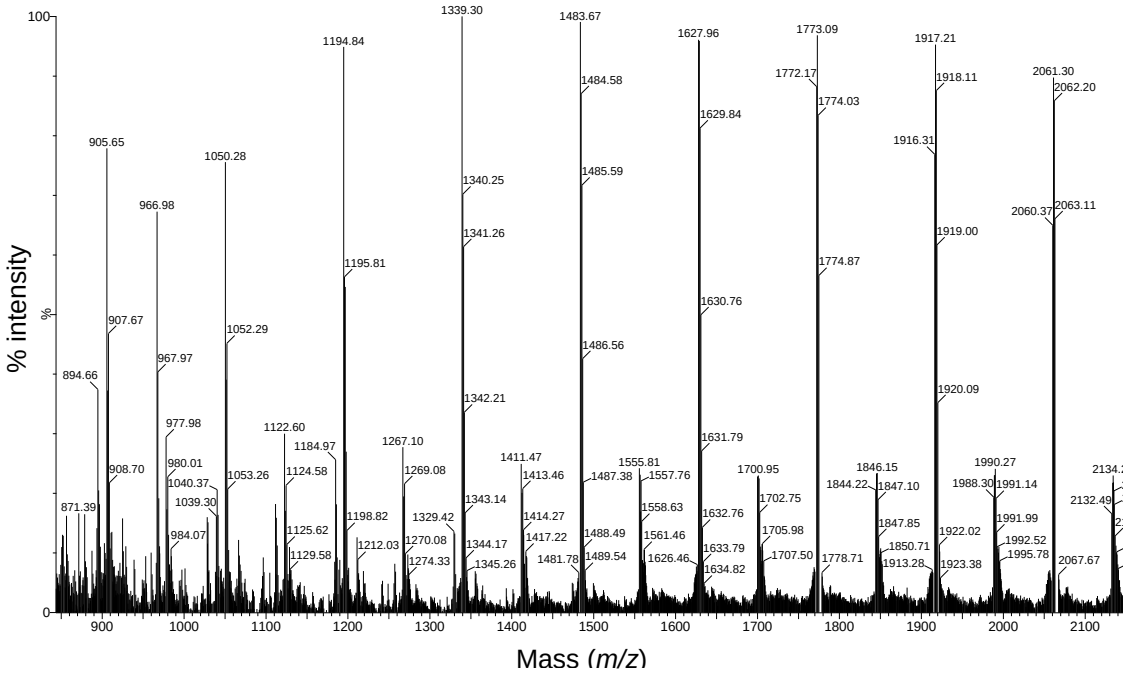


Figure 5.15 MALDI-ToF MS of PLA synthesised using (*S*,*S*)-(BOPA^{Ph})Mg(BH_4)(THF) (**(*S*,*S*)-23**). Conditions: [*rac*-LA]$_0$:[**(*S*,*S*)-23**]$_0$ = 100:1, [*rac*-LA]$_0$ = 1.0 M, [**(*S*,*S*)-23**]$_0$ = 0.01 M, 4 mL THF at room temperature. K^+ dopant.

Following the successful use of **(*S*,*S*)-23** as an initiator for the ROP of *rac*-LA, further investigations were subsequently performed with *D*- and *L*-LA (Table 5.6, Entries 2 and 3). Complex **(*S*,*S*)-23** exhibited lower catalytic activities in both cases, converting 90% of *L*-LA within 330 min and 88% of *D*-LA after 180 min (*cf*. 92% *rac*-LA in 155 min). This was indicative of the catalyst's slight preference to insert LA monomers *via* a *racemic* linkage over a *meso* dyad as a result of a chain end control mechanism. However, kinetic data were inconsistent with the operation of a pure chain end control mechanism; complex **(*S*,*S*)-23** demonstrated a slight preference in inserting *D*-LA over *L*-LA, suggesting the presence of a minor enantiomorphic site control mechanism. Regrettably, the exact rate constants could not be determined due to the polymerisation kinetics being neither first nor second order with respect to LA concentration. As observed previously in the ROP of *rac*-LA, the experimental M_n was in close agreement with the expected value for one chain being produced per metal centre at the beginning of the polymerisation followed by a decrease towards the end.

An analogous study was also performed with **(*R*,*R*)-23** to verify the monomer enchainment preference and to rule out any technical sources of error. The catalytic

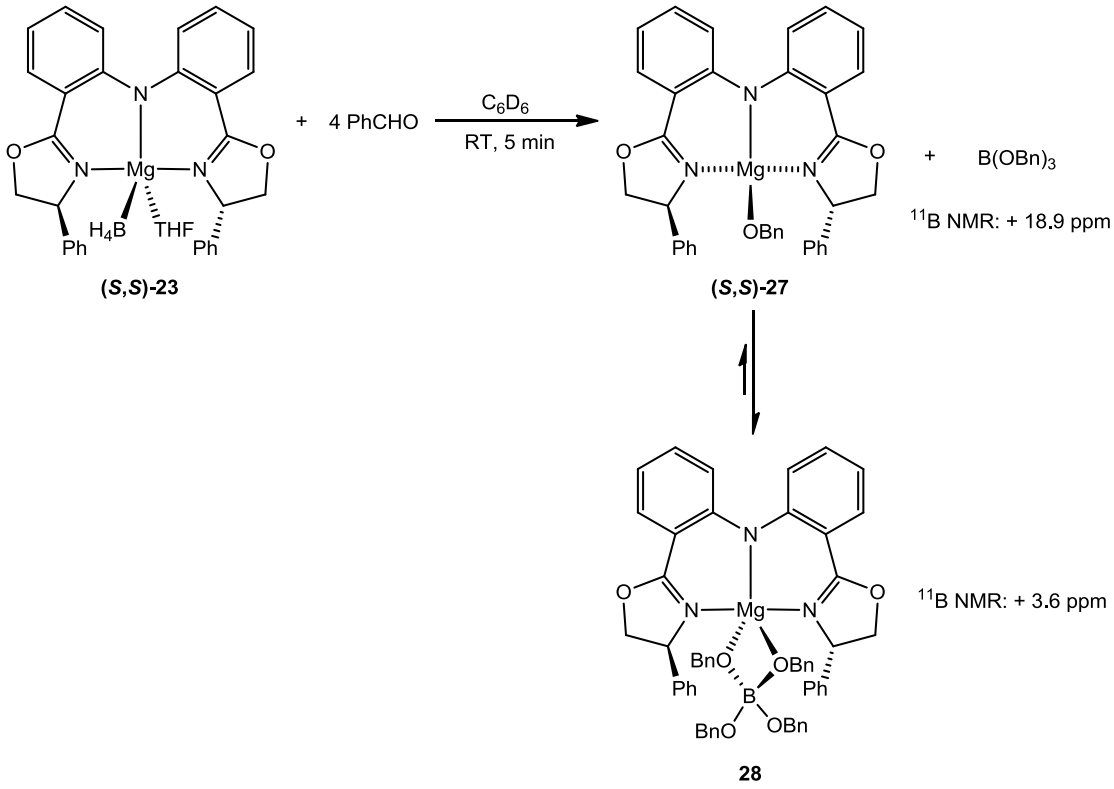
activity of **(*R*,*R*)-23** in the ROP of *rac*-LA mirrored that of **(*S*,*S*)-23**; 91% conversion was achieved after 155 min, affording slightly heterotactic (P_r = 0.63) PLA (Table 5.6, Entry 4). Complex **(*R*,*R*)-23** was found to exhibit the opposite monomer enchainment preference as **(*S*,*S*)-23** in the ROP of enantiomerically pure LA; **(*R*,*R*)-23** polymerised 88% of *L*-LA within 180 min whereas 93% conversion was achieved after 330 min for the ROP of *D*-LA (Table 5.6, Entries 5 and 6). Based on these results, it was concluded that both chain end and enantiomorphic site control mechanisms were in operation for the ROP of *rac*-LA initiated by enantiomerically pure **23**, with the former being the dominant mechanism, leading to the production of heterotactic PLA.

Complex ***rac*-23**, prepared by mixing the enantiomerically pure catalysts in a 1:1 ratio, was also employed as a catalyst in the ROP of *rac*-LA. The polymerisation rate was comparable to those using enantiomerically pure catalysts, reaching 90% conversion after 180 min (Table 5.6, Entry 7). The P_r value of the resulting polymer was found to be 0.66.

Complex **(*S*,*S*)-23** was found to be more active in the ROP of *meso*-LA than that of *rac*-LA. Although the exact rate constants could not be determined since both polymerisations were neither first nor second order with respect to LA concentration, the significant difference in rates was apparent given the fact that 89% of *meso*-LA was polymerised in 5 min (*cf*. 92% conversion of *rac*-LA in 155 min). The faster rate of polymerisation associated with *meso*-LA was due to its less stable nature in the ground state in comparison to *D*- and *L*-LA.[121] Given the fact that ROP of *rac*-LA produced heterotactic PLA, it was therefore not surprising that syndiotactic polymer was produced in the ROP of *meso*-LA. This was attributable to the catalyst's preference to insert LA *via* a *racemic* dyad instead of a *meso* linkage as a consequence of a chain end control mechanism. The trend in M_n growth *vs.* % conversion was similar to those observed previously in the ROP of *rac*-LA, namely a good agreement between the calculated and experimental M_n was observed initially followed by tailing off effects towards the end of the polymerisation.

As introduced in Chapter Four, previous work in the Mountford group has introduced a novel approach whereby a benzyloxide species could be generated *in-situ*, in conjunction with $B(OBn)_3$ upon addition of benzaldehyde to a borohydride catalyst. In order to verify whether this approach could be applied in the current system, an

NMR tube scale reaction was performed by adding 4 equiv. of benzaldehyde to 1 equiv. of **(*S*,*S*)-23** in C_6D_6. Both the ^1H and ^{11}B NMR spectra revealed the immediate transformation of **(*S*,*S*)-23** to (*S*,*S*)-(BOPA^{Ph})Mg(OBn) (**(*S*,*S*)-27**) and $B(OBn)_3$. The presence of a minor sharp signal at 18.9 ppm and a major peak at 3.6 ppm (ratio *ca*. 1:9 by integration) in the ^{11}B NMR spectrum could be attributed to $B(OBn)_3$ and the tetra-coordinated adduct (**28**), respectively, clearly indicating that the equilibrium favoured **28**. Although the ^1H NMR spectrum was not as diagnostic as the ^{11}B NMR spectrum due to the presence of overlapping signals, the singlet at 4.94 ppm could be clearly identified as $B(OBn)_3$. In addition, the peak at 4.50 ppm was tentatively assigned to the methylene protons of OBn for **28**. Unfortunately, the characteristic signals for **(*S*,*S*)-27** could not be clearly identified due to broadening. It is worth noting that no catalyst decomposition was observed, suggesting that this approach could be used to efficiently convert a borohydride to an alkoxide species given the fact that the latter could not be independently synthesised *via* conventional protonolysis or salt metathesis reactions.



Scheme 5.4 *In-situ* generated **(*S*,*S*)-27** and $B(OBn)_3$ in equilibrium with **28**.

A preliminary investigation was carried out by treating the *in-situ* generated **(*S*,*S*)-27** and $B(OBn)_3$ with 100 equiv. of *rac*-LA in THF at room temperature (Table 5.7, Entry 1). 89% conversion was achieved after 20 min, affording heterotactic PLA with P_r = 0.64. Similar to the observations made for polymerisations employing Tpm*[d] ligand-supported catalysts, the conversion of **(*S*,*S*)-23** to **(*S*,*S*)-27** and $B(OBn)_3$ resulted in a considerable increase in the rate of polymerisation. As mentioned previously, the ^{1}H NMR spectrum of the reaction between **(*S*,*S*)-23** and 10 equiv. of *rac*-LA in THF-d_8 showed the evolution of multiple side products, suggesting that not all of **(*S*,*S*)-23** had become the active species (*S*,*S*)-(BOPA^{Ph})Mg(LA-H). In contrast, the more controlled conversion of **(*S*,*S*)-23** to **(*S*,*S*)-27** and $B(OBn)_3$ (in equilibrium with **28**) circumvented the formation of side products, therefore leading to a much more efficient initiation process and hence a higher rate. It is notable that the heterotacticity of the resulting polymer remained constant throughout the course of the polymerisation (P_r = 0.62-0.64). The degree of stereocontrol exerted by the *in-situ* generated catalytic system was similar to that observed for **(*S*,*S*)-23**.

Table 5.7 Selected data for the ROP of *rac*-, *L*-, *D*- and *meso*-LA using the *in-situ* generated (*S*,*S*)-(BOPA^{Ph})Mg(OBn) (**(*S*,*S*)-27**), (*R*,*R*)-(BOPA^{Ph})Mg(OBn) (**(*R*,*R*)-27**) and *rac*-(BOPA^{Ph})Mg(OBn) (***rac*-27**) in the presence of 1 equiv. of B(OBn)$_3$ in THF.

Entry	Catalyst [a]	Monomer (LA)	Conv.[b] (%)	Time (min)	M_n(obs)[c] (g mol^{-1})	M_n(calc)[d] (g mol^{-1})	PDI[e]	P_r[b]
1	**(*S*,*S*)-27**	*rac*	89	20	9,000	3,315	1.35	0.64
2	**(*S*,*S*)-27**	*L*	90	120	6,300	3,351	1.44	/
3	**(*S*,*S*)-27**	*D*	92	10	10,290	3,423	1.32	/
4	**(*R*,*R*)-27**	*rac*	90	20	10,040	3,351	1.29	0.65
5	**(*R*,*R*)-27**	*L*	94	10	11,160	3,495	1.49	/
6	**(*R*,*R*)-27**	*D*	91	120	7,660	3,387	1.44	/
7[f]	**(*S*,*S*)-27**	*rac*	90	40	1,690	1,106	1.35	0.64
8[g]	**(*S*,*S*)-27**	*rac*	92	270	2,340	1,128	1.41	0.61
9	***rac*-27**	*rac*	89	15	9,270	3,315	1.34	0.58
10	**(*S*,*S*)-27**	*meso*	93	1.5	14,530	3,459	1.19	0.70

[a] Conditions: [LA]$_0$:[**23**]$_0$:[PhCHO]$_0$ = 100:1:4, [LA]$_0$ = 1.0 M, [**23**]$_0$ = 0.01 M, 4 mL THF at room temperature. [b] Measured by ^{1}H NMR ($CDCl_3$) analyses. [c] Molecular weights (g mol^{-1}) determined from GPC using the appropriate Mark-Houwink corrections. [d] Expected M_n (g mol^{-1}) for stated number of chains per metal and stated % conversion: M_n (calc for entries 1-6 and 9-10) = 1/4 (conversion (%) × 100 × 144.1) + 108.1. M_n (calc for entries 7 and 8) = 1/13 (conversion (%) × 100 × 144.1) + 108.1. [e] PDI = M_w/M_n. [f] 3 equiv. of B(OBn)$_3$ added. [g] 3 equiv. of B(OMe)$_3$ added.

MALDI-ToF analysis of the resulting polymer (M_n by GPC = 2280 g mol^{-1}) obtained from the ROP of *rac*-LA using *in-situ* generated **(*S*,*S*)-27** and B(OBn)$_3$ revealed the presence of the anticipated OBn end group (Figure 5.16). For example, the signal at 2309 g mol^{-1} could be assigned to OBn terminated PLA consisting of 15 repeating LA units. Intermolecular transesterification side reactions were also observed, as evidenced by peak envelopes with $\Delta m/z$ = 72 g mol^{-1}. No cyclic PLA was found. The ^{1}H NMR spectrum ($CDCl_3$, 298 K) of the isolated polymer revealed a multiplet at 4.35 ppm and a broad signal at 2.74 ppm, corresponding to the BnO[LA]$_n$C(O)CH(Me)OC(O)C<u>H</u>(Me)OH and hydroxy protons, respectively. Unfortunately, the methylene protons at the OBn end group could not be clearly distinguished due to overlapping signals with the methine protons of PLA. These assignments are fully consistent with literature reported results.[122, 123]

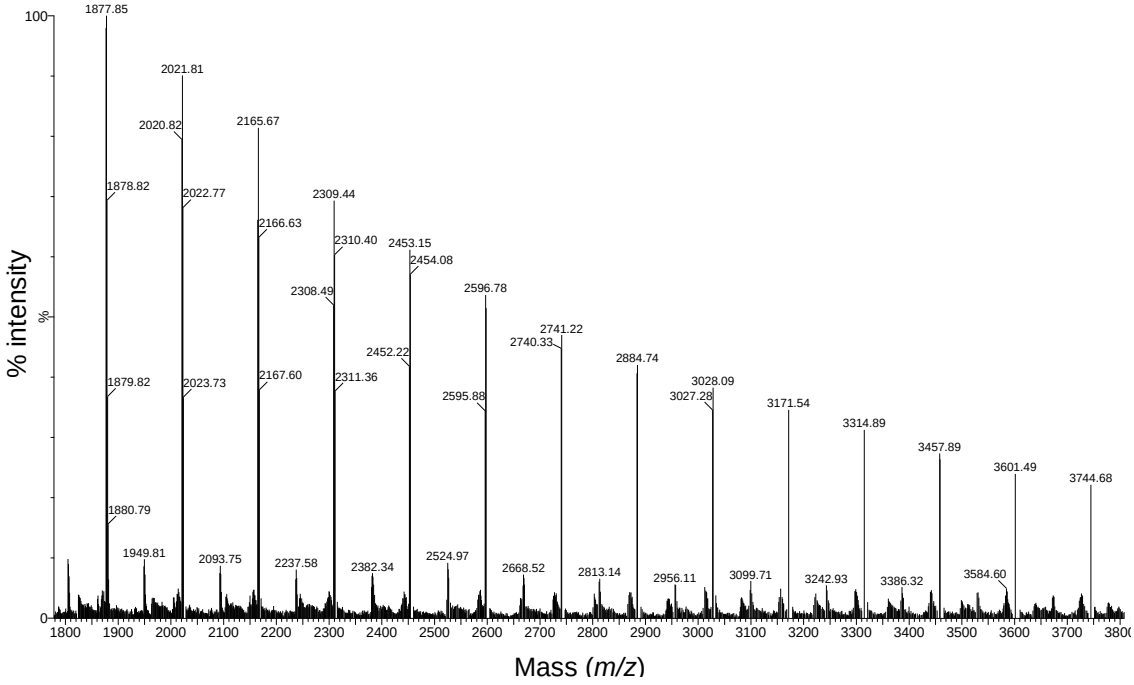


Figure 5.16 MALDI-ToF MS of PLA synthesised using *in-situ* generated (*S*,*S*)-(BOPA^{Ph})Mg(OBn) (**(*S*,*S*)-27**) and B(OBn)$_3$. Conditions: [*rac*-LA]$_0$:[**(*S*,*S*)-23**]$_0$:[PhCHO]$_0$ = 100:1:4, [*rac*-LA]$_0$ = 1.0 M, [**(*S*,*S*)-23**]$_0$ = 0.01 M, 4 mL THF at room temperature. K^+ dopant.

The experimental M_n of the PLA formed using the *in-situ* generated **(*S*,*S*)-27** was found to be slightly higher than that expected for one chain being produced per metal centre initially followed by tailing off towards the end of the polymerisation (Figure 5.17). The reduction in M_n could be attributed to two possible reasons, namely

intramolecular back-biting or chain transfer. Even though MALDI-ToF analysis of the PLA (M_n by GPC = 2280 g mol^{-1}) at 11% conversion showed no evidence for the formation of cyclic polymers (Figure 5.16), it could not be assumed that back-biting did not occur at high % conversions. The origin for this tailing off effect remains inconclusive.

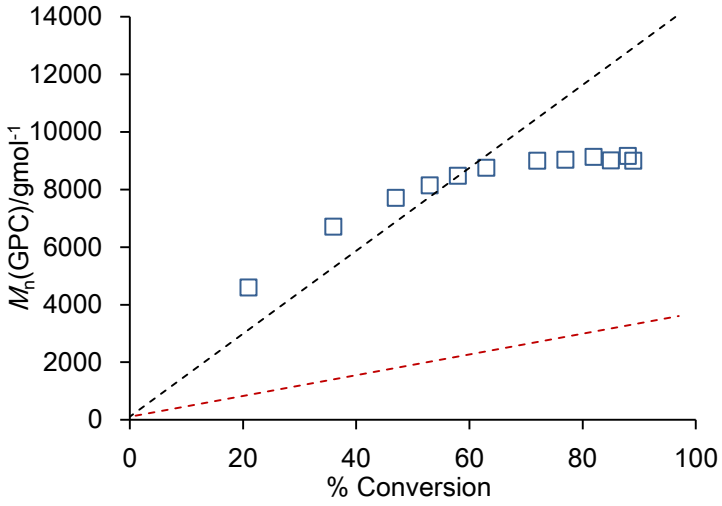


Figure 5.17 Data for the ROP of *rac*-LA using *in-situ* generated (*S*,*S*)-(BOPA^{Ph})Mg(OBn) (**(*S*,*S*)-27**) and B(OBn)$_3$. M_n (GPC) *vs.* % conversion plot. The dashed lines represent the M_n expected for one chain (black) or four chains (red) per metal centre. Conditions: [*rac*-LA]$_0$:[**(*S*,*S*)-23**]$_0$:[PhCHO]$_0$ = 100:1:4, [*rac*-LA]$_0$ = 1.0 M, [**(*S*,*S*)-23**]$_0$ = 0.01 M, 4 mL THF at room temperature.

Another polymerisation was performed by using the *in-situ* generated catalytic system in the presence of 3 equiv. of external B(OBn)$_3$ (Table 5.7, Entry 7). The addition of external B(OBn)$_3$ led to the formation of PLA whose experimental M_n values were much lower than the calculated ones based on one chain being produced per metal centre throughout the course of the polymerisation (Figure 5.18). MALDI-ToF analysis (Figure 5.19) of the polymer sample at 90% conversion (M_n by GPC = 1690 g mol^{-1}) showed no evidence for the formation of cyclic PLA, indicating that the low M_n could be attributed to chain transfer events. It is notable that the degree of chain transfer increased as the polymerisation proceeded (Figure 5.18). This could be rationalised by an increase in the relative rate of chain transfer in comparison to that of propagation; [B(OR)$_3$] (OR = OBn or polymeryl) remained constant throughout the course of the polymerisation (constant rate of chain transfer) whilst the decreasing

[*rac*-LA] resulted in a decrease in the propagation rate as the polymerisation proceeded. Previous studies in the Mountford group have suggested that a tetra-coordinated species is an essential intermediate for chain transfer to occur.[108] It was postulated that the tetra-coordinated adduct during the polymerisation in this case might feature two bridging polymeryl chains with the carbonyl oxygen chelating the magnesium centre. Such adduct species was reminiscent of several dinuclear complexes with bridging -OCH(Me)C(O)OR moieties reported in the literature.[124-127] For example, Coates *et al*. synthesised a dinuclear zinc complex with bridging methyl lactate, the carbonyl oxygen of which was found to be datively bonded to the zinc centre.[128] In this case, the polymeryl chain-bridged tetra-coordinated adduct was proposed to be the catalyst resting state. In other words, insertion of LA monomers can only occur upon dissociation of the borate ester from the metal centre. The chelating effect of the polymeryl chains resulted in a more stable adduct, hence giving a lower rate of dissociation of the borate ester and subsequent insertion of LA to occur (90% conversion in 40 min for ROP with external $B(OBn)_3$ added *cf*. 89% conversion in 20 min for the polymerisation without; Figure 5.20). Kinetic analysis revealed neither a first nor second order dependence on *rac*-LA concentration (no apparent induction period).

An analogous polymerisation was also conducted using the *in-situ* generated catalytic system in the presence of 3 equiv. of external $B(OMe)_3$ (Table 5.7, Entry 8). The experimental M_n values were slightly higher than those observed for ROP in the presence of external $B(OBn)_3$, indicating a less pronounced chain transfer effect (Figure 5.18). However, the experimental M_n values were still much lower than those in the polymerisation where no external borate ester species was added (Table 5.7, Entries 1 and 8). It was postulated that the tetra-coordinated adduct formed in this case featured one bridging polymeryl chain and one bridging OMe group. A further rate reduction was observed in this case, requiring 270 min to reach 92% conversion (Figure 5.20). This could be accounted for by the smaller size of the OMe group, hence further stabilising the tetra-coordinated adduct despite a reduced chelation effect. Interestingly, the polymerisation was found to demonstrate a first order dependence on *rac*-LA concentration (k_{obs} = 0.0095(3) min^{-1}, R^2 = 0.996) with no apparent induction period. MALDI-ToF analysis of the sample at 92% conversion (M_n by GPC = 2340 g mol^{-1}) revealed a mixture of -OMe and -OBn terminated PLA, as

well as the presence of intermolecular transesterification (peak envelopes of $\Delta m/z$ = 72 g mol^{-1}). No cyclic polymers were generated. In both polymerisations, the addition of external borate ester species had a negligible effect on the stereoselectivity of the *in-situ* generated catalytic system, as expected.

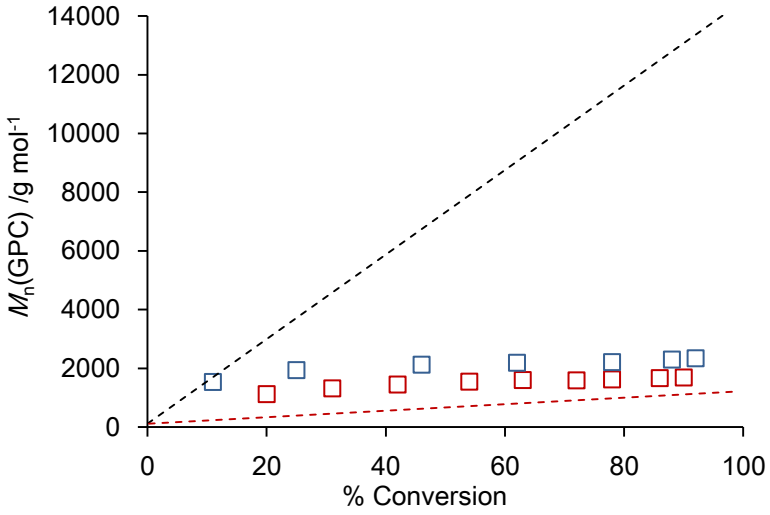


Figure 5.18 Data for the ROP of *rac*-LA using *in-situ* generated (*S*,*S*)-(BOPA^{Ph})Mg(OBn) (**(*S*,*S*)-27**) and B(OBn)$_3$ in the presence of 3 equiv. of external borate ester. M_n (GPC) *vs.* % conversion plot. The dashed lines represent the M_n expected for one chain (black) or thirteen chains (red) per metal centre. Conditions: [*rac*-LA]$_0$ = 1.0 M, [**(*S*,*S*)-23**]$_0$ = 0.01 M, 4 mL THF at room temperature. [*rac*-LA]$_0$:[**(*S*,*S*)-23**]$_0$:[PhCHO]$_0$:[B(OBn)$_3$]$_0$ = 100:1:4:3, red squares; [*rac*-LA]$_0$:[**(*S*,*S*)-23**]$_0$:[PhCHO]$_0$:[B(OMe)$_3$]$_0$ = 100:1:4:3, blue squares.

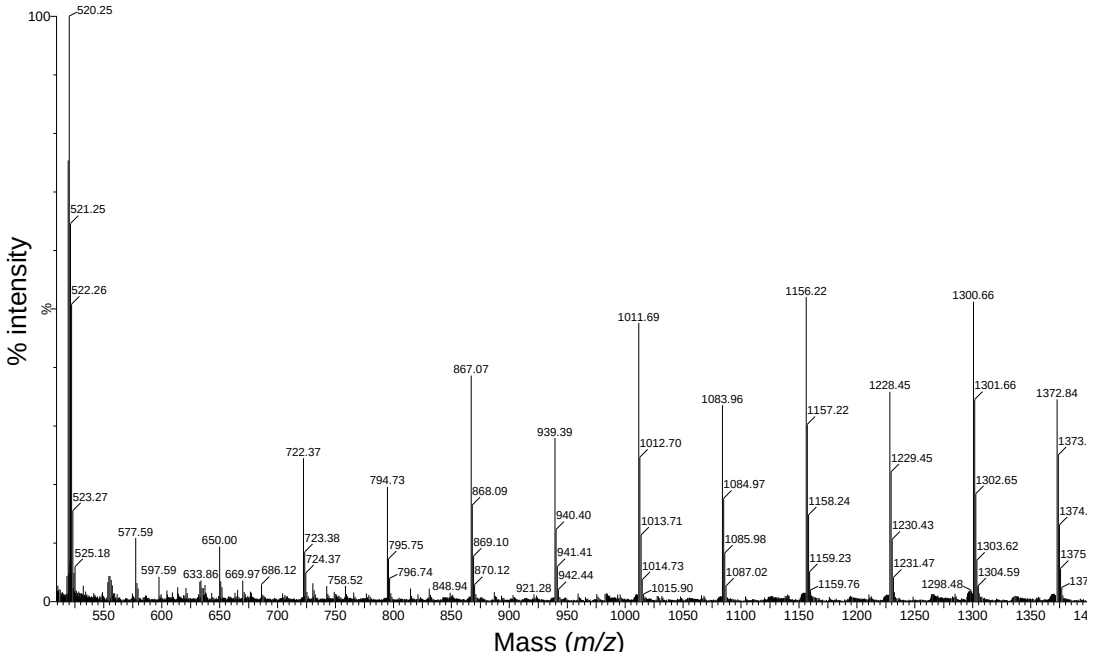


Figure 5.19 MALDI-ToF MS of PLA synthesised using *in-situ* generated (*S*,*S*)-(BOPA^{Ph})Mg(OBn) (**(*S*,*S*)-27**) and B(OBn)$_3$ in the presence of 3 equiv. of B(OBn)$_3$. Conditions: [*rac*-LA]$_0$:[**(*S*,*S*)-23**]$_0$:[PhCHO]$_0$:[B(OBn)$_3$]$_0$= 100:1:4:3, [*rac*-LA]$_0$ = 1.0 M, [**(*S*,*S*)-23**]$_0$ = 0.01 M, 4 mL THF at room temperature. K^+ dopant.

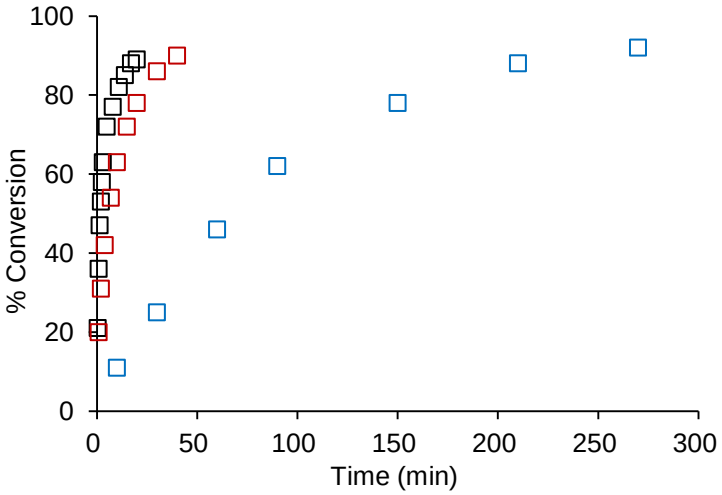


Figure 5.20 Data for the ROP of *rac*-LA using *in-situ* generated (*S*,*S*)-(BOPA^{Ph})Mg(OBn) (**(*S*,*S*)-27**) and B(OBn)$_3$ in the presence or absence of 3 equiv. of external borate ester. % conversion *vs.* time (min) plot. Conditions: [*rac*-LA]$_0$ = 1.0 M, [**(*S*,*S*)-23**]$_0$ = 0.01 M, 4 mL THF at room temperature. [*rac*-LA]$_0$:[**(*S*,*S*)-23**]$_0$:[PhCHO]$_0$ = 100:1:4, black squares; [*rac*-LA]$_0$:[**(*S*,*S*)-23**]$_0$:[PhCHO]$_0$:[B(OBn)$_3$]$_0$ = 100:1:4:3, red squares; [*rac*-LA]$_0$:[**(*S*,*S*)-23**]$_0$:[PhCHO]$_0$:[B(OMe)$_3$]$_0$ = 100:1:4:3, blue squares.

Interestingly, kinetic analysis of *rac*-LA ROP initiated by the *in-situ* generated **(*S*,*S*)-27** and $B(OBn)_3$ displayed the apparent presence of two slightly different kinetic regimes. At the early stage of the polymerisation, second order plot of $1/[rac\text{-LA}]_t$ *vs.* time (Figure 5.21) revealed a k_{obs} of 0.559(19) M^{-1} min^{-1} (R^2 = 0.997). This was followed by a decrease after 3 min (63% conversion), giving a smaller k_{obs} of 0.383(14) M^{-1} min^{-1} (R^2 = 0.997).

Despite the fact that P_r values of the resulting PLA remained in the range of 0.62-0.64 throughout the course of the ROP initiated by *in-situ* generated **(*S*,*S*)-27** and $B(OBn)_3$, kinetic analyses with *L*- and *D*-LA were also investigated to probe for any monomer enchainment preference (Figure 5.22). Complex **(*S*,*S*)-27** preferred the insertion of *D*-LA significantly over that of *L*-LA, giving a considerable relative rate (k_{rel}) of 19.5(6). In comparison to the previous study employing **(*S*,*S*)-23** as the catalyst which showed minor site selectivity, the effect of enantiomorphic site control exerted by the *in-situ* generated **(*S*,*S*)-27** was much more pronounced. It is interesting to note that the rate of *rac*-LA ROP was smaller than that of *D*-LA employing **(*S*,*S*)-27**. This was unexpected given the slight preference of the catalyst to insert LA *via* a *racemic* linkage, as evidenced by the formation of heterotactic PLA from the ROP of *rac*-LA (P_r = 0.64). A similar observation was reported by Mehrkhodavandi and co-workers for (*R*,*R*/*R*,*R*)-[(NNO)InCl]$_2$(μ-Cl)(μ-OEt) (**(*R*,*R*/*R*,*R*)-5.55**), which revealed a significant selectivity for the ROP of *L*-LA over *D*-LA (k_p for *L*-LA larger than that for *D*-LA) yet produced atactic PLA.[54] This phenomenon was rationalised by the presence of two competing rates, namely monomer coordination and subsequent propagation. It was proposed that the coordination of *D*-LA to **(*R*,*R*/*R*,*R*)-5.55** was faster than that of *L*-LA and the equilibrium favoured the formation of **(*R*,*R*/*R*,*R*)-5.55**·*D*-LA which subsequently ring-opened *D*-LA. When the rates of *D*-LA coordination and *L*-LA propagation are comparable, equal incorporation of both monomers would result in the generation of atactic PLA. It was postulated that a similar mechanism might be in operation for *rac*-LA ROP initiated by the *in-situ* generated **(*S*,*S*)-27**.

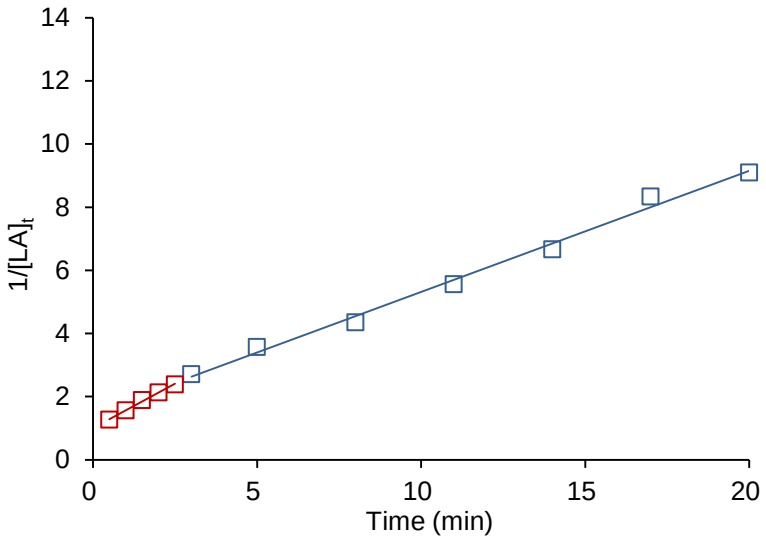


Figure 5.21 Data for the ROP of *rac*-LA using *in-situ* generated **(*S*,*S*)-27** and $B(OBn)_3$. Semilogarithmic second order plot of $1/[rac\text{-LA}]_t$ *vs.* time. Conditions: $[rac\text{-LA}]_0$ = 1.0 M, $[\mathbf{(S,S)\text{-}23}]_0$ = 0.01 M, 4 mL THF at room temperature. $[rac\text{-LA}]_0$:$[\mathbf{(S,S)\text{-}23}]_0$:$[PhCHO]_0$ = 100:1:4, k_{obs} = 0.559(19) M^{-1} min^{-1} (R^2 = 0.997) (red squares) followed by 0.383(14) M^{-1} min^{-1} (R^2 = 0.997) (blue squares).

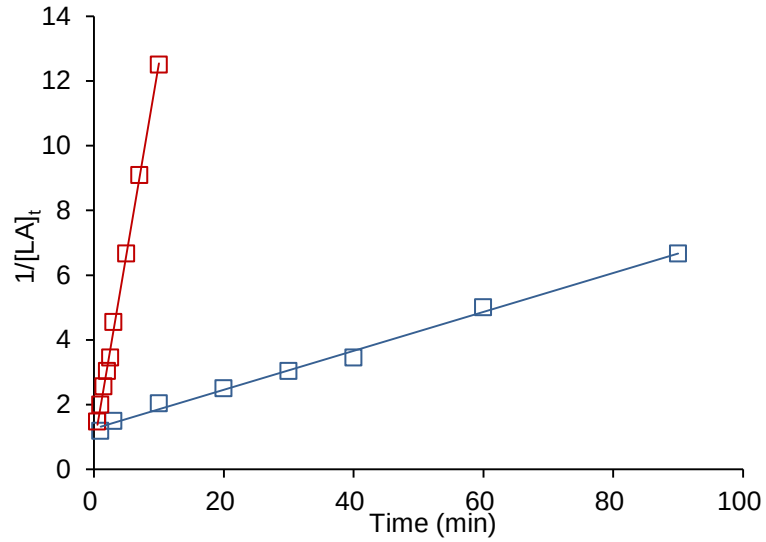


Figure 5.22 Data for the ROP of LA using *in-situ* generated **(*S*,*S*)-27** and $B(OBn)_3$. Semilogarithmic second order plot of $1/[LA]_t$ *vs.* time. Conditions: $[LA]_0$ = 1.0 M, $[\mathbf{(S,S)\text{-}23}]_0$ = 0.01 M, 4 mL THF at room temperature. $[L\text{-LA}]_0$:$[\mathbf{(S,S)\text{-}23}]_0$:$[PhCHO]_0$ = 100:1:4, k_{obs} = 0.0601(17) M^{-1} min^{-1} (R^2 = 0.995), blue squares; $[D\text{-LA}]_0$:$[\mathbf{(S,S)\text{-}23}]_0$:$[PhCHO]_0$ = 100:1:4, k_{obs} = 1.17(2) M^{-1} min^{-1} (R^2 = 0.999), red squares.

Analogous studies for the ROP of *rac*-, *L*- and *D*-LA were also performed with the *in-situ* generated **(*R*,*R*)-27** to ensure the reproducibility of the results (Table 5.7, Entries 4-6). Gratifyingly, very similar observations were obtained for the ROP of *rac*-LA using **(*R*,*R*)**- and **(*S*,*S*)-27**. In contrast, **(*R*,*R*)-27** demonstrated the opposite monomer enchainment preference to **(*S*,*S*)-27** in the ROP of enantiomerically pure LA; the k_{obs} of *L*-LA ROP (1.57(3) M^{-1} min^{-1} (R^2 = 0.997)) initiated by **(*R*,*R*)-27** was 20 times (k_{rel} = 19.9(8)) higher than that of *D*-LA (0.0789(30) M^{-1} min^{-1} (R^2 = 0.990)) whereas the reverse selectivity of the same magnitude (k_{rel} = 19.5(6)) was observed for **(*S*,*S*)-27**.

The ROP of *rac*-LA was also examined using the *in-situ* generated ***rac*-27** (prepared by the addition of 4 equiv. of benzaldehyde to ***rac*-23**), reaching 89% conversion within 15 min (Table 5.7, Entry 9). This was comparable to the ROP of *rac*-LA using enantiomerically pure **27** (89% conversion in 20 min). A P_r value of 0.58 was observed for the resulting PLA. *In-situ* generated **(*S*,*S*)-27** proved to be more active in the ROP of *meso*-LA than *rac*-LA (Table 5.7, Entry 10); 93% conversion was achieved in 1.5 min (*cf*. 89% conversion in 20 min for *rac*-LA). As mentioned previously, this was attributed to the less stable ground state structure of *meso*-LA compared to those of *D*- and *L*-LA.[121] The polymerisation was found to conform to second order kinetics, giving a k_{obs} of 12.0(5) M^{-1} min^{-1} (R^2 = 0.992). As expected, syndiotactic PLA was obtained (P_r = 0.70) due to the catalyst's preference to insert monomer *via* a *racemic* linkage as opposed to a *meso* dyad.

Polymerisations with *rac*-LA were also performed with **(*S*,*S*)-23** and *in-situ* generated **(*S*,*S*)-27** in CH_2Cl_2 and toluene to probe for any solvent effects (Table 5.8, Entries 1-4). Prior to polymerisation, **(*S*,*S*)-23** was monitored in CD_2Cl_2 or toluene-d_8 over the course of 24 h, after which time no catalyst decomposition was observed. Complex **(*S*,*S*)-23** was found to be more active in CH_2Cl_2 than in THF for the ROP of *rac*-LA; 96% conversion was reached in 35 min when the polymerisation was performed in CH_2Cl_2 whereas the analogous reaction in THF required 155 min to reach 92% conversion. This could be rationalised by the coordinating nature of THF, competing with monomer coordination and therefore slowing down the polymerisation. However, the beneficial rate enhancement in CH_2Cl_2 was accompanied by a minor decrease in the heterotacticity of the resulting polymer, giving P_r = 0.55 (*cf*. P_r = 0.60 in THF). Unfortunately, kinetic analysis of the polymerisation catalysed by **(*S*,*S*)-23** in toluene was hampered by the limited solubility of *rac*-LA in toluene. Microstructure analysis

of the isolated PLA revealed P_r = 0.60, comparable to that obtained when the polymerisation was performed in THF. *In-situ* generated **(*S*,*S*)-27** also polymerised faster ROP in CH_2Cl_2 than in THF (92% conversion at 10 min in CH_2Cl_2 *cf*. 89% conversion at 20 min in THF), affording less heterotactically enriched PLA (P_r = 0.56 in CH_2Cl_2 *vs*. 0.64 in THF).

Solvent effects also existed in the ROP of *meso*-LA (Table 5.8, Entries 5-8). **(*S*,*S*)-23** induced faster polymerisation in CH_2Cl_2 than in THF at the expense of producing less syndiotactic PLA (P_r = 0.62 in CH_2Cl_2 *vs*. 0.68 in THF). Unfortunately, kinetic analysis in toluene was not possible due to the poor solubility of *meso*-LA in toluene. However, tetrad analysis of the resulting PLA revealed P_r = 0.60. Peculiarly, *in-situ* generated **(*S*,*S*)-27** initiated *meso*-LA at a faster rate in THF than in CH_2Cl_2 (second order k_{obs} = 10(1) M^{-1} min^{-1} (R^2 = 0.992) in THF *vs*. 4.8(2) M^{-1} min^{-1} (R^2 = 0.993) in CH_2Cl_2), the origin of which remains unknown. As observed previously, PLA produced from ROP in THF demonstrated higher syndiotacticity than those generated from ROP in non-donor solvents.

Table 5.8 Selected data for the ROP of *rac*- and *meso*-LA using (*S*,*S*)-(BOPA^{Ph})Mg(BH$_4$)(THF) (**(*S*,*S*)-23**) or *in-situ* generated (*S*,*S*)-(BOPA^{Ph})Mg(OBn) (**(*S*,*S*)-27**) in CH_2Cl_2 and toluene.

Entry	Catalyst [a]	Monomer (LA)	Additives	Solvent	Conv.[b] (%)	Time (min)	M_n(obs)[c] (g mol^{-1})	M_n(calc)[d] (g mol^{-1})	PDI[e]	P_r[b]
1	**(*S*,*S*)-23**	*rac*	/	CH_2Cl_2	96	35	13,820	13,840	1.48	0.55
2	**(*S*,*S*)-23**	*rac*	4 PhCHO	CH_2Cl_2	92	10	18,530	3,423	1.35	0.56
3	**(*S*,*S*)-23**	*rac*	/	toluene	91	120	10,580	13,119	1.46	0.60
4	**(*S*,*S*)-23**	*rac*	4 PhCHO	toluene	98	60	14,800	3,639	1.29	0.59
5	**(*S*,*S*)-23**	*meso*	/	CH_2Cl_2	92	3	12,240	13,263	1.59	0.62
6	**(*S*,*S*)-23**	*meso*	4 PhCHO	CH_2Cl_2	92	2.5	16,330	3,423	1.35	0.62
7	**(*S*,*S*)-23**	*meso*	/	toluene	94	3	11,990	13,552	1.53	0.60
8	**(*S*,*S*)-23**	*meso*	4 PhCHO	toluene	94	2.5	15,430	3,387	1.33	0.62

[a] Conditions: $[LA]_0$:$[\mathbf{(S,S)\text{-}23}]_0$ = 100:1 for Entries 1,3,5 and 7; $[LA]_0$:$[\mathbf{(S,S)\text{-}23}]_0$:$[PhCHO]_0$ = 100:1:4 for Entries 2,4,6 and 8, $[LA]_0$ = 1.0 M, $[\mathbf{(S,S)\text{-}23}]_0$ = 0.01 M, 4 mL CH_2Cl_2/toluene at room temperature. [b] Measured by ^{1}H NMR ($CDCl_3$) analyses. [c] Molecular weights (g mol^{-1}) determined from GPC using the appropriate Mark-Houwink corrections. [d] Expected M_n (g mol^{-1}) for stated number of chains per metal and stated % conversion: M_n (calc for Entries 1, 3, 5 and 7) = (conversion (%) × 100 × 144.1) + 4. M_n (calc for Entries 2, 4, 6 and 8) = 1/4 (conversion (%) × 100 × 144.1) + 108.1. [e] PDI = M_w/M_n.

5.5 Summary and conclusions

This Chapter described the synthesis and characterisation of a series of magnesium complexes supported by BOPA ligands with chiral isopropyl or phenyl substituents at the oxazoline ring. The catalytic activities of (*S*,*S*)-(BOPA^{iPr})Mg{N(SiMe$_3$)$_2$} (**17**), (*S*,*S*)-(BOPA^{Ph})Mg{N(SiMe$_3$)$_2$} (**24**) and (*S*,*S*)-(BOPA^{Ph})Mg{N(SiMe$_2$H)$_2$} (**25**) featuring amide initiators were probed in the ROP of *rac*-LA. The polymerisations demonstrated poor molecular weight control, giving slightly heterotactic PLA with much higher than expected experimental M_n.

Both (*S*,*S*)-(BOPA^{Ph})Mg(BH$_4$)(THF) (**(*S*,*S*)-23**) and (*R*,*R*)-(BOPA^{Ph})Mg(BH$_4$)(THF) (**(*R*,*R*)-23**) were applied as initiators for the ROP of *rac*-LA, polymerising 100 equiv. of monomer in 155 min in THF at room temperature. The experimental M_n were in good agreement with the theoretical values based on one chain per metal centre initially followed by tailing off due to transesterification side reactions. Both **(*S*,*S*)-** and **(*R*,*R*)-23** produced slightly heterotactic PLA as a result of their preference to insert LA *via* a *racemic* linkage over a *meso* dyad. Complex **(*S*,*S*)-23** was found to favour the insertion of *D*-LA in comparison to *L*-LA whilst the opposite was observed for **(*R*,*R*)-23**. This clearly indicated the operation of enantiomorphic site control despite the dominant mechanism being chain end control. The polymerisation rate of *rac*-LA using ***rac*-23** was found to be comparable to those employing enantiomerically pure initiators. The ROP of *meso*-LA proceeded much faster than that of *rac*-LA, giving syndiotactically enriched PLA.

The mechanisms through which **(*S*,*S*)-23** polymerised *rac*-LA were also investigated. A single hydride transfer from the BH$_4$ to the carbonyl carbon of *rac*-LA generated (*S*,*S*)-(BOPA^{Ph})Mg(LA-H) and BH$_3$(THF) which underwent rapid exchange to form "B(LA-H)$_3$". The rather open coordination environment around the magnesium centre in (*S*,*S*)-(BOPA^{Ph})Mg(LA-H) allowed the formation of a major tetra-coordinated adduct (*S*,*S*)-(BOPA^{Ph})Mg(LA-H){"B(LA-H)$_3$"}, which was postulated to be the catalyst resting state. LA insertion could only occur upon dissociation into (*S*,*S*)-(BOPA^{Ph})Mg(LA-H) and "B(LA-H)$_3$".

The addition of 4 equiv. of benzaldehyde to **(*S*,*S*)-23** resulted in the *in-situ* generation of (*S*,*S*)-(BOPA^{Ph})Mg(OBn) (**(*S*,*S*)-27**) and B(OBn)$_3$, which were found to exist in equilibrium with the tetra-coordinated adduct (*S*,*S*)-(BOPA^{Ph})Mg(OBn){B(OBn)$_3$}(**28**)

(major). This *in-situ* generated catalytic system was more active than **(*S*,*S*)-23**, converting 100 equiv. of *rac*-LA in 20 min under identical conditions. The polymerisation followed two apparent kinetic regimes, with the first being faster than the second. Kinetic analysis of ROP of enantiomerically pure LA using **(*S*,*S*)-27** was subsequently investigated. A significant preference for *D*-LA over *L*-LA was observed, giving a relative rate constant (k_{rel}) of 19.5(6). This was in striking contrast to the analogous study using **(*S*,*S*)-23**, whereby very minor site selectivity was present. Kinetic analysis of ROP of enantiomerically pure LA using **(*R*,*R*)-27** was also investigated, giving complementary results. Despite the operation of enantiomorphic site control as evidenced by the preference of the enantiomerically pure catalyst to insert one LA enantiomer over the other, the major mechanism for the ROP of *rac*-LA initiated by **(*S*,*S*)**- or **(*R*,*R*)-27** was chain end control, leading to the formation of heterotactically enriched PLA.

The addition of 3 equiv. of external $B(OBn)_3$ to the *in-situ* generated **(*S*,*S*)-27** produced PLA with much lower than calculated (based on one chain per metal centre) M_n. The MALDI-ToF mass spectrum of the PLA at high % conversions suggested the absence of intramolecular transesterification, indicating that the lower than expected M_n was a consequence of chain transfer events, proceeding through a tetra-coordinated adduct. The tetra-coordinated species was postulated to be the resting state during the polymerisation and LA insertion could only occur upon dissociation of the borate ester. It was proposed that the tetra-coordinated adduct during the polymerisation featured two bridging polymeryl chains, with the carbonyl oxygen chelating the magnesium centre. This chelation effect stabilised the tetra-coordinated species, hence leading to a noticeable decrease in the polymerisation rate in comparison to the case where no external $B(OBn)_3$ was added. The addition of 3 equiv. of $B(OMe)_3$ to the *in-situ* generated **(*S*,*S*)-27** led to an even slower polymerisation as a result of the smaller size of the bridging OMe group, further stabilising the adduct species despite the reduced chelation effect. In both polymerisations involving the addition of external borate ester, no apparent induction period was observed.

In-situ generated ***rac*-27** demonstrated comparable activity and stereoselectivity to **(*S*,*S*)-27** in the ROP of *rac*-LA, producing slightly heterotactic PLA. As expected, **(*S*,*S*)-27** was more active in the ROP of *meso*-LA than *rac*-LA, as a consequence of

the less stable nature of the former compared to *L*- and *D*-LA. Syndiotactic PLA was derived from ROP of *meso*-LA due to the catalyst's preference to insert LA *via* a *racemic* linkage as opposed to a *meso* dyad.

Rac-LA ROP using **(*S*,*S*)-23** and *in-situ* generated **(*S*,*S*)-27** as catalysts were also investigated in non-donor solvents in order to probe for any solvent effects. Polymerisations proceeded faster in CH_2Cl_2 than in THF at the expense of producing PLA with a lower degree of heterotacticity. A reduction in catalyst's selectivity was also observed in polymerisations carried out in toluene compared to those in THF. Solvent effects also existed in the ROP of *meso*-LA. The polymerisation employing **(*S*,*S*)-23** as the catalyst proceeded faster in CH_2Cl_2 than in THF, affording PLA with lower syndiotacticity. Unexpectedly, *in-situ* generated **(*S*,*S*)-27** initiated faster *meso*-LA ROP in THF than in CH_2Cl_2, the origin of which remains unclear to date. The resulting PLA produced from the polymerisation carried out in THF was more syndiotactically enriched than those obtained when the polymerisations were performed in non-donor solvents.

5.6 References for Chapter Five

1. C. M. Thomas, *Chem. Soc. Rev.*, 2010, **39**, 165.
2. P. J. Dijkstra, H. Du and J. Feijen, *Polym. Chem.*, 2011, **2**, 520.
3. A. Amgoune, C. M. Thomas, T. Roisnel and J.-F. Carpentier, *Chem. Eur. J.*, 2006, **12**, 169.
4. C.-X. Cai, L. Toupet, C. W. Lehmann and J.-F. Carpentier, *J. Organomet. Chem.*, 2003, **683**, 131.
5. H. D. Dyer, S. Huijser, N. Susperregui, F. Bonnet, A. D. Schwarz, R. Duchateau, L. Maron and P. Mountford, *Organometallics*, 2010, **29**, 3602.
6. F. Bonnet, A. R. Cowley and P. Mountford, *Inorg. Chem.*, 2005, **44**, 9046.
7. X. Liu, X. Shang, T. Tang, N. Hu, F. Pei, D. Cui, X. Chen and X. Jing, *Organometallics*, 2007, **26**, 2747.
8. H. Ma, T. P. Spaniol and J. Okuda, *Angew. Chem. Int. Ed.*, 2006, **45**, 7818.
9. H. Ma, T. P. Spaniol and J. Okuda, *Inorg. Chem.*, 2008, **47**, 3328.
10. J.-C. Buffet, A. Kapelski and J. Okuda, *Macromolecules*, 2010, **43**, 10201.
11. B. M. Chamberlain, M. Cheng, D. R. Moore, T. M. Ovitt, E. Lobkovsky and G. W. Coates, *J. Am. Chem. Soc.*, 2001, **123**, 3229.

12. T. M. Ovitt and G. W. Coates, *J. Am. Chem. Soc.*, 2002, **124**, 1316.
13. T. M. Ovitt and G. W. Coates, *J. Am. Chem. Soc.*, 1999, **121**, 4072.
14. I. Peckermann, A. Kapelski, T. P. Spaniol and J. Okuda, *Inorg. Chem.*, 2009, **48**, 5526.
15. A. Sauer, J.-C. Buffet, T. P. Spaniol, H. Nagae, K. Mashima and J. Okuda, *Inorg. Chem.*, 2012, **51**, 5764.
16. A.-C. Albertsson and I. K. Varma, *Biomacromolecules*, 2003, **4**, 1466.
17. A. Södergård and M. Stolt, *Prog. Polym. Sci.*, 2002, **27**, 1123.
18. W. Amass, A. Amass and B. Tighe, *Polym. Int.*, 1998, **47**, 89.
19. J. Lunt, *Polym. Degrad. Stab.*, 1998, **59**, 145.
20. N. Nomura, J. Hasegawa and R. Ishii, *Macromolecules*, 2009, **42**, 4907.
21. Y. Ikada, K. Jamshidi, H. Tsuji and S. H. Hyon, *Macromolecules*, 1987, **20**, 904.
22. N. Yui, P. J. Dijkstra and J. Feijen, *Die Makromolekulare Chemie*, 1990, **191**, 481.
23. N. Spassky, M. Wisniewski, C. Pluta and A. Le Borgne, *Macromol. Chem. Phys.*, 1996, **197**, 2627.
24. R. Ishii, N. Nomura and T. Kondo, *Polym. J.*, 2004, **36**, 261.
25. Z. Tang, X. Chen, X. Pang, Y. Yang, X. Zhang and X. Jing, *Biomacromolecules*, 2004, **5**, 965.
26. Z. Tang, X. Chen, Y. Yang, X. Pang, J. Sun, X. Zhang and X. Jing, *J. Polym. Sci. A: Polym. Chem.*, 2004, **42**, 5974.
27. P. Hormnirun, E. L. Marshall, V. C. Gibson, R. I. Pugh and A. J. P. White, *Proceedings of the National Academy of Sciences*, 2006, **103**, 15343.
28. N. Nomura, R. Ishii, Y. Yamamoto and T. Kondo, *Chem. Eur. J.*, 2007, **13**, 4433.
29. X. Pang, H. Du, X. Chen, X. Wang and X. Jing, *Chem. Eur. J.*, 2008, **14**, 3126.
30. S. Tabthong, T. Nanok, P. Sumrit, P. Kongsaeree, S. Prabpai, P. Chuawong and P. Hormnirun, *Macromolecules*, 2015, **48**, 6846.
31. C. Bakewell, T. P. A. Cao, N. Long, X. F. Le Goff, A. Auffrant and C. K. Williams, *J. Am. Chem. Soc.*, 2012, **134**, 20577.
32. C. Bakewell, A. J. P. White, N. J. Long and C. K. Williams, *Angew. Chem. Int. Ed.*, 2014, 9226.

33. Z. Tang and V. C. Gibson, *Eur. Polym. J.*, 2007, **43**, 150.
34. S. Song, H. Ma and Y. Yang, *Dalton Trans.*, 2013, **42**, 14200.
35. W.-C. Hung and C.-C. Lin, *Inorg. Chem.*, 2009, **48**, 728.
36. H.-Y. Chen, H.-Y. Tang and C.-C. Lin, *Macromolecules*, 2006, **39**, 3745.
37. L. M. Alcazar-Roman, B. J. O'Keefe, M. A. Hillmyer and W. B. Tolman, *Dalton Trans.*, 2003, 3082.
38. C. K. A. Gregson, I. J. Blackmore, V. C. Gibson, N. J. Long, E. L. Marshall and A. J. P. White, *Dalton Trans.*, 2006, 3134.
39. C. Bakewell, A. J. P. White, N. J. Long and C. K. Williams, *Inorg. Chem.*, 2013, **52**, 12561.
40. C. Bakewell, R. H. Platel, S. K. Cary, S. M. Hubbard, J. M. Roaf, A. C. Levine, A. J. P. White, N. J. Long, M. Haaf and C. K. Williams, *Organometallics*, 2012, **31**, 4729.
41. Z. Mou, B. Liu, M. Wang, H. Xie, P. Li, L. Li, S. Li and D. Cui, *Chem. Commun.*, 2014, **50**, 11411.
42. Y. Sun, J. Xiong, Z. Dai, X. Pan, N. Tang and J. Wu, *Inorg. Chem.*, 2016, **55**, 136.
43. Z. Dai, Y. Sun, J. Xiong, X. Pan, N. Tang and J. Wu, *Catal. Sci. Technol.*, 2016, **6**, 515.
44. P. Horeglad, G. Szczepaniak, M. Dranka and J. Zachara, *Chem. Commun.*, 2012, **48**, 1171.
45. F. Hild, N. Neehaul, F. Bier, M. Wirsum, C. Gourlaouen and S. Dagorne, *Organometallics*, 2013, **32**, 587.
46. T. M. Ovitt and G. W. Coates, *J. Polym. Sci. A: Polym. Chem.*, 2000, **38**, 4686.
47. C. P. Radano, G. L. Baker and M. R. Smith, *J. Am. Chem. Soc.*, 2000, **122**, 1552.
48. Z. Zhong, P. J. Dijkstra and J. Feijen, *Angew. Chem. Int. Ed.*, 2002, **41**, 4510.
49. Z. Zhong, P. J. Dijkstra and J. Feijen, *J. Am. Chem. Soc.*, 2003, **125**, 11291.
50. A. Alaaeddine, C. M. Thomas, T. Roisnel and J.-F. Carpentier, *Organometallics*, 2009, **28**, 1469.
51. A. Pilone, K. Press, I. Goldberg, M. Kol, M. Mazzeo and M. Lamberti, *J. Am. Chem. Soc.*, 2014, **136**, 2940.

52. A. Pilone, N. De Maio, K. Press, V. Venditto, D. Pappalardo, M. Mazzeo, C. Pellecchia, M. Kol and M. Lamberti, *Dalton Trans.*, 2015, **44**, 2157.
53. A. F. Douglas, B. O. Patrick and P. Mehrkhodavandi, *Angew. Chem. Int. Ed.*, 2008, **47**, 2290.
54. I. Yu, A. Acosta-Ramírez and P. Mehrkhodavandi, *J. Am. Chem. Soc.*, 2012, **134**, 12758.
55. D. C. Aluthge, B. O. Patrick and P. Mehrkhodavandi, *Chem. Commun.*, 2013, **49**, 4295.
56. K. Matsubara, C. Terata, H. Sekine, K. Yamatani, T. Harada, K. Eda, M. Dan, Y. Koga and M. Yasuniwa, *J. Polym. Sci. A: Polym. Chem.*, 2012, **50**, 957.
57. J. Fang, I. Yu, P. Mehrkhodavandi and L. Maron, *Organometallics*, 2013, **32**, 6950.
58. H. Wang, Y. Yang and H. Ma, *Macromolecules*, 2014, **47**, 7750.
59. M. D. Jones, S. L. Hancock, P. McKeown, P. M. Schafer, A. Buchard, L. H. Thomas, M. F. Mahon and J. P. Lowe, *Chem. Commun.*, 2014, **50**, 15967.
60. K. Press, I. Goldberg and M. Kol, *Angew. Chem. Int. Ed.*, 2015, **54**, 14858.
61. M. Honrado, A. Otero, J. Fernández-Baeza, L. F. Sánchez-Barba, A. Lara-Sánchez, J. Tejeda, M. P. Carrión, J. Martínez-Ferrer, A. Garcés and A. M. Rodríguez, *Organometallics*, 2013, **32**, 3437.
62. M. Honrado, A. Otero, J. Fernández-Baeza, L. F. Sánchez-Barba, A. Garcés, A. Lara-Sánchez and A. M. Rodríguez, *Organometallics*, 2014, **33**, 1859.
63. J. Xiong, J. Zhang, Y. Sun, Z. Dai, X. Pan and J. Wu, *Inorg. Chem.*, 2015, **54**, 1737.
64. M. D. Jones, L. Brady, P. McKeown, A. Buchard, P. M. Schafer, L. H. Thomas, M. F. Mahon, T. J. Woodman and J. P. Lowe, *Chem. Sci.*, 2015, **6**, 5034.
65. S.-C. Rosca, D.-A. Rosca, V. Dorcet, C. M. Kozak, F. M. Kerton, J.-F. Carpentier and Y. Sarazin, *Dalton Trans.*, 2013, **42**, 9361.
66. R. K. Dean, A. M. Reckling, H. Chen, L. N. Dawe, C. M. Schneider and C. M. Kozak, *Dalton Trans.*, 2013, **42**, 3504.
67. J. Zhang, C. Jian, Y. Gao, L. Wang, N. Tang and J. Wu, *Inorg. Chem.*, 2012, **51**, 13380.
68. W.-Y. Lu, M.-W. Hsiao, S. C. N. Hsu, W.-T. Peng, Y.-J. Chang, Y.-C. Tsou, T.-Y. Wu, Y.-C. Lai, Y. Chen and H.-Y. Chen, *Dalton Trans.*, 2012, **41**, 3659.

69. H.-Y. Chen, L. Mialon, K. A. Abboud and S. A. Miller, *Organometallics*, 2012, **31**, 5252.
70. C.-A. Huang and C.-T. Chen, *Dalton Trans.*, 2007, 5561.
71. H.-Y. Chen, J. Zhang, C.-C. Lin, J. H. Reibenspies and S. A. Miller, *Green Chem.*, 2007, **9**, 1038.
72. M. H. Chisholm, C.-C. Lin, J. C. Gallucci and B.-T. Ko, *Dalton Trans.*, 2003, 406.
73. H. A. McManus and P. J. Guiry, *Chem. Rev.*, 2004, **104**, 4151.
74. G. Desimoni, G. Faita and K. A. Jørgensen, *Chem. Rev.*, 2006, **106**, 3561.
75. A. I. Meyers, *J. Org. Chem.*, 2005, **70**, 6137.
76. G. C. Hargaden and P. J. Guiry, *Chem. Rev.*, 2009, **109**, 2505.
77. A. K. Ghosh, P. Mathivanan and J. Cappiello, *Tetrahedron: Asymmetry*, 1998, **9**, 1.
78. B. D. Ward and L. H. Gade, *Chem. Commun.*, 2012, **48**, 10587.
79. B. D. Ward, S. Bellemin-Laponnaz and L. H. Gade, *Angew. Chem. Int. Ed.*, 2005, **44**, 1668.
80. L. Lukesova, B. D. Ward, S. Bellemin-Laponnaz, H. Wadepohl and L. H. Gade, *Dalton Trans.*, 2007, 920.
81. B. D. Ward, L. Lukešová, H. Wadepohl, S. Bellemin-Laponnaz and L. H. Gade, *Eur. J. Inorg. Chem.*, 2009, **2009**, 866.
82. Y. Pan, T. Xu, G.-W. Yang, K. Jin and X.-B. Lu, *Inorg. Chem.*, 2013, **52**, 2802.
83. S. Hong, S. Tian, M. V. Metz and T. J. Marks, *J. Am. Chem. Soc.*, 2003, **125**, 14768.
84. H. Liu, J. He, Z. Liu, Z. Lin, G. Du, S. Zhang and X. Li, *Macromolecules*, 2013, **46**, 3257.
85. A. Alaaeddine, A. Amgoune, S. Bellemin-Laponnaz, J.-F. Carpentier, S. Dagorne and C. M. Thomas, *Eur. J. Inorg. Chem.*, 2006, 3652.
86. C.-T. Chen, C.-Y. Chan, C.-A. Huang, M.-T. Chen and K.-F. Peng, *Dalton Trans.*, 2007, 4073.
87. M.-T. Chen, P.-J. Chang, C.-A. Huang, K.-F. Peng and C.-T. Chen, *Dalton Trans.*, 2009, 9068.
88. C.-T. Chen, M.-T. Chen, H.-J. Weng, C.-A. Huang and K.-F. Peng, *Eur. J. Inorg. Chem.*, 2009, 2129.

89. M.-T. Chen and C.-T. Chen, *Dalton Trans.*, 2011, **40**, 12886.
90. S. Bian, S. Abbina, Z. Lu, E. Kolodka and G. Du, *Organometallics*, 2014, **33**, 2489.
91. S. Abbina and G. Du, *Macro Lett.*, 2014, **3**, 689.
92. S. D. Bennett, B. A. Core, M. P. Blake, S. J. A. Pope, P. Mountford and B. D. Ward, *Dalton Trans.*, 2014, **43**, 5871.
93. B. A. Core, *DPhil Thesis, University of Oxford*, 2015.
94. S.-F. Lu, D.-M. Du, S.-W. Zhang and J. Xu, *Tetrahedron: Asymmetry*, 2004, **15**, 3433.
95. T. D. Nixon and B. D. Ward, *Chem. Commun.*, 2012, **48**, 11790.
96. B. Cordero, V. Gomez, A. E. Platero-Prats, M. Reves, J. Echeverria, E. Cremades, F. Barragan and S. Alvarez, *Dalton Trans.*, 2008, 2832.
97. A. W. Addison, T. N. Rao, J. Reedijk, J. van Rijn and G. C. Verschoor, *J. Chem. Soc., Dalton Trans.*, 1984, 1349.
98. C.-T. Chen, C.-A. Huang, Y.-R. Tzeng and B.-H. Huang, *Dalton Trans.*, 2003, 2585.
99. T. Roth, H. Wadepohl, E. Clot and L. H. Gade, *Chem. Eur. J.*, 2015, **21**, 18730.
100. M. G. Cushion and P. Mountford, *Chem. Commun.*, 2011, **47**, 2276.
101. R. A. Collins, J. Unruangsri and P. Mountford, *Dalton Trans.*, 2013, **42**, 759.
102. J. Jenter, P. W. Roesky, N. Ajellal, S. M. Guillaume, N. Susperregui and L. Maron, *Chem. Eur. J.*, 2010, **16**, 4629.
103. M. A. Sinenkov, G. K. Fukin, A. V. Cherkasov, N. Ajellal, T. Roisnel, F. M. Kerton, J.-F. Carpentier and A. A. Trifonov, *New J. Chem.*, 2011, **35**, 204.
104. J. Kratsch, M. Kuzdrowska, M. Schmid, N. Kazeminejad, C. Kaub, P. Oña-Burgos, S. M. Guillaume and P. W. Roesky, *Organometallics*, 2013, **32**, 1230.
105. S. Harder, *Chem. Rev.*, 2010, **110**, 3852.
106. W. Schlenk and W. Schlenk Jr, *Ber. Dtsch. Chem. Ges.*, 1929, **62**, 920.
107. D. A. Fletcher, R. F. McMeeking and D. Parkin, *J. Chem. Inf. Comput. Sci.*, 1996, **36**, 746.
108. J. Unruangsri, *D.Phil Thesis, University of Oxford*, 2014.
109. M. Schmid, S. M. Guillaume and P. W. Roesky, *Organometallics*, 2014, **33**, 5392.

110. M. Kuzdrowska, L. Annunziata, S. Marks, M. Schmid, C. G. Jaffredo, P. W. Roesky, S. M. Guillaume and L. Maron, *Dalton Trans.*, 2013, **42**, 9352.
111. T. J. Marks and J. R. Kolb, *Chem. Rev.*, 1977, **77**, 263.
112. A. Bondi, *J. Phys. Chem.*, 1964, **68**, 441.
113. M. Mantina, A. C. Chamberlin, R. Valero, C. J. Cramer and D. G. Truhlar, *J. Phys. Chem. A.*, 2009, **113**, 5806.
114. N. Romero, S.-C. Roşca, Y. Sarazin, J.-F. Carpentier, L. Vendier, S. Mallet-Ladeira, C. Dinoi and M. Etienne, *Chem. Eur. J.*, 2015, **21**, 4115.
115. A. R. Smith and T. Livinghouse, *Organometallics*, 2013, **32**, 1528.
116. H. Ma and J. Okuda, *Macromolecules*, 2005, **38**, 2665.
117. M. H. Chisholm, J. C. Gallucci and K. Phomphrai, *Inorg. Chem.*, 2005, **44**, 8004.
118. M. H. Chisholm, J. Gallucci and K. Phomphrai, *Inorg. Chem.*, 2002, **41**, 2785.
119. A. P. Dove, V. C. Gibson, E. L. Marshall, A. J. P. White and D. J. Williams, *Dalton Trans.*, 2004, 570.
120. M. S. Hill and P. B. Hitchcock, *Dalton Trans.*, 2002, 4694.
121. M. H. Chisholm, N. W. Eilerts, J. C. Huffman, S. S. Iyer, M. Pacold and K. Phomphrai, *J. Am. Chem. Soc.*, 2000, **122**, 11845.
122. Y. Wang, W. Zhao, D. Liu, S. Li, X. Liu, D. Cui and X. Chen, *Organometallics*, 2012, **31**, 4182.
123. T. Athar and A. Hakeem, *Arabian J. Chem.*, 2014, **7**, 209.
124. J. Lewiński, P. Horeglad, K. Wójcik and I. Justyniak, *Organometallics*, 2005, **24**, 4588.
125. B.-T. Ko, F.-C. Wang, Y.-L. Sun, C.-H. Lin, C.-C. Lin and C.-Y. Kuo, *Polyhedron*, 1998, **17**, 4257.
126. P. Horeglad, P. Kruk and J. Pécaut, *Organometallics*, 2010, **29**, 3729.
127. E. Grunova, E. Kirillov, T. Roisnel and J.-F. Carpentier, *Organometallics*, 2008, **27**, 5691.
128. L. R. Rieth, D. R. Moore, E. B. Lobkovsky and G. W. Coates, *J. Am. Chem. Soc.*, 2002, **124**, 15239.

Chapter Six

Experimental details and characterising data

6.1 General methods and instrumentation

All air and moisture sensitive manipulations were carried out using Schlenk line or dry-box techniques under an atmosphere of argon or dinitrogen. THF and toluene were pre-dried over activated 4 Å molecular sieves before refluxing in potassium (THF) and sodium (toluene) followed by distillation. Pentane, hexane and benzene were degassed by sparging with dinitrogen and dried by passing through a column of activated alumina.[1] Deuterated solvents were dried over sodium (C_6D_6 and toluene-d_8), potassium (THF-d_8) and P_2O_5 (CD_2Cl_2), distilled at reduced pressure and stored under argon in Teflon valve ampoules. $CDCl_3$ was used as received for non-sensitive polymer samples.

NMR samples were prepared in a dry-box in 5 mm Wilmad 507-PP tubes fitted with J. Young Teflon valves. ^{1}H, ^{2}H, $^{13}C\{^{1}H\}$, ^{11}B, $^{11}B\{^{1}H\}$ and ^{19}F NMR spectra were recorded on Bruker Advance III 400, Bruker Advance III 500 or Varian Mercury-VX 300 spectrometers at ambient temperature unless stated otherwise. ^{1}H and $^{13}C\{^{1}H\}$ spectra were referenced internally to residual protio-solvent (^{1}H) or solvent (^{13}C) resonances, and are reported relative to tetramethylsilane (δ = 0 ppm). ^{2}H NMR spectra were referenced to the natural abundance deuterium resonance of the protio-solvent. ^{11}B and $^{11}B\{^{1}H\}$ spectra were referenced externally to $BF_3(Et_2O)$. ^{19}F spectra were referenced externally to $CFCl_3$. ^{7}Li spectra were referenced externally to LiCl in D_2O (9.7 M). Chemical shifts are quoted in δ (ppm) and coupling constants (J) in Hz. Assignments were confirmed using two dimensional ^{1}H-^{1}H (COSY), ^{13}C-^{1}H (HSQC and HMBC) and one dimensional nOe NMR correlation experiments. IR spectra were recorded on a Thermo Scientific Nicolet iS5 FTIR spectrometer. Samples were prepared in a dry-box as Nujol mulls between NaCl plates or as a solution (10 mg in 0.5 mL THF) in a NaCl cell. IR data are reported in wavenumbers within the range 4000-400 cm^{-1}. Mass spectra were recorded by the departmental service of University of Oxford. Elemental analysis was carried out by the Elemental Analysis Service at the London Metropolitan University.

MALDI-ToF MS analysis was performed on a Waters MALDI micro equipped with a 337 nm nitrogen laser and an accelerating voltage of 25kV was applied. The polymer samples were dissolved in THF at a concentration of 1.0 mg mL^{-1}. The cationisation agent used was potassium trifluoroacetate (Fluka, >99%) dissolved in THF at a

concentration of 5 mg mL^{-1}. The matrix used was *trans*-2-[3-(4-*tert*-butylphenyl)-2-methy-2-propenylidene]malononitrile (DCTB) (Fluka) and was dissolved in THF at a concentration of 40.0 mg mL^{-1}. Solutions of matrix, salt and polymer were mixed in a volume ratio of 4:1:4, respectively. The mixed solution was hand-spotted on a stainless steel MALDI target and left to dry. The spectra were recorded in reflectron mode.

Polymer molecular weights (M_n, M_w and PDI) were determined by GPC using a Polymer Laboratories PL-GPC50 Plus instrument equipped with a Polymer Laboratories PLgel Mixed-D column (300 mm length, 7.5 mm diameter) and a refractive index (RI) detector. THF (Fisher, HPLC grade, stabilised with BHT, 2.5 ppm) was used as an eluent at 30 °C with a flow rate of 1.0 mL min^{-1}. Samples were dissolved in THF (Fisher, HPLC grade, stabilised with BHT, 2.5 ppm) at a concentration of 2.0 mg mL^{-1} and filtered before injection. Linear polystyrenes (Polymer Laboratories) were used as primary calibration standards and the appropriate Mark-Houwink corrections for poly(ε-CL) (K = 23.7 and α = 0.74) and poly(*rac*-LA) (K = 17.4 and α = 0.736) in THF at 30 °C were applied to calculate the experimental molecular weights.[2-4]

6.2 Literature preparations and reagent purification

Tpm*,[5] (*S*,*S*)-BOPA^{iPr},[6, 7] (*S*,*S*)-BOPA^{Ph}, (*R*,*R*)-BOPA^{Ph} and $Mg\{N(SiMe_3)_2\}_2$[8] were prepared according to or adapted from literature procedures. *Rac*-LA purchased from Sigma Alrdich was recrystallised twice from hot toluene and dried *in vacuo*. The recrystallised material was subsequently sublimed twice under reduced pressure. *L*- and *D*-LA were provided by Purac and used as received. Crude *meso*-LA was provided by Uhde Inventa-Fisher which was purified by repeated recrystallisation from isopropanol at -30 °C, followed by recrystallisation from toluene and sublimed twice under reduced pressure. Purified *rac*-, *L*-, *D*- and *meso*-LA were stored in a dry-box. BnOH (Sigma Aldrich), 2-methylcyclohexanol (Sigma Aldrich), 4-trifluoromethylbenzylaldehyde (Sigma Aldrich) and *p*-tolualdehyde (Sigma Aldrich) were drided over calcium hydride for a day at room temperature, distilled under reduced pressure and degassed prior to use. 4-methylcyclohexanone was degassed prior to use and stored under argon. Benzaldehyde (Sigma Aldrich) was purified by literature procedures and distilled prior to use.[9] Purified 1,4-dimethoxybenzene was

kindly provided by Dr Laura Stevenson and stored in a dry-box. $B(OMe)_3$ was dried over sodium at reflux overnight followed by distillation under reduced pressure. $B(OBn)_3$ purchased from Sigma Aldrich and stored in a dry-box was used without further purification. BH_3(THF) (1M in THF, Sigma Aldrich) was freshly distilled under reduced pressure prior to use. BD_3(THF) was synthesised by Dr Insun Yu *via* the reaction between 2 equiv. of $NaBD_4$ (2.5 g, 60.7 mmol) and 1 equiv. of I_2 (7.7 g, 30.3 mmol) in THF (20 mL) at 0 °C, followed by distillation under reduced pressure. BD_3(THF) was stored under argon and freshly redistilled under reduced pressure prior to use due to its tendency to ring-open THF. The concentration of BD_3(THF) (1 mL) was determined by inverse-gated $^{11}B\{^1H\}$ NMR spectroscopy using $B(C_6F_5)_3$ (5 mg, 9.8 mmol) as an internal standard. Other purified liquid reagents were stored under argon in glass ampoules fitted with J. Young Teflon valves. Other commerially available reagents were used as received.

6.3 X-ray data collection and processing parameters

Crystals were mounted on glass fibres using perfluoropolyether oil and cooled rapidly in a stream of cold dinitrogen using an Oxford Cryosystems Cryostream unit. Diffraction data were measured using an Enraf-Nonius KappaCCD diffractometer or Agilent Technologies Supernova diffractometer using Mo-κα or Cu-κα, respectively. As appropriate, absorption and decay corrections were applied to the data and equivalent reflections merged.[10, 11] The structures were solved using SIR92[12] or Superflip[13] and further refinements and all other crystallographic calculations were performed using the CRYSTALS program suite.[14] Other details of the structure solution and refinements are given in the CD Appendix.

6.4 Computational details

Computational analyses described in this Thesis were performed by Dr Matthew Blake. Gradient corrected density functional theory calculations were carried out using the PBE functional,[15, 16] as implemented in the Gaussian 09 Rev D.01 (G09) quantum chemistry code.[17] The cc-pVDZ basis set of Dunning *et al.* was used for all atoms. The ultrafine grid was employed and the SCF convergence criterion set to 10^{-6} in all cases. For geometry optimisations, the default convergence criteria were used or decreased maxstep where convergence could not otherwise be achieved. All frequency calculations were performed at optimised geometries, no imaginary

frequencies were observed. The coordinates of the geometry optimised structures are contained in the CD Appendix. Bond dissociation enthalpies and energies were calculated from frequency calculations in G09 at optimised geometries (SCF total energies modified with zero point energies and thermal corrections to 298.15 K). Quantum Theory of Atoms in Molecules analyses were performed with the AIMALL program (Version 14.04.17),[18] using wavefunction files from G09 as input. Electron densities, Laplacians and energy densities were all calculated at bond critical points. Partial atomic charges and bond delocalisation indices were also calculated.

6.5 Experimental details and characterising data for Chapter Two

(Tpm*^{d})Li(THF) (1). To a solution of Tpm* protio-ligand (4.6 g, 10.5 mmol) in THF (20 mL) was added a solution of MeLi (1.6 M in Et_2O, 9.1 mL, 14.6 mmol) dropwise at -30 °C. The resulting green solution was stirred for 0.5 h before warming up to room temperature. The dark red solution was stirred for 16 h before all volatile components were removed under reduced pressure. The residue was recrystallised in THF/hexane mixture at -30 °C and the precipitate was further washed with cold hexane (3 x 10 mL) to yield a pink solid. Yield: 2.39 g (45%). Diffraction-quality crystals were grown from a saturated THF/hexane solution at -30 °C. ^{1}H NMR (C_6D_6, 400.2 MHz, 298 K) δ 5.66 (3H, s, $\underline{H}_{pz}$), 3.64 (4H, m, OC$\underline{H}_2$CH$_2$), 2.58 (9H, s, C$\underline{H}_3$), 1.43 (4H, m, OCH$_2$C$\underline{H}_2$), 1.26 (27H, s, C(C$\underline{H}_3$)$_3$) ppm. ^{13}C{^{1}H} NMR (C_6D_6, 100.6 MHz, 298 K) δ 158.6 ($\underline{C}$-^{t}Bu), 145.1 ($\underline{C}$-CH$_3$), 99.1 ($\underline{C}$-H$_{pz}$), 74.3 ($\underline{C}$(pz)$_3$), 68.2 (O$\underline{C}$H$_2$CH$_2$), 32.0 ($\underline{C}$(CH$_3$)$_3$), 30.8 (C($\underline{C}$H$_3$)$_3$), 25.7 (OCH$_2$$\underline{C}H_2$), 12.9 (C-$\underline{C}H_3$) ppm. IR (NaCl plates, Nujol mull, cm^{-1}): 1557 (s), 1364 (s), 1250 (s), 1235 (m), 1097 (s), 1024 (s), 973 (m), 814 (s), 668 (s). EI-MS: *m/z* = 430 (20%), [$\underline{M}$]$^{+}$. Anal. found (calcd. for $C_{29}H_{47}Li_1N_6O_1$): C, 69.18 (69.29); H, 9.41 (9.42); N, 16.68 (16.72) %.

(Tpm*^{d})Mg(BH$_4$) (2). To a solution of Mg(BH$_4$)$_2$ (0.044 g, 0.80 mmol) in THF (10 mL) was added a solution of (Tpm*^{d})Li(THF) (**1**, 0.40 g, 0.80 mmol) in THF (10 mL) at room temperature. The reaction mixture was stirred for 16 h before all volatile components were removed under reduced pressure. The yellow residue was subsequently extracted into toluene (3 x 10 mL) and the volatiles were removed under reduced pressure to yield a yellow solid. This was recrystallised in a toluene/hexane mixture at -30 °C followed by washing with cold hexane (3 x 10 mL) to afford a white solid. Yield: 0.28 g (76%). Diffraction-quality crystals were grown from a

saturated toluene/hexane solution at -30 °C. ^{1}H NMR (C_6D_6, 400.2 MHz, 298 K) δ 5.59 (3H, s, $\underline{H}_{pz}$), 2.32 (9H, s, C$\underline{H}_3$), 1.42 (27H, s, C(C$\underline{H}_3$)$_3$), 1.79-1.16 (4H, br q, $^{1}J_{B\text{-}H}$ = 83.4 Hz, B$\underline{H}_4$) ppm. ^{13}C{^{1}H} NMR (C_6D_6, 100.6 MHz, 298 K) δ 163.4 ($\underline{C}$-^{t}Bu), 147.0 ($\underline{C}$-CH$_3$), 101.9 ($\underline{C}$-H$_{pz}$), 71.2 ($\underline{C}$(pz)$_3$), 32.4 ($\underline{C}$(CH$_3$)$_3$), 30.9 (C($\underline{C}$H$_3$)$_3$), 12.9 (C-$\underline{C}$H$_3$) ppm. ^{11}B NMR (C_6D_6, 128.4 MHz, 298 K) δ -38.7 (quintet, $^{1}J_{B\text{-}H}$ = 80.9 Hz, $\underline{B}$H$_4$) ppm. IR (NaCl plates, Nujol mull, cm^{-1}): 2723 (w), 2668 (w), 2359 (s), 2331 (s), 2225 (s), 2176 (s), 1598 (br), 1549 (m), 1307 (w), 1260 (s), 1235 (w), 1211 (w), 1093 (s), 1017 (s), 878 (m), 799 (s), 668 (w). IR (NaCl cell, THF, *ν*(B-H), cm^{-1}): 2386 (s, B-H$_t$ of BH$_4$), 2232 and 2175 (s, B-H$_b$ of BH$_4$; 57 cm^{-1} splitting). EI-MS: *m/z* = 462 (5%), [$\underline{M}$]$^{+}$; 447 (100%), [$\underline{M}$-BH$_4$]$^{+}$. Anal. found (calcd. for $C_{25}H_{43}B_1Mg_1N_6$): C, 64.70 (64.89); H, 9.21 (9.37); N, 17.99 (18.16) %.

Alternative synthesis of (Tpm*^{d})Mg(BH$_4$) (2). To a solution of (Tpm*^{d})Mg(OBn) (**5**, 0.22 g, 0.40 mmol) in THF (10 mL) was added BH$_3$(THF) (0.52 mL, 1 M in THF, 0.52 mmol) in a glovebox. The light yellow solution was stirred for 0.5 h before all volatile solvents were removed under reduced pressure. The residue was subsequently washed with cold hexane (3 x 10 mL) and dried *in vacuo* to yield a white powder. Yield: 0.11 g (62%).

(Tpm*^{d})Mg(Me) (3). To a solution of (Tpm*^{d})Li(THF) (**1**, 0.20 g, 0.40 mmol) in THF (10 mL) was added a solution of MeMgCl (3 M in THF, 0.13 mL, 0.40 mmol) in a glovebox. The orange solution was stirred at room temperature for 16 h before all volatile components were removed under reduced pressure. Subsequent toluene extraction and cold hexane wash (3 x 10 mL) yielded a fine cream powder. Yield: 0.16 g (87%). Diffraction-quality crystals were grown from a saturated solution of THF/hexane at -30 °C. ^{1}H NMR (C_6D_6, 400.2 MHz, 298 K) δ 5.59 (3H, s, $\underline{H}_{pz}$), 2.38 (9H, s, C$\underline{H}_3$), 1.41 (27H, s, C(C$\underline{H}_3$)$_3$), -0.11 (3H, s, Mg-C$\underline{H}_3$) ppm. ^{13}C{^{1}H} NMR (C_6D_6, 100.6 MHz, 298 K) δ 162.3 ($\underline{C}$-^{t}Bu), 146.2 ($\underline{C}$-CH$_3$), 100.9 ($\underline{C}$-H$_{pz}$), 72.4 ($\underline{C}$(pz)$_3$), 32.1 ($\underline{C}$(CH$_3$)$_3$), 30.8 (C($\underline{C}$H$_3$)$_3$), 12.7 (C-$\underline{C}$H$_3$), -6.8 (Mg-$\underline{C}$H$_3$) ppm. IR (NaCl plates, Nujol mull, cm^{-1}): 1547 (s), 1236 (m), 1260 (s), 1236 (m), 1207 (m), 1088 (s), 1017 (s), 875 (s), 817 (s), 787 (s), 673 (w). EI-MS: *m/z* = 447 (100%), [$\underline{M}$-Me]$^{+}$. Anal. found (calcd. for $C_{26}H_{42}Mg_1N_6$): C, 67.26 (67.45); H, 8.94 (9.14); N, 18.00 (18.15) %.

(Tpm*^{d})Mg(Bu) (4). To a solution of Tpm* protio-ligand (1.00 g, 2.35 mmol) in toluene (20 mL) was added a solution of $MgBu_2$ (1 M in heptane, 2.83 mL, 2.83 mmol) at room temperature. The resulting orange solution was stirred for 16 h followed by the removal of any volatile components to yield an orange residue, which was subsequently extracted with hexane (20 mL) and recrystallised at -30 °C to give a cream semi-crystalline solid. Yield: 0.67 g (56%). Diffraction-quality crystals were grown from a saturated hexane solution at -30 °C. ^{1}H NMR (C_6D_6, 400.2 MHz, 298 K) δ 5.58 (3H, s, $\underline{H}_{pz}$), 2.38 (9H, s, $C\underline{H}_3$), 2.23 (2H, m, $MgCH_2C\underline{H}_2CH_2CH_3$), 1.97 (2H, m, $MgCH_2CH_2C\underline{H}_2CH_3$), 1.39 (27H, s, $C(C\underline{H}_3)_3$), 0.89 (3H, t, $^{3}J_{H\text{-}H}$ = 7.2 Hz, $MgCH_2CH_2CH_2C\underline{H}_3$), 0.58 (2H, m, $MgC\underline{H}_2CH_2CH_2CH_3$) ppm. $^{13}C\{^{1}H\}$ NMR (C_6D_6, 100.6 MHz, 298 K) δ 162.4 ($\underline{C}$-^{t}Bu), 146.2 ($\underline{C}$-CH_3), 101.0 ($\underline{C}$-H_{pz}), 72.1 ($\underline{C}(pz)_3$), 33.2 ($MgCH_2\underline{C}H_2CH_2CH_3$), 32.8 ($MgCH_2CH_2\underline{C}H_2CH_3$), 32.1 ($\underline{C}(CH_3)_3$), 30.9 ($C(\underline{C}H_3)_3$), 14.5 ($MgCH_2CH_2CH_2\underline{C}H_3$), 14.2 ($Mg\underline{C}H_2CH_2CH_2CH_3$), 12.8 (C-$\underline{C}H_3$) ppm. IR (NaCl plates, Nujol mull, cm^{-1}): 1550 (s), 1364 (s), 1260 (w), 1238 (m), 1213 (s), 1087 (m), 1027 (w), 1016 (m), 877 (s), 820 (s), 784 (s), 735 (w). EI-MS: *m/z* = 504 (5%), [*M*]$^{+}$; 447 (100%), [*M*-Bu]$^{+}$. Anal. found (calcd. for $C_{29}H_{48}Mg_1N_6$): C, 68.84 (68.97); H, 9.50 (9.58); N, 16.54 (16.64) %.

(Tpm*^{d})Mg(OBn) (5). To a solution of (Tpm*^{d})Mg(Bu) (**4**, 0.19 g, 0.38 mmol) in benzene (10 mL) was added benzaldehyde (46 μL, 0.45 mmol) in a glovebox at room temperature. The light yellow solution was stirred for 1 h before all volatile solvents were removed under reduced pressure to give a fine light yellow solid. Yield: 0.13 g (65%). ^{1}H NMR (C_6D_6, 400.2 MHz, 298 K) δ 7.89 (2H, d, $^{3}J_{H\text{-}H}$ = 7.2 Hz, *o*-$C_6\underline{H}_5$), 7.44 (2H, app t, $^{3}J_{H\text{-}H}$ = 7.6 Hz, *m*-$C_6\underline{H}_5$), 7.25 (1H, app t, $^{3}J_{H\text{-}H}$ = 7.6 Hz, *p*-$C_6\underline{H}_5$), 5.66 (2H, s, $OC\underline{H}_2C_6H_5$), 5.56 (3H, s, $\underline{H}_{pz}$), 2.36 (9H, s, $C\underline{H}_3$), 1.42 (27H, s, $C(C\underline{H}_3)_3$) ppm. $^{13}C\{^{1}H\}$ NMR (C_6D_6, 100.6 MHz, 298 K) δ 162.5 ($\underline{C}$-^{t}Bu), 146.3 ($\underline{C}$-CH_3), 128.2 (*i*-$\underline{C}_6H_5$), 127.8 (*m*-$\underline{C}_6H_5$), 127.6 (*o*-$\underline{C}_6H_5$), 125.8 (*p*-$\underline{C}_6H_5$), 100.8 ($\underline{C}$-H_{pz}), 72.4 ($\underline{C}(pz)_3$), 68.1 ($O\underline{C}H_2C_6H_5$), 32.1 ($\underline{C}(CH_3)_3$), 30.5 ($C(\underline{C}H_3)_3$), 12.7 (C-$\underline{C}H_3$) ppm. IR (NaCl plates, Nujol mull, cm^{-1}): 2669 (m), 1547 (s), 1365 (s), 1239 (s), 1206 (s), 1155 (s), 1148 (s), 1088 (s), 1020 (s), 873 (s), 819 (s), 792 (m), 783 (m), 734 (s), 697 (s), 657 (s). EI-MS: *m/z* = 554 (1%), [*M*]$^{+}$; 447 (100%), [*M*-OBn]$^{+}$. Anal. found (calcd. for $C_{32}H_{46}Mg_1N_6O_1$): C, 69.33 (69.24); H, 8.42 (8.35); N, 15.20 (15.14) %.

(Tpm*^{d})Mg(BD_4) (2-*d_4*). To a solution of (Tpm*^{d})Mg(OBn) (**5**, 0.40 g, 0.72 mmol) in THF (2 mL) was added BD_3(THF) (5.6 mL, 0.167 M in THF, 0.94 mmol) in a

glovebox. The light yellow solution was stirred for 0.5 h before all volatile solvents were removed under reduced pressure. The residue was subsequently washed with cold hexane (3 x 10 mL) and dried *in vacuo* to yield a white powder. Yield: 0.25 g (74%). ^{1}H NMR (C_6D_6, 400.2 MHz, 298 K) δ 5.59 (3H, s, $\underline{H}_{pz}$), 2.32 (9H, s, C$\underline{H}_3$), 1.42 (27H, s, C(C$\underline{H}_3$)$_3$) ppm. ^{13}C{^{1}H} NMR (C_6D_6, 100.6 MHz, 298 K) δ 163.4 ($\underline{C}$-^{t}Bu), 146.9 ($\underline{C}$-CH$_3$), 101.9 ($\underline{C}$-H$_{pz}$), 71.2 ($\underline{C}$(pz)$_3$), 32.4 ($\underline{C}$(CH$_3$)$_3$), 30.9 (C($\underline{C}$H$_3$)$_3$), 12.9 (C-$\underline{C}$H$_3$) ppm. ^{2}H NMR (C_6H_6, 76.7 MHz, 298 K) δ 1.23-1.72 (q, $^{1}J_{B\text{-}D}$ = 12.5 Hz, B$\underline{D}_4$) ppm. ^{11}B NMR (C_6D_6, 128.4 MHz, 298 K) δ -39.3 (m, $^{1}J_{B\text{-}D}$ = 11.6 Hz, $\underline{B}D_4$) ppm. IR (NaCl plates, Nujol mull, cm^{-1}): 1834 (s), 1771 (s), 1733 (m), 1651 (m), 1549 (s), 1364 (s), 1261 (w), 1235 (s), 1216 (s), 1129 (m), 1077 (s), 1027 (m), 1017 (s), 879 (s), 819 (s), 790 (s), 790 (s), 695 (m), 658 (m). IR (NaCl cell, THF, ν(B-D), cm^{-1}): 1970 (s, B-D$_t$ of BD$_4$), 1793 and 1735 (s, B-D$_b$ of BD$_4$; 58 cm^{-1} splitting). EI-MS: *m/z* = 466 (5%), [$\underline{M}$]$^{+}$; 447 (100%), [$\underline{M}$-BD$_4$]$^{+}$. Anal. found (calcd. for $C_{25}H_{39}B_1Mg_1N_6D_4$): C, 64.42 (64.33); H, 10.31 (10.15); N, 17.93 (18.00) %.

(Tpm*^{d})Mg(Cl) (6). To a solution of Tpm* protio-ligand (0.30 g, 0.71 mmol) in benzene (10 mL) was added a solution of MeMgCl (3 M in THF, 0.28 mL, 0.85 mmol). The reaction mixture was heated at 75 °C for 96 h. All volatiles were removed under reduced pressure to produce an orange solid which was recrystallised in a mixture of toluene and hexane at -30 °C to yield a light yellow solid. Yield: 0.09 g (26%). Diffraction-quality crystals were grown from a saturated benzene solution at room temperature. ^{1}H NMR (C_6D_6, 299.9 MHz, 298 K) δ 5.55 (3H, s, $\underline{H}_{pz}$), 2.31 (9H, s, C$\underline{H}_3$), 1.47 (27H, s, C(C$\underline{H}_3$)$_3$) ppm. ^{13}C{^{1}H} NMR (C_6D_6, 75.5 MHz, 298 K) δ 163.2 ($\underline{C}$-^{t}Bu), 146.9 ($\underline{C}$-CH$_3$), 101.4 ($\underline{C}$-H$_{pz}$), 71.9 ($\underline{C}$(pz)$_3$), 32.2 ($\underline{C}$(CH$_3$)$_3$), 30.9 (C($\underline{C}$H$_3$)$_3$), 12.7 (C-$\underline{C}$H$_3$) ppm. IR (NaCl plates, Nujol mull, cm^{-1}): 1546 (s), 1365 (s), 1235 (s), 1208 (s), 1083 (s), 1029 (m), 1020 (s), 875 (s), 817 (s), 789 (s). EI-MS: *m/z* = 482 (90%), [$\underline{M}$]$^{+}$; 447 (100%), [$\underline{M}$-Cl]$^{+}$. Anal. found (calcd. for $C_{25}H_{39}Mg_1N_6Cl_1$): C, 62.28 (62.12); H, 8.06 (8.13); N, 17.24 (17.39) %.

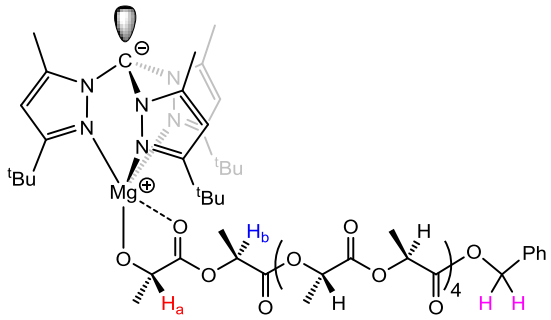
(Tpm*^{d})Mg(Br) (7). To a solution of Tpm* protio-ligand (0.30 g, 0.71 mmol) in benzene (10 mL) was added a solution of MeMgBr (3 M in Et_2O, 0.28 mL, 0.85 mmol). The reaction mixture was heated at 75 °C for 96 h. All volatiles were removed under reduced pressure to produce an orange solid. Multiple recrystallisation attempts to remove the remaining protio-ligand were unsuccessful. The pure product was not isolated and NMR characterisation was conducted in the presence of the protio-ligand.

^{1}H NMR (C_6D_6, 299.9 MHz, 298 K) δ 5.55 (3H, s, $\underline{H}_{pz}$), 2.30 (9H, s, C$\underline{H}_3$), 1.49 (27H, s, C(C$\underline{H}_3$)$_3$) ppm. ^{13}C{^{1}H} NMR (C_6D_6, 75.5 MHz, 298 K) δ 163.5 ($\underline{C}$-^{t}Bu), 146.3 ($\underline{C}$-CH$_3$), 100.9 ($\underline{C}$-H$_{pz}$), 72.3 ($\underline{C}$(pz)$_3$), 32.1 ($\underline{C}$(CH$_3$)$_3$), 30.9 (C($\underline{C}$H$_3$)$_3$), 12.5 (C-$\underline{C}$H$_3$) ppm.

[(Tpm*)Mg(Me)]Br (8). To a solution of Tpm* protio-ligand (0.50 g, 1.18 mmol) in benzene (20 mL) was added a solution of MeMgBr (3 M in Et_2O, 0.39 mL, 1.18 mmol). The cream slurry was stirred at room temperature for 16 h before the solvent was filtered. The remaining cream solid was washed with benzene (2 x 5 mL) and dried *in vacuo* to afford a white solid. Yield: 0.45 g (70%). ^{1}H NMR (CD_2Cl_2, 299.9 MHz, 298 K) δ 8.19 (1H, s, $\underline{H}$C(pz)$_3$), 6.15 (3H, s, $\underline{H}_{pz}$), 2.80 (9H, s, C$\underline{H}_3$), 1.36 (27H, s, C(C$\underline{H}_3$)$_3$), -0.77 (3H, s, Mg-C$\underline{H}_3$) ppm. ^{13}C{^{1}H} NMR (CD_2Cl_2, 75.5 MHz, 298 K) δ 168.5 ($\underline{C}$-^{t}Bu), 144.6 ($\underline{C}$-CH$_3$), 106.1 ($\underline{C}$-H$_{pz}$), 69.3 ($\underline{C}$(pz)$_3$), 32.9 ($\underline{C}$(CH$_3$)$_3$), 31.0 (C($\underline{C}$H$_3$)$_3$), 13.7 (C-$\underline{C}$H$_3$), -6.3 (Mg-$\underline{C}$H$_3$) ppm. IR (NaCl plates, Nujol mull, cm^{-1}): 1562 (s), 1303 (m), 1261 (s), 1232 (m), 1123 (s), 1017 (s), 930 (w), 813 (s). ESI^{+}-MS: *m/z* = 463, [(*Tpm*)Mg(Me)*]$^{+}$. Anal. found (calcd. for $C_{26}H_{43}Mg_1N_6Br_1$): C, 57.63 (57.42); H, 7.84 (7.97); N, 15.49 (15.45) %.

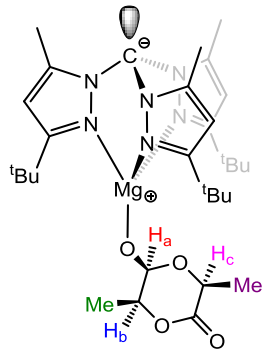
6.6 Experimental details and characterising data for Chapter Three

NMR tube scale synthesis of (Tpm*^{d})Mg[LA]$_5$OBn (9). In a glovebox, a J. Young NMR tube was charged with (Tpm*^{d})Mg(OBn) (**5**, 10 mg, 0.018 mmol) and *L*-LA (13.0 mg, 0.090 mmol) in C_6D_6 at room temperature.



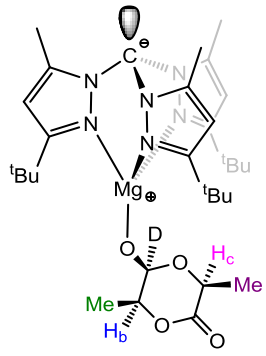
^{1}H NMR (C_6D_6, 400.2 MHz, 298 K) δ 7.10-6.98 (5H, m, C$_6\underline{H}_5$), 5.67 (3H, s, $\underline{H}_{pz}$), 5.45 (1H, m, H_b), 5.19 (1H, m, H_a), 5.04 (8H, m, remaining C$\underline{H}$(Me)), 4.91 (1H, d, $^{2}J_{H\text{-}H}$ = 9.6 Hz, H), 4.81 (1H, d, $^{2}J_{H\text{-}H}$ = 10.0 Hz, H), 2.43 (9H, s, C$\underline{H}_3$), 1.44 (27H, s, C(C$\underline{H}_3$)$_3$), 1.37-1.31 (30H, overlapping CH($\underline{Me}$)) ppm.

NMR tube scale synthesis of (Tpm*^{d})Mg(*L*-LA-H) (10). In a glovebox, a J. Young NMR tube was charged with (Tpm*^{d})Mg(BH_4) (**2**, 10 mg, 0.022 mmol) and *L*-LA (15.6 mg, 0.108 mmol) in C_6D_6 at room temperature.



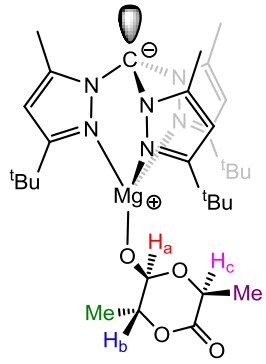
^{1}H NMR (C_6D_6, 500.0 MHz, 298 K) δ 5.80 (1H, d, $^{3}J_{H\text{-}H}$ = 2.0 Hz, H_a), 5.54 (3H, s, $\underline{H}_{pz}$), 4.59 (1H, dq, $^{3}J_{H\text{-}H}$ = 2.0 Hz, $^{3}J_{H\text{-}H}$ = 6.5 Hz, H_b), 4.45 (1H, q, $^{3}J_{H\text{-}H}$ = 6.5 Hz, H_c), 2.31 (9H, s, C$\underline{H}_3$), 1.69 (3H, d, $^{3}J_{H\text{-}H}$ = 6.5 Hz, Me), 1.63 (3H, d, $^{3}J_{H\text{-}H}$ = 6.5 Hz, Me), 1.32 (27H, s, C(C$\underline{H}_3$)$_3$) ppm.

NMR tube scale synthesis of (Tpm*^{d})Mg(*L*-LA-D) (10-d_1). In a glovebox, a J. Young NMR tube was charged with (Tpm*^{d})Mg(BD_4) (**2-d_4**, 10 mg, 0.021 mmol) and *L*-LA (15.4 mg, 0.107 mmol) in C_6D_6 at room temperature.



^{1}H NMR (C_6D_6, 500.0 MHz, 298 K) δ 5.54 (3H, s, $\underline{H}_{pz}$), 4.59 (1H, q, $^{3}J_{H\text{-}H}$ = 6.5 Hz, H_b), 4.45 (1H, q, $^{3}J_{H\text{-}H}$ = 6.5 Hz, H_c), 2.31 (9H, s, C$\underline{H}_3$), 1.69 (3H, d, $^{3}J_{H\text{-}H}$ = 6.5 Hz, Me), 1.63 (3H, d, $^{3}J_{H\text{-}H}$ = 6.5 Hz, Me), 1.32 (27H, s, C(C$\underline{H}_3$)$_3$) ppm.

NMR tube scale synthesis of (Tpm*^{d})Mg(*meso*-LA-H) (10'). In a glovebox, a J. Young NMR tube was charged with (Tpm*^{d})Mg(BH_4) (**2**, 10 mg, 0.022 mmol) and *meso*-LA (15.6 mg, 0.108 mmol) in C_6D_6 at room temperature.



^{1}H NMR (C_6D_6, 500.0 MHz, 298 K) δ 5.55 (3H, s, $\underline{H}_{pz}$), 5.22 (1H, d, $^3J_{H\text{-}H}$ = 7.0 Hz, H_a), 4.53 (1H, app quintet, $^3J_{H\text{-}H}$ = 6.5 Hz, H_b), 4.39 (1H, q, $^3J_{H\text{-}H}$ = 6.5 Hz, H_c), 2.31 (9H, s, C$\underline{H}_3$), 1.61 (3H, d, $^3J_{H\text{-}H}$ = 6.5 Hz, Me), 1.56 (3H, d, $^3J_{H\text{-}H}$ = 6.5 Hz, Me), 1.33 (27H, s, C(C$\underline{H}_3$)$_3$) ppm.

(Tp^{tBu,Me})Mg(Cy-H) (13). A mixture of *cis* and *trans* 2-methylcyclohexanol (145 µL, 1.19 mmol) was added to a solution of (Tp^{tBu,Me})Mg(Bu) (**2.18**, 0.62 g, 1.23 mmol) in benzene (15 mL) at room temperature. The reaction mixture was stirred for 2 h, after which time all volatiles were removed under reduced pressure to afford a white residue. Addition of pentane (5 mL) resulted in the formation of a white precipitate that was washed with pentane (2 × 5 mL) and dried *in vacuo*, giving a white powder. Yield: 0.50 g (75%). ^{1}H NMR (C_6D_6, 400.2 MHz, 298 K) δ 5.66 (3H, s, $\underline{H}_{pz}$), 5.65 (3H, s, $\underline{H}_{pz}$), 4.78 (2H, br s, B$\underline{H}$(pz)$_3$), 4.47 (1H, dt, $^3J_{H\text{-}H}$ = 10.4, 4.0 Hz, OC$\underline{H}$ of Cy-H, *cis*), 3.93 (1H, td, $^3J_{H\text{-}H}$ = 8.8, 4.0 Hz, OC$\underline{H}$ of Cy-H, *trans*), 2.60 (1H, m, C$\underline{H}$(CH$_3$) of Cy-H, *cis*), 2.52 (1H, m, OCHC$\underline{H}_2$ of Cy-H, *trans*), 2.13 (18H, s, overlapping C$\underline{H}_3$ of Tp), 2.11-2.05 (3H, m, C$\underline{H}_2$ of Cy-H), 2.05-1.98 (3H, m, C$\underline{H}_2$ of Cy-H), 1.94 (1H, m, OCHC$\underline{H}_2$ of Cy-H, *cis*), 1.91-1.83 (1H, m, C$\underline{H}$(CH$_3$) of Cy-H, *trans* overlapping with 1H, m, C$\underline{H}_2$ of Cy-H), 1.75 (1H, m, OCHC$\underline{H}_2$ of Cy-H, *trans*), 1.74-1.66 (1H, m, OCHC$\underline{H}_2$ of Cy-H, *cis* overlapping with 2H, m, C$\underline{H}_2$ of Cy-H), 1.61-1.58 (1H, m, C$\underline{H}_2$ of Cy-H), 1.53 (27H, s, C(C$\underline{H}_3$)$_3$), 1.52 (27H, s, C(C$\underline{H}_3$)$_3$), 1.48 (3H, d, $^3J_{H\text{-}H}$ = 6.6 Hz, CH(C$\underline{H}_3$) of Cy-H, *trans*), 1.43 (3H, d, $^3J_{H\text{-}H}$ = 7.0 Hz, CH(C$\underline{H}_3$) of Cy-H, *cis*), 1.42-1.36 (2H, m, C$\underline{H}_2$ of Cy-H) ppm. ^{13}C{^{1}H} NMR (C_6D_6, 100.6 MHz, 298 K) δ 165.6 and 164.4 (C-^{t}Bu), 144.6 and 144.4 (C-CH$_3$), 103.1 and 103.0 (C-H$_{pz}$), 77.0 (OCH of

Cy-H, *trans*), 74.5 (OCH of Cy-H, *cis*), 43.0 (CH(CH_3) of Cy-H, *trans*), 40.5 (OCHCH_2 of Cy-H, *trans*), 37.5 (CH(CH_3) of Cy-H, *cis*), 35.0, 34.5 and 33.9 (CH_2 of Cy-H), 33.0 (OCHCH_2 of Cy-H, *cis*), 32.2 and 32.0 (C(CH_3)$_3$), 31.3 and 31.3 (C(CH_3)$_3$), 27.1 and 26.8 (CH_2 of Cy-H), 21.7 (CH(CH_3) of Cy-H, *trans*), 21.1 (CH_2 of Cy-H), 13.0 and 12.9 (C-CH_3), 12.5 (CH(CH_3) of Cy-H, *cis*) ppm. ^{11}B NMR (C_6D_6, 128.4 MHz, 298 K) δ -9.4 (br d, B-H of $Tp^{tBu,Me}$) ppm. IR (NaCl plates, Nujol mull, cm^{-1}): 2550 (s), 2360 (s), 1540 (s), 1342 (s), 1244 (s), 1198 (s), 1066 (s), 1023 (m), 983 (m), 854 (w), 789 (s), 766 (s), 722 (w), 680 (m), 647 (s) . EI-MS: *m/z* = 447, [*M*-(Cy-H)]$^+$. Anal. found (calcd. for $C_{31}H_{53}B_1Mg_1N_6O_1$): C, 66.18 (66.38); H, 9.64 (9.52); N, 14.85 (14.98) %.

6.7 Experimental details and characterising data for Chapter Four

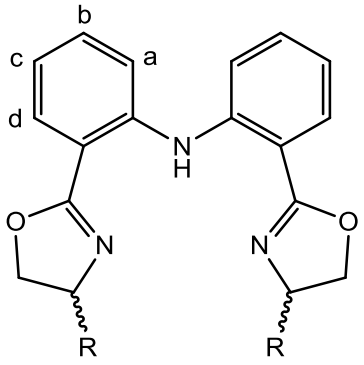
NMR tube scale synthesis of (Tpm*^{d})Mg(OBn) (5)/B(OBn)$_3$ and (Tpm*^{d})Mg(OBn){B(OBn)$_3$} (14). In a glovebox, a C_6D_6 solution of (Tpm*^{d})Mg(BH_4) (**2**, 10 mg, 0.022 mmol) in a J. Young NMR tube was treated with benzaldehyde (8.8 μL, 0.086 mmol) at room temperature. ^{1}H NMR (C_6D_6, 400.2 MHz, 298 K) δ 7.89 (2H, d, $^3J_{H-H}$ = 7.2 Hz, *o*-C_6H_5), 7.44 (2H, app t, $^3J_{H-H}$ = 7.6 Hz, *m*-C_6H_5), 7.25 (1H, app t, $^3J_{H-H}$ = 7.6 Hz, *p*-C_6H_5), 5.66 (2H, s, O$CH_2C_6H_5$), 5.56 (3H, s, H_{pz}), 4.94 (6H, s, B(OCH_2Ph)$_3$), 2.36 (9H, s, CH_3), 1.42 (27H, s, C(CH_3)$_3$) ppm. ^{11}B NMR (C_6D_6, 128.4 MHz, 298 K) δ 18.6 (s, B(OBn)$_3$), 4.0 (s, (Tpm*^{d})Mg(OBn){B(OBn)$_3$}) ppm.

(Tp^{tBu,Me})Mg(OCH$_2$C$_6$H$_4$CF$_3$) (15). A solution of ($Tp^{tBu,Me}$)Mg(Bu) (**2.18**, 0.40 g, 0.79 mmol) in benzene (15 mL) was treated with 4-trifluoromethylbenzylaldehyde (141 μL, 0.65 mmol) at room temperature. The solution mixture was stirred at room temperature for at least 4 h, after which time all volatiles were removed under reduced pressure to yield a white residue. Addition of 5 mL of pentane to the residue precipitated a white solid which was further washed with cold pentane (2 × 3 mL) and dried *in vacuo*. Yield: 0.35 g (71%). ^{1}H NMR (C_6D_6, 400.2 MHz, 298 K) δ 7.78 (2H, d, $^3J_{H-H}$ = 8.0 Hz, *o*-$C_6H_4CF_3$), 7.65 (2H, d, $^3J_{H-H}$ = 8.1 Hz, *m*-$C_6H_4CF_3$), 5.64 (3H, s, H_{pz}), 5.54 (2H, s, O$CH_2C_6H_4CF_3$), 4.78 (1H, br s, B-H), 2.12 (9H, s, CH_3), 1.44 (27H, s, C(CH_3)$_3$) ppm. ^{13}C{^{1}H} NMR (C_6D_6, 100.6 MHz, 298 K) δ 164.3 (C-^{t}Bu), 153.8 (*i*-$C_6H_4CF_3$), 144.7 (C-CH_3), 127.9 (*p*-$C_6H_4CF_3$), 127.8 (*o*-$C_6H_4CF_3$), 125.0 (q, $^1J_{C-F}$ = 3.8 Hz, $C_6H_4CF_3$), 124.9 (*m*-$C_6H_4CF_3$), 103.1 (C-H_{pz}), 67.6 (O$CH_2C_6H_4CF_3$), 32.0

($\underline{C}(CH_3)_3$), 30.7 ($C(\underline{C}H_3)_3$), 12.8 (C-$\underline{C}H_3$) ppm. ^{11}B NMR (C_6D_6, 128.4 MHz, 298 K) δ -9.1 (br d, $\underline{B}$-H) ppm. ^{19}F NMR (C_6D_6, 176.5 MHz, 298 K) δ -61.42 (s, $C_6H_4C\underline{F}_3$) ppm. IR (NaCl plates, Nujol mull, cm^{-1}): 2546 (s), 1617 (m), 1540 (s), 1343 (s), 1326 (s), 1293 (w), 1223 (s), 1180 (s), 1159 (s), 1096 (m), 1064 (s), 1029 (m), 983 (w), 819 (s), 792 (s), 782 (s), 764 (m), 679 (s), 646(s), 602 (m). EI-MS: *m/z* = 447, [$\underline{M}$-$OCH_2C_6H_4CF_3$]$^+$. Anal. found (calcd. for $C_{32}H_{46}B_1F_3Mg_1N_6O_1$): C, 61.60 (61.71); H, 7.53 (7.44); N, 13.50 (13.49) %.

(Tp^{tBu,Me})Mg(OCH$_2$C$_6$H$_4$Me) (16). A solution of (Tp^{tBu,Me})Mg(Bu) (**2.18**, 0.20 g, 0.40 mmol) in benzene (15 mL) was treated with *p*-tolualdehyde (47 μL, 0.40 mmol) at room temperature. The solution mixture was stirred for 4 h, after which time all volatiles were removed under reduced pressure to afford a white residue. Addition of 5 mL of pentane to the residue precipitated a white solid which was further washed with cold pentane (2 × 3 mL) and dried *in vacuo*. Yield: 0.21 g (92%). ^{1}H NMR (C_6D_6, 400.2 MHz, 298 K) δ 7.81 (2H, d, $^3J_{H\text{-}H}$ = 7.8 Hz, *o*-$C_6\underline{H}_4CH_3$), 7.27 (2H, d, $^3J_{H\text{-}H}$ = 7.7 Hz, *m*-$C_6\underline{H}_4CH_3$), 5.64 (3H, s, $\underline{H}_{pz}$), 5.62 (2H, s, $OC\underline{H}_2C_6H_4CH_3$), 4.78 (1H, br d, B-$\underline{H}$), 2.30 (3H, s, $C_6H_4C\underline{H}_3$), 2.12 (9H, s, $C\underline{H}_3$), 1.50 (27H, s, $C(C\underline{H}_3)_3$) ppm. $^{13}C\{^1H\}$ NMR (C_6D_6, 100.6 MHz, 298 K) δ 164.4 ($\underline{C}$-^{t}Bu), 146.4 (*i*-$\underline{C}_6H_4CH_3$), 144.5 ($\underline{C}$-CH_3), 134.6 (*p*-$\underline{C}_6H_4CH_3$), 128.7 (*o*-$\underline{C}_6H_4CH_3$), 128.2 (*m*-$\underline{C}_6H_4CH_3$), 102.9 ($\underline{C}$-H_{pz}), 68.0 ($O\underline{C}H_2C_6H_4CH_3$) 32.0 ($\underline{C}(CH_3)_3$), 30.8 ($C(\underline{C}H_3)_3$), 21.4 ($C_6H_4\underline{C}H_3$), 12.8 (C-$\underline{C}H_3$) ppm. ^{11}B NMR ($C_6D_6$, 128.4 MHz, 298 K) δ -9.2 (br d, $\underline{B}$-H) ppm. IR (NaCl plates, Nujol mull, cm^{-1}): 2544 (s), 1541 (s), 1364 (s), 1345 (s), 1243 (m), 1183 (s), 1163 (s), 1065 (s), 1028 (m), 985 (m), 854 (w), 793 (s), 765 (s), 680 (w). EI-MS: *m/z* = 447, [$\underline{M}$-$OCH_2C_6H_4CH_3$]$^+$. Anal. found (calcd. for $C_{32}H_{49}B_1Mg_1N_6O_1$): C, 67.46 (67.56); H, 8.81 (8.68); N, 14.62 (14.77) %.

6.8 Experimental details and characterising data for Chapter Five



R = ^{i}Pr, Ph

(*S*,*S*)-(BOPA^{iPr})Mg{N(SiMe$_3$)$_2$} (17). To a solution of Mg{N(SiMe$_3$)$_2$}$_2$ (0.26 g, 0.77 mmol) in toluene (20 mL) was added a solution of (*S*,*S*)-BOPA^{iPr}-H protio-ligand (0.30 g, 0.77 mmol) in toluene (20 mL). The yellow solution was stirred at room temperature for 16 h before all volatile solvents were removed under reduced pressure. The resulting solid was subsequently washed with cold pentane (3 x 5 mL) to yield a bright yellow solid. Yield: 0.28 g (63%). ^{1}H NMR (C$_6$D$_6$, 400.2 MHz, 298 K) δ 8.01 (2H, dd, $^{3}J_{H\text{-}H}$ = 8.0 Hz, $^{4}J_{H\text{-}H}$ = 1.6 Hz, Ar<u>H</u>$_d$), 7.37 (2H, app d, $^{3}J_{H\text{-}H}$ = 8.4 Hz, Ar<u>H</u>$_a$), 7.03 (2H, ddd, $^{3}J_{H\text{-}H}$ = 6.8 Hz, $^{4}J_{H\text{-}H}$ = 1.6 Hz, Ar<u>H</u>$_b$), 6.61 (2H, app t, $^{3}J_{H\text{-}H}$ = 7.6 Hz, Ar<u>H</u>$_c$), 4.09-4.04 (2H, m, OCH$_2$C<u>H</u>), 3.73-3.63 (4H, m, overlapping OC<u>H</u>$_2$CH), 2.13 (2H, m, C<u>H</u>(CH$_3$)$_2$), 0.65 (6H, d, $^{3}J_{H\text{-}H}$ = 6.6 Hz, CH(C<u>H</u>$_3$)$_2$), 0.57 (6H, d, $^{3}J_{H\text{-}H}$ = 6.6 Hz, CH(C<u>H</u>$_3$)$_2$), 0.22 (18H, s, N(Si<u>Me</u>$_3$)$_2$) ppm. ^{13}C{^{1}H} NMR (C$_6$D$_6$, 100.6 MHz, 298 K) δ 169.3 (O-<u>C</u>=N), 154.8 (MgN-<u>C</u>), 133.7 (Ar<u>C</u>$_b$), 132.1 (Ar<u>C</u>$_d$), 121.9 (Ar<u>C</u>$_a$), 117.2 (Ar<u>C</u>$_c$), 112.8 (<u>C</u>-C=N), 70.1 (OCH$_2$<u>C</u>H), 67.5 (O<u>C</u>H$_2$CH), 31.7 (<u>C</u>H(CH$_3$)$_2$), 18.1 (CH(<u>C</u>H$_3$)$_2$), 15.7 (CH(<u>C</u>H$_3$)$_2$), 6.0 (N(Si<u>Me</u>$_3$)$_2$) ppm. IR (NaCl plates, Nujol mull, cm^{-1}): 1612 (s), 1558 (w), 1535 (m), 1348 (m), 1268 (m), 1223 (s), 1159 (m), 1059 (m), 1029 (m) 968 (m), 930 (m), 883 (m), 837 (m), 744 (m). EI-MS: *m/z* = 575 (10%), [<u>*M*</u>]$^{+}$. Anal. found (calcd. for C$_{30}$H$_{46}$Mg$_1$N$_4$O$_2$Si$_2$): C, 62.47 (62.64); H, 7.83 (8.06); N, 9.77 (9.74) %.

(*S*,*S*)-(BOPA^{iPr})Mg(Cl)(THF) (18). To a solution of (*S*,*S*)-BOPA^{iPr}-H protio-ligand (0.20 g, 0.51 mmol) in THF (20 mL) was added MeMgCl (3 M in THF, 0.17 mL, 0.51 mmol) and the resulting bright yellow solution was stirred at room temperature for 30 min. All volatile components were removed under reduced pressure and the remaining solid was washed with cold pentane (3 x 5 mL) to yield a bright yellow

powder. Yield: 0.22 g (82%). ^{1}H NMR (THF-d_8, 400.2 MHz, 298 K) δ 7.72 (2H, app d, $^{3}J_{H\text{-}H}$ = 8.0 Hz, Ar$\underline{H}_d$), 7.19 (2H, d, $^{3}J_{H\text{-}H}$ = 8.8 Hz, Ar$\underline{H}_a$), 7.01 (2H, ddd, $^{3}J_{H\text{-}H}$ = 7.6 Hz, $^{4}J_{H\text{-}H}$ = 1.2 Hz, Ar$\underline{H}_b$), 6.49 (2H, app t, $^{3}J_{H\text{-}H}$ = 7.6 Hz, Ar$\underline{H}_c$), 4.98 (2H, br m, $OCH_2C\underline{H}$), 4.35 (2H, dd, $^{2}J_{H\text{-}H}$ = 8.8 Hz, $^{3}J_{H\text{-}H}$ = 5.2 Hz, $OC\underline{H}_2CH$), 4.21 (2H, app t, $J_{H\text{-}H}$ = 9.6 Hz, $OC\underline{H}_2CH$), 2.14 (2H, br m, $C\underline{H}(CH_3)_2$), 0.90 (6H, d, $^{3}J_{H\text{-}H}$ = 6.8 Hz, $CH(C\underline{H}_3)_2$), 0.73 (6H, d, $^{3}J_{H\text{-}H}$ = 6.8 Hz, $CH(C\underline{H}_3)_2$) ppm. ^{13}C{^{1}H} NMR (THF-d_8, 100.6 MHz, 298 K) δ 167.9 (O-$\underline{C}$=N), 159.6 (MgN-$\underline{C}$), 132.7 (Ar$\underline{C}_b$), 131.8 (Ar$\underline{C}_d$), 124.8 (Ar$\underline{C}_a$), 116.0 (Ar$\underline{C}_c$), 115.0 ($\underline{C}$-C=N), 71.2 ($OCH_2\underline{C}H$), 67.0 ($O\underline{C}H_2CH$), 30.6 ($\underline{C}H(CH_3)_2$), 19.9 ($CH(\underline{C}H_3)_2$), 15.0 ($CH(\underline{C}H_3)_2$) ppm. IR (NaCl plates, Nujol mull, cm^{-1}): 1614 (s), 1560 (w), 1538 (m), 1323 (m), 1265 (s), 1222 (s), 1163 (s), 1065 (m), 962 (m), 800 (w), 751 (m), 722 (m), 693 (w). EI-MS: *m/z* = 449 (90%), [$\underline{M}$-THF]$^{+}$. Anal. found (calcd. for $C_{28}H_{36}Cl_1Mg_1N_3O_3$) : C, 64.34 (64.38); H, 6.65 (6.95); N, 7.99 (8.04) %.

(*S*,*S*)-(BOPA^{iPr})Mg(Br)(THF) (19). To a solution of (*S*,*S*)-BOPA^{iPr}-H protio-ligand (0.20 g, 0.51 mmol) in THF (20 mL) was added MeMgBr (3 M in Et_2O, 0.17 mL, 0.51 mmol) and the resulting bright yellow solution was stirred at room temperature for 0.5 h. The volatile components were removed under reduced pressure and the remaining solid was washed with cold pentane (3 x 5 mL) to yield a bright yellow powder. Yield: 0.24 g (83%). ^{1}H NMR (C_6D_6, 400.2 MHz, 298 K) δ 7.99 (2H, app d, $^{3}J_{H\text{-}H}$ = 7.6 Hz, Ar$\underline{H}_d$), 7.18 (2H, d, $^{3}J_{H\text{-}H}$ = 8.4 Hz, Ar$\underline{H}_a$), 6.98 (2H, app t, $^{3}J_{H\text{-}H}$ = 7.6 Hz, Ar$\underline{H}_b$), 6.58 (2H, app t, $^{3}J_{H\text{-}H}$ = 7.6 Hz, Ar$\underline{H}_c$), 5.09 (2H, br m, $OCH_2C\underline{H}$), 3.87 (2H, dd, $^{2}J_{H\text{-}H}$ = 8.4 Hz, $^{3}J_{H\text{-}H}$ = 4.8 Hz, $OC\underline{H}_2CH$), 3.76 (2H, app t, $J_{H\text{-}H}$ = 9.2 Hz, $OC\underline{H}_2CH$), 3.68 (2H, m, $OC\underline{H}_2CH_2$), 3.44 (2H, m, $OC\underline{H}_2CH_2$), 2.17 (2H, m, $C\underline{H}(CH_3)_2$), 1.01 (4H, m, $OCH_2C\underline{H}_2$), 0.75 (6H, d, $^{3}J_{H\text{-}H}$ = 6.8 Hz, $CH(C\underline{H}_3)_2$), 0.63 (6H, d, $^{3}J_{H\text{-}H}$ = 6.8 Hz, $CH(C\underline{H}_3)_2$) ppm. ^{13}C{^{1}H} NMR (C_6D_6, 100.6 MHz, 298 K) δ 167.5 (O-$\underline{C}$=N), 157.5 (MgN-$\underline{C}$), 133.1 (Ar$\underline{C}_b$), 131.2 (Ar$\underline{C}_d$), 123.4 (Ar$\underline{C}_a$), 116.4 (Ar$\underline{C}_c$), 113.6 ($\underline{C}$-C=N), 70.0 ($OCH_2\underline{C}H$), 69.3 ($O\underline{C}H_2CH_2$), 67.1 ($O\underline{C}H_2CH$), 31.6 ($\underline{C}H(CH_3)_2$), 24.8 ($OCH_2\underline{C}H_2$), 18.7 ($CH(\underline{C}H_3)_2$), 15.1 ($CH(\underline{C}H_3)_2$) ppm. IR (NaCl plates, Nujol mull, cm^{-1}): 1615 (s), 1561 (w), 1538 (w), 1325 (m), 1265 (m), 1222 (s), 1163 (s), 1066 (m), 1031 (w), 962 (m), 751 (m), 722 (w), 694 (w). EI-MS: *m/z* = 494 (100%), [$\underline{M}$-THF]$^{+}$. Anal. found (calcd. for $C_{28}H_{36}Br_1Mg_1N_3O_3$): C, 59.60 (59.33); H, 6.26 (6.40); N, 7.56 (7.41) %.

K(*S*,*S*)-(BOPA^{iPr}) (20). To a solution of (*S*,*S*)-BOPA^{iPr}-H protio-ligand (0.20 g, 0.51 mmol) in THF (10 mL) was added to a solution of $KN(SiMe_3)_2$ (0.12 g, 0.61 mmol) in THF (20 mL) to form a canary yellow solution. This was stirred for 16 h before all volatile components were removed under reduced pressure. The resulting residue was washed with toluene (3 x 10 mL) to yield a bright yellow powder. Yield: 0.18 g (68%). ^{1}H NMR (THF-d_8, 400.2 MHz, 298 K) δ 7.36 (2H, d, $^3J_{H\text{-}H}$ = 7.6 Hz, Ar$\underline{H}_d$), 6.77 (2H, m, Ar$\underline{H}_a$ overlapping with 2H, m, Ar$\underline{H}_b$), 6.09 (2H, m, Ar$\underline{H}_c$), 4.06 (2H, m, OC$\underline{H}_2$CH), 3.93-3.82 (2H, m, OCH_2C$\underline{H}$ overlapping with 2H, m, OC$\underline{H}_2$CH), 1.63 (2H, m, C$\underline{H}(CH_3)_2$), 0.90 (6H, d, $^3J_{H\text{-}H}$ = 6.8 Hz, CH(C$\underline{H}_3)_2$), 0.83 (6H, d, $^3J_{H\text{-}H}$ = 6.8 Hz, CH(C$\underline{H}_3)_2$) ppm. ^{13}C{^{1}H} NMR (THF-d_8, 100.6 MHz, 298 K) δ 166.5 (O-$\underline{C}$=N), 158.9 (KN-$\underline{C}$), 132.3 (Ar$\underline{C}_d$), 131.3 (Ar$\underline{C}_b$), 121.0 (Ar$\underline{C}_a$), 116.6 ($\underline{C}$-C=N), 111.6 (Ar$\underline{C}_c$), 74.1 (OCH$_2\underline{C}$H), 68.3 (O$\underline{C}$H$_2$CH), 34.0 ($\underline{C}$H(CH$_3$)$_2$), 19.6 (CH($\underline{C}$H$_3$)$_2$), 18.4 (CH($\underline{C}$H$_3$)$_2$) ppm. IR (NaCl plates, Nujol mull, cm^{-1}): 1616 (s), 1583 (m), 1547 (m), 1326 (s), 1201 (s), 1159 (s), 1036 (s), 974 (m), 908 (s), 846 (w), 800 (w), 743 (s), 722 (w), 693 (m), 663 (w). EI-MS: *m/z* = 429 (30%), [$\underline{M}$]$^+$; 391 (100%), [$\underline{M}$-K]$^+$. Anal. found (calcd. for $C_{24}H_{28}K_1N_3O_2$): C, 66.97 (67.10); H, 6.64 (6.57); N, 9.72 (9.78) %.

{(*S*,*S*)-(BOPA^{iPr})}$_2$Mg (21). To a solution of K(*S*,*S*)-(BOPA^{iPr}) (**20**, 0.80 g, 1.86 mmol) in THF (20 mL) was added a solution of $Mg(BH_4)_2$ (0.051 g, 0.94 mmol) in THF (10 mL). The resulting yellow solution was stirred for 16 h before all volatile components were removed under reduced pressure. The solid was extracted into toluene (2 x 10 mL) and all volatiles were removed under reduced pressure to afford a spongy yellow residue. This was washed with cold pentane (3 x 10 mL) to give a bright yellow solid. Yield: 0.63 g (84%). ^{1}H NMR (C_6D_6, 400.2 MHz, 298 K) δ 8.13 (4H, dd, $^3J_{H\text{-}H}$ = 8.0 Hz, $^4J_{H\text{-}H}$ = 1.2 Hz, Ar$\underline{H}_d$), 7.28 (4H, d, $^3J_{H\text{-}H}$ = 8.8 Hz, Ar$\underline{H}_a$), 6.96 (4H, ddd, $^3J_{H\text{-}H}$ = 6.8 Hz, $^4J_{H\text{-}H}$ = 1.6 Hz, Ar$\underline{H}_b$), 6.55 (4H, app t, $^3J_{H\text{-}H}$ = 7.6 Hz, Ar$\underline{H}_c$), 3.74-3.64 (8H, m, overlapping OC$\underline{H}_2$CH), 3.46 (4H, m, OCH$_2$C$\underline{H}$), 1.78 (4H, m, C$\underline{H}(CH_3)_2$), 0.58 (12H, d, $^3J_{H\text{-}H}$ = 6.8 Hz, CH(C$\underline{H}_3)_2$), 0.56 (12H, d, $^3J_{H\text{-}H}$ = 6.8 Hz, CH(C$\underline{H}_3)_2$) ppm. ^{13}C{^{1}H} NMR (C_6D_6, 100.6 MHz, 298 K) δ 167.3 (O-$\underline{C}$=N), 160.3 (MgN-$\underline{C}$), 132.5 (Ar$\underline{C}_b$), 132.0 (Ar$\underline{C}_d$), 125.6 (Ar$\underline{C}_a$), 115.9 (Ar$\underline{C}_c$), 115.3 ($\underline{C}$-C=N), 70.6 (OCH$_2\underline{C}$H), 67.2 (O$\underline{C}$H$_2$CH), 30.2 ($\underline{C}$H(CH$_3$)$_2$), 19.5 (CH($\underline{C}$H$_3$)$_2$), 14.7 (CH($\underline{C}$H$_3$)$_2$) ppm. IR (NaCl plates, Nujol mull, cm^{-1}): 1610 (s), 1560 (w), 1536 (m), 1428 (w), 1333 (m), 1265 (m), 1218 (s), 1055 (m), 970 (m), 801 (m), 748 (m). EI-MS:

m/z = 805 (15%), [*M*]$^+$; 414 (90%), [*M*-BOPA]$^+$. Anal. found (calcd. for $C_{48}H_{56}Mg_1N_6O_4$): C, 71.47 (71.59); H, 6.90 (7.01); N, 10.30 (10.44) %.

Alternative route to {(*S*,*S*)-(BOPA^{iPr})}$_2$Mg (21). To a solution of Mg[N(SiMe$_3$)$_2$]$_2$ (0.18 g, 0.51 mmol) in toluene (20 mL) was added a solution of (*S*,*S*)-BOPA^{iPr}-H protio-ligand (0.40 g, 1.02 mmol) in toluene (20 mL). The yellow solution was heated at 70 °C for 48 h before all volatile solvents were removed under reduced pressure. The resulting solid was washed with cold pentane (3 x 10 mL) to yield a bright yellow solid. Yield: 0.32 g (78%).

[(*S*,*S*)-(BOPA^{Ph})Li]$_2$(THF) ((*S*,*S*)-22). To a solution of (*S*,*S*)-BOPA^{Ph}-H (0.50 g, 1.09 mmol) in THF (20 mL) was added a solution of MeLi (1.6 M in Et$_2$O, 0.68 mL, 1.09 mmol). The orange red solution was stirred for 2 h before all volatile components were removed under reduced pressure. The resulting solid was washed with cold pentane (3 x 10 mL) and dried *in vacuo* to afford a bright yellow powder. Yield: 0.43 g (78%). Diffraction-quality crystals were grown from a saturated THF/pentane solution at room temperature. ^{1}H NMR (C$_6$D$_6$, 400.2 MHz, 298 K) δ 8.18 (4H, m, Ar$\underline{H}_d$), 7.85 (2H, d, $^3J_{H\text{-}H}$ = 8.4 Hz, Ar$\underline{H}_a$), 7.14-7.04 (4H, m, Ar$\underline{H}_b$ overlapping with 2H, m, Ar$\underline{H}_a$ and 2H, m, *p*-C$_6\underline{H}_5$), 6.98 (4H, m, *o*-C$_6\underline{H}_5$), 6.85-6.69 (4H, m, *m*-C$_6\underline{H}_5$ overlapping with 4H, m, *o*-C$_6\underline{H}_5$ and 2H, m, *p*-C$_6\underline{H}_5$), 6.65 (4H, m, Ar$\underline{H}_c$), 6.54 (4H, m, *m*-C$_6\underline{H}_5$), 4.46 (2H, app t, $^3J_{H\text{-}H}$ = 8.8 Hz, OCH$_2$C$\underline{H}$), 4.04 (2H, m, OCH$_2$C$\underline{H}$ overlapping with 2H, m, OC$\underline{H}_2$CH), 3.97 (2H, app t, $J_{H\text{-}H}$ = 8.8 Hz, OC$\underline{H}_2$CH), 3.71 (2H, app t, $J_{H\text{-}H}$ = 8.0 Hz, OC$\underline{H}_2$CH), 3.63 (2H, m, OC$\underline{H}_2$CH), 3.34 (4H, m, OC$\underline{H}_2$CH$_2$), 1.27 (4H, m, OCH$_2$C$\underline{H}_2$). ^{13}C{^{1}H} NMR (C$_6$D$_6$, 100.6 MHz, 298 K) δ 168.0 and 167.6 (O-$\underline{C}$=N), 162.6 and 157.1 (MgN-$\underline{C}$), 143.2 and 142.9 (*i*-$\underline{C}_6$H$_5$), 132.5 and 132.3 (Ar$\underline{C}_b$), 131.8 and 131.6 (Ar$\underline{C}_d$), 128.8 and 128.5 (*o*-$\underline{C}_6$H$_5$), 127.6 and 126.9 (*p*-$\underline{C}_6$H$_5$), 126.8 and 125.5 (*m*-$\underline{C}_6$H$_5$), 120.3 and 117.4 (Ar$\underline{C}_a$), 115.8 and 114.4 (Ar$\underline{C}_c$), 114.3 ($\underline{C}$-C=N), 73.9 and 73.0 (O$\underline{C}$H$_2$CH), 69.5 and 68.0 (OCH$_2\underline{C}$H), 67.8 (O$\underline{C}$H$_2$CH$_2$), 25.7 (OCH$_2\underline{C}$H$_2$) ppm. ^{7}Li NMR (C$_6$D$_6$, 155.5 MHz, 298 K) δ 2.22 (N-$\underline{Li}$) ppm. ^{1}H NMR (THF-*d*$_8$, 400.2 MHz, 298 K) δ 7.66 (2H, dd, $^3J_{H\text{-}H}$ = 8.0 Hz, $^4J_{H\text{-}H}$ = 1.2 Hz, Ar$\underline{H}_d$), 7.28 (2H, d, $^3J_{H\text{-}H}$ = 8.4 Hz, Ar$\underline{H}_a$), 7.19 (2H, m, *p*-C$_6\underline{H}_5$ overlapping with 4H, m, *o*-C$_6\underline{H}_5$), 7.06 (4H, m, *m*-C$_6\underline{H}_5$), 6.96 (2H, app t, $J_{H\text{-}H}$ = 8.4 Hz, Ar$\underline{H}_b$), 6.32 (2H, app t, $J_{H\text{-}H}$ = 7.6 Hz, Ar$\underline{H}_c$), 5.02 (2H, dd, $^3J_{H\text{-}H}$ = 7.6 Hz, $^3J_{H\text{-}H}$ = 9.6 Hz, OCH$_2$C$\underline{H}$), 4.56 (2H, app t, $J_{H\text{-}H}$ = 8.4 Hz, OC$\underline{H}_2$CH), 4.07 (2H, app t, $J_{H\text{-}H}$ = 8.0 Hz, OC$\underline{H}_2$CH) ppm. ^{13}C{^{1}H} NMR (THF-*d*$_8$, 100.6 MHz, 298 K) δ 167.7 (O-$\underline{C}$=N), 157.3

(MgN-C), 144.3 (*i*-C_6H_5), 132.0 (ArC_b), 131.8 (ArC_d), 129.4 (*o*-C_6H_5), 128.2 (*p*-C_6H_5), 127.7 (*m*-C_6H_5), 120.0 (ArC_a), 115.1 (C-C=N), 113.7 (ArC_c), 73.9 (OCH_2CH), 70.7 (OCH_2CH) ppm. ^{7}Li NMR (THF-d_8, 155.5 MHz, 298 K) δ 1.86 (N-Li) ppm. IR (NaCl plates, Nujol mull, cm^{-1}): 1630 (s), 1613 (s), 1584 (w), 1532 (s), 1430 (s), 1348 (s), 1292 (w), 1263 (m), 1221 (s), 1202 (w), 1158 (m), 1139 (w), 1057 (m), 1038 (m), 953 (s), 745 (s), 700 (s). EI-MS: *m/z* = 465 (50%), [(*S*,*S*)-BOPA^{Ph}Li]$^+$. Anal. found (calcd. for $C_{64}H_{56}Li_2N_6O_5$): C, 75.96 (76.63); H, 5.72 (5.63); N, 7.91 (8.38) %.

[(*R*,*R*)-(BOPA^{Ph})Li]$_2$(THF) ((*R*,*R*)-22). To a solution of (*R*,*R*)-BOPA^{Ph}-H (0.50 g, 1.09 mmol) in THF (20 mL) was added a solution of MeLi (1.6 M in Et_2O, 0.68 mL, 1.09 mmol). The orange red solution was stirred for 2 h before all volatile components were removed under reduced pressure. The resulting solid was washed with cold pentane (3 x 10 mL) and dried *in vacuo* to afford a bright yellow powder. Yield: 0.41 g (75%). Diffraction-quality crystals were grown from a saturated THF/pentane solution at room temperature. ^{1}H NMR (C_6D_6, 400.2 MHz, 298 K) δ 8.18 (4H, m, ArH_d), 7.84 (2H, d, $^3J_{H-H}$ = 8.4 Hz, ArH_a), 7.14-7.03 (4H, m, ArH_b overlapping with 2H, m, ArH_a and 2H, m, *p*-C_6H_5), 6.98 (4H, m, *o*-C_6H_5), 6.83-6.69 (4H, m, *m*-C_6H_5 overlapping with 4H, m, *o*-C_6H_5 and 2H, m, *p*-C_6H_5), 6.65 (4H, m, ArH_c), 6.54 (4H, m, *m*-C_6H_5), 4.46 (2H, app t, $^3J_{H-H}$ = 8.8 Hz, OCH_2CH), 4.04 (2H, m, OCH_2CH overlapping with 2H, m, OCH_2CH), 3.95 (2H, app t, J_{H-H} = 8.8 Hz, OCH_2CH), 3.71 (2H, app t, J_{H-H} = 8.0 Hz, OCH_2CH), 3.63 (2H, m, OCH_2CH), 3.34 (4H, m, OCH_2CH_2), 1.26 (4H, m, OCH_2CH_2). ^{13}C{^{1}H} NMR (C_6D_6, 100.6 MHz, 298 K) δ 168.0 and 167.7 (O-C=N), 162.6 and 157.1 (MgN-C), 143.2 and 143.0 (*i*-C_6H_5), 132.4 (ArC_b), 131.8 and 131.6 (ArC_d), 128.8 and 128.5 (*o*-C_6H_5), 127.6 and 126.9 (*p*-C_6H_5), 126.9 and 125.5 (*m*-C_6H_5), 120.2 and 117.4 (ArC_a), 115.8 and 114.3 (ArC_c), 114.3 (C-C=N), 73.9 and 73.0 (OCH_2CH), 69.6 and 68.0 (OCH_2CH), 67.8 (OCH_2CH_2), 25.7 (OCH_2CH_2) ppm. ^{7}Li NMR (C_6D_6, 155.5 MHz, 298 K) δ 2.22 (N-Li) ppm. ^{1}H NMR (THF-d_8, 400.2 MHz, 298 K) δ 7.65 (2H, dd, $^3J_{H-H}$ = 8.0 Hz, $^4J_{H-H}$ = 1.2 Hz, ArH_d), 7.28 (2H, d, $^3J_{H-H}$ = 8.4 Hz, ArH_a), 7.19 (2H, m, *p*-C_6H_5 overlapping with 4H, m, *o*-C_6H_5), 7.04 (4H, m, *m*-C_6H_5), 6.97 (2H, app t, J_{H-H} = 8.0 Hz, ArH_b), 6.32 (2H, app t, J_{H-H} = 7.6 Hz, ArH_c), 5.02 (2H, dd, $^3J_{H-H}$ = 7.6 Hz, $^3J_{H-H}$ = 9.2 Hz, OCH_2CH), 4.56 (2H, app t, J_{H-H} = 8.4 Hz, OCH_2CH), 4.08 (2H, app t, J_{H-H} = 8.0 Hz, OCH_2CH) ppm. ^{13}C{^{1}H} NMR (THF-d_8, 100.6 MHz, 298 K) δ 167.5 (O-C=N), 157.6 (MgN-C), 144.3 (*i*-C_6H_5), 132.0 (ArC_b), 131.7 (ArC_d), 129.8 (*o*-C_6H_5), 128.1 (*p*-

$\underline{C}_6H_5$), 127.7 (*m*-$\underline{C}_6H_5$), 120.1 (Ar$\underline{C}_a$), 115.1 ($\underline{C}$-C=N), 113.7 (Ar$\underline{C}_c$), 73.7 (O$\underline{C}H_2$CH), 70.7 (OCH$_2\underline{C}$H) ppm. ^{7}Li NMR (THF-d_8, 155.5 MHz, 298 K) δ 1.86 (N-$\underline{Li}$) ppm. IR (NaCl plates, Nujol mull, cm^{-1}): 1633 (s), 1613 (s), 1557 (w), 1530 (m), 1430 (s), 1340 (m), 1259 (s), 1223 (s), 1203 (m), 1158 (s), 1062 (s), 950 (s), 744 (s), 695 (s). EI-MS: *m/z* = 465 (100%), [(*R*,*R*)-BOPA^{Ph}Li]$^+$. Anal. found (calcd. for $C_{64}H_{56}Li_2N_6O_5$): C, 75.92 (76.63); H, 5.88 (5.63); N, 8.00 (8.38) %.

(*S*,*S*)-(BOPA^{Ph})Mg(BH$_4$)(THF) ((*S*,*S*)-23). To a solution of Mg(BH$_4$)$_2$ (0.031 g, 0.56 mmol) in THF (20 mL) was added a solution of [(*S*,*S*)-(BOPA^{Ph})Li]$_2$(THF) (**(*S*,*S*)-22**, 0.30 g, 0.29 mmol) in THF (10 mL). The yellow solution was stirred for 3 h before all volatile components were removed under reduced pressure. The resulting residue was extracted with toluene (3 x 10 mL) and heated at 60 °C for 16 h. All volatile components were removed under reduced pressure and dried *in vacuo* for at least 2 h. This is followed by toluene extraction (3 x 10 mL) and washing with cold pentane (3 x 5 mL) to yield a bright yellow solid. Yield: 0.17 g (50%). Diffraction-quality crystals were grown from a saturated THF/pentane solution at room temperature. ^{1}H NMR (C_6D_6, 400.2 MHz, 298 K) δ 7.97 (2H, dd, $^3J_{H\text{-}H}$ = 8.0 Hz, $^4J_{H\text{-}H}$ = 1.6 Hz, Ar$\underline{H}_d$), 7.25-7.20 (2H, m, Ar$\underline{H}_a$ overlapping with 4H, m, *m*-$C_6\underline{H}_5$), 7.00 (2H, ddd, $^3J_{H\text{-}H}$ = 8.4 Hz, $^4J_{H\text{-}H}$ = 1.2 Hz, Ar$\underline{H}_b$), 6.96 (4H, m, *o*-$C_6\underline{H}_5$), 6.89 (2H, app t, $^3J_{H\text{-}H}$ = 7.2 Hz, *p*-$C_6\underline{H}_5$), 6.60 (2H, app t, $^3J_{H\text{-}H}$ = 7.6 Hz, Ar$\underline{H}_c$), 5.87 (2H, dd, $^3J_{H\text{-}H}$ = 9.6 Hz, $^3J_{H\text{-}H}$ = 4.8 Hz, OCH$_2$C$\underline{H}$), 3.92-3.83 (4H, m, overlapping O$\underline{C}H_2$CH), 3.29 (2H, m, O$\underline{C}H_2$CH$_2$), 2.97 (2H, m, O$\underline{C}H_2$CH$_2$), 0.80 (4H, m, OCH$_2$C$\underline{H}_2$), 1.07-0.30 (4H, br q, $^1J_{B\text{-}H}$ = 72.4 Hz, B$\underline{H}_4$) ppm. ^{13}C{^{1}H} NMR (C_6D_6, 100.6 MHz, 298 K) δ 168.7 (O-$\underline{C}$=N), 157.9 (MgN-$\underline{C}$), 143.0 (*i*-$\underline{C}_6H_5$), 133.2 (Ar$\underline{C}_b$), 131.5 (Ar$\underline{C}_d$), 128.8 (*o*-$\underline{C}_6H_5$), 127.8 (*p*-$\underline{C}_6H_5$), 127.4 (*m*-$\underline{C}_6H_5$), 123.6 (Ar$\underline{C}_a$), 116.5 (Ar$\underline{C}_c$), 113.8 ($\underline{C}$-C=N), 74.1 (O$\underline{C}H_2$CH), 68.4 (O$\underline{C}H_2$CH$_2$), 68.2 (OCH$_2\underline{C}$H), 24.7 (OCH$_2\underline{C}$H$_2$) ppm. ^{11}B NMR (C_6D_6, 128.4 MHz, 298 K) δ -37.9 (quintet, $^1J_{B\text{-}H}$ = 80.4 Hz, $\underline{B}H_4$) ppm. IR (NaCl plates, Nujol mull, cm^{-1}): 2353 (s), 2305 (s), 2194 (br), 2177 (br), 1614 (s), 1534 (w), 1429 (m), 1330 (s), 1263 (s), 1241 (w), 1228 (w), 1218 (m), 1154 (s), 1119 (w), 1066 (m), 1044 (w), 1027 (w), 948 (w), 927 (w), 875 (m), 746 (s), 721 (w), 697 (s). IR (NaCl cell, THF, *v*(B-H), cm^{-1}): 2375 and 2324 (s, B-H$_t$ of BH$_4$; 51 cm^{-1} splitting), 2173 (s, B-H$_b$ of BH$_4$). EI-MS: *m/z* = 497 (90%), [$\underline{M}$-THF]$^+$; 482 (100%), [$\underline{M}$-BH$_4$-THF]$^+$. Anal. found (calcd. for $C_{34}H_{36}B_1Mg_1N_3O_3$): C, 71.68 (71.67); H, 6.36 (6.37); N, 7.27 (7.37) %.

(*R*,*R*)-(BOPA^{Ph})Mg(BH$_4$)(THF) ((*R*,*R*)-23).To a solution of $Mg(BH_4)_2$ (0.031 g, 0.56 mmol) in THF (20 mL) was added a solution of [(*R*,*R*)-(BOPA^{Ph})Li]$_2$(THF) (**(*R*,*R*)-22**, 0.30 g, 0.29 mmol) in THF (10 mL). The yellow solution was stirred for 3 h before all volatile components were removed under reduced pressure. The resulting residue was extracted with toluene (3 x 10 mL) and heated at 60 °C for 16 h. All volatile components were removed under reduced pressure and dried *in vacuo* for at least 2 h. This is followed by toluene extraction (3 x 10 mL) and washing with cold pentane (3 x 5 mL) to yield a bright yellow solid. Yield: 0.19 g (56%). Diffraction-quality crystals were grown from a saturated THF/pentane solution at room temperature. ^{1}H NMR (C_6D_6, 400.2 MHz, 298 K) δ 7.96 (2H, dd, $^3J_{H-H}$ = 8.0 Hz, $^4J_{H-H}$ = 1.6 Hz, Ar$\underline{H}_d$), 7.26-7.19 (2H, m, Ar$\underline{H}_a$ overlapping with 4H, m, *m*-$C_6\underline{H}_5$), 7.00 (2H, ddd, $^3J_{H-H}$ = 8.0 Hz, $^4J_{H-H}$ = 1.2 Hz, Ar$\underline{H}_b$), 6.96 (4H, m, *o*-$C_6\underline{H}_5$), 6.89 (2H, app t, $^3J_{H-H}$ = 7.2 Hz, *p*-$C_6\underline{H}_5$), 6.59 (2H, app t, $^3J_{H-H}$ = 8.0 Hz, Ar$\underline{H}_c$), 5.86 (2H, dd, $^3J_{H-H}$ = 9.2 Hz, $^3J_{H-H}$ = 4.8 Hz, $OCH_2C\underline{H}$), 3.92-3.83 (4H, m, overlapping $OC\underline{H}_2CH$), 3.27 (2H, m, $OC\underline{H}_2CH_2$), 2.96 (2H, m, $OC\underline{H}_2CH_2$), 0.78 (4H, m, $OCH_2C\underline{H}_2$), 1.05-0.35 (4H, br q, $^1J_{B-H}$ = 74.4 Hz, B$\underline{H}_4$) ppm. ^{13}C{^{1}H} NMR (C_6D_6, 100.6 MHz, 298 K) δ 168.8 (O-$\underline{C}$=N), 157.8 (MgN-$\underline{C}$), 142.8 (*i*-$\underline{C}_6H_5$), 133.2 (Ar$\underline{C}_b$), 131.5 (Ar$\underline{C}_d$), 128.8 (*o*-$\underline{C}_6H_5$), 127.9 (*p*-$\underline{C}_6H_5$), 127.3 (*m*-$\underline{C}_6H_5$), 123.5 (Ar$\underline{C}_a$), 116.5 (Ar$\underline{C}_c$), 113.7 ($\underline{C}$-C=N), 74.1 ($O\underline{C}H_2CH$), 68.4 ($O\underline{C}H_2CH_2$), 68.2 ($OCH_2\underline{C}H$), 24.6 ($OCH_2\underline{C}H_2$) ppm. ^{11}B NMR (C_6D_6, 128.4 MHz, 298 K) δ -38.0 (quintet, $^1J_{B-H}$ = 80.5 Hz, $\underline{B}H_4$) ppm. IR (NaCl plates, Nujol mull, cm^{-1}): 2354 (s), 2305 (s), 2195 (br), 1619 (s), 1557 (m), 1534 (w), 1430 (s), 1330 (s), 1258 (s), 1241 (w), 1228 (w), 1217 (s), 1154 (s), 1119 (w), 1063 (s), 1044 (w), 1027 (w), 954 (m), 927 (m), 876 (m), 836 (w), 746 (s), 697 (s). IR (NaCl cell, THF, *ν*(B-H), cm^{-1}): 2361 and 2329 (s, B-H$_t$ of BH_4, 32 cm^{-1} splitting), 2171 (s, B-H$_b$ of BH_4). EI-MS: *m/z* = 483 (60%), [$\underline{M}$-BH$_4$-THF]$^+$. Anal. found (calcd. for $C_{34}H_{36}B_1Mg_1N_3O_3$): C, 71.69 (71.67); H, 6.28 (6.37); N, 7.36 (7.37) %.

(*S*,*S*)-(BOPA^{Ph})Mg{N(SiMe$_3$)$_2$} (24). To a solution of Mg{N(SiMe$_3$)$_2$}$_2$ (0.15 g, 0.44 mmol) in toluene (20 mL) was added a solution of (*S*,*S*)-BOPA^{Ph}-H protio-ligand (0.20 g, 0.44 mmol) in toluene (10 mL). The resulting orange solution was stirred at room temperature for 16 h before all volatile components were removed under reduced pressure. The remaining solid was washed with cold pentane (3 x 10 mL) to yield a bright yellow powder. Yield: 0.15 g (54%). ^{1}H NMR (C_6D_6, 400.2 MHz, 298 K) δ 8.00 (2H, app d, $^3J_{H-H}$ = 8.0 Hz, Ar$\underline{H}_d$), 7.52 (2H, d, $^3J_{H-H}$ = 8.4 Hz, Ar$\underline{H}_a$), 7.11

(2H, app t, $^{3}J_{H\text{-}H}$ = 8.4 Hz, Ar$\underline{H}_b$), 7.07-7.00 (4H, m, *o*-$C_6\underline{H}_5$ overlapping with 2H, m, *p*-$C_6\underline{H}_5$), 6.94 (4H, m, *m*-$C_6\underline{H}_5$), 6.67 (2H, app t, $^{3}J_{H\text{-}H}$ = 8.0 Hz, Ar$\underline{H}_c$), 4.48 (2H, dd, $^{3}J_{H\text{-}H}$ = 9.6 Hz, $^{3}J_{H\text{-}H}$ = 7.6 Hz, $OCH_2C\underline{H}$), 3.82 (2H, app t, $J_{H\text{-}H}$ = 8.8 Hz, $OC\underline{H}_2CH$), 3.51 (2H, app t, $J_{H\text{-}H}$ = 8.0 Hz, $OC\underline{H}_2CH$), 0.03 (18H, s, $N(Si\underline{Me}_3)_2$) ppm. $^{13}C\{^{1}H\}$ NMR (C_6D_6, 100.6 MHz, 298 K) δ 170.3 (O-$\underline{C}$=N), 154.4 (MgN-$\underline{C}$), 141.7 (*i*-$\underline{C}_6H_5$), 133.8 (Ar$\underline{C}_b$), 131.8 (Ar$\underline{C}_d$), 129.0 (*o*-$\underline{C}_6H_5$), 128.5 (*p*-$\underline{C}_6H_5$), 127.4 (*m*-$\underline{C}_6H_5$), 121.6 (Ar$\underline{C}_a$), 117.3 (Ar$\underline{C}_c$), 113.6 ($\underline{C}$-C=N), 74.3 ($O\underline{C}H_2CH$), 68.5 ($OCH_2\underline{C}H$), 5.9 ($N(Si\underline{Me}_3)_2$) ppm. IR (NaCl plates, Nujol mull, cm^{-1}): 1629 (s), 1608 (s), 1590 (w), 1574 (m), 1559 (w), 1534 (s), 1350 (s), 1272 (w), 1230 (s), 1167 (m), 1073 (m), 1052 (m), 1016 (s), 950 (m), 886 (s), 842 (s), 824 (w), 760 (m), 745 (m), 697 (s), 667 (w). EI-MS: *m/z* = 570 (100%), $[\underline{M}\text{-}SiMe_3]^+$; 482 (60%), $[\underline{M}\text{-}N(SiMe_3)_2]^+$. Anal. found (calcd. for $C_{36}H_{42}Mg_1N_4O_2Si_2$): C, 67.13 (67.22); H, 6.63 (6.58); N, 8.61 (8.71) %.

(*S*,*S*)-(BOPA^{Ph})Mg{N(SiMe$_2$H)$_2$} (25). To a solution of (*S*,*S*)-(BOPA^{Ph})Mg{$N(SiMe_3)_2$} (**24**, 0.20 g, 0.31 mmol) in toluene (20 mL) was added $HN(SiMe_2H)_2$ (56 μL, 0.31 mmol). The resulting yellow solution was stirred at room temperature for 16 h followed by the removal of all volatile components. The yellow solid was washed with cold pentane (3 x 10 mL) to afford a bright yellow powder. Yield: 0.15 g (78%). ^{1}H NMR (C_6D_6, 400.2 MHz, 298 K) δ 8.01 (2H, dd, $^{3}J_{H\text{-}H}$ = 8.0 Hz, $^{4}J_{H\text{-}H}$ = 1.6 Hz, Ar$\underline{H}_d$), 7.57 (2H, d, $^{3}J_{H\text{-}H}$ = 8.8 Hz, Ar$\underline{H}_a$), 7.10 (2H, ddd, $^{3}J_{H\text{-}H}$ = 8.8 Hz, $^{4}J_{H\text{-}H}$ = 2.0 Hz, Ar$\underline{H}_b$), 7.06-7.00 (4H, m, *o*-$C_6\underline{H}_5$ overlapping with 2H, m, *p*-$C_6\underline{H}_5$), 6.88 (4H, m, *m*-$C_6\underline{H}_5$), 6.67 (2H, app t, $^{3}J_{H\text{-}H}$ = 7.6 Hz, Ar$\underline{H}_c$), 4.67 (2H, sept, $^{3}J_{H\text{-}H}$ = 2.8 Hz, $N(SiMe_2\underline{H})_2$), 4.58 (2H, dd, $^{3}J_{H\text{-}H}$ = 10.0 Hz, $^{3}J_{H\text{-}H}$ = 7.6 Hz, $OCH_2C\underline{H}$), 3.86 (2H, dd, $^{2}J_{H\text{-}H}$ = 9.6 Hz, $^{3}J_{H\text{-}H}$ = 8.8 Hz, $OC\underline{H}_2CH$), 3.57 (2H, app t, $J_{H\text{-}H}$ = 8.0 Hz, $OC\underline{H}_2CH$), 0.12 (6H, d, $^{3}J_{H\text{-}H}$ = 2.8 Hz, $N(Si\underline{Me}_2H)_2$), 0.05 (6H, d, $^{3}J_{H\text{-}H}$ = 2.8 Hz, $N(Si\underline{Me}_2H)_2$) ppm. $^{13}C\{^{1}H\}$ NMR (C_6D_6, 100.6 MHz, 298 K) δ 170.3 (O-$\underline{C}$=N), 154.8 (MgN-$\underline{C}$), 141.0 (*i*-$\underline{C}_6H_5$), 133.7 (Ar$\underline{C}_b$), 131.7 (Ar$\underline{C}_d$), 129.1 (*o*-$\underline{C}_6H_5$), 128.4 (*p*-$\underline{C}_6H_5$), 127.2 (*m*-$\underline{C}_6H_5$), 121.8 (Ar$\underline{C}_a$), 117.3 (Ar$\underline{C}_c$), 113.1 ($\underline{C}$-C=N), 74.3 ($O\underline{C}H_2CH$), 68.3 ($OCH_2\underline{C}H$), 4.6 ($N(Si\underline{Me}_2H)_2$), 3.8 ($N(Si\underline{Me}_2H)_2$) ppm. IR (NaCl plates, Nujol mull, cm^{-1}): 2018 (br), 1609 (m), 1592 (w), 1578 (w), 1533 (s), 1433 (s), 1347 (s), 1263 (w), 1226 (s), 1073 (s), 1051 (w), 1027 (w), 949 (m), 839 (s), 745 (s), 696 (s). EI-MS: *m/z* = 600 (10%), $[\underline{M}\text{-}Me]^+$; 556 (100%), $[\underline{M}\text{-}SiMe_2H]^+$. Anal. found (calcd. for $C_{34}H_{38}Mg_1N_4O_2Si_2$): C, 66.21 (66.38); H, 6.36 (6.23); N, 8.94 (9.11) %.

(*S*,*S*)-(BOPA^{Ph})Mg(Br)(THF) (26). To a solution of (*S*,*S*)-BOPA^{Ph}-H protio-ligand (0.20 g, 0.44 mmol) in toluene (20 mL) was added MeMgBr (3 M in Et_2O, 0.15 mL, 0.44 mmol). The resulting bright yellow solution was stirred for 1 h before all volatile components were removed under reduced pressure. The remaining solid was washed with cold pentane (3 x 10 mL) to yield a bright yellow powder. Yield: 0.21 g (75%). ^{1}H NMR (C_6D_6, 400.2 MHz, 298 K) δ 7.97 (2H, dd, $^3J_{H\text{-}H}$ = 8.0 Hz, $^4J_{H\text{-}H}$ = 1.2 Hz, Ar$\underline{H}_d$), 7.34 (4H, d, $^3J_{H\text{-}H}$ = 7.6 Hz, *m*-$C_6\underline{H}_5$), 7.18 (2H, d, $^3J_{H\text{-}H}$ = 7.2 Hz, Ar$\underline{H}_a$), 7.02-6.94 (2H, m, Ar$\underline{H}_b$ overlapping with 4H, m, *o*-$C_6\underline{H}_5$), 6.87 (2H, app t, $^3J_{H\text{-}H}$ = 7.6 Hz, *p*-$C_6\underline{H}_5$), 6.60 (2H, app t, $^3J_{H\text{-}H}$ = 7.6 Hz, Ar$\underline{H}_c$), 6.17 (2H, app t, $^3J_{H\text{-}H}$ = 7.2 Hz, $OCH_2C\underline{H}$), 3.82 (4H, m, overlapping $OC\underline{H}_2CH$), 3.37 (2H, m, $OC\underline{H}_2CH_2$), 2.83 (2H, m, $OC\underline{H}_2CH_2$), 0.77 (4H, m, $OCH_2C\underline{H}_2$) ppm. $^{13}C\{^1H\}$ NMR (C_6D_6, 100.6 MHz, 298 K) δ 168.1 (O-$\underline{C}$=N), 157.8 (MgN-$\underline{C}$), 143.3 (*i*-$\underline{C}_6H_5$), 133.1 (Ar$\underline{C}_b$), 131.4 (Ar$\underline{C}_d$), 128.8 (*o*-$\underline{C}_6H_5$), 127.8 (*p*-$\underline{C}_6H_5$), 127.6 (*m*-$\underline{C}_6H_5$), 123.6 (Ar$\underline{C}_a$), 116.4 (Ar$\underline{C}_c$), 113.7 ($\underline{C}$-C=N), 73.9 ($O\underline{C}H_2CH$), 68.8 ($O\underline{C}H_2CH_2$), 68.5 ($OCH_2\underline{C}H$), 24.6 ($OCH_2\underline{C}H_2$) ppm. IR (NaCl plates, Nujol mull, cm^{-1}): 1614 (s), 1557 (s), 1535 (m), 1428 (s), 1333 (w), 1315 (m), 1262 (s), 1199 (s), 1165 (s), 1060 (s), 1037 (s), 953 (s), 912 (w), 875 (m), 750 (s), 698 (s). EI-MS: *m/z* = 562 (50%), [$\underline{M}$-THF]$^+$; 482 (5%), [$\underline{M}$-THF-Br]$^+$. Anal. found (calcd. for $C_{34}H_{32}Br_1Mg_1N_3O_3$: C, 64.33 (64.32); H, 4.95 (5.08); N, 6.57 (6.62) %.

NMR tube scale synthesis of (*S*,*S*)-(BOPA^{Ph})Mg(OBn) ((*S*,*S*)-27)/B(OBn)$_3$ and (*S*,*S*)-(BOPA^{Ph})Mg(OBn){B(OBn)$_3$} (28). In a glovebox, a C_6D_6 solution of (*S*,*S*)-(BOPA^{Ph})Mg(BH_4)(THF) (**(*S*,*S*)-23**, 10 mg, 0.018 mmol) in a J. Young NMR tube was treated with benzaldehyde (7.1 μL, 0.070 mmol) at room temperature. The ^{1}H NMR spectrum gave a complex mixture of products. ^{11}B NMR (C_6D_6, 128.4 MHz, 298 K) δ 18.9 (s, $\underline{B}(OBn)_3$), 3.6 (s, (*S*,*S*)-(BOPA^{Ph})Mg(OBn){$\underline{B}(OBn)_3$}).

6.9 Polymerisation procedures

General procedure for the polymerisation of ε-CL (Chapter Three and Chapter Four). In a dry box, a solution of ε-CL (0.378 g, 3.3 mmol) in THF or toluene (2.5 mL) was added rapidly in one portion to a stirred THF or toluene solution (0.8 mL) of catalyst (0.0166 mmol) at room temperature. $[\varepsilon\text{-CL}]_0$:$[\text{initiator}]_0$ = 200:1. Aliquots (approx. 0.1 mL) were taken at appropriate time intervals and quenched outside the dry box with wet THF (1 mL) or inside the dry box with degassed, wet THF (1 mL).

The volatiles were evaporated to dryness to give PCL. The monomer to polymer % conversion was determined using ^{1}H NMR spectroscopy ($CDCl_3$), and measured by integration of the resonances of PCL and unreacted ε-CL. Aliquots were recovered for GPC and MALDI-ToF MS analyses. The polymer was isolated by addition of hexane to a concentrated THF solution of PLA to yield a precipitate which was washed with hexane and dried *in vacuo*.

General procedure for the polymerisation of ε-CL with additives (Chapter Four). In a dry box, a solution of ε-CL (0.378 g, 3.3 mmol) in THF or toluene (2.5 mL) was added rapidly in one portion to a 5 min stirred THF or toluene solution (0.8 mL) of catalyst (0.0166 mmol) and additive at room temperature. $[\varepsilon\text{-CL}]_0$:$[\text{initiator}]_0$ = 200:1. Aliquots (approx. 0.1 mL) were taken at appropriate time intervals and quenched outside the dry box with wet THF (1 mL) or inside the dry box with degassed, wet THF (1 mL). The volatiles were evaporated to dryness to give PCL. The monomer to polymer % conversion was determined using ^{1}H NMR spectroscopy ($CDCl_3$), and measured by integration of the resonances of PCL and unreacted ε-CL. Aliquots were recovered for GPC and MALDI-ToF MS analyses. The polymer was isolated by addition of hexane to a concentrated THF solution of PLA to yield a precipitate which was washed with hexane and dried *in vacuo*.

General procedure for the polymerisation of *rac*-, *L*-, and *meso*-LA (Chapter Three and Chapter Four). In a dry box, a solution of lactide (0.432 g, 3.0 mmol) in THF (5 mL) was added rapidly in one portion to a stirred THF solution (1 mL) of catalyst (0.03 mmol) at room temperature. $[\text{LA}]_0$:$[\text{initiator}]_0$ = 100:1. Aliquots (approx. 0.1 mL) were taken at appropriate time intervals and quenched outside the dry box with wet THF (1 mL) or inside the dry box with degassed, wet THF (1 mL). The volatiles were evaporated to dryness to give PLA. The monomer to polymer % conversion was determined using ^{1}H NMR spectroscopy ($CDCl_3$), and measured by integration of the C<u>H</u>Me resonances of the unreacted monomer and PLA. Aliquots were recovered for GPC and MALDI-ToF MS analyses. The polymer was isolated by addition of pentane to a concentrated THF solution of PLA to yield a precipitate which was washed with pentane and dried *in vacuo*.

General procedure for the polymerisation of *rac*-LA with additives (Chapter Three and Chapter Four). In a dry box, a solution of *rac*-lactide (0.432 g, 3.0 mmol) in THF (5 mL) was added rapidly in one portion to a 5 min stirred THF solution (1 mL) of catalyst (0.03 mmol) and additive at room temperature. $[LA]_0$:$[initiator]_0$ = 100:1. Aliquots (approx. 0.1 mL) were taken at appropriate time intervals and quenched outside the dry box with wet THF (1 mL) or inside the dry box with degassed, wet THF (1 mL). The volatiles were evaporated to dryness to give PLA. The monomer to polymer % conversion was determined using ^{1}H NMR spectroscopy ($CDCl_3$), and measured by integration of the C<u>H</u>Me resonances of the unreacted monomer and PLA. Aliquots were recovered for GPC and MALDI-ToF MS analyses. The polymer was isolated by addition of pentane to a concentrated THF solution of PLA to yield a precipitate which was washed with pentane and dried *in vacuo*.

General procedure for the polymerisation of *rac*-, *L*-, *D*- and *meso*-LA in THF or dichloromethane (Chapter Five). In a dry box, a solution of lactide (0.576 g, 4.0 mmol) in THF or dichloromethane (3 mL) was added rapidly in one portion to a stirred THF or dichloromethane solution (1 mL) of catalyst (0.04 mmol) at room temperature. $[LA]_0$:$[initiator]_0$ = 100:1. Aliquots (approx. 0.1 mL) were taken at appropriate time intervals and quenched outside the dry box with wet THF (1 mL) or inside the dry box with degassed, wet THF (1 mL). The volatiles were evaporated to dryness to give PLA. The monomer to polymer % conversion was determined using ^{1}H NMR spectroscopy ($CDCl_3$), and measured by integration of the C<u>H</u>Me resonances of the unreacted monomer and PLA. Aliquots were recovered for GPC and MALDI-ToF MS analyses. The polymer was isolated by addition of pentane to a concentrated THF solution of PLA to yield a precipitate which was washed with pentane and dried *in vacuo*.

General procedure for the polymerisation of *rac*-, *L*-, *D*- and *meso*-LA with additives in THF or dichloromethane (Chapter Five). In a dry box, a solution of lactide (0.576 g, 4.0 mmol) in THF or dichloromethane (3 mL) was added rapidly in one portion to a 5 min stirred THF or dichloromethane solution (1 mL) of catalyst (0.04 mmol) and additive at room temperature. $[LA]_0$:$[initiator]_0$ = 100:1. Aliquots (approx. 0.1 mL) were taken at appropriate time intervals and quenched outside the dry box with wet THF (1 mL) or inside the dry box with degassed, wet THF (1 mL). The volatiles were evaporated to dryness to give PLA. The monomer to polymer %

conversion was determined using ^{1}H NMR spectroscopy ($CDCl_3$), and measured by integration of the C<u>H</u>Me resonances of the unreacted monomer and PLA. Aliquots were recovered for GPC and MALDI-ToF MS analyses. The polymer was isolated by addition of pentane to a concentrated THF solution of PLA to yield a precipitate which was washed with pentane and dried *in vacuo*.

General procedure for the polymerisation of *rac*- and *meso*-LA in toluene (Chapter Five). In a dry box, a toluene solution (1 mL) of catalyst (0.04 mmol) was added rapidly in one portion to a suspension of lactide (0.576 g, 4.0 mmol) in toluene (3 mL) at room temperature. $[LA]_0$:$[initiator]_0$ = 100:1. An Aliquot (approx. 0.1 mL) was taken at the end of the polymerisation and quenched outside the dry box with wet THF (1 mL). The volatiles were evaporated to dryness to give PLA. The monomer to polymer % conversion was determined using ^{1}H NMR spectroscopy ($CDCl_3$), and measured by integration of the C<u>H</u>Me resonances of the unreacted monomer and PLA. Aliquots were recovered for GPC and MALDI-ToF MS analyses. The polymer was isolated by addition of pentane to a concentrated THF solution of PLA to yield a precipitate which was washed with pentane and dried *in vacuo*.

General procedure for the polymerisation of *rac*- and *meso*-LA with additives in toluene (Chapter Five). In a dry box, a 5 min stirred toluene solution (1 mL) of catalyst (0.04 mmol) and additive was added rapidly in one portion to a suspension of lactide (0.576 g, 4.0 mmol) in toluene (3 mL) at room temperature. $[LA]_0$:$[initiator]_0$ = 100:1. An aliquot (approx. 0.1 mL) was taken at the end of the polymerisation and quenched outside the dry box with wet THF (1 mL). The volatiles were evaporated to dryness to give PLA. The monomer to polymer % conversion was determined using ^{1}H NMR spectroscopy ($CDCl_3$), and measured by integration of the C<u>H</u>Me resonances of the unreacted monomer and PLA. Aliquots were recovered for GPC and MALDI-ToF MS analyses. The polymer was isolated by addition of pentane to a concentrated THF solution of PLA to yield a precipitate which was washed with pentane and dried *in vacuo*.

6.10 References for Chapter Six

1. A. B. Pangborn, M. A. Giardello, R. H. Grubbs, R. K. Rosen and F. J. Timmers, *Organometallics*, 1996, **15**, 1518.
2. A. Rudin and H. L. W. Hoegy, *J. Polym. Sci. A: Polym. Chem.*, 1972, **10**, 217.

3. I. Barakat, P. Dubois, R. Jérôme and P. Teyssié, *J. Polym. Sci. A: Polym. Chem.*, 1993, **31**, 505.
4. J. R. Dorgan, J. Janzen, D. M. Knauss, S. B. Hait, B. R. Limoges and M. H. Hutchinson, *J. Polym. Sci. B: Polym. Phys.*, 2005, **43**, 3100.
5. D. L. Reger, T. C. Grattan, K. J. Brown, C. A. Little, J. J. S. Lamba, A. L. Rheingold and R. D. Sommer, *J. Organomet. Chem.*, 2000, **607**, 120.
6. S.-F. Lu, D.-M. Du, S.-W. Zhang and J. Xu, *Tetrahedron: Asymmetry*, 2004, **15**, 3433.
7. T. D. Nixon and B. D. Ward, *Chem. Commun.*, 2012, **48**, 11790.
8. Y. Sarazin, R. H. Howard, D. L. Hughes, S. M. Humphrey and M. Bochmann, *Dalton Trans.*, 2006, 340.
9. W. L. F. Armarego and C. L. L. Chai, *Purification of Laboratory Chemicals*, Elsevier, 7th edn.
10. *Agilent Technologies* Oxford, 2011.
11. Z. Otwinowski and W. Minor, *Processing of X-ray Diffraction Data Collected in Oscillation Mode*, Academic Press, New York, 1997.
12. A. Altomare, G. Cascarano, C. Giacovazzo, A. Guagliardi, M. C. Burla, G. Polidori and M. Camalli, *J. Appl. Crystallogr.*, 1994, **27**, 435.
13. L. Palatinus and G. Chapuis, *J. Appl. Crystallogr.*, 2007, **40**, 786.
14. P. W. Betteridge, J. R. Carruthers, R. I. Cooper, K. Prout and D. J. Watkin, *J. Appl. Crystallogr.*, 2003, **36**, 1487.
15. J. P. Perdew, K. Burke and M. Ernzerhof, *Phys. Rev. Lett*, 1996, **77**, 3865.
16. J. P. Perdew, K. Burke and M. Ernzerhof, *Phys. Rev. Lett*, 1997, **78**, 1396.
17. M. J. Frisch, G. W. Trucks, H. B. Schlegel, G. E. Scuseria, M. A. Robb, J. R. Cheeseman, G. Scalmani, V. Barone, B. Mennucci, G. A. Petersson, H. Nakatsuji, M. Caricato, X. Li, H. P. Hratchian, A. F. Izmaylov, J. Bloino, G. Zheng, J. L. Sonnenberg, M. Hada, M. Ehara, K. Toyota, R. Fukuda, J. Hasegawa, M. Ishida, T. Nakajima, Y. Honda, O. Kitao, H. Nakai, T. Vreven, J. A. Montgomery Jr., J. E. Peralta, F. Ogliaro, M. J. Bearpark, J. Heyd, E. N. Brothers, K. N. Kudin, V. N. Staroverov, R. Kobayashi, J. Normand, K. Raghavachari, A. P. Rendell, J. C. Burant, S. S. Iyengar, J. Tomasi, M. Cossi, N. Rega, N. J. Millam, M. Klene, J. E. Knox, J. B. Cross, V. Bakken, C. Adamo, J. Jaramillo, R. Gomperts, R. E. Stratmann, O. Yazyev, A. J. Austin, R. Cammi, C. Pomelli, J. W. Ochterski, R. L. Martin, K. Morokuma, V. G.

Zakrzewski, G. A. Voth, P. Salvador, J. J. Dannenberg, S. Dapprich, A. D. Daniels, Ö. Farkas, J. B. Foresman, J. V. Ortiz, J. Cioslowski and D. J. Fox, *Gaussian 09, Revision D.01*, Gaussian, Inc., Wallingford, CT, USA, 2009.

18. T. A. Keith, *AIMALL*, 2014.

Appendix

A1. NMR tube scale synthesis of "B(LA-H)$_3$" *via* the reaction between 1 equiv. of BH$_3$(THF) and 5 equiv. of *L*-LA in C$_6$D$_6$

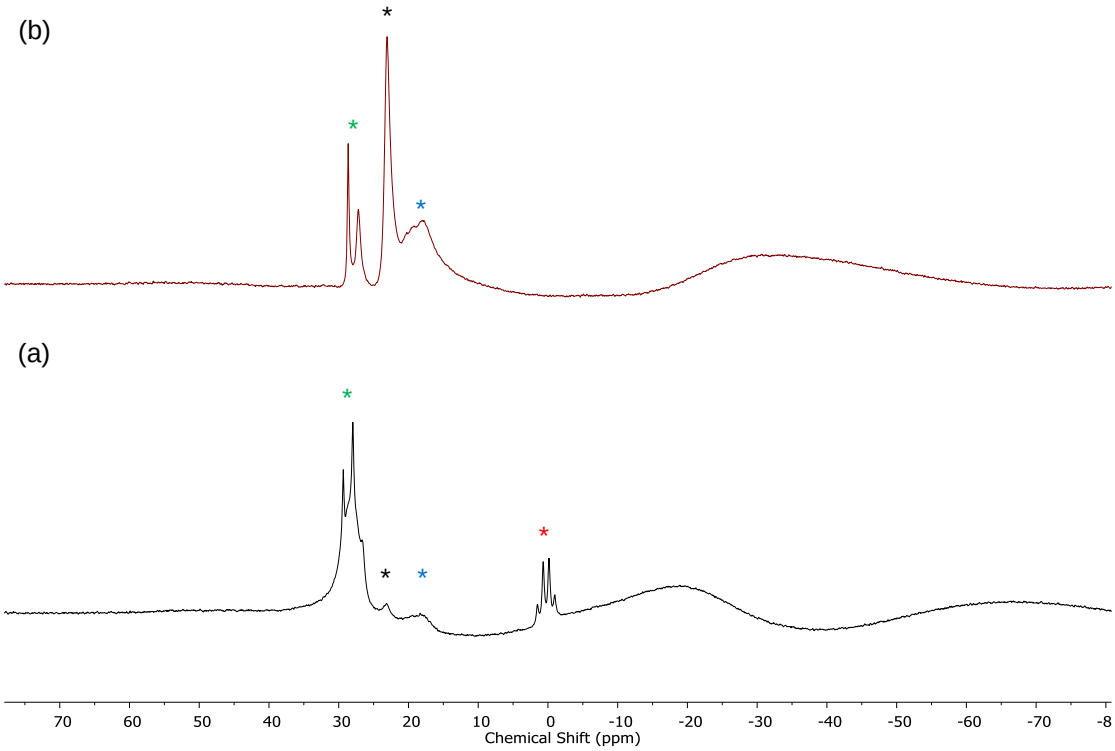


Figure A1.1 ^{11}B NMR spectrum (C$_6$D$_6$, 160.4 MHz, 298 K) (a) of the reaction between 1 equiv. of BH$_3$(THF) and 5 equiv. of *L*-LA recorded 5 min after the reaction at room temperature. ^{11}B NMR spectrum (C$_6$D$_6$, 160.4 MHz, 298 K) (b) recorded after heating the reaction between 1 equiv. of BH$_3$(THF) and 5 equiv. of *L*-LA at 60 ℃ for 3 h. "*" denotes unreacted BH$_3$(THF). "*" denotes "B(LA-H)$_3$". "*" denotes "BH(LA-H)$_2$". "*" denotes "BH$_2$(LA-H)".

A2. NMR tube scale reaction between 1 equiv. of (Tpm*^{d})Mg(BH$_4$) (2) and 5 equiv. of *L*-LA in C_6D_6 at room temperature

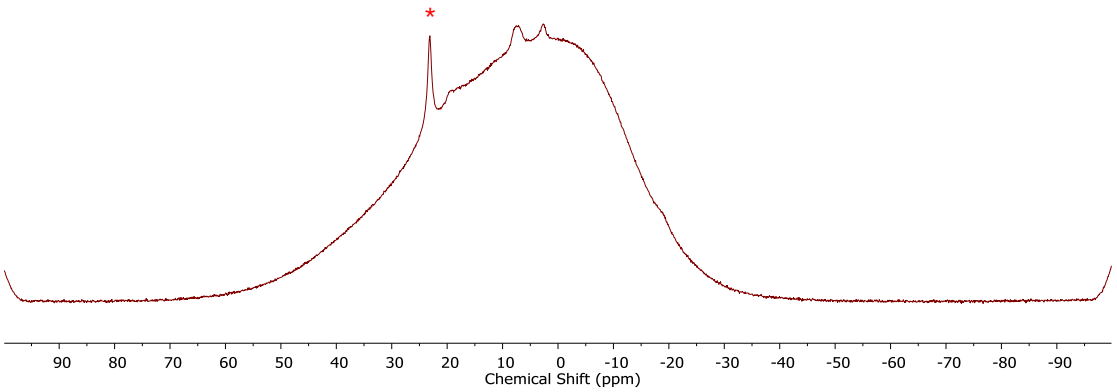


Figure A2.1 ^{11}B NMR spectrum (C_6D_6, 160.4 MHz, 298 K) of the reaction between 1 equiv. of (Tpm*^{d})Mg(BH$_4$) (**2**) and 5 equiv. of *L*-LA recorded 5 min after the reaction. "*" denotes "B(LA-H)$_3$". The identities of all other signals remain unknown.

A3. NMR tube scale reactions between 1 equiv. of BH_3(THF) and 3 equiv. of ketones and aldehydes

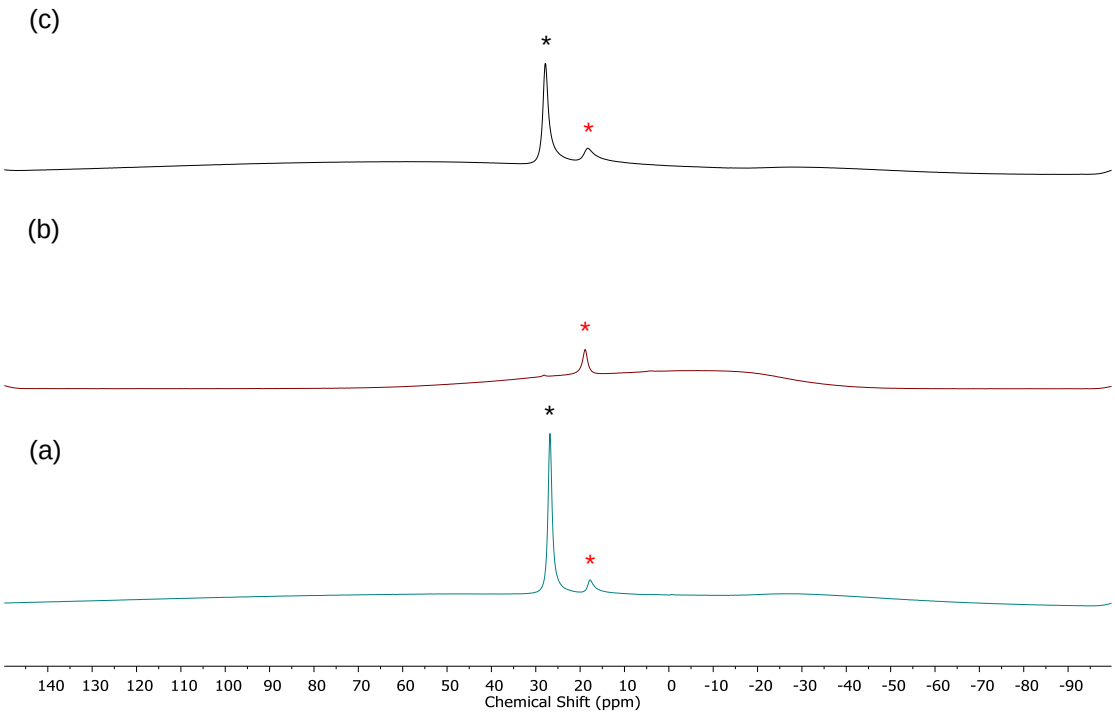


Figure A3.1 $^{11}B\{^1H\}$ NMR spectrum (THF-d_8, 128.4 MHz, 298 K) of the reaction between 1 equiv. of BH_3(THF) and 3 equiv. of (a) 2-methylcyclohexanone, (b) *p*-tolualdehyde and (c) terephthalaldehyde recorded 16 h after the reaction at room temperature. "*" denotes $B(OR)_3$ (OR = corresponding alkoxide). "*" denotes $BH(OR)_2$.

A4. NMR tube scale reaction between 1 equiv. of (Tpm*^{d})Mg(BH$_4$) (2) and 4 equiv. of 2-methylcyclohexanone

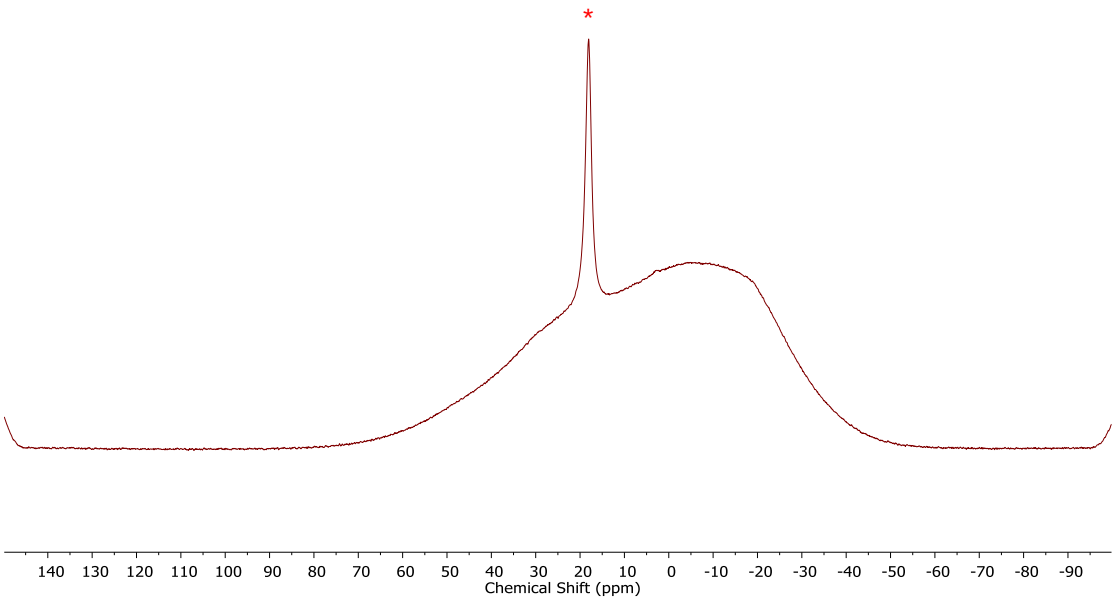


Figure A4.1. ^{11}B NMR spectrum (C_6D_6, 160.4 MHz, 298 K) of the reaction between 1 equiv. of (Tpm*^{d})Mg(BH$_4$) (**2**) and 4 equiv. of 2-methylcyclohexanone recorded 5 min after the reaction. "*" denotes B(Cy-H)$_3$.

A5. *In-situ* generation of (Tpm*^{d})Mg(OBn) (5) and B(OBn)$_3$

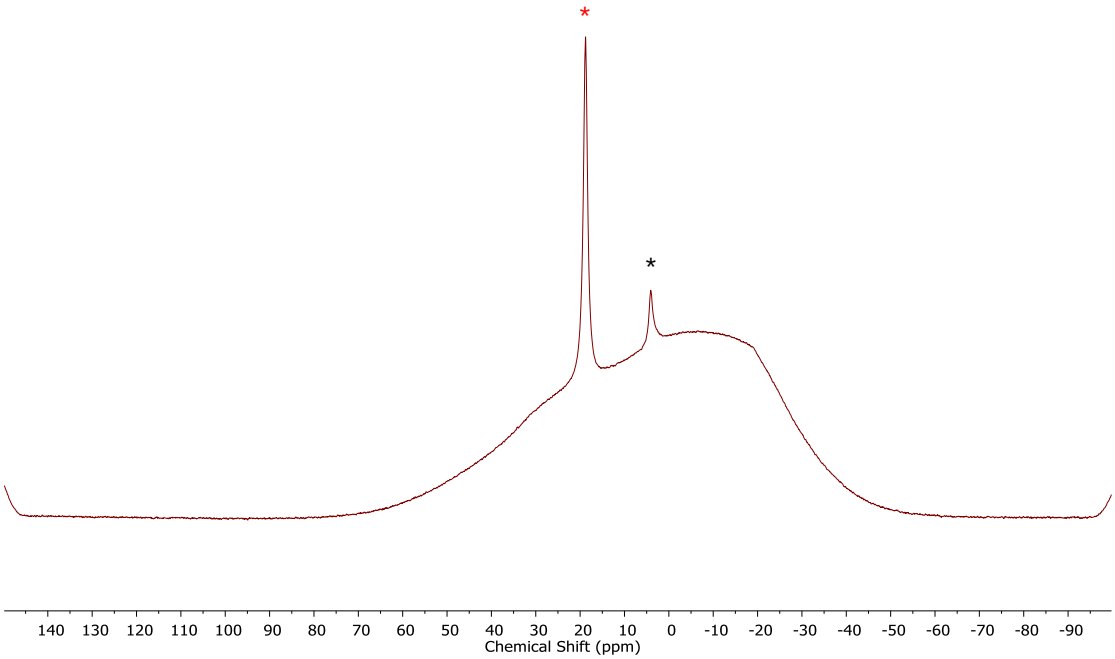


Figure A5.1. ^{11}B NMR spectrum (C_6D_6, 160.4 MHz, 298 K) of the reaction between 1 equiv. of (Tpm*^{d})Mg(BH_4) (**2**) and 4 equiv. of benzaldehyde recorded 5 min after the reaction. "*" denotes B(OBn)$_3$. "*" denotes (Tpm*^{d})Mg(OBn){B(OBn)$_3$}.

A6. NMR tube scale reaction between ($Tp^{tBu,Me}$)Mg(Cy-H) (13) and $B(Cy\text{-}H)_3$

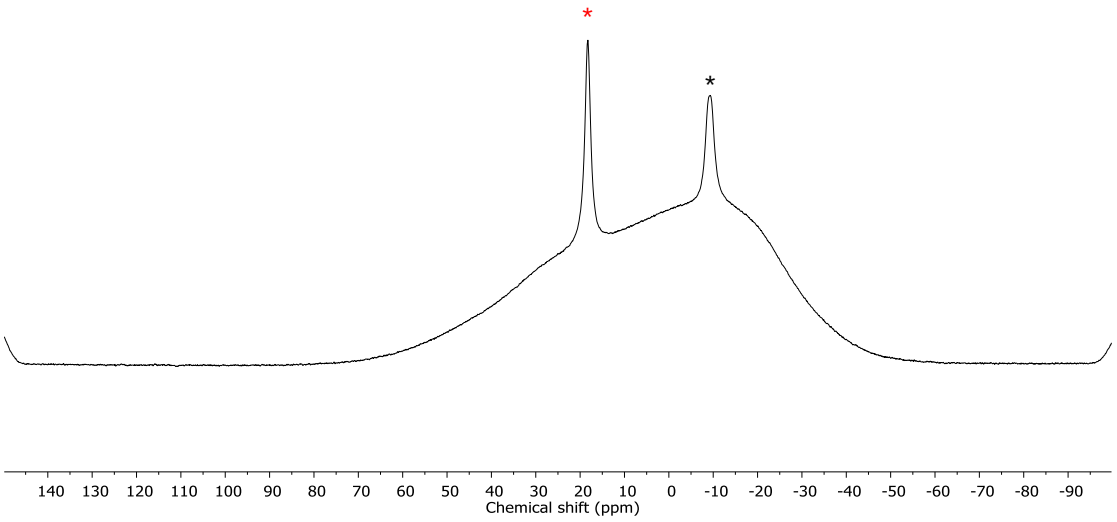


Figure A6.1. ^{11}B NMR spectrum (C_6D_6, 160.4 MHz, 298 K) of the equimolar reaction between ($Tp^{tBu,Me}$)Mg(Cy-H) (**13**) and $B(Cy\text{-}H)_3$. "*" denotes $B(Cy\text{-}H)_3$. "*" denotes the apical B-H of **13**.

A7. NMR tube scale reaction between (*S*,*S*)-(BOPA^{Ph})Mg(BH$_4$)(THF) ((*S*,*S*)-23) and 10 equiv. of *rac*-LA

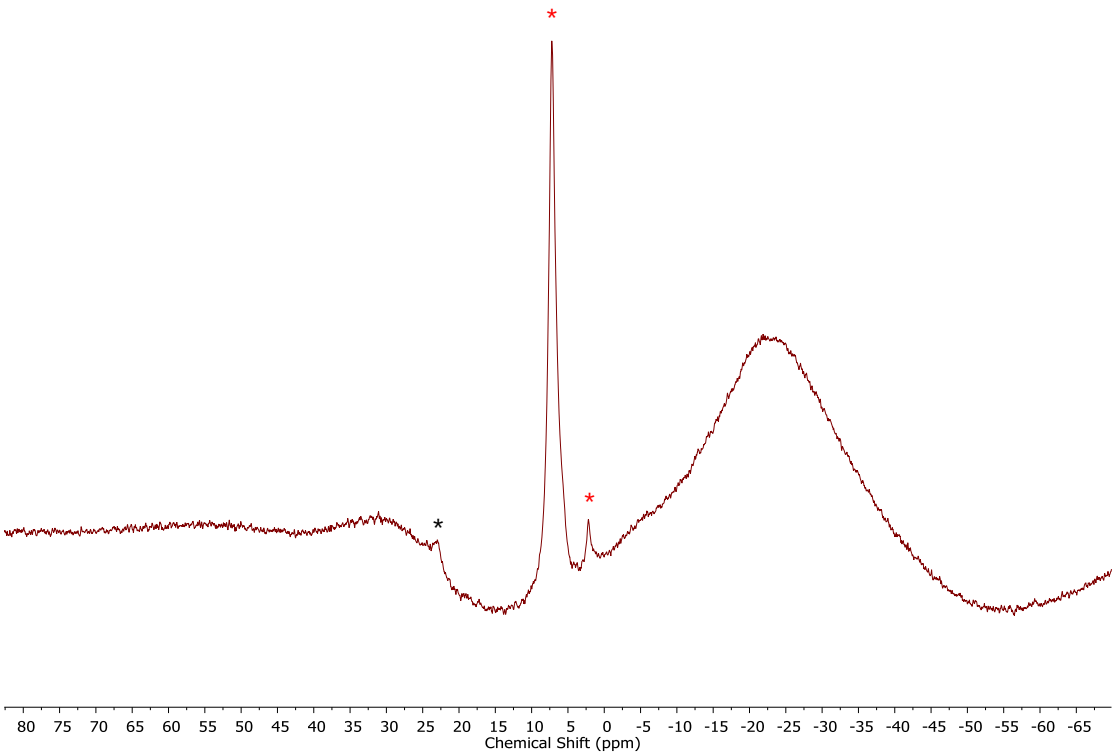


Figure A7.1. ^{11}B NMR spectrum (THF-d_8, 128.4 MHz, 298 K) of the reaction between (*S*,*S*)-(BOPA^{Ph})Mg(BH$_4$)(THF) (**(*S*,*S*)-23**) and 10 equiv. of *rac*-LA. "*" denotes tetra-coordinated adduct species. "*" denotes "B(LA-H)$_3$".

A8. NMR tube scale reaction between (*S*,*S*)-(BOPA^{Ph})Mg(BH$_4$)(THF) ((*S*,*S*)-23) and 4 equiv. of benzaldehyde

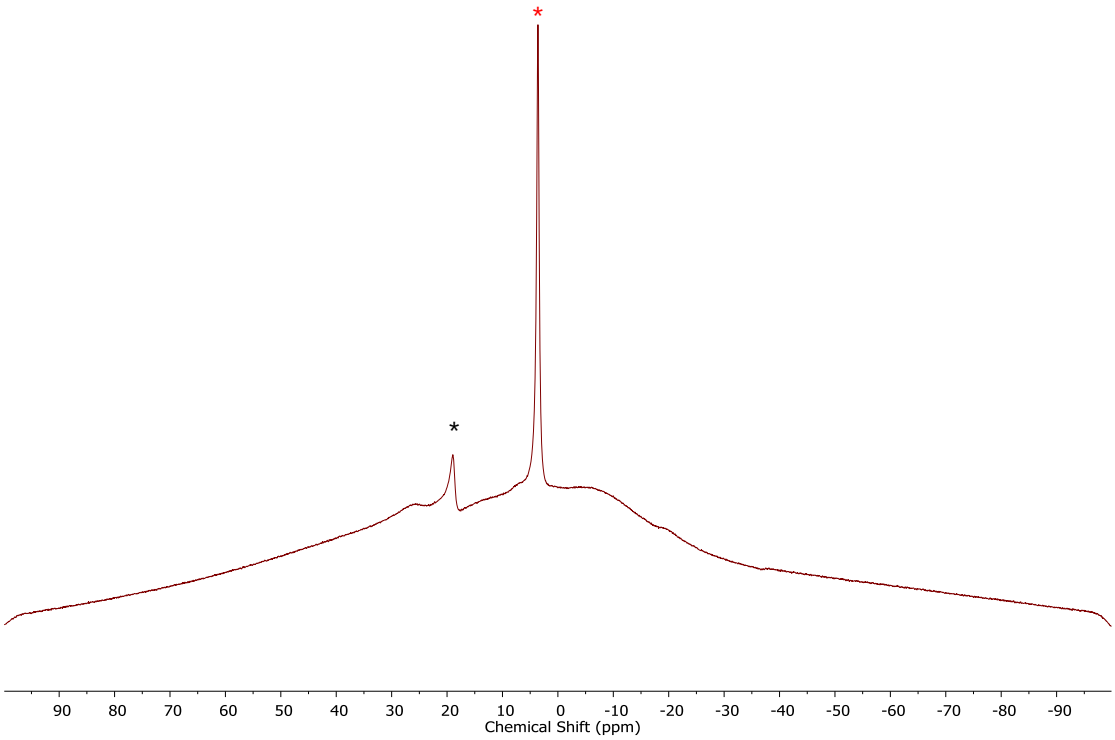


Figure A8.1. ^{11}B NMR spectrum (C_6D_6, 128.4 MHz, 298 K) of the reaction between (*S*,*S*)-(BOPA^{Ph})Mg(BH$_4$)(THF) (**(*S*,*S*)-23**) and 4 equiv. of benzaldehyde. "*" denotes (*S*,*S*)-(BOPA^{Ph})Mg(OBn){B(OBn)$_3$} (**28**). "*" denotes B(OBn)$_3$.

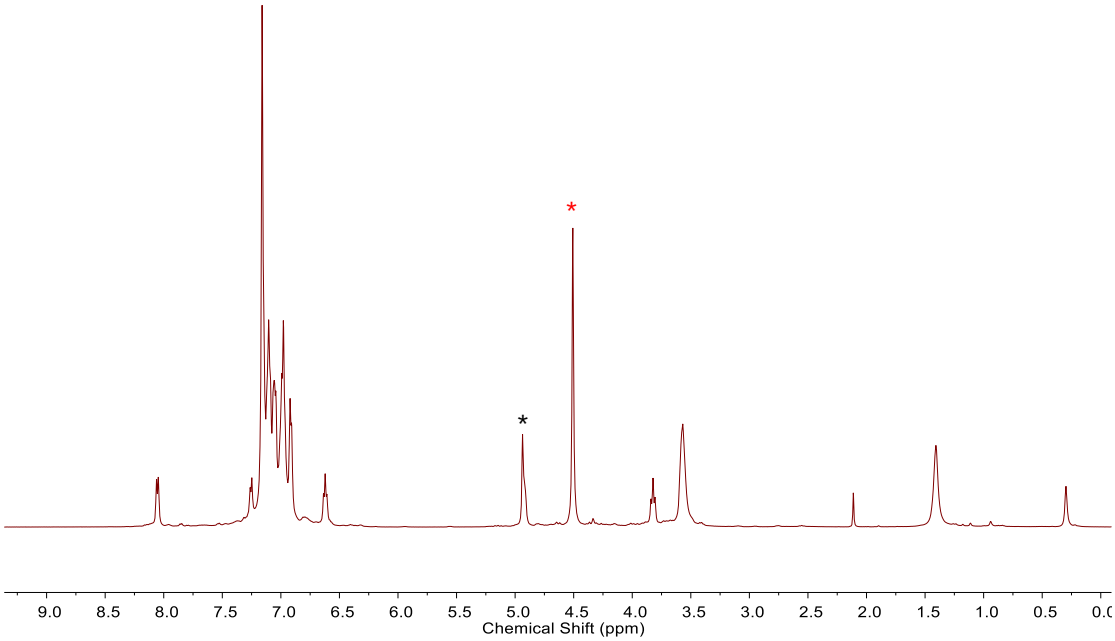


Figure A8.2. ^{1}H NMR spectrum (C_6D_6, 400.2 MHz, 298 K) of the reaction between (*S*,*S*)-(BOPA^{Ph})Mg(BH_4)(THF) (**(*S*,*S*)-23**) and 4 equiv. of benzaldehyde. "*" denotes methylene protons on the bridging and terminal OBn fragments of (*S*,*S*)-(BOPA^{Ph})Mg(OBn){$B(OBn)_3$} (**28**). "*" denotes $B(OBn)_3$.